DISSERTATION

DEVELOPMENT OF LEWIS PAIR METHODOLOGIES FOR ADVANCED POLYMER SYNTHESIS AND APPLICATION

Submitted by

Michael Lawrence McGraw

Department of Chemistry

In partial fulfillment of the requirements

For the Degree of Doctor of Philosophy

Colorado State University

Fort Collins, Colorado

Spring 2022

Doctoral Committee:

Advisor: Eugene Y.-X. Chen

Travis S. Bailey
Anthony K. Rappe
James C. Linden

Copyright by Michael L. McGraw 2022
All Rights Reserved

ABSTRACT

DEVELOPMENT OF LEWIS PAIR METHODOLOGIES FOR ADVANCED POLYMER SYNTHESIS AND APPLICATION

This dissertation describes the development of new chemistries related to Lewis pair polymerization methodology with emphasis on chemical selectivity and control. Selectivity is defined as the ability to promote desirable chemistry while simultaneously discouraging unwanted chemistry. Control is defined as the ability to target specific and highly sophisticated products from the outset and the ability to reliably achieve that desired product as a consequence of predictable reaction behavior. The themes contained herein relate to catalysis, mechanism elucidation and application, polymer synthesis, and green chemistry.

Chapter 1 introduces LPP and includes sections from my published perspective article *Lewis Pair Polymerization: Perspective on a Ten-Year Journey*. This chapter includes a brief history of the technique, as well as mechanistic fundamentals and key features of the method. Chapters 2 & 3 describes the LPP of the challenging biorenewable monomer methyl crotonate. Chapter 4 describes the invention of the compounded sequence control (CSC) LPP method. Chapter 5 discusses the application of CSC to the synthesis of more advanced cyclic diblock structures using by utilizing a unique sorbate-based initiation system. Chapter 6 details the mechanism by which the sorbate-based initiation system effects cyclization to produce cyclic polymers with spatial and temporal control. Finally, chapter 7 offers some conclusions and future directions.

ACKNOWLEDGEMENTS

Chapter 1. This dissertation chapter contains selections from the perspective article published in Macromolecules [McGraw, M. L.; Chen, E. Y.-X. Lewis Pair Polymerization: Perspective on a Ten-Year Journey. *Macromolecules* **2020**, *53*, 6102− 6122]. This work was supported by the U.S. National Science Foundation (NSF-1904962).

Chapter 2. This dissertation chapter contains the article published in ACS Catalysis [McGraw, M.; Chen, E. Y.-X. Catalytic Lewis Pair Polymerization of Renewable Methyl Crotonate to High-Molecular-Weight Polymers. *ACS Catal*. **2018**, *8*, 9877−9887]. This work was supported by the U.S. National Science Foundation (NSF-1507702).

Chapter 3. This work was supported by the US National Science Foundation (NSF-1507702). This dissertation chapter contains the manuscript of a full paper published in Tetrahedron [McGraw, M. L. & Chen, E. Y.-X. Borane/silane frustrated Lewis pairs for polymerization of β-substituted Michael acceptors. *Tetrahedron* **2019**, *75*, 1475–1480].

Chapter 4. This work was supported by the United States National Science Foundation, grant NSF-1904962. This dissertation chapter contains the manuscript of a communication published in the Journal of the American Chemical Society [McGraw, M. L.; Clarke, R. W.; Chen, E. Y.-X. Compounded Sequence Control in Polymerization of One-Pot Mixtures of Highly Reactive Acrylates by Differentiating Lewis Pairs. *J. Am. Chem. Soc.* **2020**, *142*, 5969−5973].

Chapter 5. This work was supported by the United States National Science Foundation, grant NSF-1904962. This dissertation chapter contains the manuscript of a communication published in the Journal of the American Chemical Society [McGraw, M. L.; Clarke, R. W.; Chen, E. Y.-X. Synchronous Control of Chain Length/Sequence/Topology for Precision Synthesis of Cyclic Block Copolymers from Monomer Mixtures. *J. Am. Chem. Soc.* **2021**, *143*, 3318–3322].

Chapter 6. This work was supported by the United States National Science Foundation, grant NSF-1904962. This dissertation chapter contains the manuscript of a full paper that is under review during the writing of this dissertation [Towards Spatial and Temporal Control in Precision Cyclic Polymer Synthesis by Lewis Pair Polymerization]

DEDICATION

This work is dedicated to my family.

TABLE OF CONTENTS

Chapter 1
Introduction to Lewis Pair Polymerization

1.1 Background and Significance

Lewis Pair polymerization (LPP),[1-3] a polymerization method introduced in 2010,[4] uniquely utilizes both Lewis acid (LA) and Lewis base (LB) components to cooperatively and synergistically activate and polymerize a diverse scope of monomers. Through balancing the relative strength of LAs and LBs as well as steric interplays of Lewis pairs (LPs), chain initiation (k_i), propagation (k_p), termination (k_t), and transfer (k_{tr}) events can be significantly affected by Lewis pairing (during k_i) and ion pairing (after k_i) dynamics, thus modulating *activity*, *control* (initiation efficiency, livingness, chain structure, topology, sequence), and *selectivity* (regio, chemo and stereoselectivity). The simple yet sophisticated chemistry of LPP has notably advanced synthetic polymer chemistry over the last ten years and continually inspired us and many other researchers to solve modern polymerization problems. By the time of the writing of this dissertation, LPP has been exploited to enable living polymerizations of many polar vinyl monomers[5-7] and controlled polymerizations of some of the most challenging vinyl monomers.[8-11] LPP has also been used to effect polymerizations of heterocyclic monomers, such as lactones,[2,12] epoxides,[13,14] cyclic carbonates,[15,16] and cyclic anhydrides.[17] The control of polymer topology,[14,18] architecture,[7] and sequence[19] has also been achieved by the LPP method.

Despite the significant advances already made over the past ten years, LPP is still a relatively young field as compared to other well-developed polymerization methods, and many features and opportunities for discovery are still unexplored. Just to highlight two frontiers at the outset, the chemoselectivity of LPP has been utilized to polymerize biorenewable monomers that are not polymerizable or polymerized effectively otherwise. As biomass conversion technology advances,

many new bio-based monomers will become accessible and affordable. Utilization of such monomers represents not only a carbon-neutral strategy towards sustainable plastics but also an abundant, yet underexploited, source of carbon. However, biorenewable monomers are typically highly functionalized, as compared to petroleum-derived monomers before downstream functionalization, and therefore difficult to polymerize due to chemoselectivity challenges by conventional polymerization methods. In this context, LPP has successfully solved some notable challenges, polymerizing bio-based, multi-functional monomers such as sorbates,[18] crotonates,[9,20,21] cinnamates,[10] vinyl-functionalized α-methylene-γ-butyrolactones,[22] and β-angelica lactone,[8] effectively and chemoselectively by suitable LPs. On the second frontier in the synthesis of sequence-controlled polymers, most recently LPP enabled the rapid and scalable synthesis of a record 53-block copolymer (BCP) at room temperature (RT) through sequential additions of comonomers, demonstrating the remarkable robustness and living/ immortal features of the LPs employed in that system.[23] Another powerful demonstration of the unique utility of LPP in the sequence-controlled polymer synthesis is direct polymerization of one-pot mixtures of highly reactive acrylates to well-defined and resolved di- or tri-BCPs through LPP's uniquely compounded thermodynamic and kinetic differentiation.[19]

As mentioned in the abstract, the key advantages of LPP revolve around themes of ***selectivity*** and ***control***. Thus, to understand the source of such selectivity and control we must first discuss ***mechanism*** and ***kinetics***. Accordingly, this chapter examines these fundamental features of LPP, with an emphasis placed on the identification and strategic application of the key, unique features characteristic of LPP, to give perspective on how they are applied in the later chapters, and how they are made useful amongst the broader picture of polymer chemistry.

1.2 Mechanism

1.2.1 General considerations: Lewis paring, initiation, and propagation

All LPP systems employ both LA and LB components. The LA component is typically an electrophile with a single coordination site, so that when the terminal growing anions such as an enolate or alkoxide binds to the LA, the LA is saturated with electrons and cannot bind another free monomer. Thus, typically one LA is used to stabilize the active species while another activates the incoming monomer. The most frequently employed LAs are electro-deficient, coordinatively unsaturated compounds of group 13 elements (Al, B), which have smaller ionic radii compared to transition metals and complete an octet after coordination of a single monomer. Cationic silylium (R_3Si^+) species behave in a similar way. Transition metal LAs are rarely used, but complexes of some rare-earth elements[24-26] have been used. Many other common and readily available LAs have been used for ring-opening polymerization (ROP), including complexes or salts of Zn^{2+}, Li^+, Mg^{2+}, and Y^{3+} ions (Figure 1.1).

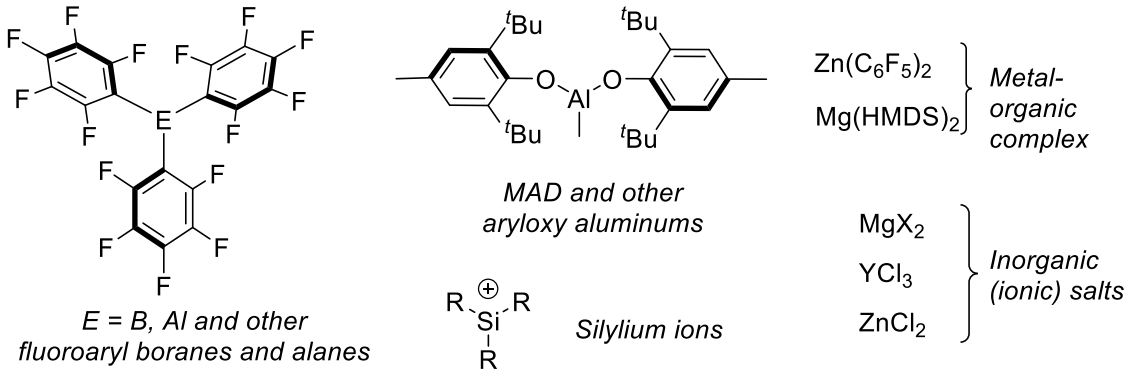

Figure 1.1. Classes of LAs.

The LB component is typically a neutral base, predominately organic compounds, such as phosphines (PR_3), tertiary amines (R_3N), pyridines (Py), phosphazine superbases (PSB), *N*-heterocyclic carbenes (NHC), *N*-heterocyclic olefins (NHO), *N*-heterocyclic imines (NHI),

hydrosilanes (R_3SiH), and silyl ketene acetals (SKA) (Figure 1.2). Most of them are strong neutral bases, and often also nucleophiles, which become cationic following attack on an electrophile.

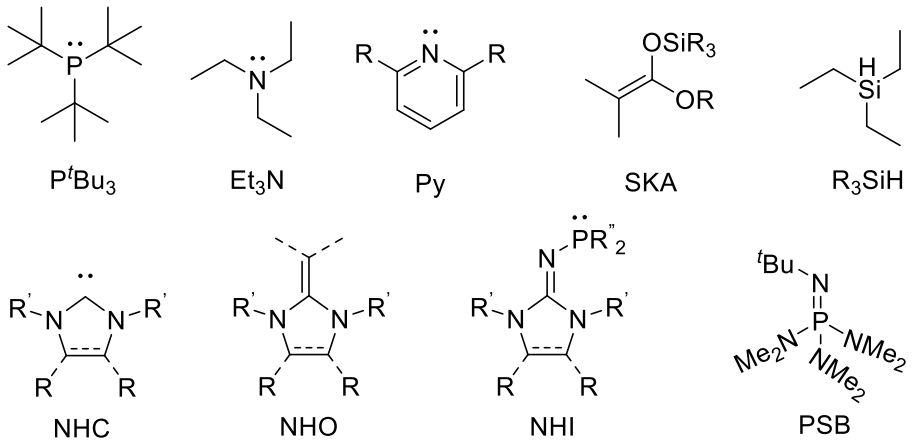

Figure 1.2. Classes of LBs.

One factor always worth considering is the possibility of the LB attacking the LA to form a stable classical Lewis adduct (CLA). If this interaction is irreversible, a fraction of the LP will be poisoned, leading to low initiator efficiency, and this is the case for several reported LPP systems.[2-4] It is therefore advantageous, if the LP interaction is weak and reversible (i.e., the case of interacting LPs), or better yet, if the LP is sterically frustrated (Figure 1.3). In almost all non-frustrated Lewis pair (FLP) cases, the best way to avoid initiation inhibition due to strong Lewis paring is to first premix the LA (employed in a catalytic amount relative to monomer) and the monomer, so that the LA is coordinated to a monomer before exposure to the LB.

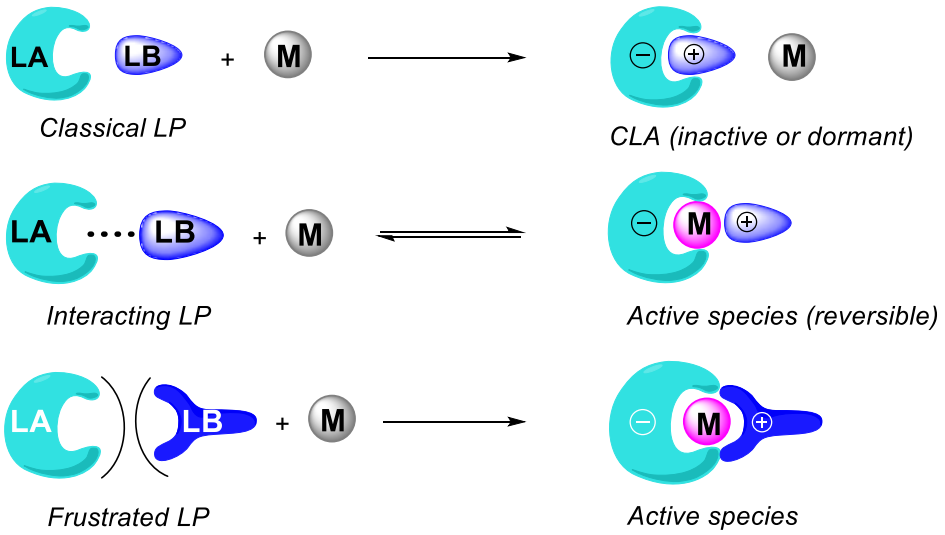

Figure 1.3. Effects of degree of the Lewis pairing on initiation.

One key advantage of LPP is the extraordinary degree of tunability inherent to it. Individual aspects of a polymerization, such as events involving initiation (k_i), propagation (k_p), termination (k_t), and chain transfer (k_{tr}), can be targeted and manipulated with an unprecedented level of selectivity. The tunability of this system is a consequence of many factors. (1) The ability to manipulate both the LA and LB components *independently* grants a higher level of control to LPP in comparison to other methods. Both the LA and LB structures render significant impact on the polymerization character. Thus, being able to manipulate one but not the other in any particular scenario, is extremely useful. (2) The very nature of LA and LB structures is a very sensitive and delicate relationship between structure and reactivity. As a consequence, a great variety in reactivity can be obtained by simple structural changes. (3) The rapid growth of independent fields of organocatalysis[27-34] and main-group FLP chemistry[35-39] has provided the LPP field with a massive library of LP structures available for synthesis or commercial availability. (4) The LA and LB components commonly have simple structures, accessible in only a few synthetic steps, making a great variety of structures and therefore reactivities accessible with little investment.

Although many variations on the mechanism of LPP exist, there is a common thread that unites and defines all LPPs: the LA propagation cycle, generally involving first activation of a free monomer (M) by a free LA followed by addition of active growing chain (P_n^*) to the activated monomer (M^*) as the rate-determining step (*r.d.s.*) and finally release of the LA (Figure 1.4). The LA cycle is critical to the way we think about these polymerizations. In particular, the two-step activation process (activation followed by chain addition) fundamentally changes the kinetics and the selectivity of polymerization. Consequently, much of our work is related to ways upon which one can exploit the kinetic and selective advantages associated with this two-step activation.

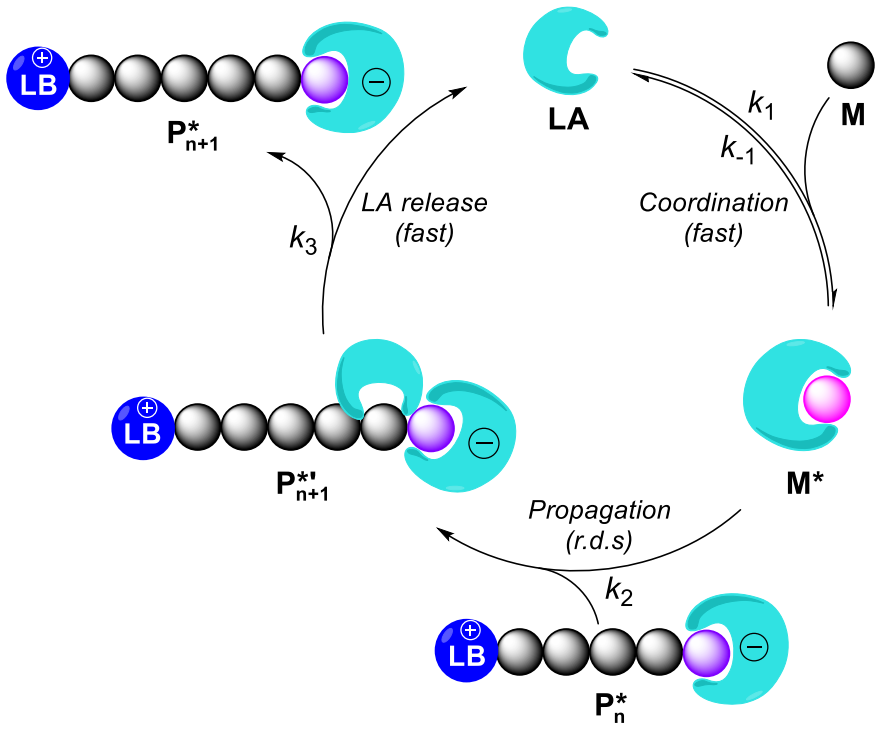

Figure 1.4. Propagation cycle defining LPP

To illustrate the contrast between LPP and typical chain-growth polymerization, here we first consider two analogous polymerization reactions (Figure 1.5), one being the organocatalytic conjugate-addition polymerization of methyl methacrylate (MMA. Note that, for simplicity and

consistency, we use MMA to represent common polar vinyl monomers throughout this chapter) by an NHC,[40,41] and the other being LPP of MMA by an NHC/$Al(C_6F_5)_3$ LP.[2] The former, has been commonly referred to as *zwitterionic polymerization*, as both positive and negative charges are covalently tethered on the active species. Such zwitterionic species can adopt both the open chain form (active for further monomer additions) and the cyclic, spiro form (dormant state), the relative stability of which depends on the NHC and monomer structures as well as the solvent polarity. And although both of these examples do contain zwitterionic active species, the latter must be distinguished as LPP because the contrast in reactivity provided by the LA. In the LPP case, the zwitterionic active species do not react with free monomer, but only an activated equivalent of monomer, *making the free monomer essentially solvent molecules* to dissipate heat in a bulk LPP. This scenario gives the polymerization zero-order rate dependence on $[MMA]_t$ and first order in $[LA]_t$ (typically this is understood as $[LA]_0$). As a consequence, the conversion vs time profile of the LPP reaction would be a linear curve from start to finish. In contrast, the zwitterionic polymerization propagates with any free monomer in solution. Thus, the rate has first-order dependence on $[MMA]_t$ and therefore experiences a first-order decay as MMA is consumed. This first-order decay is present in almost any other chain-growth polymerization method, including typical anionic, coordination, and radical methods. Thus, it is an important distinction which has led to several innovations (*following chapters*). Likewise, the stabilization of the zwitterionic intermediate is key for selectivity and control in that it is generally very stable and not prone to unwanted side reactions such as chain-termination and chain-transfer. As a general rule, the LA-stabilized nucleophilic chain end does not react with any carbonyl other than a carbonyl activated by a 2nd equivalent of LA.

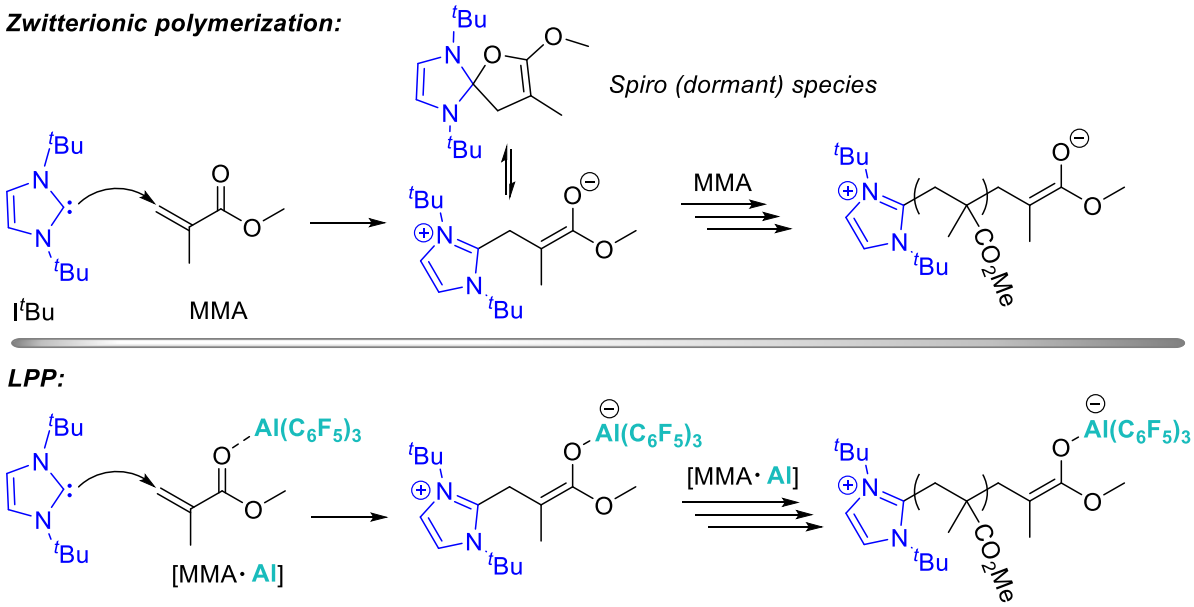

Figure 1.5. Mechanistic comparisons of zwitterionic polymerization and LPP

Next, we should compare LA-mediated anionic polymerization[42,43] and LPP (Figure 1.6) to point out some important distinctions as well. (1) The anionic active species is comprised of an anionic enolate and a metal (M_t) cation derived from initiation by a charged, anionic nucleophile. This results in a very tight ion pairing with little spatial separation between ions, thus lowering the energy of the active species through electrostatic stabilization. In comparison, the zwitterionic active species typically found in LPP is comprised of a highly separated ion pair, with anion and cation found on opposite ends of the growing polymer chain, thus the looser ion pairing (Figure 1.6) results in a more reactive enolate. (2) The cationic initiating group attached to the α-terminus during LPP can potentially act as a leaving group, opening up the possibility of cyclic polymer formation and chain transfer, while the inert Nu (e.g., alkyl) initiating end-group found in anionic polymerization will not react and can be therefore forgotten. In other words, the Nu in LA-mediated anionic polymerization plays a role only in chain initiation, while the LB in LPP can play a role in not only chain initiation but also propagation and transfer. This is concept is largely

disputed in chapter 6, but is certainly relevant to ring-opening polymerization examples and may be relevant to vinyl addition LPP in the future. (3) The LA-mediated anionic polymerization can be tuned by the choice of LA, and has perhaps a few metal ions to choose from, while the LPP has an enormous library of LBs to choose from which not only change the character of chain initiation and propagation but also provide access to different mechanisms. (4) Organic LBs are usually soluble in organic solvents inorganic (ionic) initiators, leading to more convenient system preparation, compatibility, and smoother initiation processes.

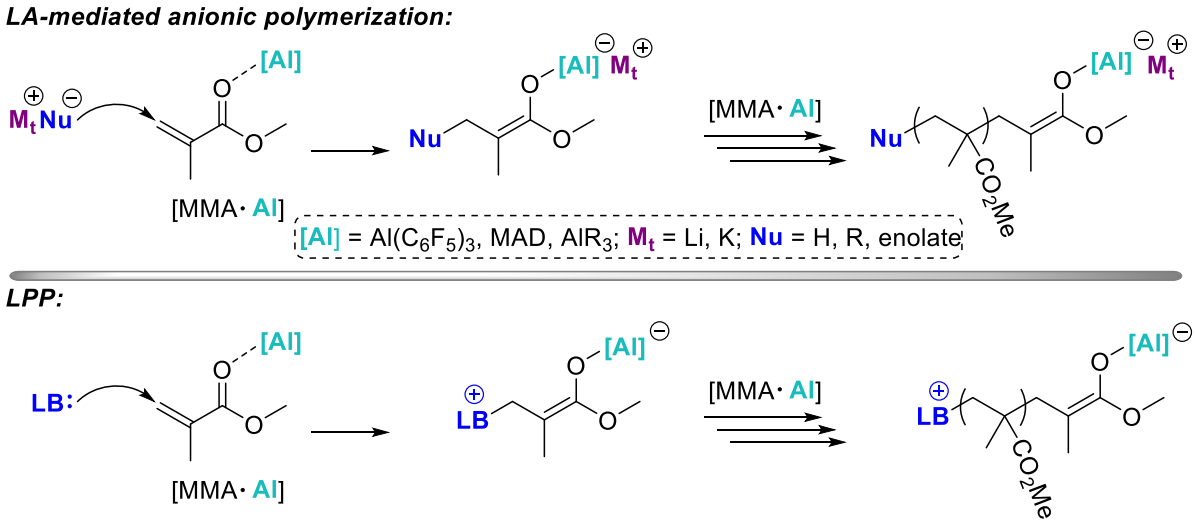

Figure 1.6. Mechanistic comparisons of LA-mediated anionic polymerization and LPP

One might be tempted to think the LB is important during the initiation step but negligible thereafter. However, this would be a mistake as the *LB plays a critical role in not only initiation but also in propagation and chain transfer*. For example, in our recent study on the LPP of methyl crotonate (MC),[9] we performed a direct comparison between several LBs while keeping the LA constant throughout. In particular, two LBs, an NHO, 1,3-dimethyl-4,5-diphenyl-2-(propan-2-ylidene)-2,3-dihydro-1H-imidazole), and an NHC, 1,3,4-triphenyl4,5-dihydro-1H-1,2,4-triazol-5-ylidene (TPT), both operated by the same zwitterionic LPP mechanism and the cationic end groups

generated by them were similar in structure, containing 5-membered heterocycles with phenyl substitutions. The only differences, apart from the exact phenyl substitution, were that the NHO contained an imidazolium frame while TPT a triazolium. This seemingly subtle change imparted notable changes on both the activity of polymerization and propensity for chain transfer. For example, the TPT cation promoted a slower, but a more controlled, polymerization with low dispersity ($Đ$ = 1.18), presumably due to formation of a tighter ion pair with the enolaluminate anion and therefore being less prone to transfer. Similarly, Rieger[44] found in LPP of *tert*-butyl methacrylate (^{t}BMA), that the sterics associated with the phosphine LB employed had an effect on the chain-end controlled stereo-selectivity of the LPP, with PCy_3 providing noticeably higher syndioselectivity than PEt_3, presumably due to the proximity of the bulky cyclohexanyl ligands to the transition state of propagation. In general, it should be assumed that ion-pairing exists between the cationic LB end group and the anionic enolate or alkoxide end group, whether inter- or intramolecular (Figure 1.7), or solvent-separated states, depending on the nature of solvent and added additives if any (such as salts),[1] and has a significant effect on the transition state of propagation.

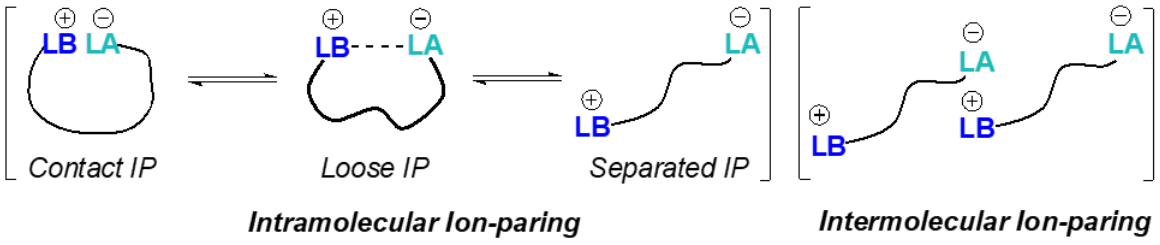

Figure 1.7. Zwitterionic ion-pairing modes during chain propagation in LPP (IP = ion pair).

1.2.2 Vinyl-addition LPP

The aforementioned case, *zwitterionic* mode (Figure 1.8), was not only the first mode discovered, but is also most common.[2-5,6,9,11,18,19,44-56] In the zwitterionic mode (Z-LPP), a neutral LB undergoes a nucleophilic attack on an activated monomer to generate a zwitterionic active species. The active species containing an enolate goes on to propagate with an activated monomer. Z-LPP is typically highly active and chemoselective, making it a robust option. For example, several extended polar vinyl monomer families including acrylamides,[3,6,44,57] vinyl phosphonates,[44,57] vinyl pyridines,[44-57] and vinyl oxazolines,[44,45] and most recently acrylates[58] have been effectively polymerized by the zwitterionic mode. It is most common because typical polar vinyl monomers have an electrophilic site most prone to nucleophilic addition by the LB.

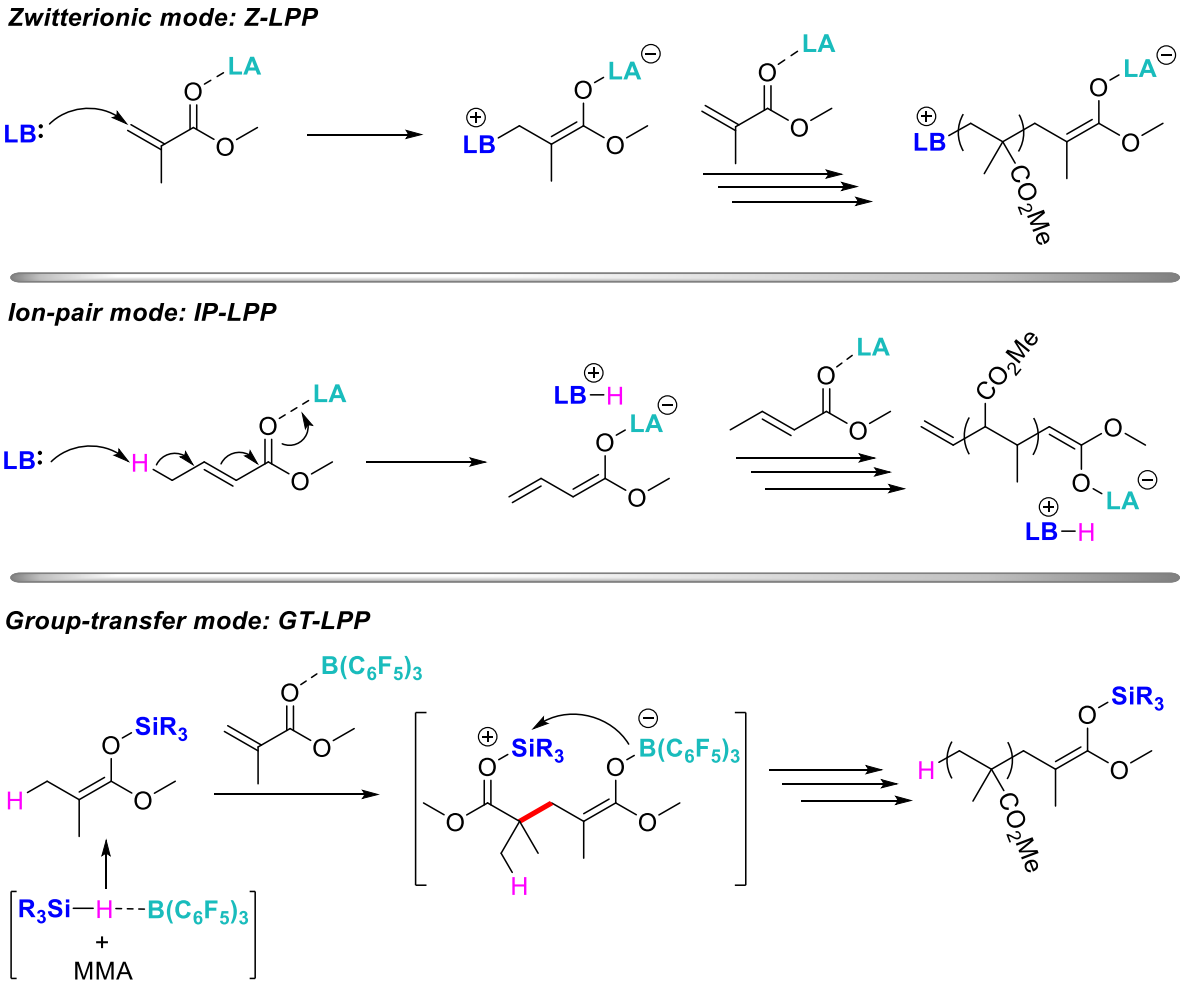

Figure 1.8. Mechanism of vinyl-addition LPP operating in three different modes

The second case, *ion-pair* mode (Figure 1.8),[8,9,44] can occur if there is an acidic proton on the activated monomer. In this event, the LB deprotonates the activated monomer, generating an enolate stabilized by the protonated LB cation. In the case of crotonates, IP-LPP reactions are notably more reactive than their zwitterionic analogues and are also prone to chain transfer via deprotonation of the protonated LB by the LA-stabilized enolate and subsequent re-initiation by the released free LB. This unique reaction sequence allows polymers to be synthesized in a catalytic fashion.

In the third case, LPP can operate in *group transfer* mode—GT-LPP (Figure 1.8), which can be considered a special case (LA-mediated) group transfer polymerization (GTP).[59-63] Although there are several GTP mechanisms,[1] the LA-catalyzed variant, or GT-LPP, is unique in that it relies on a *r.d.s.* being the conjugate addition to LA-activated monomer. Therefore, the selectivity and kinetic themes discussed herein are only relevant to this particular group transfer variant. GT-LPP can either be executed by an SKA coupled with an auxiliary LA,[20,64-70] such as $B(C_6F_5)_3$, or through an SKA/SiR_3^+ pair. In the former case, an SKA at the ω-terminus acts as a nucleophile and does a conjugate addition on an LA-activated monomer. The result is a zwitterionic intermediate containing a cationic silylium and an anionic auxiliary LA-stabilized enolate. The enolate oxygen then quickly recaptures the silylium moiety and releases a free LA. GT-LPP can be initiated by FLP-type hydrosilylation of a polar vinyl monomer or using a monomeric SKA directly. These reactions are typically less active than their zwitterionic counterparts and are the most selective of any mode, due to the stability of the neutral SKA. On the other hand, an SKA/SiR_3^+ pair can be generated through hydride abstraction, or from deprotonation[71-74] of a strong Brønsted organic acid by an SKA. The activity of these reactions can be tuned by the degree of interaction with the charge

compensating anion. For example, silylium $[SiR_3]^+[B(C_6F_5)_4]^-$ can be generated by hydride abstraction[75-78] of an SKA or a hydrosilane. The formal cation will render a highly reactive system. In contrast, $(Tf)_2NH$ can be deprotonated by an SKA to render $[SiR_3]^+[(Tf)_2N]^-$, which exists as a weakly bonded (and thus much more stable) $(Tf)_2N—SiR_3$.[7,10,21,79]

1.3 Kinetics

1.3.1 General considerations: Lewis paring, initiation, and propagation

The unique LPP mechanism which disposes itself to several exploitable features (Figure 1.4) follows:

1. $$rate = k_2[LA]_0[LB]_0 \approx k_2[M^*]_t[P^*]_t$$

(where $[LB]_0 \sim [P^*]_t$, the concentration of zwitterionic active species; and $[LA]_0 \propto [M^*]_t$, the concentration of activated monomers) and subsequently gives linear conversion vs time plots. It should be noted that one equivalent of LA is consumed at the start of the reaction to generate the active species. Thus, in an experimental scenario, a 2/1 LA/LB ratio actually yields a 1/1 $[M^*]/[P^*]$ ratio, but for the purposes of this discussion, that will be neglected. Equation 2 differs from typical (nearly inescapable) chain-growth kinetics which follow rate = $k_p[P^*]_t[M]_t$, where $[P^*]_t$ (active growing chains). Several interesting conceptual advancements follow. First, the kinetics of LPP allow the targeted MW ($[M]_0/[LB]_0$) and the targeted polymerization activity ($[LA]_0$) to be split between two different handles. For example, should there be a desire to increase the MW of any given LPP, one could simply decrease the $[LB]_0$, while compensating the $[LA]_0$ to maintain the reasonable reaction times and full monomer conversion. In theory, *ultra-high MW can be achieved by this strategy without compromise in activity and conversion*, simply by independent manipulation of the [LA]/[LB] ratio.

To illustrate this point, Figure 1.9 shows four different simulated LPP reactions, all making DP = 1000 polymers with varying activity as a consequence of different $[LA]_0$. Correlation of this activity dependence on $[LA]_0$ reveals a 1st order relationship. Although not shown, a similar manipulation of the $[LB]_0$ concentration would also reveal a 1st order dependence on $[LB]_0$. For comparison, with typical 1st order chain-growth kinetics, should there be a desire to increase MW, one would do so by decreasing the initiator loading and in doing so would also decrease the activity since the active species ($[P^*]_t$) is in lower concentration. This strategy of two-component manipulation can be used when polymerization is thermodynamically feasible but kinetically slow to push polymerizations to completion, which was demonstrated during the synthesis of high MW PMC, where M/LA/LB ratios of 2000/64/1 were employed to force polymerization of unreactive MC to occur in a reasonable timeframe.[9]

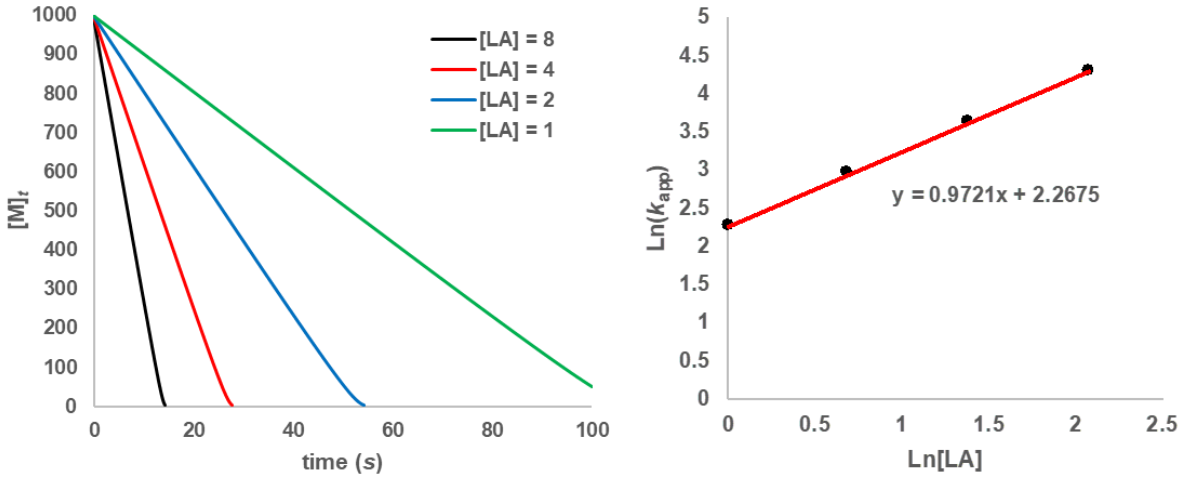

Figure 1.9. COPASI (Complex Pathway Simulator) simulation (left) of generalized LPP according to Figure 1.4, with differing $[LA]_0$. Conditions: K_{eq} (k_1/k_{-1}) = 1; k_2 = 10; k_3 = 100; $[M]_0$ = 1000; $[LB]_0$ = 1; $[LA]_0$ = {1, 2, 4, 8}. And (right) Ln$[LA]_0$ vs Ln(k_{app}) plot, k_{app} calculated from the slope of each line.

Likewise, this strategy can be used to slow down polymerizations of highly reactive monomers in order to obtain a more controlled system. This is relevant to solvent-free, bulk or neat

polymerizations, which are considered to be more environmentally friendly. Since the LA-stabilized active species cannot interact with the unactivated free monomer, the free monomer is not included in the rate law and can therefore be considered a solvent. Thus, (even highly reactive and exothermic) liquid monomers can theoretically be polymerized without solvent to any desired MW if the $[LA]_0$ is appropriately lowered to an extent where polymerization is slow and controlled, and *the inert free monomer, acting as a solvent, will dissipate the heat produced by polymerization and ensuring even mixing.*

Of course, with the conditions illustrated in Figure 1.9—and in most reported cases—it is reasonable to make the assumption that $[LA]_0 = [M^*]_t$, because in most cases the equilibrium k_1/k_{-1} is shifted far to the right, and most of the LA's time is occupied by coordination to monomer. However, this is not exactly true. The rate determining step, written as $k_2[M^*]_t[P^*]_t$, contains $[M^*]_t$ which is in fact a function of monomer concentration, solved for by a simple pre-equilibrium approximation:

1. $$[M^*]_t = \frac{k_1[M]_t[LA]_t}{k_{-1}}$$

And since $[LA]_t$ is in catalytic concentration, its time dependence will be neglected since any change in $[LA]_t$ would be dwarfed by the change in $[M]_t$ for intents and purposes related to the overall rate law. Thus, we can consider $[M]_t$ as the only variable.

2. $$[M^*]_t = [M]_t\left(\frac{k_1[LA]_0}{k_{-1}}\right)$$

It can be seen from eq. 4 that as $[M]_t$ decreases, $[M^*]_t$ decreases. Careful observation of Figure 1.9 will reveal a slight deviation from linearity near full conversion, which is due to the $[M^*]_t$ dependence on $[M]_t$. Note that, the K_{eq} for this modeled system, or the ratio of k_1/k_{-1}, is set simply to 1. Thus, even at a conservative estimate of the LA/monomer coordination affinity, there is

substantial constancy to the prior assumptions that $[M^*]_t = [LA]_0$ (as judged by the linearity of the $[M]_t$ vs time plot). We generally assume that this K_{eq} is much higher than 1, therefore $[M^*]_t = [LA]_0$ is a good assumption. However, we normally judiciously choose solvents for LPP, such as toluene or methylene chloride, because they rarely interact with the LA (except $Al(C_6F_5)_3$ that, in the absence of monomer, binds toluene and reacts with methylene chloride). If the solvent can foreseeably interact with the LA, then the $[M^*]_t/[M]_t$ equilibrium may be dramatically driven to the left. Likewise, if there is interaction between the LA/LB, this would also drive the equilibrium to the left. This kind of interaction would present itself as being either 1st order or pseudo-1st order with respect to monomer. Figure 1.10 shows the simulated curve of a LPP where the M---LA coordination is weak, with the k_1/k_{-1} (or K_{eq}) being 0.01 and 0.001. The former ($K_{eq} = 0.01$) yields a pseudo-1st order plot, where the $[M]_t$ vs time plot shows a mostly linear curve that becomes nonlinear towards the end of the reaction. The latter ($K_{eq} = 0.001$) is seemingly nonlinear throughout the course of the reaction and has a near ideal fit to the 1st order plot ($-Ln([M]_t/[M]_0)$ vs time).

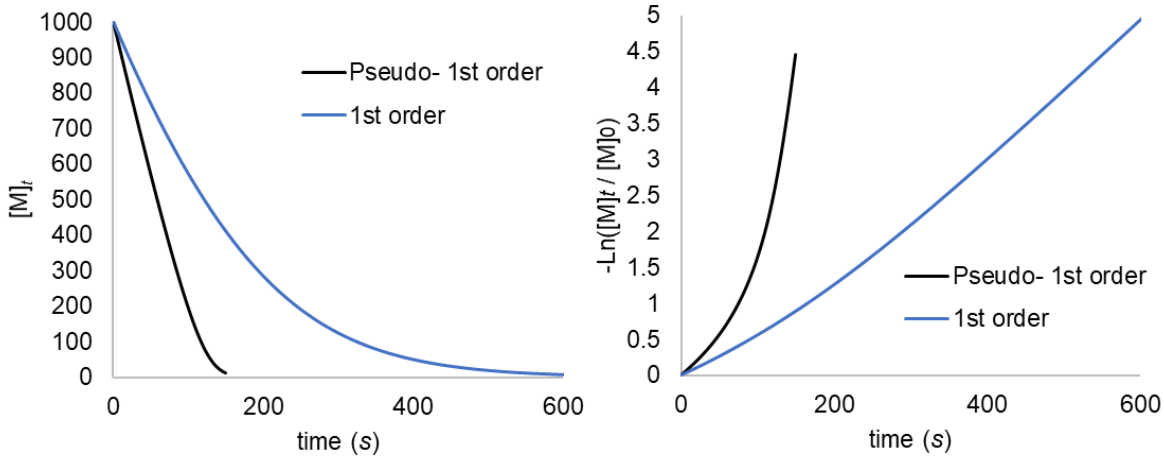

Figure 1.10. COPASI simulation (left) of LPP according to Figure 1.4, with exceptionally low K_{eq}, showing departure from zero-order $[M]_t$ dependence and gradual adoption of 1st-order $[M]_t$

dependence. Conditions: (k_1/k_{-1}) K_{eq} = {0.01 (black), 0.001 (blue); k_2 = 10; k_3 = 100; $[M]_0$ = 1000; $[LB]_0$ = 1; $[LA]_0$ = 1. And (right) 1st order plots of both curves, showing a linear fit at K_{eq} = 0.001.

If the reaction is 1st order, yet still following the LPP mechanism, the differential concentration of the activated monomer must now be considered in the rate law giving:

3. $$rate = k_2[P^*]_t \frac{k_1[M]_t[LA]_t}{k_{-1}}$$

Since both LA and LB are at catalytic concentrations and hardly change throughout the course of the reaction, $[P^*]_t$ and $[LA]_t$ can be made $[LB]_0$ and $[LA]_0$, respectively. Lastly, k_1/k_{-1} can be understood as K_{eq}, the equilibrium constant of coordination, giving:

4. $$rate = K_{eq}k_2[M]_t[LA]_0[LB]_0$$

Thus, if the coordination of monomer to LA is weak, or K_{eq} is far less than one, it will follow the above rate law and have 1st-order dependence on $[LB]_0$, $[LA]_0$, and $[M]_t$. When the K_{eq} is far below 1, there might be a tendency to expect the *r.d.s.* to be coordination, misleading one into thinking the LB is completely uninvolved in the *r.d.s.* and thus not involved in the rate law. This would be an incorrect treatment of the coordination step's nature as an equilibrium. And as Figure 1.11 shows, even when $[M]_t$ becomes 1st order due to weak coordination, there is still a 1st-order dependence on the LB.

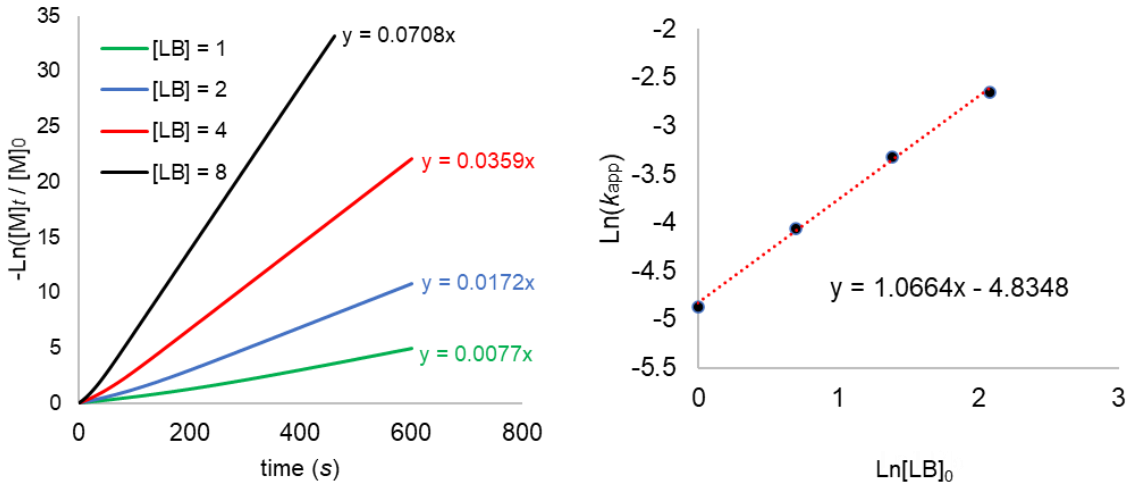

Figure 1.11. COPASI simulation (left) of LPP according to Figure 1.4, with exceptionally low K_{eq} = 0.001, showing 1st order plots of Ln($[M]_t/[M]_0$) vs time at different $[LB]_0$ with conditions: (k_1/k_{-1}) K_{eq} = 0.001; k_2 = 10; k_3 = 100; $[M]_0$ = 1000; $[LB]_0$ = {1, 2, 4, 8}; $[LA]_0$ = 1. And (right) Ln(k_{app}) vs Ln$[LB]_0$, k_{app} calculated from the slope of each line.

There is a kinetic limitation related to the dilution of the LP catalyst. Since the *r.d.s.* involves a statistical collision between M^* and P^*, dilution of the system results in rapid second-order decay of activity. Or, in other words, dilution of the system decreases the concentration of two factors in the rate law. Figure 1.12 illustrates the rapid decay in activity as both the LA and LB are diluted, while keeping monomer concentration constant. In terms of component ratios, this series represents M/LA/LB = {1000/1/1; 2000/1/1; 4000/1/1; 8000/1/1}. The log/log plot on the right shows the expected 2nd order dependence on the sum of LA + LB. This makes high turnover numbers difficult to achieve with LPP in a timely manner. And since it makes economic sense to use extremely low catalyst loadings, this aspect of LPP seems limited. Nonetheless, the immortal LPP reported by Zhang was capable of polymerizing MMA at a M/LA/LB ratio of 20,000/2/1 and achieved 89% conversion in 48 h.[55]

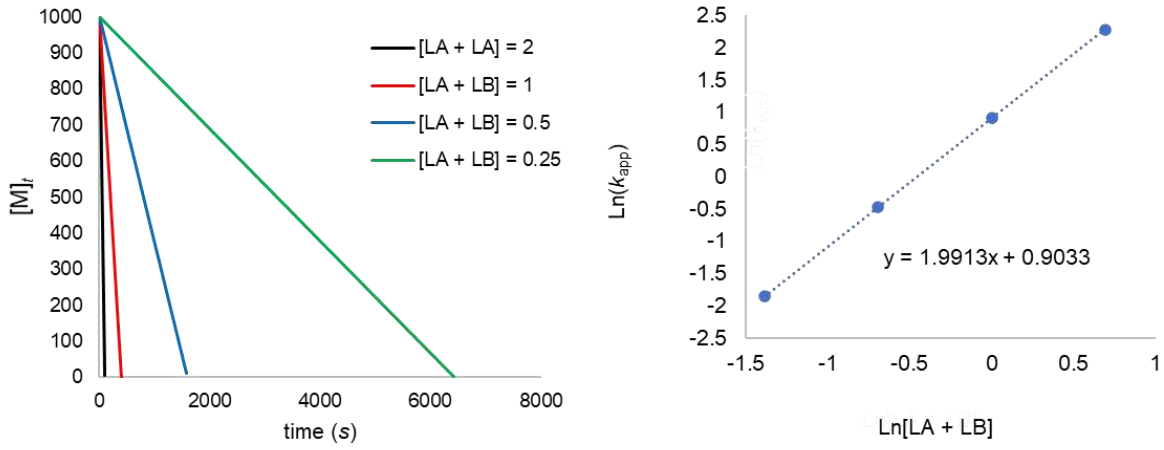

Figure 1.12. COPASI simulation (left) of LPP according to Figure 1.4, showing rapid second order decay of activity when both LA and LB are diluted: K_{eq} (k_1/k_{-1}) = 10; k_2 = 10; k_3 = 100; $[M]_0$ = 1000; $[LB]_0$ = $[LA]_0$ = {1; 0.5; 0.25; 0.125}. And (right) Ln(k_{app}) vs Ln$[LB]_0$, k_{app} calculated from the slope of each line.

1.3.2 Compounded Sequence Control (CSC) block copolymerization

While this chemistry was invented by the author and the details of its invention are described in Chapter 4. This section includes a kinetic simulation study that thoroughly develops the CSC concept from a theoretical standpoint. The author chose to include this section here since it nicely fits with the themes of **Chapter 1** and the material was taken from the same source text. However, the reader might consider reading this section after or with Chapter 4.

Most recently,[19] we developed a strategy that exploits LPP kinetics to implement compounded sequence-control (CSC) block copolymerizations from one-pot mixed comonomers (Figure 1.13). This strategy relies on the two-step LPP propagation mechanism that involves coordination followed by bimolecular conjugate addition (Figure 1.4). Since the addition step is rate determining, the monomer coordination process has time to establish an equilibrium prior to the *r.d.s.*

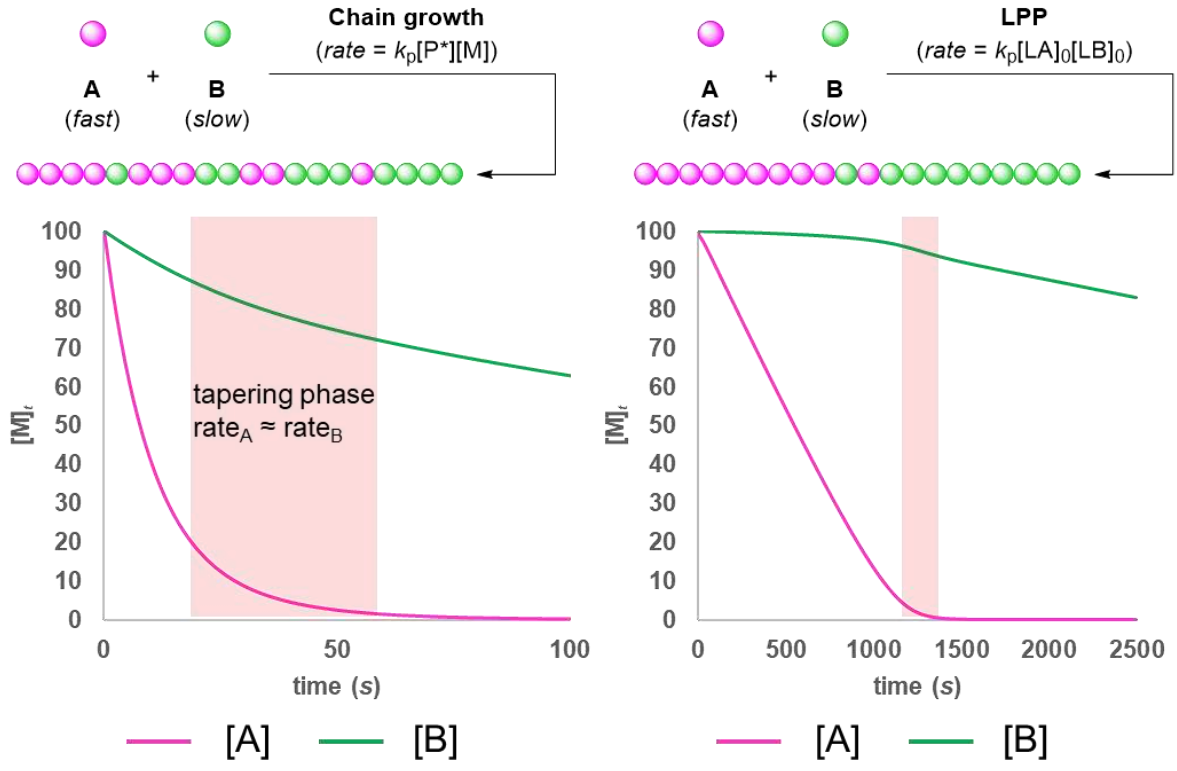

Figure 1.13. COPASI simulation (left) of chain-growth one-pot copolymerization of A (fast) and B (slow) monomers according to rate = $k_p[P^*]_t[M]_t$, showing 1st order decay in both A and B, and (right) LPP of one-pot copolymerization of A and B monomers, with $K_{eq} = 30$, according to Figure 1.4, showing zero-order decay of A, while B is locked out of the reaction until depletion of A. Conditions: (for both) $k_{p,A/A} = 0.1$; $k_{p,A/B} = 0.01$; $k_{p,B/B} = 0.0033$; $k_{p,B/A} = 0.05$; $[M]_0 = 100$; $[I]_0$ or $[LB]_0 = 1$; (for LPP only) ($[A^*][B]/[B^*][A]$) $K_{eq} = 30$, $[LA]_0 = 1$.

When more than one monomer is present, the LA then has time to select the preferable comonomer for coordination prior to the *r.d.s.*, and thus biases which monomer is available for the *r.d.s.* (Figure 1.14). This scenario differs from metal-mediated coordination-addition polymerization, where coordination typically is the *r.d.s.* and is immediately followed by addition,[80] which does not allow enough time for a prior equilibrium (K_{eq}) to establish.

Additionally, any propagating active species, when exposed to two different monomers with inherently different reactivity, will have some selectivity towards one monomer over the other (differing propagation rates, k_p), resulting in a tapered or gradient copolymer structure. The shaded area in Figure 1.13 marks the tapering phase at which point $rate_A$ is approximately equal to $rate_B$, resulting in a significant tapering effect (sequence error) for any typical first-order chain-growth polymerization. This "natural" k_p selectivity is also present in LPP, but occurs during the *r.d.s.* of bimolecular addition. Therefore, there are two different events of selectivity occurring at two different steps. If these two events operate constructively (i.e. the same monomer is selected for during coordination and propagation), the two selectivity probabilities will compound (thus the name *compounded sequence control*, Figures 1.10 and 1.11). This compounded thermodynamically biased prior K_{eq} and kinetically differing k_p sequence control, unique to LPP, drastically suppresses the tapering effect (i.e., no sequence error until very late in the copolymerization, see Figures 1.9), thereby enabling the synthesis of highly resolved BCPs.[19]

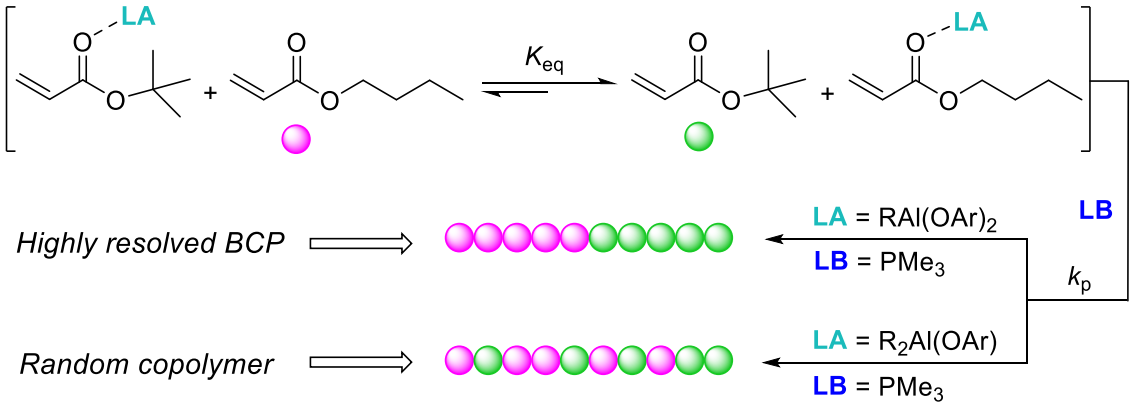

Figure 1.14. Illustrated K_{eq} differentiation

To demonstrate the equal importance of both prior K_{eq} and differing k_p, we have performed a thorough simulation study to isolate each variable. In Figure 1.15, we show three reactions, all containing the same K_{eq} = 15, but with differing reactivity ratios. For all reactions, the reactivity ratios represent the $k_{p,A/A}/k_{p,B/B}$ ratio, or the ratio of the homopolymer k_p's and can be measured. Thus, the cross-polymerization rates ($k_{p,A/B}$ and $k_{p,B/A}$) are considered *and important* but chosen judiciously and arbitrarily for the purposes of the simulation study, and we have not endeavored to measure them experimentally. Thus, it can be seen from Figure 1.15 that various degrees of selectivity derived from differing propagation rates lead to different levels of block resolution.

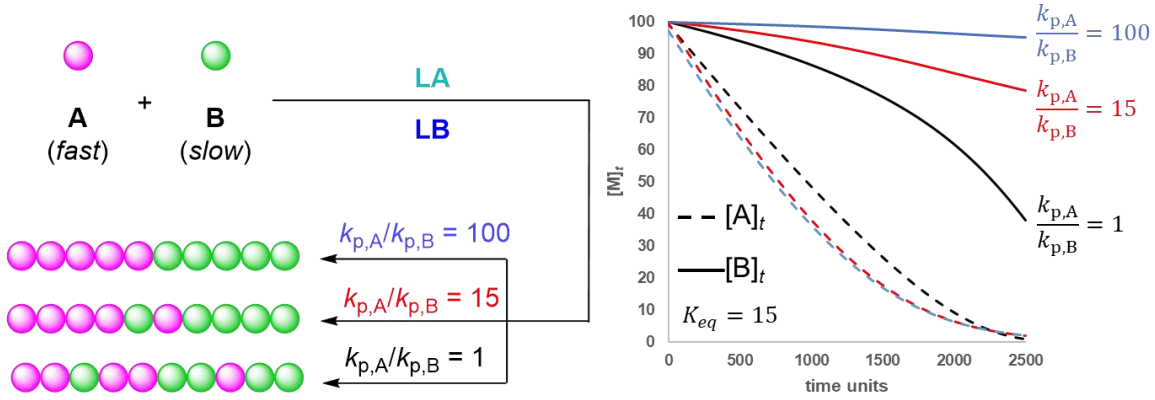

Figure 1.15. Comparative simulation of CSC-LPP at different reactivity ratios. Conditions: ([A*][B]/[B*][A]) K_{eq} = 30; [M]$_0$ = 100; [LA]$_0$ = 1; [LB]$_0$ = 1; (blue) $k_{p,A/A}/k_{pB/B}$ = 100: $k_{p,A/A}$ = 1; $k_{p,A/B}$ = 0.1; $k_{p,B/B}$ = 0.01; $k_{p,B/A}$ = 0.5; (red) $k_{p,A/A}/k_{pB/B}$ = 15: $k_{p,A/A}$ = 1; $k_{p,A/B}$ = 0.2; $k_{p,B/B}$ = 0.066; $k_{p,B/A}$ = 0.5; (black) $k_{p,A/A}/k_{pB/B}$ = 1: $k_{p,A/A}$ = $k_{p,A/B}$ = $k_{p,B/B}$ = $k_{p,B/A}$ = 1. X-axis is artificially scaled so that each run can be evenly overlaid.

In a similar fashion, the reactivity ratios, $k_{p,A/A}/k_{p,B/B}$, were kept constant at 30 while the K_{eq} was manipulated (Figure 1.16). Here, we see a similar trend where a higher K_{eq} results in higher block resolution. Notably, at K_{eq} = 100, the B monomer is completely locked out of polymerization until A has been depleted. Likewise, for this reaction, A shows an almost perfectly linear conversion vs time plot from start to finish. This can be attributed to the constancy of the [A*]$_t$ shown on the right, where due to a high K_{eq} value, its concentration does not significantly change over the course of the polymerization until [A]$_t$ approaches depletion. In contrast, when K_{eq} = 5, such constancy is not observed, and the [A*]$_t$ is much more variable, leading to lower block resolution. This contrasts starkly with the K_{eq} = 1 case, where [A*]$_t$ is virtually always less than [B*]$_t$, resulting in a poor block resolution reminiscent of a typical chain-growth polymerization (Figure 1.16).

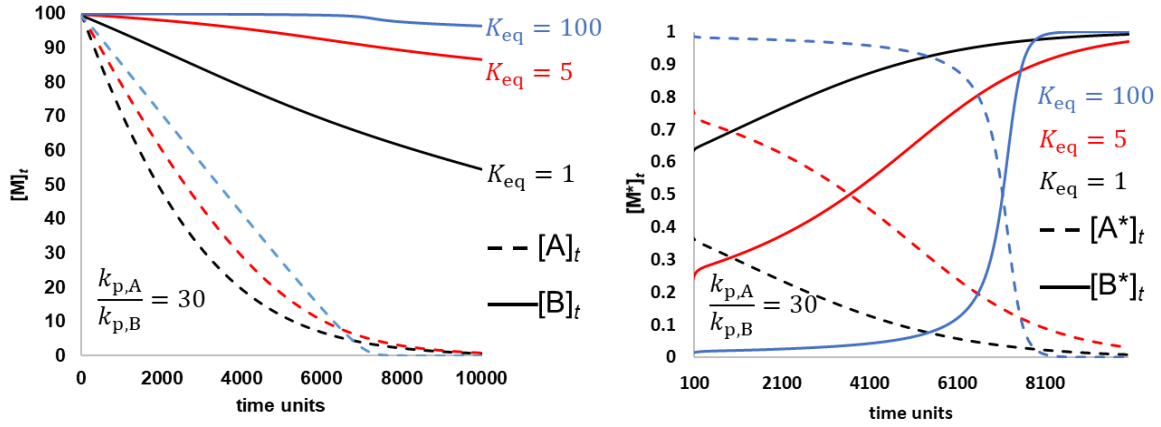

Figure 1.16. Comparative simulation of CSC-LPP at different K_{eq}, with monomer depletion vs time (left) and activated monomer vs time (right). Conditions: $[M]_0 = 100$; $[LA]_0 = 1$; $[LB]_0 = 1$; $k_{p,A/A} = 0.1$; $k_{p,A/B} = 0.01$; $k_{p,B/B} = 0.0033$; $k_{p,B/A} = 0.05$; (blue) ($[A^*][B]/[B^*][A]$) $K_{eq} = 100$; (red) $K_{eq} = 5$; (black) $K_{eq} = 1$. X-axis is artificially scaled so that each run can be evenly overlaid.

Hypothetical extrapolation of this concept leads to many intriguing possibilities. (1) Two-step A-B-A triblocks include the aforementioned *slow-fast-slow* triblock and equally feasible *fast-slow-fast* triblocks involving initiation of a *fast*/*slow* comonomer mixture, followed by addition of a second quantity of the fast monomer. (2) The A-B-A tri-BCPs should be made in one-pot by initiating polymerization on a mixture of comonomers with using a dinuclear LB. (3) The one-pot A-why highly sophisticated multiblock copolymers. As for diblock copolymerizations, this method not only saves an addition step, but also saves a purification step, as two monomers can be packaged in the same container, presumably with some form of a stabilizer, and purified in a one-pot setup.

Conclusions

As mentioned in the abstract, application of LPP is generally concerned with *selectivity* and *control*. With a solid understanding of the LPP fundamentals, the reader can now consider the unique chemistry of LPP and appreciate the mechanisms by which such reactivity is derived. The forthcoming chapters will showcase LPP in action.

References cited in Chapter 1

[1] Hong, M.; Chen, J.; Chen, E.Y.-X. Polymerization of Polar Monomers Mediated by Main-Group Lewis Acid-Base Pairs. *Chem. Rev.* **2018**, *118*, 10551−10616.

[2] Chen, E. Y.-X. "Polymerization by Classical and Frustrated Lewis Pairs", *Top. Curr. Chem.* **2013**, *334*, 239–260.

[3] Zhang, Y. T.; Miyake, G. M.; John, M. G.; Falivene, L.; Caporaso, L.; Cavallo, L.; Chen, E. Y.-X. Lewis Pair Polymerization by Classical and Frustrated Lewis Pairs: Acid, Base and Monomer Scope and Polymerization Mechanism. *Dalton Trans*. **2012**, *41*, 9119−9134.

[4] Zhang, Y. T.; Miyake, G. M.; Chen, E. Y.-X. Alane-Based Classical and Frustrated Lewis Pairs in Polymer Synthesis: Rapid Polymerization of MMA and Naturally Renewable Methylene Butyrolactones into High-Molecular-Weight Polymers. *Angew. Chem., Int. Ed*. **2010**, *49*, 10158−10162.

[5] Wang, Q.; Zhao, W.; Zhang, S.; He, J.; Zhang, Y.; Chen, E. Y.-X. Living Polymerization of Conjugated Polar Alkenes Catalyzed by N-Heterocyclic Olefin-Based Frustrated Lewis Pairs. *ACS Catal*. **2018**, *8*, 3571−3578.

[6] Wang, H.; Wang, Q.; He, J.; Zhang, Y. Living polymerization of acrylamides catalysed by N-heterocyclic olefin-based Lewis pairs. *Polym. Chem*. **2019**, *10*, 3597−3603.

[7] Takada, K.; Ito, T.; Kiano, K.; Tsuchida, S.; Takagi, Y.; Chen, Y.; Satoh, T.; Kakuchi, T. Synthesis of Homopolymers, Diblock Copolymers, and Multiblock Polymers by Organocatalyzed Group Transfer Polymerization of Various Acrylate Monomers. *Macromolecules* **2015**, *48*, 511−519.

[8] Wang, X.-J.; Hong, M. Lewis-Pair-Mediated Selective Dimerization and Polymerization of Lignocellulose-Based β-Angelica Lactone into Biofuel and Acrylic Bioplastic. *Angew. Chem., Int. Ed.* **2020**, *59*, 2664-2668.

[9] McGraw, M.; Chen, E. Y.-X. Catalytic Lewis Pair Polymerization of Renewable Methyl Crotonate to High-Molecular-Weight Polymers. *ACS Catal*. **2018**, *8*, 9877−9887.

[10] Imada, M.; Takenaka, Y.; Hatanaka, H.; Tsuge, T.; Abe, H. Unique Acrylic Resins with Aromatic Side Chains by Homopolymerization of Cinnamic Monomers. *Commun. Chem*. **2019**, *2*, 109.

[11] R. W. Clarke, M. L. McGraw, R. R. Gowda, E. Y.-X. Chen, *Macromolecules* **2020**, *53*, 640-648

[12] Wang, Q. Y.; Zhao, W. C.; He, J. H.; Zhang, Y. T.; Chen, E. Y.- X. Living Ring-Opening Polymerization of Lactones by N-Heterocyclic Olefin/Al(C_6F_5)$_3$ Lewis Pairs: Structures of Intermediates, Kinetics, and Mechanism. *Macromolecules* **2017**, *50*, 123−136.

[13] Walther, P.; Krauß, A.; Naumann, S. Lewis Pair Polymerization of Epoxides via Zwitterionic Species as a Route to High-Molar-Mass Polyethers. *Angew. Chem., Int. Ed.* **2019**, *58*, 10737-10741.

[14] Chen, Y.; Shen, J.; Liu, S.; Zhao, J.; Wang, Y.; Zhang, G. High Efficiency Organic Lewis Pair Catalyst for Ring-Opening Polymerization of Epoxides with Chemoselectivity. *Macromolecules* **2018**, *51*, 8286−8297.

[15] Piedra-Arroni, E.; Brignou, P.; Amgoune, A.; Guillaume, S. M.; Carpentier, J. F.; Bourissou, D. A Dual Organic/Organometallic Approach for Catalytic Ring-Opening Polymerization. *Chem. Commun*. **2011**, *47*, 9828−9830.

[16] Brignou, P.; Guillaume, S. M.; Roisnel, T.; Bourissou, D.; Carpentier, J. F. Discrete Cationic Zinc and Magnesium Complexes for Dual Organic/Organometallic-Catalyzed Ring-Opening Polymerization of Trimethylene Carbonate. *Chem. - Eur. J.* **2012**, *18*, 9360− 9370.

[17] Ji, H. Y.; Wang, B.; Pan, L.; Li, Y. S. Lewis Pairs for Ring-Opening Alternating Copolymerization of Cyclic Anhydrides and Epoxides. *Green Chem.* **2018**, *20*, 641−648.

[18] Hosoi, Y.; Takasu, A.; Matsuoka, S.-I.; Hayashi, M. N-Heterocyclic Carbene Initiated Anionic Polymerization of (E,E)- Methyl Sorbate and Subsequent Ring-Closing to Cyclic Poly(alkyl sorbate). *J. Am. Chem. Soc.* **2017**, *139*, 15005−15012.

[19] McGraw, M. L.; Chen, E. Y.-X. Compounded Sequence Control in Polymerization of One-Pot Mixtures of Highly Reactive Acrylates by Differentiating Lewis Pairs. *J. Am. Chem. Soc.* **2020**, *13*, 5969-5973.

[20] McGraw, M. L. & Chen, E. Y.-X. Borane/silane frustrated Lewis pairs for polymerization of β-substituted Michael acceptors. *Tetrahedron* **2019**, *75*, 1475–1480.

[21] Takenaka, Y. & Abe, H. Group-transfer polymerization of various crotonates using organic acid catalysts. *Macromolecules* **2019**, *52*, 4052–4058.

[22] Gowda, R. R.; Chen, E. Y.-X. Chemoselective Lewis Pair Polymerization of Renewable Multivinyl-Functionalized γ-Butyrolactones. *Phil. Trans. R. Soc. A.* **2017**, *375*, 2101/1−2101/14.

[23] Bai, Y.; Wang, H.; He, J.; Zhang, Y. Rapid and Scalable Access to Sequence-Controlled DHDM Multiblock Copolymers by FLP Polymerization. *Angew. Chem., Int. Ed.* **2020**, *10*, 10.1002/anie.202004013

[24] Xu, P. F.; Yao, Y. M.; Xu, X. Frustrated Lewis Pair-Like Reactivity of Rare-Earth Metal Complexes: 1,4-Addition Reactions and Polymerizations of Conjugated Polar Alkenes. *Chem. - Eur. J*. **2017**, *23*, 1263−1267.

[25] Xu, P. F.; Xu, X. Homoleptic Rare-Earth Aryloxide Based Lewis Pairs for Polymerization of Conjugated Polar Alkenes. *ACS Catal*. **2018**, *8*, 198−202.

[26] Xu, P. F.; Wu, L.; Dong, L. Q.; Xu, X. Chemoselective Polymerization of Polar Divinyl Monomers with Rare-Earth/ Phosphine Lewis Pairs. *Molecules* **2018**, *23*, 360.

[27] MacMillan, D. W. C. The Advent and Development of Organocatalysis. *Nature* **2008**, *455*, 304−308.

[28] Kiesewetter, M. K.; Shin, E. J.; Hedrick, J. L.; Waymouth, R. M. Organocatalysis: Opportunities and Challenges for Polymer Synthesis. *Macromolecules* **2010**, *43*, 2093−2107.

[29] Naumann, S. Synthesis, properties & applications of N-heterocyclic olefins in catalysis. *Chem. Commun*. **2019**, *55*, 11658-11670.

[30] Schuldt, R.; Kästner, J.; Naumann, S. Proton Affinities of N-Heterocyclic Olefins and Their Implications for Organocatalyst Design. *J. Org. Chem*. **2019**, *84*, 2209−2218.

[31] *Organic Catalysis for Polymerization*; Dove, A. P., Sardon, H., Naumann, S., Eds.; RSC Polymer Chemistry Series, RSC: London, **2018**.

[32] Fevre, M.; Pinaud, J.; Gnanou, Y.; Vignolle, J.; Taton, D. N-` Heterocyclic Carbenes (NHCs) as Organocatalysts and Structural Components in Metal-Free Polymer Synthesis. *Chem. Soc. Rev.* **2013**, *42*, 2142−2172.

[33] Naumann, S.; Dove, A. P. N-Heterocyclic Carbenes for Metal-Free Polymerization Catalysis: An Update. *Polym. Int.* **2016**, *65*, 16− 27.

[34] Flanigan, D. M.; Romanov-Michailidis, F.; White, N. A.; Rovis, T. Organocatalytic Reactions Enabled by N-Heterocyclic Carbene. *Chem. Rev*. **2015**, *115*, 9307−9387.

[35] Stephan, D. W. The Broadening Reach of Frustrated Lewis Pair Chemistry. *Science* **2016**, *354*, No. aaf7229.

[36] Stephan, D. W.; Erker, G. Frustrated Lewis Pair Chemistry: Development and Perspectives. *Angew. Chem., Int. Ed*. **2015**, *54*, 6400−6441.

[37] Stephan, D. W. Frustrated Lewis Pairs: From Concept to Catalysis. *Acc. Chem. Res.* **2015**, *48*, 306−316.

[38] Frustrated Lewis Pairs I & II. *Topics in Current Chemistry*; Stephan, D. W., Erker, G., Eds.; Springer: New York, 2013; Vols. 332, 334.

[39] Jupp, A. R.; Stephan, D. W. New Directions for Frustrated Lewis Pair Chemistry. *Trends in Chemistry* **2019**, *1*, 35−48.

[40] Zhang, Y.; Miyake, G. M.; Chen, E. Y.-X. Conjugate-Addition Organopolymerization: Rapid Production of Acrylic Bioplastics by N-Heterocyclic Carbenes. *Angew. Chem., Int. Ed.* **2012**, *51*, 2465−2469.

[41] Zhang, Y.; Schmitt, M.; Falivene, L.; Caporaso, L.; Cavallo, L.; Chen, E. Y.-X. Organocatalytic Conjugate-Addition Polymerization of Linear and Cyclic Acrylic Monomers by N-Heterocyclic Carbenes: Mechanisms of Chain Initiation, Propagation, and Termination. *J. Am. Chem. Soc*. **2013**, *135*, 17925−17942.

[42] Hu, Y.; Gustafson, L. O.; Zhu, H.; Chen, E. Y.-X. Anionic Polymerization of MMA and Renewable Methylene Butyrolactones by Resorbable Potassium Salts. *J Polym Sci A Polym Chem* **2011**, *49*, 2008-2017.

[43] Rodriguez-Delgado, A.; Chen, E. Y.-X. Single-Site Anionic Polymerization. Monomeric Ester Enolaluminate Propagator Synthesis, Molecular Structure, and Polymerization Mechanism, *J. Am. Chem. Soc.* **2005**, *127*, 961−974.

[44] Knaus, M. G. M.; Giuman, M. M.; Pöthig, A.; Rieger, B. End of Frustration: Catalytic Precision Polymerization with Highly Interacting Lewis Pairs. *J. Am. Chem. Soc.* **2016**, *138*, 7776−7781.

[45] He, J. H.; Zhang, Y. T.; Chen, E. Y. X. Synthesis of Pyridine and 2-Oxazoline-Functionalized Vinyl Polymers by Alane-Based Frustrated Lewis Pairs. *Synlett* **2014**, *25*, 1534−1538.

[46] He, J. H.; Zhang, Y. T.; Falivene, L.; Caporaso, L.; Cavallo, L.; Chen, E. Y. X. Chain Propagation and Termination Mechanisms for Polymerization of Conjugated Polar Alkenes by [Al]-Based Frustrated Lewis Pairs. *Macromolecules* **2014**, *47*, 7765−7774.

[47] Gowda, R. R.; Chen, E. Y.-X. Chemoselective Lewis Pair Polymerization of Renewable Multivinyl-Functionalized γ-Butyrolactones. *Philos. Trans. R. Soc., A* **2017**, *375*, 20170003.

[48] Chen, J.; Chen, E. Y.-X. Lewis Pair Polymerization of Acrylic Monomers by N-Heterocyclic Carbenes and $B(C_6F_5)_3$. *Isr. J. Chem*. **2015**, *55*, 216−225.

[49] Ottou, W. N.; Conde-Mendizabal, E.; Pascual, A.; Wirotius, A. L.; Bourichon, D.; Vignolle, J.; Robert, F.; Landais, Y.; Sotiropoulos, J. M.; Miqueu, K.; Taton, D. Organic Lewis Pairs Based on Phosphine and Electrophilic Silane for the Direct and Controlled Polymerization of Methyl Methacrylate: Experimental and Theoretical Investigations. *Macromolecules* **2017**, *50*, 762−774.

[50] Wang, X. J.; Zhang, Y. X.; Hong, M. Controlled and Efficient Polymerization of Conjugated Polar Alkenes by Lewis Pairs Based on Sterically Hindered Aryloxide-Substituted Alkylaluminum. *Molecules* **2018**, *23*, 442.

[51] Jia, Y. B.; Ren, W. M.; Liu, S. J.; Xu, T. Q.; Wang, Y. B.; Lu, X. B. Controlled Divinyl Monomer Polymerization Mediated by Lewis Pairs: A Powerful Synthetic Strategy for Functional Polymers. *ACS Macro Lett*. **2014**, *3*, 896−899.

[52] Jia, Y. B.; Wang, Y. B.; Ren, W. M.; Xu, T. Q.; Wang, J.; Lu, X. B. Mechanistic Aspects of Initiation and Deactivation in N-Heterocyclic Olefin Mediated Polymerization of Acrylates with Alane as Activator. *Macromolecules* **2014**, *47*, 1966−1972.

[53] Xu, T. Q.; Chen, E. Y.-X. Probing Site Cooperativity of Frustrated Phosphine/Borane Lewis Pairs by a Polymerization Study. *J. Am. Chem. Soc*. **2014**, *136*, 1774−1777.

[54] Chen, J.; Chen, E. Y.-X. Reactivity of Amine/E(C6F5)3 (E = B, Al) Lewis Pairs toward Linear and Cyclic Acrylic Monomers: Hydrogenation vs. Polymerization. *Molecules* **2015**, *20*, 9575−9590.

[55] Bai, Y.; He, J.; Zhang, Y. Ultra-High-Molecular-Weight Polymers Produced by the Immortal Phosphine-Based Catalyst System. *Angew. Chem., Int. Ed.* **2018**, *57*, 17230−17234.

[56] Jia, Y. B.; Wang, Y. B.; Ren, W. M.; Xu, T. Q.; Wang, J.; Lu, X. B. Mechanistic Aspects of Initiation and Deactivation in N-Heterocyclic Olefin Mediated Polymerization of Acrylates with Alane as Activator. *Macromolecules* **2014**, *47*, 1966−1972.

[57] Watson, I. C.; Zhou, Y.; Ferguson, M. J.; Kränzlein, M.; Rieger, B.; Rivard, E. Trialkylaluminum N-Heterocyclic Olefin (NHO) Adducts as Catalysts for the Polymerization of Michael-Type Monomers. *Z. Anorg. Allg. Chem*. **2020**, *646*, 1–6.

[58] Zhang, Z.-H.; Wang, X.; Wang, X.-J.; Li, Y.; Hong, M. Tris(2,4-difluorophenyl)borane/Triisobutylphosphine Lewis Pair: A Thermostable and Air/Moisture-Tolerant Organic Catalyst for the Living Polymerization of Acrylates. *Macromolecules* **2021**, *54*, 8495-8502.

[59] Fuchise, K.; Chen, Y. G.; Satoh, T.; Kakuchi, T. Recent Progress in Organocatalytic Group Transfer Polymerization. *Polym. Chem.* **2013**, *4*, 4278–4291.

[60] Webster, O. W. Group Transfer Polymerization: Mechanism and Comparison with Other Methods for Controlled Polymerization of Acrylic Monomers. *Adv. Polym. Sci.* **2004**, *167*, 1–34.

[61] Webster, O. W. The Discovery and Commercialization of Group Transfer Polymerization. *J. Polym. Sci., Part A: Polym. Chem.* **2000**, *38*, 2855–2860.

[62] Hertler, W. R.; Sogah, D. Y.; Webster, O. W.; Trost, B. M. Group-Transfer Polymerization. 3. Lewis Acid Catalysis. *Macromolecules* **1984**, *17*, 1415-1417.

[63] Webster, O. W.; Hertler, W. R.; Sogah, D. Y.; Farnham, W. B.; Rajanbabu, T. V. Group-Transfer Polymerization. 1. A New Concept for Addition Polymerization with Organo-Silicon Initiators. *J. Am. Chem. Soc.* **1983**, *105*, 5706–5708.

[64] Fuchise, K.; Tsuchida, S.; Takada, K.; Chen, Y. G.; Satoh, T.; Kakuchi, T. $B(C_6F_5)_3$-Catalyzed Group Transfer Polymerization of *n*-Butyl Acrylate with Hydrosilane through In-Situ Formation of Initiator by 1,4-Hydrosilylation of *n*-Butyl Acrylate. *ACS Macro Lett*. **2014**, *3*, 1015−1019.

[65] Kikuchi, S.; Chen, Y. G.; Kitano, K.; Sato, S.; Satoh, T.; Kakuchi, T. $B(C_6F_5)_3$-Catalyzed Group Transfer Polymerization of N,N-Disubstituted Acrylamide Using Hydrosilane: Effect of Hydrosilane and Monomer Structures, Polymerization Mechanism, and Synthesis of α-End-Functionalized Polyacrylamides. *Macromolecules* **2016**, *49*, 3049−3060.

[66] Chen, Y. G.; Kitano, K.; Tsuchida, S.; Kikuchi, S.; Takada, K.; Satoh, T.; Kakuchi, T. $B(C_6F_5)_3$-Catalyzed Group Transfer Polymerization of Alkyl Methacrylates with Dimethylphenylsilane through In Situ Formation of Silyl Ketene Acetal by $B(C_6F_5)_3$-Catalyzed 1,4- Hydrosilylation of Methacrylate Monomer. *Polym. Chem*. **2015**, *6*, 3502−3511.

[67] Chen, Y.; Jia, Q.; Ding, Y.; Sato, S.-I.; Xu, L.; Zang, C.; Shen, X.; Kakuchi, T. $B(C_6F_5)_3$-Catalyzed Group Transfer Polymerization of Acrylates Using Hydrosilane: Polymerization Mechanism, Applicable Monomers, and Synthesis of Well-Defined Acrylate Polymers. *Macromolecules* **2019**, *52*, 844-856.

[68] Hu, L.; Zhao, W.; He, J.; Zhang, Y. Silyl Ketene Acetals/ B(C6F5)3 Lewis Pair-Catalyzed Living Group Transfer Polymerization of Renewable Cyclic Acrylic Monomers. *Molecules* **2018**, *23*, 665.

[69] Hu, L.; He, J. H.; Zhang, Y. T.; Chen, E. Y.-X. Living Group Transfer Polymerization of Renewable α-Methylene-γ-butyrolactones Using $Al(C_6F_5)_3$ Catalyst. *Macromolecules* **2018**, *51*, 1296−1307.

[70] Li, J.; Kikuchi, S.; Sato, S.-I.; Chen, Y.; Xu, L.; Song, B.; Duan, Q.; Wang, Y.; Kakuchi, T.; Shen, X. Core-First Synthesis and Thermoresponsive Property of Three-, Four-, and Six-Arm Star-Shaped Poly(N,N-diethylacrylamide)s and Their Block Copolymers with Poly(N,N-dimethylacrylamide). *Macromolecules* **2019**, *52*, 7207-7217.

[71] Kikuchi, S.; Chen, Y. G.; Kitano, K.; Takada, K.; Satoh, T.; Kakuchi, T. Organic Acids as Efficient Catalysts for Group Transfer Polymerization of N,N-Disubstituted Acrylamide with Silyl Ketene Acetal: Polymerization Mechanism and Synthesis of Diblock Copolymers. *Polym. Chem.* **2015**, *6*, 6845−6856.

[72] Fuchise, K.; Chen, Y. G.; Takada, K.; Satoh, T.; Kakuchi, T. Effect of Counter Anions on Kinetics and Stereoregularity for the Strong Bronsted Acid-Promoted Group Transfer Polymerization of N,N-Dimethylacrylamide. *Macromol. Chem. Phys.* **2012**, *213*, 1604− 1611.

[73] Kakuchi, R.; Chiba, K.; Fuchise, K.; Sakai, R.; Satoh, T.; Kakuchi, T. Strong Bronsted Acid as a Highly Efficient Promoter for Group Transfer Polymerization of Methyl Methacrylate. *Macromolecules* **2009**, *42*, 8747−8750.

[74] Takada, K.; Fuchise, K.; Chen, Y. G.; Satoh, T.; Kakuchi, T. Controlled Polymerization of Methyl Acrylate for High-Molecular Weight Polymers by Pentafluorophenylbis(triflyl)methane-Promoted Group Transfer Polymerization Using Triisopropylsilyl Ketene Acetal. *J. Polym. Sci., Part A: Polym. Chem.* **2012**, *50*, 3560−3566.

[75] Zhang, Y.; Chen, E. Y.-X. Controlled Polymerization of Methacrylates to High Molecular Weight Polymers Using Oxidatively Activated Group Transfer Polymerization Initiators. *Macromolecules* **2008**, *41*, 36−42.

[76] Zhang, Y. T.; Lay, F.; Garcia-Garcia, P.; List, B.; Chen, E. Y.-X. High-Speed Living Polymerization of Polar Vinyl Monomers by Self-Healing Silylium Catalysts. *Chem. - Eur. J.* **2010**, *16*, 10462−10473.

[77] Xu, T.; Chen, E. Y.-X. Silylium Dual Catalysis in Living Polymerization of Methacrylates via In Situ Hydrosilylation of Monomer. *J. Polym. Sci., Part A: Polym. Chem.* **2015**, *53*, 1895−1903.

[78] Zhang, Y.; Gustafson, L. O.; Chen, E. Y.-X. Dinuclear Silylium-Enolate Bifunctional Active Species: Remarkable Activity and Stereoselectivity toward Polymerization of Methacrylate and Renewable Methylene Butyrolactone Monomers. *J. Am. Chem. Soc.* **2011**, *133*, 13674−13684.

[79] Chen, Y. G.; Takada, K.; Fuchise, K.; Satoh, T.; Kakuchi, T. Synthesis of Syndiotactic-Rich Star-Shaped Poly(methyl methacrylate) by Core-First Group Transfer Polymerization Using N-(Trimethylsilyl)bis(trifluoromethanesulfonyl)imide. *J. Polym. Sci., Part A: Polym. Chem.* **2012**, *50*, 3277−3285.

[80] Chen, E. Y.-X. Coordination Polymerization of Polar Vinyl Monomers by Single-Site Metal *Catalysts. Chem. Rev.* **2009**, *109*, 5157−5214.

Chapter 2
Lewis Pair Polymerization of Renewable Methyl Crotonate

2.1 Background and Significance

The demand to develop new chemistries associated with small molecule building blocks sourced from renewable carbon cycles has led to many fascinating advances in catalysis.[1] Economically competitive and environmentally benign methods of converting naturally abundant and annually renewable biomass into discrete products have put emphasis on certain small molecules and their transformations.[2] One of the most practically feasible ways to utilize these renewable chemicals is to build them up into useful polymeric materials.[3] Therefore, it is of great interest to develop efficient catalytic or controlled polymerization methods and processes that can effectively convert such renewable building blocks or monomers into practically useful materials.

Recently, much research has been devoted to the biosynthesis of polyhydroxyalkanoates (PHA) [4a-b] from various microorganisms as a useful means of converting raw biomass into useful polymers.[4c] Poly(3-hydroxybutyrate) (PHB) has received the most attention due to its structural simplicity, and because it can be synthesized by a large number of bacteria and plants.[4d] Although PHB itself can be used as a biodegradable plastic, it can also be converted to *trans*-crotonic acid through catalytic pyrolysis or methyl crotonate (MC) by transesterification.[5] Interestingly, there are no practical methods of polymerizing crotonates directly to polymers with useful molecular weight, thus making them a rather unexploited class of biorenewable monomers. Moreover, poly(crotonate)s are of interest due to their *ditactic* structures, which if controlled could lead to materials with advanced physical and mechanical properties. This property makes crotonates suitable candidates for investigation into chain-end and site-control mechanisms for producing

disyndiotactic, threo-diisotactic, erythro-diisotactic, or diheterotactic polymers, which is a largely underdeveloped area of polymer chemistry.[6]

Polymerization of crotonates and other β-substituted monomers such as cinnamates has proven to be difficult under the same conditions suitable for acrylates and methacrylates such as methyl methacrylate (MMA).[7] Crotonic esters, being constitutional isomers of methacrylic esters (only differing by position of the methyl group) and having the same α, β-unsaturated ester functionality as industrially important acrylic and methacrylic monomers, should be polymerizable by similar addition polymerization mechanisms. However, the increased stability of the α, β-double bond and sterics at the β-carbon due to β-substitution makes the β-carbon relatively less susceptible to nucleophilic attack (Figure 2.1).

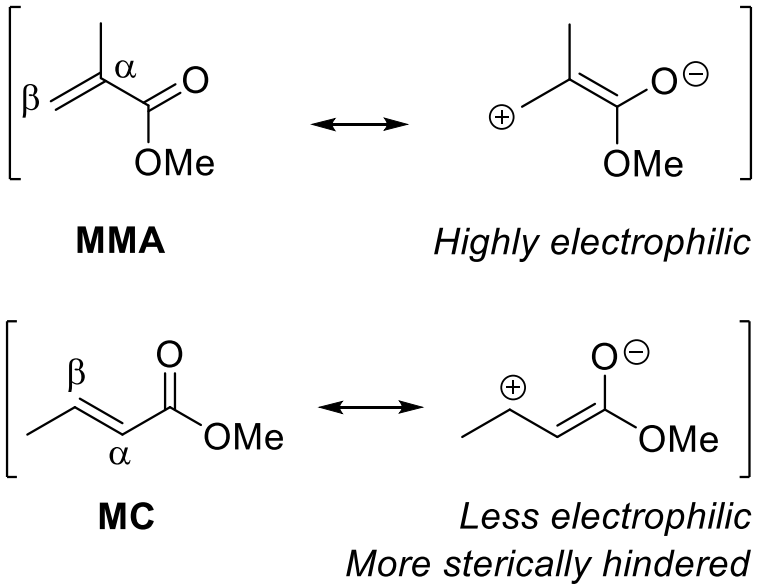

Figure 2.1. Differences in electronics and sterics between MMA and MC congeners.

Early attempts to polymerize crotonates anionically with organolithium reagents were unsuccessful, presumably because of early termination due to lithium chelation to internal

carbonyls.[7a] Sterically hindered *t*-butyl crotonate was polymerized in lithium/ammonia solution,[7b] up to 75 % conversion (M_n < 3 kg/mol). Nagasawa et al. showed that *t*-butyl crotonate can be polymerized anionically by 2-MeBuLi in THF at -78 °C to high molecular weight polymer (M_n = 302 kg/mol). [7c] Tanabe et al. reported a coordination polymerization of MC using $CaZnEt_4$ which achieved low conversion to form oligomers.[7d] Hatada and co-workers[7e-g] reported group transfer polymerization (GTP) of MC facilitated by HgI_2 Lewis acid (LA) which produced polymers with M_n up to 12.9 kg/mol. This polymerization was later improved by Kitayama et al. to make polymers with M_n up to 32.4 kg/mol and enhanced disyndiotacticity.[7f-g]

Recently, Lewis basic organocatalysts[8,9,10,11] such as *N*-heterocyclic carbenes (NHCs) and *N*-heterocyclic olefins (NHOs) have enabled the zwitterionic polymerization[12] of acrylates,[12b,e] epoxides,[12a] lactides,[12c-d] and lactones.[10a] This strategy utilizes neutral nucleophiles which become cationic following addition to Michael acceptors or ester carbonyls. The imidazolium or triazolium cation present in the zwitterionic polymerization renders a much higher energy enolate or alkoxy species when compared to those stabilized by alkali metal cations in anionic methods. Organocatalysts alone, especially those such as NHCs and NHOs which are potent bases, can generate enolates that are too reactive. The great distance between the anion and cation within the zwitterion affords a highly reactive enolate that results in early termination or chain transfer.[12b,d] These side reactions can be made useful in coupling reactions,[9] but are problematic in polymerizations.

To tune the reactivity of the enolate generated by organocatalysts, LAs can be employed to both stabilize the enolate and activate the monomer, thus promoting selective and controlled polymerization. This strategy is related to the polymerization method known as Lewis pair polymerization (LPP)[13,14] by classical Lewis adducts (CLAs) or frustrated Lewis pairs (FLPs)[15]

and has shown to be an effective strategy for polymerizing polar vinyl monomers,[14b,16,17,18,19,20] such as MMA and *γ*-methyl-*α*-methylene-*γ*-butyrolactone (γMMBL), and for ring-opening polymerization (ROP) of lactide[21] and lactones.[22,23,24] LPP differs from zwitterionic polymerization in that it exploits the cooperative reactivity of neutral LAs such as alanes, [18,19,25] boranes,[26,16b] $Zn(C_6F_5)_2$,[21] metal halides, [20, 23] and rare earth aryl oxides,[27] together with neutral Lewis bases (LBs) such as amines,[14,21] phosphines,[14b] silyl ketene acetals,[26] NHCs,[25] and NHOs.[16] Introduction of the LA has afforded a more controlled zwitterionic polymerization by ideally stabilizing the active enolate chain end enough to preclude termination reactions and reactions with unactivated monomers[16c,18a] and advanced chemoselectivity towards highly functionalized monomers.[17,18b] We previously reported detailed investigation of the LPP of a number of conjugated polar alkenes by the Lewis pairs (LPs) based on the highly Lewis acidic and sterically encumbered alane $Al(C_6F_5)_3$.[14b] Among the LBs tested, NHCs, including 1,3-di-*tert*-butylimidazolin-2-ylidene (I^{t}Bu), 1,3-di-mesityl-butylimidazolin-2-ylidene (IMes), and 1,3,4-triphenyl4,5-dihydro-1H-1,2,4-triazol-5-ylidene (TPT), proved to be highly active with many monomers including MMA, α-methylene-γ-butyrolactone (MBL), and γMMBL. Strongly nucleophilic I^{t}Bu alone can initiate zwitterionic polymerization of MMA and γMMBL in DMF.[12b]

Weymouth et al.[28] recently showed that crotonate esters can be organocatalytically dimerized in a head-to-tail fashion into unsaturated diesters by employing NHCs. That work revealed two key pathways that explain why the zwitterionic polymerization was *not* observed for crotonates: the first being 1,2-proton transfer within the zwitterionic LB-monomer adduct (**1**) to the single monomer addition product and the second being 1,3-elimination of the LB in the zwitterionic dimer (**2**) to the dimerization product, Figure 2.2. In light of our continued interested in addressing challenging polymerization issues using the LPP approach, we reasoned that if LAs are employed

to stabilize NHC zwitterions **1** and **2**, proton transfer/elimination pathways could be avoided, and the extended lifetime of the zwitterion could then allow for propagation to occur. We also hypothesized that $Al(C_6F_5)_3$, $B(C_6F_5)_3$, and methyl aluminum bis(2,6-di-*tert*-butyl-4-methylphenoxide) (MAD) would be suitable LAs given their proven ability to facilitate bimetallic conjugate addition through enolaluminate[14,16] and enolborate[16b,e] intermediates. Indeed, our study described herein showed that the LPP strategy is effective in generating relatively high molecular weight poly(methyl crotonate) (PMC) with M_n up to 161 kg/mol under ambient temperature and solvent free conditions. This study also revealed some intriguing mechanistic features unique to the LPP of β-substituted acrylic monomers.

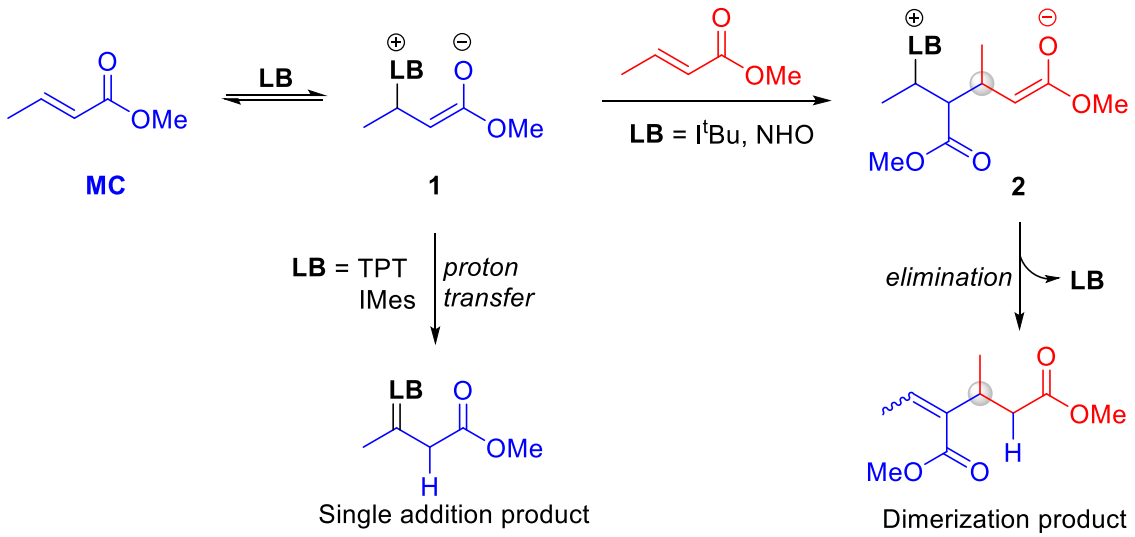

Figure 2.2. Reactivity of LBs (NHC and NHO) with MC

2.2 Results and Discussion

2.2.1 Results of Polymerization of MC by Lewis Pairs (LPs). As described above, NHCs alone will react with MC to form either the single addition product from zwitterionic enolate intermediate **1** in the case of TPT and IMes, or the dimerization product from zwitterionic dimeric

enolate intermediate **2** in the case of I^{t}Bu or NHO (Figure 2.2).[28] Guided by the above hypothesis, we first examined our initial strategy of employing LAs to stabilize enolates **1** and **2** so that the proton transfer and elimination pathways could be suppressed or shut down and thus only propagation proceeds via repeated Michael additions of propagating zwitterionic enolate **5** and its homologs to LA-activated monomer **4** to produce PMC **6** (Figure 2.3).

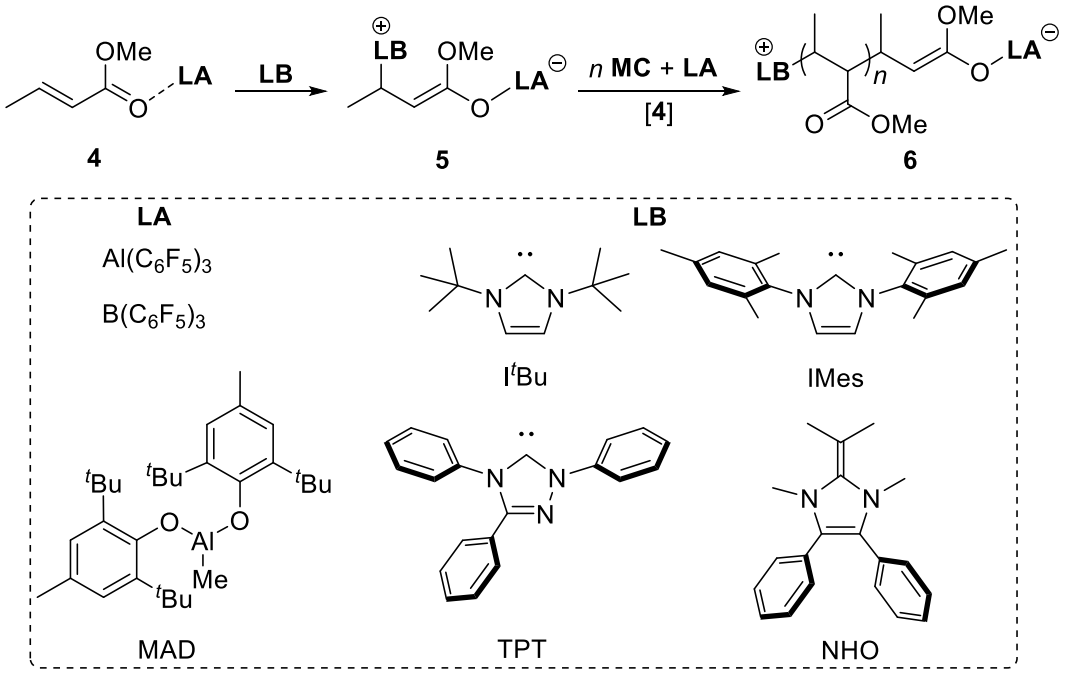

Figure 2.3. Proposed Route to PMC by LPP and the LAs and LBs Employed in This Study.

Starting with the most acidic LA of the series, $Al(C_6F_5)_3$, and using the MC:LA:LB ratio of 100:2:1, reactions were screened with all four LBs listed in Figure 2.3. To prevent direct contact between the free LA and LB and promote the clean generation of zwitterionic active species **5**, followed by propagation to give zwitterionic polymer **6**, these reactions were carried out by first premixing MC and LA to generate activated monomer **4**, followed by addition of the MC/LA solution to the LB. The 2:1 LA:LB ratio was kept constant so that 1 equivalent of the LA generates the zwitterionic active species while the second activates the incoming monomer. The I^{t}Bu

reactions resulted in a trace amount of polymer/oligomer formation after 24 h. It was later found in a stoichiometric NMR scale reaction of MC:Al(C_6F_5)$_3$:I^{t}Bu 1:1:1 (Figure A1) that I^{t}Bu deprotonates the LA-activated monomer at the γ-position to form an unreactive enolaluminate. The deprotonation of MC using NHC alone was also proposed by Waymouth et al. as the competing mechanism for the dimerization of MC, involving the deprotonation of MC to form conjugated enolate **3**, followed by subsequent addition, chain transfer (proton exchange), and isomerization steps (Figure 2.4).[28] On the other hand, TPT was found to rapidly polymerize MC at the 100:2:1 MC:LA:LB ratio, causing the solution to gel instantaneously but with the conversion being less than 50%. Stoichiometric reactions of MC:Al(C_6F_5)$_3$:TPT (1:1:1) cleanly produced zwitterionic enolate species **5**, which quickly rearranged at room temperature to form an isomeric thermodynamic product (Figures A5), as indicated by a color change from yellow to dark violet and corresponding spectral changes. The thermodynamic isomer was found inactive toward further propagation. In light of the above issues associated with the LPP of MC by Al(C_6F_5)$_3$ based LPs, this LP system was not studied in detail or employed for further mechanistic studies.

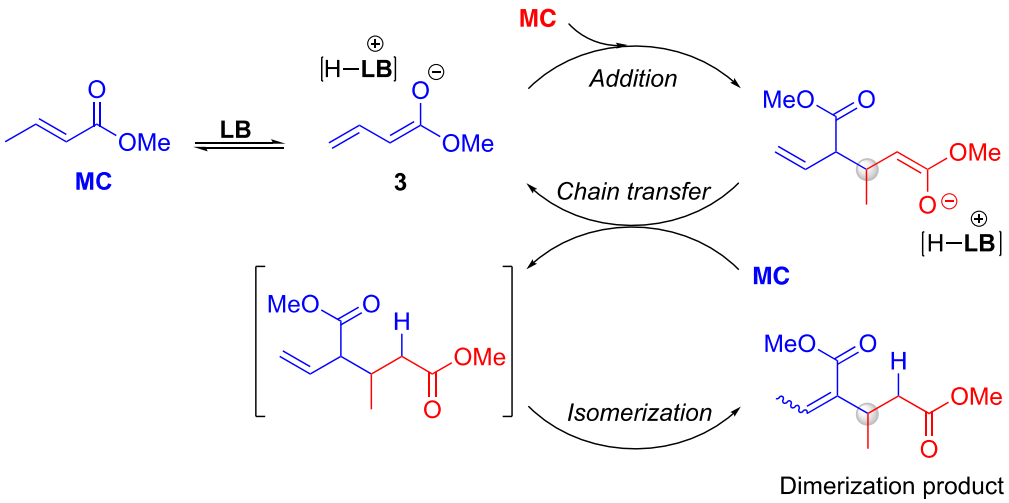

Figure 2.4. Proposed Basic Pathway for Dimerization of MC.

Next, a milder LA, $B(C_6F_5)_3$, was screened against different LBs. Gratifyingly, I^{t}Bu, TPT, and NHO were all effective at polymerizing MC at the MC/LA/LB ratio up to 200:2:1, while IMes was found to be only marginally active and thus not thoroughly studied or used further. Gel permeation chromatography (GPC) traces for these polymers were often bimodal, and initiation efficiencies (I*) were rather low (<50%). Attempts to synthesize $B(C_6F_5)_3$ variants of zwitterionic active species **5** in C_6D_6 resulted in CLA formation as the major product when TPT or I^{t}Bu was used as the LB, which is assumed to be irreversible in these cases. Thus, if MC coordinates weakly to $B(C_6F_5)_3$, and the lifetime of the free LA is significant enough to facilitate CLA formation, it is conceivable that a fraction of the LP is deactivated at the start of polymerization, giving rise to low I* values. Table A1 summarizes the results of selected MC polymerization runs with $B(C_6F_5)_3$-based LPs with I^{t}Bu, TPT, and NHO.

Following the successful polymerization of MC with $B(C_6F_5)_3$-based LPs, MAD, with a Lewis acidity between that of $B(C_6F_5)_3$ and $Al(C_6F_5)_3$, was screened with several LBs (Table 2.1) as MAD has recently proven to be a highly effective LA for facilitating living or controlled bimetallic propagation in several LPP systems[16,19,25]. The increased steric hindrance provided by the bulky phenoxy ligands was reasoned to suppress side reactions such as LA-assisted Claisen-type cyclization, thereby effecting living MMA polymerization with the MAD/NHO LP system. MAD also forms a true FLP with NHO,[16a] and there was no background polymerization activity by MAD alone up to 24 h with MAD concentrations up to 8 mol % relative to MC.

The results summarized in Table 2.1 show a significant increase in polymerization activity for the MAD/LB system compared to the $B(C_6F_5)_3$/LB system. In particular, the MAD/I^{t}Bu LP displayed an extremely high turnover frequency (TOF) of 42 min^{-1}, achieving gelation in under 50 s at the 100:2:1 MC/LA/LB ratio (run 1, Table 2.1), but the activity dropped drastically when the ratio was

increased to 500/2/1 (run 3, Table 2.1). Lower-than-expected-molecular-weight values and correspondingly high *I** values (276 – 1140%, runs 1- 3, Table 2.1) are suggestive of a chain transfer mechanism (*vide infra*).

Table 2.1. Results of Polymerization of MC by MAD-based LPs

Run #	[MC]:[MAD]:[LB]	LB or MC-LP	t_{gel}[b] (min)	Conv (%)	M_n[c] (kg/mol)	$Đ$[c] (M_w/M_n)	I^*[d] (%)	TOF (min^{-1})[e]
1	100:2:1	I^{t}Bu	0.8	>99	3.63	1.35	276	42
2	200:2:1		8	>99	3.98	1.84	503	
3	500:2:1		>180	74	3.25	1.43	1140	
4	100:2:1	TPT	18	>99	13.3	1.12	75	1.3
5	200:2:1		40	>99	21.3	1.22	94	
6	500:2:1		>180	93	52.3	2.05	89	
7	100:2:1	NHO	10	>99	15.9[f]	1.10	65[g]	3.6
8	200:2:1		30	>99	33.4	1.09	60	
9	500:2:1		>180	95	11.0	1.90	432	
10	100:1:1	^{TPT}**5**	14	>99	20.7	1.03	50	1.9

[a] Conditions: [MC] = 0.53 mL (5.0 mmol); neat; temperature = 25 ºC; time = 24 h; MC was pre-mixed with MAD followed by addition of 10-50 µL of 0.094 M LB stock solution in toluene. [b] Approximate time of gelation. [c] Number-average molecular weight (M_n) and dispersity indices ($Đ$) determined by GPC at 40 °C in $CHCl_3$ coupled with a DAWN HELEOS II multi (18)-angle light scattering detector and an Optilab TrEX *d*RI detector for absolute molecular weights. [d] Initiation efficiency (I^*) = M_n(calcd)/M_n(exptl), where M_n(calcd) = MW(MC) × [MC]/[LB] × conversion% + MW of chain-end groups. [e] Turnover frequency (TOF) calculated by slopes of linear regions in conversion vs time kinetic plots (Figure 2.2). [f] Bimodal distribution: M_n = 15.9 kg/mol and $Đ$ = 1.10 (45.7%); M_n = 15.0 kg/mol and $Đ$ = 1.04 (54.3%). [g] Composite I^* based on two GPC peaks, where M_n(exptl) = (% composition A) × (M_n)A + (% composition B) × (M_n)B.

In comparison, NHO and TPT LBs exhibited much lower TOFs (runs 4 and 7, Table 2.1) but both achieved much higher conversions (93-95%) at the 500:2:1 ratio. TPT did not appear to chain transfer and thus produced relatively high molecular weight polymers with M_n up to 52.3 kg/mol and *I** values less than 100% (75-94%, runs 4-6, Table 2.1). On the other hand, NHO had a high *I** value of 432 % at the 500:2:1 ratio (run 9, Table 2.1), suggesting that chain transfer was involved at low LA concentrations. The ^{1}H NMR spectra of runs where chain transfer was implied by *I**

values, such as runs 1-3 by I^{t}Bu, showed visible end olefin end groups (*vide infra*). It is noteworthy however, that these same end groups were also visible in the NMR spectrum of run 7 by NHO (Figure A27). Although the composite *I** value was still less than 100 %, the bimodal GPC trace for run 7 (Figure A30) suggested two distinct types of polymers: the first being the polymer initiated directly by the LB, while the second being the polymer initiated through chain transfer (*vide infra*).

It is quite clear from the 500:2:1 run (runs 3, 6, 9, Table 2.1) that there was a rapid decay in polymerization activity with increasing the monomer loading. This observation can be explained by the propagation step's reliance on the concentrations of both **4** and **6** based on the proposed bimetallic propagation in Figure 2.3, giving the rate law k_p[**4**][**6**] which has been observed in LPP systems.[14b,16a,d,22] Since [**6**] is related to the initial LB concentration and [**4**] is related to the initial LA concentration, increasing the monomer loading dilutes both factors in the rate law, resulting in a rapid rate decay, thus preventing efficient polymerization past a minimum precatalyst concentration. The use of solvents has the same effect on the rate law, which was shown kinetically (*vide infra*). It's worth pointing out that solvents that are more polar than MC, such as DMF or DMSO, will competitively coordinate with the free LA and result in only dimerization products, while dichloromethane is known to react with NHCs and NHOs. Solvents less polar than MC such as toluene and THF drastically limit polymerization by diluting the precatalyst.

To address the conversion limitation at increased monomer loadings, we hypothesized that decreasing the initial concentration of LB while keeping the LA concentration constant around 2 mol % should be a promising strategy for synthesizing high molecular weight PMC. By keeping the LA concentration constant, the experienced TOF of propagation for each individual chain should remain constant. Thus, by decreasing the initial LB concentration, the total number of

chains produced would be lowered. Therefore, there is a larger monomer reservoir to support greater chain lengths. This strategy is also beneficial because there is more total solution volume per growing chain to dissipate the heat generated by the reaction, thereby controlling runaway character which was observed in run 1. Another advantage of this strategy is that by premixing the monomer with an excess of LA such as MAD, any protic impurities still present in the monomer will be scavenged by the LA prior to contact with LB or active species.

Table 2.2 summarizes the results of independently lowering LB concentration while keeping MAD concentration at 2.00 mol % for I^{t}Bu polymerizations and 3.25 mol % for other LBs. All LBs converted MC quantitatively in less than 24 h and gelled in less than 1 h. I^{t}Bu (run 11) formed a gel within 5 min (gelation has been shown kinetically to occur between 45 and 55 % conversion). GPC data for these runs showed that I^{t}Bu generated polymers that undergo chain transfer frequently while TPT generated polymers with much higher molecular weight with M_n up to 124 kg/mol (I^* = 81%, run 15, Table 2.2). NHO underwent chain transfer but to a lesser extent than I^{t}Bu (runs 17-19 vs. 11-13). All LBs can achieve quantitative or near quantitative MC conversion with the $[MC]_0$:$[I^tBu]_0$ ratio ranging from moderate 500:1 to high 4000:1.

Table 2.2. Results of MC Polymerization by MAD-Based LPs with High [MC]/[LB] Ratios [a]

Run	Base	[MC]:[MAD]:[LB]	t_{gel} (min)	Conv (%)	M_n (kg/mol)	$Đ$ (M_w/M_n)	I^* (%)
11	I^{t}Bu	1000:20: 1	5	>99	23.6	4.52	432
12		2000:40: 1	9	>99	21.8	6.43	848
13		4000:80:1	30	98	78.3	4.39	511
14	TPT	500:16:1	25	>99	48.8	1.18	103
15		1000:32:1	70	>99	124	2.82	81
16		2000:64:1	180	99	104	3.90	193
17	NHO	500:16:1	20	>99	35.3	1.88	142
18		1000:32:1	40	99	52.7	4.76	190
19		2000:64:1	120	99	70.3	4.49	285
20	KO^{t}Bu	1000:32:1	5	>99	97.1	3.47	103

[a] Conditions: [MC] = 1.00 mL (9.43 mmol); neat; temperature = 25 ºC; time = 24 h; MC+MAD solutions were first prepared by serial dilution of 8.0 mol % MAD stock solution in MC, and 10-100 μL of 0.094 M LB stock solution in toluene was then added; see footnotes in Table 2.1 for other explanations or abbreviations.

2.2.2 Chain Propagation Mechanism. The chain propagation mechanism via bimetallic conjugate addition should be the same in all the LPP systems herein. Zero order monomer dependence kinetics are predicted, at least before gelation occurs, based on the following rate law:

$$1.) -\frac{d[\mathrm{MC}]}{dt} = k_\mathrm{p}[\mathbf{4}][\mathbf{6}] \approx k_\mathrm{p}[\mathrm{MAD}]_0[\mathrm{LB}]_0$$

[**4**] and [**6**] can be treated as constants since they are regenerated each turnover. Linear monomer conversion vs time plots are expected and indeed observed under neat conditions for $[MC]_0$:$[MAD]_0$:$[LB]_0$ = 100:2:1 polymerizations at room temperature (RT) and without temperature control (Figure 2.5). It is noteworthy that all profiles in Figure 2.5 exhibited a slightly positive deviation from linearity, attributable to the exothermic nature of this polymerization causing gradual increase in propagation rates over time under neat conditions.

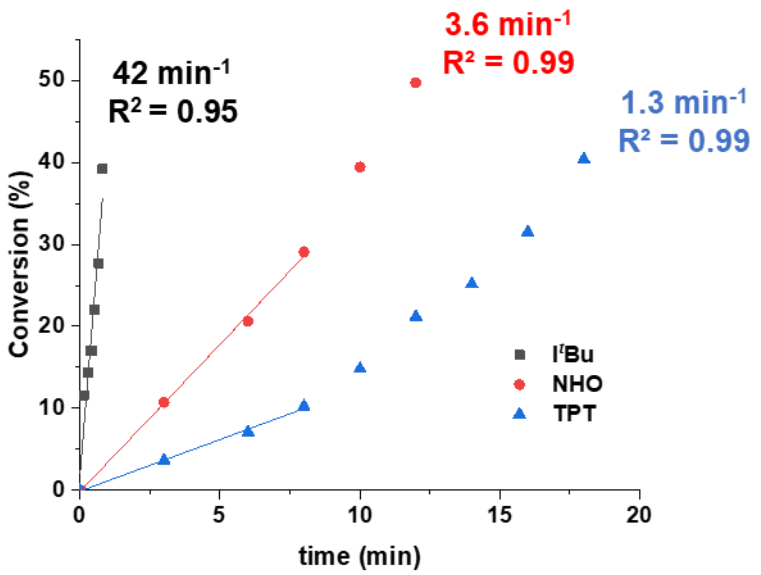

Figure 2.5. Kinetic Profiles of MC:MAD:LB = 100:2:1 runs under neat conditions and calculated TOF values from the slopes of initial linear regions of the kinetic plots.

The kinetic experiments were also carried out in solution. Polymerization of MC with MAD/I^{t}Bu when performed in toluene was observed to be first order in monomer concentration, at least when [LA] + [LB] was above a certain threshold (Figures 2.6 and 2.7). When $[LA]_0$ and $[LB]_0$ were lowered while maintaining a 2:1 ratio and keeping [MC] constant, first order behavior ceased and polymerization rate decayed at low conversion. The first-order kinetics implies that the rate-determining step is actually recombination of MC and LA to form **4** under such conditions. In toluene, there is probably an entropically driven equilibrium between the free LA and **4** due to dilution of [MC] and [MAD] and possible interaction between the solvent molecule and strongly acidic aluminum LA.

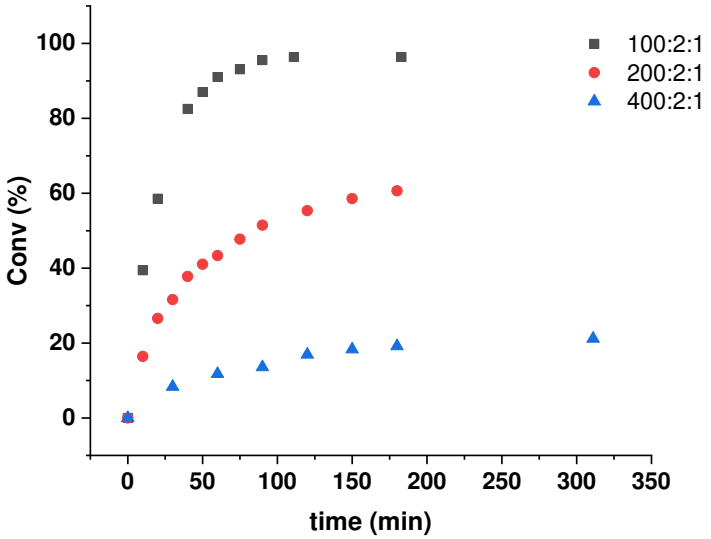

Figure 2.6. Conversion vs time profiles for MC:MAD:I^{t}Bu = 100:2:1, 200:2:1, 400:2:1. [MC] = 2.17 M in toluene, RT.

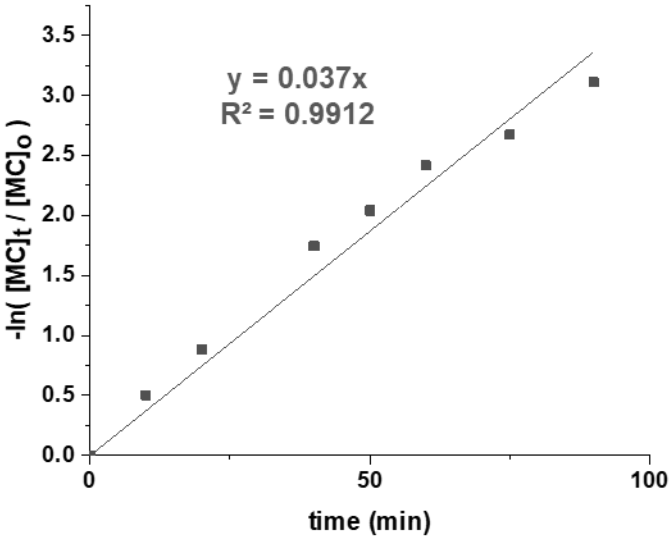

Figure 2.7. First-order plot for MC:MAD:I^{t}Bu = 100:2:1 polymerizations. [MC] = 2.17 M in toluene, RT.

2.2.3 Chain Initiation Mechanisms. The MAD/TPT system is proposed to predominantly undergo the nucleophilic initiation pathway outlined in Figure 2.3. This mechanism was evidenced by the formation of the single-addition product when the LA was absent (*c.f.*, Figure 2.2), and the clean formation of MC/MAD/TPT zwitterionic species ^{TPT}**5** (Figures 2.8 and A11-13), upon addition of premixed 1:1 MC:MAD to 1 equiv. of TPT in C_6D_6. This intermediate was isolated as a powder by crystallization from toluene/hexane. Significantly, addition of 1 equiv. of the isolated ^{TPT}**5** to 100:1 MC:MAD promoted rapid polymerization and achieved a somewhat higher TOF (1.9 min^{-1}, run 10) than the polymerization by addition of TPT directly to MC+MAD (1.3 min^{-1}, run 4), demonstrating the kinetic competency of zwitterionic intermediate **5**. NHO is also proposed to initiate the polymerization primarily through nucleophilic addition; ^{NHO}**5** can also be generated through the same procedure as ^{TPT}**5** (Figures A14 and A15) and, however, it is thermally unstable and could not be isolated at RT. Intermediates $^{\mathbf{TPT}}$**5** and $^{\mathbf{NHO}}$**5** are analogous to several previously reported structures from other LPP systems.[14b,16a-b,24]

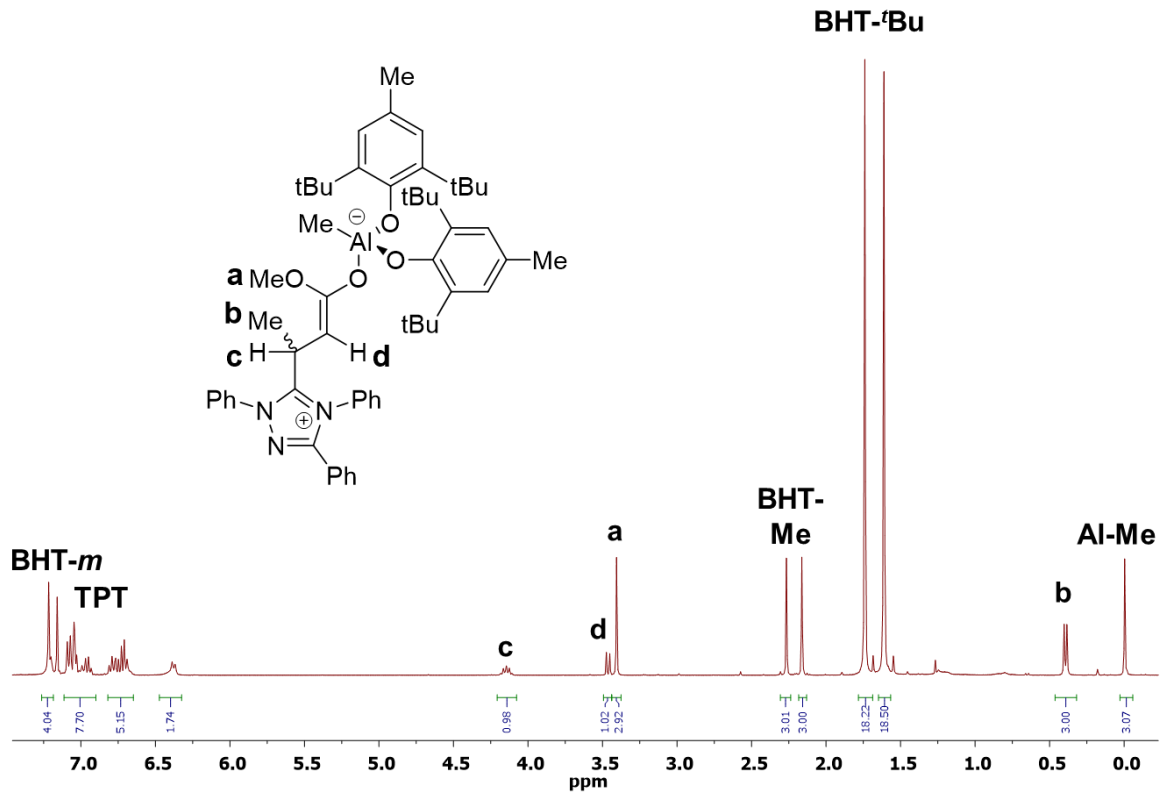

Figure 2.8. ^{1}H NMR (C_6D_6, RT) spectrum of active species ^{TPT}**5** generated through nucleophilic initiation.

On the other hand, the MAD/I^{t}Bu system is proposed to initiate the polymerization via the basic (deprotonation) pathway (Figure 2.11), based on the observations of the vinyl end group by NMR and substantial chain transfer by the large *I** values (*vide supra*). To search for corroborating evidence of chain ends, matrix-assisted laser desorption/ionization time-of-flight mass spectroscopy (MALDI-TOF MS) was used to analyze the resulting polymers. Interestingly, only one set of molecular ion peaks was observed for the MAD/I^{t}Bu-generated polymer (run 11, Table 2.2) corresponding to absent end groups (y-intercept of 23 Da, the mass of a sodium atom, Figure 2.9). On the other hand, the polymer produced by MAD/NHO (run 18, Table 2.2) showed two sets of peaks, one corresponding to no end groups (y-intercept = 23 Da) and the other with end groups corresponding the mass of the NHO plus a proton (y-intercept = 291 Da, Figure A18). Only

one set of MS peaks was observed for the polymer produced by MAD/TPT (run 15, Figure 2.10) corresponding to the attached TPT cation and proton.

Based on the above results, it was then proposed that TPT and NHO follow the nucleophilic initiation pathway outlined in Figure 2.3, while I^{t}Bu initiates the polymerization by deprotonating **4** to generate enolaluminate **7** (Figure 2.11) as opposed to the zwitterionic addition product **5**. This basic pathway is also consistent with the fact there being an undetectable amount of the I^{t}Bu$^+$ bound polymer. In addition, attempts to synthesize $^{I^tBu}$**5**, the postulated nucleophilic initiation product, resulted in the exclusive formation of enolate **7** (Figures A8-A10), the basic initiation product.

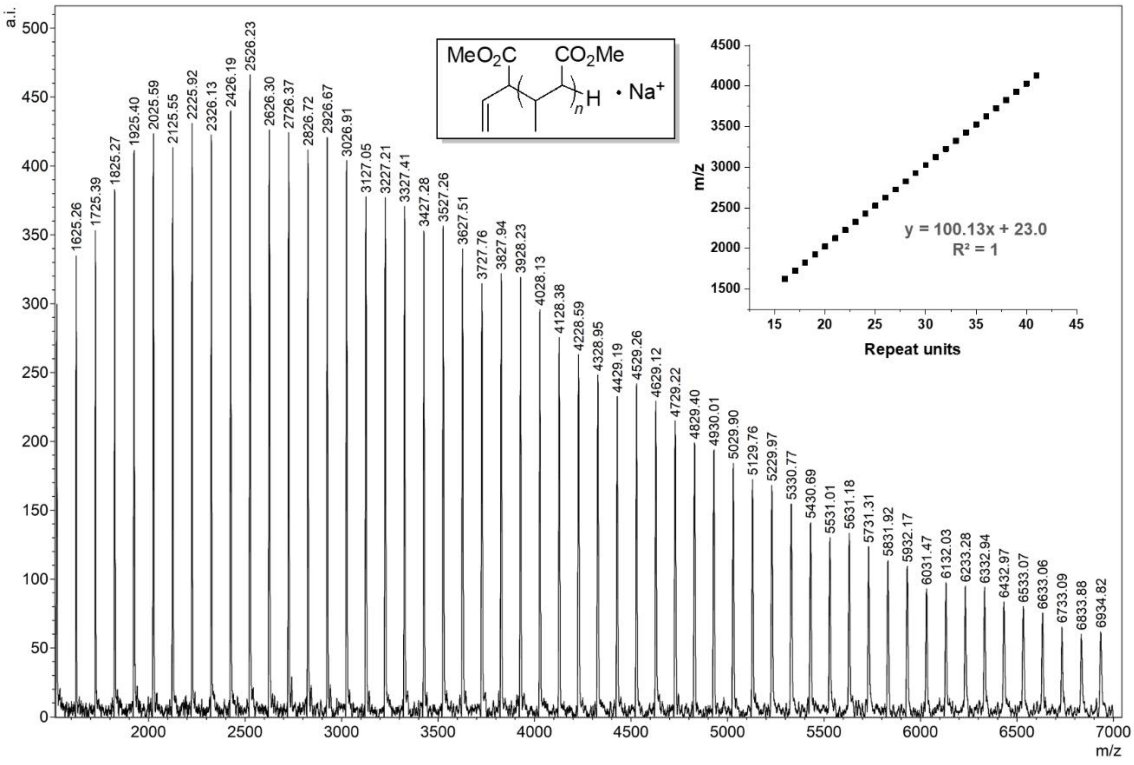

Figure 2.9. MALDI-TOF MS spectrum and end group calculations for PMC by MAD/I^{t}Bu.

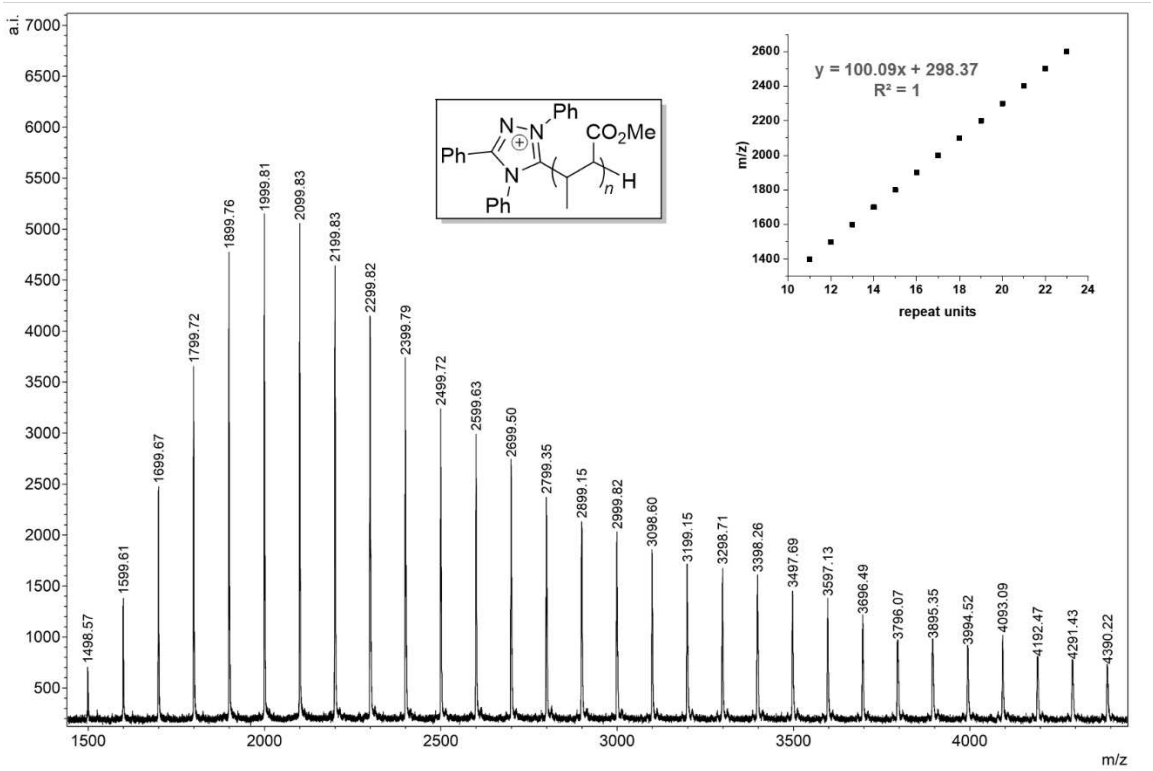

Figure 2.10. MALDI-TOF MS spectrum and end group calculations for the oligomers produced by MAD/TPT.

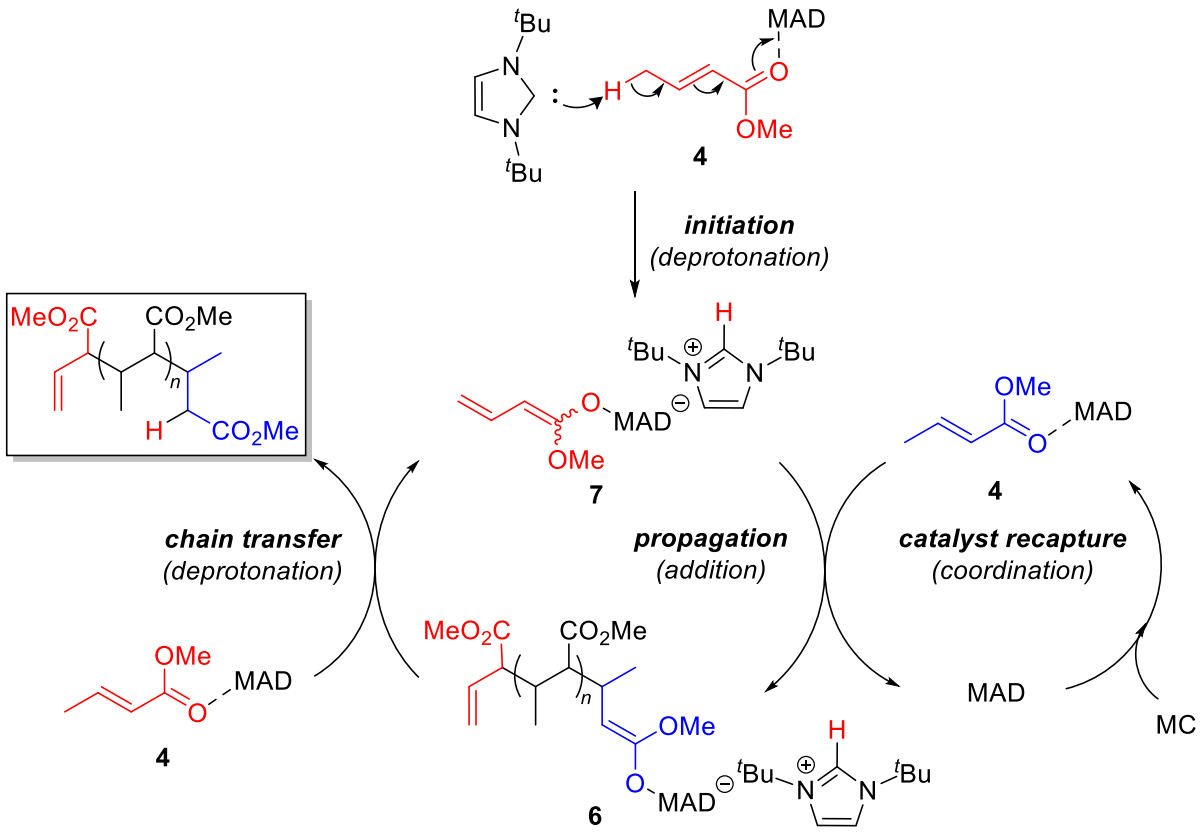

Figure 2.11. Proposed Mechanism for MC Polymerization by MAD/I^{t}Bu, Involving Basic Initiation as well as Bimetallic Chain Propagation and Transfer (not Including Unimolecular Chain Transfer).

To further probe whether initiation can occur through deprotonation, we reacted MC:MAD (100:2) with 1 equiv. of a Brønsted base, KO^{t}Bu, which resulted in efficient polymerization reaching gelation in 30 min. The ^{1}H NMR of the KO^{t}Bu- generated polymer exhibited the vinyl end group matching with that generated by I^{t}Bu (Figure A24), thus providing additional, strong evidence that I^{t}Bu initiates the polymerization according to the basic pathway outlined in Figure 2.11. Since this strategy represents a practically feasible method of making vinyl-functionalized PMC, we attempted the synthesis of high M_n PMC using MC:MAD:KO^{t}Bu = 1000:32:1; the polymerization gelled in 5 min and reached quantitative MC conversion eventually, producing PMC with a high M_n of 97.1 kg/mol and a near quantitative initiation efficiency of I^* = 103 % (run 20, Table 2.2).

2.2.4 Chain Transfer Mechanisms. The PMC products with no detectable end groups as judged by MALDI-TOF MS spectra were first suspected to be cyclic. There have been recent reports[10a,12b,21,25] of a S_N2 ring-closing mechanism where the growing enolate chain end gets a backside attack on the β-carbon bonded to the LB^+ initiating group. The LB^+ dissociates taking the electrons with it to reform the original NHC. However, macrocyclization seems unlikely in the case of the MC/I^{t}Bu system based on the absence of a leaving group at the α-terminus (Figure 2.11). Alternative mechanisms for chain transfer in the MC/I^{t}Bu system include the deprotonation of an activated monomer shown in Figure 2.11, or the deprotonation of the imidazolium cation to reform the original NHC (Figure 2.12).

To further interrogate the chain transfer mechanism, we synthesized low molecular weight polymers using a MC:MAD:LB ratio of 30:2:1 in toluene, and let the reaction mixture stir for 12 h. These polymers were then isolated and analyzed by NMR and MALDI-TOF MS (Figures 2.10 and A19-A20). Since the live zwitterionic polymers are expected to reach 100 % conversion well before 12 h, they should spend a long time period stirring in toluene in the absence of monomer, which should invoke cyclization if any. Likewise, if 100 % conversion is reached quickly, there should not be any chain transfer product generated by the deprotonation pathway because there is no free monomer left to deprotonate. The results showed that the polymer again by I^{t}Bu displayed only one set of *m*/*z* peaks corresponding to no end groups (Figure A19), consistent with the current deprotonation mechanism (Figure 2.11). NHO (Figure A20) and TPT (Figure 2.10) also showed only one set of *m*/*z* peaks corresponding to attached LB and H^+. These results suggest again that NHO and TPT initiate exclusively through the nucleophilic mechanism and do not chain transfer by cyclization, at least in toluene.

^{1}H NMR spectra were obtained for the 30:2:1 polymers and analyzed. Supposed vinyl end groups can be observed in the PMC produced by MAD/I^{t}Bu (Figures A21-A23) in the olefin region that are not present in analogous spectra of the PMC by MAD/TPT or MAD/NHO. These peaks correspond to the alkene at the α-terminus of the polymers initiated by deprotonation. This result provides additional evidence that I^{t}Bu initiates polymerization by deprotonation and does not cyclize.

We also sought for ways to distinguish chain transfer mechanisms kinetically. Because one has the unique ability to manipulate [LA] independently in LPP systems, propagation rate can be manipulated without changing the size of the monomer reservoir or the theoretical M_n. By invoking the following proportionality, one can use M_n as a proxy for the rate of chain transfer with respect to differing propagation rates.

$$2.) M_n \propto \frac{rate\ of\ propagation}{rate\ of\ chain\ transfer}$$

Using the same bimetallic rate expression for propagation discussed earlier, one can write two different forms, distinguished by chain transfer's reliance on **4**. In all cases, it seems reasonable to assume [**4**] is a function of initial $[LA]_0$ and [**6**] is a function of initial $[LB]_0$.

$$3.) M_n \propto \frac{k_p[\mathbf{4}][\mathbf{6}]}{k_{CT}[\mathbf{4}][\mathbf{6}]}$$

$$4.) M_n \propto \frac{k_p[\mathbf{4}][\mathbf{6}]}{k_{CT}[\mathbf{6}]}$$

Proportionality 3 describes chain transfer by bimetallic deprotonation (Figure 2.11), where propagation and chain transfer both have reliance on activated monomer **4**. In this case, one would expect all concentration terms to cancel, making M_n fairly independent of initial $[LA]_0$.

On the other hand, one would expect chain transfer by S_N2 macrocyclization to follow proportionality 4. Since **4** is not involved in macrocyclization, increasing initial $[LA]_0$ should increase propagation rate without affecting chain transfer rate. Therefore, it is foreseeable that increasing $[LA]_0$ should result in higher M_n polymers. Similar logic can be applied to the I^{t}Bu system to differentiate between bimetallic deprotonation (Figure 2.11) and deprotonation of the imidazolium cation (Figure 2.12) as the former should follow proportionality 3 while the latter should follow proportionality 4.

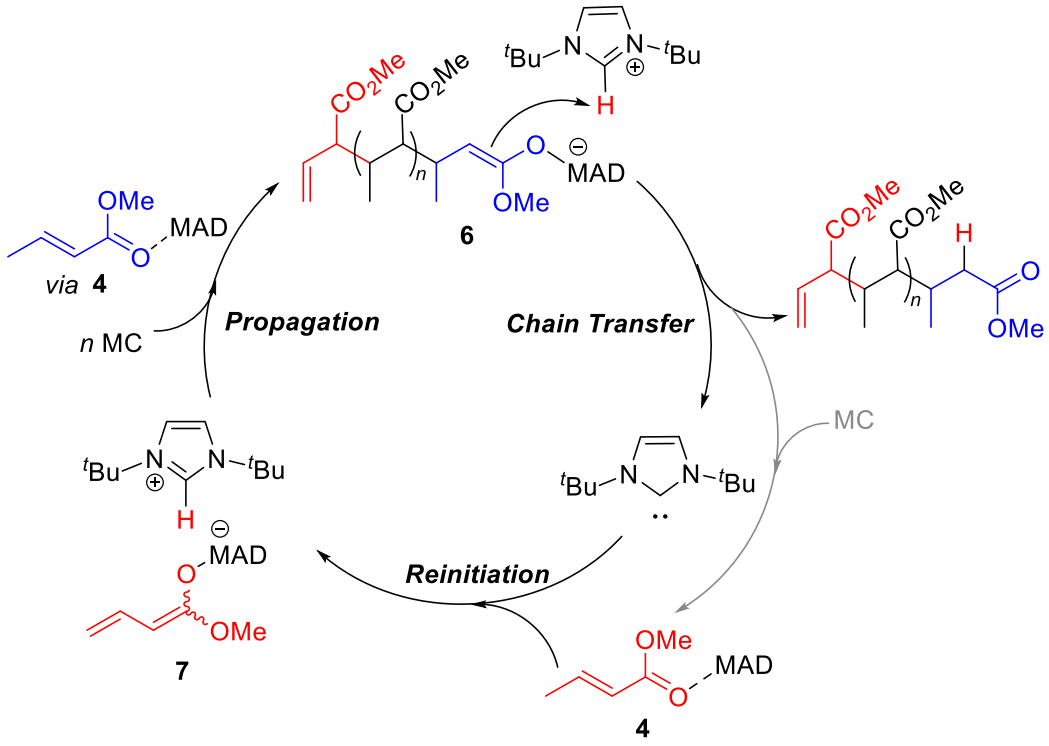

Figure 2.12. Proposed Unimolecular Chain Transfer for the MAD/I^{t}Bu System Involving deprotonation of I^{t}Bu$^+$ to Reform the Carbene.

Guided by the above hypotheses, MC/MAD/LB systems were examined at varying $[MAD]_0$, from 1000:20:1 to 1000:40:1, to 1000:80:1. Reactions were prepared by diluting an 8.0 mol % MC/MAD stock solution to the appropriate concentration. Then, to each MC/MAD solution, a

constant volume of a LB/toluene stock solution was added. Each reaction was given a full 24 h to complete and all conversions were quantitative by NMR. Figure 2.13 and Table 2.3 show the M_n dependence on $[MAD]_0$.

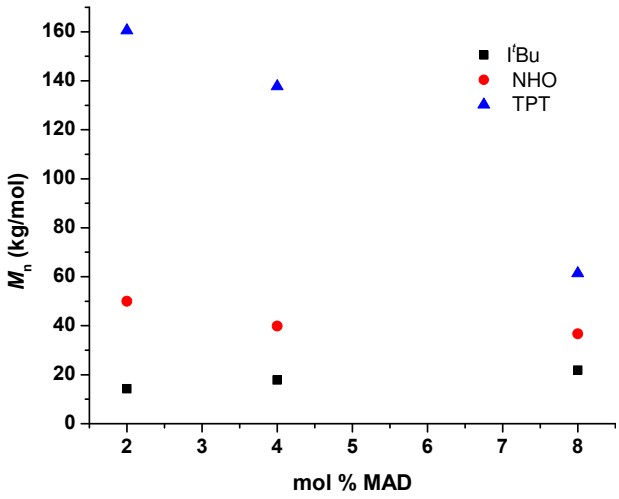

Figure 2.13. M_n vs $[MAD]_0$ Plots for MC:MAD:LB = 1000:X:1.

The initial negative slope present in the M_n vs [LA] curve followed by subsequent stabilization around 38 kg/mol (by NHO) is strong evidence that S_N2 cyclization did not occur, and that chain transfer is [LA] dependent. Bimetallic deprotonation of **4** was hypothesized to be the main contributor for the NHO and TPT systems. This feature also implies that in the NHO and TPT systems, cationic LB end groups would be stabilizing the enolaluminate end group of a growing chain (Figure 2.14), as opposed to an I^{t}Bu imidazolium cation (Figure 2.11). High molecular weight chains with the cationic LB end groups might experience serious drop in TOF from the loss of mobility, especially after gelation. The increased mobility of the imidazolium cation to exit the polymer phase during chain transfer and reenter solution might explain why it has such a high TOF

of I^{t}Bu compared to NHO or TPT. For the TPT series, the 1000:20:1 ratio produced the highest molecular weight PMC with M_n = 161 kg/mol and $Đ$ = 1.62 (run 27, Table 2.3). Intriguingly, increasing the ratio to 1000:40:1 and 1000:80:1 reduced M_n value to 138 kg/mol and 61.4 kg/mol, respectively. One hypothesis for the observed larger negative slope for TPT is that when TOF is higher due to higher [LA], the temperature increases more rapidly, effectively lowering the pK_a of MC and increasing the rate of chain transfer. To test this hypothesis, the conditions from run 16 (Table 2.2) were scaled up to 8.0 mL of MC, and the resulting polymer had a M_n of only 15.8 kg/mol (vs. 104 kg/mol) correlating to a high I^* value of 1266 %. Under these conditions, gelation occurred very fast (30 min) compared to run 16 (3 h), and the reactor was rather hot late in the reaction.

The slightly positive slope in the M_n vs $[MAD]_0$ plot by I^{t}Bu (doubling $[LA]_o$ resulted in approx. 25 % M_n increase) suggests a significant contribution from a [LA] independent chain transfer. These reactions (runs 21-23) gelled in less than 5 min and experienced rapid temperature changes. It does seem likely that both bimetallic deprotonation (Figure 2.11) and deprotonation of the imidazolium (Figure 2.12) are significant contributors to the rate of chain transfer. This hypothesis is consistent with the run 3 results, where [LA] was only 0.4 mol % and the PMC produced was rather small (M_n = 3.25 kg/mol), suggesting the [LA] independent chain transfer route (Figure 2.12) is less neglectable when [LA] is very small.

Table 2.3. Results of MC Polymerization Investigating M_n Dependence on [MAD]$_0$ [a]

Run #	LB	MC:MAD:LB	Conv (%)	M_n (kg/mol)	$Đ$ (M_w/M_n)	I^* (%)
21	I^{t}Bu	1000:20:1	100	14.3	1.92	700
22		1000:40:1	100	17.8	1.43	562
23		1000:80:1	100	21.9	1.52	457
24	NHO	1000:20:1	100	49.9	2.49	201
25		1000:40:1	100	39.9	1.96	251
26		1000:80:1	100	36.7	1.93	273
27	TPT	1000:20:1	100	161	1.62	62
28		1000:40:1	100	138	2.02	73
29		1000:80:1	100	61.4	1.76	163

[a] [MC] = 0.50 mL (4.7 mmol); see footnotes in Table 2.1 for conditions and explanations.

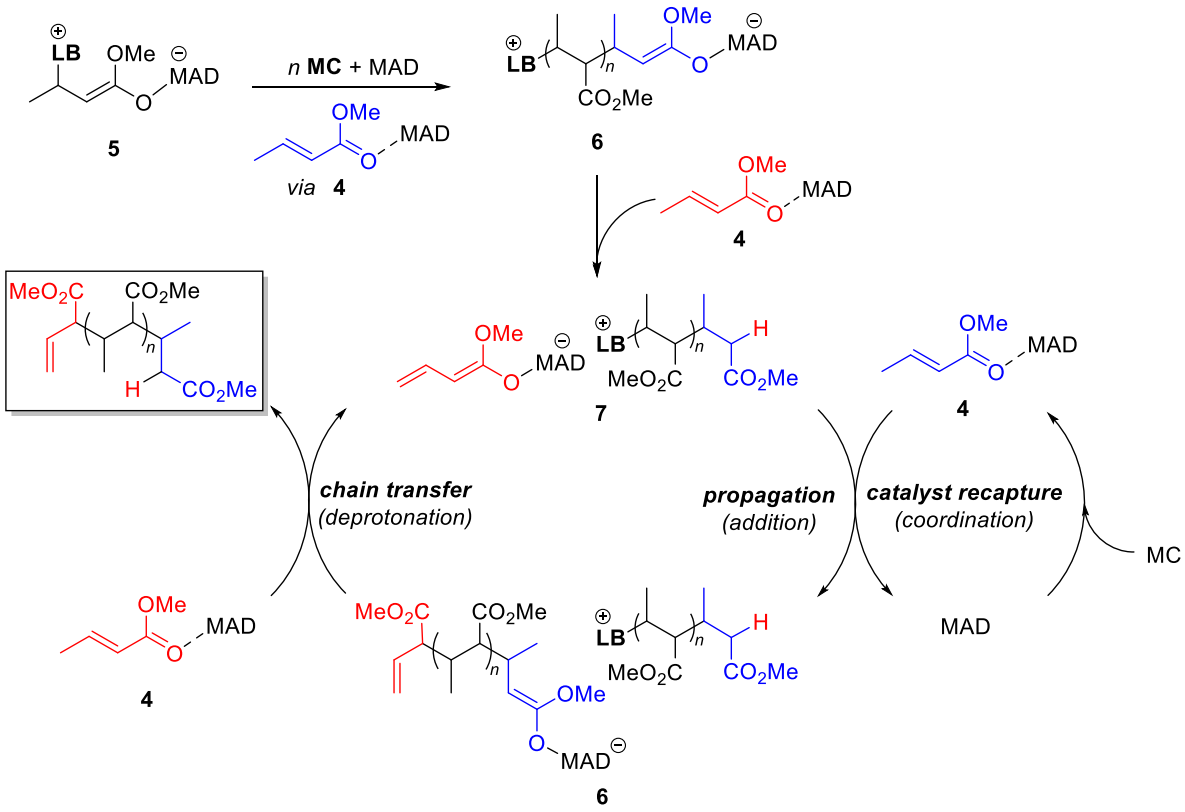

Figure 2.14. Proposed Mechanism for MC Polymerization by MAD/NHO and MAD/TPT, Involving Nucleophilic Initiation and Bimetallic Chain Transfer.

2.2.5 Polymer Tacticity and Thermal Stability. PMC materials produced by the current LPs exhibited similar stereochemistry regardless of the LA or LB, as indicated by NMR spectra of the polymers synthesized with $Al(C_6F_5)_3$, $B(C_6F_5)_3$, and MAD (Figure A25). Integration of the *β*-methyl peak gave approximately 70 % disyndiotacticity, based on comparison with NMR spectra reported by Kitayama.[7f] This polymer microstructure is consistent with analysis of Newman projection shown in Figure 2.15, where both hydrogens are located on the same side of the bond forming alkenes, and the prochiral enolate face opposite to the *β*-methyl is preferred. This analysis may suggest that manipulation of sterics at *β*-substituent could enhance the disyndioselectivity of the resulting polymer.

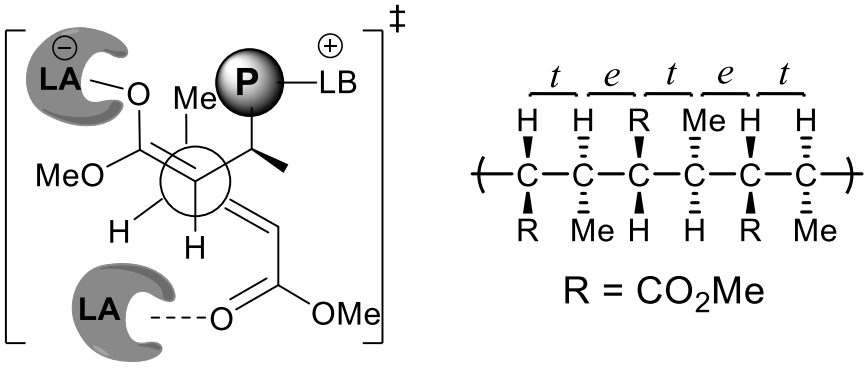

Figure 2.15. Predicted transition state responsible for disyndioselectivity (*t* = threo, *e* = erythro).

Selected PMC samples were analyzed by differential scanning calorimetry (DSC) and thermal gravimetric analysis (TGA). No obvious glass-transition temperature (T_g) was observed up to 280 °C on DSC curves (Figure A34), while all polymers showed nearly identical TGA profiles with minor deviations of decomposition temperature (T_d), with all around 354 °C (Figure 2.16).

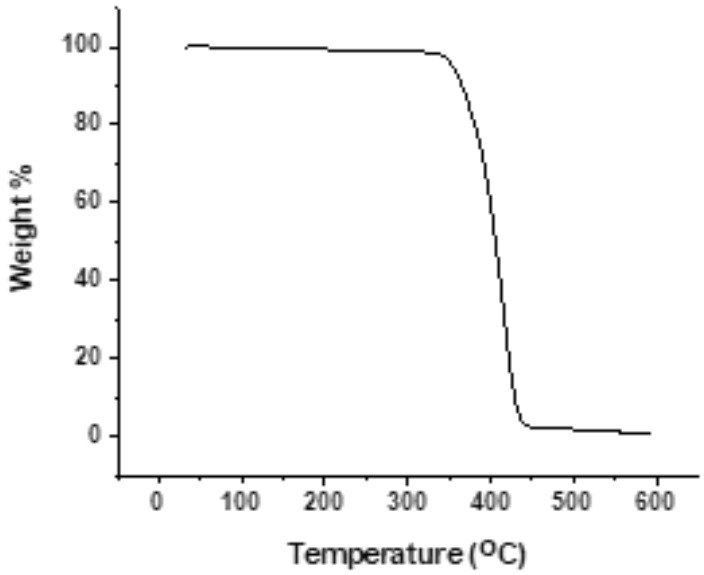

Figure 2.16. A representative TGA curve of PMC (run 15, Table 2.2).

2.3 Conclusions

In summary, this contribution uncovers LA/LB LP structures and reaction conditions under which the biorenewable MC undergoes conjugate addition polymerization to low, medium, and high molecular weight polymers. The LBs examined in this work, I^{t}Bu, NHO, and TPT, were all found to be active for polymerization of MC in the presence of a strong LA, including $E(C_6F_5)_3$ (E = Al, B) and especially MAD. Unoptimized conditions have produced polymers with M_n up to 161 kg/mol. Mechanistic studies have revealed two different initiation mechanisms, basic and nucleophilic pathways. I^{t}Bu prefers the basic initiation pathway, while the other LBs (NHO and TPT) prefer the nucleophilic initiation pathway. Chain transfer is found to be present in all cases to varying degrees. The ability of I^{t}Bu to affect basic initiation allows for a unique chain transfer mechanism where the growing enolate chain end deprotonates the imidazolium cation, resulted from the basic initiation, to reform carbene I^{t}Bu that reinitiates new chains. This mechanistic

scenario makes the rate of chain transfer especially high in the MAD/I^{t}Bu system, allowing for polymers to be synthesized *catalytically* with high initiation efficiencies over 1000%. A second chain transfer mechanism, which is ubiquitous in all the present LPP systems, bimolecular deprotonation of the activated monomer, is highly dependent on temperature. If high molecular weights of PMC are desired, temperature control is needed to slow down the rate of chain transfer.

Realizing the susceptibility of MC to deprotonation by an organic or inorganic base, we developed a facile approach to PMC, simply using KO^{t}Bu as initiator in combination with MAD. This simple LA facilitated anionic polymerization was exploited to produce unique vinyl-functionalized PMC with a relatively high molecular weight of M_n = 97.1 kg/mol.

Lastly, we have shown in a broader context of LPP that, by using large $[LA]_0$ with respect to $[LB]_0$, one can force slow polymerizations via bimolecular propagation under dilute conditions to occur in reasonable timeframes. This strategy is particularly useful when activating less reactive monomers, where polymerization is thermodynamically favorable but kinetically slow.

References cited in Chapter 2

[1] Selected reviews: (a) Sheldon, R. A. Green and Sustainable Manufacture of Chemicals from Biomass, State of the Art. *Green Chem.* **2014**, *16*, 950–963. (b) Tuck, C. O.; Pérez, E.; Horváth, I. T.; Sheldon, R. A.; Poliakoff, M. Valorization of Biomass: Deriving More Value from Waste. *Science* **2012**, *337*, 695–699. (c) Gallezot, P. Conversion of Biomass to Selected Chemical Products. *Chem. Soc. Rev.* **2012**, *41*, 1538-1558. (d) Corma, A.; Iborra, S.; Velty, A. Chemical Routes for the Transformation of Biomass into Chemicals. *Chem. Rev.* **2007**, *107*, 2411−2502.

[2] Jang, Y.-S.; Kim, B.; Shin, J. H.; Choi, Y. J. Choi, S.; Song, C. W.; Lee, J.; Park, H. G.; Lee, S. Y. Bio-Based Production of C2–C6 Platform Chemicals. *Biotechnol. Bioeng.* **2012**, *109*, 2437-2459.

[3] Zhang, X.; Fevre, M.; Jones, G. O.; Waymouth R. M. Catalysis as an Enabling Science for Sustainable Polymers. *Chem. Rev.* **2018**, *118*, 839–885.

[4] (a) Saharan, B. S.; Grewal, A.; Kumar, P. Biotechnological Production of Polyhydroxyalkanoates: A Review on Trends and Latest Developments. *Chin. J. Bio.* **2014**, *2014*, 802984. (b) Poirier, Y.; Nawrath, C.; Somerville, C. Production of Polyhydroxyalkanoates, a Family of Biodegradable Plastics and Elastomers, in Bacteria and Plants. *Bio/Technology, **1995***, *13*, 142–150. (c) Rathore, P. Bioprospects of PHB: A Review. *IJETST*, **2014**, *1*, 529-532. (d) Somleva, M. N.; Peoples, O. P.; Snell, K. D.; PHA Bioplastics, Biochemicals, and Energy from Crops. *Plant Biotechnol. J.* **2013**, *11*, 233-252.

[5] (a) Spekreijse, J.; Le Notre, J.; Sanders, J. P. M.; Scott, E. L. Conversion of Polyhydroxybutyrate (PHB) to Methyl Crotonate for the Production of Biobased Monomers. *J. Appl. Polym. Sci.* **2015**, *132*, 42462/1-42462/8. (b) Ariffin, H.; Nishida, H.; Shirai, Y.; Hassan, M. A. Highly Selective

Transformation of Poly[(R)-3-hydroxybutyric acid] into Trans-crotonic Acid by Catalytic Thermal Degradation. (c) Grassie, N.; Murray, E. J.; Holmes, P. A. The Thermal Degradation of Poly(-(D)-β-Hydroxybutyric Acid): Part 3—The Reaction Mechanism. *Polym. Degrad. Stab.* **1984**, *6*, 127-134. (d) Flanagan, J. C. A.; Myung, J.; Criddle, C. S., Waymouth, R. M. Poly(hydroxyalkanoate)s from Waste Biomass: A Combined Chemical–Biological Approach. *ChemistrySelect* **2016**, *1*, 2327 – 2331.

[6] Ute, K.; Asada, T.; Nabeshima, Y.; Hatada, K. Stereospecific Synthesis of Ditactic Polymers. *Polym. Bull.* **1993**, *30*, 171-178.

[7] (a) Bockman, O. C.; Schuerch, C. Anionic Polymerizations via the Michael Reaction. *Polym. Lett*. **1963**, *1*, 145-151. (b) Miller, M. L.; Skogman, J. Polymerization of *tert*-Butyl Crotonate. *J. Polym., Sci. A*. **1964**, *2*, 4551-4558. (c) Kitano, T.; Fujimoto, T.; Nagasawa, M. Preparation and Characterization of a Monodisperse, Semiflexible Polymer, Poly(*tert*-butyl crotonate). *Macromolecules* **1974**, *7*, 719-724. (d) Tsuruta, T.; Makimoto, T.; Tanabe, K. Anionic Polymerization of β- Substituted Acrylic Esters. *Makromol. Chem.* **1968**, *114*, 182-200. (e) Ute, K.; Tarao, T.; Hatada, K. Group Transfer Polymerization of Methyl Crotonate. *Polym. J.* **1997**, *29*, 957–958. (f) Ute, K.; Tarao, T.; Hongo, S.; Ohnuma, H.; Hatada, K.; Kitayama, T. Preparation of Disyndiotactic Poly(methyl crotonate) by Stereospecific Group Transfer Polymerization. *Polym J.* **1999**, *31*, 177-183. (g) Ute, K.; Tarao, T.; Kitayama, T. Enhanced Stereocontrol in Disyndiotactic-Specific Group Transfer Polymerization of Methyl Crotonate—Stereochemical Evidence of Group Transfer. *Polym. J*. **2005**, *37*, 578-583.

[8] Roy, M. M. D.; Rivard, E. Pushing Chemical Boundaries with N-Heterocyclic Olefins (NHOs): From Catalysis to Main Group Element Chemistry. *Acc. Chem. Res*. **2017**, *50*, 2017−2025.

[9] Flanigan, D. M.; Romanov-Michailidis, F.; White, N. A.; Rovis, T. Organocatalytic Reactions Enabled by N-Heterocyclic Carbene. *Chem. Rev.* **2015**, *115*, 9307−9387.

[10] (a) Naumann, S.; Dove, A. N-Heterocyclic Carbenes as Organocatalysts for Polymerizations: Trends and Frontiers. *Polym. Chem.* **2015**, *6*, 3185-3200. (b) Naumann, S.; Dove, A. P. N-Heterocyclic Carbenes for Metal-free Polymerization Catalysis: an Update. *Polym. Int.* **2016,** *65*, 16–27. (c) Fevre, M.; Pinaud, J.; Gnanou, Y.; Vignolle, J.; Taton, D. *N*-Heterocyclic Carbenes (NHCs) as Organocatalysts and Structural Components in Metal-Free Polymer Synthesis. *Chem. Soc. Rev.* **2013**, *42*, 2142-2172.

[11] (a) Brown, H. A.; Waymouth, R. M. Zwitterionic Ring-Opening Polymerization for the Synthesis of High Molecular Weight Cyclic Polymers. *Acc. Chem. Res.* **2013**, *46*, 2585–2596. (b) Kiesewetter, M. K.; Shin, E. J.; Hedrick, J. L.; Waymouth, R. M. Organocatalysis: Opportunities and Challenges for Polymer Synthesis. *Macromolecules* **2010**, *43*, 2093–2107. (c) Kamber, N. E.; Jeong, W.; Waymouth, R. M.; Pratt, R. C.; Lohmeijer, B. G. G.; Hedrick, J. L. Organocatalytic Ring-Opening Polymerization. *Chem. Rev.* **2007**, *107*, 5813-5840.

[12] (a) Naumann, S.; Thomas, A. W.; Dove, A. P. N-Heterocyclic Olefins as Organocatalysts for Polymerization: Preparation of Well-Defined Poly(propylene oxide). *Angew. Chem. Int. Ed*. **2015**, *54*, 9550–9554. (b) Zhang, Y.; Schmitt, M.; Falivene, L.; Caporaso, L.; Cavallo, L.; Chen, E. Y.-X. Organocatalytic Conjugate-Addition Polymerization of Linear and Cyclic Acrylic Monomers by N-Heterocyclic Carbenes: Mechanisms of Chain Initiation, Propagation, and Termination. *J. Am. Chem. Soc*. **2013**, *135*, 17925–17942. (c) Dove, A.P. Organic catalysis for Ring-opening polymerization. *ACS Macro Lett*. **2012**, *1*, 1409–1412. (d) Jeong, W.; Shin, E. J.; Culkin, D. A.; Hedrick, J. L.; Waymouth, R. M. Zwitterionic Polymerization: A Kinetic Strategy for the Controlled Synthesis of Cyclic Polylactide. *J. Am. Chem. Soc.* **2009**, *131*, 4884–4891.

[13] Li, X.; Chen, C.; Wu, J. Lewis Pair Catalysts in the Polymerization of Lactide and Related Cyclic Esters. *Molecules* **2018**, *23*, 189.

[14] (a) Chen, E. Y.-X. Polymerization by Classical and Frustrated Lewis Pairs. In Frustrated Lewis Pairs II: Expanding the Scope. Erker, G.; Stefan, D. W. Springer-Verlag Berlin Heidelberg, **2013**, *334*, 244-260. (b) Zhang, Y.; Miyake, G. M.; John, M. G.; Falivene, L.; Caporaso, L.; Cavallo, L.; Chen, E. Y.-X. Lewis Pair Polymerization by Classical and Frustrated Lewis Pairs: Acid, Base and Monomer Scope and Polymerization Mechanism. *Dalton Trans*. **2012**, *41*, 9119-9134. (c) Zhang, Y.; Miyake, G. M.; Chen, E. Y.-X. Alane-Based Classical and Frustrated Lewis Pairs in Polymer Synthesis: Rapid Polymerization of MMA and Naturally Renewable Methylene Butyrolactones into High-Molecular-Weight Polymers. *Angew. Chem.* Int. Ed. **2010**, *49*, 10158 –10162.

[15] Selected reviews: (a) Stephan, D. W. The Broadening Reach of Frustrated Lewis Pair Chemistry. *Science* **2016**, *354*, aaf7229, DOI: 10.1126/science.aaf7229. (b) Stephan, D. W.; Erker, G. Frustrated Lewis Pair Chemistry: Development and Perspectives. *Angew. Chem., Int. Ed.* **2015**, *54*, 6400–6441. (c) Stephan, D. W. Frustrated Lewis pairs. *J. Am. Chem. Soc.*, **2015**, *137*, 10018–10032. (d) Stephan, D. W. Frustrated Lewis Pairs: From Concept to Catalysis. *Acc. Chem. Res.* **2015**, *48*, 306–316. (e) Frustrated Lewis Pairs I & II; Stephan, D. W.; Erker, G. Eds. *Topics in Current Chemistry*; Springer: New York, **2013**, Vols. 332 & 334.

[16] (a) Wang, Q.; Zhao, W.; Zhang, S.; He, J.; Zhang, Y.; Chen E. Y.-X. Living Polymerization of Conjugated Polar Alkenes Catalyzed by N-Heterocyclic Olefin-Based Frustrated Lewis Pairs. *ACS Catal*. **2018**, *8*, 3571–3578. (b) Chen, J.; Chen, E. Y.-X. Lewis Pair Polymerization of Acrylic Monomers by N-Heterocyclic Carbenes and $B(C_6F_5)_3$. *Isr. J. Chem*. **2015**, *55*, 216–225. (c) Chen, J.; Chen, E. Y.-X. Reactivity of Amine/$E(C_6F_5)_3$ (E = B, Al) Lewis Pairs toward Linear and Cyclic Acrylic Monomers: Hydrogenation vs. Polymerization. *Molecules* **2015**, *20*, 9575-9590. (d) He,

J.; Zhang, Y.; Falivene, L.; Caporaso, L.; Cavallo, L.; Chen, E. Y.-X. Chain Propagation and Termination Mechanisms for Polymerization of Conjugated Polar Alkenes by [Al]-Based Frustrated Lewis Pairs. *Macromolecules* **2014**, *47*, 7765−7774. (e) Xu, T.; Chen, E. Y.-X. Probing Site Cooperativity of Frustrated Phosphine/Borane Lewis Pairs by a Polymerization Study. *J. Am. Chem. Soc.* **2014**, *136*, 1774–1777. (f) He, J. H.; Zhang, Y. T.; Chen, E. Y.-X. Synthesis of Pyridine- and 2-Oxazoline-Functionalized Vinyl Polymers by Alane-Based Frustrated Lewis Pairs. *Synlett* **2014**, *25*, 1534-1538.

[17] Gowda, R. R.; Chen, E. Y.-X. Chemoselective Lewis Pair Polymerization of Renewable Multivinyl-Functionalized γ-Butyrolactones. *Phil. Trans. R. Soc. A*, **2017**, 375, 2101.

[18] (a) Jia, Y.-B.; Wang, Y.-B.; Ren, W.-M.; Xu, T.; Wang, J.; Lu, X.-B. Mechanistic Aspects of Initiation and Deactivation in N-Heterocyclic Olefin Mediated Polymerization of Acrylates with Alane as Activator. *Macromolecules* **2014**, *47*, 1966–1972. (b) Jia, Y.-B.; Ren, E.-M.; Liu, S.-J.; Xu, T.; Wang, Y.-B.; Lu, X.-B. Controlled Divinyl Monomer Polymerization Mediated by Lewis Pairs: A Powerful Synthetic Strategy for Functional Polymers. *ACS Macro lett.* **2014**, *3*, 896-899.

[19] Wang, X.; Zhang, Y.; Hong, M. Controlled and Efficient Polymerization of Conjugated Polar Alkenes by Lewis Pairs Based on Sterically Hindered Aryloxide-Substituted Alkylaluminumitle. *Molecules* **2018**, *23*, 442.

[20] Knaus, M. G. M.; Giuman, M. M.; Pöthig, A.; Rieger, B. End of Frustration: Catalytic Precision Polymerization with Highly Interacting Lewis Pairs. *J. Am. Chem. Soc*. **2016**, 138, 7776–7781.

[21] (a) Wang, B.; Pan, L.; Ma, Z.; Li, Y. S. Ring-Opening Polymerization with Lewis Pairs and Subsequent Nucleophilic Substitution: A Promising Strategy to Well-Defined Polyethylene-like Polyesters without Transesterification. *Macromolecules* **2018**, *51*, 836-845. (b) Li, X.-Q.; Wang,

B.; Jia, H.-Y.; Li, Y.-S. Insights into the mechanism Mechanism for ringRing-opening polymerization Polymerization of lactide Lactide Catalyzed Catalyzed by $Zn(C_6F_5)_2$/organic Superbase Lewis Pairs. *Catal. Sci. Technol.* **2016**, *6*, 7763–7772. (c) Piedra-Arroni, E.; Ladaviere, C.; Amgoune, A.; Bourissou, D. Ring-Opening Polymerization with $Zn(C_6F_5)_2$-Based Lewis Pairs: Original and Efficient Approach to Cyclic Polyesters. *J. Am. Chem. Soc.* **2013**, *135*, 13306-13309.

[22] Wang, Q. Y.; Zhao, W. C.; He, J. H.; Zhang, Y. T.; Chen, E. Y.-X. Living Ring-Opening Polymerization of Lactones by *N*-Heterocyclic Olefin/$Al(C_6F_5)_3$ Lewis Pairs: Structures of Intermediates, Kinetics, and Mechanism. *Macromolecules* **2017**, *50*, 123-136.

[23] (a) Meisner, J.; Karwounopoulos, J.; Walther, P.; Kästner, J.; Naumann, S. The Lewis Pair Polymerization of Lactones Using Metal Halides and N-Heterocyclic Olefins: Theoretical Insights. *Molecules* **2018**, *23*, 432. (b) Walther, P.; Naumann, S. *N*-Heterocyclic Olefin-Based (Co)polymerization of a Challenging Monomer: Homopolymerization of ω-Pentadecalactone and Its Copolymers with γ-Butyrolactone, δ-Valerolactone, and ε-Caprolactone. *Macromolecules* **2017**, *50*, 8406-8416. (c) Naumann, S.; Wang, D. R. Dual Catalysis Based on *N*-Heterocyclic Olefins for the Copolymerization of Lactones: High Performance and Tunable Selectivity. *Macromolecules* **2016**, *49*, 8869-8878. (d) Naumann, S.; Scholten, P. B. V.; Wilson, J. A.; Dove, A. P. Dual Catalysis for Selective Ring-Opening Polymerization of Lactones: Evolution toward Simplicity. *J. Am. Chem. Soc.* **2015**, *137*, 14439-14445.

[24] Kreitner, C.; Geier, S. J.; Stanlake, L. J. E.; Caputo C. B.; Stephan, D. W. Ring Openings of Lactone and Ring Contractions of Lactide by Frustrated Lewis Pairs. *Dalton Trans.* **2011**, *40*, 6771–6777.

[25] Hosoi, Y.; Takasu, A.; Matsuoka, S.; Hayashi, M. *N*-Heterocyclic Carbene Initiated Anionic Polymerization of (*E,E*)-Methyl Sorbate and Subsequent Ring-Closing to Cyclic Poly(alkyl sorbate). *J. Am. Chem. Soc.* **2017**, *139*, 15005–15012.

[26] Hu, L.; Zhao, W.; He, J.; Zhagn, Y. Silyl Ketene Acetals/$B(C_6F_5)_3$ Lewis Pair-Catalyzed Living Group Transfer Polymerization of Renewable Cyclic Acrylic Monomers. *Molecules* **2018**, *23*, 665.

[27] Xu, P. F.; Xu, X. Homoleptic Rare-Earth Aryloxide Based Lewis Pairs for Polymerization of Conjugated Polar Alkenes. *ACS Catal.* **2018**, *8*, 198-202.

[28] Flanagan, J. C. A.; Kang, E. J.; Strong, N. I.; Waymouth, R. M. Catalytic Dimerization of Crotonates. *ACS Catal*. **2015**, *5*, 5328–5332.

Chapter 3
Living Lewis Pair Polymerization of Crotonates by Group Transfer

3.1 Background and Significance

In **Chapter 2**, we described our use of Aluminum-based Lewis acids (LA), most notably methyl aluminum bis(2,6-di-*tert*-butyl-4-methylphenoxide) (MAD), and *N*-heterocyclic carbene (NHC) Lewis base (LB) Lewis pairs (LPs) to accomplish LPP of β-substituted Michael acceptors such as methyl crotonate (MC),[1] which are difficult to polymerize under the typical conditions suitable for α-substituted Michael acceptors.[2,3,4,5,6] Chapter 2 describes how the subtlety of adding even a seemingly innocuous methyl substitution at the β-carbon generates so much chaos that special efforts must be taken to address chemoselectivity. In that LPP of MC, depending on the LB used, the polymerization operates in either an ion-paired (IP) mode that is highly prone to chain transfer (CT), or a zwitterionic mode that generates high number-average molecular weight (M_n) poly(MC) (PMC). Even in the zwitterionic mode, CT by deprotonation (γ-proton) of the activated monomer is still challenging to avoid, thus negatively impacting the ability of this LPP to control the polymer M_n and dispersity ($Đ$) values. Hence, this work sought a LPP method that would be chemoselective only for repeated conjugate additions and mechanistically prohibit deprotonation of the activated monomer. We hypothesized that an LP of $B(C_6F_5)_3$ and a silyl ketene acetal (SKA) as the LB should achieve this goal and thus provide a process for controlled, or even living, MC polymerization.

This hypothesis was based on the fact that the $B(C_6F_5)_3$/SKA LP system has historically achieved controlled or living polymerization of several similar monomers[7,8,9,10,11,12] based on a variety of causes. First and foremost, the unique group transfer polymerization mechanism[13,14] by which the propagation proceeds has powerful implications in chemoselectivity. Unlike the IP and

zwitterionic modes (which proceed through LA-capped anionic enolate growing chains), the SKA/LA system proceeds through neutral SKA intermediates which become momentarily zwitterionic following addition to an LA-activated monomer but are quickly neutralized by the transfer of the silylium moiety to the enolate (Figure 3.1). Our reasoning was that SKAs, being neutral, will have lower basicity in contrast to the LA-complexed enolate anion chain ends, thus making them inherently more selective for propagation (vs CT). Moreover, continuous group transfer of the silylium moiety to the chain end will ensure chemoselectivity in that the nature of the nucleophile can be tuned by structural manipulations of the LB, while the nature of the electrophile can be tuned by structural manipulations of the LA. Conversely, both nucleophile and electrophile are responsive to structural changes to the LA in zwitterionic and IP modes. The utility of this strategy lies in the ability to both lower the reactivity of the growing chain end by employing the SKA (protecting growing chains from CT and termination side reactions) while simultaneously increasing the reactivity of the activated monomer by using a stronger LA, thus compensating reactivity in a way that increases chemoselectivity without sacrificing activity. Second, the SKA LB or initiator, which can be added in its pure form to initiate polymerization, can also be generated through a convenient LA-catalyzed 1,4-hydrosilylation of Michael acceptors (monomers), and thus the polymerization can be executed directly by using the LA/[SiH] LP or FLP.[12,15,16,17,18] This strategy enables access to a large library of synthetically feasible or commercially available hydrosilane reagents.

3.2 Results and discussion

3.2.1. Mechanistic consideration of LPP by [B]/[SiH] FLPs

To actualize these postulated advantages, the LA-catalyzed 1,4-hydrosilylation mechanism—which is functionally the initiation step of the LPP employing the borane /silane FLPs—must be

carefully considered. The mechanism first proposed by Piers in 1996[19] describing the 1,2-hydrosilylation of carbonyls, which we refer to as FLP activation, relies on weak Lewis pairing between $B(C_6F_5)_3$ and the hydrosilane [SiH]. This interaction generates a highly acidic silylium center, which activates the substrate carbonyl for hydride delivery by $[HB(C_6F_5)_3]^-$ (Figure 3.1). This mechanism was proposed to explain a decreased hydrosilylation activity observed in response to increased Lewis basicity of the substrate carbonyl. When the strength of the substrate-LA bond increases, the amount of the "free" LA catalyst for the FLP activation of the silane decreases. Convincing evidence for this mechanism was provided by Rendler and Oestreich, who demonstrated that hydrosilylation of acetophenone using an enantiopure chiral hydrosilane results in 97 % stereoinversion at the silicon center. Stereoinversion implies S_N2-type substrate coordination to the FLP-activated silylium center and dissociation of the hydridoborate.[20] Furthermore, structural evidence of borane/hydrosilane[21] and alane/hydrosilane[18] LPs has been obtained by X-ray crystallography. If the same logic is applied to the 1,4-hydrosilylation of Michael acceptors for LPP, it follows that increasing the strength of the LA should slow down the rate of initiation because a larger fraction of the LA will be stuck to monomer and reluctant to reenter the initiation cycle. If we also apply the principle that increasing LA strength increases monomer activation for propagation and thus polymerization activity, which has been true for the LPP of several monomers,[1,22,23] it is realized that any attempts to increase polymerization rate by increasing LA strength comes at the expense of initiation rate. Recent studies on the LPP of γ-methyl-α-methylene-butyrolactone (γMMBL) and MC congener methyl methacrylate (MMA) with $Al(C_6F_5)_3$/SKA LPs illustrates this concept of *conflicting LA roles*. For example, the LPP initiated by $PhMe_2SiH$ and $Al(C_6F_5)_3$ had initiation efficiency (I^*) around 35 %, while the I^* value was enhanced to 75 % when the polymerization was carried out using the preformed SKA

(Me_2C=C(Ome)$OsiMe_2Ph$). Other SKAs such as (Me_2C=C(Ome)Osi^iBu_3) were able to achieve near quantitative *I** and produced high M_n (179 kg/mol) PMMBL with low dispersity ($Đ$ = 1.08) but only when initiated with the preformed SKA. Since it is more convenient and economical to use hydrosilanes rather than the preformed SKAs for LPP, it is of both fundamental and technological interest to study the monomer hydrosilylation mechanism thoroughly to find conditions that cleanly generate these highly active SKA-based LP structures. Accordingly, we report here the results of MC polymerization using the $B(C_6F_5)_3$/[SiH] FLP in the context of its initiation mechanism to generate the SKA *in-situ* and its subsequent propagation cycle (Figure 3.1), as well as comparative studies using the preformed discrete SKAs and NHCs that involve IP and zwitterionic modes.

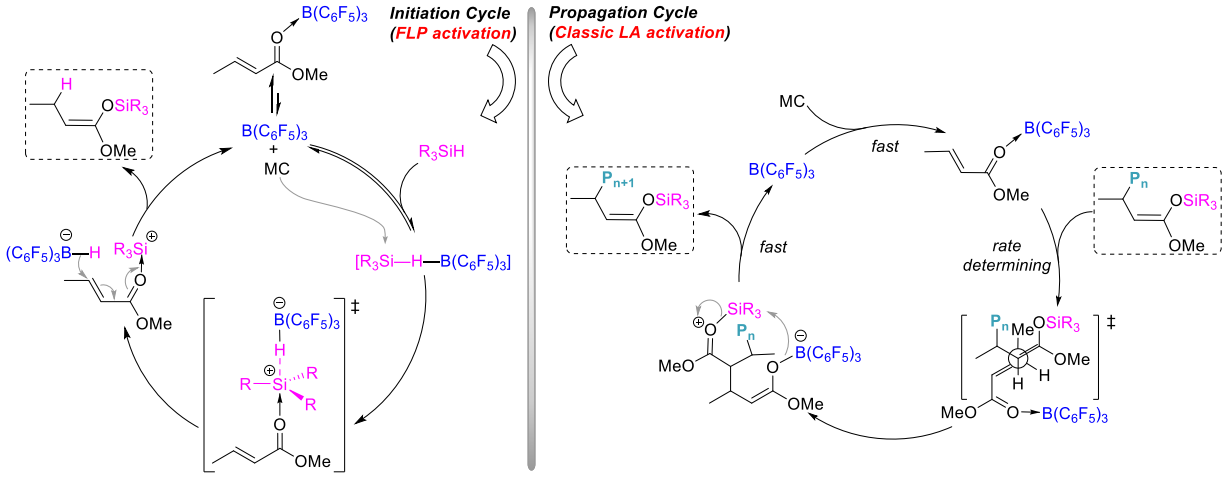

Figure 3.1. Left: proposed 1,4-hydrosilylation mechanism for MC; and right: propagation mechanism for LPP of MC in group transfer mode, highlighting dual and yet contrasting roles of the LA in initiation and propagation cycles.

3.2.2. Results of polymerization of MC by $B(C_6F_5)_3$/[SiH] FLPs

LPP of MC was carried out in neat and room temperature (RT) using either the $B(C_6F_5)_3$/[SiH] FLP ([SiH] = Et_3SiH, $PhMe_2SiH$) or $B(C_6F_5)_3$ with a preformed SKA, (Me_2C=C(Ome)$OsiMe_3$) (**1**) or (Et(H)C=C(Ome)$OsiEt_3$) (**2**) as control. Polymerizations were typically performed by

premixing 4 mol % $B(C_6F_5)_3$ in neat MC to make a colorless solution, followed by addition to a preweighed liquid silane or SKA, followed by stirring at room temperature until gelation. Polymerizations initiated by Et_3SiH and $PhMe_2SiH$ remained transparent and colorless throughout the polymerization even in the gel. Gelation has been shown to occur between 45-55 % conversion and was used in this study to compare activities (Table 3.1). Other mixing and addition sequences were also investigated, the results of which were summarized in Table B1.

At a MC:$B(C_6F_5)_3$:Et_3SiH ratio of 50:2:1, the solution gelled in 2 h. Similar polymerizations using $PhMe_2SiH$ and **1** gelled in 4 h. The relatively high activity of Et_3SiH (based on t_{gel}) is most likely a consequence of higher I^* rather than intrinsic activity. It is clear that there is a deactivation pathway, due to I^* being only 64 % for the polymerizations initiated by Et_3SiH (run 1, Table 3.1). However, it is unclear whether deactivation occurs before or after hydrosilylation because the preformed SKAs **1** and **2** also exhibited a low I^* of 52 % (run 4) and 16 % (run 3), respectively. $PhMe_2SiH$ had a very low I^*, but was still active enough to reach similar conversion (91%) as Et_3SiH. The low $Đ$ value of $PhMe_2SiH$ generated PMC, despite the low I^*, suggests that a large majority of the $PhMe_2SiH$ did not participated in initiation, and only a small fraction that effected initiation subsequently propagated in a controlled fashion.

Table 3.1. Selected results of MC polymerization by LPs consisting of $B(C_6F_5)_3$ and [SiH] or preformed SKA[a]

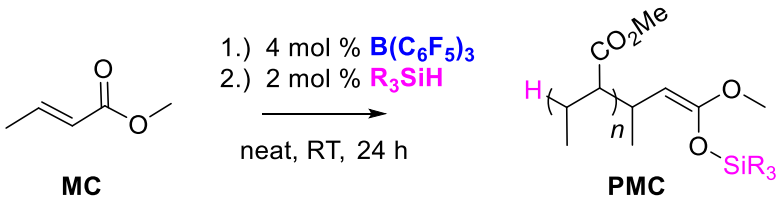

Run	LB	MC:LA:LB	[b] t_{gel} (h)	Conv (%)	[c] M_n (kg/mol)	[c] $Đ$	[d] I^* (%)
1	Et_3SiH	50:2:1	2	91	7.14	1.13	64
2	$PhMe_2SiH$	50:2:1	4	91	29.9	1.08	15
3	**2**	50:2:1	n.d	88	26.9	1.33	16
4	**1**	50:2:1	4	94	9.54	1.16	52
5	Et_3SiH	100:4:1	6	66	23.6	1.15	42
6	Et_3SiH	50:2:1	-	0	-	-	-

[a] Conditions: $[MC]_0$ = 0.53 mL (5.0 mmol); LA = $B(C_6F_5)_3$ (except for run 6 with BPh_3) neat; RT (except for run 5 at 50 °C); time = 24 h; n.d. = not determined. [b] Approximate time of gelation. [c] Absolute M_n and $Đ$ values determined by GPC at 40 °C in $CHCl_3$ coupled with a DAWN HELEOS II multi-angle light scattering detector and an Optilab TrEX dRI detector. [d] I^* = M_n(calcd)/M_n(exptl), where M_n(calcd) = MW(MC) × [MC]/[LB] × conversion % + MW of chain-end groups.

To provide key proof of concept that the growing SKA chain ends are chemoselective for addition and devoid of CT by deprotonation of the activated monomer, a polymerization reaction was set up with an MC:$B(C_6F_5)_3$:Et_3SiH ratio of 100:4:1, sealed in a pressure vessel, and heated in an oil bath at 50 °C. The reaction gelled in 6 h and the crude product was a soft gel after 24 h (66 % conv). Analysis of the isolated sample by gel-permeation chromatograph (GPC) revealed a moderate I^* (M_n = 23.6 kg/mol, I^* = 42 %), but an impressively low $Đ$ of 1.15 (run 5, Table 3.1). This result is significant because, in the absence of solvent or treating at a relatively high temperature for a long time, polymerizations often experience broadened dispersity due to heterogenous propagation in the gel phase or decomposition of the active species; thus, it shows the robustness of the SKA chain end to endure 24 h at 50 °C while maintaining a low $Đ$. The observation that solution gelled after 6 h yet only 66 % conversion was observed after 24 h implies that the SKA nucleophile is not potent enough to be active in the gel phase, where collision

frequency is drastically reduced. Importantly, no vinyl end groups (an indicator for initiation/CT by deprotonation) were detected by NMR (Figure B2); this result, coupled with the observed low *Đ*, suggests that CT had been shut down. Furthermore, increasing the temperature in LPP by [Al]/NHC has been shown to increase the rate of CT in MC polymerizations.[1] The reluctance of the growing PMC chain to transfer under the $B(C_6F_5)_3$/[SiH] conditions, even at elevated temperature, is convincing evidence that continual neutralization of the zwitterionic addition product via the group transfer mechanism is a promising strategy for achieving a living LPP.

It is worth noting that the limited degree of polymerization achieved in the MC polymerization by $B(C_6F_5)_3$/[SiH] FLPs was also observed with similar, more reactive acrylic monomers such as methyl methacrylate (MMA). For example, Kakuchi et. al.[16] reported the polymerization of MMA using $B(C_6F_5)_3$ and $^{i}Pr_3SiH$ to produce PMMA with M_n = 10 kg/mol and the polymerization of *N,N*-diethylacrylamide to yield the polymer with M_n = 25.4 kg/mol.[17] Most recently, Zhang et. al. reported living polymerization of γMMBL using $B(C_6F_5)_3$/SKA LPs,[8] suggesting that the $B(C_6F_5)_3$/SKA system is capable of promoting a living polymerization, but needs to be structurally tuned for MC.

3.2.3. Initiation Mechanism

LPP of MC by $B(C_6F_5)_3/R_3SiH$ LPs is proposed to proceed through the *in situ* $B(C_6F_5)_3$-catalyzed 1,4-hydrosilylation of MC to form the corresponding SKA, which participates in repeated conjugate addition and group transfer propagation steps (Figure 3.1). The 1,4-hydrosilylation initiation mechanism and subsequent propagation by the *in situ* generated SKA is supported by the following *three lines of evidence*. First, the hydrosilylation product of MC/$PhMe_2SiH$, (Et(H)C=C(Ome)O$SiMe_2$Ph) (**3**) (and **2**, Figure B4), was readily generated by addition of a catalytic amount of $B(C_6F_5)_3$ (0.0014 equiv) to a 1:1 mixture of MC/$PhMe_2SiH$. ^1H NMR of this

intermediate shows predominately one geometric isomer, (*Z*) with minor peaks attributable to the I-isomer (Figure 3.2, B5). Second, the preformed SKAs **1** and **2** were found to be active for MC polymerization only in the presence of $B(C_6F_5)_3$ (run 3, Table 3.1). Third, the matrix-assisted laser desorption/ionization time-of-flight mass spectroscopy (MALDI-TOF MS) spectrum (Figure 3.3) of resulting polymer showed one polymer species end-capped by hydrogen atoms: the initiating end, being the hydride originally delivered by R_3SiH during initiation and the terminal end being the proton abstracted during the methanol quench.

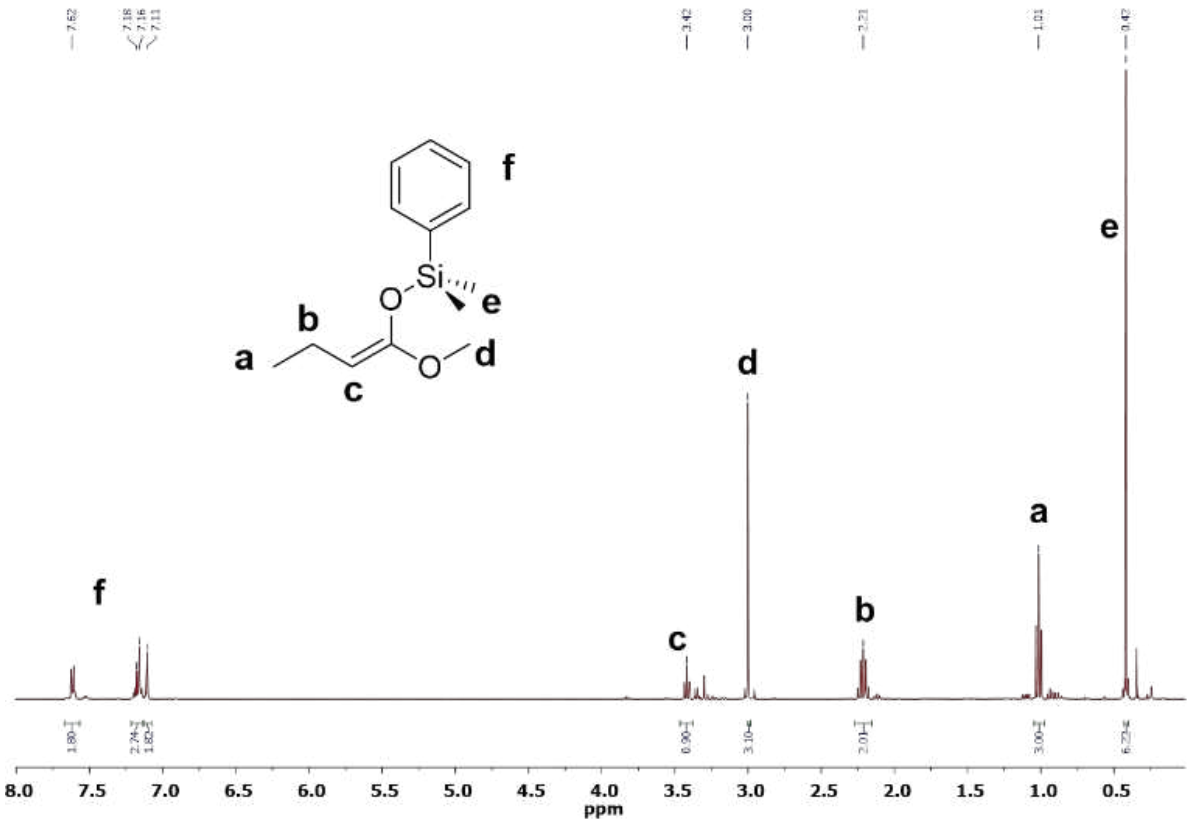

Figure 3.2. ^1H NMR (C_6D_6) of **3**, generated *in situ* by mixing MC, $PhMe_2SiH$, and $B(C_6F_5)_3$ at a ratio of 1:1:0.0014, showing predominately (*Z*)-isomer (~92 %), with small peaks corresponding to the I-isomer (~8%). Spectrum was acquired in 13 min after mixing when quantitative conversion was achieved. Absolute stereochemistry determined by HH NOESY NMR analysis (Figure B5).

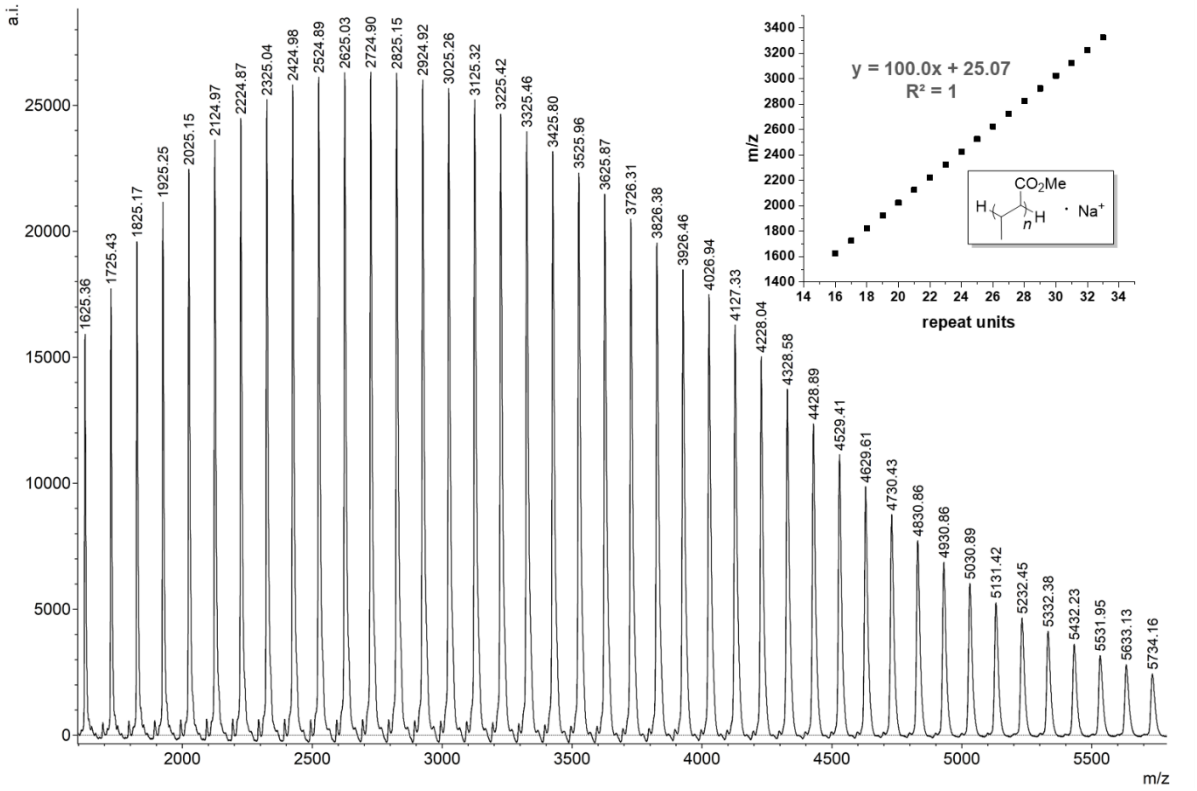

Figure 3.3. MALDI-TOF MS spectrum of PMC oligomers prepared from MC:$B(C_6F_5)_3$:Et_3SiH = 20:2:1. End groups, calculated by plotting *m*/*z* values vs repeat units, were determined to be two hydrogen atoms, based on a y-intercept of 25.07 Da (mass of Na atom plus two hydrogen atoms).

3.2.4. Propagation mechanism

The chain propagation cycle depicted in Figure 3.1 is proposed to proceed through neutral bimolecular conjugate addition between the nucleophilic SKA growing chain end and electrophilic $B(C_6F_5)_3$ activated monomer to form a zwitterionic oxonium intermediate, which is quickly neutralized by the group transfer of the silylium to the enolate oxygen. This propagation mechanism is consistent with the LPP mechanism well-established for many other monomers and the following *three lines of evidence* for the current MC polymerization system. First, the

polymerization of MC that only ensues in the presence of *both* $B(C_6F_5)_3$ and the preformed SKA implies that the neutral SKA molecule *selectively* attacks the LA-activated MC. Second, the predicted and observed zero order kinetics (Figure 3.4)—which imply that the group transfer step is fast and that bimolecular conjugate addition is rate limiting—are consistent with previously reported LPPs,[1] where the rate of polymerization follows k_p[LA][LB]. Third, ^{1}H NMR spectra of the MC:$B(C_6F_5)_3$:Et_3SiH 20:2:1 polymerization process before and after quenching with methanol were compared, revealing that the spectrum of the unquenched polymer contained peaks attributable to the SKA end group, while the spectrum of the polymer after quenching contained no such SKA end groups (Figure B7).

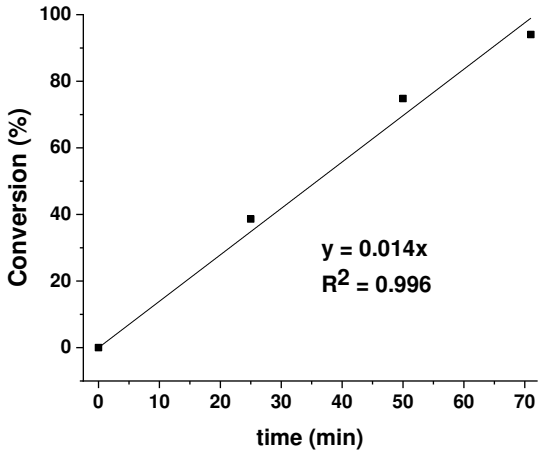

Figure 3.4. Zero-order kinetics as shown by linear conversion vs time plot for MC polymerization with [MC]:[$B(C_6F_5)_3$]:[Et_3SiH] = 25:2:1. MC:DCM = 1:1 (v/v).

3.2.5. Comparison of [B]/[SiH] with [B]/NHC systems

NHC LBs such as 1,3-di-*tert*-butylimidazolin-2-ylidene (I^tBu) and 1,3,4-triphenyl4,5-dihydro-1H-1,2,4-triazol-5-ylidene (TPT) (Figure 3.5) were also studied with $B(C_6F_5)_3$ for LPP of MC as a direct comparison to [SiH] conditions (Table 3.2). As expected, the rate of polymerization is considerably lower for the [SiH] based system when compared to the NHC based systems (as

judged by gel times, Table 3.2), due to decreased nucleophilicity of the neutral SKA chain end relative to anionic enolborate chain ends and the high energy oxonium/zwitterionic intermediate generated following propagation (Figure 3.5). A similar line of reasoning is that the propagation step is much more balanced in the case of IP and zwitterionic modes because the enolborate that is generated after propagation is identical to the enolborate prior to propagation, and the exchange happens in a single concerted step. Conversely, the propagation step for the $B(C_6F_5)_3$/[SiH] (or SKA) system must first form the zwitterionic intermediate (*c.f.* Figure 3.1). Although this step is thermodynamically favorable due to C-C bond formation, the silylium experiences a jump in energy while it is in the zwitterionic intermediate. This reasoning is further supported by our previous study[12] where SKA based LPP was performed on MMA using silylium LAs generated by hydride abstraction. That system proved to be more active than analogous $B(C_6F_5)_3$/SKA systems[16] because in that scenario, the silylium cation activating the incoming monomer is identical to the silylium capping the SKA. Therefore, propagation can proceed without the formation of a high energy zwitterionic intermediate.

Table 3.2. Results of LPP with [SiH] and NHC LBs with different LPP modes [a]

Run	LB	MC:LA:LB	t_{gel} (h)	Conv (%)	M_n (kg/mol)	$Đ$	I^* (%)
7	I^{t}Bu	50:2:1	0.17	94	8.90	1.17	56
8	TPT	50:2:1	0.56	94	23.9	1.12	20
9	Et_3SiH	50:2:1	2	91	7.14	1.13	70

[a] Conditions: $[MC]_0$ = 0.53 mL (5.0 mmol); LA = $B(C_6F_5)_3$; neat; RT; time = 24 h; MC was premixed with $B(C_6F_5)_3$, followed by addition of liquid or solid LB.

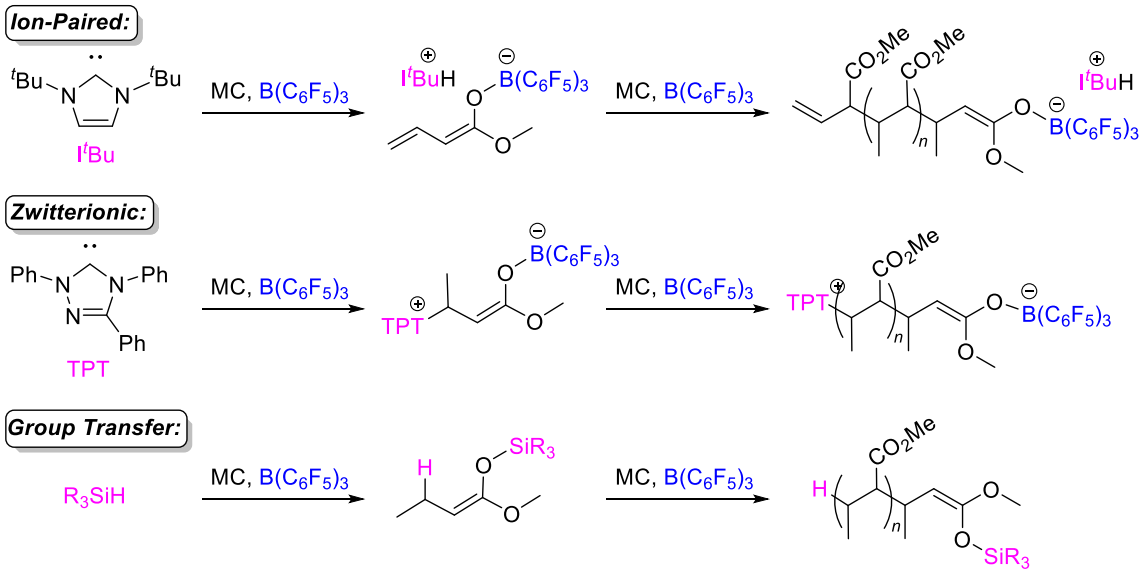

Figure 3.5. Three different LPP pathways to PMC based on different LBs (NHC and [SiH]).

3.3 Conclusions

Through this work we have developed a new and convenient method for synthesizing low to medium M_n PMC through LPP of a challenging β-substituted Michael acceptor, MC, using $B(C_6F_5)_3$/[SiH] FLPs. The 1,4-hydrosilylation of MC via the FLP-type activation was utilized to achieve initiation through *in-situ* SKA formation, enabling the use of readily available silanes as the LB precursor. Corroborating experimental evidence has been disclosed to support our current understanding of the LPP mechanism and the group transfer mechanism unique to SKA-based LBs. The results reported herein underscore the inherent challenge of the conflicting roles of the LA in the FLP activation during the initiation cycle and the classic LA activation during the chain propagation cycle: the FLP activation during chain initiation calls for weak LA-substrate (monomer) interaction while the classic LA activation during chain propagation requires strong LA-monomer interaction. This work also serves as a foundation for future works toward the

development of living polymerization of MC, by exploiting the group transfer mechanism as a means of shutting down CT.

References cited in Chapter 3

[1] McGraw, M.; Chen, E. Y.-X. *ACS Catal*. **2018**, *8*, 9877−9887.

[2] Flanagan, J. C. A.; Kang, E. J.; Strong, N. I.; Waymouth, R. M. *ACS Catal*. **2015**, *5*, 5328–5332.

[3] Ute, K.; Tarao, T.; Kitayama, T. *Polym. J*. **2005**, *37*, 578-583.

[4] Ute, K.; Tarao, T.; Hongo, S.; Ohnuma, H.; Hatada, K.; Kitayama, T. *Polym J.* **1999**, *31*, 177-183.

[5] Ute, K.; Tarao, T.; Hatada, K. *Polym. J.* **1997**, *29*, 957–958.

[6] Tsuruta, T.; Makimoto, T.; Tanabe, K. *Makromol. Chem.* **1968**, *114*, 182-200.

[7] Hu, L.; He, J.; Zhang, Y.; Chen, E. Y.-X. *Macromolecules* **2018**, *51*, 1296−1307.

[8] Hu, L.; Zhao, W.; He, J.; Zhang, Y. *Molecules* **2018**, *23*, 665.

[9] Zhang, Y.; Chen, E. Y.-X. *Macromolecules* **2008**, *41*, 36−42.

[10] Zhang, Y.; Chen, E. Y.-X. *Macromolecules* **2008**, *41*, 6353−6360.

[11] Zhang, Y.; Gustafson, L. O.; Chen, E. Y.-X. *J. Am. Chem. Soc.* **2011**, *133*, 13674−13684.

[12] Xu, T.; Chen, E. Y.-X. *J. Polym. Sci., Part A: Polym. Chem.* **2015**, *53*, 1895−1903.

[13] Webster, O. W. *Adv. Polym. Sci.* **2004**, *167*, 1-34

[14] Webster, O. W.; Hertler, W. R.; Sogah, D. Y.; Farnham, W. B.; Rajanbabu, T. V. *J. Am. Chem. Soc.* **1983**, *105*, 5706-5708.

[15] Fuchise, K.; Tsuchida, S.; Takada, K.; Chen, Y. G.; Satoh, T.; Kakuchi, T. *ACS Macro Lett.* **2014**, *3*, 1015−1019.

[16] Chen, Y. G.; Kitano, K.; Tsuchida, S.; Kikuchi, S.; Takada, K.; Satoh, T.; Kakuchi, T. *Polym. Chem.* **2015**, *6*, 3502−3511.

[17] Kikuchi, S.; Chen, Y. G.; Kitano, K.; Sato, S.; Satoh, T.; Kakuchi, T. *Macromolecules* **2016**, *49*, 3049−3060.

[18] Chen, J.; Chen, E. Y.-X. *Angew. Chem. Int. Ed.* **2015**, *54*, 6842–6846.

[19] Parks, D. J.; Piers, W. E. *J. Am. Chem. Soc.* **1996**, *118*, 9440−9441.

[20] Rendler, S.; Oestreich, M. *Angew. Chem. Int. Ed*. **2008**, *47*, 5997 –6000.

[21] Houghton, A. Y.; Hurmalainen, J.; Mansikkamaki, A.; Piers, W. E.; Tuononen, H. M. *Nature Chemistry* **2014**, *6*, 983-988.

[22] Zhang, Y. T.; Miyake, G. M.; John, M. G.; Falivene, L.; Caporaso, L.; Cavallo, L.; Chen, E. Y. X. *Dalton Trans.* **2012**, *41*, 9119−9134.

[23] Chen, J.; Chen, E. Y.-X. *Molecules* **2015**, *20*, 9575−9590.

Chapter 4
Discovery of Compounded Sequence Control Lewis Pair Polymerization

4.1 Background and Significance

Lewis pair polymerization (LPP)[1] is a versatile technique that has continuously evolved by revealing fundamental insights that translate into useful and applicable solutions to polymerization problems. By exploiting the cooperative and synergistic interplay of both Lewis acid (LA) and Lewis base (LB) components, polymerization characteristics can be targeted and manipulated with tunability, selectivity, and predictability.[1] The accumulation of research on LPP[2-9] and frustrated Lewis pair (FLP) chemistry[10-15] have provided a wealth of variety in Lewis pair (LP) structure and reactivity that can be exploited to solve polymerization challenges.

The scope of LPP has been expanded to include many types of polar monomers.[4-6,16-22] While the reactivity varies considerably, the propagation mechanism generally remains the same, involving (rate-determining) attack on the LA-activated monomer by the LA-stabilized zwitterion (via initiation by LB) with zero-order kinetics in [monomer] (Figure 4.1). Here we invoke these mechanistic nuances to demonstrate that LPP provides a unique strategy for gaining precise sequence control[23-35] in polymerizing mixtures of highly reactive, side-reaction prone acrylates into well-defined and resolved BCPs.

4.2 Mechanistic Considerations Regarding Sequence Control

Several groups have explored methyl aluminum-di(2,6-di-*tert*-butyl-4-methyl-phenoxy) (MAD) as an effective bulky LA for the controlled LPP of polar monomers.[2,3,36-41] With MAD's high acidity coupled with high steric hindrance, we hypothesized that mixing MAD with two different comonomers should result in preferential coordination of MAD to one over the other. If there is a

large enough free energy difference between the two MAD/comonomer adducts, an equilibrium would be established that biases which comonomer is available for propagation before entering the rate determining step (Figure 4.1). Accordingly, we surmised that LPP could be exploited to gain precise sequence control in copolymerizing one-pot comonomer mixtures based on biased prior equilibrium differentiation (K_{eq}) during the coordination step *compounding* with differing monomer propagation rates (k_p) at the addition step.

Furthermore, the unique kinetics of LPP predisposes copolymerizations to highly resolved block structures, largely absent of the common *tapering effect* (Figure 4.2). In comparison to LPP which is zero order with respect to monomer (rate = $k_p[LB]_0[LA]_0$),[1] conventional polymerizations are first order in [M] (rate = $k_p[P^*]_t[M]_t$).

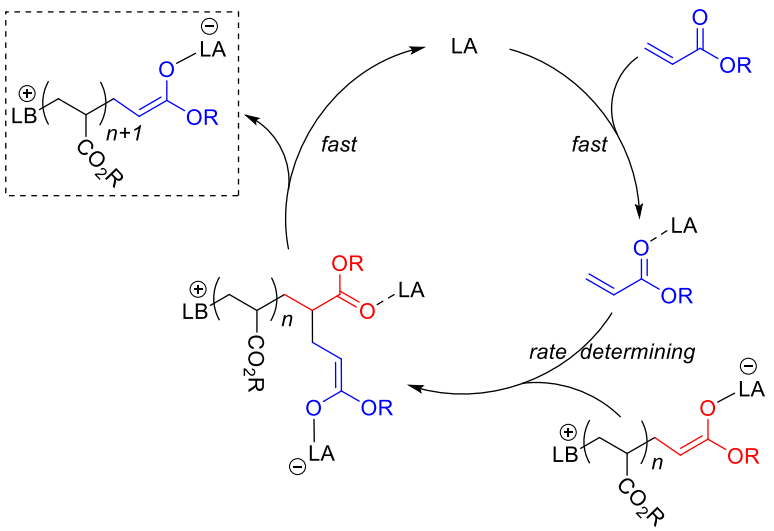

Figure 4.1. Propagation mechanism for the LPP of acrylates (M) via zwitterionic intermediates with zero-order kinetics in [M].

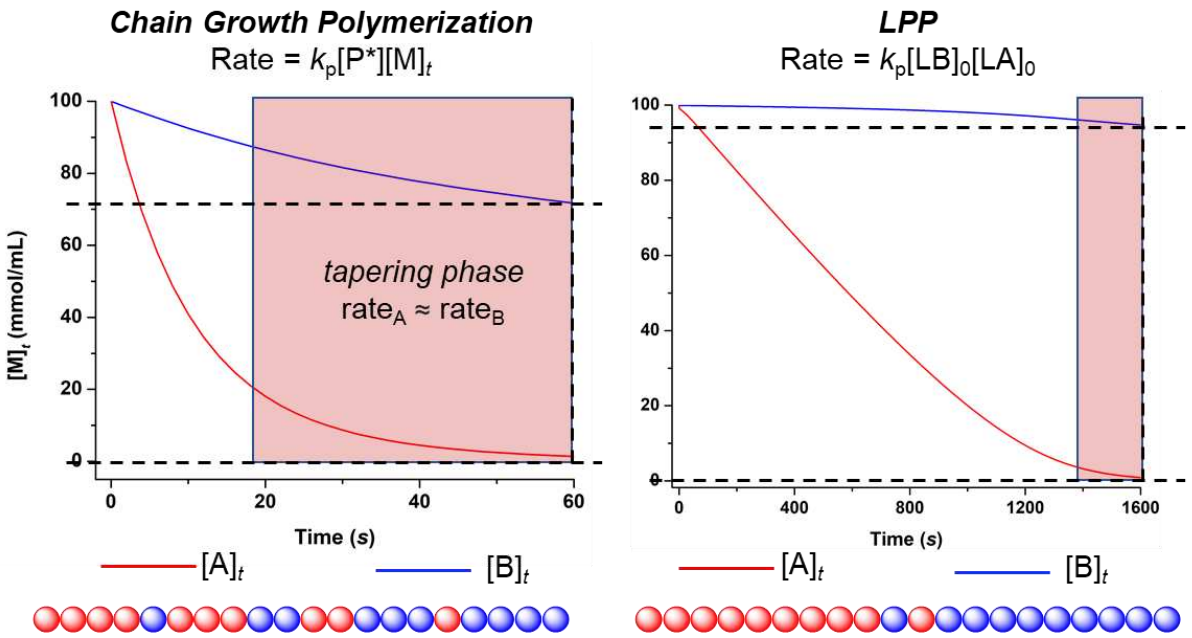

Figure 4.2. COPASI (complex pathway simulator) simulations of typical chain-growth polymerization and LPP, illustrating the significant prior equilibrium differentiation effect in LPP (A = more reactive M, B = less reactive M, $K_{eq} = 4$).

When the rate is dependent on $[M]_t$, even when $k_A > k_B$, there will be some point in the reaction when $[A]_t$ is very low compared to $[B]_t$. At this point, $rate_A$ will be approximately equal to $rate_B$, resulting in a tapering effect (Figure 4.2). Conversely, in LPP, there is no rate dependence on $[M]_t$. If incorporation of A is preferable to B at the start of the reaction, it will be so until A is at a concentration comparable to $[LA]_t$, at which point the K_{eq} of the prior equilibrium between comonomer/LA adducts begins to shift in favor of B (Figure C23). If the initial K_{eq} is considerably high, the aforementioned shift in K_{eq} will be negligible and block resolution will approach ideal (Figure C24). LA-monomer binding affinity was exploited in copolymerization of lactones, but no block copolymer (BCP) was generated.[16,17]

4.3 Results and Discussion

4.3.1. Sequential Addition LPP of Acrylates

To test this hypothesis, we chose acrylates as they are industrially important but their high reactivity and propensity for termination or transfer side reactions presents a challenge to control, especially in BCP synthesis by anionic or coordination polymerization methods.[42] Specifically, we chose a comonomer pair of *n*-butyl acrylate (^{n}BA) and *tert*-butyl acrylate (^{t}BA), with their corresponding polymers P^{n}BA and P^{t}BA serving as soft and hard blocks.[43,44] Acrylates also present challenges to LPs[6] due to the facile Claisen-type backbiting termination.[9,45-47] Although BCPs have been synthesized by sequential additions of acrylates/methacrylates[46,48] or acrylates by carbene- or LA-mediated group-transfer polymerization, and methacrylates by LPP,[3,40] the synthesis of all acrylate tri-BCP containing both ^{n}BA (highly reactive) and ^{t}BA (prone to decomposition)[47,49,50] has remained a challenge, not to mention via more difficult one-pot additions. All these factors make these acrylates ideal candidates to showcase the unique capability of LPP with specially designed LPs.

We found that, using MAD and less hindered (mesityloxy)diisobutylaluminum (**1**) and (2,6-di-*tert*-butyl-4-methylphenoxy)diisobutylaluminum (**2**) LAs, combined with sterically unhindered LB PMe_3, ^{t}BA was effectively polymerized, yielding full conversion in seconds (**Table C1**). Near ideal initiation efficiency and low dispersity ($Đ$) values were obtained from ^{t}BA/**2**/PMe_3 = 200/2/1, and using MAD as the LA, high molecular weight P^{t}BA (M_n = 256 kg/mol, $Đ$ = 1.02) was obtained in just 100 s. A kinetic profile of ^{t}BA/MAD/PMe_3 = 400/4/1 showed a linear curve in the conversion-time plot (Figure C2), consistent with the general mechanism of LPP (Figure 4.1) that exhibits zero-order dependence on [M]. The challenge associated with ^{n}BA is its extreme reactivity, making its polymerization harder to control and prone to chain termination with less hindered LAs **1** and **2**. With MAD, full conversion with ^{n}BA/MAD/PMe_3 = 800/2/1 can be achieved in seconds, but bimodal molecular-weight distributions were observed (**Table C2**).

Next, we investigated sequential block copolymerizations of ^{t}BA with ^{n}BA (**Table C3**). The 300/300 and 300/300/300 block copolymerizations afforded well-defined di- and tri-BCPs, P^{t}BA-*b*-P^{n}BA and P^{t}BA-*b*-P^{n}BA-*b*-P^{t}BA, with M_n = 128 kg/mol, $Đ$ = 1.07 and crossover efficiency = 91%, and M_n = 200 kg/mol, $Đ$ = 1.08 and crossover efficiency = 96%, respectively. However, gel-permeation chromatography (GPC) traces of the aliquots of the BCPs exhibited a low molecular weight shoulder (Figure 4.3a), representing terminated P^{t}BA. We reasoned that this termination occurs only after monomer is completely consumed and not during the polymerization. The aforementioned backbiting termination requires the LA to activate an in-chain ester carbonyl. And if there is free monomer left in solution, the LA will preferentially coordinate to it instead. This hypothesis has been confirmed by a more convenient mixed monomer addition strategy detailed below.

4.3.2. Compounded Sequence Control LPP of Acrylates

Based on the following three arguments, here we present the corresponding evidence to support our original hypothesis that LPP can be used to differentiate between multiple comonomers in a one-pot mixture to yield highly resolved BCPs.

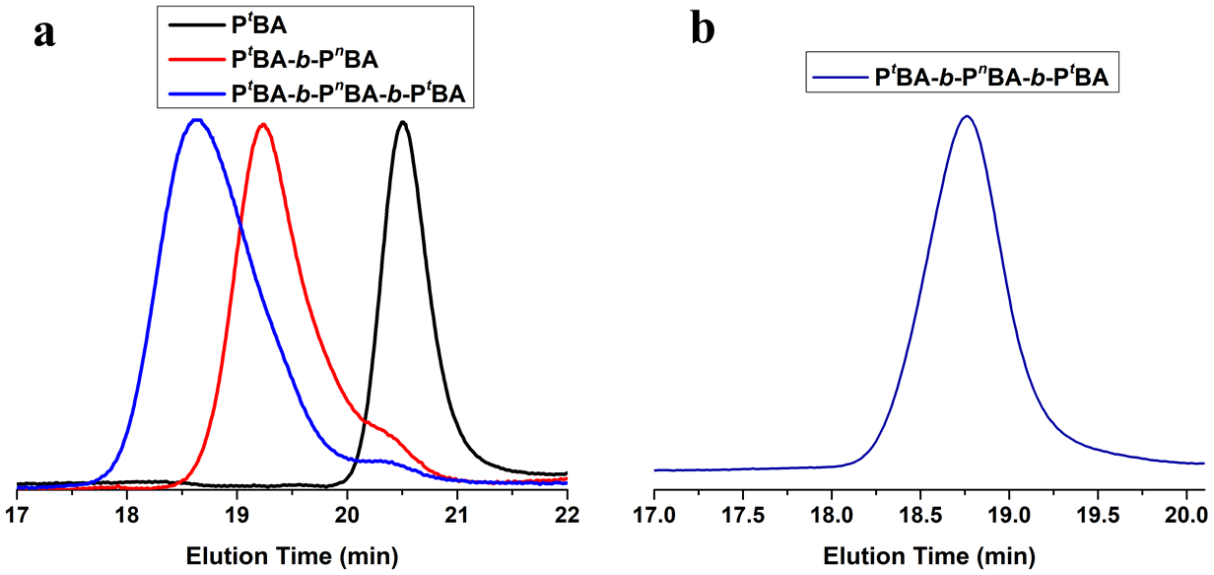

Figure 4.3. GPC traces of monoblock, diblock, and triblock aliquots of ^{t}BA/^{n}BA/^{t}BA sequential triblock copolymerization (300-300-300) (**a**) and P^{t}BA-*b*-P^{n}BA-*b*-P^{t}BA synthesized by mixed addition (**b**).

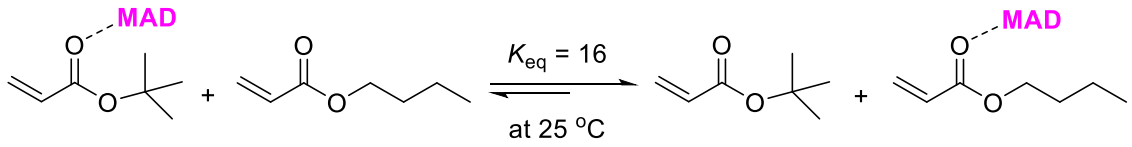

Figure 4.4. Prior equilibrium differentiation between ^{t}BA and ^{n}BA biased by MAD.

The first argument, *preferential coordination* of the LA to one comonomer over the other, was quantified for a ^{t}BA/^{n}BA/MAD (1/1/1) mixture by variable temperature ^{1}H NMR in toluene-d_8 between -70 and -30 °C. A Van't Hoff plot yielded K_{eq} = 16 and ΔH_{rxn} = -2.3 kJ/mol for the equilibrium between ^{t}BA/MAD and ^{n}BA/MAD adducts at RT (Figure 4.4). Thus, in a LPP where ^{t}BA and ^{n}BA are mixed with MAD, initially 80 % of the MAD is occupied by ^{n}BA and that amount gradually decreases as ^{n}BA is preferentially consumed. Therefore, when both monomers are present, there is approximately a 1/17 probability that the LPP will misincorporate a ^{t}BA unit into the growing polymer chain based on this argument alone.

For the second argument, *differing monomer* k_p, we can compare turnover frequencies (TOFs) of the LPP of each monomer. The kinetic profile (Figure C2) of a polymerization with ^{t}BA/MAD/PMe$_3$ = 400/4/1 gave a TOF of 10.3 s^{-1}. An identical experiment with ^{n}BA gave a TOF of 310 s^{-1}. Thus, the k_p for ^{n}BA is ~30 times greater than that of ^{t}BA, implying that there is roughly a 1/30 probability that the LPP will make the mistake of incorporating a ^{t}BA unit into the growing P^{n}BA chain based on kinetics. However, for a ^{t}BA unit to be mistakenly incorporated into the growing chain while the ^{n}BA block is polymerizing*, two mistakes must be made consecutively*: MAD must coordinate to ^{t}BA followed by chain addition to the ^{t}BA/MAD adduct. Hence, both probability values compound to establish roughly a 1/510 chance (without considering cross-propagation rates) of misincorporation.

For the third argument, *suppressed tapering*, since LPP does not have kinetic dependence on [M], these assumptions are true throughout the linear course of the polymerization and are not subject to the tapering effect until very late in the reaction. The simulated LPP curve shape (Figure 4.2) was experimentally confirmed by monitoring the polymerization of the ^{t}BA + ^{n}BA (1/1) mixture with MAD/PMe$_3$. Figure C25 gives a realistic picture of the polymer structure and an approximation for block resolution of a ^{n}BA/^{t}BA diblock with ^{n}BA/^{t}BA/MAD/PMe$_3$ = 100/100/2/1, where by the time the first aliquot was taken at 2.7 s, the ^{n}BA reservoir was completely depleted while only 3.0 % of the ^{t}BA reservoir had been consumed. Therefore, it can be assumed that an amount less than 3.0 % of ^{t}BA misincorporates into the ^{n}BA block.

Table 4.1. Results of diblock and triblock copolymerizations [a]

Run	LA	[^{t}BA]/[^{n}BA]/ [LA]/[PMe$_3$]	Time (s)	Conv. (%)	M_n (kg/mol)	$Đ$ (M_w/M_n)
1	**1**	100/100/2/1	4	100	32.3	1.68
2	MAD	400/400/2/1	59	100	109	1.05
3	MAD	100/900/2/1	15	100	127	1.02
4	MAD	300/300/6/1	40	100	90.1	1.06
5	MAD	800/800/8/1	20 [b]	100	272	1.03
6	MAD	600/300/6/1	50 [b]	100	204	1.02

[a] Conditions: 23°C, for diblock copolymerizations (runs 1-4), $[M]_0$ = 0.59 M in toluene ($[M]_0 = [^n\text{BA}]_0 + [^n\text{BA}]_0$), ^{t}BA, ^{n}BA, and LA premixed, followed by addition of PMe$_3$. For triblock copolymerizations, [M] = 1.18 M (run 5) and [M] = 0.59 M (run 6). ^{t}BA and LA were premixed, followed by addition of PMe$_3$. [b] Time corresponds to the approximate time of 50 % conv of ^{t}BA when ^{n}BA was added.

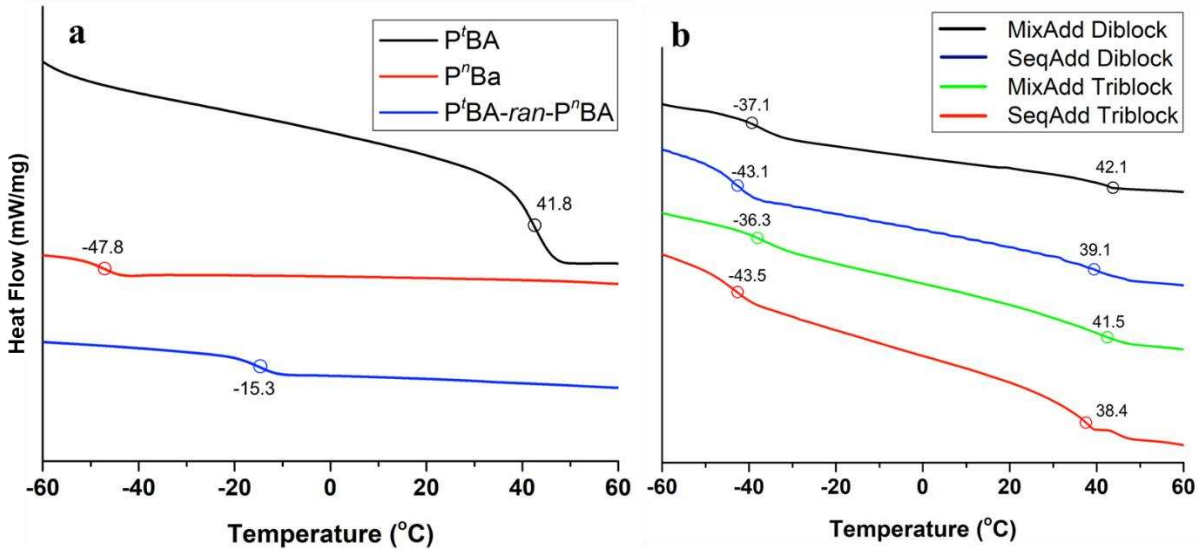

Figure 4.5. DSC plots (endo down) of (**a**) P^{t}BA, P^{n}BA, and P^{t}BA-*ran*-P^{n}BA and (**b**) P^{t}BA-*b*-P^{n}BA synthesized from sequential addition (SeqAdd) and mixed addition (MixAdd), and P^{t}BA-*b*-P^{n}BA-*b*-P^{t}BA synthesized from SeqAdd and MixAdd.

To further test our hypothesis, diblock copolymerizations of the ^{t}BA + ^{n}BA mixture were compared with non-differentiating **1** and differentiating MAD (Table 4.1, runs 1-4). Predominantly due to no differing k_p for ^{n}BA and ^{t}BA, **1** yielded a random copolymer (P^{t}BA-*ran*-P^{n}BA), as evidenced by both differential scanning calorimetry (DSC) (Figure 4.5) and ^{13}C NMR (Figure C17). The ^{13}C spectrum of P^{t}BA-*ran*-P^{n}BA shows two unresolved peaks in the carbonyl region corresponding to randomly incorporated ^{t}BA and ^{n}BA units, while the DSC trace shows a single

glass-transition temperature (T_g) at -15.3 °C, which lies between the T_g's of the two homopolymers at 41.8 °C for P^{t}BA and -47.8 °C for P^{n}BA. In contrast, MAD led to well-resolved di-BCPs. The high resolution of these diblocks is supported by the above arguments as well as DSC (Figure 4.5) and ^{13}C NMR (Figure C17). Thus, P^{t}BA-*b*-P^{n}BA synthesized from sequential and mixed additions both exhibit two T_g's with values close to their homopolymers. The ^{13}C NMR also indicates independent ^{t}BA and ^{n}BA domains as signatures nearly identical to the homopolymers were observed. Furthermore, P^{t}BA-*b*-P^{n}BA (M_n = 127 kg/mol, run 3) showed a unimodal GPC, symmetric bell curve with essentially ideal initiation efficiency (100%) and $Đ$ (1.02) values, suggesting that when ^{t}BA is present in the ^{n}BA polymerization, it prevents a bimodal distribution.

With well-define di-BCPs synthesized by mixed comonomer addition, we reasoned that tri-BCP P^{t}BA-*b*-P^{n}BA-*b*-P^{t}BA should be made in two addition steps by initiating LPP on the entire sum of less reactive ^{t}BA, and adding the more reactive ^{n}BA at ~50 % conversion of ^{t}BA, at which point the more reactive monomer will selectively polymerize until depleted. Then, the remaining fraction of the less reactive comonomer will continue to polymerize to yield tri-BCP. Indeed, this strategy produced well-defined tri-BCP with high M_n (272 kg/mol) and low $Đ$ (1.03, run 5) values. The high resolution of these triblocks is supported again by DSC (Figure 4.5) and ^{13}C NMR (Figure C17). Furthermore, P^{t}BA-*b*-P^{n}BA-*b*-P^{t}BA (run 6, Figure 4.3b) showed a symmetric GPC bell curve without shouldering, unlike the tri-BCP prepared by sequential addition. This result further highlights an important advantage of this strategy that can prevent LA-activated chain termination by occupying the free LA with a comonomer at all block-constructing stages.

4.4 Conclusions

In summary, we have established LPP as a unique and powerful method to polymerize one-pot comonomer mixtures of highly reactive and side-reaction prone acrylates into well-defined and

resolved di- or tri-BCPs. A preliminary result also indicated this method can be applied to acrylate/methacrylate mixtures. Three distinctive features of LPP have been exploited to accomplish this challenging task. *First*, preferential coordination of the LA to one comonomer over the other imposes the significant prior equilibrium differentiation (K_{eq}) effect. *Second*, zero-order kinetic dependence on [M] substantially suppresses tapering in BCP formation. *Third*, compounding the biased K_{eq} with differing monomer k_p further diminishes the probability for misincorporation errors. The principles described in this report should be generally applicable to catalysis and other polymerization systems, especially concerning sequence control, kinetic resolution, and block resolution.

References cited in Chapter 4

[1] Hong, M.; Chen, J.; Chen, E.Y.-X. Polymerization of Polar Monomers Mediated by Main-Group Lewis Acid–Base Pairs. *Chem. Rev*. **2018**, *118*, 10551-10616.

[2] McGraw, M.; Chen, E. Y.-X. Catalytic Lewis Pair Polymerization of Renewable Methyl Crotonate to High-Molecular-Weight Polymers. *ACS Catal*. **2018**, *8*, 9877−9887.

[3] Wang, Q.; Zhao, W.; Zhang, S.; He, J.; Zhang, Y.; Chen, E. Y.-X. Living Polymerization of Conjugated Polar Alkenes Catalyzed by N-Heterocyclic Olefin-Based Frustrated Lewis Pairs. *ACS Catal*. **2018**, *8*, 3571−3578.

[4] Wang, Q. Y.; Zhao, W. C.; He, J. H.; Zhang, Y. T.; Chen, E. Y.- X. Living Ring-Opening Polymerization of Lactones by N-Heterocyclic Olefin/$Al(C_6F_5)_3$ Lewis Pairs: Structures of Intermediates, Kinetics, and Mechanism. *Macromolecules* **2017**, *50*, 123−136.

[5] Knaus, M. G. M.; Giuman, M. M.; Pöthig, A.; Rieger, B. End of Frustration: Catalytic Precision Polymerization with Highly Interacting Lewis Pairs. *J. Am. Chem. Soc.* **2016**, *138*, 7776−7781.

[6] Zhang, Y.; Miyake, G. M.; John, M. G.; Falivene, L.; Caporaso, L.; Cavallo, L.; Chen, E. Y.-X. Lewis Pair Polymerization by Classical and Frustrated Lewis Pairs: Acid, Base and Monomer Scope and Polymerization Mechanism. *Dalton Trans*. **2012**, *41*, 9119−9134.

[7] Zhang, Y.; Miyake, G. M.; Chen, E. Y.-X. Alane-Based Classical and Frustrated Lewis Pairs in Polymer Synthesis: Rapid Polymerization of MMA and Naturally Renewable Methylene Butyrolactones into High-Molecular-Weight Polymers. *Angew. Chem., Int. Ed*. **2010**, *49*, 10158−10162.

[8] Jia, Y.-B.; Ren, W.-M.; Liu, S.-J.; Xu, T.; Wang, Y.-B.; Lu, X.-B. Controlled Divinyl Monomer Polymerization Mediated by Lewis Pairs: A Powerful Synthetic Strategy for Functional Polymers. *ACS Macro Lett.* **2014**, *3*, 896−899.

[9] Jia, Y.-B.; Wang, Y.-B.; Ren, W.-M.; Xu, T.; Wang, J.; Lu, X.-B. Mechanistic Aspects of Initiation and Deactivation in N-Heterocyclic Olefin Mediated Polymerization of Acrylates with Alane as Activator. *Macromolecules* **2014**, *47*, 1966−1972.

[10] Stephan, D. W. The Broadening Reach of Frustrated Lewis Pair Chemistry. *Science* **2016**, *354*, aaf7229.

[11] Stephan, D. W.; Erker, G. Frustrated Lewis Pair Chemistry: Development and Perspectives. *Angew. Chem., Int. Ed.* **2015**, *54*, 6400−6441.

[12] Stephan, D. W. Frustrated Lewis pairs. *J. Am. Chem. Soc*. **2015**, *137*, 10018−10032.

[13] Stephan, D. W. Frustrated Lewis Pairs: From Concept to Catalysis. *Acc. Chem. Res*. **2015**, *48*, 306−316.

[14] Frustrated Lewis Pairs I & II; Stephan, D. W., Erker, G., Eds.; Topics in Current Chemistry; Springer: New York, 2013; Vols. 332, 334.

[15] Jupp, A. R.; Stephan, D. W. New Directions for Frustrated Lewis Pair Chemistry. *Trends in Chemistry* **2019**, *1*, 35-48.

[16] Walther, P.; Naumann, S. N-Heterocyclic Olefin Based (Co)polymerization of a Challenging Monomer: Homopolymerization of ω-Pentadecalactone and Its Copolymers with γ-Butyrolactone, δ-Valerolactone, and ε-Caprolactone. *Macromolecules* **2017**, *50*, 8406−8416.

[17] Naumann, S.; Scholten, P. B. V.; Wilson, J. A., Dove, A. P. Dual Catalysis for Selective Ring-Opening Polymerization of Lactones: Evolution toward Simplicity. *J. Am. Chem. Soc*. **2015**, *137*, 14439−14445.

[18] Lewis Pair Catalysts in the Polymerization of Lactide and Related Cyclic Esters. *Molecules* **2018**, *23*, 189 (1-13).

[19] Li, X.-Q.; Wang, B.; Ji, H.-Y.; Li, Y.-S. Insights Into the Mechanism for Ring-Opening Polymerization of Lactide Catalyzed by $Zn(C_6F_5)_2$/ Organic Superbase Lewis Pairs. *Catal. Sci. Technol.* **2016**, *6*, 7763–7772.

[20] Piedra-Arroni, E.; Ladavière, C.; Amgoune, A.; Bourissou, D. Ring-Opening Polymerization with $Zn(C_6F_5)_2$-Based Lewis Pairs: Original and Efficient Approach to Cyclic Polyesters. *J. Am. Chem. Soc*. **2013**, *135*, 13306−13309.

[21] Walther, P.; Krauβ, A.; Naumann, S. Lewis Pair Polymerization of Epoxides via Zwitterionic Species as a Route to High-Molar-Mass Polyethers. *Angew. Chem. Int. Ed*. **2019**, *58*, 10737–10741.

[22] Naumann, S.; Thomas, A. W.; Dove, A. P. N-Heterocyclic Olefins as Organocatalysts for Polymerization: Preparation of Well-Defined Poly(propylene oxide*). Angew. Chem., Int. Ed.* **2015**, *54*, 9550−9554.

[23] Tang, X.; Westlie, A. H.; Watson, E. M.; Chen, E. Y.-X. Stereosequenced Crystalline Polyhydroxyalkanoates from Diastereomeric Monomer Mixtures, *Science* **2019**, *366*, 754−758.

[24] Ji, H.-Y.; Song, D.-P.; Wang, B.; Pan, L.; Li, Y.-S. Organic Lewis Pairs for Selective Copolymerization of Epoxides with Anhydrides to Access Sequence-Controlled Block Copolymers. *Green Chem.* **2019**, *21*, 6123–6132.

[25] Stöber, T.; Williams, C. K. Selective Polymerization Catalysis from Monomer Mixtures: Using a Commercial Cr-Salen Catalyst to Access ABA Block Polyesters *Angew. Chem. Int. Ed*. **2018**, *57*, 6337 –6341.

[26] Lutz, J. F.; Ouchi, M.; Liu, D. R.; Sawamoto, M. Sequence-Controlled Polymers. *Science* **2013**, *341*, 1238149.

[27] Badi, N.; Lutz, J. F. Sequence control in polymer synthesis. *Chem. Soc. Rev.* **2009**, *38*, 3383–3390.

[28] Satoh, K.; Matsuda, M.; Nagai, K.; Kamigaito, M. AAB-Sequence living radical chain copolymerization of naturally occurring limonene with maleimide: an end-to-end sequence-regulated copolymer. *J. Am. Chem. Soc.* **2010**, *132*, 10003–10005.

[29] Huang, Z.; Noble, B. B.; Corrigan, N.; Chu, Y.; Satoh, K.; Thomas, D. S.; Hawker, C. J.; Moad, G.; Kamigaito, M.; Coote, M. L.; Boyer, C.; Xu, J. Discrete and stereospecific oligomers prepared by sequential and alternating single unit monomer insertion. *J. Am. Chem. Soc.* **2018**, *140*, 13392–13406.

[30] Ji, H.-Y.; Wang, B.; Pan, L.; Li, Y.-S. One-step access to sequence-controlled block copolymers by self-switchable organocatalytic multicomponent polymerization. *Angew. Chem. Int. Ed.* **2018**, *57*, 16888–16892.

[31] Lin, F.; Wang, M.; Pan, Y.; Tang, T.; Cui, D.; Liu, B. Sequence and regularity controlled coordination copolymerization of butadiene and styrene: strategy and mechanism. *Macromolecules* **2017**, *50*, 849−856.

[32] Liu, B.; Cui, D.; Tang, T. Stereo- and temporally controlled coordination polymerization triggered by alternating addition of a Lewis acid and base. *Angew. Chem. Int. Ed.* **2016**, *55*, 11975−11978.

[33] Liu, D.; Wang, M.; Wang, Z.; Wu, C.; Pan, Y.; Cui, D. Stereoselective copolymerization of unprotected polar and nonpolar styrenes by an yttrium precursor: control of polar-group distribution and mechanism. *Angew. Chem. Int. Ed.* **2017**, *56*, 2714−2719.

[34] Liu, S.; Bai, T.; Ni, K.; Chen, Y.; Zhao, J.; Ling, J.; Ye, X.; Zhang, G. Biased Lewis Pairs: A General Catalytic Approach to Ether-Ester Block Copolymers with Unlimited Ordering of Sequences. *Angew. Chem. Int. Ed.* **2019**, *58*, 15478 – 15487.

[35] Nowalk, J. A.; Fang, C.; Short, A. L.; Weiss, R. M.; Swisher, J. H.; Liu, P.; Meyer, T. Y. Sequence-Controlled Polymers Through Entropy-Driven Ring Opening Metathesis Polymerization: Theory, Molecular Weight Control, and Monomer Design. *J. Am. Chem. Soc.* **2019**, *141*, 5741−5752.

[36] Wang, X.; Zhang, Y.; Hong, M. Controlled and Efficient Polymerization of Conjugated Polar Alkenes by Lewis Pairs Based on Sterically Hindered Aryloxide-Substituted Alkylaluminumitle. *Molecules* **2018**, *23*, 442.

[37] Wang, H.; Wang, Q.; He, J.; Zhang, Y. Living polymerization of acrylamides catalysed by *N*-heterocyclic olefin-based Lewis pairs. *Polym. Chem.* **2019**, *10*, 3597–3603.

[38] Bai, Y.; He, J.; Zhang, Y. Ultra-High-Molecular-Weight Polymers Produced by the Immortal Phosphine-Based Catalyst System. *Angew. Chem. Int. Ed.* **2018**, *57*,17230–17234.

[39] Zhao, W.; Wang, Q.; He, J.; Zhang, Y. Chemoselective and Living/Controlled Polymerization of Polar Divinyl Monomers by N-heterocyclic Olefin Based Classical and Frustrated Lewis Pairs. *Polym. Chem.* **2019**, *10*, 4328–4335.

[40] Zhang, P.; Zhou, H.; Lu, X.-B. Living and Chemoselective (Co)polymerization of Polar Divinyl Monomers Mediated by Bulky Lewis Pairs. *Macromolecules* **2019**, *52*, 4520−4525.

[41] Hosoi, Y.; Takasu, A.; Matsuoka, S.-I.; Hayashi, M. N-Heterocyclic Carbene Initiated Anionic Polymerization of (E,E)-Methyl Sorbate and Subsequent Ring-Closing to Cyclic Poly(alkyl sorbate). *J. Am. Chem. Soc.* **2017**, *139*, 15005−15012.

[42] Chen, E. Y.-X. Coordination Polymerization of Polar Vinyl Monomers by Single-Site Metal Catalysts. *Chem. Rev.* **2009**, *109*, 5157-5214.

[43] Luo, Y.; Wang, X.; Zhu, Y.; Li, B.-G.; Zhu, S. Polystyrene-*block*-poly(*n*-butyl acrylate)-*block*-polystyrene Triblock Copolymer Thermoplastic Elastomer Synthesized via RAFT Emulsion Polymerization. *Macromolecules* **2010**, *43*, 7472-7481.

[44] Tong, J. D.; Jerôme, R. Synthesis of Poly(methyl methacrylate)-b-poly(n-butyl acrylate)-b-poly(methyl methacrylate) Triblocks and Their Potential as Thermoplastic Elastomers. *Polymer* **2000**, *41*, 2499–2510.

[45] He, J.; Zhang, Y.; Falivene, L.; Caporaso, L.; Cavallo, L.; Chen, E. Y.-X. Chain Propagation and Termination Mechanisms for Polymerization of Conjugated Polar Alkenes by [Al]-Based Frustrated Lewis Pairs. *Macromolecules* **2014**, *47*, 7765−7774.

[46] Raynaud, J.; Gnanou, Y.; Taton, D. Group Transfer Polymerization of (Meth)acrylic Monomers Catalyzed by N-Heterocyclic Carbenes and Synthesis of All Acrylic Block Copolymers: Evidence for an Associative Mechanism. *Macromolecules* **2009**, *42*, 5996-6005.

[47] Takenaka, Y.; Abe, H. Group-Transfer Polymerization of Various Crotonates Using Organic Acid Catalysts. *Macromolecules* **2019**, *52*, 4052−4058.

[48] Raynaud, J.; Gnanou, Liu, N.; Fèvre, M.; Gnanou, Y.; Taton, D. No Matter the Order of Monomer Addition for the Synthesis of Well-Defined Block Copolymers by Sequential Group Transfer Polymerization Using N-Heterocyclic Carbenes as Catalysts. *Polym. Chem.* **2011**, *2*, 1706–1712.

[49] Takada, K.; Ito, T.; Kiano, K.; Tsuchida, S.; Takagi, Y.; Chen, Y.; Satoh, T.; Kakuchi, T. Synthesis of Homopolymers, Diblock Copolymers, and Multiblock Polymers by Organocatalyzed

Group Transfer Polymerization of Various Acrylate Monomers. *Macromolecules* **2015**, *48*, 511−519.

[50] Chen, Y.; Kitano, K.; Tsuchida, S.; Kikuchi, S.; Takada, K.; Satoh, T.; Kakuchi, T. $B(C_6F_5)_3$-Catalyzed Group Transfer Polymerization of Alkyl Methacrylates with Dimethylphenylsilane through In Situ Formation of Silyl Ketene Acetal by $B(C_6F_5)_3$-Catalyzed 1,4-Hydrosilylation of Methacrylate Monomer. *Polym. Chem.* **2015**, *6*, 3502–3511.

Chapter 5
Synchronous Control of Sequence and Topology

5.1 Background and Significance

Lewis pair polymerization (LPP) utilizes both Lewis acid (LA) and Lewis base (LB) components to cooperatively facilitate polymerization reactions, delivering exquisite control and tunability.[1-3] Recent LPP examples that have noticeably advanced the polymerization methodology include living and immortal polymerizations,[4-6] polymerizations of bio-based monomers with high functionality,[7-10] as well as precise comonomer sequence[11] and topological[10-14] control. Most recently, Takasu utilized LPP to synthesize cyclic polar vinyl polymers.[12] Methyl sorbate (MS), which can be effectively polymerized by LA methyl aluminum di(2,6-di-*tert*-butyl-4-methylphenoxy) (MAD) and LB 1,3-di-*tert*-butylimidazolin-2-ylidene (I^{t}Bu) pair, cyclizes, proposed by S_N2 attack from the enolate at the ω-terminus to the carbon bonded to the cationic LB initiating group at the α-terminus.[10] When excess methyl methacrylate (MMA) was added to a stoichiometric MS/MAD/I^{t}Bu mixture, LPP took place followed by ring closure, presumably through S_N2 attack from the polymeric MMA (PMMA) enolate anion to the MS/I^{t}Bu cation, to form cyclic PMMA with number-average molecular weight (M_n) ranging from low (7.3 kDa) to medium (29.1 kDa), dispersity ($Đ$) from 1.56 to 1.16, and initiation efficiency (I*) from ~20-55%[12] (Figure 5.1). This strategy suppressed H-transfer events encountered in the direct MMA polymerization by I^{t}Bu alone, which limited cyclic PMMA formation.[15] Herein, we disclose our findings that Takasu's sorbate-based methodology for cyclic vinyl polymers coupled with our LPP methodology for compounded sequence control (CSC)[2,11] enables the exquisite chain length-, sequence-, and topology-controlled synthesis of well-defined cyclic block copolymers (*c*BCPs)

with high M_n (247 kDa), low $Đ$ (1.04), and high I^* (95%) values, from one-pot monomer mixtures using pre-mixed ethyl sorbate (ES)/MAD/I^{t}Bu mixture **1** (Figure 5.1).

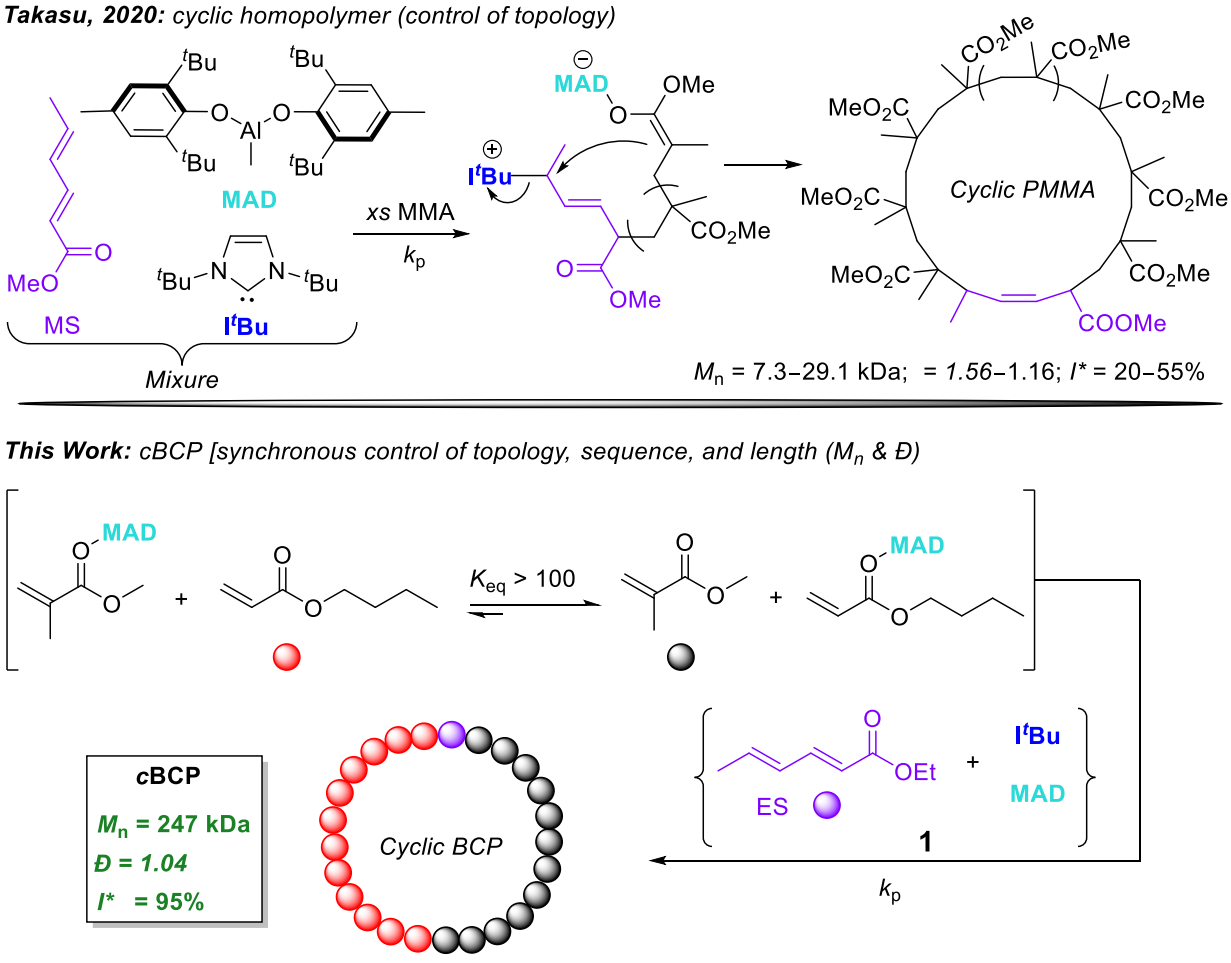

Figure 5.1. General synthetic route to cyclic polar vinyl homopolymers (top)[12] and synthetic route to *c*BCPs by CSC-LPP (bottom)

A classic strategy for cyclic polymer[16] synthesis[17-19] involves anionic polymerization wherein the initiating species acts not only as a nucleophilic initiator but also as a leaving group for ring-closure. This strategy works well for coordinative[20-24] and zwitterionic[25-27] ring-opening polymerization (ROP). In this case, if the activity of ring-closure (which is usually considered a chain transfer) is similar to the activity of propagation, then the M_n and $Đ$ values of the polymerization will be uncontrolled due to a reliance on proportionality eq. 1,[2] where k_p and k_{ct}

are the activities of propagation and chain transfer (cyclization), respectively, $[M]_t$ is the time dependent monomer concentration, and $[I]_0$ the initial initiator (I) concentration (a reasonable proxy for the number of propagating species).

1. $$M_n \propto \frac{k_p[M]_t[I]_0}{k_{ct}[I]_0}$$

Since this logic gives an average molecular weight, it should rather be understood as a statistical likelihood of chain transfer distributed across a broad range of molecular weights (that average to M_n). Moreover, the time dependent nature of $[M]_t$ means that the statistically predicted M_n will be variable with respect to time. Thus, M_n and $Đ$ can hardly be controlled in a reaction governed by proportionality 1. In contrast, LPP is well equipped to control the cyclic polymer M_n and $Đ$ due to its unique zero order in $[M]_t$ propagation kinetics shown (by the absence of $[M]_t$) in the numerator of proportionality eq. 2.

2. $$M_n \propto \frac{k_p[LA]_0[LB]_0}{k_{ct}[LB]_0}$$

Therefore, the propagation rate (numerator) can be tuned independently with respect to the chain transfer (ring-closure) rate by manipulation of $[LA]_0$. If the propagation rate is considerably higher than the chain transfer rate, proportionality 2 can be completely circumvented because chain transfer will statistically occur long after monomer depletion. *Thus, cyclic polymers with specific M_n values and low Đ indices can be targeted and achieved by LPP.*

Likewise, *c*BCPs are challenging to synthesize by chain-growth methods, especially with the classical sequential addition method, due to the event that cyclization can occur prematurely after the first comonomer sequence, resulting in either a mixture cyclic homopolymers or *c*BCPs contaminated with cyclic homopolymers. Only a few examples exist by ROP[21,22] that we are aware

of, and to our knowledge, *c*BCPs from olefinic monomers by purely chain growth methodologies are absent from the literature, with the exception of post-functionalized ring-closing by click-reactions or other privileged processes and highly dilute conditions.[28-34] To this end, a one-pot sequence-controlled methodology would seamlessly transition from one comonomer to the next, thereby minimizing total polymerization time during which cyclization can occur prematurely. We recently devised a one-pot sequence controlled diblock copolymerization of *n*-butyl and *tert*-butyl acrylate (^{n}BA and ^{t}BA) based on thermodynamic bias (K_{eq}) between the two monomers during the first step (LA-activation) constructively compounding with kinetic bias (k_p) during the second step (conjugate addition), hence the name CSC.[2,11] The result was rapid polymerization of ^{n}BA with exclusion of ^{t}BA until ^{n}BA was near depletion, followed by eventual polymerization of ^{t}BA.

5.2 Results and Discussion

Upon optimization in LB, we found that tri-cyclohexyl phosphine (PCy_3) works for the synthesis of the linear di-BCP via CSC diblock polymerization of ^{n}BA/MMA mixtures (runs 1 and 2, Table D1) since ^{n}BA is predisposed to termination during the course of polymerization. We found that sterically hindered LBs greatly diminish the activity of the Claisen-type termination common amongst acrylic monomers. I^{t}Bu works well for the linear copolymerization as well but since it has a tendency to cyclize and undergo H-transfer reactions, we opted to use PCy_3 to ensure we had a reliable linear comparison. Our attempt to measure the K_{eq} value for the ^{n}BA/MAD vs MMA/MAD equilibrium showed the equilibrium bias is shifted so far in favor of ^{n}BA/MAD that MMA/MAD could not be detected (Figure D1). Thus, we postulated that a heavily biased equilibrium K_{eq} for the ^{n}BA/MAD adduct compounding with the heavy k_p bias of ^{n}BA vs MMA (acrylates by MAD/LB convert on the order of seconds, while methacrylates convert on the order of minutes) will result in a high degree of block resolution in the mixed, one-pot copolymerization.

Indeed, the one-pot CSC method works well for the *n*BA/MMA mixture as evidenced by the presence of two glass-transition temperature (T_g) values (-46, 122 °C) observed from differential scanning calorimetry (DSC, Figure 5.2**A**), suggesting the presence of individual P*n*BA and PMMA domains, and by well-resolved ^{13}C NMR peaks of the BCP which strongly resemble the signatures of the individual homopolymers (Figure D3). The polymer sequencing can actually be observed qualitatively by a color change that occurs a few seconds after initiation from brilliant yellow to light yellow (signaling full conversion of *n*BA) followed by a color change from yellow to clear after a few minutes (signaling full conversion of MMA). Thus, high M_n P*n*BA-*b*-PMMA (up to 286 kDa) was synthesized from one-pot in one-step with low $Đ$ values (1.06–1.12) rapidly (in mins).

Next, we endeavored to synthesize the postulated cyclic *n*BA/MMA di-BCPs by initiating the same polymerization with the sorbate-derived mixture **1**. Here we simply dissolved MAD into a mixture of *n*BA and MMA in toluene and added initiator **1** to reach the pre-determined molar ratio of *n*BA/MMA/MAD/**1** (runs 3 and 4, Table D1). The polymerization was complete in less than 5 min (as indicated by color change) but the reaction was left to stir for 3 h to ensure complete cyclization before quenching with benzoic acid in MeOH. As in the linear BCPs, the resulting cyclic analogs also exhibited two distinct T_g values, and the polymer M_n can be controlled by the molar ratio of *n*BA/MMA/MAD/**1**, producing BCPs with M_n = 82.6 and 247 kDa (Table D1, runs 3 and 4, respectively). Noteworthy also is the extremely low $Đ$ value (1.04) for the resulting *c*BCPs. The presumed *c*BCPs were further characterized using hydrodynamic volume (V_h) and intrinsic viscosity [η] measurements by triple-detection gel permeation chromatography (GPC) to determine polymer topology since cyclic polymers are known to have lower V_h, thus lower [η], compared to their linear counterparts.[35] A d*n*/d*c* method was used to determine absolute molecular

weight data for both linear and *c*BCPs, therefore the individual d*n*/d*c* values were measured and were found indeed different. For example, a linear BCP (run 1) and cyclic analogue (run 3) containing the same comonomer ratio eluted at nearly the exact same time (Figure 5.2**B**). However, the measured d*n*/d*c* value for the cyclic polymer (0.0643 mL/g, Figure D14) was considerably lower than that of its linear counterpart (0.0737 mL/g, Figure D6). When the weight-average molecular weight (M_w) of these linear and cyclic analogues is compared per elution volume (as a function of hydrodynamic radius), *c*BCPs have a higher M_w than their linear analogues by a factor of 1.14 on average and thus a lower V_h (Figure 5.2**E** and **F**), supporting the cyclic structure of the BCPs. The radius of gyration (R_g) per M_w measured by multi-angle light scattering, was also higher for linear polymers compared to their cyclic analogues. Lastly, we compared the [η] per M_w and the bulk rheological viscosity (Figure 5.2**C** and **D**) and in both cases cyclic polymers exhibited lower viscosity since they have a lower degree of chain entanglement.[35]

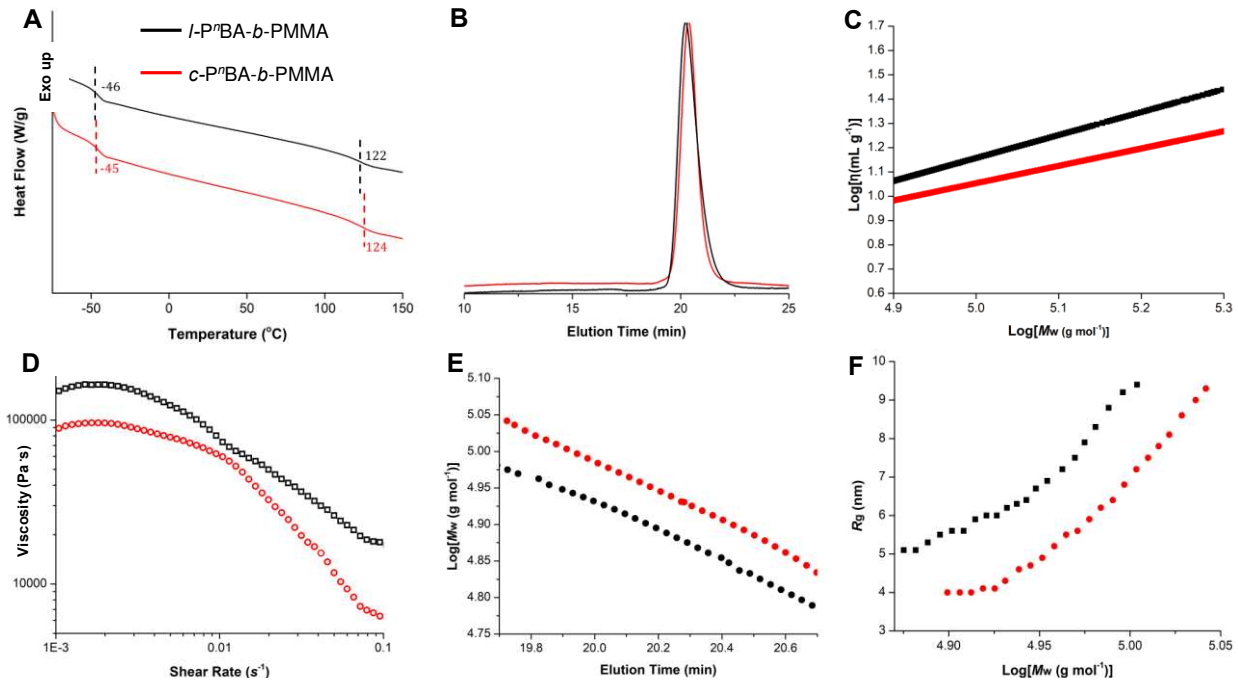

Figure 5.2. Comparative characterizations of linear (run 1, black) and cyclic (run 2, red) diblock P*n*BA-*b*-PMMA counterparts. (**A**) DSC traces of linear (*l*) and cyclic (*c*) P*n*BA-*b*-PMMA showing

two T_g's corresponding to P^{n}BA (-45 to -46 ^{o}C) and PMMA (122 and 124 ^{o}C) domains. (**B**) GPC elution time for *l*- and *c*-P^{n}BA-*b*-PMMA showing a narrow molecular weight distribution for both topologies. (**C**) Mark-Houwink-Sakurada plots for *l*- and *c*-P^{n}BA-*b*-PMMA showing higher [η] for the *l*-structure, especially at the higher M_w region. (**D**) Rheological viscosity of *l*- and *c*-P^{n}BA-*b*-PMMA. (**E**) Log(M_w) vs elution time plots of *l*- and *c*-P^{n}BA-*b*-PMMA. (**F**) R_g vs Log(M_w) plots showing higher R_g for the *l*-structure.

High molecular weight *c*BCPs can be made by simply decreasing the LP loading, as judged by all lines of evidence including M_w vs elution time, R_g vs M_w, a similarly lower d*n*/d*c*, higher T_g's, and lower bulk rheological viscosity for the *c*BCPs compared to the linear BCP counterpart (Figures D24-27). However, for the high monomer/initiator ratio run, ^{n}BA/MMA/MAD/**1** = 1200/800/10/1 (run 4), we opted to use a 10/1 MAD/LB ratio to increase polymerization activity relative to cyclization (eq. 2), which increases the likelihood of Claisen termination (as MAD is required to catalyze termination). Thus, one might expect that this *c*BCP may contain some unquantified linear contaminant. However, the identically low $Đ$ value (1.04) of this BCP to that produced by the 2/1 MAD/LB ratio (run 3) appears to indicate that both *c*BCPs are similarly well-controlled. Lastly, we included a 5-point demonstration of control over M_n and $Đ$ by this system (Table D2, Figure D28).

5.3 Direct Observation of *c*BCPs

Direct observation of the *c*BCPs topology by high resolution transmission electron microscopy (TEM) would provide more direct evidence for not only cyclization but also block resolution enabled by CSC. By using the method employed by Takasu[13] and utilizing the exquisite chemoselctivity of LPP,[1,2,36-38] we substituted allyl methacrylate (AMA) for MMA in the block-copolymerization and synthesized cyclic P^{n}BA-*b*-PAMA (M_n = 170 kDa, $Đ$ = 1.28). Next, we grafted octadecanethiol onto the allyl pendant groups of the *c*BCP via the thiol-ene click reaction to the corresponding grafted brush *c*BCP, P^{n}BA-*b*-PAMA$_g$ (M_n = 720 kDa, $Đ$ = 1.39) (Figure 5.3**A**). Now, expecting the octadecanthiol-grafted block to be visible by TEM, we anticipated

seeing "half-circle" shaped *c*BCP images. Indeed, we were able to directly observe half-circles with a diameter of 50 nm (Figure 5.3**B**). Owing to the packing of the octadecanethiol-grafted BCP into crystalline (Figure D35) domains, we could more easily observe large polymer crystalline domains that intriguingly retain the half-circle shape from 0.5 to 1 μm in diameter (Figure 5.3**C**). To ensure these "half-circle" shapes are a consequence of the *c*BCPs topology, we synthesized the linear BCP P^{n}BA-*b*-PAMA$_g$ analogue using PCy_3 instead of **1**, and subsequently observed columns of linear "worm-like" polymer domains of various sizes (Figure 5.3**D**, Figures D36-37).

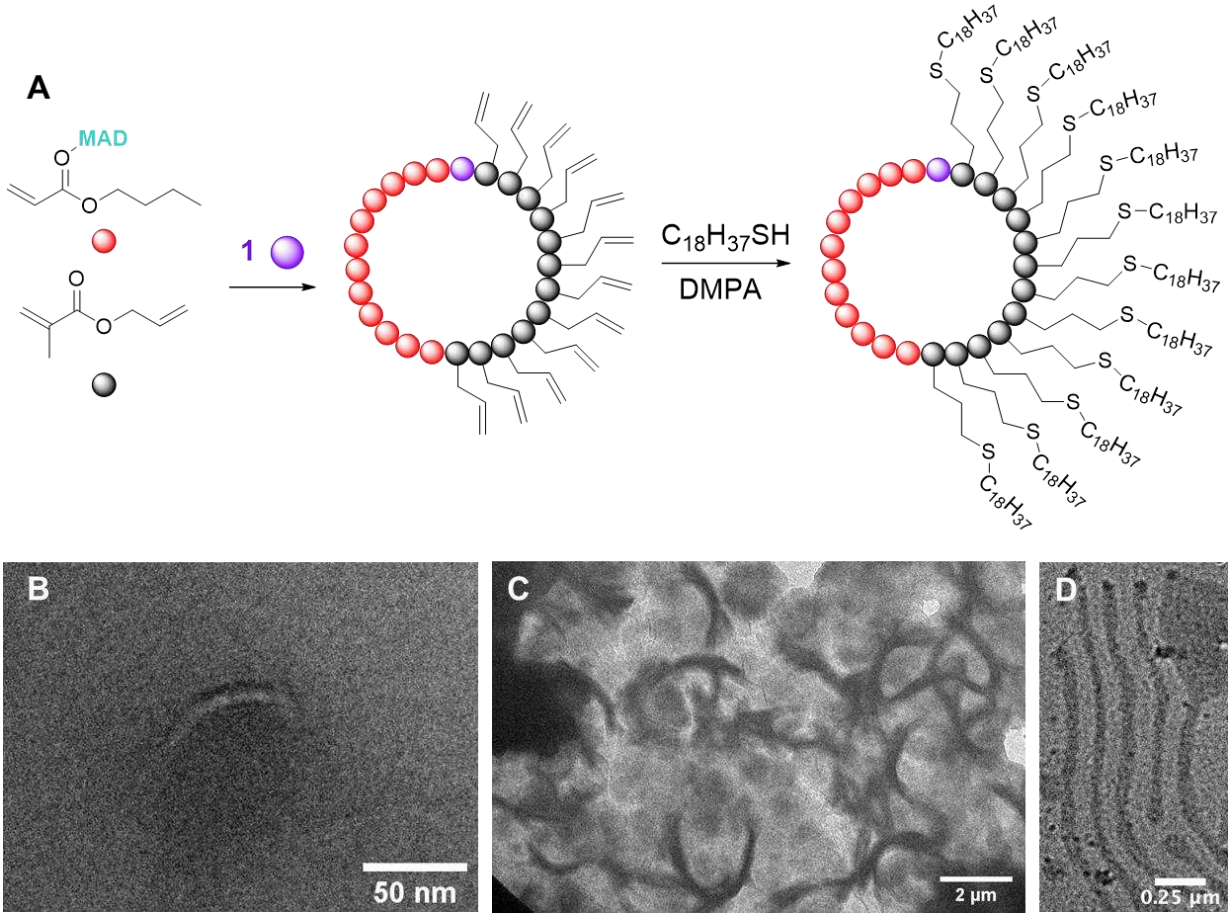

Figure 5.3. Direct observation of cyclic and linear BCP morphologies by TEM. (**A**) Synthetic route to cyclic "half-circle" brush copolymers. (**B**) TEM image of a single cyclic half-circle P^{n}BA-*b*-PAMA$_g$ chain. (**C**) TEM image of large half-circle shaped crystalline cyclic P^{n}BA-*b*-PAMA$_g$ domains. (**D**) TEM image of self-organized linear P^{n}BA-*b*-PAMA$_g$ analogue for comparison.

5.4 Conclusion

In summary, we have developed a general method for making well-defined *c*BCPs selectively and precisely from a one-pot monomer mixture. Acrylic *c*BCPs were expediently (in mins), conveniently (one pot, room temperature, normal concentration), and efficiently (I^* = 95%) synthesized to medium and high molecular weight (M_n = 247 kDa) with low dispersity ($Đ$ = 1.04). Considering the well-recognized challenges even in controlling M_n and $Đ$ values of cyclic homopolymers by rapid chain-growth polymerizations, not even mentioning *c*BCPs, this method showcases the potential of LPP to conquer longstanding precision polymer synthesis challenges and also the broad applicability of the CSC methodology.

References Cited in Chapter 5

[1] Hong, M.; Chen, J.; Chen, E.Y.-X. Polymerization of Polar Monomers Mediated by Main-Group Lewis Acid-Base Pairs. *Chem. Rev*. **2018**, *118*, 10551−10616.

[2] McGraw, L. M.; Chen, E. Y.-X. Lewis Pair Polymerization: Perspective on a Ten-Year Journey. *Macromolecules* **2020**, *53*, 6102–6122.

[3] Zhang, Y. T.; Miyake, G. M.; John, M. G.; Falivene, L.; Caporaso, L.; Cavallo, L.; Chen, E. Y.-X. Lewis Pair Polymerization by Classical and Frustrated Lewis Pairs: Acid, Base and Monomer Scope and Polymerization Mechanism. *Dalton Trans*. **2012**, *41*, 9119−9134.

[4] Wang, Q.; Zhao, W.; Zhang, S.; He, J.; Zhang, Y.; Chen, E. Y.-X. Living Polymerization of Conjugated Polar Alkenes Catalyzed by N-Heterocyclic Olefin-Based Frustrated Lewis Pairs. *ACS Catal.* **2018**, *8*, 3571−3578.

[5] Bai, Y.; He, J.; Zhang, Y. Ultra-High-Molecular-Weight Polymers Produced by the Immortal Phosphine-Based Catalyst System. *Angew. Chem., Int. Ed.* **2018**, *57*, 17230−17234.

[6] Bai, Y.; Wang, H.; He, J.; Zhang, Y. Rapid and Scalable Access to Sequence-Controlled DHDM Multiblock Copolymers by FLP Polymerization. *Angew. Chem., Int. Ed.* **2020**, *59*, 11613-11619.

[7] McGraw, M.; Chen, E. Y.-X. Catalytic Lewis Pair Polymerization of Renewable Methyl Crotonate to High-Molecular-Weight Polymers. *ACS Catal*. **2018**, *8*, 9877−9887.

[8] Wang, X.-J.; Hong, M. Lewis-Pair-Mediated Selective Dimerization and Polymerization of Lignocellulose-Based β-Angelica Lactone into Biofuel and Acrylic Bioplastic. *Angew. Chem., Int. Ed*. **2020**, *59*, 2664−2668.

[9] Imada, M.; Takenaka, Y.; Hatanaka, H.; Tsuge, T.; Abe, H. Unique Acrylic Resins with Aromatic Side Chains by Homopolymerization of Cinnamic Monomers. *Commun. Chem*. **2019**, *2*, 109.

[10] Hosoi, Y.; Takasu, A.; Matsuoka, S.-I.; Hayashi, M. N-Heterocyclic Carbene Initiated Anionic Polymerization of (E,E)- Methyl Sorbate and Subsequent Ring-Closing to Cyclic Poly(alkyl sorbate). *J. Am. Chem. Soc.* **2017**, *139*, 15005−15012.

[11] McGraw, M. L.; Clarke, R. W.; Chen, E. Y.-X. Compounded Sequence Control in Polymerization of One-Pot Mixtures of Highly Reactive Acrylates by Differentiating Lewis Pairs. *J. Am. Chem. Soc.* **2020**, *142*, 5969−5973.

[12] Oga, Y.; Hosoi, Y.; Takasu, A. Synthesis of cyclic Poly(methyl methacrylate) via N-Heterocyclic carbene (NHC) initiated-anionic polymerization and subsequent ring-closing without need of highly dilute conditions. *Polymer* **2020**, *186*, 122019.

[13] Naruse, K.; Takasu, A.; Higuchi, M. Direct Observation of a Cyclic Vinyl Polymer Prepared by Anionic Polymerization using N-Heterocyclic Carbene and Subsequent Ring-Closure without Highly Diluted Conditions. *Macromol. Chem. Phys.* **2020**, *221*, 2000004.

[14] Muramatsu, Y.; Takasu, A.; Higuchi, M.; Hayashi, M. Direct observation of the formation of a cyclic poly(alkyl sorbate) via chain-growth polymerization by an N-heterocyclic carbene initiator and ring-closing without extreme dilution. *J Polym Sci.* **2020**, *58*, 2936–2942.

[15] Zhang, Y.; Schmitt, M.; Falivene, L.; Caporaso, L.; Cavallo, L.; Chen, E. Y.-X. Organocatalytic Conjugate-Addition Polymerization of Linear and Cyclic Acrylic Monomers by *N*-Heterocyclic Carbenes: Mechanisms of Chain Initiation, Propagation, and Termination, *J. Am. Chem. Soc.* **2013**, *135*, 17925–17942.

[16] Yamamoto, T.; Tezuka, Y. Topological polymer chemistry: a cyclic approach toward novel polymer properties and functions. *Polym. Chem.* **2011**, *2*, 1930-1941.

[17] Kricheldorf, H. R. Cyclic polymers: Synthetic strategies and physical properties. *J. Polym. Sci. A Polym Chem* **2010**, *48*, 251-284.

[18] Haque, F. M.; Grayson, S. M. The synthesis, properties and potential applications of cyclic polymers. *Nat. Chem* **2020**, *12*, 433-444.

[19] Endo, K. Synthesis and Properties of Cyclic Polymers. In *New Frontiers in Polymer Synthesis*; Kobayashi, S., Ed.; Springer-Verlag: Berlin, Heidelberg, 2008; pp 121-185.

[20] Li, X. Q.; Wang, B.; Ji, H. Y.; Li, Y. S. Insights into the Mechanism for Ring-Opening Polymerization of Lactide Catalyzed by $Zn(C_6F_5)_2$/Organic Superbase Lewis Pairs. *Catal. Sci. Technol.* **2016**, *6*, 7763−7772.

[21] Piedra-Arroni, E.; Ladaviere, C.; Amgoune, A.; Bourissou, D. Ring-Opening Polymerization with $Zn(C_6F_5)_2$-Based Lewis Pairs: Original and Efficient Approach to Cyclic Polyesters. *J. Am. Chem. Soc.* **2013**, *135*, 13306−13309.

[22] Wang, B.; Pan, L.; Ma, Z.; Li, Y. Ring-Opening Polymerization with Lewis Pairs and Subsequent Nucleophilic Substitution: A Promising Strategy to Well-Defined Polyethylene-like Polyesters without Transesterification. *Macromolecules* **2018**, *51*, 836−845.

[23] Zhu, J.-B.; Watson, E. M.; Tang, J.; Chen, E. Y.-X. A Synthetic Polymer System with Repeatable Chemical Recyclability. *Science* **2018**, *360*, 398−403.

[24] Hong, M.; Chen, E. Y.-X. Completely Recyclable Biopolymers with Linear and Cyclic Topologies via Ring-Opening Polymerization of γ-Butyrolactone. *Nat. Chem.* **2016**, *8*, 42−49.

[25] Brown, H. A.; Waymouth, R. M. Zwitterionic Ring-Opening Polymerization for the Synthesis of High Molecular Weight Cyclic Polymers. *Acc. Chem. Res*. **2013**, *46*, 2585−2596.

[26] Culkin, D. A.; Jeong, W.; Csihony, S.; Gomez, E. D.; Balsara, N. P.; Hedrick, J. L.; Waymouth, R. M. Zwitterionic Polymerization of Lactide to Cyclic Poly(Lactide) by Using N-Heterocyclic Carbene Organocatalysts. *Angew. Chem., Int. Ed.* **2007**, *46*, 2627−2630.

[27] Shi, C.; McGraw, M. L.; Li, Z.-C.; Cavallo, L.; Falivene, L.; Chen, E. Y.-X. High-Performance Pan-Tactic Polythioesters with Intrinsic Crystallinity and Chemical Recyclability. *Science Advances* **2020**, *6*, eabc0495.

[28] Jones, F. R. Cyclics in Styrene-Dimethyl Siloxane Block Copolymers. *Eur. Polym. J.* **1974**, *10*, 249-254.

[29] Yin, R.; Hogen-Esch, T. E. Synthesis and Characterization of Narrow Molecular Weight Distribution Polystyrene-Poly(dimethylsiloxane) Macrocyclic Block Copolymers and Their Isobaric Precursors. *Macromolecules* **1993**, *26*, 6952-6957.

[30] Ma, J. Synthesis of well-defined macrocyclic block copolymers using living coupling agent method. *Macromol. Symp.* **1995**, *95*, 41-49.

[31] Deffieux, A.; Schappacher, M.; Rique-Lurbet, L. New routes to macrocyclic polymers of controlled dimensions. *Polymer* **1994**, *35*, 4562-4568.

[32] Lecommandoux, S.; Borsali, R.; Schappacher, M.; Deffieux, A.; Narayanan, T.; Rochas, C. Microphase separation of linear and cyclic block copolymers poly(styrene-b-isoprene): SAXS experiments. *Macromolecules* **2004**, *37*, 1843–1848.

[33] Poelma, J. E. Ono, K.; Miyajima, D.; Aida, T.; Satoh, K.; Hawker, C. J. Cyclic block copolymers for controlling feature sizes in block copolymer lithography. *ACS Nano* **2012**, *6*, 10845–10854.

[34] Zhang, B., Zhang, H., Li, Y., Hoskins, J. N. & Grayson, S. M. Exploring the effect of amphiphilic polymer architecture: synthesis, characterization, and self-assembly of both cyclic and linear poly(ethylene glycol)-b-polycaprolactone. *ACS Macro Lett.* **2013**, *2*, 845–848.

[35] Roovers, J. Organic Cyclic Polymers. In *Cyclic Polymers*; Semlyen, J. A., Ed.; Kluwer Academic Press: Dordrecht, Boston, London, 2000; Chapter 10, pp 347-385.

[36] Zhang, P.; Zhou, H.; Lu, X.-B. Living and Chemoselective (Co)polymerization of Polar Divinyl Monomers Mediated by Bulky Lewis Pairs. *Macromolecules* **2019**, *52*, 4520−4525.

[37] Zhao, W.; Wang, Q.; He, J.; Zhang, Y. Chemoselective and living/controlled polymerization of polar divinyl monomers by N-heterocyclic olefin based classical and frustrated Lewis pairs. *Polym. Chem.* **2019**, *10*, 4328−4335.

[38] Zhao, W.; He, J.; Zhang, Y. Lewis pairs polymerization of polar vinyl monomers. *Sci. Bull*. **2019**, *64*, 1830−1840.

Chapter 6
Origins of Spatial and Temporal Control in Cyclic LPP by Sorbate Initiation System

6.1 Background and Significance

Cyclic polymers have gained increased attention in recent years.[1,2,3,4,5,6,7,8,9] This excitement is partly due to availability of more diverse classes of cyclic polymers made possible by emerging methodologies, such as zwitterionic ring-opening polymerization,[10,11, 12,13,14] ring-expansion polymerization,[15,16,17,18,19,20,21] Lewis pair polymerization (LPP),[22,23,24,25,26] and coordinative insertion/back-biting ring closure.[27,28,29] Added to this development are the advances in more traditional techniques such as unimolecular and bimolecular coupling reactions used for ring closure, most notably the click reactions.[2,30,31,32,33,34,35,36,37] Additionally, materials properties unique to cyclic polymers (with respect to linear analogues), such as lower intrinsic viscosity (η),[38,39,40,41,42] faster crystallization kinetics,[43,44,45] and sometimes higher resistance to chemical[46,47] and thermal degradation, can be exploited. Perhaps most intriguing is the role of cyclic block copolymers (BCPs) in self-assembly where the dynamics of phase segregation differ from their linear counterparts in their degree of entanglement and degrees of rotational and translational freedom.[37,47,48,49,50]

The principal synthetic challenge in precision synthesis of cyclic polymers lies in the cyclization or ring-closure step, where a chemical path is necessary to bond the two termini. If the cyclization step is available during the polymerization (propagation), then *the ring-closing event will be in competition with propagation* and will thus occur statistically over a broad range of molecular weights (Figure 6.1), usually in the form of a chain transfer.[10,13,14,17] On the other hand, the ring closing event can be reserved until a later step, and triggered by an exogenous reagent. For example, polymerizations can be executed by controlled radical methods while installing a

coupling node (such as an alkyne) on the initiating molecule and installing a second node (such as an azide) on the opposite terminus either with a functionalized quenching molecule or an additional post-functional step.[31] Then, in a final step, a click reaction can be triggered to bond the termini together.[30-37] Although these methods afford more control over number-average molecular weight (M_n) and dispersity ($Đ$), they require multiple steps and privileged chemistries restricting them to largely academic interests. A more ideal methodology, in our opinion, is to make available the potential for ring-closing during the polymerization step, while installing some chemo- or spatial and temporal control[51] that allows the polymerization to achieve full conversion (i.e., monomer depletion) and only then execute the cyclization event to occur at the specific site of the chain (Figure 6.1).

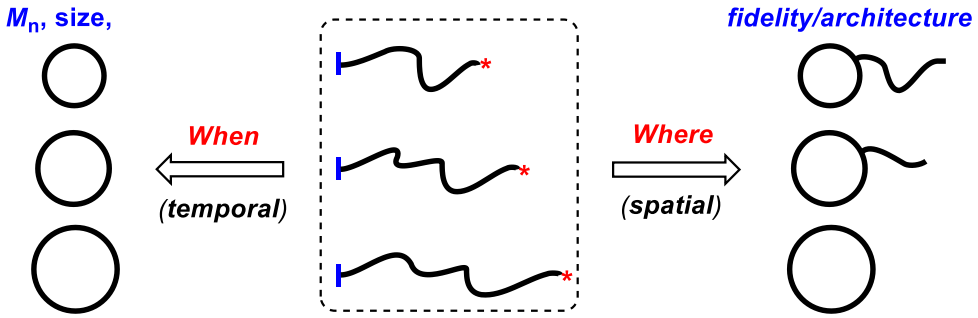

Figure 6.1. Schematic illustration of spatial and temporal control that regulates where and when cyclization takes place to achieve precision cyclic polymers with predictable M_n and low $Đ$ values as well as high structural fidelity.

In this context, Takasu and co-workers recently disclosed a facile route to cyclic polar polyolefins from LPP of the biorenewable monomer class of alkyl sorbates.[26] The sorbate monomer is a conjugated diene involving a complex electron system with complicated regio- and stereochemistry associated with its polymerization. Anionic routes were first explored on this monomer class by Takasu and Hirabayashi[52,53,54] where much of the regio and stereochemistry was defined spectroscopically. Those reports showed that employment of the bulky Lewis Acid (LA)

methyl aluminum-di(2,6-di-*tert*-butyl-4-methyl-phenoxy) (MAD) can restrict the regiochemistry of the resulting polysorbates to the 1,4-addition structure while cold temperatures and various other conditions could yield more stereoselective polymers. When Takasu and Hayashi employed an organic Lewis base (LB), 1,3-di-*tert*-butylimidazolin-2-ylidene (I^{t}Bu), instead of traditional alkyl lithium bases, the resulting polymers were found to be cyclic, as determined by matrix assisted laser desorption ionization time-of-flight mass spectrometry (MALDI-TOF-MS), viscometry,[26] and later by direct observation with transmission electron microscopy (TEM) upon thiol-ene click post-functionalization.[55]

The proposed mechanism (Figure 6.2) was that nucleophilic conjugate addition of the initiating LB (I^{t}Bu) to the electrophilic alkyl sorbate δ-carbon results in the formation of a zwitterionic enolate, which then after repeated conjugate additions to other sorbate molecules (aided by MAD) a polysorbate is produced with an imidazolium cationic α-terminus and an anionic enolaluminate ω-terminus. This *nucleophilic-initiation*-based mechanistic hypothesis then afforded the enticing nuance that the two termini electrostatically draw each other into proximity, where an S_N2-type ring-closure can occur to regenerate the neutral I^{t}Bu and yield a neutral cyclic polysorbate.

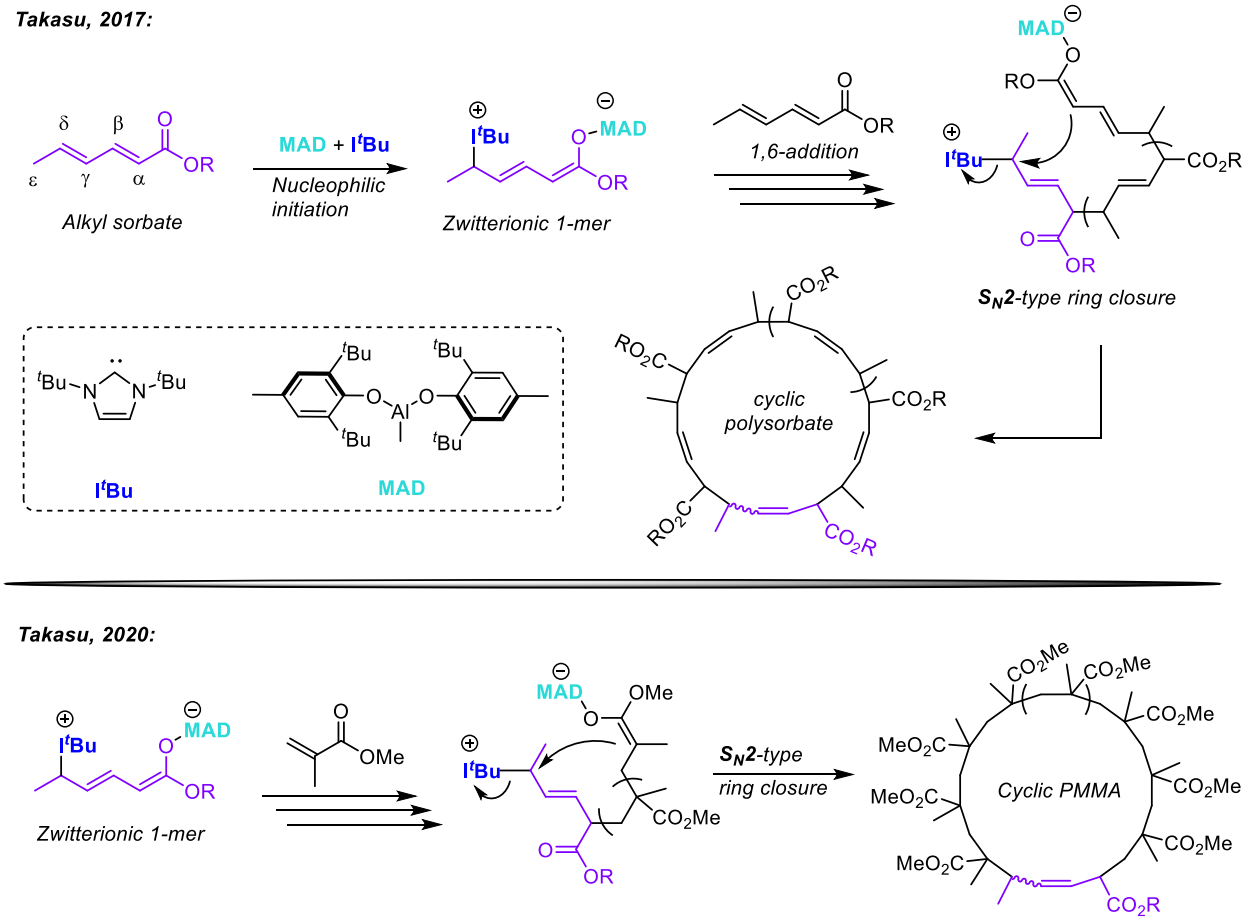

Figure 6.2. Originally proposed path to cyclic polysorbates (top) and more generalized route to cyclic poly(methacrylate)s (bottom), with both mechanisms operating through a zwitterionic propagating species and an S_N2-type ring-closure

This method was later utilized by Takasu to render a more generalized method to synthesize cyclic poly(methacrylate)s by simply preforming the sorbate-derived active species (presumed at the time to be the zwitterionic 1-mer, Figure 6.2) by premixing MAD, methyl sorbate (MS), and I^{t}Bu together at a 1/1/1 molar ratio followed by addition of methyl methacrylate (MMA) with some additional MAD catalyst.[56] Polymerization then proceeded from the sorbate 1-mer to grow polymethacrylate chains that would eventually ring-close presumably via the same S_N2 step, displacing the I^{t}Bu$^+$ leaving group and forming a bond between the once methacrylic enolate ω-terminus and the sorbate δ-carbon. The result was indeed cyclic poly(methyl methacrylate) (*c*-

PMMA), as judged by the MALDI-TOF-MS and viscometry. Later, allyl methacrylate was employed so that 1-octadecanethiol (1-ODT) chains could be clicked onto the pendant allyl groups to make cyclic-brush-polymethacrylates which can be directly observed by TEM.[55,57]

Intrigued by this hypothesized mechanism, we most recently adapted Takasu's methodology for our compounded sequence control (CSC) LPP method [58,59] to make cyclic di-BCPs of *n*-butyl acrylate (^{n}BA) and MMA in one pot and one step.[22] By utilizing this unique strategy, we successfully synthesized high molecular weight (M_n up to 267 kDa) cyclic P^{n}BA-*b*-PMMA with narrow dispersity ($Đ$ = 1.03) at room temperature (RT) and without highly dilute conditions. By several lines of evidence including hydrodynamic radius (V_h), radius of gyration (R_g), solution viscometry, bulk viscometry, and TEM, we supported the cyclic topology of these di-BCPs.

However, when we checked the proton NMR of the preformed sorbate initiating species (generated by 1/1/1 mixing of ethyl sorbate (ES), MAD, and I^{t}Bu), we noticed that the 1-mer was not a zwitterionic product of nucleophilic attack, but rather an ion pair product of basic deprotonation (Figures 6.3 and E1). After rigorously assigning the structure of the [I^{t}Bu·H]$^{+}$[MAD·ES]$^{-}$ ion pair **1** using ^{1}H and HH-COSY NMR techniques as well as mass spectrometry, we concluded that the mechanism first proposed by Takasu et al. needed to be revisited and revised. If an ion pair is the species initiating polymerization of sorbates and (meth)acrylates, then there is no leaving group to facilitate S_N2 ring-closure. Hence, without that enticing S_N2 ring-closure event, the fundamental question is: how does the cyclization actually take place to form the cyclic polymer?

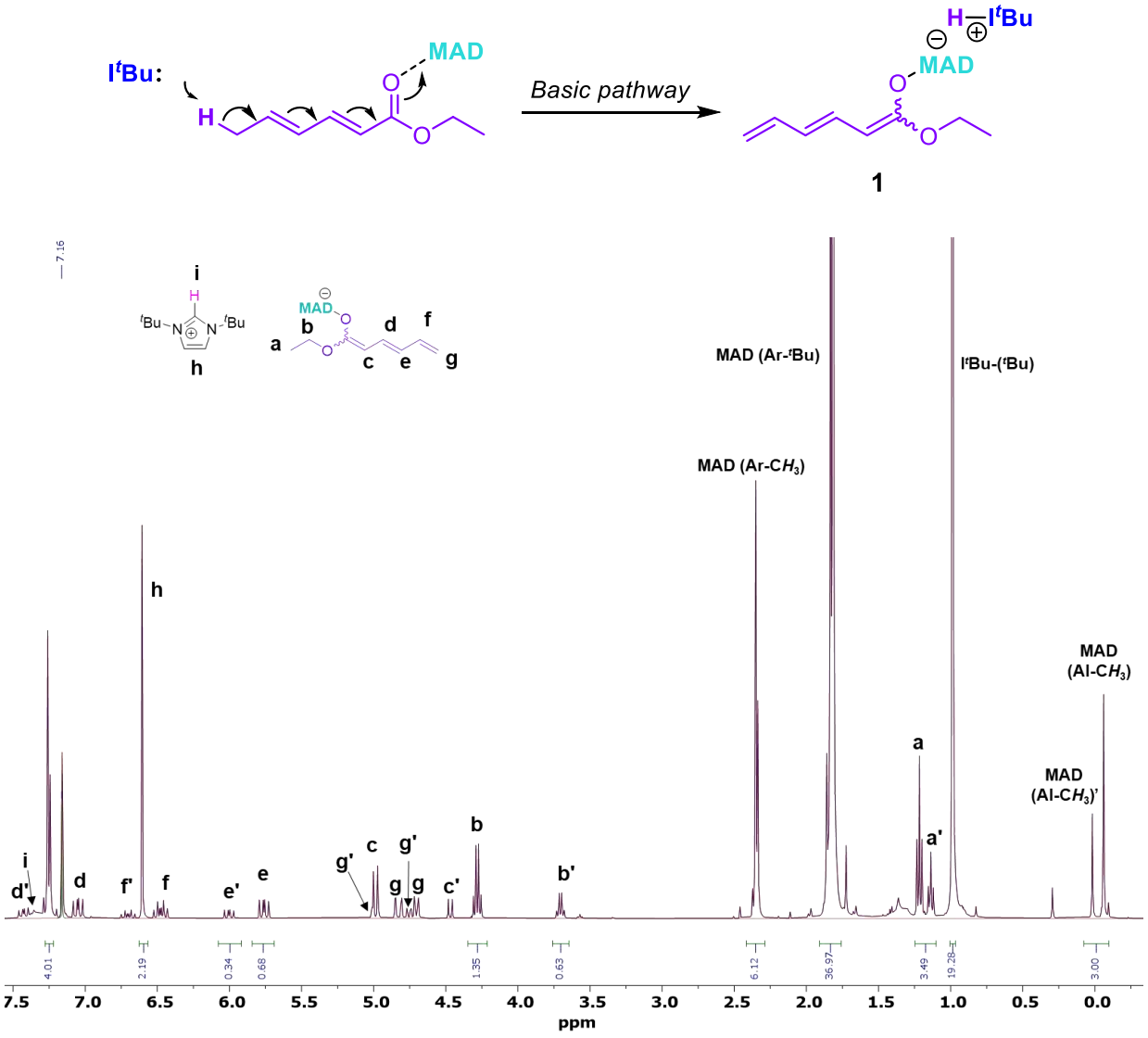

Figure 6.3. Deprotonative mechanism by which the initiating species **1** is generated via the basic pathway (top) and ^{1}H NMR (C_6D_6) of ion pair **1**, showing two geometric isomers.

After reviewing all of the evidence again, including MALDI-TOF-MS, viscometry, R_g and V_h, differential refractive index, glass transitions, TEM, and most convincingly the MALDI-TOF-MS evidence from the original report[26] featuring mass calculations before and after hydrogenation of cyclic polysorbates, we were convinced that this method produces cyclic polymers by an *unknown mechanism* of which we needed to elucidate. Herein we disclose the results of this investigation and present what we believe is a strong case for an alternative mechanism.

6.2 Results and Discussion

6.2.1. Distinguishing Basic *vs* Nucleophilic Initiation Pathways by I^{t}Bu

As mentioned in the Introduction we first noticed by ^{1}H NMR that **1** was not a zwitterion but rather an ion pair. This ion pair was prepared by mixing MAD/ES/I^{t}Bu together in C_6D_6, toluene, or dichloromethane (DCM) at a molar ratio of 1/1/1. We generally premix MAD and the sorbate molecule together first, and only then add the mixture to I^{t}Bu. Solubilities are best in DCM, which is what we used for most polymerization runs. However, due to side reactions between I^{t}Bu and DCM, we took precautions to not expose I^{t}Bu to DCM unless the MAD/ES adduct was already present. Figure 6.3 shows the ^{1}H NMR spectrum of this ion pair **1** as a mixture of some *E*/*Z* isomer pair. Although there are technically two alkenes that could express geometric isomerism (α and γ), the α (enolate) alkene is the one assumed to be expressing isomerism. This assumption is based on a similar ion pair formed when methyl crotonate (MC) is reacted with MAD/I^{t}Bu, which also forms an analogous *E*/*Z* ion pair. However, the crotonate ion pair only has one alkene from which geometric isomerism can exist and it is the enolate. Thus, we assume the same for the more ambiguous sorbates. When **1** was synthesized in DCM (Figure E4), the compositional ratio of the isomer pair was 1/1. When **1** was synthesized in C_6D_6, the ratio was 2/1. When the *E*/*Z* = 1/1 solution in DCM was diluted into C_6D_6, the *E*/*Z* ratio remained 1/1 indefinitely vs time and did not drift towards 2/1. Thus, it seems as though when I^{t}Bu deprotonates the ES·MAD adduct, the reaction is irreversible.

The **1** synthesized in DCM (Figure E4) clearly showed the I^{t}Bu$^+$-*H* proton peak at 7.51 ppm. Additionally, the terminal ε-protons of the deprotonated ES can be correlated to the rest of the structure with the HH-COSY (Figures E4 and E3), and as one would expect, both protons have their own peaks since it is an asymmetric alkene. The fact that two unique doublets for these

terminal ε-methyl protons can be observed, as well as two unique nuclear overhauser effect (NOE) signals with the δ-proton on the HH-COSY, strongly supports the deprotonative mechanism. And since Takasu et al. ran the polymerizations at -20 ^{o}C, we checked to ensure that the synthesis of **1** at -20 ^{o}C would give the same product, and it does (Figure E5). We also want to point out that Takasu et al. mainly used MS in their studies while we used ES. We chose ES as it has a lower boiling point (making purification by distillation more convenient), and it might better stabilize the ion pair **1**, making it more durable for our studies. In any case, we made sure MS behaves the same as ES and synthesized the MAD/MS/I^{t}Bu ion pair (Figure E6), and it gave an identical set of ^{1}H NMR peaks (with the exception of a slightly different *E*/*Z* ratio) indicating that it forms the ion pair just like ES and does not form the zwitterion by the nucleophilic initiation. Additionally, we found further evidence for this ion pair **1** structure when we performed time of flight mass spectrometry on this molecule (Figure E7). In the absence of any ionizing agent, we found that the imidazolium cation was the major *m*/*z* peak observed in positive mode (*m*/*z* = 181.17), while the MAD capped sorbate was the only peak observed in negative mode (*m*/*z* = 619.43).

6.2.2. Determining Initiation and Termination Chain Ends

Next, we ensured that the deprotonative initiation pathway was in fact the real mechanism in a polymerization scenario. Here, we initiated polymerization on 200 equiv of ES simply by using I^{t}Bu as the initiator so that the deprotonation (or conjugate addition) would occur *in-situ*. The ES/MAD/I^{t}Bu ratio used was 200/2/1 with $[ES]_0$ = 0.60 M in toluene. However, we quenched aliquots of the reaction at various time points. An aliquot quenched at 27 % conversion yielded a poly(ethyl sorbate) (PES) with the degree of polymerization (DP) equal to approximately 54. Crucially here, the PES chains are still growing and would not have cyclized yet. Therefore, one of two outcomes is expected. First, if the polymerization is initiating nucleophilically (according

to Takasu's mechanism) and cyclizes by S_N2 attack on the carbon bearing the I^tBu^+, premature quenching of the reaction should yield a polymer with the I^tBu^+ initiating group still attached, the weight of which would be detectable via MALDI-TOF-MS and most likely represented by an end group mass near m/z =181 (I^tBu^+ + H). Alternatively, if the initiation step is basic, no end groups should be detected and the MALDI-TOF-MS would give an intercept of near 23 (the mass of Na^+, Figure 6.5). The polymer we gathered after premature quenching at 27 % conversion gave a MALDI-TOF-MS spectrum which had one set of peaks characterized by a $m/z = 140n + 23$ (Figure 6.4). Thus, it is suggested by this experiment that the deprotonative mechanism is indeed correct.

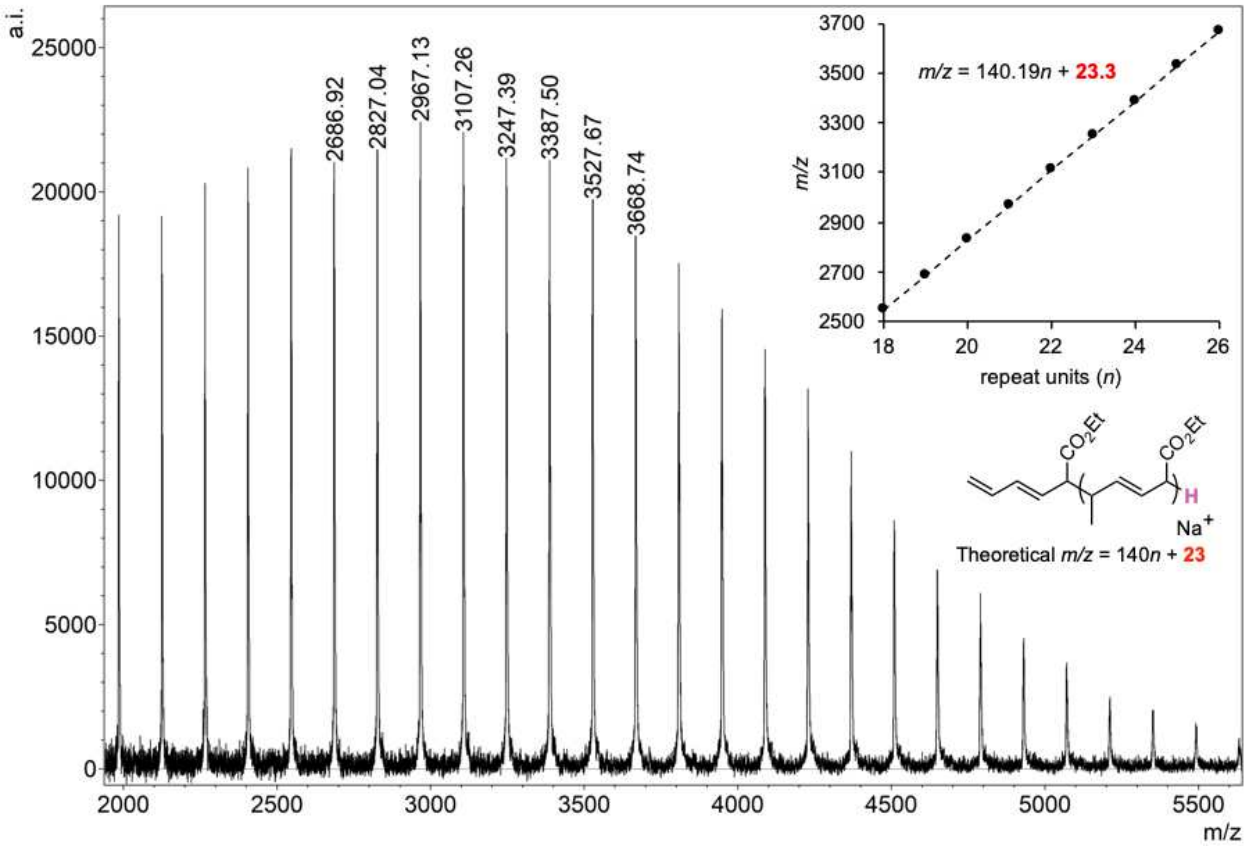

Figure 6.4. MALDI-TOF-MS spectrum of PES initiated by ion pair **1** but quenched prematurely at 27 % conversion. One set of peaks with an intercept of 23 reveals the basic initiation pathway. Note that the shown chemical structures only represent one of several regiochemical possibilities.

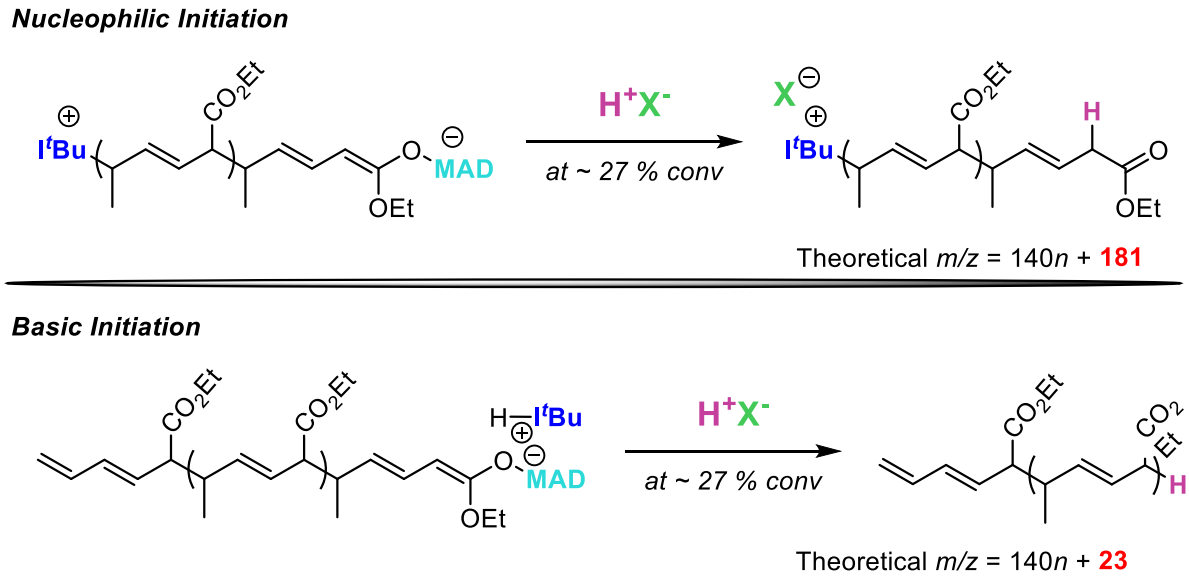

Figure 6.5. Premature quenching of an ES/MAD/I^{t}Bu LPP hypothesized to yield a binary result to distinguish between basic/nucleophilic initiation

Next, we chose some other LBs that we know from our prior and literature work have higher tendencies to operate through the nucleophilic path rather than the basic initiation pathway and conducted similar LPP on ES attempting to observe the S_N2 ring closing step. In our earlier report on the LPP of MC,[60] which also has both nucleophilic and basic pathways available, we found that 1,3,4-triphenyl-4,5-dihydro-1H-1,2,4-triazol-5-ylidene (TPT) exclusively operates through the nucleophilic path, while I^{t}Bu exclusively operates through the basic path. Additionally, we and others have observed TPT acting as a leaving group in several umpolung-type coupling reactions.[61,62,63,64,65] We hypothesized that this same behavior might be expressed in the sorbate system. When we attempted to synthesize the TPT/ES/MAD 1/1/1 zwitterionic species in C_6D_6, we obtained an extremely convoluted ^{1}H NMR that was inconclusive (Figure E8). We surmised that the complicated NMR spectrum was a product of the number of possible regio- and stereoisomers that could be obtained when there are two points of attack (β and δ) and two alkenes with *E*/*Z* isomers available for ES. Accordingly, we added this presumed non-selective cocktail of

isomeric zwitterions (**2**) to an MMA/MAD solution in toluene so that the calculated MMA/MAD/**2** concentration was 40/1/1 with $[MMA]_0 = 0.60$ M. We acquired an aliquot after 1 h which showed full monomer conversion but left the reaction to stir for a full 24 h so that if the S_N2-type cyclization step was at all accessible, the step had plenty of time to execute (Figure 6.7). After 24 h, the reaction was quenched and isolated, then prepped for MALDI-TOF-MS analysis. The resulting polymer yielded a mass spectrum (Figure 6.6) with one set of peaks that correlated to $m/z = 100.19n + 438.7$, with 100.19 accounting for an MMA repeat unit and 438.7 accounting for an end group involving TPT^+ (297.4 Da), ES (140.2 Da) and a proton (1.0 Da). The fact that a Na^+ was not accounted for in the mass of the intercept implies that the TPT initiating group was still cationic after 24 h so it can be assumed that the commonly observed proton exchange, which yields a neutral enamine, is not operative here.[66,67] Although inconclusive, this experiment demonstrates that (in accordance with many other LPP studies) of vinyl monomers when an N-heterocyclic carbene (NHC) initiates LPP along the nucleophilic path, the NHC bond is rather strong and not readily susceptible to substitution reactions and ES is not an exception. We performed a similar experiment wherein ES was polymerized by tricyclohexyl phosphine (PCy_3) at an ES/MAD/PCy_3 ratio of 40/2/1 with $[ES]_0 = 0.60$ M in toluene and a full 24 h of stirring before quenching. Similarly, cationic PCy_3^+ end groups were exclusively found in the MALDI-TOF-MS spectrum as an intercept of $m/z = 281.4$ ($PCy_3^+ + H$) was detected (Figure E10).

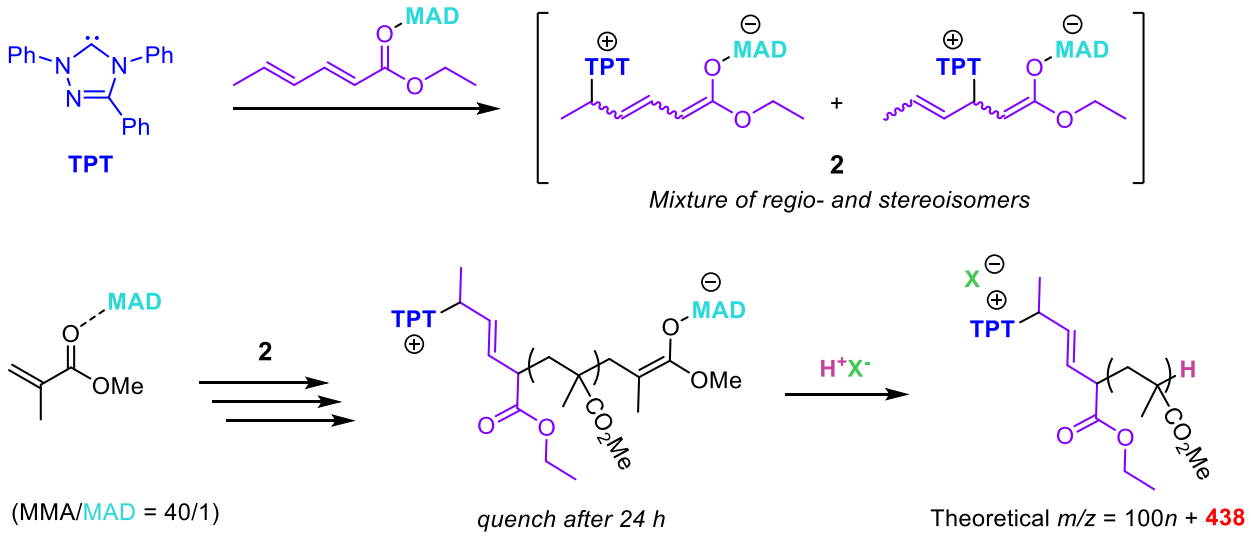

Figure 6.6. Investigation into the true nucleophilic path using the uniquely nucleophilic but less basic TPT

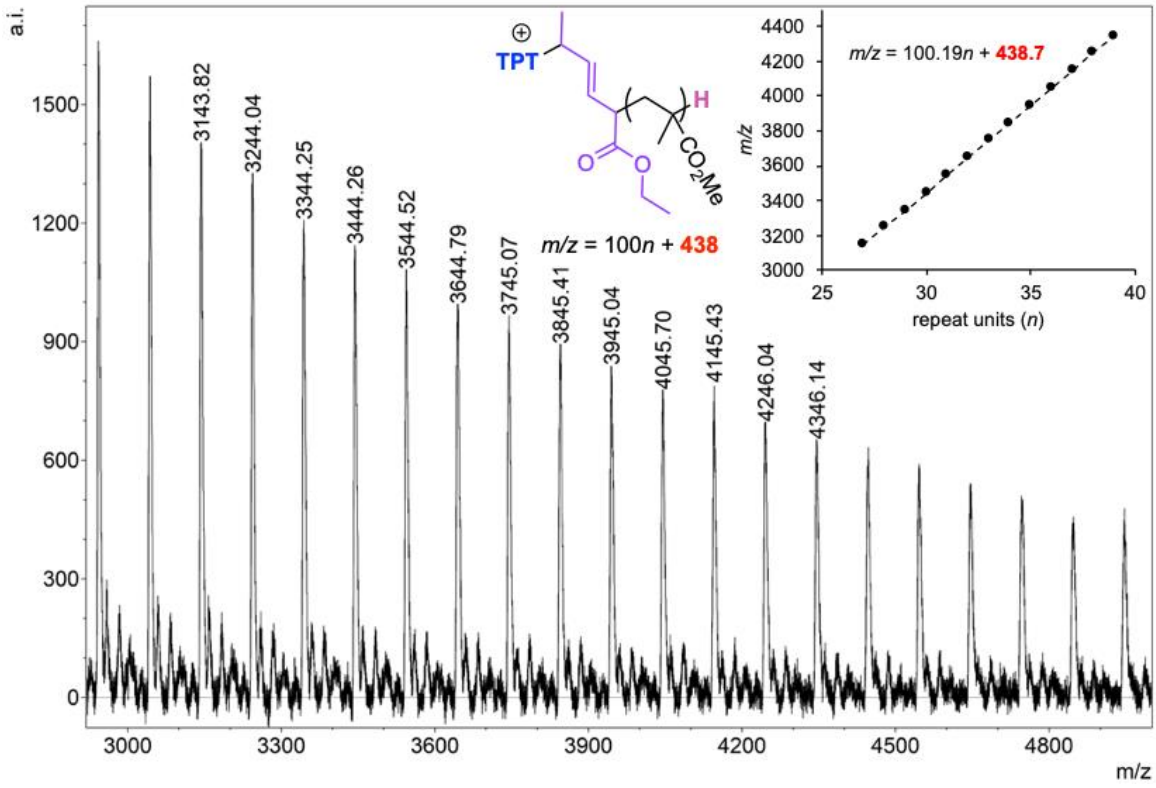

Figure 6.7. MALDI-TOF-MS Spectrum of linear PMMA (*l*-PMMA) initiated by species **2**, quenched after 24 h, showing one dominant set of peaks with an end group mass correlating to the expected mass of TPT, and ES unit, and a proton, supporting our claim that S_N2-type ring closure is improbable for the nucleophilic pathway. Shown chemical structures only represent one of several regiochemical possibilities.

6.2.3. Elucidating Mechanism of Ring Closure

Guided by the above-described results, we then formulated a few alternative hypotheses. First, if sorbate ion pair **1** initiated LPP by attack of monomer from either the nucleophilic γ or ε carbon of the enolate in **1**, there would be an alkene conjugated to the sorbate carbonyl which might act as an electrophile for eventual conjugate addition from the enolate at the opposite terminus. This hypothesis seems promising especially when considering the effect of MAD coordination to the conjugated sorbate unit providing additional activation. This hypothesis would yield a cyclic polymer bearing an enolate on the sorbate unit (Figure 6.8). We reasoned that this enolate might be detected if we quenched the reaction with a deuterated acid. Importantly, an ES LPP initiated by I^{t}Bu normally gives a set of MALDI-TOF-MS peaks with an intercept of m/z = 23 (the mass of just Na^+). The cyclic PES hypothetically generated by Takasu's original mechanism (Figure 6.2) would also have an intercept of m/z = 23. However, Takasu's S_N2 ring-closing step gives a neutral polymer that should not even react with the quenching acid. Therefore, when a deuterium is used as the acid quench, an intercept of m/z = 24 would be additional evidence that the S_N2 mechanism is improbable as it implies that the product interacts with the quenching medium and is thus basic, as well as a strong piece of evidence that the ring-closing step is indeed a conjugate addition since any other ring closing step would not result in a basic (enolate) product. We performed a LPP of ES at an ES/MAD/I^{t}Bu ratio of 40/2/1 with $[ES]_0$ = 0.60 M and gave a full 24 h for cyclization to occur. We then partitioned the reaction solution into two different vials. One of the vials was quenched with benzoic acid/MeOH, while the other was quenched with D_2O/MeOD. Both samples were analyzed by MALDI-TOF-MS. The sample quenched with benzoic acid/MeOH gave an intercept of m/z = 23 while the sample quenched with D_2O/MeOD gave an intercept of m/z = 24 (Figure 6.9), thus supporting our hypothesis.

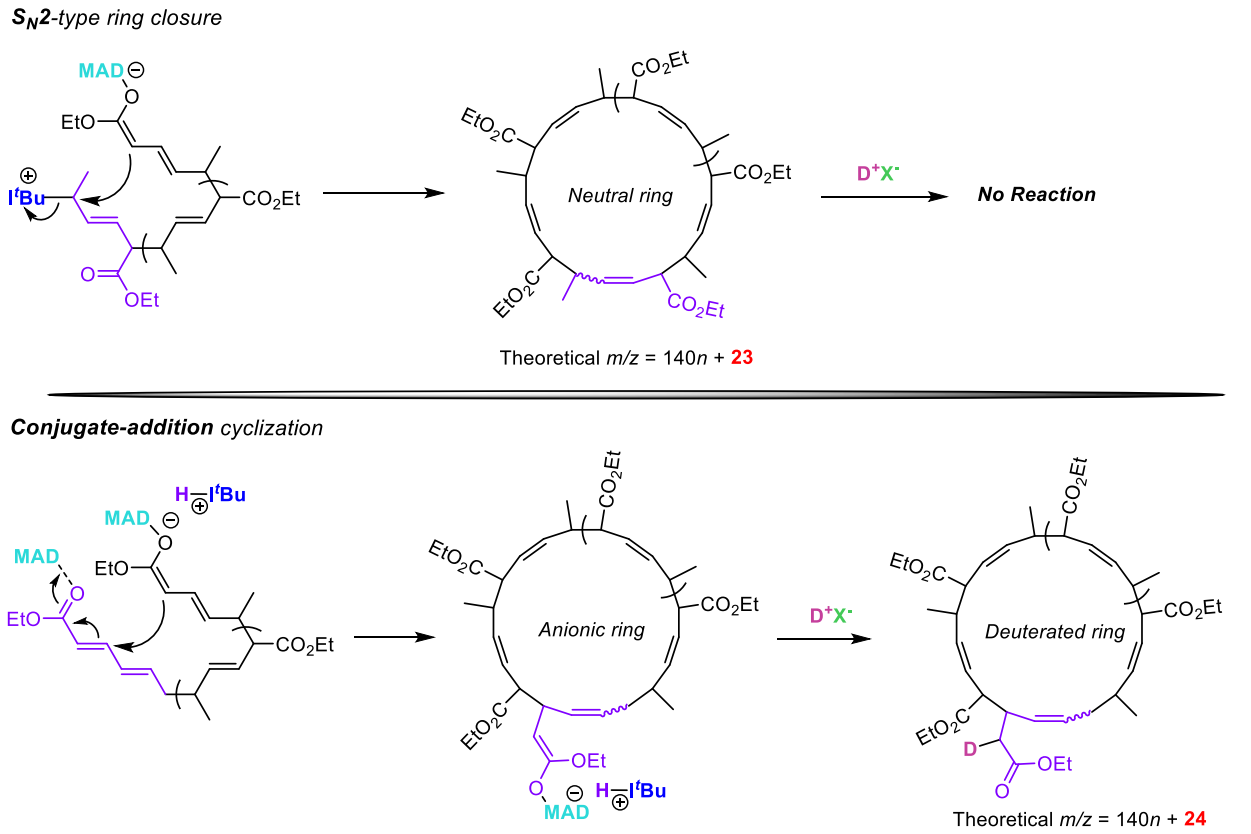

Figure 6.8. Deuterium labeling experiment used to determine the chemical nature of the post-cyclized product

While the conjugate addition mechanism in Figure 6.8 is viable if initiation is either γ- or ε-selective, we questioned whether the first addition is regioselective. Our work on the related crotonate system[60] and Waymouth's similar work[68] of the dimerization of crotonates was highly suggestive of α-addition, and several small molecule synthesis reports[69,70] also gave convincing evidence that the Li^+ enolate of alkyl sorbates yielded an α-addition product. Thus, it is reasonable to suspect a mixture of both ε- and α- initiation with the ε-initiated cyclic polymer accounted for within the current mechanism. Therefore, it is necessary for us to deal with the possibility of α-initiation which would render a pendant diene that is not conjugated to the carbonyl, thus preventing it from being a target for conjugate addition from the opposite enolaluminate terminus.

We then considered the possibility of an α-proton migration to the ε-carbon which would then put the diene into conjugation with the carbonyl.

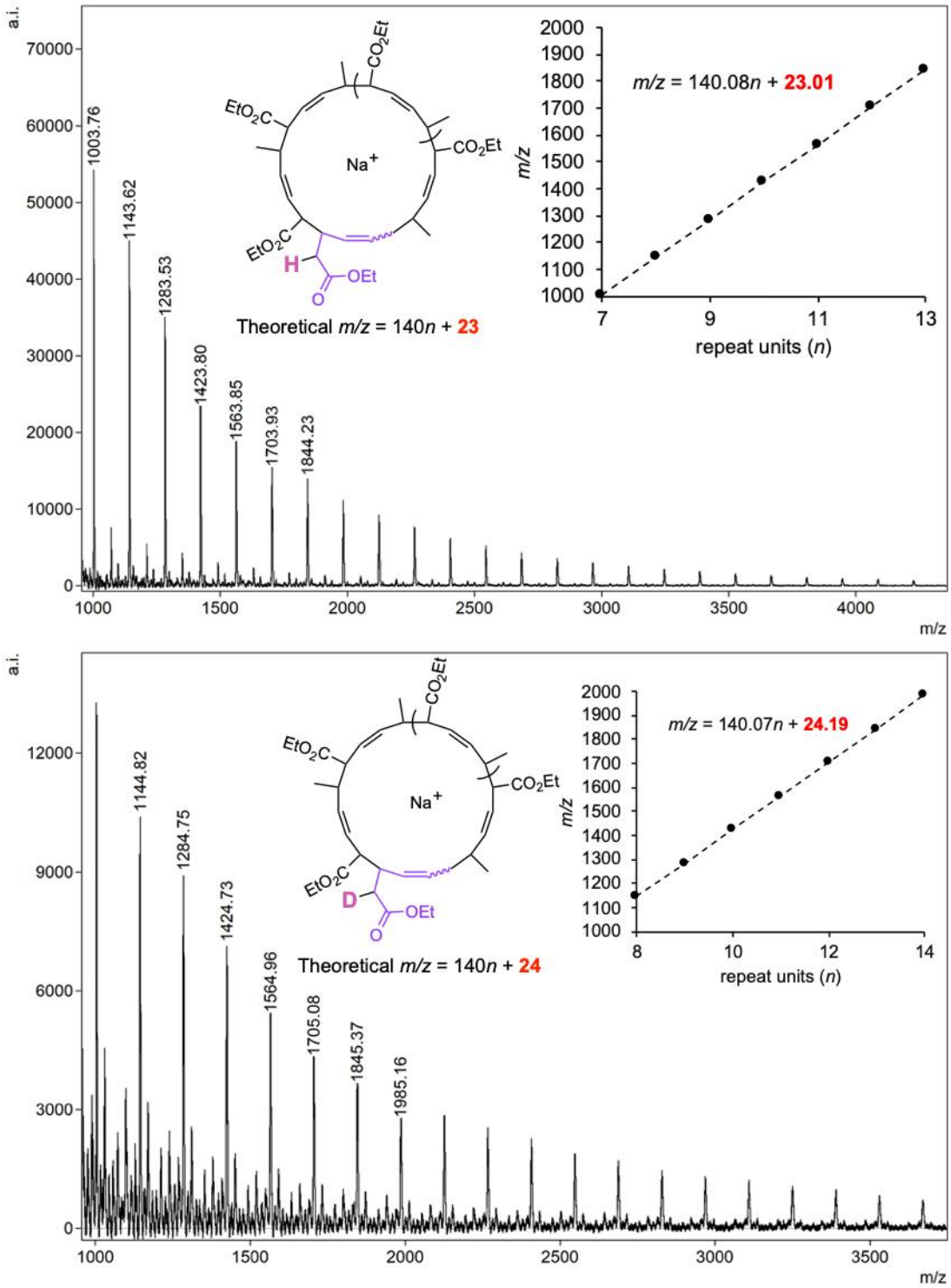

Figure 6.9. MALDI-TOF-MS spectra of presumably cyclic PES initiated by ion pair **1** and given 24 h to react before quenching by benzoic acid (top) and D_2O/MeOD (bottom) supporting the enolate product of ring-closure by conjugate addition. Shown chemical structures only represent one of several regiochemical possibilities.

We considered this possibility after recalling an observation in Waymouth's previous work[68] on the dimerization of crotonates, wherein a similar isomerization is observed (Figure 6.10). In this example, a terminal alkene is repositioned to into conjugation, presumably by a base-catalyzed proton exchange. Since the conjugated alkene is clearly thermodynamically favored over the terminal alkene due to conjugation, similar logic would suggest the sorbate analogue would be equally, if not more, disposed to this type of transformation if there is a path to overcome the energy barrier for such a proton exchange.

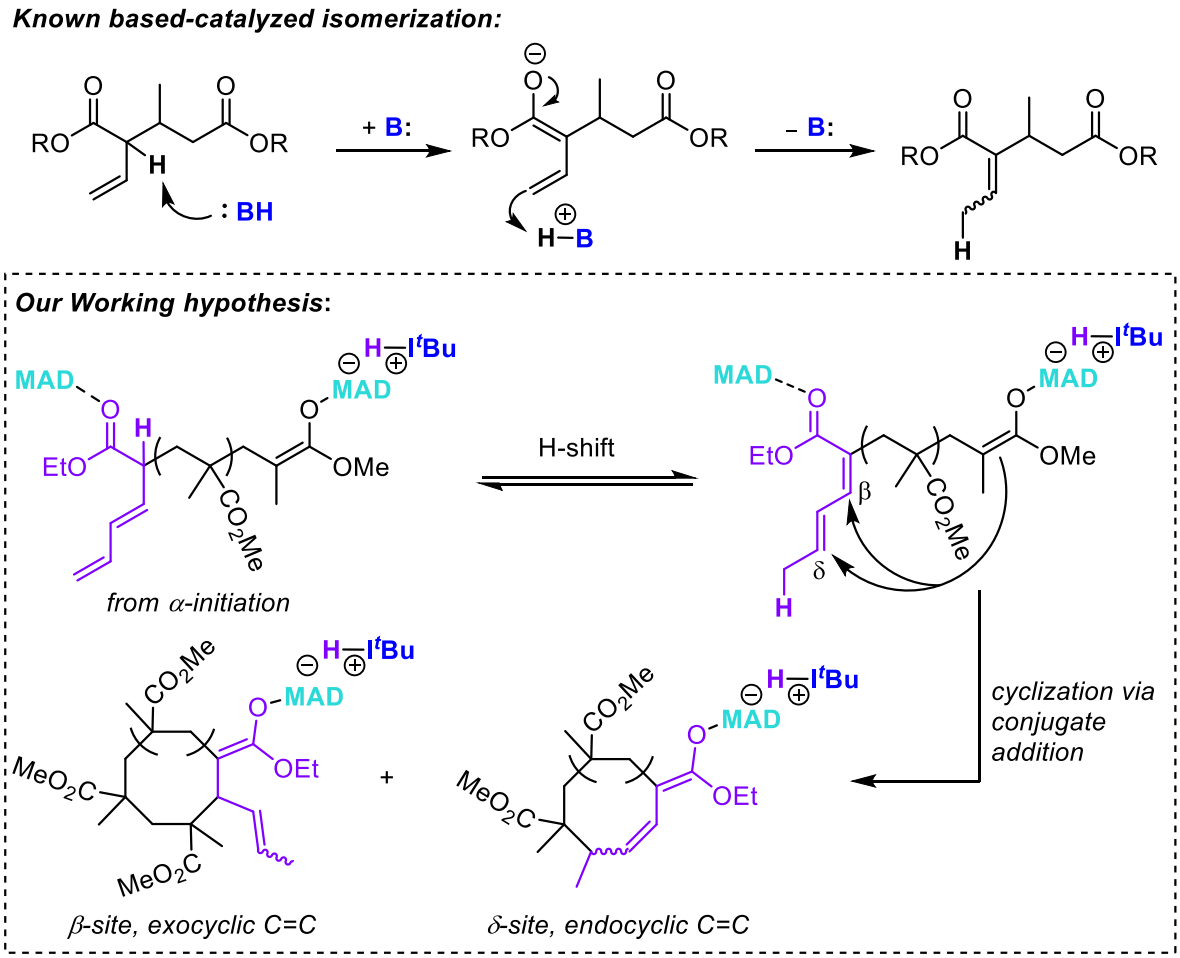

Figure 6.10. Necessary proton shifts required to reposition terminal alkenes into conjugation if α-initiation prevails

Accordingly, we designed an experiment to study the evolution of the alkenyl protons constituting the sorbate end group vs time. We set up a polymerization with an MMA/MAD/**1** molar ratio of 25/0.50/1.00 where $[MMA]_0$ = 0.45 M in toluene. We quenched half of the reaction at 1 min and found that the conversion was 99 %. The other half of the reaction was quenched at 24 h and interestingly the reaction was still at 99 % conversion, while a normal LPP at this point would have gone to completion. Our hypothesis here is that the residual 1 % of MMA is a result of competitive MAD coordination by the ester carbonyl on the sorbate initiating group which becomes prohibitively dominant once $[MMA]_t$ gets very low. More interesting is that at 1 min, there was an abundance of peaks in the alkenyl region (Figure 6.11, top; also see Figures E11 and E14). The pair of doublets at 5.05 and 5.2 ppm are indicative of terminal alkenyl protons since they have similar integration, different J-coupling constants, and both couple to the multiplet at 6.25 ppm on the HH-COSY (Figure E12). Thus, we can speculate that the presence of a terminal alkene is suggestive of either α- or γ- initiation but not ε. We might also speculate that these peaks represent an extent of the reaction before the proton exchange proposed in Figure 6.10 has occurred. After 24 h all of these peaks disappeared except for one clump of peaks at 5.4 ppm, in accordance with Takasu's data.[56] We then obtained MALDTI-TOF-MS spectra for both these samples and found the *m/z* trend to be identical at $m/z = 100n + 163$ (Figures E13 and E15). Thus, to account for the loss of unsaturation while maintaining the exact same molecular weight (Figure 6.11, bottom; Figures E11-E15), ring closure by conjugate addition seems the most reasonable.

Furthermore, we repeated the experiment but tracked the vinyl peaks over time, taking aliquots every few hours and could gradually observe the disappearance of vinyl peaks over the course of 24 h (Figure E11). The lack of any convincing new peaks led us to think that the proton exchange

intermediate is transient and quickly undergoes cyclization once it is formed. We interrogated the possibility of a LA-catalyzed proton shift by mixing a model small molecule, ethyl 2-(cyclohex-1-en-1-yl)butanoate, which should have considerable thermodynamic incentive to undergo proton shift by a similar path, with 10 mol% MAD in toluene but no proton shift was observed. Thus, our favorite hypothesis is a proton shift that involves cooperative effort from the LA and basic enolates (*vide infra*).

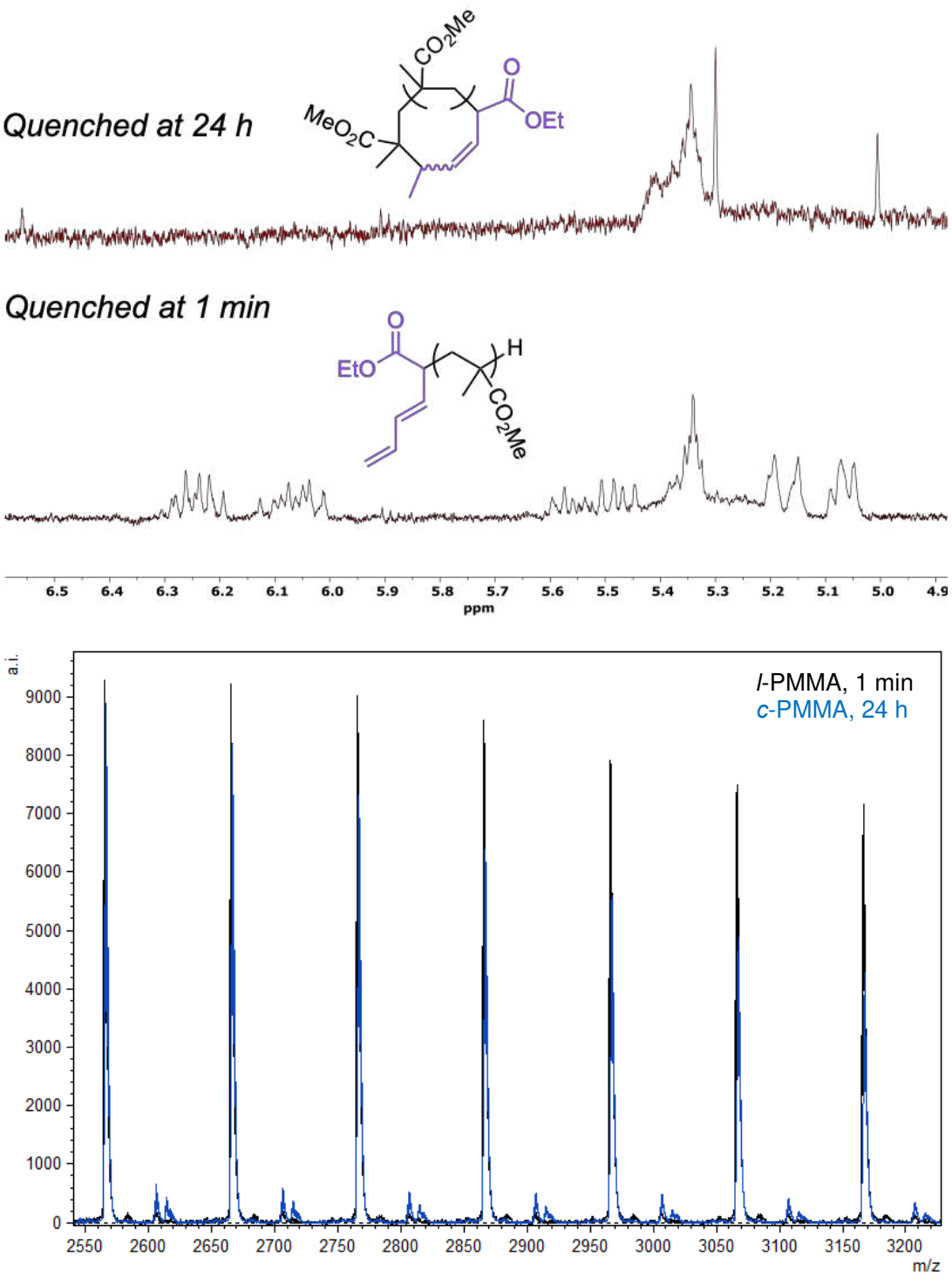

Figure 6.11. Top: ^{1}H NMR ($CDCl_3$) of isolated PMMA initiated by **1** quenched after 1 min and 24 h (both at 99 % conversion), expanded to the alkenyl region, showing the presence of many alkene peaks after 1 min and disappearance of those peaks after 24 h. Bottom: overlayed MALDI-TOF-MS spectra for *l*-PMMA quenched at 1 min and *c*-PMMA quenched after 24 h, showing nearly identical spectra for both polymers.

6.3 Considerations Regarding Spatial and Temporal control

We mentioned in our previous work[59,22] on this topic that many comparable cyclization strategies (especially those related to zwitterionic polymerization) contain an internal limitation in that the cyclization step will become competitive with propagation, thereby yielding cyclic polymers with broad molecular weight distributions. Our latest work seemed to overcome this limitation by providing cyclic di-BCPs of MMA and ^{n}BA with M_n up to 267 kg/mol and $Đ$ as low as 1.03.[22] It is now quite clear that this exquisite control is the consequence of a temporal control (i.e., when cyclization occurs) that arises from the necessity for LA activation during the proton transfer/cyclization steps. When there is a considerable amount of free monomer present in the system, the monomer will outcompete the sorbate terminus for control over the LA and thus propagation will continue. Only when monomer is depleted (or near depletion) can the sorbate terminus begin to control the LA. Thus, the cyclization step must wait for propagation to finish before it becomes appreciable. One caveat here is that the ES sorbate **1** might not be the optimal initiator for obtaining temporal control. Since MMA is a weak donor and its coordination to MAD is less competitive than most monomers,[22] it is not unreasonable to suspect the sorbate terminus will become active for cyclization earlier than expected, thus generating some broadening of $Đ$. To test this limit, the LPP at a high MMA/MAD/**1** ratio of 2000/10/1 and $[MMA]_0$ = 0.45 M in toluene led to PMMA with M_n = 201 kg/mol and $Đ$ = 1.61. After 24 h, the reaction remained at 98.6 % conversion, suggesting that cyclization occurred with some monomer still present. To optimize temporal control and thus reclaim narrow $Đ$ during high MMA ratio polymerizations, it might be necessary to further tune the sorbate molecule (perhaps by tuning the sterics of the ester). On the other hand, optimal temporal control can be achieved by copolymerizing MMA with ^{n}BA.[22]

The mechanism by which spatial control (i.e., where cyclization takes place) is achieved by the MAD/I^{t}Bu/sorbate system is more subtle to explain. It would be convenient if the zwitterionic mechanism by nucleophilic initiation could be invoked, which would give the termini electrostatic attraction and put the electrophilic carbon in line with the leaving I^{t}Bu$^+$ to guide the point of attack by the terminal enolate (Figure 6.2). However, since we must now consider the revised ion-pair mechanism, the spatial control arises from conjugate addition of the terminal enolate to the initiating sorbate terminus (Figure 6.10) at the δ-site (*vide infra*). A possible side reaction of this preferential intramolecular addition (ring-closing) is intermolecular addition (linear chain coupling). The intermolecular chain coupling product (most likely followed up by another ring-closure) can be ascertained by MALDI-TOF-MS and can be seen in Figure 6.11 (the small set of peaks near the baseline that appeared in the *c*-PMMA spectrum) according to $m/z = 100n + 303$ (Figure E15; y-intercept corresponds to ES + ES + Na$^+$), but this side product seems quite negligible for polymerizations ran even at a relatively high concentration of $[MMA]_0 = 0.45$ M.

6.4 Achieving Spatiotemporal Cyclization Beyond Sorbates

In light of these new mechanistic insights, we decided to revisit our aforementioned crotonate chemistry to investigate whether similar structure and reactivity of crotonates with respect to sorbates would render a similar cyclization pathway. Previously, we showed that the homopolymerization of crotonates by MAD/I^{t}Bu produced linear polymers with a vinyl chain end due to the acidic protons on the γ-methyl which render the homopolymerization more predisposed to chain transfer.[60] However, if the discretely synthesized crotonate ion pair **3** is used to initiate polymerization of methacrylates, then the deprotonative chain transfer is no longer available, thus preserving the potential for a ring-closing step analogous to the sorbate system. Guided by this hypothesis, we isolated ion pair **3** and concluded based on ^{1}H NMR characterization that it was a

fairly even mixture of geometric isomers based on the asymmetric enolate alkene (Figure E9). Our previous study provided evidence that **3** initiates from the α- carbon of the enolate giving a polymer with a vinyl end group.[60] Thus, a similar proton shift would be needed to move the terminal alkene into conjugation with the crotonate carbonyl before cyclization can take place (Figure 6.12).

With the above hypotheses formulated, we attempted MMA polymerization by applying an MMA/MAD/**3** ratio of 25/0.50/1.0 with $[MMA]_0$ = 0.87 M in toluene. This reaction was partitioned into two equal volume reactors, with one of the reactors being completely quenched after 1 min. This quenched polymer was isolated and characterized by ^{1}H NMR and HH COSY to define the vinyl end group peaks (~5.2 ppm and ~5.7-5.9 ppm in $CDCl_3$). Meanwhile, the unquenched reactor was monitored vs time via ^{1}H NMR to track the disappearance of the vinyl end groups (Figure 6.13).

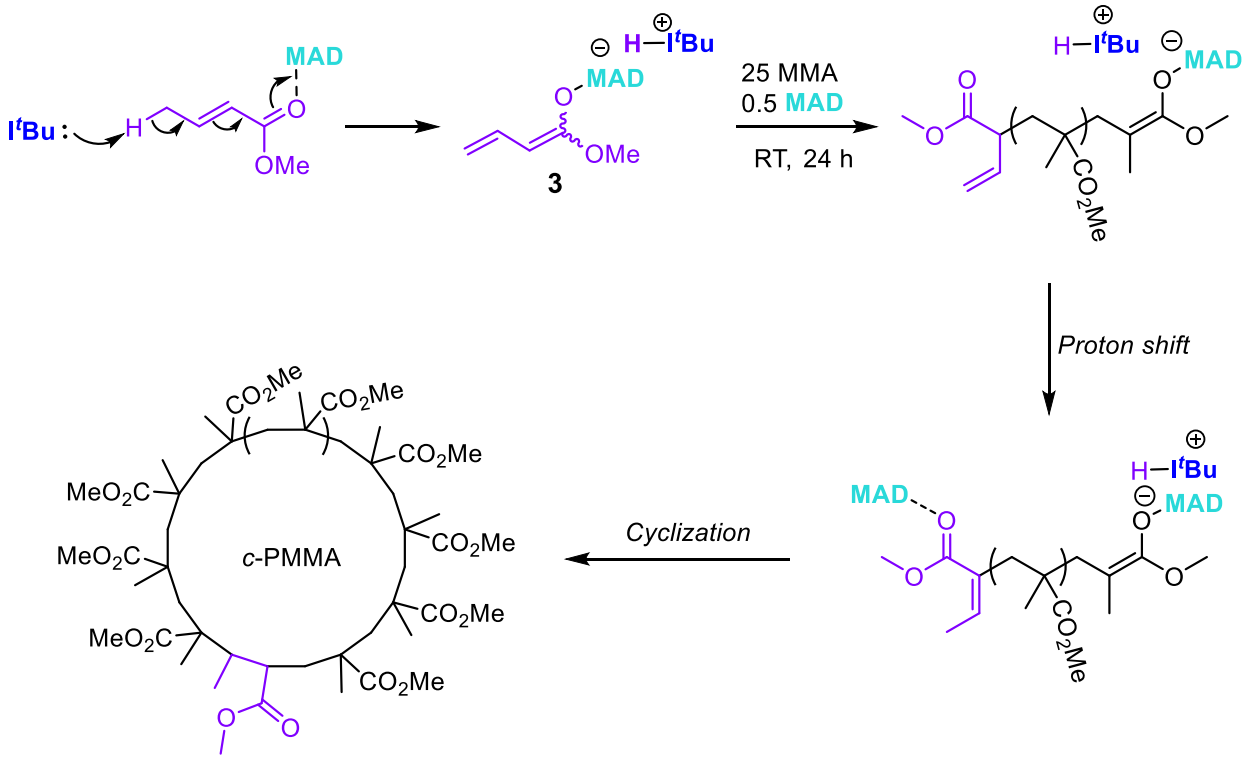

Figure 6.12. Proposed route to *c*-PMMA by crotonate ion pair 3, involving a proton shift which generates a conjugated ester followed by cyclization via conjugate addition

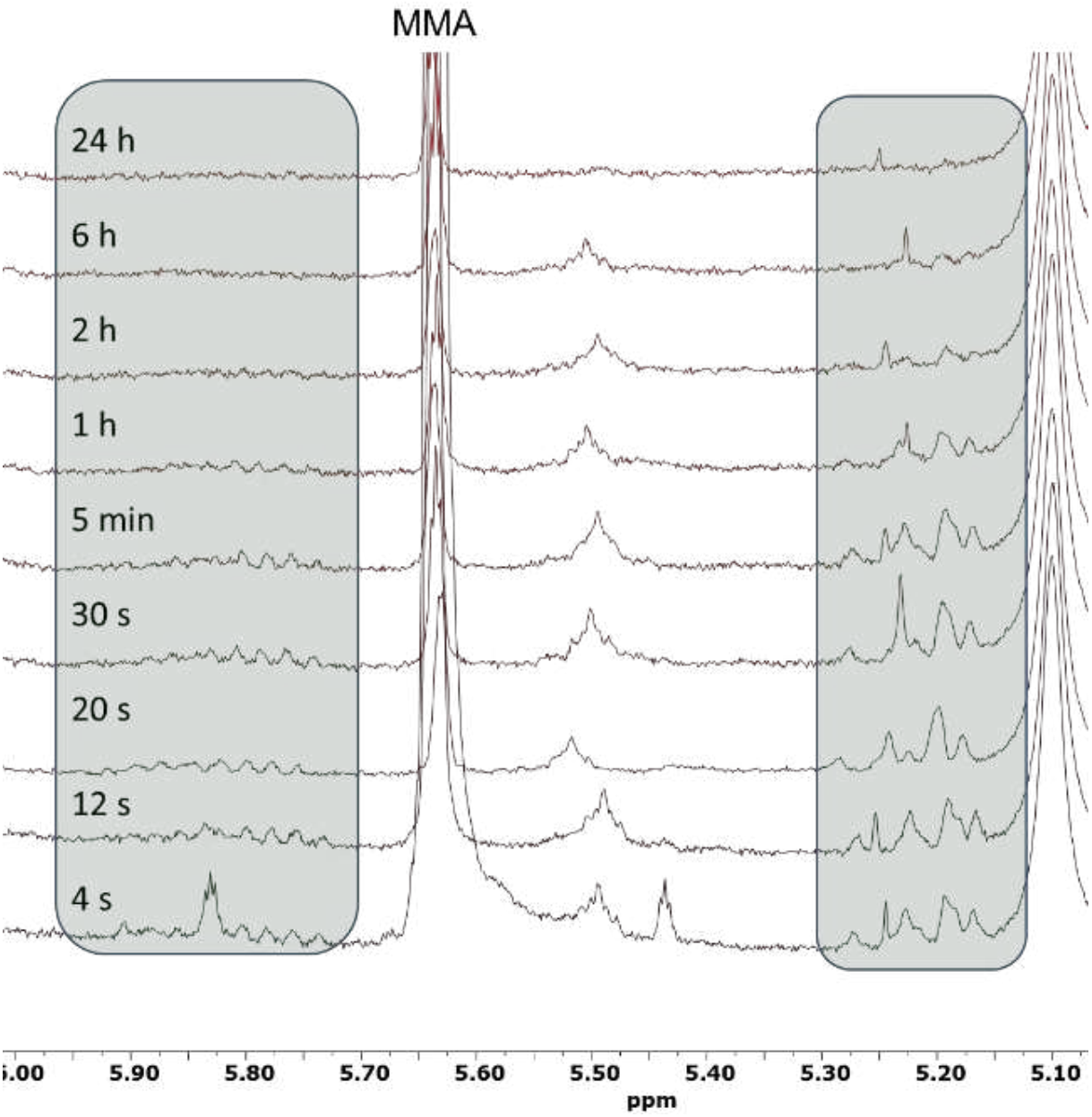

Figure 6.13. ^{1}H NMR ($CDCl_3$) of the MMA polymerization by **3** at various time points, showing gradual disappearance of vinyl end groups over time, indicating ring-closing.

As expected, the vinyl peaks disappeared over time and vanished after 24 h. This is consistent with the mechanistic scenario outlined in Figure 6.12 and strikingly similar to the analogous experiment performed by the sorbate ion pair **1**. Another important clue here is that the MMA was never

completely consumed but concluded at 98.6 % conversion after 24 h. Again, this contrasts drastically from a typical LPP of methacrylates to linear polymers wherein monomer will generally convert quantitatively. The incomplete monomer conversion is highly indicative of a scenario such as that shown in Figure 6.12, where the conjugated product following the proton shift has a stronger affinity for MAD relative to MMA. Thus, at low monomer concentrations, the conjugated crotonate end group outcompetes the residual MMA for MAD coordination and propagation stops shy of full conversion as a consequence.

To confirm that **3** does indeed produce cyclic polymers, we substituted allyl methacrylate (AMA) for MMA and performed a polymerization using a ratio AMA/MAD/**3** = 200/2/1 with $[AMA]_0$ = 0.45 M in toluene and gave 24 h of reaction time to produce cyclic PAMA (*c*-PAMA) with M_n = 45.3 kg/mol and $Đ$ = 1.08. The isolated *c*-PAMA was subjected to post-functionalization by the thiol-ene click reaction using 1-ODT as the substrate to quantitatively convert the allyl pendant groups into long alkyl chains, affording grafted *c*-PAMA (*c*-$PAMA_g$, theoretical M_n = 148 kg/mol), which might make the ring polymers large enough to be directly observable by TEM. To our satisfaction, we directly observed the cyclic structures by TEM and obtained several example images of *c*-$PAMA_g$ (Figure 6.14; see also Figures E24-E26), strongly supporting our conclusion that crotonates, like sorbates, are capable of spatio-temporally controlled macrocyclization via a proton transfer/conjugate addition mechanism.

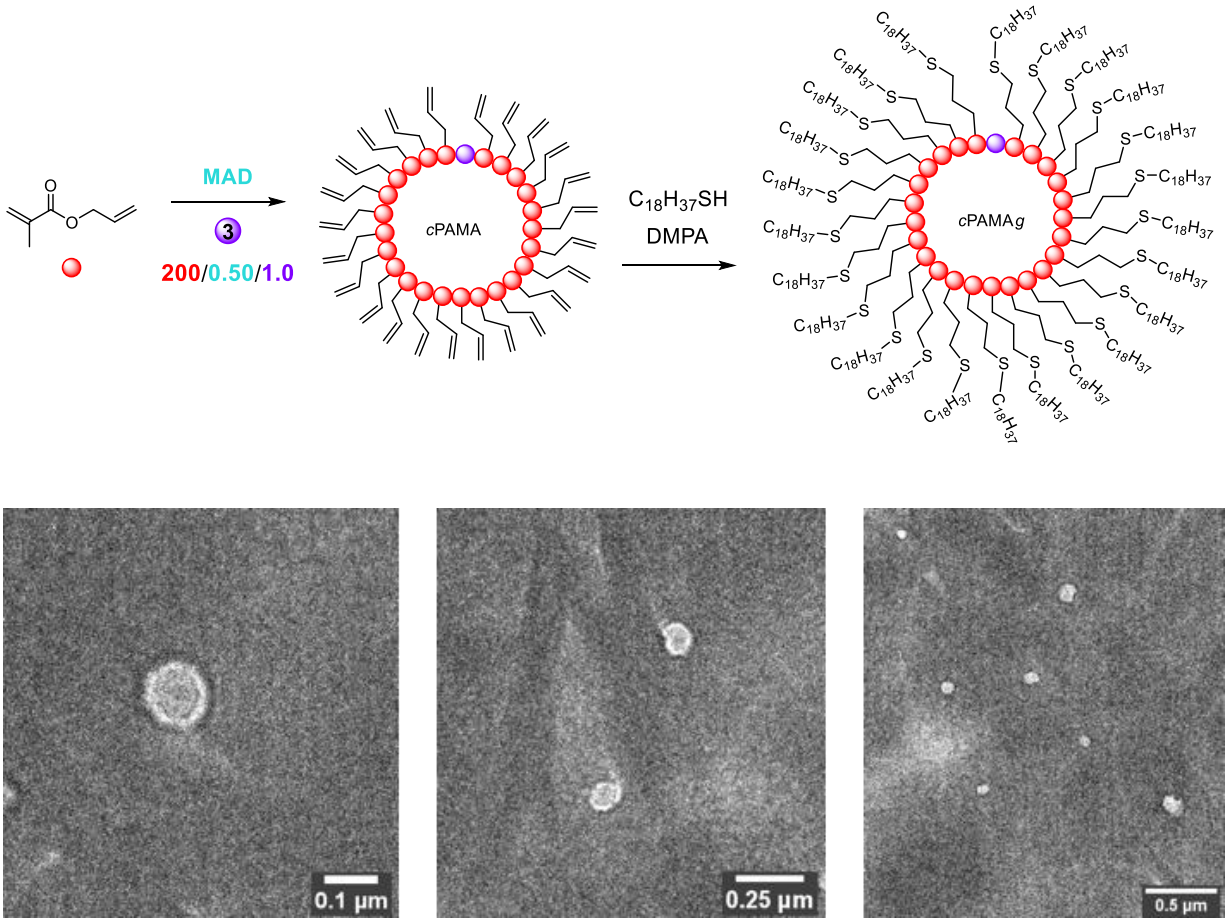

Figure 6.14. Synthesis of *c*-PAMA$_g$ and corresponding TEM images of the resulting cyclic polymers showing singular and clustered cyclic polymers that average 100 nm in diameter.

6.5 Understanding Active Species Generation, Chain Initiation, and Cyclization by a Density Functional Theory (DFT) Study.

6.5.1. Generation of Active Species

As discussed in the previous sections, the nature of LB (i.e., I^{t}Bu vs. TPT) employed in the polymerization allows different mechanistic pathways (i.e., basic vs. nucleophilic pathway) to proceed in the polymerization of MMA by the LB/sorbate/MAD system. To assist the DFT discussion, Figure 6.15 compares the basic pathway, which involves the abstraction of an ε-methyl proton of the activated MS by the LB to generate the corresponding ion pair *active species*, with

the nucleophilic pathway that proceeds through conjugate addition of the LB to the δ (or β) carbon of the MS·MAD adduct to form the corresponding zwitterionic active species. As showed in Figure 6.15, for the sterically hindered, strong base I^{t}Bu, the basic pathway is kinetically favored over the nucleophilic pathway, judged by a 2.4 kcal/mol lower kinetic barrier [16.6 vs. 19.0 kcal/mol transition state (TS) energy]. On the other hand, the nucleophilic addition product, the zwitterionic species, is thermodynamically favored by 2.5 kcal/mol with respect to the ion pair, afforded via the basic pathway (-5.7 vs. -3.2 kcal/mol product energy). Nevertheless, the key competition occurs at the TS level since, once the active species is generated, it will quickly react with the MMA present in abundance in the reaction environment, shifting the reaction towards the overall downhill chain growth to form thermodynamically stable polymer products (*vide infra*). Moreover, experimental evidence implies that this deprotonation is irreversible.

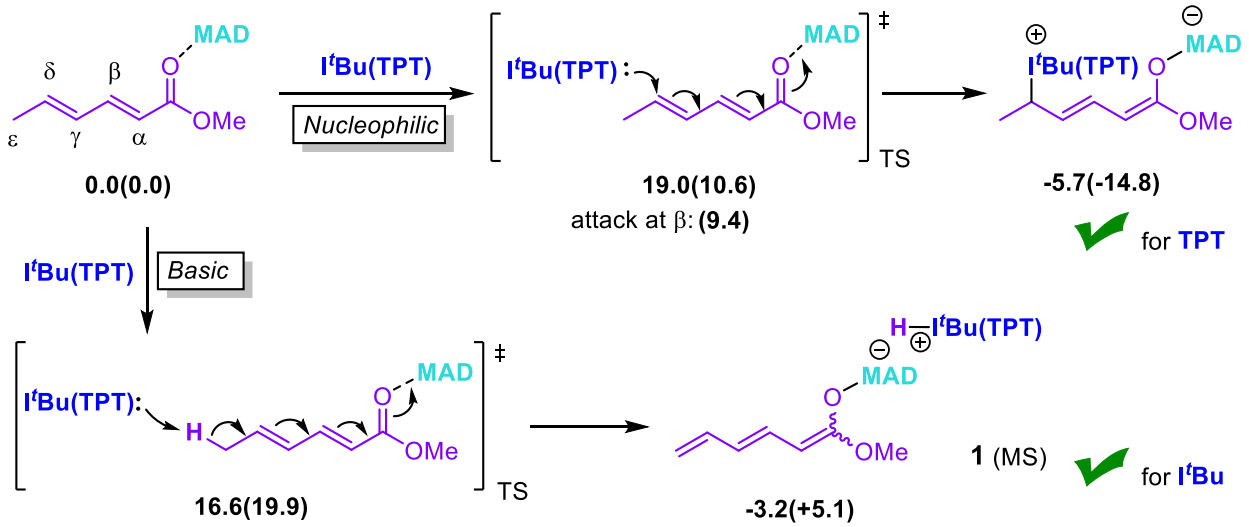

Figure 6.15. Energetic profiles of basic vs nucleophilic pathway in generation of active species as a function of LB. Free energies reported in toluene and kcal/mol

In contrast, in the case of the uniquely nucleophilic but less basic TPT, the preferred reaction pathway is reversed, resulting in an inversion of selectivity. In fact, the nucleophilic addition is now almost 10 kcal/mol more favored than the proton abstraction barrier (10.6 vs. 19.9 kcal/mol

TS energy). This strong kinetic preference for the nucleophilic pathway by TPT is also synergistically coupled with its resulting zwitterionic species being thermodynamically favored by almost 20 kcal/mol relative to the basic pathway product, thus ruling out the basic pathway for TPT (-14.8 vs. +5.1 kcal/mol product energy). These DFT results on the opposite selectivity between I^{t}Bu and TPT for the active species generation step are consistent with, and provide a better understanding of, the above described, experimentally observed selectivity inversion.

6.5.2. Regioselectivity of Initiation

Focusing on the kinetically favored basic pathway by I^{t}Bu, the system that actually produces the cyclic polymer, we examined the next fundamental step of the polymerization reaction, which is the *monomer initiation* to generate the propagating enolate species that undergoes repeated conjugate addition in the chain propagation cycle. In this monomer (MMA) initiation step involving nucleophilic addition of the sorbate enolate **1** (MS) to the MMA·MAD adduct, three possible *regioselectivity* scenarios must be considered (Figure 6.16): the nucleophilic attack of the MMA·MAD adduct by the α, γ, and ε-carbon sites of enolate **1**.

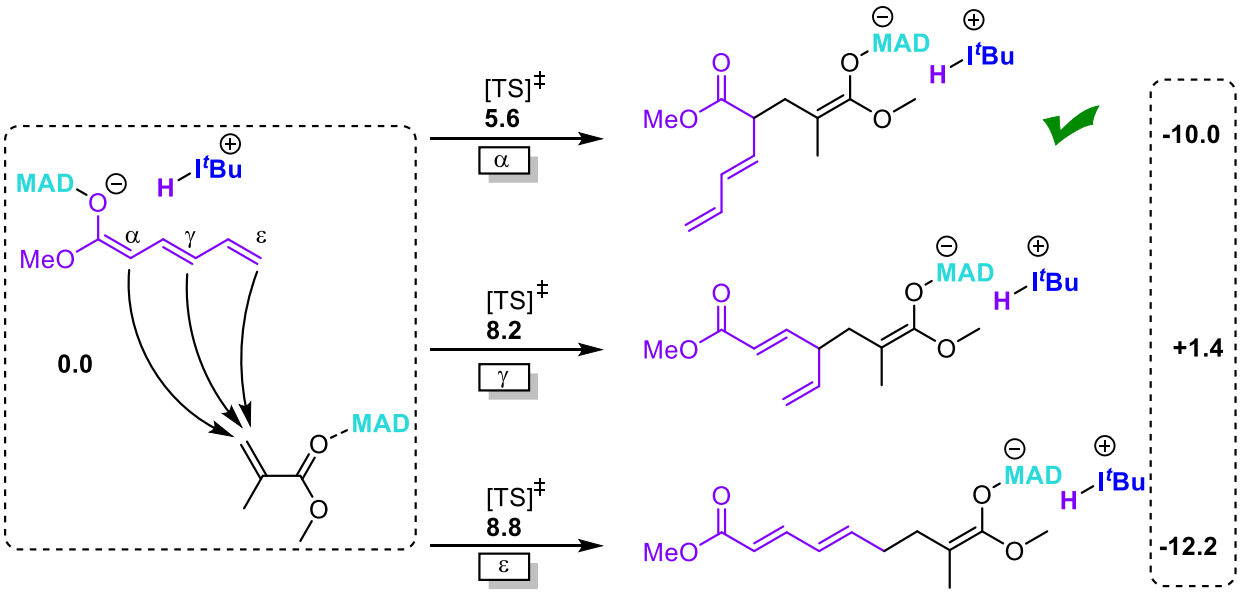

Figure 6.16. Regioselectivity considerations for the monomer initiation step to generate the propagating enolate. Free energies reported in toluene and kcal/mol

From a kinetic standpoint, both γ and ε-site attacks need to overcome a relative energy barrier of 8-9 kcal/mol with the ε-carbon addition product being thermodynamically much more favored (by more than 10 kcal/mol). However, the α-site attack is clearly kinetically controlled with a relative energy barrier of only 5.6 kcal/mol, about 3 kcal/mol lower than the other two pathways. In addition, the α-selectivity also produces the initiated MMA enolate propagation species with good stability, 10 kcal/mol lower in energy with respect to the ion pair and the MMA·MAD adduct considered at infinite distance (Figure 6.16). However, the above computed initiation regioselectivity brought about an intriguing question: since the preferred α-selectivity generates the active propagating species that contains neither the conjugated Michael acceptor terminus (*c.f.*, Figure 6.16) required for cyclization via conjugate addition ring closure nor a leaving group required for S_N2 type ring-closure, how does the cyclization actually take place to form the cyclic polymer?

6.5.3. Mechanism of Cyclization

To address this question while avoiding complex conformation issues when modeling the cyclization step of the favored "α-initiated" growing chain, we computed this step by using two separated fragments simulating the two chain ends, the same approach we had used in our previous work.[67] One fragment in Figure 6.17 represents the initiation chain-end with the methyl group at the α-carbon simulating the polymer chain, and the other fragment is the ion pair formed by the protonated LB and the anionic chain end representing the last enchained MMA unit. To generate the diene conjugated with the ester carbonyl (i.e., the Michael acceptor), we considered a proton transfer from the α-carbon to the ε-carbon of the sorbate chain end fragment. Since the direct 1,6-H transfer requires an energy barrier of 26.4 kcal/mol, which is much higher than those required in the other steps of the scenarios considered, we focused on a two-step pathway involving the anionic chain end fragment. At first, the proton at the α-carbon transfers from the initiation fragment to the α-carbon of the enolate fragment, forming an anionic sorbate unit paired with the positively charged $[I^tBu\text{-}H]^+$ moiety and a neutral MMA-MAD chain-end. Next, a further H-transfer from the α-carbon of the neutral fragment to the ε-carbon of the anionic sorbate unit leads to a new conjugated Michael acceptor terminus (Figure 6.17).

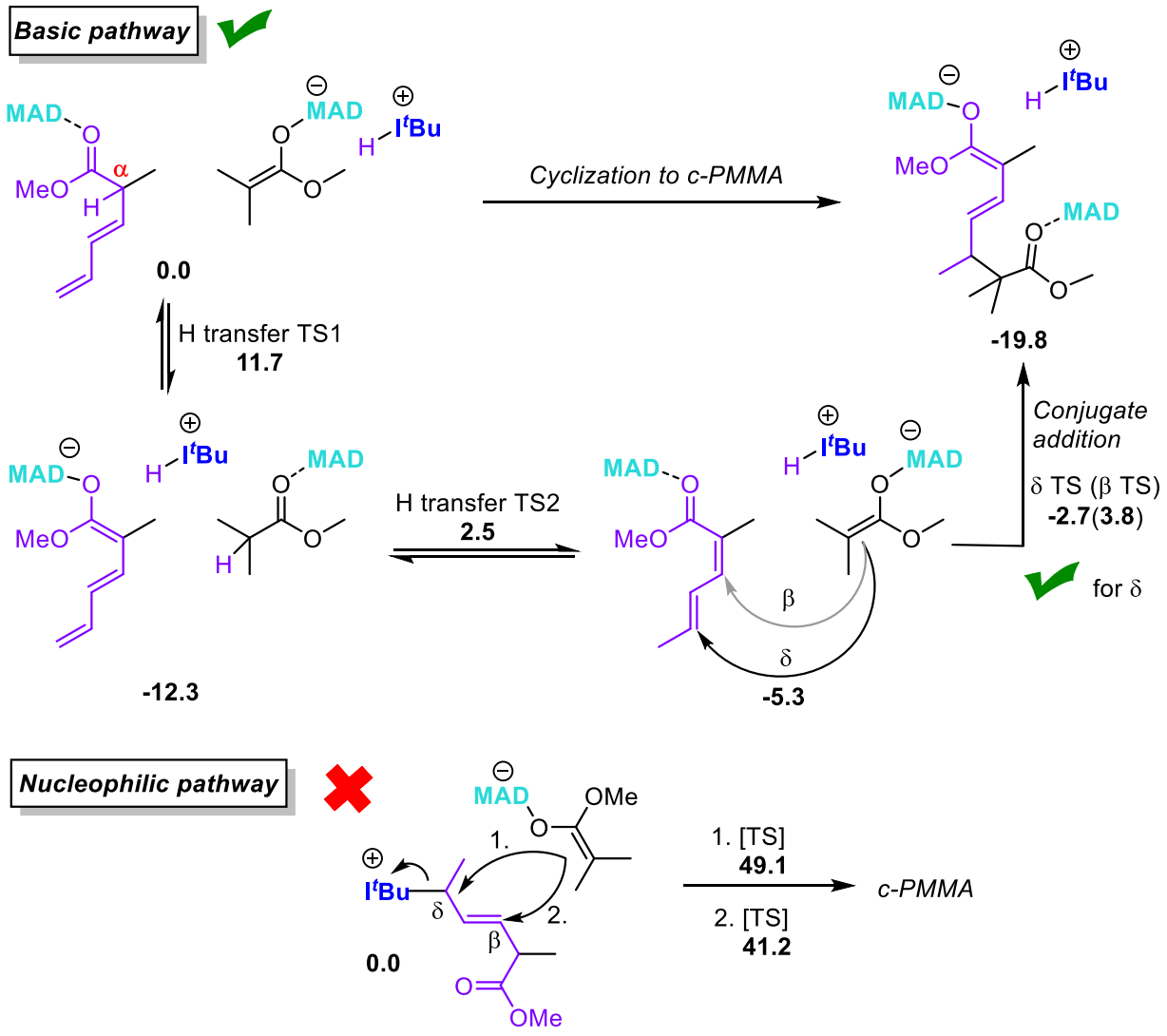

Figure 6.17. Cyclization considerations for the ring-closure step leading to the cyclic polymer formation. Free energies reported in toluene and kcal/mol

The energies reported in Figure 6.17 indicate the H-transfer steps as energetically feasible, requiring ~12 and ~15 kcal/mol for the first and the second step, respectively, with the transient intermediate and the final isomerization conjugate product being ~12 and ~5 kcal/mol more stable than the starting species, respectively. Noteworthy here is that the barrier of 12-15 kcal/mol for H-transfer is considerably higher than the propagation step (5-8 kcal/mol); thus, these events that lead to cyclization have to wait until essentially all monomer is consumed, thus the temporal control of cyclization. The final cyclization step involving the conjugate addition to the δ-carbon

is almost 7 kcal/mol more kinetically favored than the one involving the β-carbon, leading to a strong kinetic selectivity towards the formation of the *c*-PMMA with an endocyclic double bond, consistent with the above-described experimental result. The overall reaction is about 20 kcal/mol downhill relative to the starting species, providing a strong thermodynamic driving force for the ring closure. It is worth noting that the cyclization scenarios computed along the nucleophilic pathway occurring via S_N2 type ring-closure by back-biting attack of the enolate chain end at either the δ- or β-carbon of the sorbate unit, with concomitant elimination of I^{t}Bu, are considered as energetically inaccessible, with energy barriers higher than 49 or 41 kcal/mol (Figure 6.17).

6.6 Conclusions

Key takeaways and conclusions drawn from the herein combined experimental and theoretical study towards establishing the highly demanding spatial and temporal control for the precision synthesis of cyclic polymers with predictable M_n and low $Đ$ values as well as high structural fidelity by the LPP methodology, here represented by a prototype system comprising [LB (I^{t}Bu, TPT) + LA (MAD) + substrate (sorbates, crotonates, methacrylates)], are summarized as follows:

(1) For the *active species generation step*, the nature of the LB determines the mechanistic pathway by which the LPP operates on monomers and thus ultimately the topology of the resulting polymers. While the steric hindered, strong base I^{t}Bu activates the sorbate·LA adduct via proton abstraction (i.e., basic pathway) to produce the corresponding ion pair propagating species that lead to formation of cyclic polymers, the uniquely nucleophilic but less basic TPT proceeds with conjugate addition to the activated monomer (i.e., nucleophilic pathway) to afford the corresponding zwitterionic species that only lead to linear polymer formation.

(2) For the *monomer initiation* step along the cyclic-polymer-forming basic pathway to generate the ion-pair propagating species, the regioselectivity is confirmed to be the unanticipated attack from the α-site of the sorbate enolate to generate an unconjugated terminus, rather than the attacks from γ and ε-carbon sites of the enolate that would afford the conjugated terminus. The surprise here is largely due to the follow-up question of how the subsequent cyclization could occur since the α-initiated terminus contains neither the conjugated Michael acceptor terminus required for cyclization via conjugate-addition ring closure, nor a leaving group required for S_N2 type ring-closure.

(3) The *cyclization* step to form cyclic polymers is also surprising and counterintuitive. The preferred α-selectivity during chain initiation leads to the active propagating species that contains no apparent structural motifs typically thought to be required for ring-closing events. Hence, the realization of isomerization of the non-conjugated initiating terminus to the conjugated one via a two-step H-transfer is significant in twofold. First, this process provides the suitable motif for cyclization to occur and complete ring-closure. Second, the considerably higher energy barrier for the isomerization than the chain propagation encourages temporal control of cyclization, that is, it does not occur until after essentially all monomers have been consumed. Convincing lines of combined experimental and theoretical evidence also show that the nucleophilic pathway does not lead to cyclic polymers because the S_N2 type ring-closure proposed in literature are considered as energetically inaccessible, with energy barriers higher than 41 kcal/mol.

(4) The LPP methodology is uniquely equipped for achieving spatiotemporal control in the precision cyclic polymer synthesis, which has been realized with the successful synthesis of well-defined cyclic homopolymers such as *c*-PES and *c*-PMMA, as well as cyclic BCP P^{n}BA-*b*-PMMA with M_n up to 267 kDa and $Đ$ as narrow as 1.03. The key features of LPP that enabled such

exquisite control include CSC, selective K_{eq} binding of the LA to specific sites for activation to trigger programmable chemical events, and largely differentiated kinetic barriers between chain propagation and cyclization, thus allowing the polymerization to achieve essentially full monomer conversion and only then execute the cyclization event to occur at the specific site of the chain. Overall, the discrete, individual roles of the LA and LB, as well as their synergy and cooperativity, are essential for the successful implementation of LPP for precision cyclic polymer synthesis.

(5) A mechanistic understanding of LPP for precision cyclic polymer synthesis enabled us to expand the built-in initiating/ring-closing moiety from sorbates to crotonates. However, under high monomer to initiator ratio conditions, for both sorbate and crotonate cases the polymerization of MMA (i.e., a monomer with weak binding to the LA MAD) stops at ~99 % monomer conversion, a result of the isomerized conjugated sorbate or crotonate initiating terminus that outcompetes the residual MMA for MAD coordination. These results suggest that cyclization occurred with a trace amount of monomer still present, shy of the ideal, complete MMA conversion.

The above discussed complex dynamics of this polymerization system point to the need for continued study that aims to optimize temporal control under high monomer loading conditions for weakly LA-binding monomers, investigates the effects of sorbate and crotonate structures (by tuning the sterics and electronics of the ester) and LA structures (by tuning the differential binding between monomer and the initiating terminus) on the temporal control, and explores other monomer classes. Research along these lines is underway.

References cited in Chapter 6

[1] Haque, F. M.; Grayson, S. M. The synthesis, properties and potential applications of cyclic polymers. *Nat. Chem.* **2020**, *12*, 433-444.

[2] Liénard, R.; Winter, J. D.; Coulembier, O. Cyclic polymers: Advances in their synthesis, properties, and biomedical applications. *J. Polym Sci.* **2020**, *58*,1481–1502.

[3] Laurent, B. A.; Grayson, S. M. Synthetic approaches for the preparation of cyclic polymers. *Chem. Soc. Rev.* **2009**, *38*, 2202–2213.

[4] Wang, T.-W. & Golder, M. R. Advancing macromolecular hoop construction: recent developments in synthetic cyclic polymer chemistry. *Polym. Chem.* **2021**, *12*, 958-969.

[5] Tu, X.-Y.; Liu, M.-Z.; Wei, H. Recent progress on cyclic polymers: Synthesis, bioproperties, and biomedical applications. *J. Polym. Sci. A Polym. Chem.* **2016**, *54*, 1447–1458.

[6] Jia, Z.; Monteiro, M. J. Cyclic Polymers: Methods and Strategies. *J. Polym. Sci. A Polym. Chem.* **2012**, *50*, 2085-2097.

[7] Endo, K. Synthesis and Properties of Cyclic Polymers. *Adv. Polym. Sci.* **2008**, *217*, 121-183.

[8] Kricheldorf, H. R. Cyclic polymers: Synthetic strategies and physical properties. *J. Polym. Sci., Part A: Polym. Chem.* **2010**, *48*, 251−284.

[9] Josse, T.; De Winter, J.; Gerbaux, P.; Coulembier, O. Cyclic Polymers by Ring-Closure Strategies. *Angew. Chem. Int. Ed.* **2016**, *55*, 13944-13958.

[10] Brown, H. A.; Waymouth, R. M. Zwitterionic Ring-Opening Polymerization for the Synthesis of High Molecular Weight Cyclic Polymers. *Acc. Chem. Res.* **2013**, *46*, 2585−2596.

[11] Culkin, D. A.; Jeong, W.; Csihony, S.; Gomez, E. D.; Balsara, N. P.; Hedrick, J. L.; Waymouth, R. M. Zwitterionic Polymerization of Lactide to Cyclic Poly(Lactide) by Using N-Heterocyclic Carbene Organocatalysts. *Angew. Chem., Int. Ed.* **2007**, *46*, 2627−2630.

[12] Shi, C.; McGraw, M. L.; Li, Z.-C.; Cavallo, L.; Falivene, L.; Chen, E. Y.-X. High-performance pan-tactic polythioesters with intrinsic crystallinity and chemical recyclability. *Sci. Adv*. **2020**, *6*, 0495.

[13] Jeong, W.; Hedrick, J. L.; Waymouth, R. M. Organic Spirocyclic Initiators for the Ring-Expansion Polymerization of β-Lactones J. *Am. Chem. Soc.* **2007**, *129*, 8414–8415.

[14] Jeong, W.; Shin, E. J.; Culkin, D. A.; Hedrick, J. L.; Waymouth, R. M. Zwitterionic Polymerization: A Kinetic Strategy for the Controlled Synthesis of Cyclic Polylactide. *J. Am. Chem. Soc.* **2009**, *131*, 4884−4891.

[15] Kricheldorf, H. R.; Weidner, S. M. High molar mass cyclic poly(L-lactide) via ring-expansion polymerization with cyclic dibutyltin bisphenoxides. *Eur. Polym.* **2018**, *105*, 158-166.

[16] Chang, Y. A.; Waymouth, R. M. Recent Progress on the Synthesis of Cyclic Polymers via Ring-Expansion Strategies. *J. Polym. Sci. A Polym. Chem.* **2017**, *55*, 2892–2902.

[17] Bielawski, C. W.; Benitez, D.; Grubbs, R. H. An "Endless" Route to Cyclic Polymers. *Science* **2002**, *297*, 2041−2044.

[18] C. D. Roland, H. Li, K. A. Abboud, K. B. Wagener, A. S. Veige, Cyclic polymers from alkynes. *Nat. Chem.* **2016**, *8*, 791–796.

[19] Kricheldorf, H. R.; Lee, S.-R. Polylactones. 35. Macrocyclic and Stereoselective Polymerization of β-D,L-Butyrolactone with Cyclic Dibutyltin Initiators. *Macromolecules* **1995**, *28*, 6718– 6725.

[20] Miao, Z.; Gonsales, S. A.; Ehm, C.; Mentink-Vigier, F.; Bowers, C. R.; Sumerlin, B. S.; Veige, A. S. Cyclic polyacetylene. *Nat. Chem.* **2021**, *13*, 792-799.

[21] Wang, T.-W.; Huang, P.-R.; Chow, J. L.; Kaminsky, W.; Golder, M. R. A Cyclic Ruthenium Benzylidene Initiator Platform Enhances Reactivity for Ring-Expansion Metathesis Polymerization. *J. Am. Chem. Soc* **2021**, *143*, 7314-7319.

[22] McGraw, M. L.; Clarke, R. W.; Chen, E. Y.-X. Synchronous Control of Chain Length/Sequence/Topology for Precision Synthesis of Cyclic Block Copolymers from Monomer Mixtures. *J. Am. Chem. Soc.* **2021**, *143*, 3318–3322.

[23] Li, X. Q.; Wang, B.; Ji, H. Y.; Li, Y. S. Insights into the Mechanism for Ring-Opening Polymerization of Lactide Catalyzed by $Zn(C_6F_5)_2$/Organic Superbase Lewis Pairs. *Catal. Sci. Technol.* **2016**, *6*, 7763−7772.

[24] Piedra-Arroni, E.; Ladaviere, C.; Amgoune, A.; Bourissou, D. Ring-Opening Polymerization with $Zn(C_6F_5)_2$-Based Lewis Pairs: Original and Efficient Approach to Cyclic Polyesters. *J. Am. Chem. Soc.* **2013**, *135*, 13306−13309.

[25] Wang, B.; Pan, L.; Ma, Z.; Li, Y. Ring-Opening Polymerization with Lewis Pairs and Subsequent Nucleophilic Substitution: A Promising Strategy to Well-Defined Polyethylene-like Polyesters without Transesterification. *Macromolecules* **2018**, *51*, 836−845.

[26] Hosoi, Y.; Takasu, A.; Matsuoka, S.; Hayashi, M. N-Heterocyclic Carbene Initiated Anionic Polymerization of (E,E)- Methyl Sorbate and Subsequent Ring-Closing to Cyclic Poly(alkyl sorbate). *J. Am. Chem. Soc.* **2017**, *139*, 15005−15012.

[27] Zhu, J.-B.; Watson, E. M.; Tang, J.; Chen, E. Y.-X. A Synthetic Polymer System with Repeatable Chemical Recyclability. *Science* **2018**, *360*, 398−403.

[28] Hong, M.; Chen, E. Y.-X. Completely Recyclable Biopolymers with Linear and Cyclic Topologies via Ring-Opening Polymerization of γ-Butyrolactone. *Nat. Chem.* **2016**, *8*, 42−49.

[29] Shi, C.; Li, Z.-C.; Caporaso, L.; Cavallo, L.; Falivene, L.; Chen, E. Y.-X. Hybrid Monomer Design for Unifying Conflicting Polymerizability, Recyclability, and Performance Properties. *Chem.* **2021**, *7*, 670−685.

[30] Schappacher, M.; Defeux, A. Synthesis of macrocyclic poly(2-chloroethyl vinyl ether)s. *Makromol. Chem. Rapid Commun*. **1991**, *12*, 447–453.

[31] Laurent, B. A.; Grayson, S. M. An Efficient Route to Well-Defined Macrocyclic Polymers via "Click" Cyclization. *J. Am. Chem. Soc.* **2006**, *128*, 4238-4239.

[32] Misaka, H.; Kakuchi, R.; Zhang, C. H.; Sakai, R.; Satoh, T.; Kakuchi, T. Synthesis of Well-Defined Macrocyclic Poly(δ-valerolactone) by "Click Cyclization" *Macromolecules* **2009**, *42*, 5091–5096.

[33] Stanford, M. J.; Pflughaupt, R. L.; Dove, A. P. Synthesis of Stereoregular Cyclic Poly(lactide)s via "Thiol−Ene" Click Chemistry. *Macromolecules* **2010**, *43*, 6538–6541.

[34] Glassner, M.; Blinco, J. P.; Barner-Kowollik, C. Diels–Alder reactions as an efficient route to high purity cyclic polymers. *Macromol. Rapid Commun*. **2011**, *32*, 724–728.

[35] Josse, T.; Altintas, O.; Oehlenschlaeger, K. K.; Dubois, P.; Gerbaux, P.; Coulembier, O.; Barner-Kowollik, C. Ambient temperature catalyst-free light-induced preparation of macrocyclic aliphatic polyesters. *Chem. Commun*. **2014**, *50*, 2024–2026.

[36] Sun, P.; Tang, Q.; Wang, Z.; Zhao, Y.; Zhang, K. Cyclic polymers based on UV-induced strain promoted azide–alkyne cycloaddition reaction. *Polym. Chem*. **2015**, *6*, 4096–4101.

[37] Polymeropoulos, G.; Bilalis, P.; Hadjichristidis, N. Well-Defined Cyclic Triblock Terpolymers: A Missing Piece of the Morphology Puzzle. *ACS Macro Lett.* **2016**, *5*, 1242-1246.

[38] Roovers, J. Viscoelastic properties of polybutadiene rings. *Macromolecules* **1988**, *21*, 1517–1521.

[39] Carl, W. Configurational and rheological properties of cyclic polymers. *Faraday Trans.* **1995**, *91*, 2525−2530.

[40] Pasquino, R.; Vasilakopoulos, T. C.; Jeong, Y. C.; Lee, H.; Rogers, S.; Sakellariou, G.; Allgaier, J.; Takano, A.; Brás, A. R.; Chang, T.; Gooßen, S.; Pyckhout-Hintzen, W.; Wischnewski, A.; Hadjichristidis, N.; Richter, D.; Rubinstein, M.; Vlassopoulos, D. Viscosity of Ring Polymer Melts. *ACS Macro Lett*. **2013**, *2*, 874−878.

[41] Parisi, D.; Costanzo, S.; Jeong, Y.; Ahn, J.; Chang, T.; Vlassopoulos, D.; Halverson, J. D.; Kremer, K.; Ge, T.; Rubinstein, M.; Grest, G. S.; Srinin, W.; Grosberg, A. Y. Nonlinear Shear Rheology of Entangled Polymer Rings. *Macromolecules* **2021**, *54*, 2811–2827.

[42] Tsamopoulos, A. J.; Katsarou, A. F.; Tsalikis, D. G.; Mavrantzas, V. G. Shear Rheology of Unentangled and Marginally Entangled Ring Polymer Melts from Large-Scale Nonequilibrium Molecular Dynamics Simulations. *Polymer* **2019**, *11*, 1194.

[43] Shin, E. J.; Jeong, W.; Brown, H. A.; Koo, B. J.; Hedrick, J. L.; Waymouth, R. M. Crystallization of Cyclic Polymers: Synthesis and Crystallization Behavior of High Molecular Weight Cyclic Poly(ε-caprolactone)s. *Macromolecules* **2011**, *44*, 2773−2779.

[44] Zaldua, N.; Lienard, R.; Josse, T.; Zubitur, M.; Mugica, A.;́ Iturrospe, A.; Arbe, A.; De Winter, J.; Coulembier, O.; Müller, A. J. Influence of Chain Topology (Cyclic versus Linear) on the Nucleation and Isothermal Crystallization of Poly(L-lactide) and Poly(d-lactide). *Macromolecules* **2018**, *51*, 1718−1732.

[45] Lorenzo, A. T.; Cordova, M. E.; Grayson, S. M.; Müller, A. J.; Hoskins, J. N. A comparative study on the crystallization behavior of analogous linear and cyclic poly(ε-caprolactones). *Macromolecules* **2011**, *44*, 1742–1746.

[46] Hoskins, J. N.; Grayson, S. M. Synthesis and degradation behavior of cyclic poly(ε-caprolactone). *Macromolecules* **2009** *42*, 6406–6413.

[47] Zhang, B.; Zhang, H.; Li, Y.; Hoskins, J. N.; Grayson, S. M. Exploring the effect of amphiphilic polymer architecture: synthesis, characterization, and self-assembly of both cyclic and linear poly(ethylene glycol)-*b*-polycaprolactone. *ACS Macro Lett.* **2013**, *2*, 845–848.

[48] Marko, J. F. Microphase separation of block copolymer rings. *Macromolecules* **1993**, *26*, 1442–1444.

[49] Lecommandoux, S.;Borsali, R.; Schappacher, M.; Deffieux, A.; Narayanan, T.; Rochas, C. Microphase separation of linear and cyclic block copolymers poly(styrene-b-isoprene): SAXS experiments. *Macromolecules* **2004**, *37*, 1843–1848.

[50] Poelma, J. E. Ono, K.; Miyajima, D.; Aida, T.; Satoh, K.; Hawker, C. J. Cyclic block copolymers for controlling feature sizes in block copolymer lithography. *ACS Nano* **2012**, *6*, 10845–10854.

[51] Aubert, S.; Bezagu, M.; Spivey, A. C.; Arseniyadis, S. Spatial and temporal control of chemical processes. Nat. Rev. Chem. **2019**, *3*, 706-722.

[52] Hirabayashi, T.; Yamamoto, H.; Kojima, T.; Takasu, A.; Inai, Y. Synthesis of Head-to-Tail and Head-to-Head Poly(propylene-alt-methyl methacrylate)s via Anionic Polymerization of Methyl 2,4- Alkadienoates. *Macromolecules* **2000**, *33*, 4304−4306.

[53] Takasu, A.; Ishii, M.; Inai, Y.; Hirabayashi, T. Highly Threo Diastereoselective Anionic Polymerization of (E,E)-Methyl Sorbate Catalyzed by a Bulky Organoaluminum Lewis Acid. *Macromolecules* **2001**, *34*, 6548−6550.

[54] Takasu, A.; Ishii, M.; Inai, Y.; Hirabayashi, T.; Inomata, K. Threo-Disyndiotactic Polymerization of (E,E)-Alkyl Sorbates Assisted by Bulky Organoaluminum Lewis Acid via "Alternating Turning over Polymerization (ATOP)" Mechanism. *Macromolecules* **2003**, *36*, 7055−7064.

[55] Muramatsu, Y.; Takasu, A.; Higuchi, M.; Hayashi, M. Direct observation of the formation of a cyclic poly(alkyl sorbate) via chain growth polymerization by an N-heterocyclic carbene initiator and ring-closing without extreme dilution. *J. Polym. Sci.* **2020**, *58*, 2936− 2942.

[56] Oga, Y.; Hosoi, Y.; Takasu, A. Synthesis of cyclic Poly(methyl methacrylate) via N-Heterocyclic carbene (NHC) initiated-anionic polymerization and subsequent ring-closing without need of highly dilute conditions. *Polymer* **2020**, *186*, 122019.

[57] Naruse, K.; Takasu, A.; Higuchi, M. Direct Observation of a Cyclic Vinyl Polymer Prepared by Anionic Polymerization using N-Heterocyclic Carbene and Subsequent Ring-Closure without Highly Diluted Conditions. *Macromol. Chem. Phys*. **2020**, *221*, 2000004.

[58] McGraw, M. L.; Clarke, R. W.; Chen, E. Y.-X. Compounded Sequence Control in Polymerization of One-Pot Mixtures of Highly Reactive Acrylates by Differentiating Lewis Pairs. *J. Am. Chem. Soc.* **2020**, *142*, 5969−5973.

[59] McGraw, L. M.; Chen, E. Y.-X. Lewis Pair Polymerization: Perspective on a Ten-Year Journey. *Macromolecules* **2020**, *53*, 6102− 6122.

[60] McGraw, M.; Chen, E. Y.-X. Catalytic Lewis Pair Polymerization of Renewable Methyl Crotonate to High-Molecular-Weight Polymers. *ACS Catal.* **2018**, *8*, 9877−9887.

[61] Zang, H. J.; Chen, E. Y. X. Organocatalytic upgrading of furfural and 5-hydroxymethyl furfural to C10 and C12 furoins with quantitative yield and atom-efficiency. *Int. J. Mol. Sci.* **2015**, *16*, 7143−7158.

[62] Hong, M.; Tang, X. Y.; Falivene, L.; Caporaso, L.; Cavallo, L.; Chen, E. Y.-X. Proton-Transfer Polymerization by N-Heterocyclic Carbenes: Monomer and Catalyst Scopes and Mechanism for Converting Dimethacrylates into Unsaturated Polyesters. *J. Am. Chem. Soc.* **2016**, *138*, 2021−2035.

[63] Liu, D.; Zhang, Y.; Chen, E. Y.-X. Organocatalytic Upgrading of the Key Biorefining Building Block by a Catalytic Ionic Liquid and N-heterocyclic Carbenes, *Green Chem.* **2012**, *14*, 2738–2746.

[64] Biju, A. T.; Padmanaban, M.; Wurz, N. E.; Glorius, F. *Angew. Chem. Int. Ed.* **2011**, *50*, 8412–8415.

[65] Matsuoka, S.-I.; Ota, Y.; Washio, A.; Katada, A.; Ichioka, K.; Takagi, K.; Suzuki, M. *Org. Lett.* **2011**, *13*, 3722–3725.

[66] Zhang, Y.; Miyake, G. M.; Chen, E. Y.-X. Conjugate-Addition Organopolymerization: Rapid Production of Acrylic Bioplastics by N-Heterocyclic Carbenes. *Angew. Chem., Int. Ed*. **2012**, *51*, 2465−2469.

[67] Zhang, Y.; Schmitt, M.; Falivene, L.; Caporaso, L.; Cavallo, L.; Chen, E. Y.-X. Organocatalytic Conjugate-Addition Polymerization of Linear and Cyclic Acrylic Monomers by N-Heterocyclic Carbenes: Mechanisms of Chain Initiation, Propagation, and Termination. *J. Am. Chem. Soc.* **2013**, *135*, 17925−17942.

[68] Flanagan, J. C. A.; Kang, E. J.; Strong, N. I.; Waymouth, R. M. Catalytic Dimerization of Crotonates. *ACS Catal*. **2015**, *5*, 5328−5332.

[69] Haag, D.; Chen, X. T.; Fraser-Reid, B. Carbohydrate Based IMDA/aldol Strategy Towards the Densely Functionalized trans-Decalin Subunit of Azadirachtin, *Chem. Commun.* **1998**, 2577-2578.

[70] Sato, M.; Kahn, M. A convenient preparation of 1-phenylsulfonyl-3-iodomethylindole. *Tetrahedron Lett.* **1990**, *31*, 4697-4698.

Chapter 7
Summary and Outlook

7.1 Summary and Outlook

As of the time of this dissertation's publication, the story of LPP is still young and far from over. Yet, the 5 years of work spent by the author has accumulated several important advancements that embody the themes of control and selectivity which foreshadow the future directions of the growing field. Thus, we will thematically discuss the key points of each chapter and give a broader perspective that relates the authors work to contemporary works as well as possible future ideas.

7.1.1 Chemoselectivity of highly functionalized bio-sourced monomers

Chapters 2 and 3 both deal with the LPP of methyl crotonate, a biorenewable monomer that features a β-methyl substitution which, compared to classical Michael acceptor monomers such as acrylates and methacrylates, is unique. This seemingly harmless variation introduces the chaotic presence of an acidic γ-proton which renders most anionic polymerization methods problematic. This substitution also stabilizes the alkene making polymerization less downhill, which, likely accounts for the crotonates' resistance to radical methods. Furthermore, crotonates' tendency to dimerize either by deprotonative chain transfer or by elimination of the initiating group prevent polymerization by modern zwitterionic methods.[1] In chapter 2, we showcase the chemoselectivity of LPs by solving these problems. The main ingredient of this selectivity is the stabilization of the enolate active species by MAD, which inhibits elimination of the initiating LB group and slows down the deprotonative chain transfer by reducing the basicity of the enolate. However, to compensate for this enolate stabilization, propagation is promoted by the activation of incoming monomers by MAD-coordination. Thus one of the key concepts of LPP is demonstrated: reactivity of the propagating species is transferred to the incoming monomer, protecting the growing chain

while simultaneously preserving overall activity. We expanded on this concept in chapter 3, where instead of stabilizing the enolate with an aluminum LA, a neutral silyl group was used to further stabilize the enolate. This method completely shut down the deprotonative chain transfer event to yield a living polymerization, albeit by sacrificing quite a bit of activity.

This method has been adopted by several other groups to solve similar problems. In 2020 the Hong group used our exact strategy to polymerize the renewable β-angelica lactone which, similar to crotonates, has an acidic γ-proton and an even smaller thermodynamic driving force for polymerization.[2] Similar to our crotonate chemistry, a deprotonative initiation mechanism was useful to induce a LPP by the ion-pair mode. But more importantly, by lowering the enolate basicity through LA-stabilization, the γ-deprotonation can be avoided during propagation. We also connected these ideas to the sorbate chemistry which was actually published by Takasu shortly before our crotonate work in 2017,[3] but with the incorrect initiation mechanism. When we figured out the behavior of the acidic γ-proton found in crotonates, we were able to correct the sorbate story by realizing that sorbates' analogous acidic ε-protons also play a role in the sorbate polymerization as well as the cyclization mechanism discussed in chapters 5 and 6.

Furthermore, the Abe group adopted our crotonate chemistry and improved on our group transfer method to make the living reaction much more practical and also expanded the scope to crotonates other than the methyl ester.[4] Further studies compatibilized the crotonate monomer with methacrylates and various other comonomers to generate an impressive suite of bio-sourced materials. [5] Lastly, Abe was able to use the group-transfer based LPP to polymerize the bio-sourced cinnamates which like crotonates are β-substituted but with an even more challenging phenyl group. Although β-phenyl substitution does not have acidic protons, it further stabilizes the alkene

and provides even more steric hindrance. Yet by utilizing a sterically unhindered silylium LA the unprecedented polymerization of cinnamates was accomplished.[6]

As biomass reformation technology continues improving, more and more monomers will become available and economically viable. As markets shift more away from petroleum-based plastics and towards more sustainable options, LPP will be important because it has the unique capability to deal with these highly functionalized monomers. LPP technology should continue to improve its capabilities with respect to chemoselectivity and control over these challenging monomers. Itaconates for example are an inexpensive and underutilized monomer with hardly any methodology suitable for its polymerization. The author recommends further study in this direction.

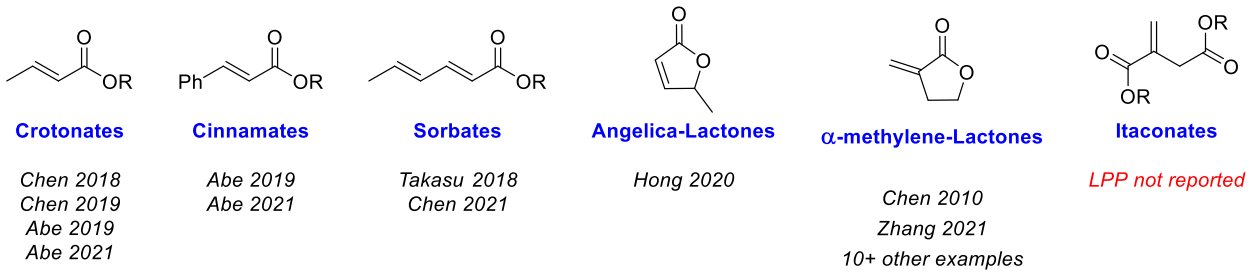

Figure 7.1. Scope of bio-renewable acrylic monomers.

While the homopolymerization of these monomer types is important to understand, it is equally important to design practically useful products from them. Often times the homopolymers of highly functionalized bio-acrylics does not result in an immediately useful polymer. For example, crotonates, cinnamates, and lactone-based acrylic polymers are often extremely brittle and unfit for most applications while sorbates are typically too soft. LPP, having the capability to polymerize the homopolymers individually should have the potential to compatibilize multiple bio-based

comonomers to make copolymers or sophisticated architectures/topologies that approach more ideal material properties.

7.1.2 Control of Polymer Sequence

In order to make sustainable materials that are competitive with legacy materials, we need strategies that improve the performance, practicality, and economy of our sustainable options. Copolymerization is one tool at our disposal in the effort to optimize mechanical performance and the practical utility of our materials. By combining property elements of two homopolymers into one hybrid copolymer, we can target specific characteristics or produce a diverse suite of materials.

Of the several types of copolymers, including random-, alternating-, tapered-, and block-assemblies, block copolymers are especially interesting due to their ability to form microphase self-assembly such as lamellar, gyroid, or cylinders. This concept adds a new layer of complexity to the study and application of these materials, especially when considering that separated phases might have different mechanical properties such as strength and flexibility, but also various chemical properties such as solubility, gas permeation, light absorption etc. Hard materials can be hybridized with soft materials to form copolymers with a multi-domain structure wherein hard domains provide structure and rigidity while soft domains provide flexibility and durability. Thermoplastic elastomers are often ABA triblock copolymers wherein the hard A domains are linked together by the soft B domain, yielding a network effect. Certain chemistries can also be localized within a single domain, such as crosslinking, bond-exchange, post-functionalization, photochemistry etc. All these points are made simply to express the fact that material function and property can be affected by more than just the monomer structure. Thus it is important to develop methodologies that are *controlled* enough to access these complex architectures.

One challenging aspect of block copolymerizations are that the polymerization method must be living. Otherwise, termination after the first block would result in incomplete crossover to the second comonomer and thus homopolymer contaminant. Our compounded sequence control (CSC) methodology presented in chapters 4 and 5 deliver solutions to this problem, at least concerning acrylates. Acrylate polymerizations are notoriously difficult to control due to their propensity to terminate via in-chain Claisen condensation. In the LPP scenario, we demonstrated that the presence of unreacted free monomer inhibits the Claisen via LA sequestration. Thus in CSC, where acrylates are usually the preferential monomer that sequences first, the acrylate block can seamlessly crossover to polymerize the comonomer block with low risk of termination since the comonomer is actively sequestering the LA. Another advantage of CSC is the ability to package, transport and store mixtures of monomers. Since acrylics are typically packaged with a radical inhibitor that requires a purification step prior to polymerization, classical sequential addition copolymerization methods require two purification steps. With CSC, the monomer mixture can be packaged at any desired ratio so that both monomers can be purified simultaneously through a single step.

While Chapter 4 discusses CSC copolymerizations[7] of two different acrylates and chapter 5[8] discusses the acrylate/methacrylate combination, we hope this technology will be expanded to a much broader scope of substrates and applications. The acrylate/methacrylate combination, which has nearly ideal sequencing, is a promising platform for several proof-of-concept ideas. For example, the use of a bifunctional initiator with an acrylate/methacrylate pair would in theory produce a nice ABA triblock in one step, with the hard methacrylates being the outside blocks. Similar logic can be used with multi-functional initiators for the synthesis of star polymers.

Combining any of these ideas with either the allyl substituted acrylate or methacrylate opens the door for endless post-functionalization ideas.

There are also ideas involving timed additions of comonomers (Figure 7.2). for example, to make an ABA triblock copolymer of P^{t}BA-*b*-P^{n}BA-*b*-P^{t}BA, We showed in chapter 3 that we can simply initiate polymerization on a quantity of ^{t}BA, and then add ^{n}BA when this reaction reaches 50 % conversion. The higher priority ^{n}BA will then selectively polymerize until its depletion, at which point polymerization of ^{t}BA will resume. We used this concept in a recent work which capitalizes on the unique chemistry of ^{t}BA to make ABA thermoplastic elastomers that selectively crosslink in the A domains. [9]

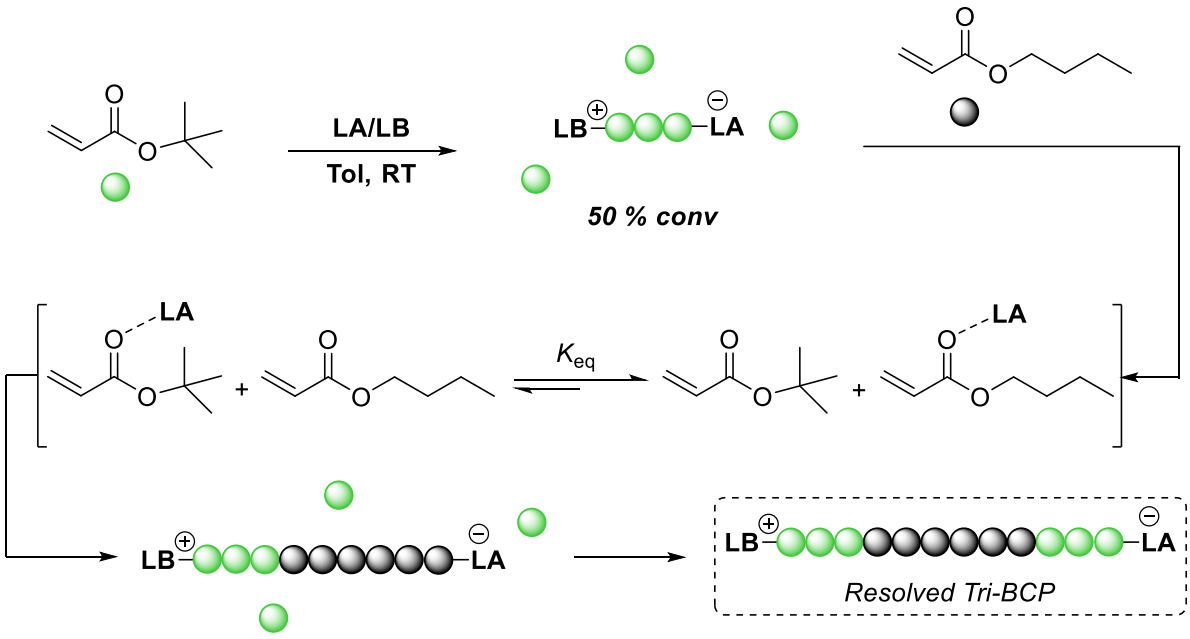

Figure 7.2. Timed addition method for ABA triblock copolymer synthesis by CSC-LPP.

Although unpublished, the author has found combinations of 3 monomers that sequence. While hard data for this system will not be discussed herein, it should not be a stretch for the reader

familiar with chapters 4 and 5 to consider that a 3 part mixture of ^{n}BA, ^{t}BA, and MMA will in fact sequence into an ABC triblock copolymer in one-pot and one-step. Thus extension of this logic reveals that the use of a bifunctional initiator will yield a CBABC pentablock in one step (Figure 7.3).

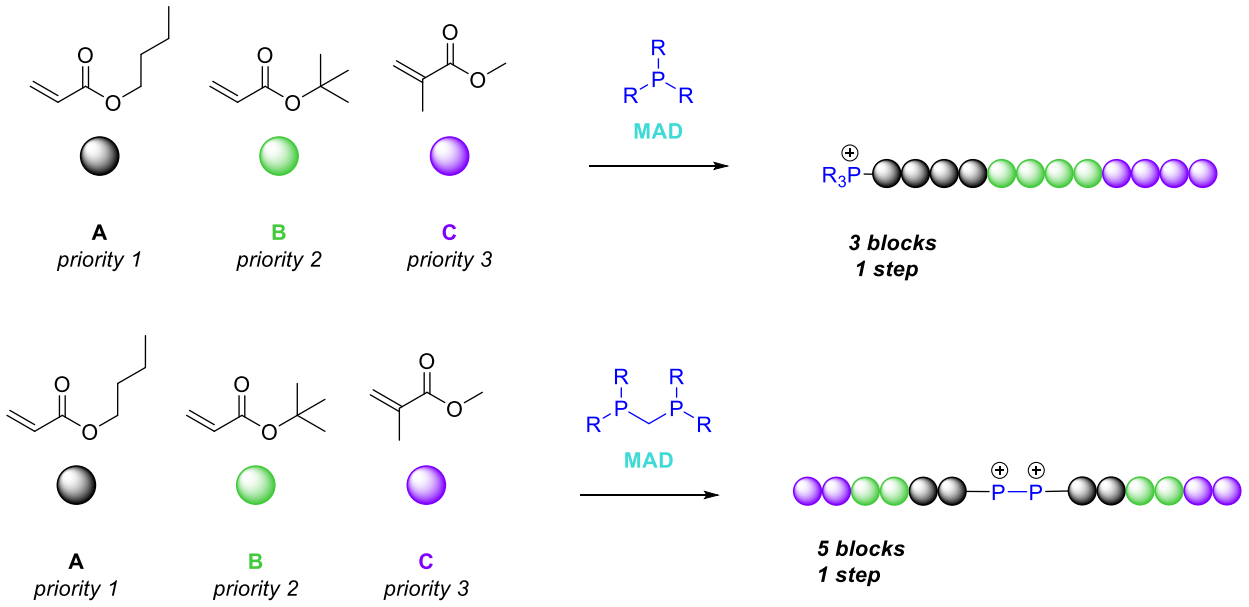

Figure 7.3. Hypothetical synthesis of ABC triblock and CBABC pentablocks by CSC-LPP

By incorporating a timed addition strategy with a bifunctional initiator and 3 monomers, one can envision a scenario where A, B, and C are polymerized by CSC together to sequence a CBABC pentablock, but after partial conversion of C, another charge of A and B are added. This second charge would actually yield 6 more blocks, giving an 11-block CBACBABCABC copolymer in only two steps (Figure 7.4).

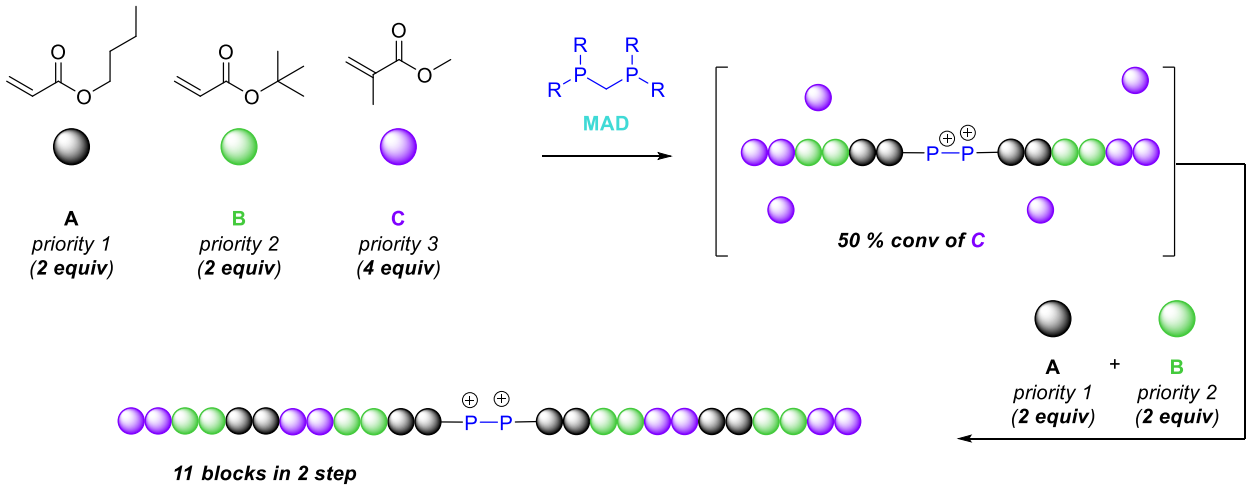

Figure 7.4. Hypothetical synthesis of 11-block CBACBABCABC copolymer in two steps by CSC-LPP.

Lastly, there is potential for a scenario where an infinite number of repeating blocks can be achieved by using a metered addition of comonomers (Figure 7.5). Most simply, polymerization can be initiated on a low priority monomer such as MMA, while a high priority monomer such as ^{n}BA can be dripped into the reaction at a steady rate. In this case, every time a drop of ^{n}BA enters the reaction, it will polymerize selectively until it is depleted, at which point MMA polymerization will resume. The size and number of blocks is determined by the drop rate and the drop size with respect to the total MMA reservoir. This could also be extrapolated to 3 or more monomers. Obviously, CSC-LPP quickly adds layers of complexity and has potential to make highly sophisticated polymers. Hopefully this technology helps improve next generation materials and provides solutions to modern polymerization problems. The future holds many exciting advancements for CSC. Especially when it is applied to the full monomer scope of Michael acceptors and is applied more broadly to even ROP polymerization systems.

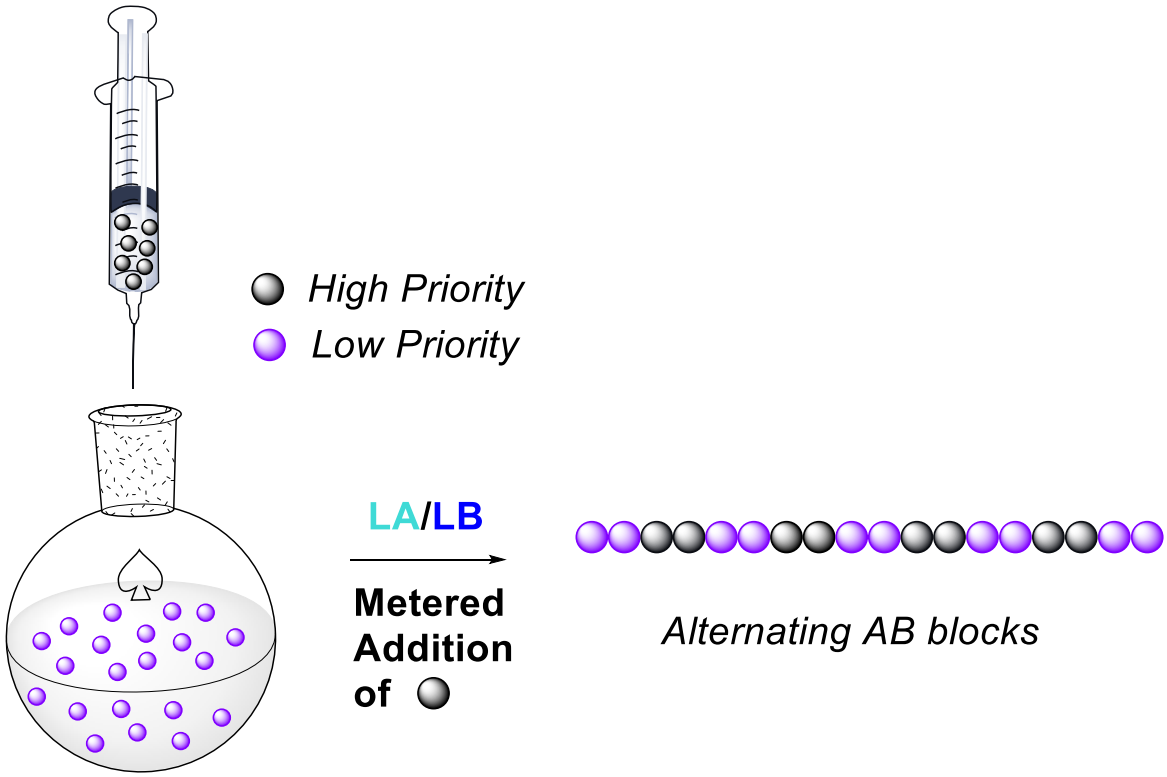

Figure 7.5. Hypothetical infinite alternating block copolymerization strategy by CSC-LPP through metered comonomer addition.

7.1.4 Control of Polymer Topology

While the function and application of topology is not within the scope of the author's dissertation, many of the ideas and methodologies presented within this work enable new routes to complex topological structures that were before inaccessible. For example, Chapter 5 includes a new method for synthesizing high molecular weight block copolymers with good control, while Chapter 6 elucidates mechanistic details for the key ring closure step and explains how such control over spatial and temporal elements of the reaction is achieved. While the cyclic topology is perhaps one of the most challenging targets in the topological repertoire, there are many topologies that LPP has yet to conquer. Multi-armed star polymers for example have not yet been reported in the literature but seem possible after optimization of a multi-functional Lewis base initiator, while branch or hyper-branched topologies seem much harder to achieve. While the literature has plenty

of examples of all of the aforementioned topologies, LPP offers not only the homopolymerization of challenging topologies but also their block copolymerization. For example, by combining CSC-LPP with the sorbate-based ring-closure methodologies (Chapter 5), we could make cyclic block copolymers. The same logic could be applied in the future for other topology-controlled methodologies such as star polymers. We also showed in Chapter 5 and Chapter 6 that the chemoselective LPP of vinyl or allyl (meth)acrylates is compatible with CSC, enabling not just the synthesis of brush topologies but also the option to include specific brush blocks within a larger copolymer structure of any given topology.

7.2 Conclusions

The authors work related to LPP has been presented so that our most important advancements are clearly described within each chapter. These advances are described within the greater themes of LPP of *selectivity* and *control*. With these themes in mind, several future directions and possibilities were proposed within the confines of reasonable potential. The future of LPP (by the author's estimation) will have the most impact in (1) enabling the chemoselective polymerization of challenging biorenewable monomers which will then hopefully provide sustainable alternatives to legacy petroleum-based materials and (2) enabling the convenient/economical synthesis of high-performance copolymers from biorenewable monomers.

I want to end this dissertation on a note of encouragement and gratitude. Studying this system has been such an unforgettable experience that I am so thankful for. These past 5 years I've spent working on these projects have exposed me to so many types of chemistry including mechanism, catalysis, synthesis, thermodynamics/kinetics, spectroscopy, intermediate isolation, polymer characterization, material testing, material design, optimization, logic, and philosophy. I encourage

other students and scientists to get involved with LPP as it will challenge you, while igniting your passion for research and problem solving. It is still a young field and there is still so much to do.

References cited in Chapter 7

[1] Flanagan, J. C. A.; Kang, E. J.; Strong, N. I.; Waymouth, R. M. Catalytic Dimerization of Crotonates. *ACS Catal*. **2015**, *5*, 5328–5332.

[2] Wang, X.-J.; Hong, M. Lewis-Pair-Mediated Selective Dimerization and Polymerization of Lignocellulose-Based β-Angelica Lactone into Biofuel and Acrylic Bioplastic. *Angew. Chem., Int. Ed.* **2020**, *59*, 2664-2668.

[3] Hosoi, Y.; Takasu, A.; Matsuoka, S.-I.; Hayashi, M. N-Heterocyclic Carbene Initiated Anionic Polymerization of (E,E)- Methyl Sorbate and Subsequent Ring-Closing to Cyclic Poly(alkyl sorbate). *J. Am. Chem. Soc.* **2017**, *139*, 15005−15012.

[4] Takenaka, Y. & Abe, H. Group-transfer polymerization of various crotonates using organic acid catalysts. *Macromolecules* **2019**, *52*, 4052–4058.

[5] Imada, M.; Takenaka, Y.; Tsuge, T.; Abe, H. Copolymers incorporated with β-substituted acrylate synthesized by organo-catalyzed group-transfer polymerization. *Polym. J.* **2021**, *53*, 989-999.

[6] Imada, M.; Takenaka, Y.; Hatanaka, H.; Tsuge, T.; Abe, H. Unique Acrylic Resins with Aromatic Side Chains by Homopolymerization of Cinnamic Monomers. *Commun. Chem*. **2019**, *2*, 109.

[7] McGraw, M. L.; Clarke, R. W.; Chen, E. Y.-X. Compounded Sequence Control in Polymerization of One-Pot Mixtures of Highly Reactive Acrylates by Differentiating Lewis Pairs. *J. Am. Chem. Soc*. **2020**, *142*, 5969−5973.

[8] McGraw, M. L.; Clarke, R. W.; Chen, E. Y. X. Synchronous Control of Chain Length/Sequence/Topology for Precision Synthesis of Cyclic Block Copolymers from Monomer Mixtures. *J. Am. Chem. Soc.* **2021**, *143,* 3318−3322.

[9] Clarke, R. W.; McGraw, M. L.; Newell, B. S.; Chen, E. Y.-X. Thermomechanical activation achieving orthogonal working/healing conditions of nanostructured tri-block copolymer thermosets. *Cell Reports Physical Science* **2021**, *2*, 100483.

Appendix A
Supplementary Information Corresponding to Chapter 2

Taken verbatim from:

McGraw, M.; Chen, E. Y.-X. Catalytic Lewis Pair Polymerization of Renewable Methyl Crotonate to High-Molecular-Weight Polymers. *ACS Catal*. **2018**, *8*, 9877−9887.

Materials

All syntheses and manipulations of air and moisture sensitive materials were carried out in flame dried Schlenk-type glassware on a dual-manifold Schlenk line or in an inert gas (Ar or N_2)-filled glovebox. Methyl crotonate (MC) was purchased from Sigma-Aldrich and dried for 24 h over CaH_2 followed by vacuum distillation at 45 °C at reduced pressure. It was then titrated by dropwise addition of $AlEt_3$ until the solution turned pale yellow and redistilled. All experiments were performed within 1 week of monomer purification. *N*-Heterocyclic carbenes (NHCs), 1,3-di-*tert*-butylimidazolin-2-ylidene (I^{t}Bu) and 1,3-di-mesityl-butylimidazolin-2-ylidene (IMes) were purchased from VWR and used as received. NHC 1,3,4-triphenyl4,5-dihydro-1H-1,2,4-triazol-5-ylidene (TPT),[1] *N*-heterocyclic olefin (NHO) 1,3-dimethyl-4,5-diphenyl-2-(propan-2-ylidene)-2,3-dihydro-1H-imidazole, [2] $Al(C_6F_5)_3$·0.5(toluene)[3] and methylaluminum bis(2,6-di-*tert*-butyl-4-methylphenoxide) (MAD) [4] were synthesized according to literature procedures. *Extra caution should be exercised when handling* $Al(C_6F_5)_3$ *due to its thermal and shock sensitivity. Preparation of unsolvated form of this reagent should be avoided.* Toluene and benzene were dried with NaK and filtered through a 0.2 μm filter just prior to use. The same procedure was used to purify pentane, benzene-d_6, and toluene-d_8. KO^{t}Bu was purchased from Sigma-Aldrich and purified by sublimation at 200 °C under high vacuum. $B(C_6F_5)_3$ was obtained from Boulder Scientific Co. as a research gift and purified twice by sublimation at 40 °C under vacuum.

Analytical methods

NMR Spectroscopy. Monomer conversion as well as structure characterizations of intermediates and polymers were carried out by ^{1}H NMR and HH-COSY experiments using a Varian Inova 400 MHz (FT 400 MHz, ^{1}H; 100 MHz, ^{13}C) or a or Bruker AVIII 400 MHz spectrometer (400 MHz, ^{1}H; 100 MHz, ^{13}C). Chemical shifts were referenced to internal solvent resonances corresponding to 7.26 ppm (chloroform) and 7.16 ppm (benzene) and reported as parts per million relative to $SiMe_4$.

Elemental Analysis. Elemental analysis was performed by Robertson Microlit Laboratories.

Gel Permeation Chromatography (GPC). Measurements of polymer absolute weight-average molecular weight (M_w), number-average molecular weight (M_n), and molecular weight distributions or dispersity indices ($Đ = M_w/M_n$) were performed via GPC. The GPC instrument consisted of an Agilent HPLC system equipped with one guard column and two PL gel 5 μm mixed-C gel permeation columns and coupled with a Wyatt DAWN HELEOS II multi (18)-angle light scattering detector and a Wyatt Optilab TrEX dRI detector; the analysis was performed at 40 °C using chloroform as the eluent at a flow rate of 1.0 mL/min, using Wyatt ASTRA 7.1.2 molecular weight characterization software. The refractive index increment (dn/dc) of the poly(methyl crotonate) (PMC) was determined to be 0.0426 mL/g obtained by batch experiments using Wyatt Optilab TrEX *d*RI detector and calculated using ASTRA software. Polymer solutions were prepared in chloroform and injected into *d*RI detector by Harvard Apparatus pump 11 at a flow rate of 0.25 mL/min. A series of known concentrations were injected and the change in refractive index was measured to obtain a plot of change in refractive index versus change in

concentration ranging from 0.5 to 5.0 mg/mL. The slope from a linear fitting of the data was the d*n*/d*c* of PMC.

Matrix-assisted Laser Desorption/ionization Time-of-flight Mass Spectroscopy (**MALDI-TOF MS**). MALDI−TOF MS was used to analyze low molecular weight PMC samples, using an Ultraflex MALDI-TOF mass spectrometer (Bruker Daltonics) operated in positive ion, reflector mode using a Nd:YAG laser at 355 nm and 25 kV accelerating voltage. A thin layer of a 1% NaI solution was first deposited on the target plate, followed by 0.6 μL of both PMC (2 mg/ml in $CHCl_3$) and matrix (dithranol, 20 mg/mL in $CHCl_3$). External calibration was done using a peptide calibration mixture (4 to 6 peptides) on a spot adjacent to the sample. The raw data was processed in the FlexAnalysis software (version 2.4, Bruker Daltonics), and the Figures were potted using mMass software.

Thermal Analysis. Differential scanning calorimetry (DSC) was performed on thoroughly dried PMC samples on an Auto Q20, TA Instrument. DSC plots represent data obtained from a second scan after the thermal history was removed from the first scan. The second heating rate was 20 °C/min and cooling rate was 20 °C/min. Thermal gravimetric analysis (TGA) was used to measure decomposition temperatures (T_d) on a Q50 TGA Analyzer, TA Instrument. Polymer samples were heated from ambient temperature to 500 °C at a heating rate of 10 °C/min. T_d is the temperature at which the sample experiences 5.0% weight loss.

Experimental Details

Polymerization procedure. Typical polymerizations consisted of first premixing 5.0 mmol of MC (0.53 mL, 0.501 g) with a certain amount of LA and stirring for 10 min followed by addition of

the MC/LA solution to a certain amount of solid LB. For polymerizations related to kinetic experiments, large MC/LA stock solutions were prepared and used for several polymerizations so that experimental error would be the same throughout. For polymerizations with MC:LB ratios greater than or equal to 1000:1, a 0.0944 M stock solution of LB in toluene was first prepared. 10-100 μL of the LB solution was added to the 1.0 mL or 0.5 mL of MC/LA solution (1 mL of 2 mol% MAD in MC + 100; 50; 25 μL of 0.0944 M I^{t}Bu in toluene corresponds to MC:MAD:I^{t}Bu = 1000:20:1; 2000:20:1; 4000:40:1). This method was adopted to minimize errors associated with weighing out small quantities of LB and assure precise stoichiometry for comparable data. The small amount of toluene added was considered neglectable. Polymers were typically quenched with 2-3 mL of $CDCl_3$ spiked with benzoic acid (approx. 500 ppm). If polymerization went to full conversion, the resulting polymer product was a solid block that normally would take several hours to dissolve in $CDCl_3$. Once dissolved, a few drops of the crude product was diluted in 0.5 mL $CDCl_3$ and analyzed with ^{1}H NMR. Conversion was calculated by comparison of monomer and polymer signal integration. The remaining dissolved polymer could be crashed with methanol, however the gel like consistency of the resulting solid makes it difficult to isolate by filtration. Because of this, we chose to centrifuge the solid polymer several times with fresh methanol to remove decomposed catalyst. Typical ^{1}H NMR spectral data of PMC are listed as follows: ^{1}H NMR (400 MHz, $CDCl_3$): δ (ppm) = 3.49-3.79 (br. 3H, OCH_3), 2.00-2.67 (br. 2H -CH(CO_2CH_3)CH(CH_3)-), 0.70-1.13 (br. 3H, -CH(CH_3)).

Synthesis and Isolation of Zwitterionic Intermediate ^{TPT}5. 0.472 M stock solutions of MC, MAD, and TPT were prepared in benzene-d_6. 1 mL of MC stock solution (0.496 g, 0.50 mmol) was mixed with 1 mL of MAD stock solution (0.238 g, 0.50 mmol), and the mixture was allowed to stir for 10 min. It was then added dropwise with stirring to 1 mL of the TPT stock solution

(0.147 g, 0.50 mmol) over a period of 5 min. The product was then layered with 5 mL of pentane, at which point precipitation was observed in the pentane layer. The layered mixture was put in a –30 °C freezer, and small white beads formed of the product ^{TPT}**5**. The beads were filtered and washed with pentane and dried *in vacuo* for 4 h to give 0.2944 g of isolate ^{TPT}**5**, 68 % yield. Crystals were grown from dissolving 0.2 g of the isolated product in 3 mL of toluene layered with 2 mL of hexane but none were high enough quality for X-ray diffraction. Elemental analysis was performed on a sample that was recrystallized from toluene/hexane and dried for 16 h *in vacuo*. Elemental composition data are consistent with the calculated composition of ^{TPT}**5**·(toluene). Elemental composition calculated: % C = 77.98; % H = 8.31 %; % N = 4.33 %. Elemental composition found: % C = 77.57; % H = 8.48 %; % N = 5.09 %.

The spectrum in Figure 2.5 was obtained by a similar method, where all stock solutions were 0.080 M in benzene-d_6. 0.25 mL of MC stock solution was added to a 0.25 mL of MAD stock solution and stirred for 10 min. Then the MC/MAD 1:1 solution was added dropwise to the 0.25 mL of TPT stock solution over 5 min. The resulting solution was added to an NMR tube (calculated 0.0175 g ^{TPT}**5** in 0.75 mL of benzene-d_6) for analysis. ^{1}H NMR spectral data of ^{TPT}**5** are listed as follows: ^{1}H NMR (400 MHz, C_6D_6): δ (ppm) = 7.2, 7.22 (s, 4H, BHT-*m*), 6.92-7.12 (m, 8H, TPT^+), 6.64-6.84 (m, 5H, TPT^+), 6.32-6.47 (d, br, 2H, TPT^+), 4.11-4.18 (p, 1H (TPT^+)C*H*(CH_3)), 3.45-3.47 (d, 1H ($CH(CH_3)$C*H*C(OCH_3)), 3.41 (s, 3H, OCH_3), 2.16, 2.27 (s, 3H, BHT-CH_3), 1.61, 1.74 (s, 18H, BHT-^{t}*Bu*), 0.384-0.402 (d, 3H (TPT^+)CH(CH_3)), 0.00 (s, 3H, AlCH_3).

Kinetics. Experiments were performed by spiking the premixed MC/MAD 100:2 solution with 10-20 mg of hexamethyl benzene as an internal standard. Aliquots were taken at different time points and quenched in C_6D_6 (with 500 ppm benzoic acid), then filtered through a 0.2 μm filter to remove polymer. Conversion was calculated by comparing ^{1}H NMR integration of monomer signal at time

t, normalized by the integration of the internal standard peak at 2.13 ppm at time *t*, to the integration of the monomer signal at time = 0 relative to integration of internal standard.

Table A1. Results of MC Polymerization by $B(C_6F_5)_3$/LB [a]

Run	MC:$B(C_6F_5)_3$:LB	LB	t_{gel}[b] (min)	Conversion (%)	M_n[c] (kg/mol)	$Đ$[c] (M_w/M_n)	I^*[d] (%)
31	100:2:1	I^{t}Bu	35	>99	14.1	1.19	71
32	200:2:1		>3 h	>99	30.9	1.06	65
33	500:2:1		-	40	18.0	1.19	111
34	100:2:1	TPT	45	>99	16.3	1.21	62
35	200:2:1		> 3 h	>99	17.8 (97.3 %) 245 (2.7 %)	1.28 1.25	95[e]
36	500:2:1		-	23	12.8 (51 %) 13.5 (49 %)	1.13 1.09	88[e]
37	100:2:1	NHO	30-35	>99	25.1 (20.4 %) 21.2 (79.6 %)	1.09 1.06	47[e]
38	200:2:1		2-3 h	>99	0.820	1.85	244
39	500:2:1		-	21	1.41	1.09	74

[a] Conditions: [MC] = 0.53 mL (5.0 mmol); neat; temperature = 25 ºC; time = 24 h; MC was pre-mixed with $B(C_6F_5)_3$ followed by addition of LB. [b] Approximate time of gelation monomer. [c] M_n and $Đ$ determined by GPC. [d] Initiator efficiency (I^*) = M_n(calcd)/M_n(exptl), where M_n(calcd) = MW(monomer) × [monomer]/[LB] × conversion% + MW of chain-end groups. [e] Composite I^* based on two GPC peaks, where M_n(calcd) = (% composition A) × $(M_n)_A$ + (% composition B) × $(M_n)_B$.

In-situ Generation of $^{Al(C6F5)3}$7

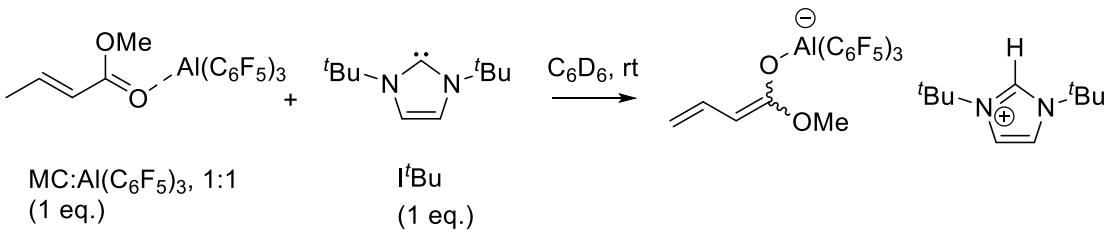

0.080 M stock solutions of MC, $Al(C_6F_5)_3$, and I^{t}Bu were first prepared in C_6D_6. Then, 0.25 mL of MC stock solution was mixed with 0.25 mL of $Al(C_6F_5)_3$ stock solution in a 5 mL scintillation vial and allowed to mix for 10 min. Then the MC:$Al(C_6F_5)_3$ 1:1 solution was added dropwise to 0.25 mL of I^{t}Bu stock solution with stirring via Pasteur pipette. The 1:1:1 solution was then pipetted back and forth several times between vials to ensure exact stoichiometry, then pipetted into an NMR tube and sealed for NMR analysis.

^{1}H NMR spectrum of the MC:$Al(C_6F_5)_3$:I^{t}Bu 1:1:1 product shown in Figure A1 revealed no clean products. Peaks in the olefin region correspond to the α- and γ-protons of the enolaluminate product $^{Al(C6F5)3}$**7** (5.0-4.4 ppm, Figure A2). Two singlets at 6.41 and 8.26 ppm with integrals of 1.81 and 1.00, respectively, represent the three sp^2-carbon protons on the protonated imidazolium. These peaks couple in the HH-COSY spectrum (Figure A3). Since very little polymer was produced from MC/$Al(C_6F_5)_3$/I^{t}Bu polymerization reactions, it is assumed that $^{Al(C6F5)3}$**7** is ineffective for polymerization.

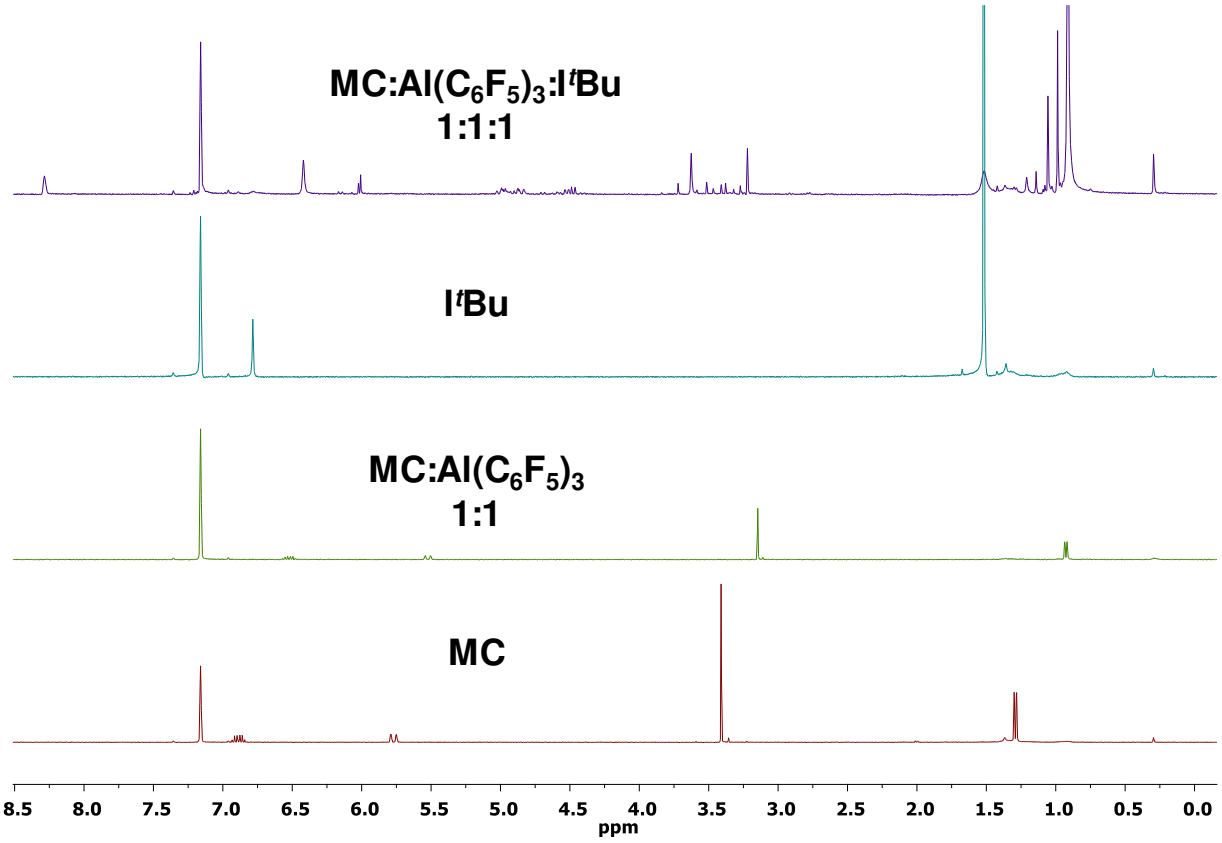

Figure A1. ^{1}H NMR spectrum of $^{Al(C6F5)3}$**7** overlaid with controls.

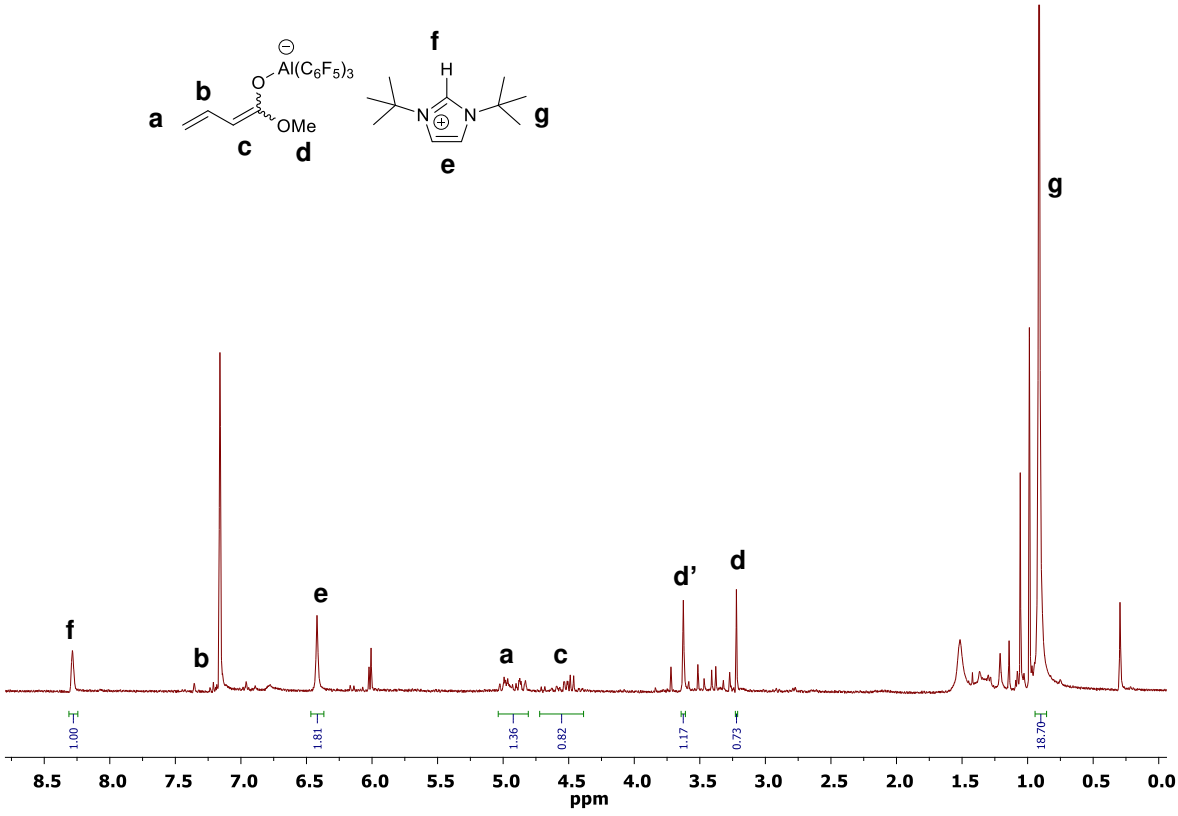

Figure A2. ^{1}H NMR spectrum of *in-situ* generated enolaluminate $^{Al(C6F5)3}$**7**.

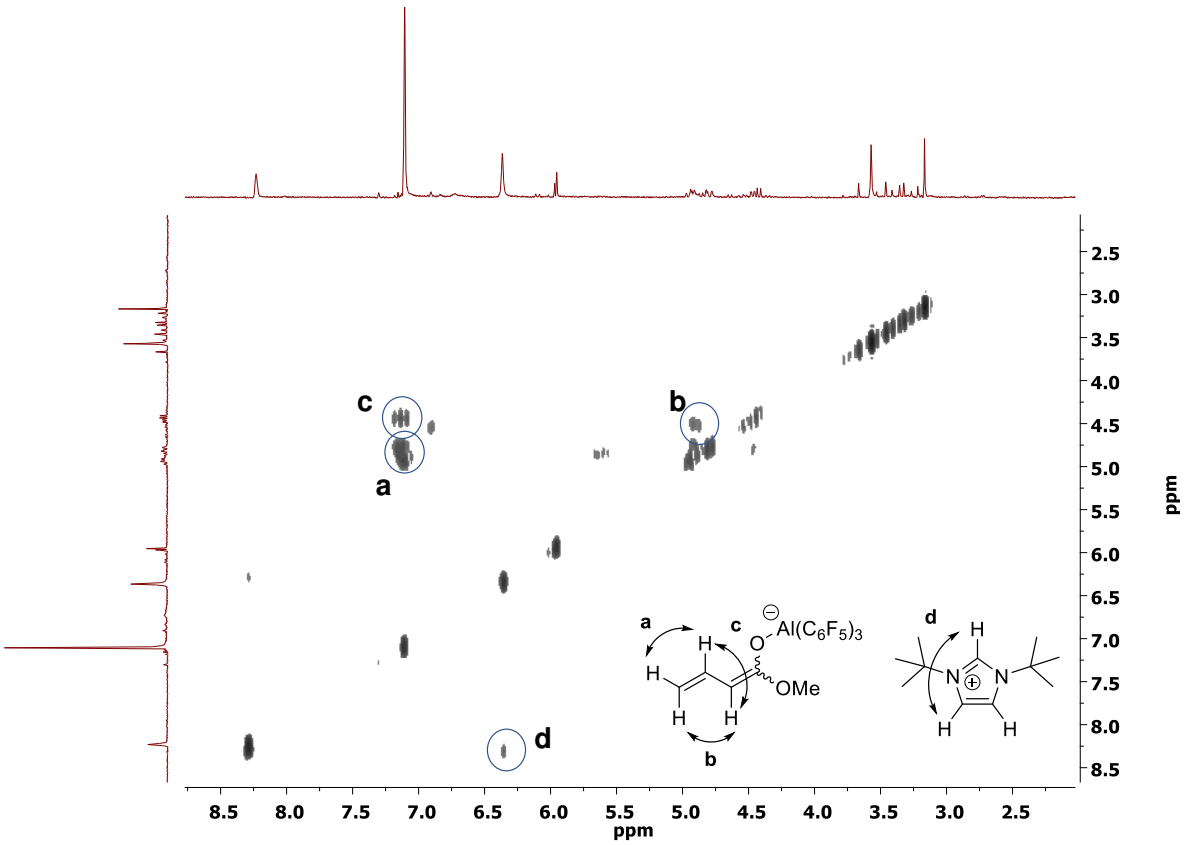

Figure A3. HH-COSY spectrum of *in-situ* generated enolaluminate $^{Al(C6F5)3}$**7**.

MC/TPT Single Addition Product

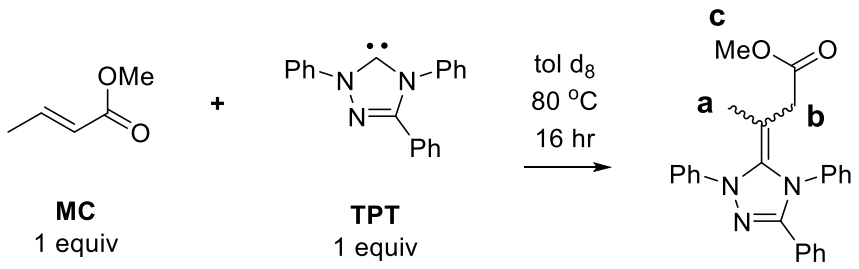

0.080 M stock solutions of MC and TPT were first prepared in toluene-d_8. Then, 0.50 mL of MC stock solution was mixed with 0.50 mL of TPT stock solution in a J-Young type NMR tube, sealed, and inverted several times. It was heated in an oil bath at 80 °C for 16 h, then analyzed by NMR.

Similarly, 0.0149 g of TPT (50 μmol) was added to 1.0 mL of 0.05 M MC in toluene (50 μmol MC) in a 25 mL Schlenk flask and heated to 80 °C in an oil bath while under N_2 for 16 h. Then, after allowing to cool to RT, 0.53 mL of 2 mol % $Al(C_6F_5)_3$ in MC was added by syringe through a septum, to make the overall stoichiometry 100:2:1. No polymerization ensued.

The ^{1}H NMR results (Figure A4) are the same as previously reported.[5] Later, another experiment was performed involving premixing MC:TPT 100:1 for 30 min followed by addition of 2 eq of MAD. Polymerization ensued (100 % conv, M_n = 20.6 kg/mol, I^* = 48 %), however I^* was much lower than the normal addition sequence in run 4 (I^* = 75 %). It is unclear on what time scale enamine formation occurs or if it is relevant to normal polymerization conditions.

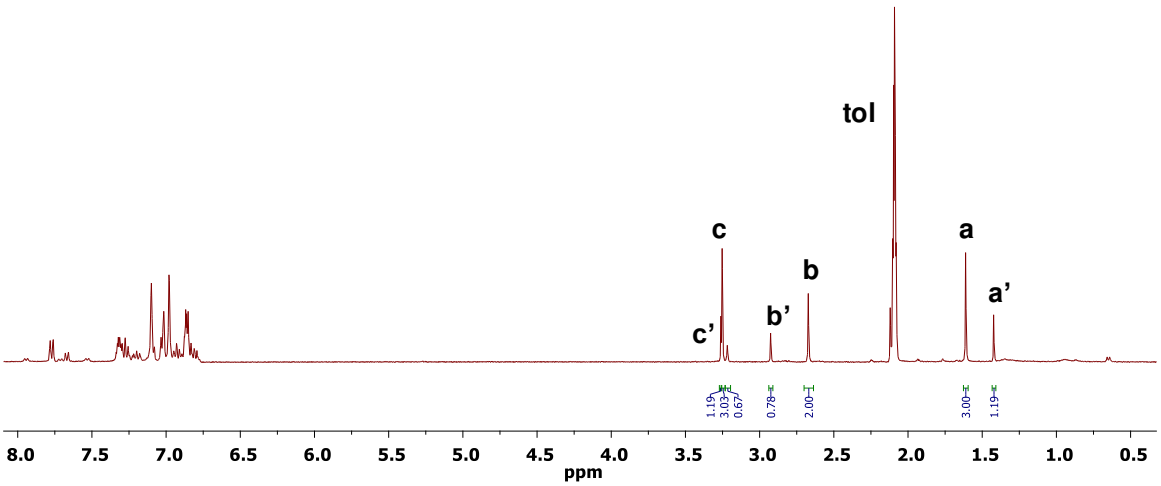

Figure A4. ^{1}H NMR spectrum of MC/TPT single addition product.

In situ Generation of $^{Al(C6F5)3/TPT}$5 and its Decomposition

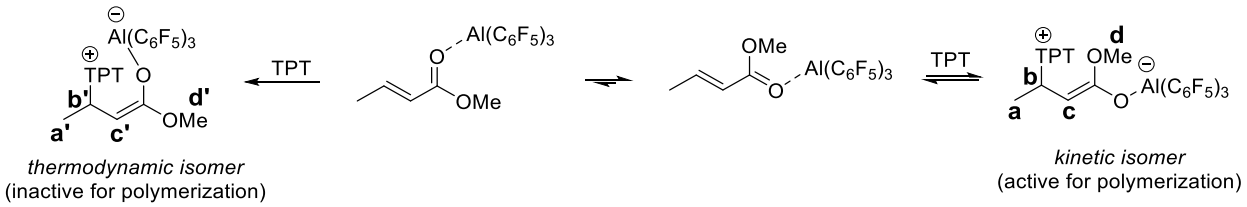

0.080 M stock solutions of MC, $Al(C_6F_5)_3$, and TPT were first prepared in C_6D_6. Then, 0.25 mL of MC stock solution was mixed with 0.25 mL of $Al(C_6F_5)_3$ stock solution in a 5 mL scintillation vial and allowed to mix for 10 min. Then the MC:$Al(C_6F_5)_3$ 1:1 solution was added dropwise to 0.25 mL of TPT stock solution with stirring via Pasteur pipette. The 1:1:1 solution was then pipetted back and forth several times between vials to ensure exact stoichiometry, then pipetted into an J-Young type NMR tube, sealed, and immediately analyzed by NMR. It was then heated at 60 °C for 90 min and analyzed by NMR. It was again heated at 90 °C for 3 h and analyzed by NMR to show the formation of the more stable thermodynamic product. Then, the crude thermodynamic isomer was added to MC:$Al(C_6F_5)_3$ (100:2). No polymerization ensued.

^{1}H NMR spectrum of the MC:$Al(C_6F_5)_3$:TPT 1:1:1 product shown in Figure A5 with different heat exposures revealed two isomeric products, presumably the *cis*/*trans* isomers of zwitterionic $^{Al(C6F5)3/TPT}$**5**. The kinetically favored species at RT is converted to a thermodynamic isomer at high temperatures, or even long periods at RT, and the kinetic product isomerizes seemingly irreversibly. The kinetic product is pale yellow, while the thermodynamic product is a brilliant violet color. One hypothesis is that the *cis* isomer might be the thermodynamic product since it allows for closer proximity between the two opposite charges

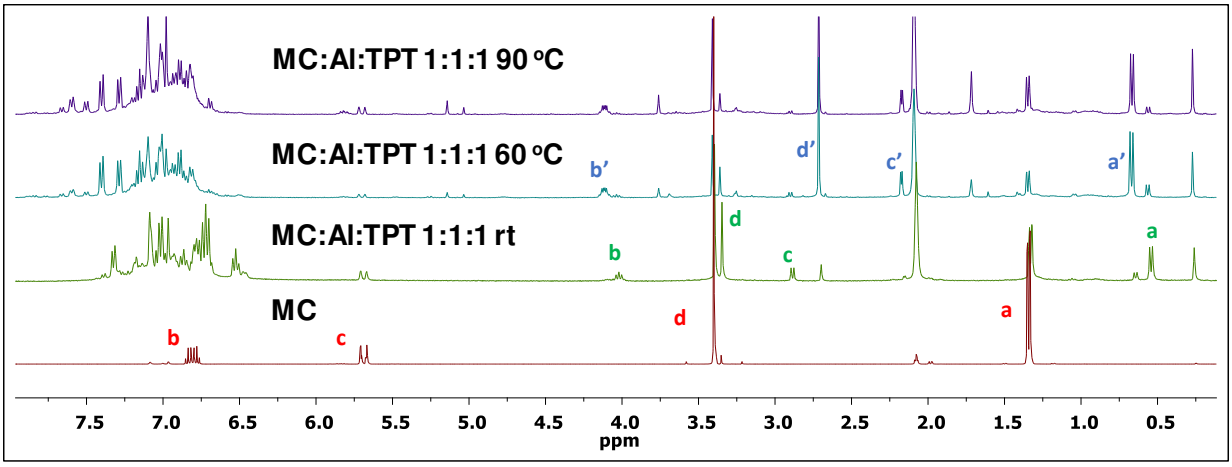

Figure A5. ^{1}H NMR spectra of the proposed zwitterionic product from the reaction of MC:Al(C_6F_5)$_3$:TPT 1:1:1 and its corresponding rearrangement to thermodynamically favored isomer.

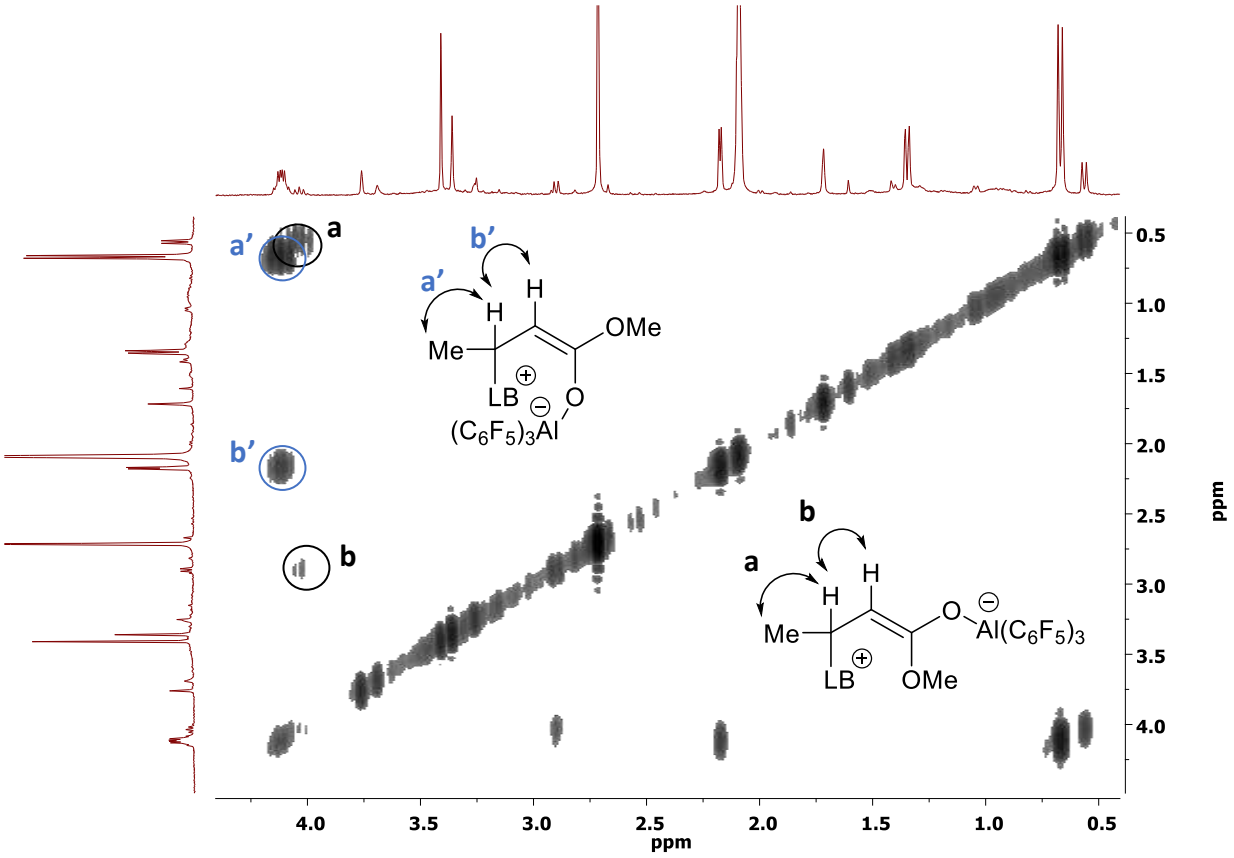

Figure A6. HH-COSY spectrum of MC:$Al(C_6F_5)_3$:TPT 1:1:1 zwitterion (0.80 M in C_6D_6), heated to 60 °C for 90 min, allowing for easy deconvolution of both isomers.

Attempted Generation of $^{B(C6F5)3/TPT}$5

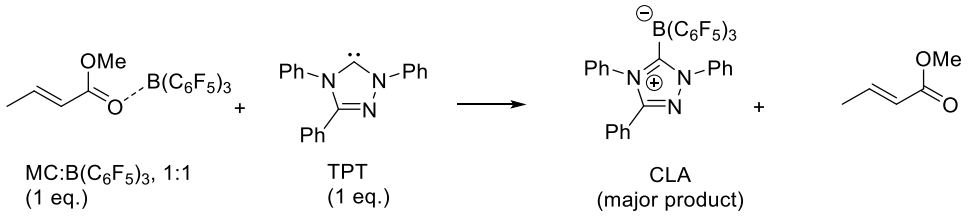

0.080 M stock solutions of MC, $B(C_6F_5)_3$, and TPT were first prepared in C_6D_6. Then, 0.25 mL of MC stock solution was mixed with 0.25 mL of $B(C_6F_5)_3$ stock solution in a 5 mL scintillation vial

and stirred for 10 min. Then the 1:1 MC:$B(C_6F_5)_3$ solution was added dropwise to 0.25 mL of TPT stock solution with stirring via Pasteur pipette. The 1:1:1 solution was then pipetted back and forth several times between vials to ensure exact stoichiometry, then pipetted into an NMR tube, sealed, and immediately analyzed by NMR. MC:$B(C_6F_5)_3$ (1:1) and $B(C_6F_5)_3$:TPT (1:1) controls were performed with similar procedures.

The major product is the CLA (Figure A7). CLA formation is likely the result of insufficient coordination between MC and $B(C_6F_5)_3$. It is assumed that CLA formation is irreversible and leads to low I^* in the MC polymerization using the TPT/$B(C_6F_5)_3$ LP.

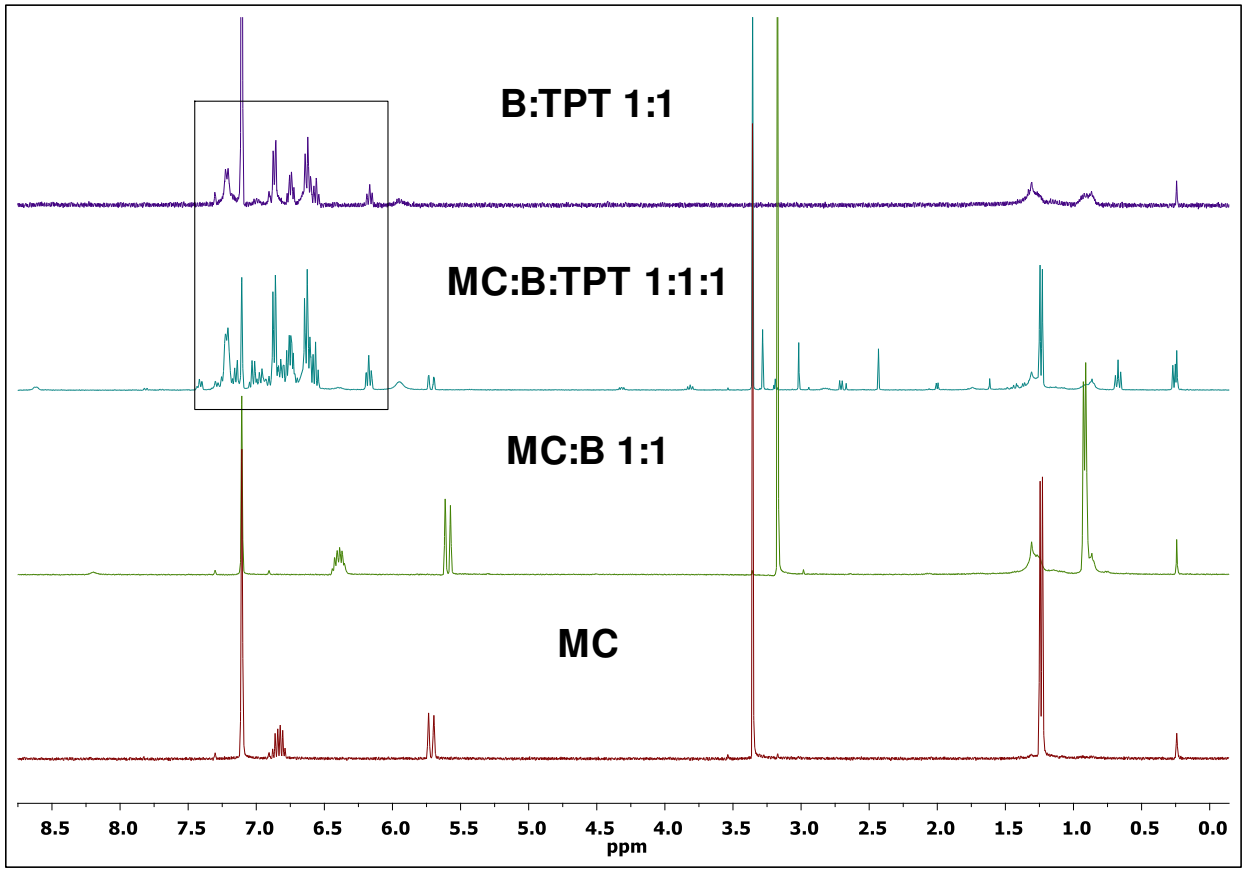

Figure A7. ^{1}H NMR results of attempted synthesis of zwitterionic active species from the reaction of MC:$B(C_6F_5)_3$:TPT (1:1:1) and actual formation of inactive CLA major product.

***In-situ* Generation of Enolaluminate ^{MAD}7**

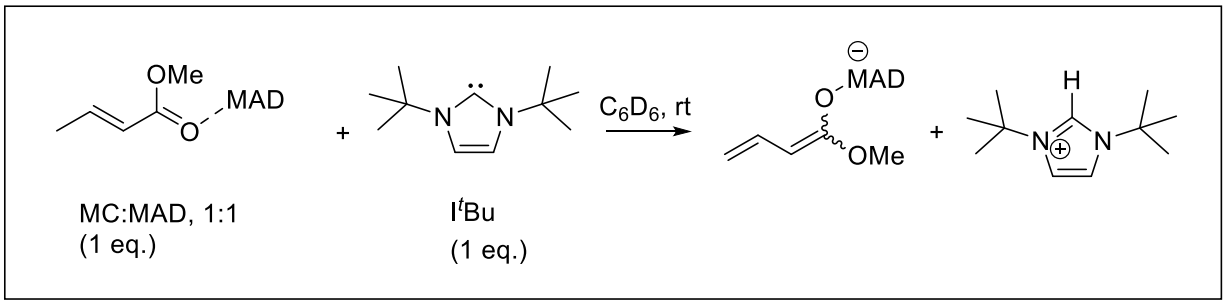

Approximately 2 mL of 0.080 M stock solutions of MC, MAD, and I^{t}Bu were prepared in C_6D_6. To a 5 mL scintillation vial, 0.25 mL of the MAD stock solution was mixed with 0.25 mL of the MC stock solution. The mixture was stirred for 10 min. The 0.50 mL of MC:MAD 1:1 solution was then added dropwise by Pasteur pipette into 0.25 mL of I^{t}Bu stock solution, with stirring. The solution then pipetted back and forth between vials to ensure exact stoichiometry. The MC:MAD:I^{t}Bu 1:1:1 solution was pipetted into an NMR tube, sealed, and immediately analyzed by NMR.

The ^{1}H NMR (Figure A8) shows the relatively clean formation of ^{MAD}**7**. Both isomers are similarly represented. This result provided strong evidence that polymerization with the MAD/I^{t}Bu LP proceeds through basic initiation.

^{1}H NMR spectral data of ^{MAD}**7** are listed as follows: ^{1}H NMR (400 MHz, C_6D_6): δ (ppm) = -0.083, -0.052 ppm (s 3H, Al-CH_3); 1.01, 1.07 (s, 18H, I^{t}Bu-^{t}*Bu*); 1.82, 1.84 (s, 36H, BHT-^{t}*Bu*); 2.24, 2.35 (s, 6H, BHT-CH_3). **Isomer 1**: 3.32, 3.36 (s, *i* = 1.53, OCH_3); 4.55-4.58 (d, *i* = 0.75, CH_2CHCHC(OCH$_3$)); 4.79, 4.87 (d, *i* = 0.54, CH$_2$CHC*H*C(OCH$_3$)); 7.39-7.5 (m, *i* = 0.65, CH$_2$C*H*CHC(OCH$_3$)). **Isomer 2**: 3.74, 3.77 (s, *i* = 1.04, OCH_3); 4.43-4.46 (d, *i* = 0.50, CH_2CHCHC(OCH$_3$)); 4.92, 4.87 (d, *i* = 0.44, CH$_2$CHC*H*C(OCH$_3$)); 6.96-7.06 (m, *i* = 0.52,

$CH_2CHCHC(OCH_3)$). 6.62, 6.70 (s, 2H, -N(^{t}Bu)-CH-N(^{t}Bu)-C*H*-C*H*-); 7.48, 7.58 (s, 1H, -N(^{t}Bu)-C*H*-N(^{t}Bu)-CH); 7.25, 7.26 (s, 4H, BHT-*m*), 4.325 (m, *i* = 0.41).

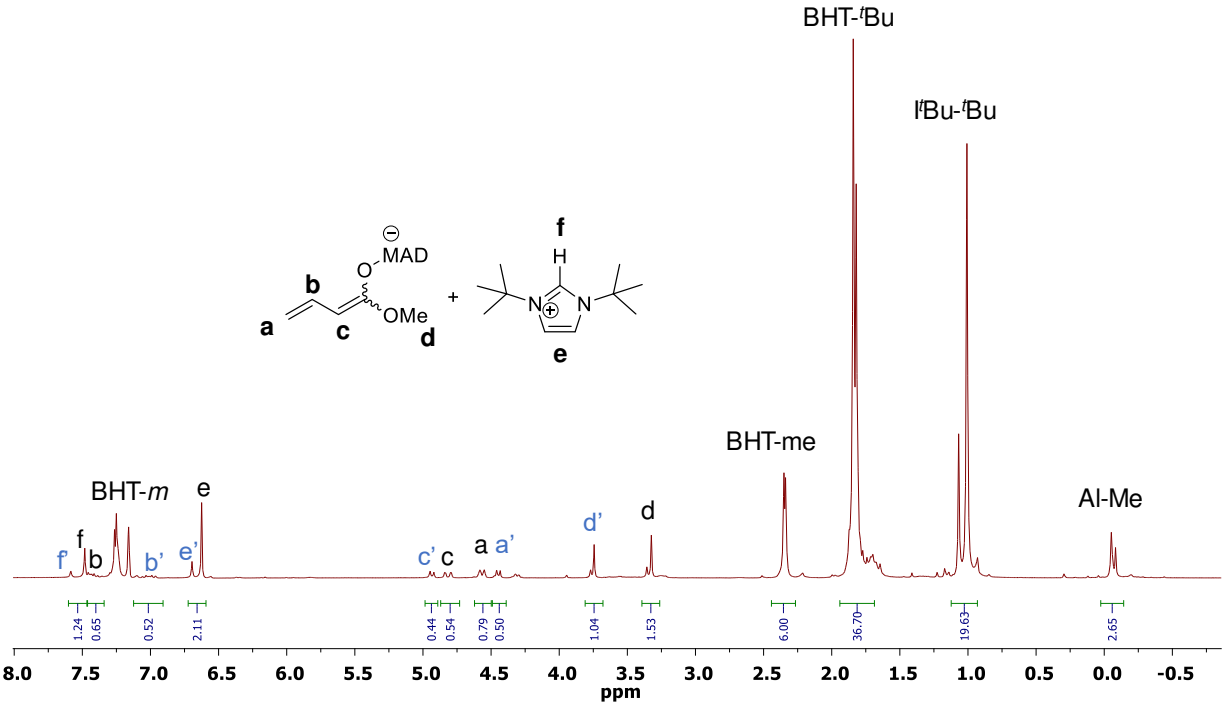

Figure A8. ^{1}H NMR spectrum of ^{MAD}**7**.

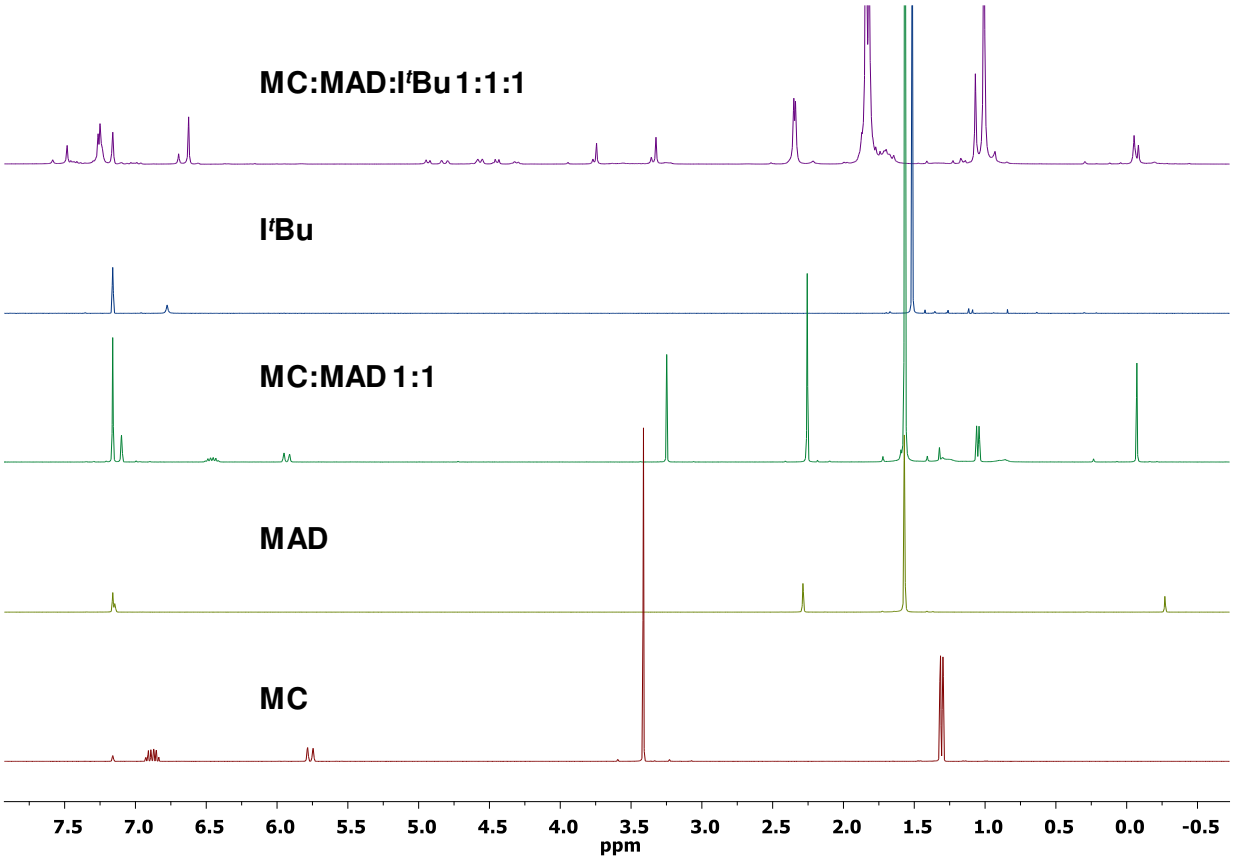

Figure A9. ^{1}H NMR controls, supporting the formation of ^{MAD}**7**.

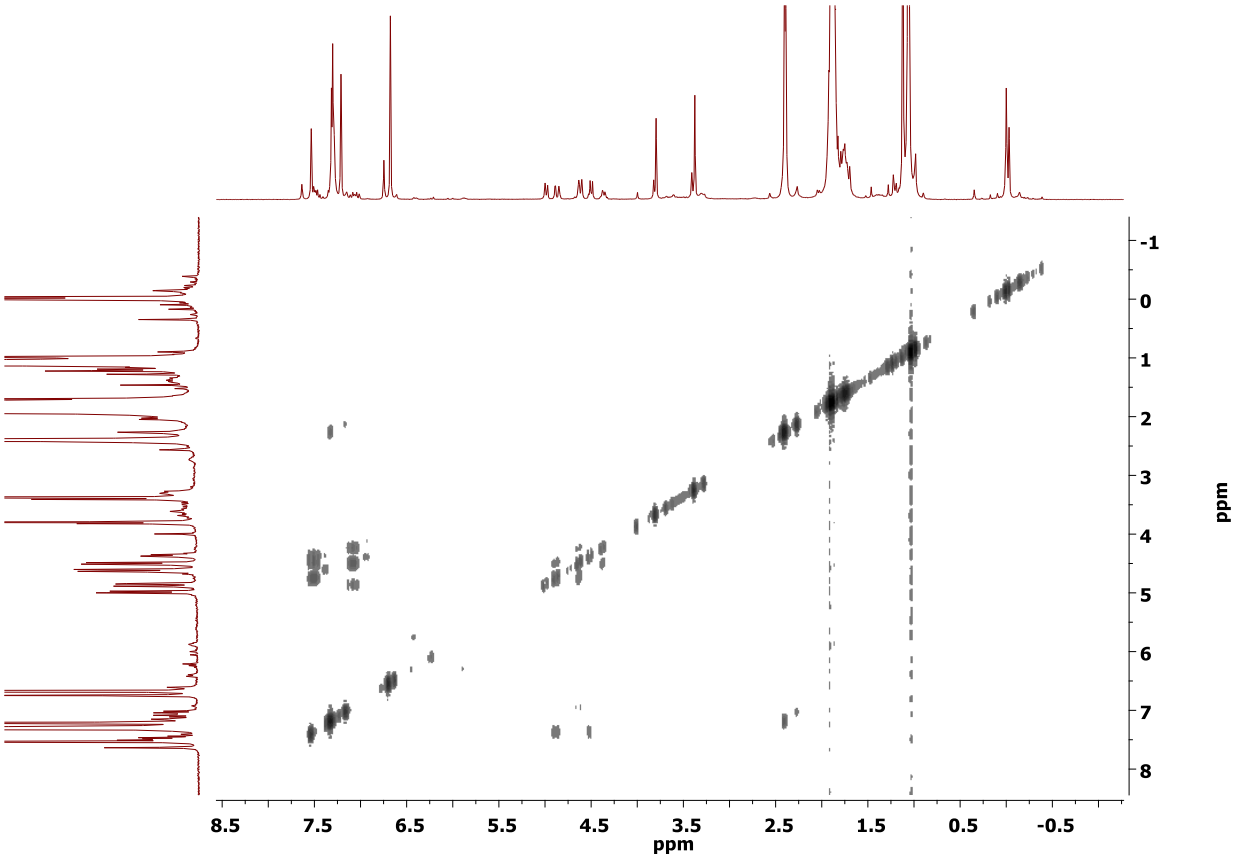

Figure A10. HH-COSY spectrum of ^{MAD}**7**.

***In-situ* Generation of ^{TPT}5**

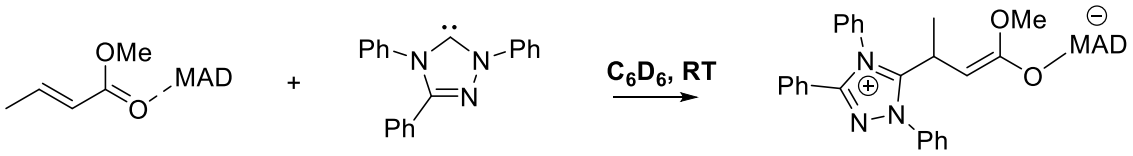

MC:MAD 1:1 | **TPT 1 equiv** | **^{TPT}5**

Approximately 2 mL of 0.080 M stock solutions of MC, MAD, and TPT were prepared in C_6D_6. To a 5 mL scintillation vial, 0.25 mL of the MAD stock solution was mixed with 0.25 mL of the MC stock solution. The mixture was stirred for 10 min. The 0.50 mL of MC:MAD 1:1 solution was then added dropwise by Pasteur pipette into 0.25 mL of TPT stock solution, with stirring. The solution was then pipetted back and forth between vials to ensure exact stoichiometry. The MC:MAD:TPT 1:1:1 solution was pipetted into an NMR tube, sealed, and analyzed immediately by NMR. In a similar fashion, 0.50 mL of MC stock solution was mixed with 0.50 mL of MAD stock solution and stirred for 10 min, then slowly added dropwise to 0.25 mL of TPT stock solution. The resulting MC:MAD:TPT 2:2:1 solution was pipetted back and forth between both vials, then analyzed by NMR.

The ^{1}H NMR spectra clearly show the clean formation of ^{TPT}**5**, which provided strong evidence that MAD/TPT initiates the MC polymerization via the nucleophilic pathway. Especially since the isolated ^{TPT}**5** is active for polymerization when added to MC:MAD 100:1. The MC:MAD:TPT 2:2:1 experiment was also performed in attempt to synthesize the zwitterionic dimer. However, the resulting product was 1 equiv. of ^{TPT}**5**, and 1 eq of activated monomer **4**. Greater monomer concentrations are needed for propagation.

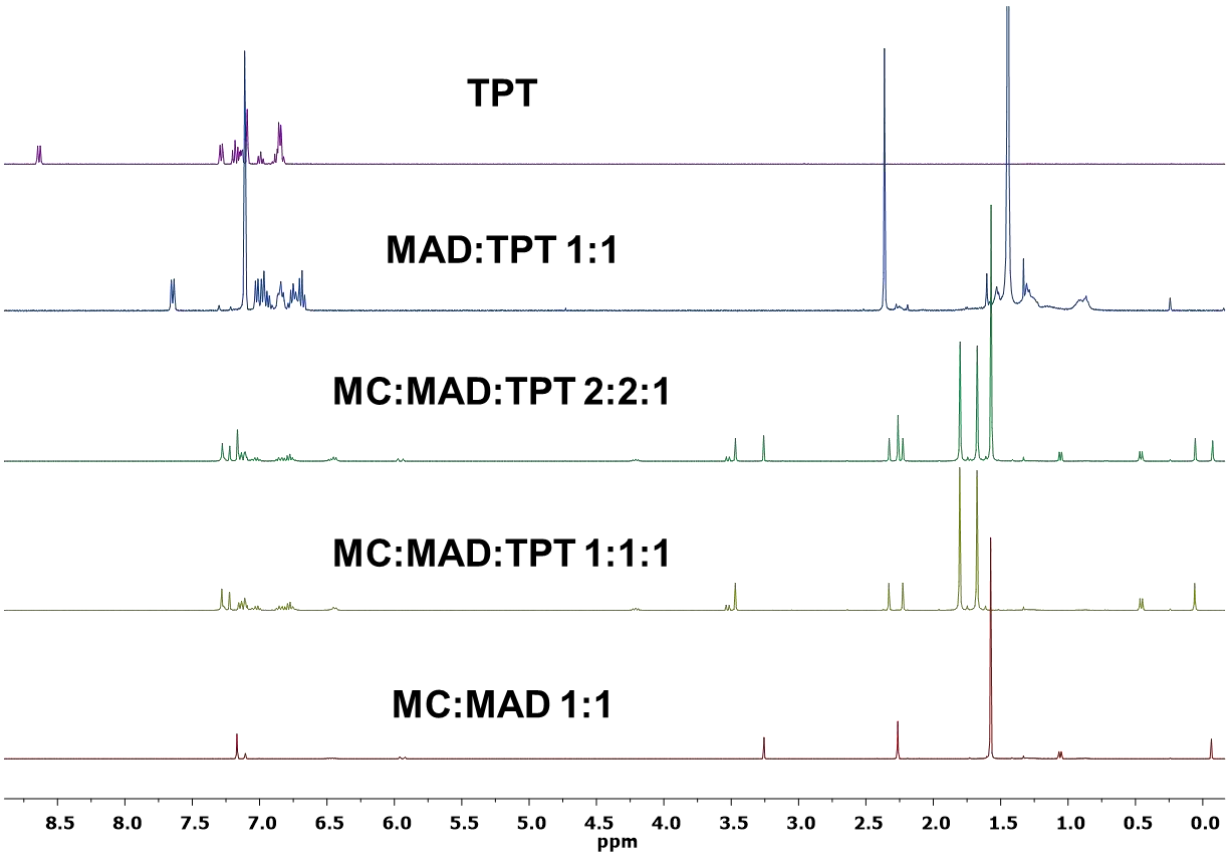

Figure A11. ^{1}H NMR controls, supporting the formation of ^{TPT}**5**.

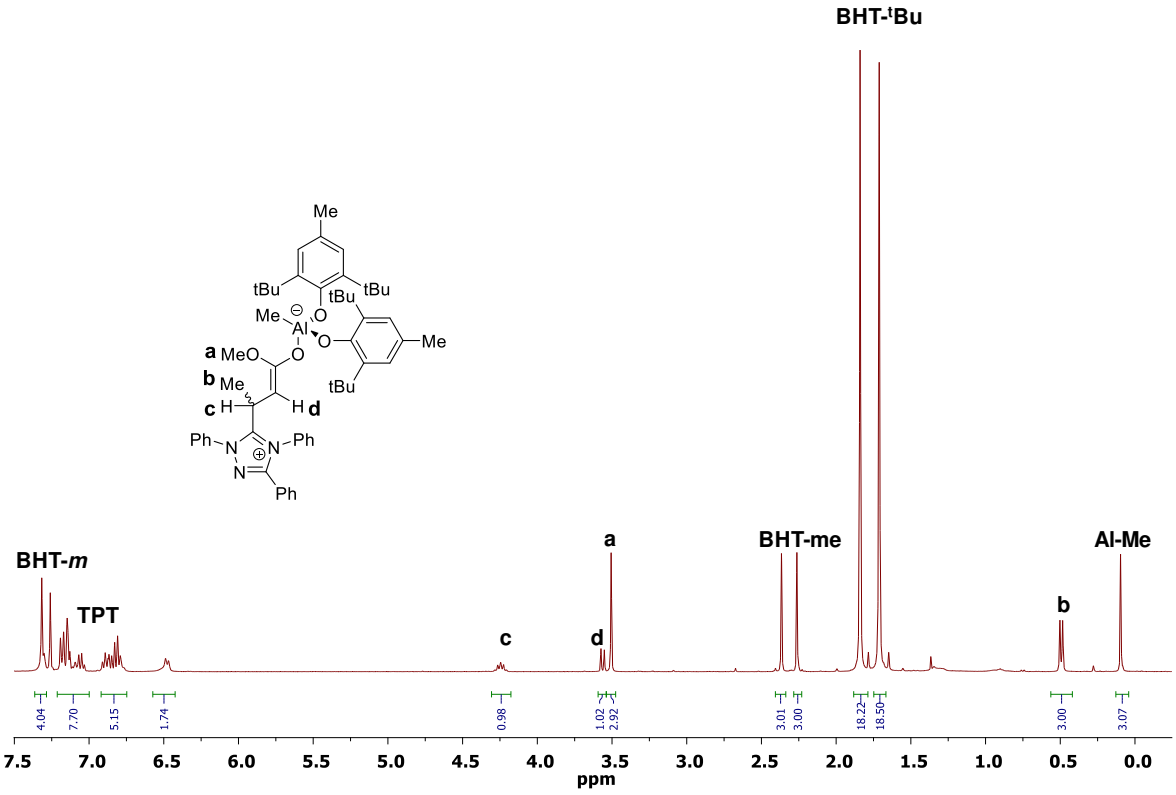

Figure A12. ^{1}H NMR spectrum of ^{TPT}**5**.

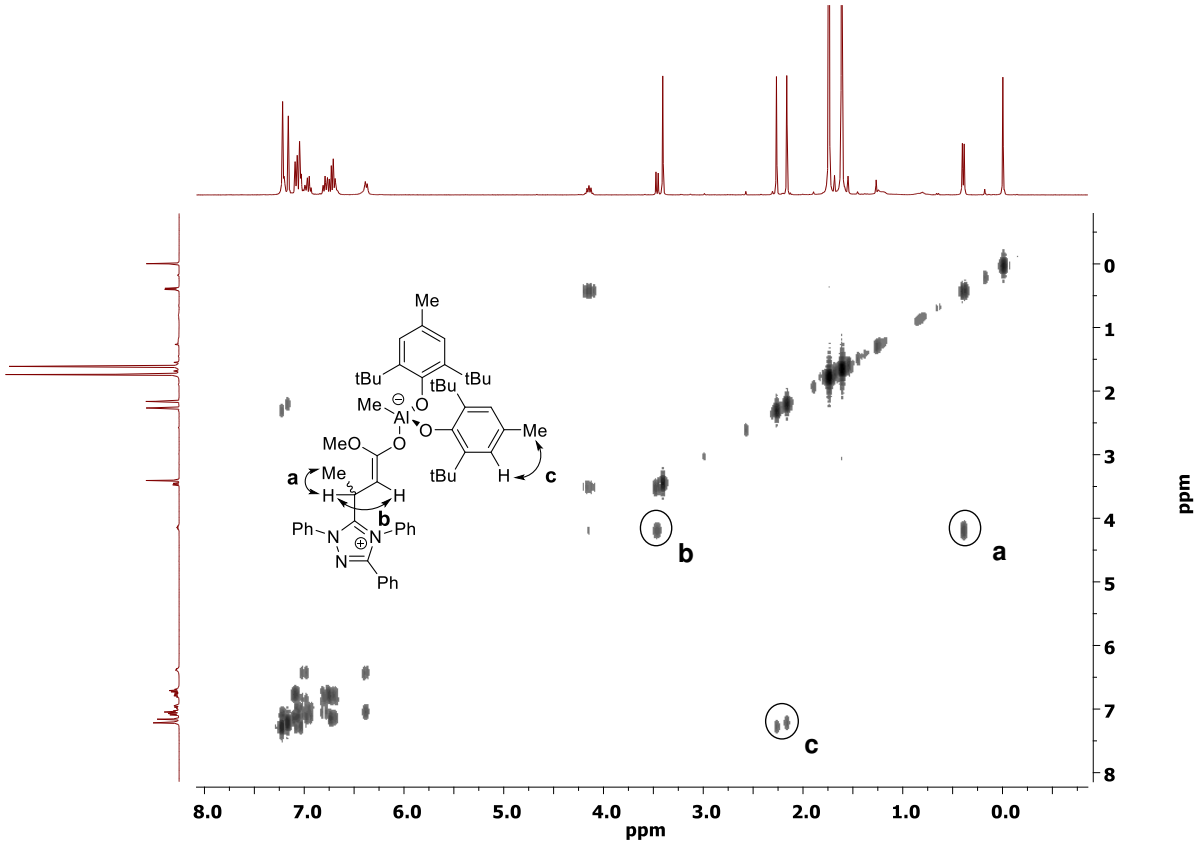

Figure A13. HH-COSY of ^{TPT}**5**.

***In-situ* Generation of ^{NHO}5**

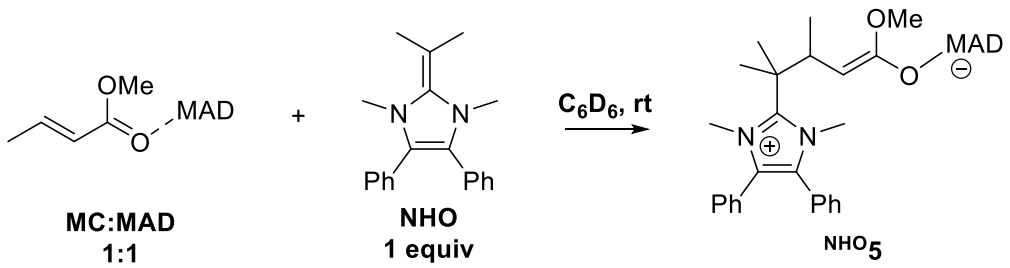

Approximately 2 mL of 0.080 M stock solutions of MC, MAD, and NHO were prepared in C_6D_6. Into a 5 mL scintillation vial, 0.25 mL of the MAD stock solution was mixed with 0.25 mL of the MC stock solution. The mixture was stirred for 10 min. The 0.50 mL of MC:MAD 1:1 solution was then added dropwise by Pasteur pipette into 0.25 mL of NHO stock solution, with stirring. The solution was then pipetted back and forth between vials to ensure exact stoichiometry. The MC:MAD:NHO 1:1:1 solution was pipetted into an NMR tube, sealed, and analyzed immediately by NMR. Attempts to isolate ^{NHO}**5** by precipitation with hexane result in decomposition of the crude product.

The ^{1}H NMR shows the relatively clean formation of ^{NHO}**5** with some other minor co-products. ^{1}H NMR spectral data of ^{NHO}**5** are listed as follows: ^{1}H NMR (400 MHz, C_6D_6): δ (ppm) = 7.29, 7.32 (s, 4H, BHT-*m*), 6.32-6.47 (m, br. *i* = 11.54, C(C_6H_5)C(C_6H_5)), 3.47, 3.48 (s, 4H, (C*H*C(OCH_3)), 2.96-3.21 (br, 6H, C(CH_3)$_2$R), 2.82-2.89 (p, 1H, (NHO$^+$)C*H*(CH_3)), 2.36, 2.39 (s, 3H BHT-CH_3), 1.82, 1.88 (s, 18H BHT-^{t}*Bu*), 1.08 (s, 3H, N(CH_3)), 0.91 (s, 3H, N(CH_3)C(C(CH_3)$_2$R)N(CH_3)), 0.84-0.85 (d, 3H (NHO$^+$)CH(CH_3)), 0.02 (s 3H, Al-CH_3).

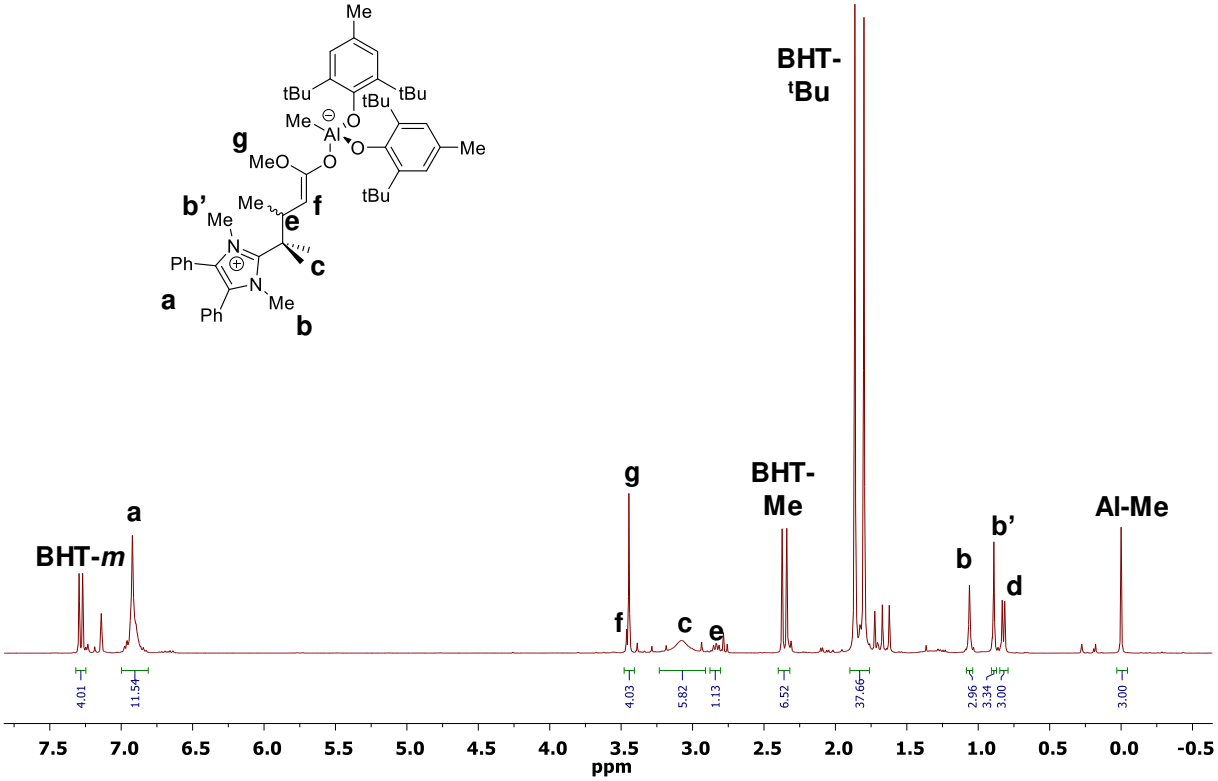

Figure A14. ^{1}H NMR spectrum of *in-situ* generated ^{NHO}**5**.

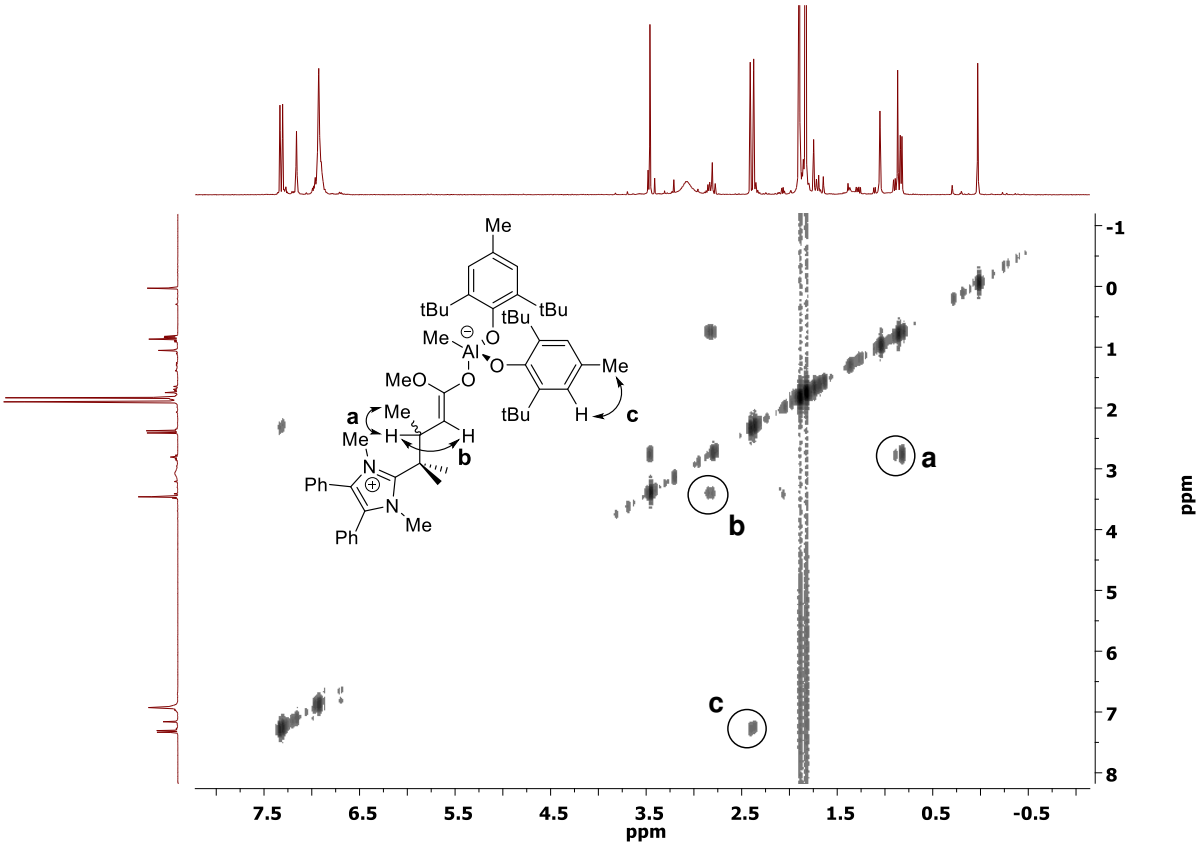

Figure A15. HH-COSY spectrum of *in-situ* generated ^{NHO}**5**.

MALDI-TOF MS Spectra of PMC

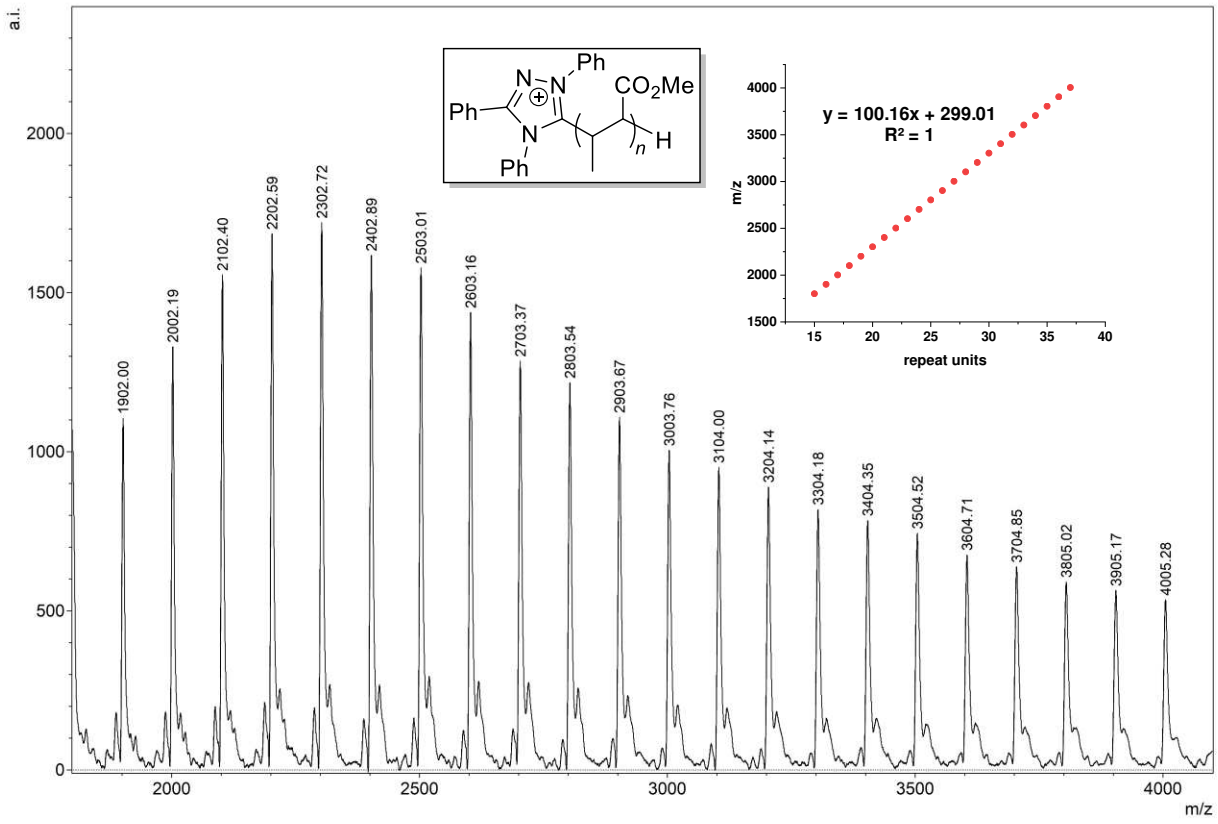

Figure A16. MALDI-TOF MS spectrum and end group calculations for the PMC produced by MC:MAD:TPT = 1000:32:1 (run 15).

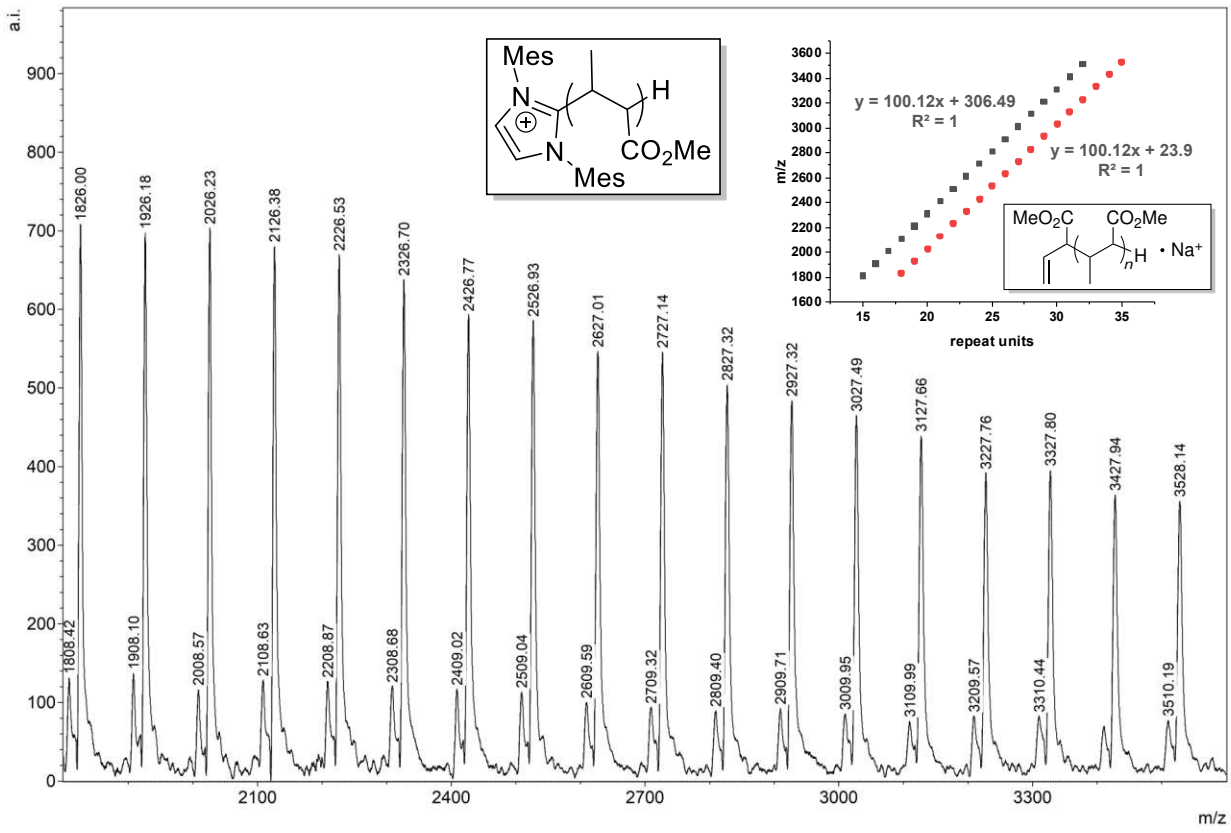

Figure A17. MALDI-TOF MS spectrum and end group calculations for the PMC produced by MC:MAD:IMes = 1000:20:1.

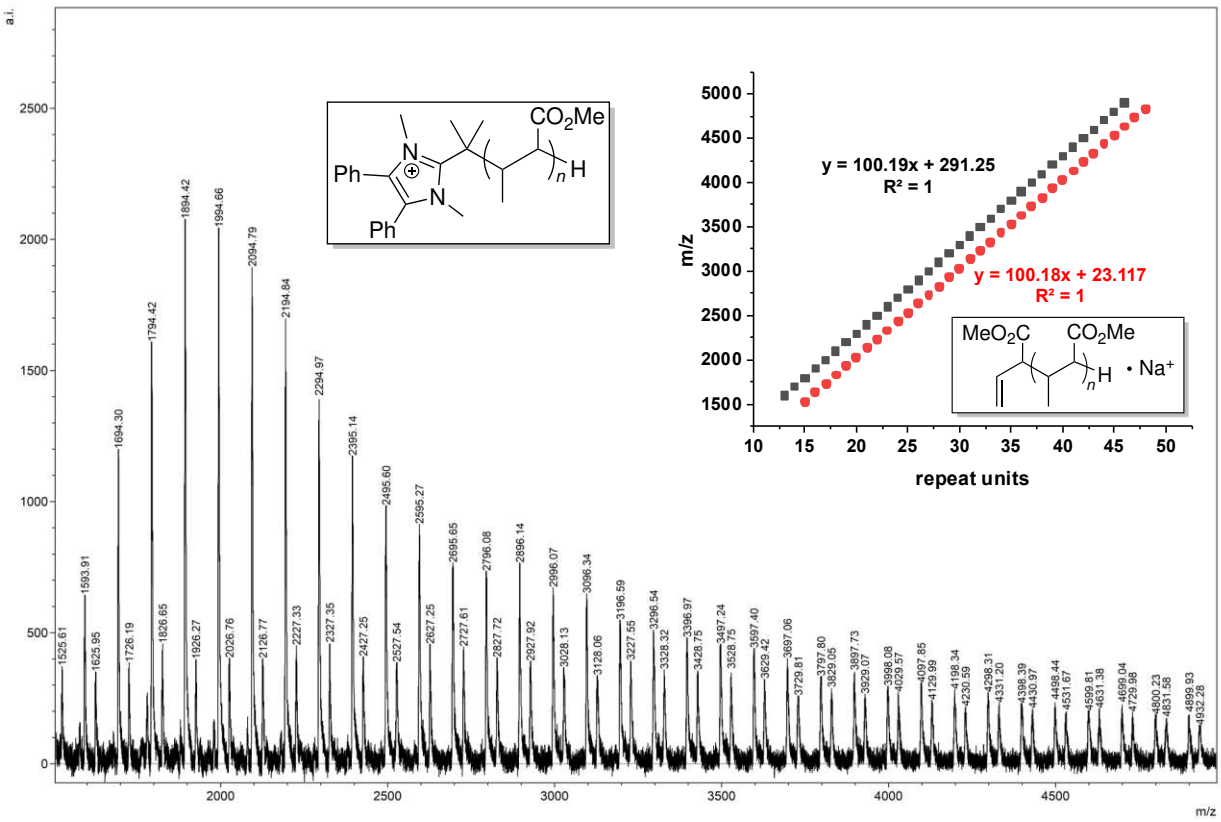

Figure A18. MALDI-TOF MS spectrum and end group calculations for the PMC produced by MC:MAD:NHO = 1000:20:1.

Synthesis of Low Molecular Weight Polymers for End Group Analysis

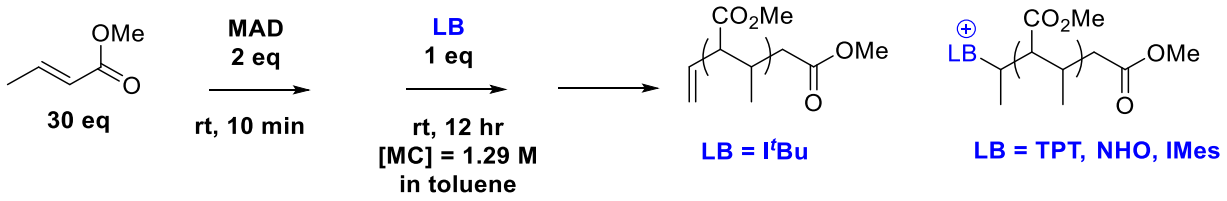

Conditions: 0.0480 g of MAD was dissolved in 0.16 mL of MC (6.6 mol % MAD). Then, 1 mL of 0.050 M LB solution was added to the MC/MAD solution to make total stoichiometry MC:MAD:LB 30:2:1.

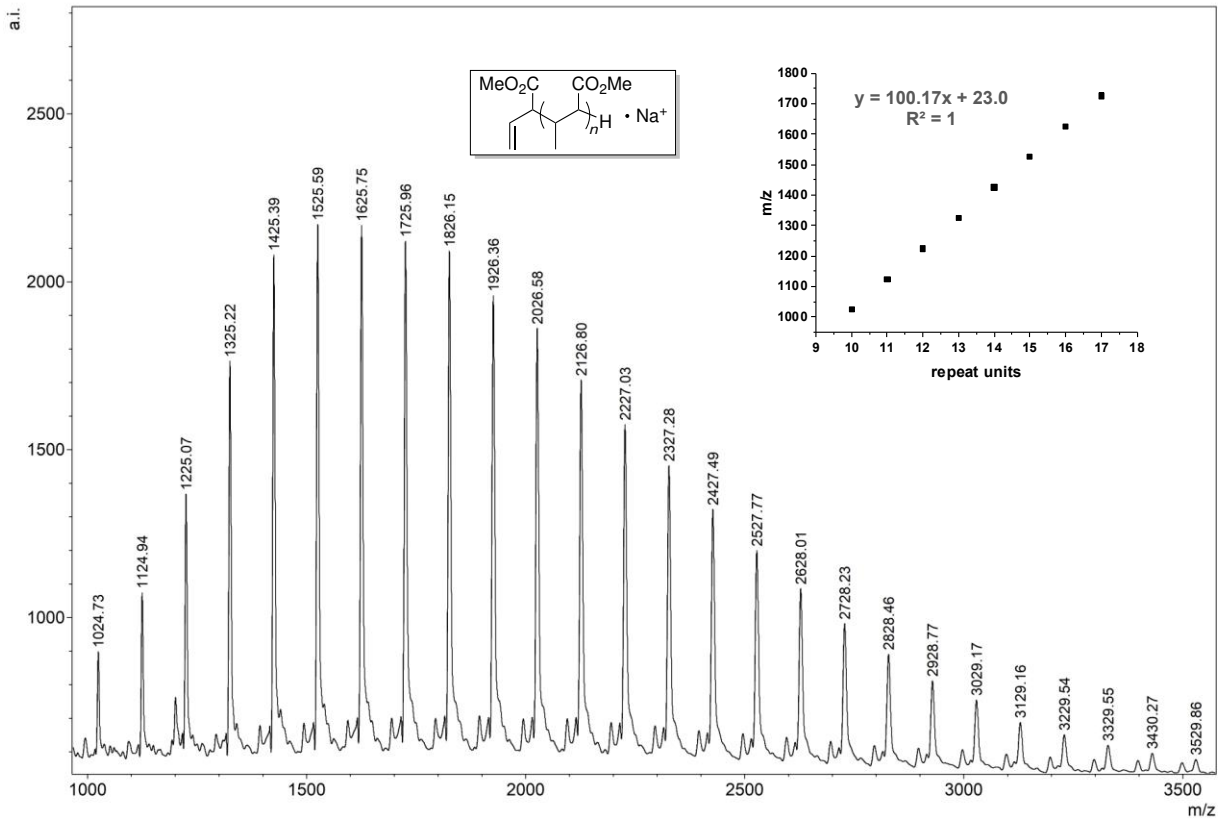

Figure A19. MALDI-TOF MS spectrum and end group calculations for low molecular weight PMC produced by MC:MAD:I^{t}Bu = 30:2:1 ([MC] = 1.43 M in toluene, RT, 12 h).

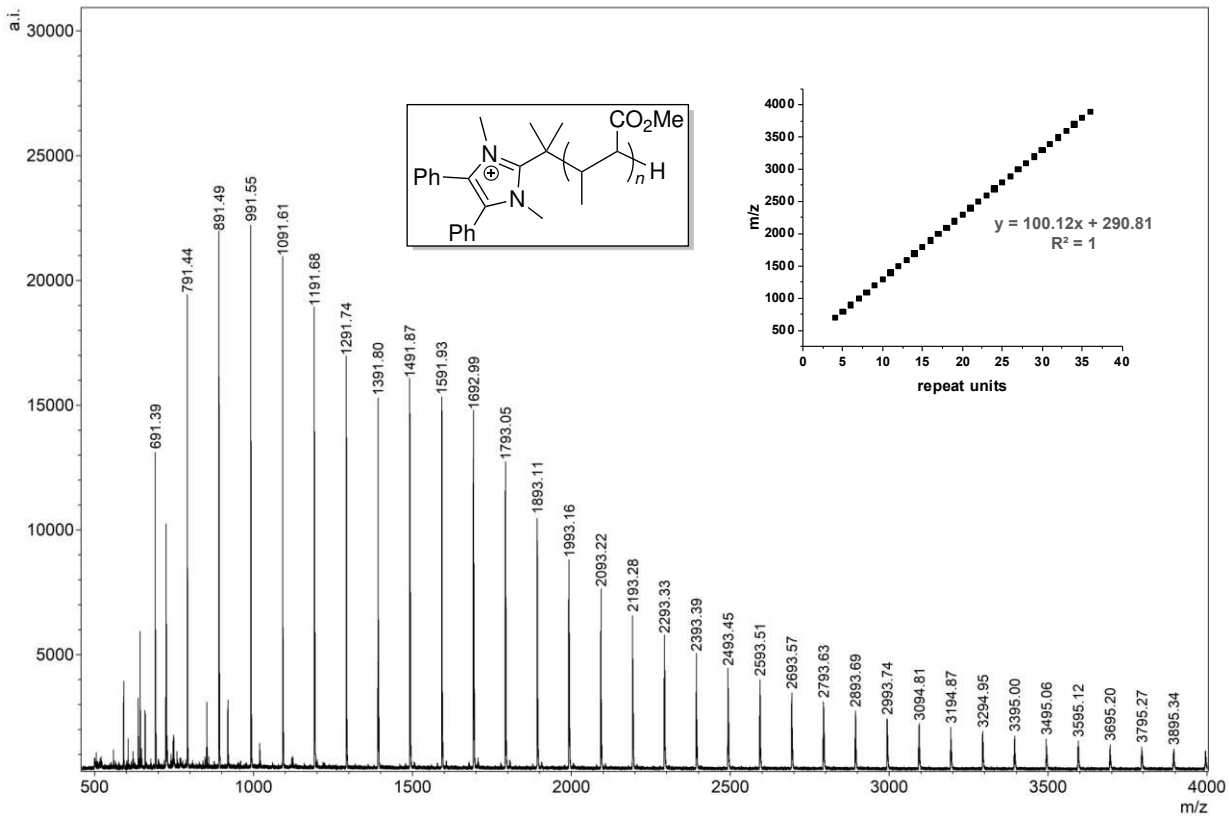

Figure A20. MALDI-TOF MS spectrum and end group calculations for low molecular weight PMC produced by MC:MAD:NHO = 30:2:1 ([MC] = 1.43 M in toluene, RT, 12 h).

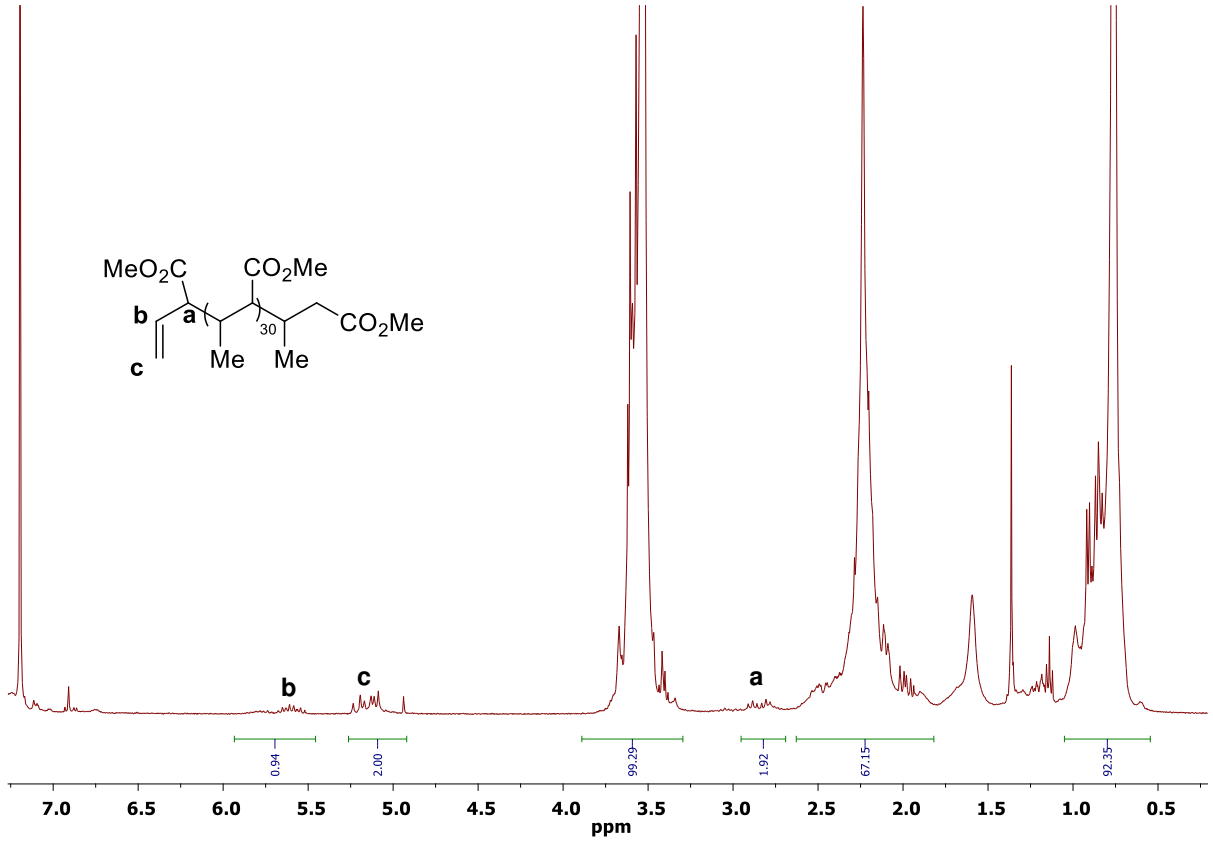

Figure A21. ^{1}H NMR spectrum of the oligomerization product by MC:MAD:I^{t}Bu = 30:2:1, [MC] = 1.43 M in toluene, RT, 12 h. ($CDCl_3$)

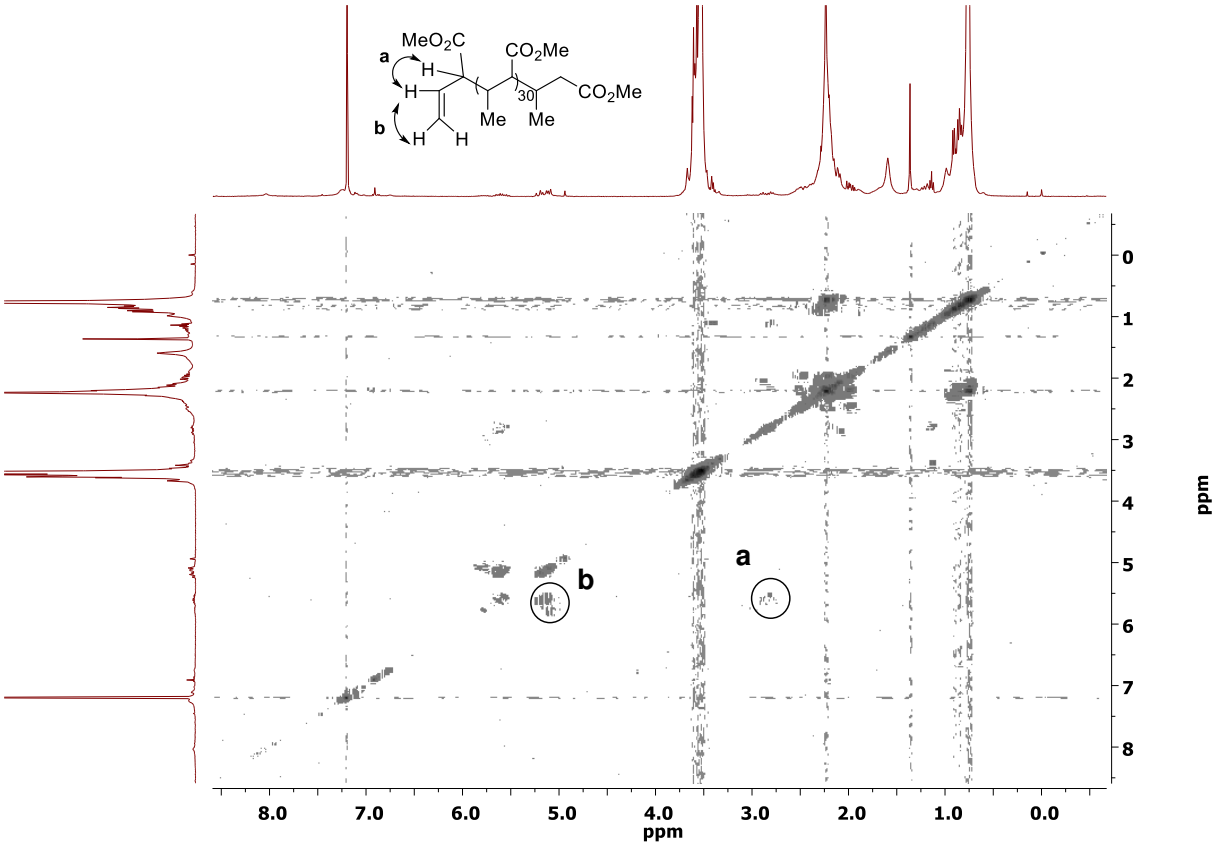

Figure A22. HH-COSY spectrum of the oligomerization product by MC:MAD:I^{t}Bu = 30:2:1, [MC] = 1.43 M in toluene, RT, 12 h. ($CDCl_3$)

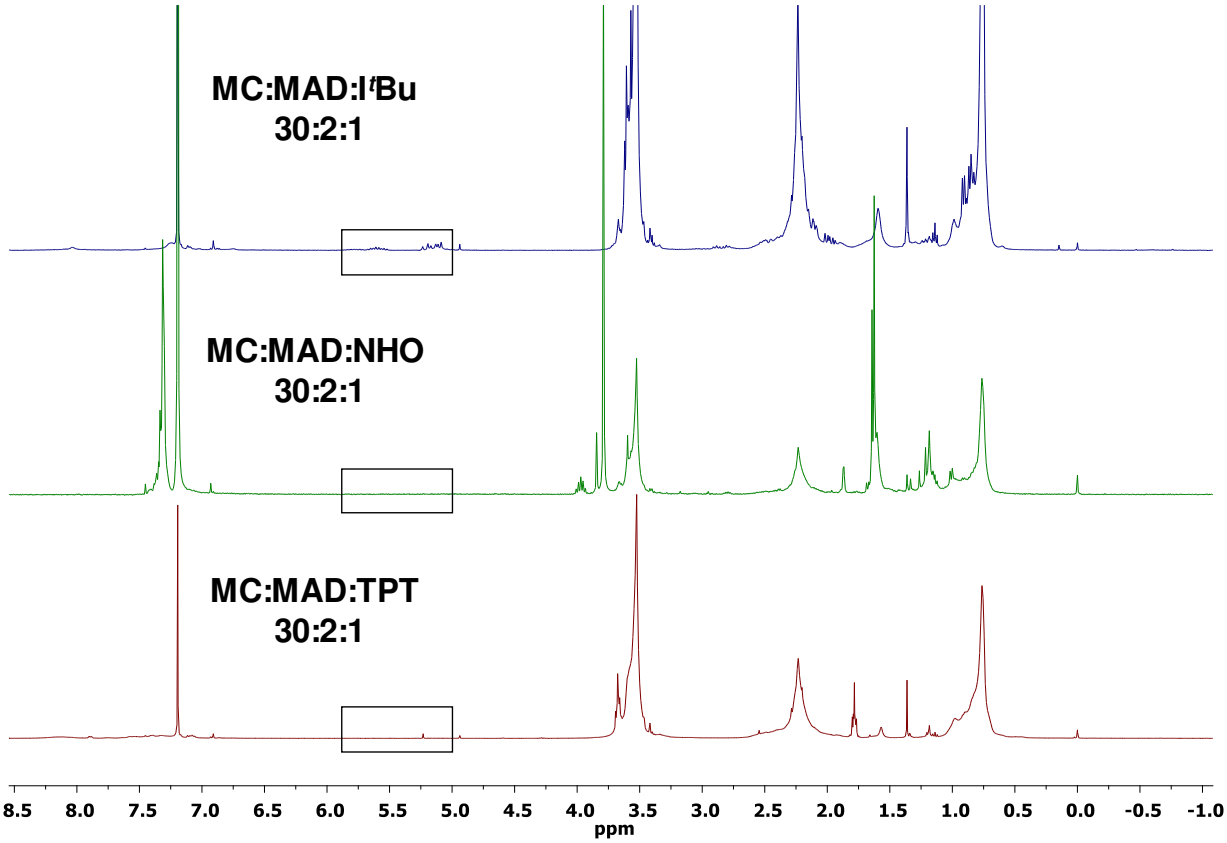

Figure A23. ^{1}H NMR spectral comparison of the oligomerization products by MC:MAD:LB = 30:2:1, [MC] = 1.43 M in toluene, RT, 12 h. ($CDCl_3$)

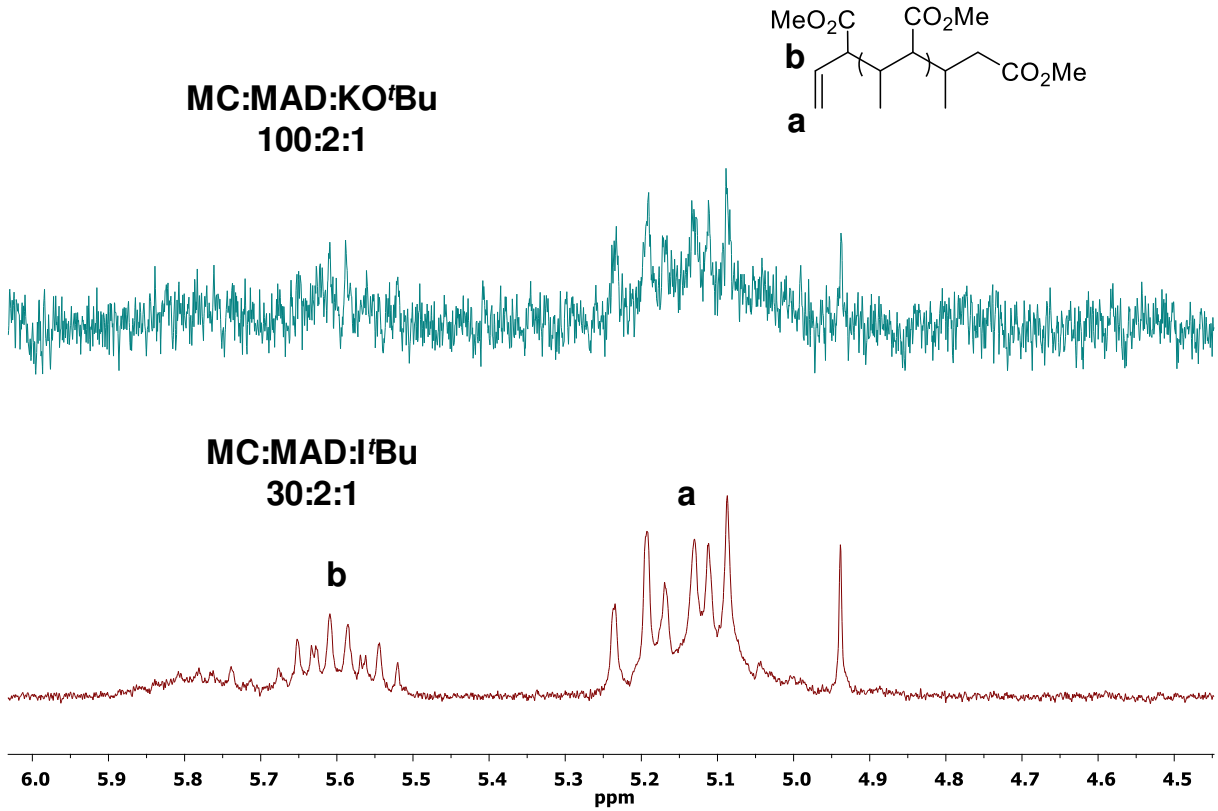

Figure A24. ^{1}H NMR Spectral comparison of the oligomerization product by MC:MAD:I^{t}Bu = 30:2:1 and the polymerization product by MC:MAD:KO^{t}Bu = 100:2:1 with expanded olefin region to show the common vinyl end group. ($CDCl_3$)

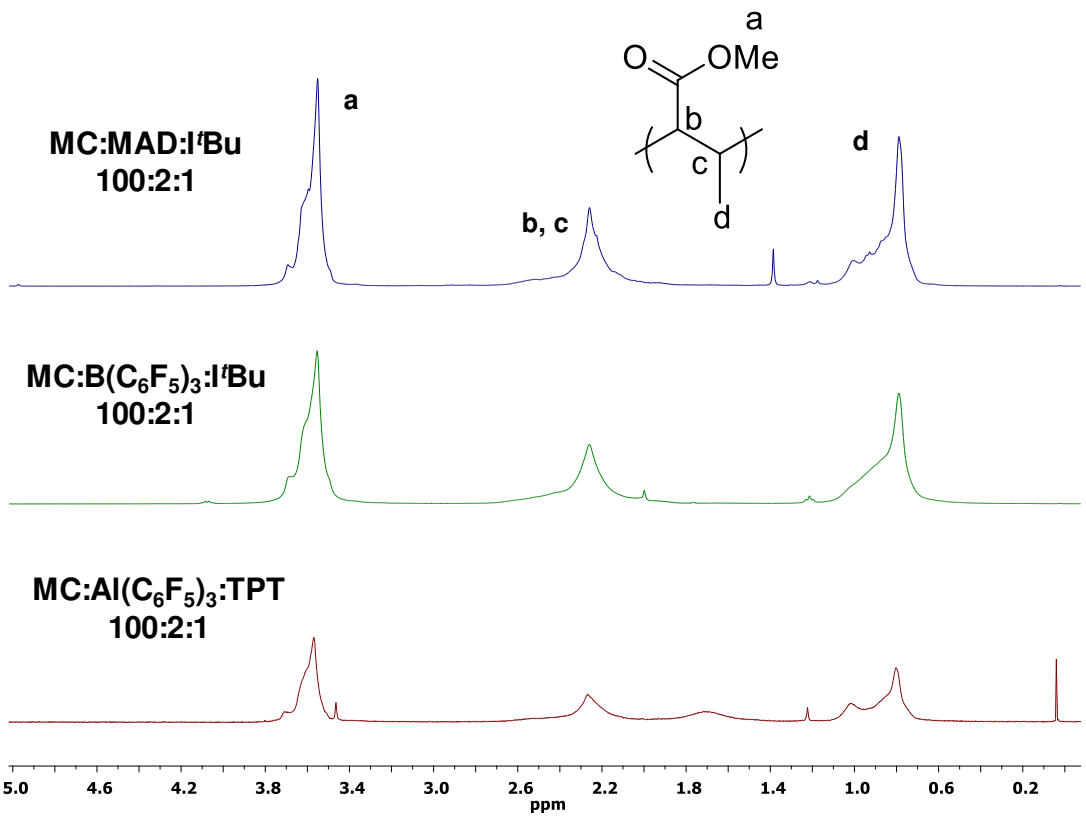

Figure A25. ^{1}H NMR spectra of PMC produced by MC:LA:LB = 100:2:1, showing similar stereochemical signature regardless of LA. ($CDCl_3$)

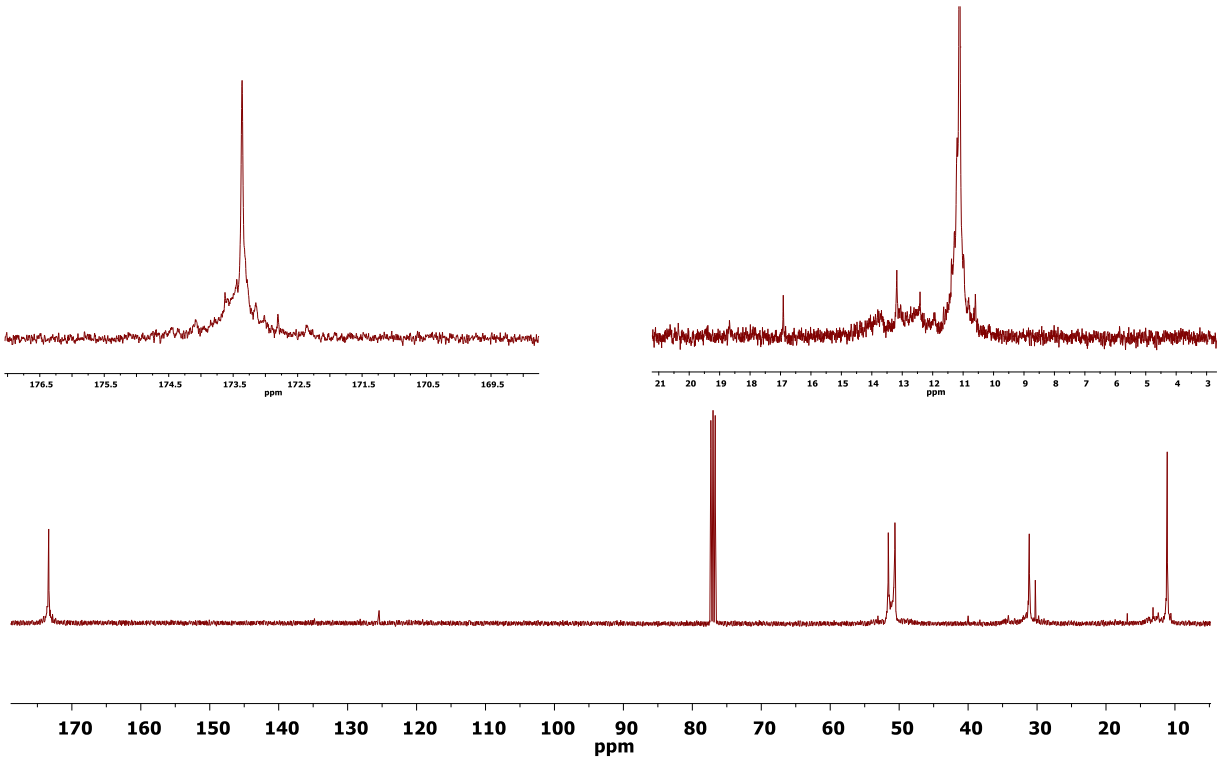

Figure A26. ^{13}C NMR spectrum of PMC by MC:MAD:I^{t}Bu = 100:2:1. ($CDCl_3$)

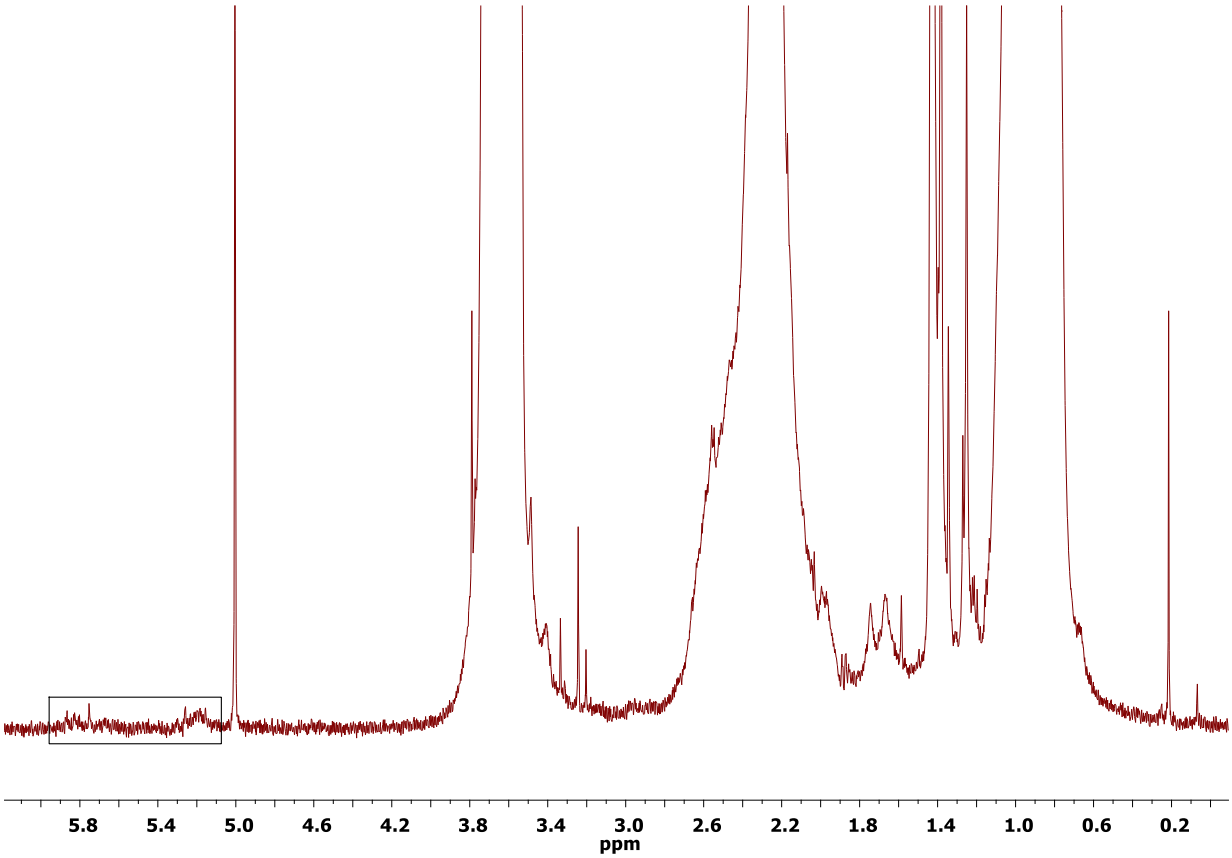

Figure A27. ^{1}H NMR spectra of PMC produced by MC:MAD:NHO = 100:2:1 (run 7), showing faint outline of olefin end groups (Mn = 16 kg/mol). ($CDCl_3$)

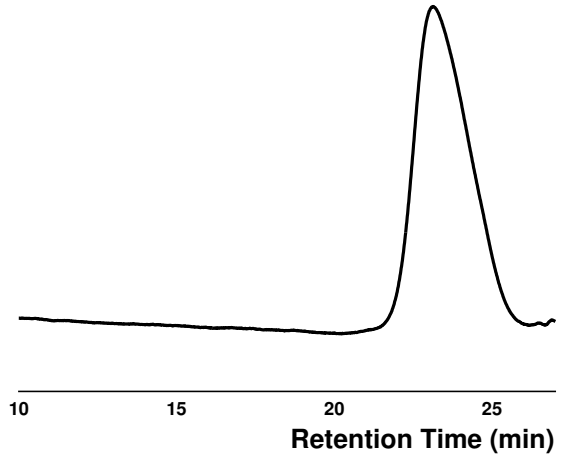

Figure A28. GPC trace of Run 1 (Table 2.1), obtained by MC/MAD/I^{t}Bu = 100:2:1, M_n = 3.63 kg/mol $Đ$ = 1.35

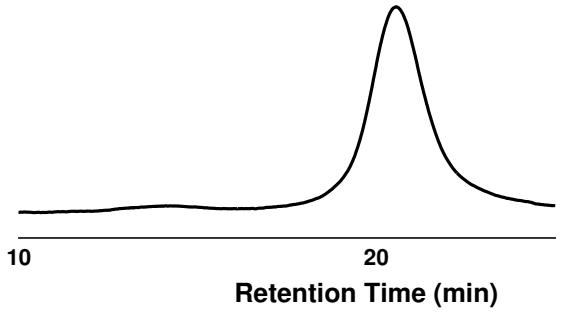

Figure A29. GPC trace of Run 5 (Table 2.1), obtained by MC/MAD/TPT = 200:2:1, M_n = 21.3 kg/mol $Đ$ = 1.22

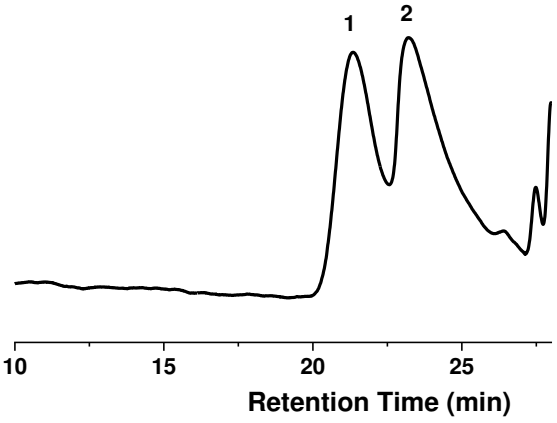

Figure A30. GPC trace of Run 7 (Table 2.1), obtained by MC/MAD/NHO = 100:2:1. Peak 1 M_n = 15.9 kg/mol $Đ$ = 1.10 (45.7%); Peak 2 M_n = 15.0 kg/mol $Đ$ = 1.04 (54.3%)

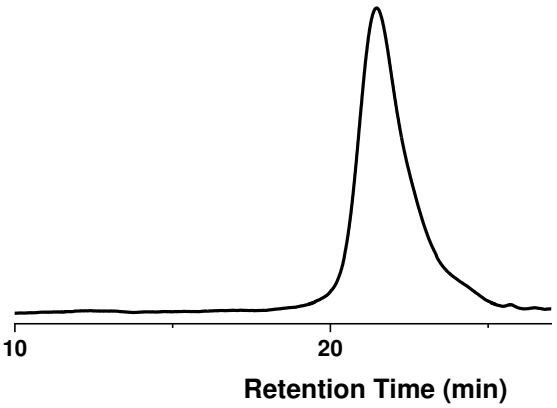

Figure A31. GPC trace of Run 10 (Table 2.1), obtained by MC/MAD/^{TPT}**5** = 100:1:1. M_n = 20.7 kg/mol $Đ$ = 1.10

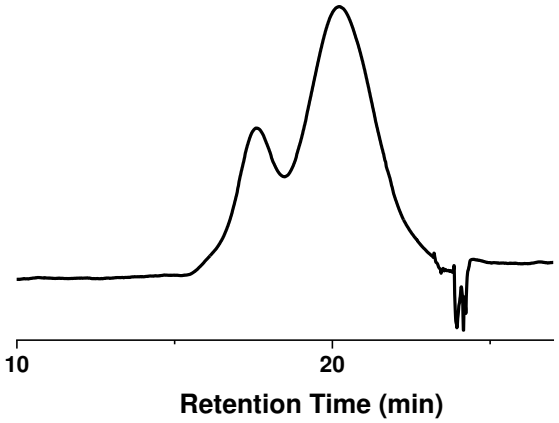

Figure A32. GPC trace of Run 13 (Table 2.2), obtained by MC/MAD/I^{t}Bu = 4000:80:1. M_n = 78.3 kg/mol $Đ$ = 4.39

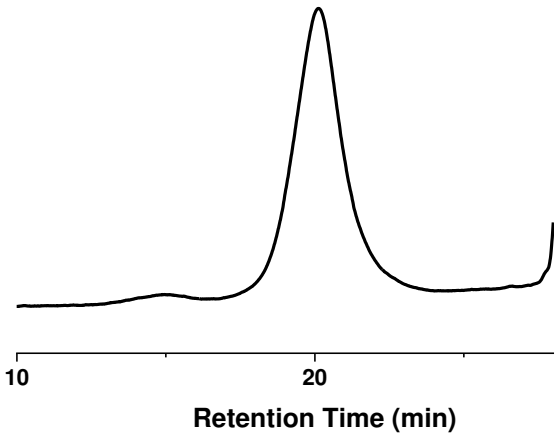

Figure A33. GPC trace of Run 14 (Table 2.2), obtained by MC/MAD/TPT = 500:16:1. M_n = 48.8 kg/mol $Đ$ = 1.18

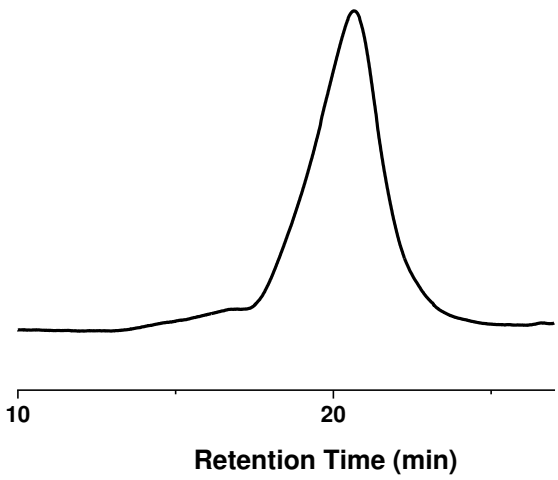

Figure A34. GPC trace of Run 17 (Table 2.2), obtained by MC/MAD/NHO = 500:16:1. M_n = 35.3 kg/mol $Đ$ = 1.88

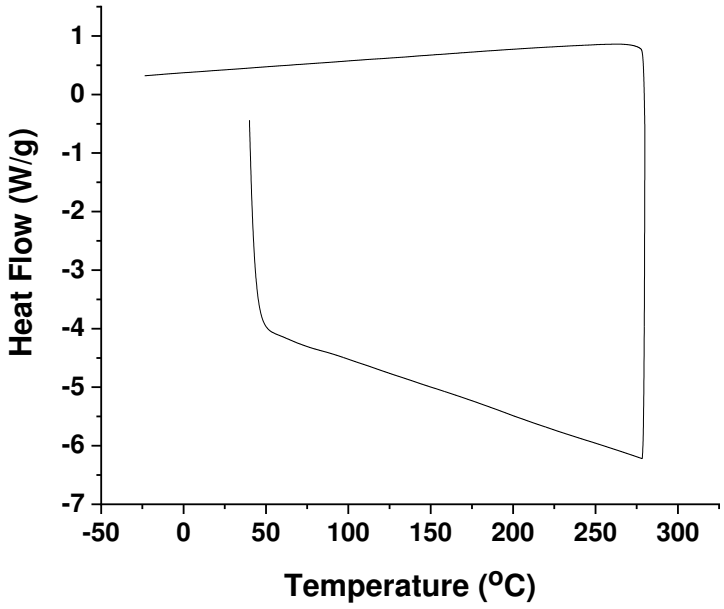

Figure A35. A representative DSC curve of PMC (run 15, Table 2.2).

References cited in Appendix A

[1] (a) Enders, D.; Breuer, K.; Raabe, G.; Runsink, J.; Teles, J. H.; Melder, J. P.; Ebel, K.; Brode, S. Preparation, Structure, and Reactivity of 1,3,4-Triphenyl-4,5-dihydro-1H-1,2,4-triazol-5-ylidene, a New Stable Carbene. *Angew. Chem. Int. Ed. Engl.* **1995**, *34*, 1021– 1023; (b) Enders, D.; Breuer, K.; Kallfass, U.; Balensiefer, T. Preparation and Application of 1,3,4-Triphenyl-4,5-dihydro-1H-1,2,4-triazol-5-ylidene, A Stable Carbene. *Synthesis*, **2003**, 1292–1295.

[2] Wang, Q. Y.; Zhao, W. C.; He, J. H.; Zhang, Y. T.; Chen, E. Y.-X. Living Ring-Opening Polymerization of Lactones by *N*-Heterocyclic Olefin/Al(C_6F_5)$_3$ Lewis Pairs: Structures of Intermediates, Kinetics, and Mechanism. *Macromolecules* **2017**, *50*, 123-136.

[3] Feng, S.; Roof, G. R.; Chen, E. Y.-X. Tantalum(V)-Based Metallocene, Half-Metallocene, and Non-Metallocene Complexes as Ethylene–1-Octene Copolymerization and Methyl Methacrylate Polymerization Catalysts. *Organometallics* **2002**, *21*, 832−839.

[4] Shreve, A. P.; Mulhaupt, R.; Fultz, W.; Calabrese, J.; Robbins, W.; Ittel, S. Sterically Hindered Aryloxide-substituted Alkylaluminum Compounds. *Organometallics* **1988**, *7*, 409–416.

[5] Flanagan, J. C. A.; Kang, E. J.; Strong, N. I.; Waymouth, R. M. Catalytic Dimerization of Crotonates. *ACS Catal*. **2015**, *5*, 5328–5332.

Appendix B

Supplementary Information Corresponding to Chapter 3

Taken verbatim from:

McGraw, M. L. & Chen, E. Y.-X. Borane/silane frustrated Lewis pairs for polymerization of β-substituted Michael acceptors. *Tetrahedron* **2019**, *75*, 1475–1480.

Materials and methods

Methyl crotonate was purchased from Sigma-Aldrich and dried for 24 h over CaH_2 followed by vacuum distillation at 45 °C at reduced pressure. The distillate MC was then titrated by dropwise addition of $AlEt_3$ until the solution turned pale yellow, and redistilled, and stored in a brown bottle inside a glovebox prior to use (within one week of monomer purification). 1 was purchased from Sigma-Aldrich and stored over molecular sieves at –30 °C inside the glovebox freezer. NHC 1,3-di-*tert*-butylimidazolin-2-ylidene (I^tBu) was purchased from VWR and used as received, and NHC 1,3,4-triphenyl4,5-dihydro-1H-1,2,4-triazol-5-ylidene (TPT) was synthesized according to literature procedures.

[1] Toluene was dried with NaK alloy and filtered through a 0.2 μm filter just prior to use. The same procedure was used to purify benzene-d_6. Dichloromethane (DCM) was dried for 48 h with CaH_2 and distilled at 1 atm. $B(C_6F_5)_3$ was obtained from Boulder Scientific Co. as a research gift and purified twice by sublimation at 40 °C under vacuum. BPh_3 was purchased from Sigma-Aldrich and purified by sublimation at 110 °C. Et_3SiH and $PhMe_2SiH$ were purchased from Sigma-Aldrich and stored over molecular sieves prior to use.

All syntheses and manipulations of air and moisture sensitive materials were carried out in flame dried Schlenk-type glassware on a dual-manifold Schlenk line or in an inert gas (Ar or N_2)-filled glovebox. NMR-scale reactions were performed using Teflon valve sealed J-Young type NMR tubes.

Monomer conversion as well as structure characterizations of intermediates and polymers were carried out by ^{1}H NMR experiments using a Varian Inova 400 MHz (FT 400 MHz, ^{1}H; 100 MHz, ^{13}C) or a or Bruker AVIII 400 MHz spectrometer (400 MHz, ^{1}H; 100 MHz, ^{13}C). Chemical shifts were referenced to internal solvent resonances corresponding to 7.26 ppm (chloroform) and 7.16 ppm (benzene) and reported as parts per million relative to $SiMe_4$.

Measurements of polymer absolute weight-average molecular weight (M_w), number-average molecular weight (M_n), and molecular weight distributions or dispersity indices ($Đ = M_w/M_n$) were performed via GPC. The GPC instrument consisted of an Agilent HPLC system equipped with one guard column and two PL gel 5 μm mixed-C gel permeation columns and coupled with a Wyatt DAWN HELEOS II multi (18)-angle light scattering detector and a Wyatt Optilab TrEX dRI detector; the analysis was performed at 40 °C using chloroform as the eluent at a flow rate of 1.0 mL/min, using Wyatt ASTRA 7.1.2 molecular weight characterization software. The refractive index increment (d*n*/d*c*) of the poly(methyl crotonate) (PMC) was determined to be 0.0426 mL/g obtained by batch experiments described in our previous report.[1]

MALDI−TOF MS was used to analyze low molecular weight PMC samples, using an Ultraflex MALDI-TOF mass spectrometer (Bruker Daltonics) operated in positive ion, reflector mode using a Nd:YAG laser at 355 nm and 25 kV accelerating voltage. A thin layer of a 1% NaI solution was first deposited on the target plate, followed by 0.6 μL of both PMC (2 mg/ml in $CHCl_3$) and matrix (dithranol, 20 mg/mL in $CHCl_3$). External calibration was done using a peptide calibration mixture

(4 to 6 peptides) on a spot adjacent to the sample. The raw data was processed in the FlexAnalysis software (version 2.4, Bruker Daltonics), and the figures were potted using mMass software.

Polymerization procedure

Neat polymerizations were carried out by first premixing 5.0 mmol of MC (0.53 mL, 0.501 g) with 4 mol % $B(C_6F_5)_3$ (0.2048 g) and stirring for 10 min, followed by addition of the MC/$B(C_6F_5)_3$ solution to a pre-weighed amount of liquid hydrosilane (0.0116 g Et_3SiH) to make the ratio of [MC]:[$B(C_6F_5)_3$]:[R_3SiH] = 50:2:1. Solution-based polymerizations were carried out by premixing MC with the hydrosilane and $B(C_6F_5)_3$ in DCM, then mixing the two solutions together either instantly, or by dropwise addition of $B(C_6F_5)_3$/DCM to MC/R_3SiH. In the MC:$B(C_6F_5)_3$:R_3SiH = 25:2:1 runs, 20-30 % of the MC loading was added to the $B(C_6F_5)_3$/DCM solution to help dissolve all of the $B(C_6F_5)_3$ before exposing it to R_3SiH.

Polymerizations were typically quenched with 2-3 mL of $CDCl_3$ spiked with benzoic acid (approx. 500 ppm). Once fully dissolved, a few drops of the crude product were diluted in 0.5 mL $CDCl_3$ and analyzed by ^1H NMR. Conversion was calculated by comparison of monomer and polymer signal integration. The remaining dissolved polymer was crashed with methanol and isolated by filtration or centrifuge. ^1H NMR (400 MHz, $CDCl_3$) of PMC: δ (ppm) = 3.49-3.79 (br. 3H, OCH_3), 2.00-2.67 (br. 2H -CH(CO_2CH_3)CH(CH_3)-), 0.70-1.13 (br. 3H, -CH(CH_3)).

Isolation of 2 from Hydrosilylation of MC

Et_3SiH (1.57 mL, 9.84 mmol) and MC (1.00 mL, 9.84 mmol) were added to 100 mL of DCM at RT. $B(C_6F_5)_3$ (0.075 g) was dissolved in 10 mL of DCM and added over 1 min to the MC/Et_3SiH mixture. The solution was stirred for 1 h. An aliquot of the crude mixture taken for ^1H NMR

analysis and conversion was found to be quantitative. Next, DCM was removed by vacuum, and the liquid 2 was further purified by vacuum distillation at 50 ^{o}C under N_2. A relatively large sacrificial amount was left behind in the distillation and the isolated yield was 78 % (1.66 g, 2), 60 % major isomer. Major isomer was found to be the (*Z*)-isomer by HH-NOESY (Fig. S5) in the case of SKA 3, but was not determined for 2. ^{1}H NMR (major isomer) (400 MHz, $CDCl_3$): δ (ppm) = 3.42 (t. 1H, α-C*H*), 3.13 (s. 3H -OCH_3), 2.27 (p. 2H, β-CH_2), 1.10 (t. 3H, γ-CH_3), 1.04 (t. 12H, Si-CH_2CH_3), 0.74 (q. 4H, Si-C$H_2$$CH_3$).

2 and 3 can also be generated *in-situ*. Stock solutions (0.080 M) were prepared for $PhMe_2SiH$ and MC in C_6D_6. A 0.0080 M stock solution was prepared of $B(C_6F_5)_3$ which was diluted to 0.0008 M. MC (0.35 mL) and $PhMe_2SiH$ were added to a J-Young type NMR tube. The tube was immediately sealed and analyzed by ^{1}H NMR.

Polymerization Kinetics

Polymerization kinetics were obtained by running a polymerization according to the DCM conditions described above. Fig. 3 was generated by using the immediate addition protocol (not the dropwise protocol). These runs were scaled up to 1.00 g of MC as more solution volume was needed for taking aliquots. Aliquots (0.05 mL) at time points were taken via a syringe and quickly flushed into 0.70 mL $CDCl_3$ spiked with 500 ppm benzoic acid. Aliquots were transferred to NMR tubes and analyzed by NMR methods.

Table B1. Results of solution polymerization of MC with $B(C_6F_5)_3$/LB (LB = Et3SiH, **2**) based LPs with different addition protocols [a]

Run	MC:LA:LB	LB	protocol	Conv (%)	M_n (kg/mol)	$Đ$	I^* (%)
[b]1	25:2:1	Et_3SiH	[b]Drip	98	8.17	1.06	31
2	25:2:1	Et_3SiH	[c]Splash	98	7.84	1.03	32
3	25:1:1	Et_3SiH	Drip	98	5.89	1.08	42
4	25:1:1	Et_3SiH	Splash	98	6.88	1.08	36
[c]5	25:1:1	**2**	Drip	98	10.2	1.12	25

[a] Conditions: $[MC]_0$ = 4.72 M in DCM, LA = $B(C_6F_5)_3$; RT; time = 24 h; DCM/$B(C_6F_5)_3$ solution added to MC/Et_3SiH solution

[b] DCM/$B(C_6F_5)_3$ solution added dropwise over 3 min to MC/Et_3SiH solution

[c] DCM/$B(C_6F_5)_3$ solution added quickly to MC/Et_3SiH solution

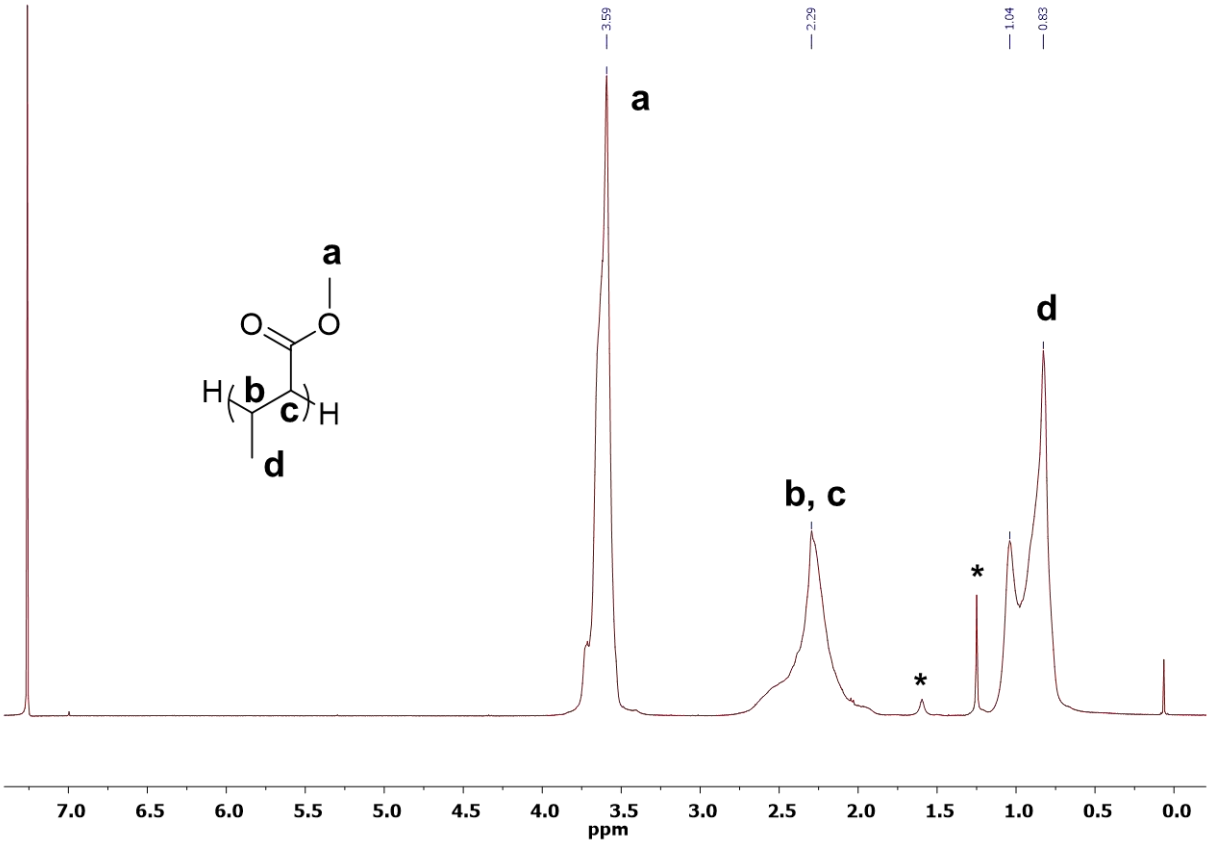

Figure B1. A representative ^1H NMR ($CDCl_3$) spectrum of isolated PMC (M_n = 7.14 kg/mol, $Đ$ = 1.13; run 1, Table 1). Peaks marked with * are for H_2O (1.56 ppm) and unknown impurity (1.25 ppm) brought into the system.

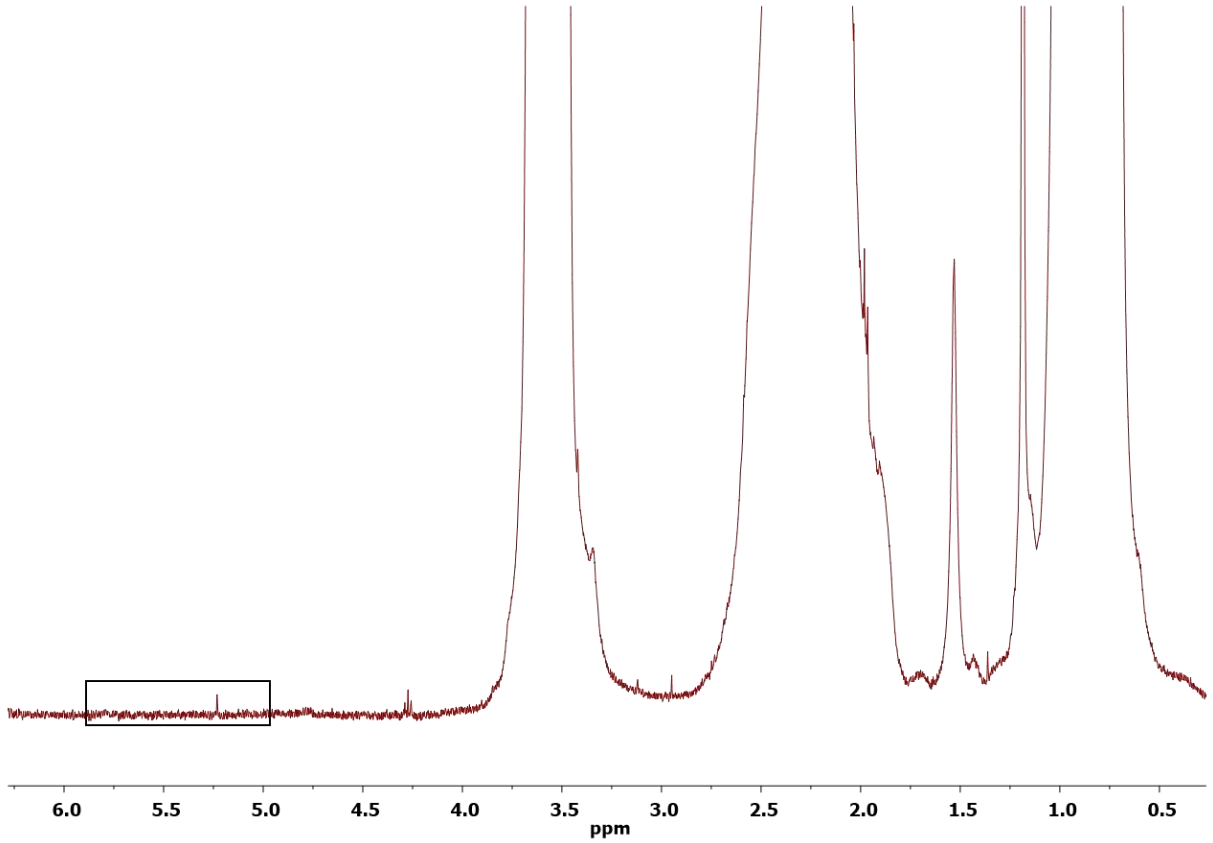

Figure B2. ^{1}H NMR ($CDCl_3$) of PMC produced by MC:$B(C_6F_5)_3$:Et_3SiH ratio of 100:4:1, run 5, Table 3.1, expanded to show lack of peaks associated with a vinyl end group.

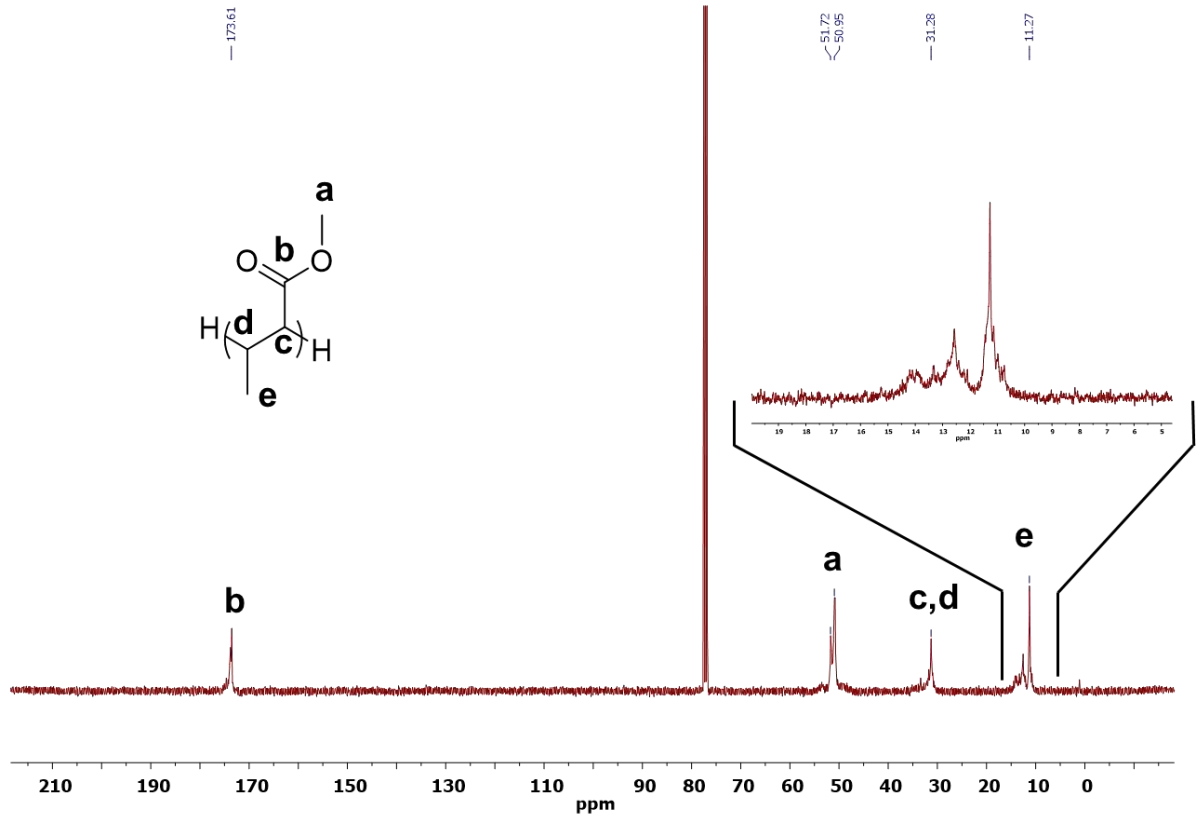

Figure B3. ^{13}C NMR ($CDCl_3$) of PMC prepared by MC:$B(C_6F_5)_3$:Et_3SiH ratio of 100:4:1, run 5, Table 3.1.

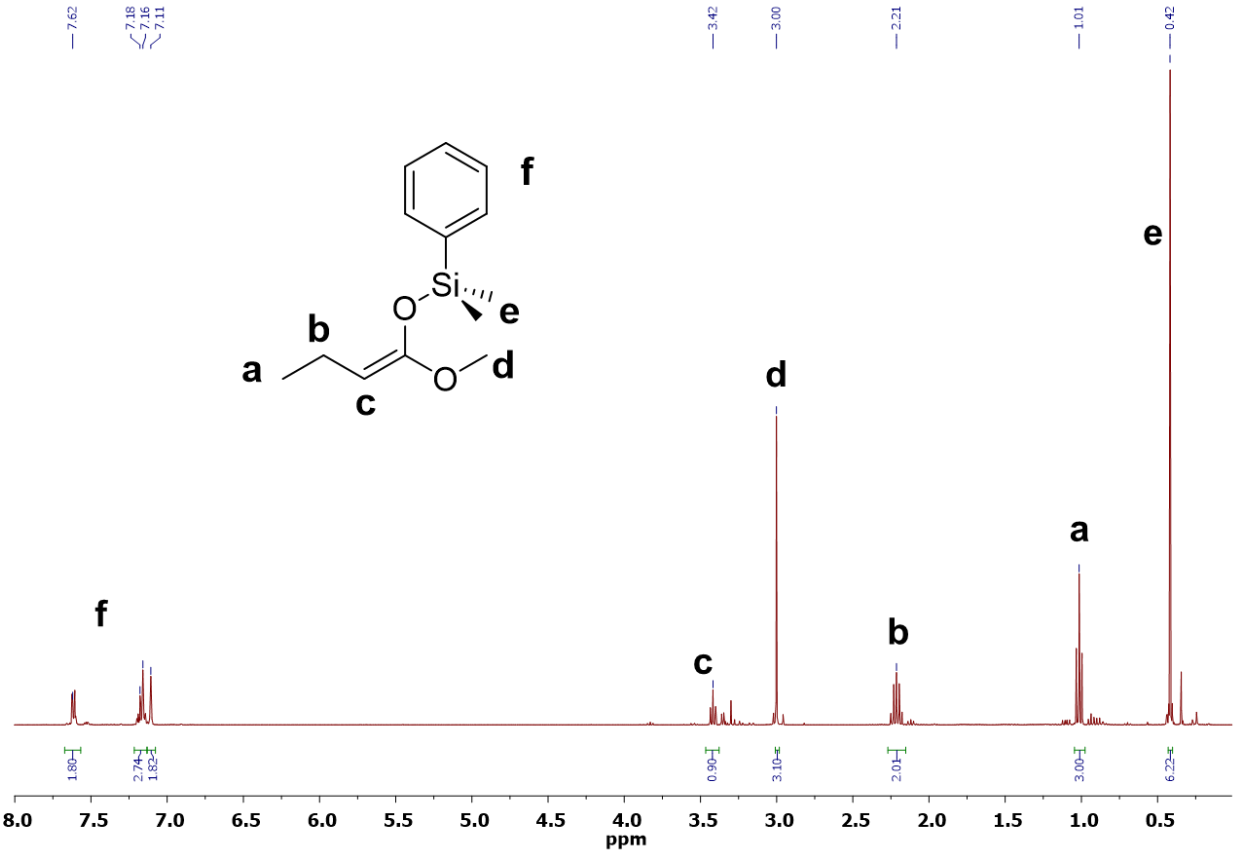

Figure B4. ^{1}H NMR (C_6D_6) of **3**.

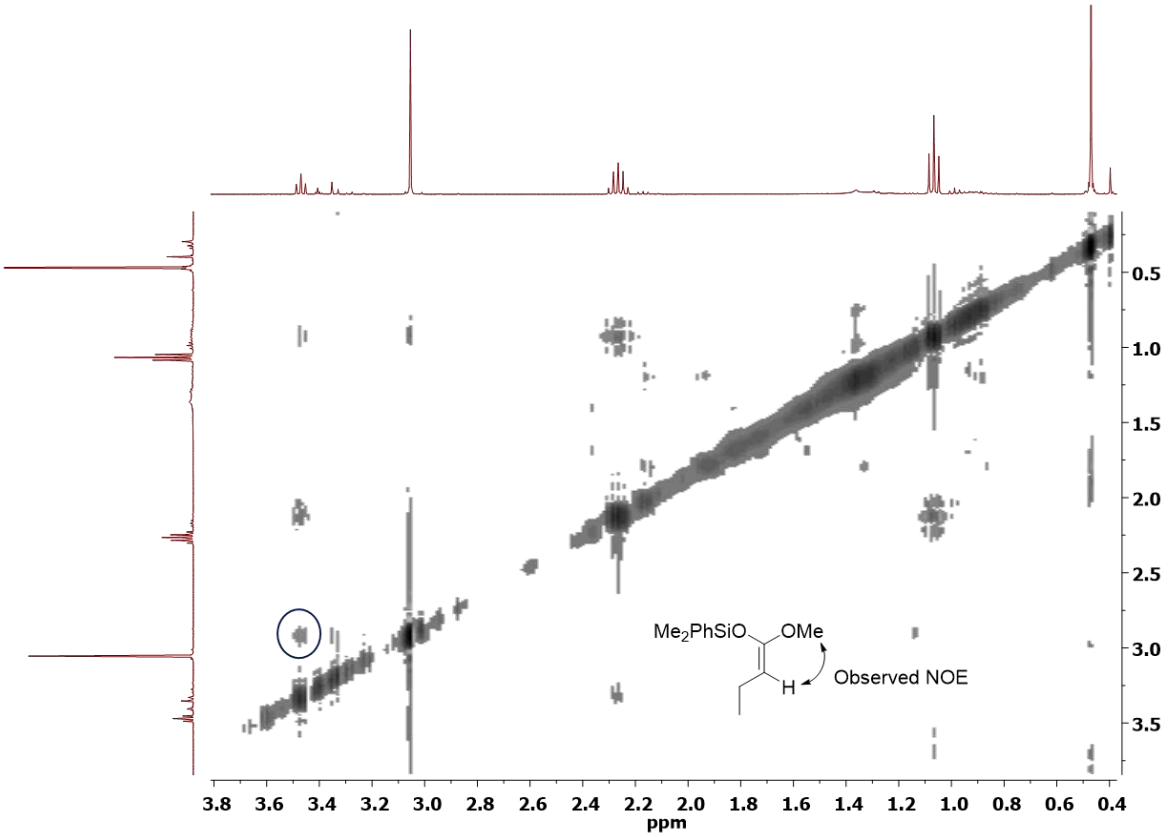

Figure B5. HH NOESY NMR (C_6D_6) of **3** (Calcd. [**3**] = 0.026 M), used for determination of absolute stereochemistry. Observable coupling between enolate α-proton and methoxy protons—as well as lack of coupling between α-proton and silyl methyl protons—imply the major product is the (*Z*)-isomer.

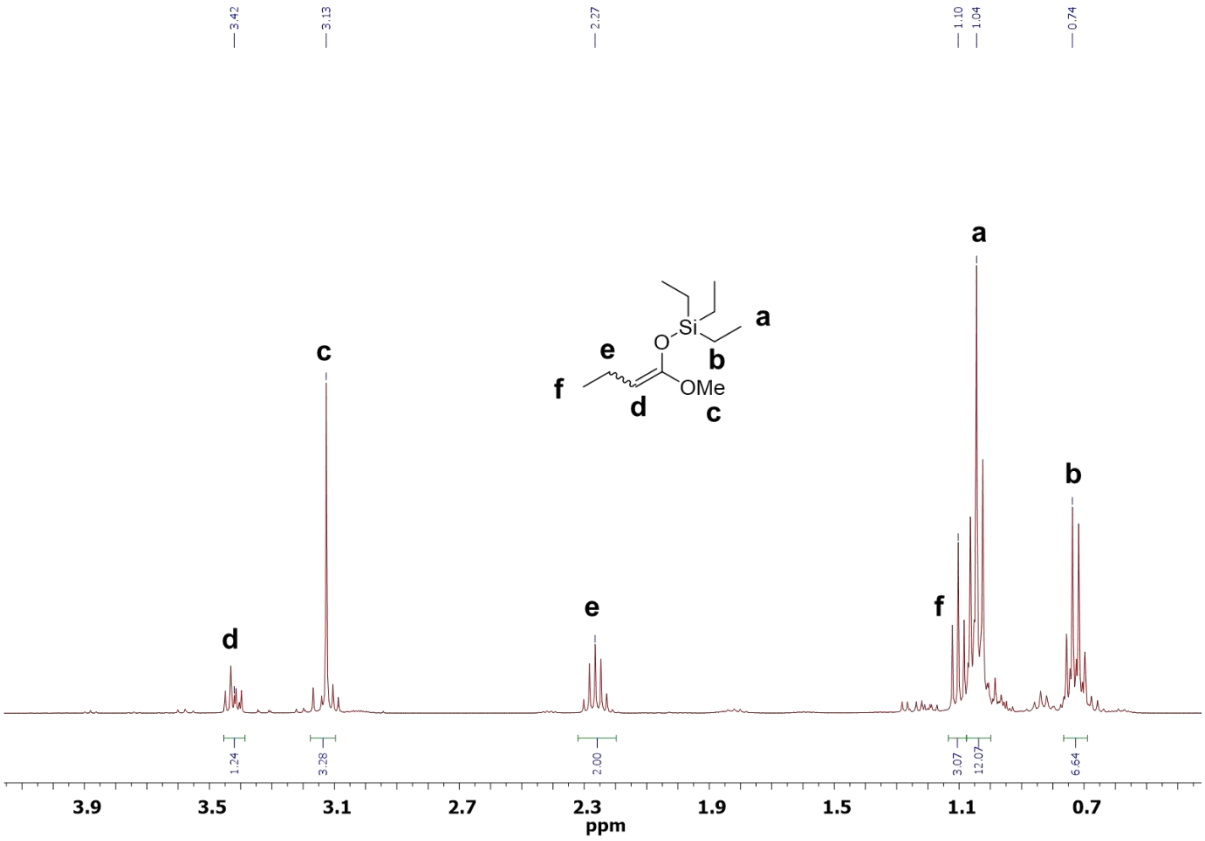

Figure B6. ^{1}H NMR (C_6D_6) of **2**, generated *in situ* by mixing MC, Et_3SiH, and $B(C_6F_5)_3$ at a ratio of 1:1:0.01, showing predominately one isomer (the minor isomer can be identified by the small peaks). Spectrum acquired 10 min after addition. Calcd. [**2**] = 0.026 M.

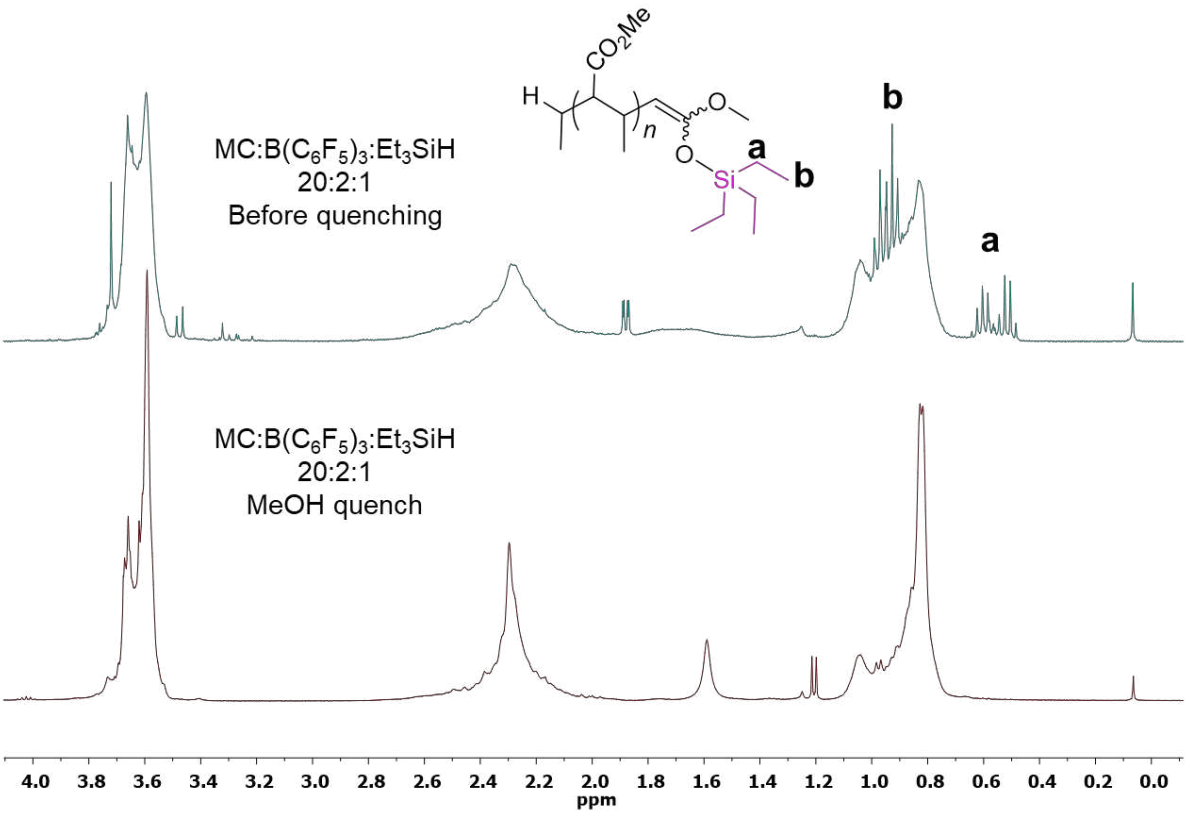

Figure B7. ^{1}H NMR ($CDCl_3$) spectra of PMC before and after quenching with MeOH. This sample was prepared from an MC:B(C_6F_5)$_3$:Et_3SiH ratio of 20:2:1 in neat at RT for 24 h, which was also analyzed by MALDI-TOF MS (Fig. 2) after MeOH quenching.

References cited in Appendix B

1 Enders, D.; Breuer, K.; Kallfass, U.; Balensiefer, T. *Synthesis*, **2003**, 1292–1295.

Appendix C

Supplementary Information Corresponding to Chapter 4

Taken verbatim from:

McGraw, M. L.; Clarke, R. W.; Chen, E. Y.-X. Compounded Sequence Control in Polymerization of One-Pot Mixtures of Highly Reactive Acrylates by Differentiating Lewis Pairs. *J. Am. Chem. Soc.* **2020**, *142*, 5969−5973.

Materials

All syntheses and manipulations of air- and moisture-sensitive materials were carried out in flame-dried Schlenk-type glassware on a dual-manifold Schlenk line or in an inert gas (Ar or N_2)-filled glovebox. Monomers *n*-butyl acrylate (^{n}BA) and *tert*-butyl acrylate (^{t}BA) were purchased from TCI. All monomers were purified by titration with triethyl aluminum followed by vacuum distillation in the absence of light, and stored in amber bottles inside a -30 ^{o}C freezer inside an inert glovebox. Trimethylphosphine (PMe_3) was purchased from Alfa Aesar, stored at -30 ^{o}C inside an inert glovebox, and used as received. Phenoxy aluminum alkyl compounds, (2,6-di-*tert*-butyl-4-methylphenoxy)diisobutylaluminum (^{i}Bu$_2$Al(BHT) and methylaluminum bis(2,6-di-*tert*-butyl-4-methylphenoxide) (MAD), were synthesized according to literature procedures.[1]

Analytical Methods

NMR Spectroscopy. Monomer conversion as well as structural characterizations of catalysts, intermediates and polymers were carried out by ^{1}H NMR, and ^{13}C NMR experiments using a Varian Inova 400 MHz (FT 400 MHz ^{1}H; 100 MHz ^{13}C) or a Bruker AVIII 400 MHz spectrometer

(400 MHz ^{1}H; 100 MHz ^{13}C). Variable temperature ^{1}H NMR experiments were used to obtain Van't Hoff plots and subsequent K_{eq} values. Chemical shifts were referenced to internal solvent resonances corresponding to 7.26 ppm ($CHCl_3$) and 7.16 (C_6D_6) and reported as parts per million, relative to $SiMe_4$.

Gel Permeation Chromatography (GPC). Measurements of polymer absolute weight-average molecular weight (M_w), number-average molecular weight (M_n), and molecular weight distributions or dispersity indices ($Đ = M_w/M_n$) were performed via GPC. The GPC instrument consisted of an Agilent HPLC system equipped with one guard column and three PL-gel 5 μm mixed-C gel permeation columns running THF as eluent at 1.0 mL/min at 40 °C. The detectors used were a Wyatt Technology TrEX differential refractometer (dRI) and a Wyatt Technology miniDAWN Treos light scattering detector (MALS). The d*n*/d*c* values were determined experimentally, through analysis of known-concentration samples, to be 0.0527 for poly(*tert*-butyl acrylate) and 0.0651 for poly(*n*-butyl acrylate). Diblock and triblock specimens d*n*/d*c* values were calculated based on weighted average with respect to co-monomer composition.

Thermal Analysis. Differential Scanning Calorimetry (DSC) was performed on a thoroughly dried polymer samples on an Auto Q20, TA Instrument. DSC Plots represent the data obtained from a second heating scan after the thermal history was removed on the first heating scan. The second heating scan was performed at a heating rate of 20 °C/min following a cooling scan at a rate of 10 °C/min.

Experimental Details

Synthesis and isolation of (^{i}Bu)$_2$Al(OMes). In a 200 mL schlenk flask and inside an Ar-filled glovebox, 6.43 mL of triisobutylaluminum was dissolved in 60 mL hexane. In a 20 mL scintillation

vial, 3.47 g hydroxymesityl was dissolved in 20 mL of DCM. The hydroxymesityl/DCM was added dropwise to the triisobutylaluminum over 5 min at room temperature (RT) with stirring. After mixing, the reaction was continued for 20 min, and then concentrated by vacuum to quarter volume, at which point most of the (^{i}Bu)$_2$Al(OMes) had precipitated. The mixture was then filtered over a fine frit and washed 3 times with 20 mL of hexane. After drying the solid product (5.02 g, 71.3 % yield) for 2 h by vacuum, it was stored in a scintillation vial at -30 ^{o}C inside an inert glovebox.

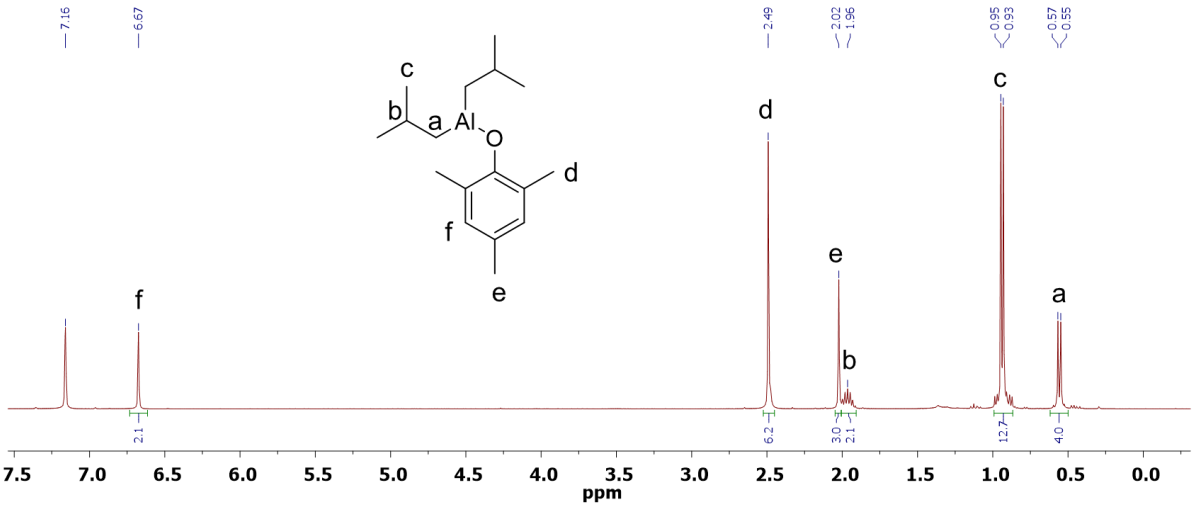

Figure C1. ^{1}H NMR (C_6D_6) of (^{i}Bu)$_2$Al(OMes).

Homopolymerization procedure. Typical homopolymerizations were performed by first mixing 0.50 mL of monomer (^{t}BA or ^{n}BA) with an appropriate amount of solid LA, and then diluting the monomer/LA solution with toluene until the total solution volume was either 3 mL or 6 mL. A 0.50 mL monomer to 5.50 mL solvent ratio (0.62 M) seemed to work better at preventing crosslinking side reactions and was therefore used in copolymerizations. Then, a 0.175 M PMe_3 solution was prepared in toluene, and an appropriate quantity of the PMe_3 solution was added to

the monomer/LA/toluene solution to initiate polymerization. As a typical example, a ^{t}BA/MAD/PMe_3 = 100/2/1 reaction (Table 4.1, run 3) was executed by mixing 0.50 mL of ^{t}BA, 2.50 mL of toluene, and 0.0335 g MAD followed by addition of 0.20 mL of 0.175 M PMe_3 in toluene. The reaction was stirred vigorously and watched carefully for a color change from yellow to clear signaling full conversion. Immediately after color change, 5 mL of methanol spiked with benzoic acid (1000 ppm) was added to quench the reaction. Failure to quench the active species following full conversion will lead to insoluble, crosslinked product. For purification, the quenched reaction was dried via rotary evaporation and redissolved in acetone. An equal portion of water was added, and the solution was again evaporated until all the acetone was removed, at which point the polymer crashed out, and the water was decanted. The polymer was washed with water several more times by adding water to the same vial, and decanting. Finally, the wet polymer was dried in a vacuum oven at 80 ^{o}C for 12 h. For extra pure polymer product, dialysis in acetone was employed.

Sequential addition triblock copolymerization. Sequential addition copolymerizations were executed by first dissolving ^{t}BA and MAD into a quantity of toluene that would be appropriate for the volume of all three blocks combined. For example, for the synthesis of P(^{t}BA-*b*-^{n}BA-*b*-^{t}BA), (theoretical DP = 300-300-300; Table 4.2, run 8), 0.50 mL of ^{t}BA was added to 16.5 mL of toluene with 0.0335 g of MAD. Then, 0.883 mg of PMe_3 was added as 66 μL of a 0.175 M PMe_3/toluene stock solution to initiate polymerization. The polymerization was watched vigilantly until a color change from yellow to clear was observed, followed by immediate addition of 0.50 mL of ^{n}BA. Again, the reaction was monitored until color change to clear and then 0.50 mL of ^{t}BA was added. When the reaction finally turned clear once more, 10 mL of methanol spike with benzoic acid (1000 ppm) was added to quench the reaction. Thus, 15.5 mL of solvent was used in the beginning

because it corresponds to 5.50 mL of solvent per 0.50 mL monomer. It was found that at least 5.5 mL of solvent was needed per 0.50 mL monomer to stop the reaction from getting too viscous. The crude reaction mixture was dried by rotary evaporation, redissolved in 5 mL of acetone followed by addition of 5 mL of water. The acetone was removed by rotary evaporation, at which point the polymer crashed out of the water. The water was decanted. The wet polymer was washed several times by addition and decantation of water. Finally, the wet polymer was dried in a vacuum oven at 80 °C for 12 h.

Mixed addition diblock copolymerization (Table 4.3, Run 12). For mixed addition, both monomers (0.50 mL ^{t}BA and 0.50 mL ^{n}BA) were mixed in 16.5 mL of toluene with 0.0335 g MAD. The solution had a very brilliant yellow color (corresponding to the ^{n}BA/MAD adduct). With vigorous stirring, 67 μL of 0.175 M PMe_3 in toluene was added to the solution (^{t}BA/^{n}BA/MAD/PMe_3 = 300/300/6/1). After 3-4 s, the solution color changed from brilliant yellow (^{n}BA/MAD) to faint yellow (^{t}BA/MAD), signaling that ^{n}BA conversion was complete. After 40 s, the solution became clear, signaling full conversion of both monomers, at which point it was quenched with 10 mL of methanol (1000 ppm benzoic acid). The crude reaction mixture was dried by rotary evaporation, redissolved in 5 mL of acetone followed by addition of 5 mL of water. The acetone was removed by rotary evaporation, at which point the polymer crashed out of the water. The water was decanted. The wet polymer was washed several times by addition and decantation of water. Finally, the wet polymer was dried in a vacuum oven at 80 °C for 12 h.

Mixed addition triblock copolymerization (Table 4.3, Run 14). For mixed addition P(^{t}BA-*b*-^{n}BA-*b*-^{t}BA) (theoretical DP = 300-300-300) triblock, the entire quantity of ^{t}BA (1.0 mL) was mixed with 16.5 mL of toluene and 0.0335 g MAD. Then 67 μL of 0.175 M PMe_3 was added to this solution to initiate polymerization (^{t}BA/MAD/PMe_3 = 600/6/1). This polymerization reached

full conversion in 100 s. Therefore, we estimated that half conversion would be around 50 s. We then repeated an identical reaction, except at exactly t = 50 s, 0.50 mL of ^{n}BA was rapidly added, at which point the solution color changed from faint yellow to brilliant yellow for about 3-4 s and then changed back to faint yellow for about another 40 s. The second half of the ^{t}BA polymerization (following ^{n}BA addition) was always a little bit faster since the solution temperature increased after ^{n}BA polymerization. The reaction was quenched after turning clear with 10 mL methanol (1000 ppm benzoic acid). The crude reaction mixture was dried by rotary evaporation, redissolved in 5 mL of acetone followed by addition of 5 mL of water. The acetone was removed by rotary evaporation, at which point the polymer crashed out of the water. The water was decanted. The wet polymer was washed several times by addition and decantation of water. Finally, the wet polymer was dried in a vacuum oven at 80 ^{o}C for 12 h.

Kinetics. Kinetics (shown in Figure C2) was performed by mixing 0.50 mL of ^{t}BA with 5.5 mL of toluene and 0.0168 g of MAD in a scintillation vial. Then 0.050 mL of 0.175 M PMe_3 in toluene was added to start the reaction (^{t}BA/MAD/PMe_3 = 400/4/1). The time of the precise reaction was known ahead of time from an identical reaction (36 s). Aliquots were taken as frequently as possible by withdrawing about 0.5 mL of the reaction into a syringe and quenching it in a vial of $CDCl_3$/benzoic acid (500 ppm) while noting the exact time. Conversion of each aliquot was measured by comparison of monomer β-proton peak (5.21 ppm) with toluene satellite peak (1.95 ppm).

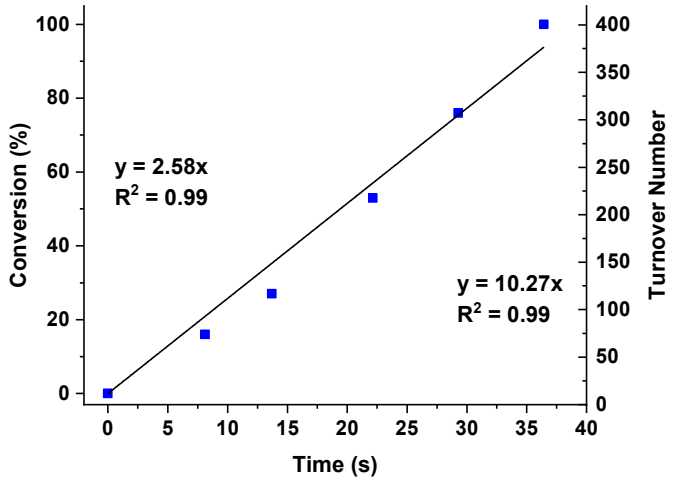

Figure C2. Kinetic profile of ^{t}BA/MAD/PMe$_3$ = 400/4/1. [^{t}BA] = 0.590 M in toluene, room temperature.

Table C1. Results of homopolymerization of acrylates by LPs [a]

Run #	M	LA	[M]/[LA] /[PMe$_3$]	Time (s)	Conv[b] (%)	M_n[c] (kg/mol)	$Đ$[c]	I*[d]
1	^{t}BA	**1**	200/2/1	1	100	26.0	1.15	99
2	^{t}BA	**2**	200/2/1	3	100	25.5	1.12	101
3	^{t}BA	MAD	100/2/1	4.2	100	14.8	1.05	85
4	^{t}BA	MAD	200/2/1	13	100	36.6	1.03	70
5	^{t}BA	MAD	1600/8/1	99	100	256	1.02	80
6	^{n}BA	MAD	200/2/1	<1	100	31.7	1.18[e]	70

[a] Conditions: 23°C, $[M]_0$ = 1.18 M in toluene, monomer and LA premixed followed by addition of PMe$_3$ from a stock solution. [b] Conversion calculated by ^{1}H NMR. [c] M_n and $Đ$ determined by GPC at 40 °C in THF coupled with a multi-angle light scattering detector and a *d*RI detector for absolute molecular weights. [d] $I^* = M_{n(calcd)}/M_{n(exptl)}$, where $M_{n(calcd)}$ = MW(M) × [M]/[LB] × conversion% + MW of chain-end groups.

Table C2. Additional results of LPP of acrylates [a]

Run #	M	LA	[M]/[LA]/[PMe_3]	Time	Conv[b] (%)	M_n[c] (kg/mol)	$Đ$[c]	I^*[d]
7	^{t}BA	(^{i}Bu)$_2$Al(OMes)	100/2/1	1 s	100	15.2	1.15	85
8	^{t}BA	(^{i}Bu)$_2$Al(OMes)	200/2/1	1 s	100	26.0	1.15	99
9	^{t}BA	(^{i}Bu)$_2$Al(BHT)	100/2/1	2 s	100	12.6	1.10	102
10	^{t}BA	(^{i}Bu)$_2$Al(BHT)	200/2/1	3 s	100	25.5	1.12	101
11	^{t}BA	MAD	100/2/1	4 s	100	14.8	1.05	85
12	^{t}BA	MAD	200/2/1	13 s	100	36.6	1.03	70
13	^{t}BA	MAD	400/2/1	49 s	100	64.1	1.01	80
14	^{t}BA	MAD	1600/8/1	99 s	100	256	1.02	80
15	^{n}BA	MAD	100/2/1	<1 s	100	26.7 300 (14%)	1.26 1.53	-
16	^{n}BA	MAD	200/2/1	<1 s	100	31.7 497 (15%)	1.18 1.74	-
17	^{n}BA	MAD	400/2/1	2 s	100	52.4 1610 (26%)	1.09 1.2	-
18	^{n}BA	MAD	800/2/1	4 s	100	98.6 1130 (15%)	1.01 1.12	-

[a] Conditions: $[M]_0$ = 1.18 M in toluene. For all polymerizations, monomer and LA were premixed followed by addition of PMe_3 from a 0.0175 M stock solution. [b] Conversion calculated by H-NMR integration of crude reaction, or full conversion were assumed by color change from yellow to clear. [c] Number-average molecular weight (M_n) and dispersity indices ($Đ$) determined by GPC at 40 °C in THF coupled with a DAWN HELEOS II multi-angle light scattering detector and an Optilab TrEX dRI detector for absolute molecular weights. [d] Initiation efficiency (I^*) = $M_{n(calcd)}/M_{n(exptl)}$, where $M_{n(calcd)}$ = MW(monomer) × [monomer]/[LB] × conversion% + MW of chain-end groups.

Table C3. Results of sequential addition diblock and triblock copolymerizations of ^{t}BA with ^{n}BA [a]

Run	[^{t}BA]/[^{n}BA]/ [MAD]/[PMe_3]	Time (s)	Conv (%)	M_n (kg/mol)	$Đ$
19a	100/0/2/1	21	100	16.2	1.05
19b	100/200/2/1	21/1	100	50.4	1.06
19c	200/200/2/1	21/1/17	100	67.9	1.02
20a	300/0/6/1	50	100	58.1	1.01
20b	300/300/6/1	50/2	100	128	1.07
20c	600/300/6/1	50/2/46	100	200	1.08

[a] Conditions: 23°C, $[M]_0$ = 0.59 M in toluene after final monomer addition, total solution volume = 18 mL. For all triblock polymerizations, ^{t}BA and MAD were premixed in toluene followed by addition of PMe_3 from a stock solution. Aliquots were taken just after complete conversion of each block.

Selected GPC Traces of Polymer Products

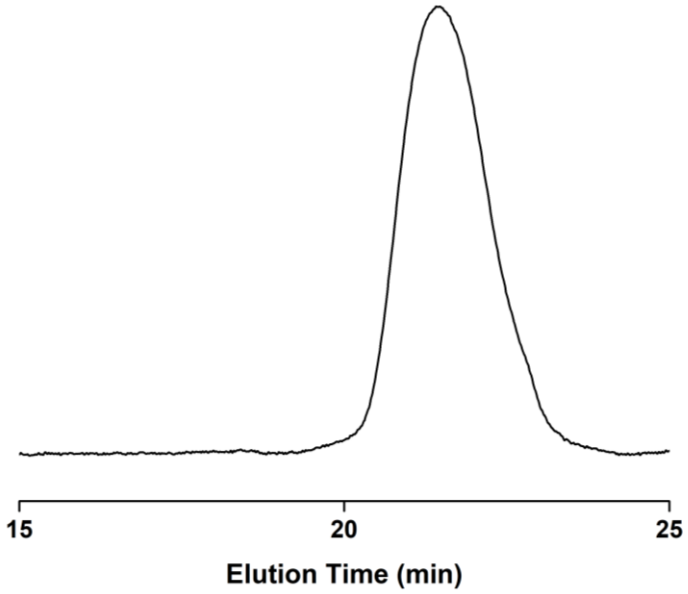

Figure C3. GPC (dRI) trace of P^{t}BA synthesized by ^{t}BA/(^{i}Bu)$_2$Al(OMes)/PMe$_3$ = 200/2/1 (Table C1, run 1; M_n = 26.0 kg/mol, $Đ$ = 1.15).

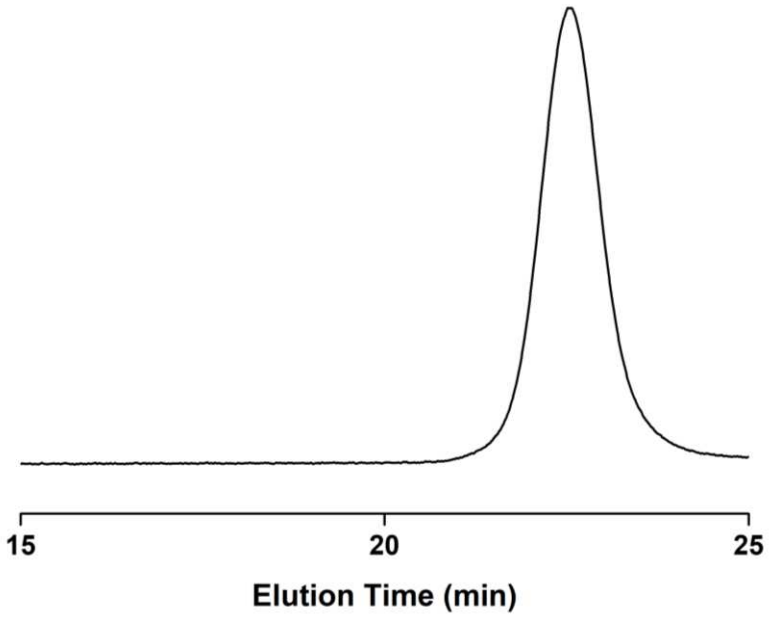

Figure C4. GPC (dRI) trace of P^{t}BA synthesized by ^{t}BA/(^{i}Bu)$_2$Al(BHT)/PMe$_3$ = 100/2/1 (Table C2, run 9; M_n = 12.6 kg/mol, $Đ$ = 1.10).

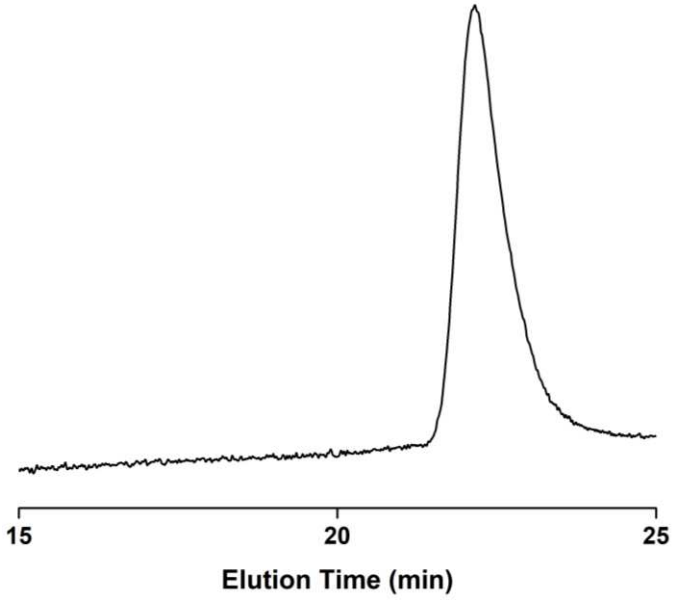

Figure C5. GPC (dRI) trace of P^{t}BA synthesized by ^{t}BA/MAD/PMe$_3$ = 100/2/1 (Table C1, run 3; M_n = 14.8 kg/mol, $Đ$ = 1.05).

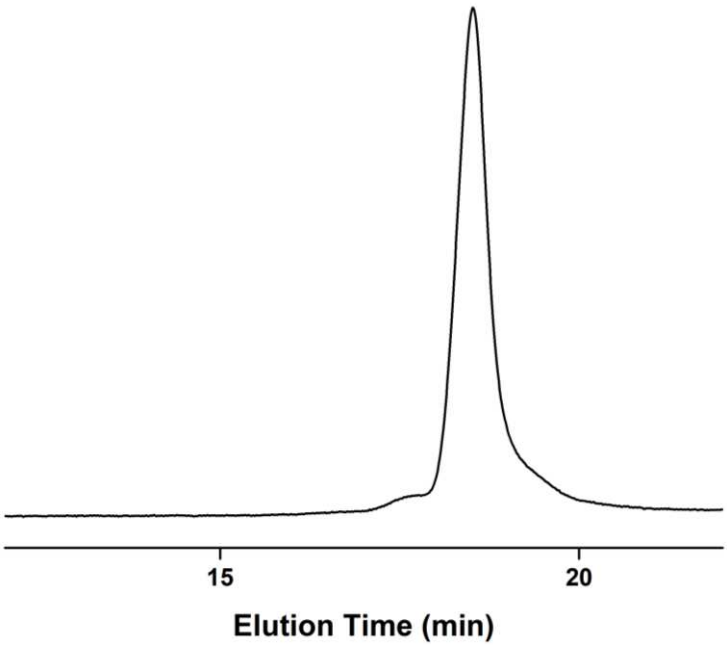

Figure C6. GPC (dRI) trace of P^{t}BA synthesized by ^{t}BA/MAD/PMe$_3$ = 1600/2/1 (Table C1, run 5; M_n = 256 kg/mol, $Đ$ = 1.02).

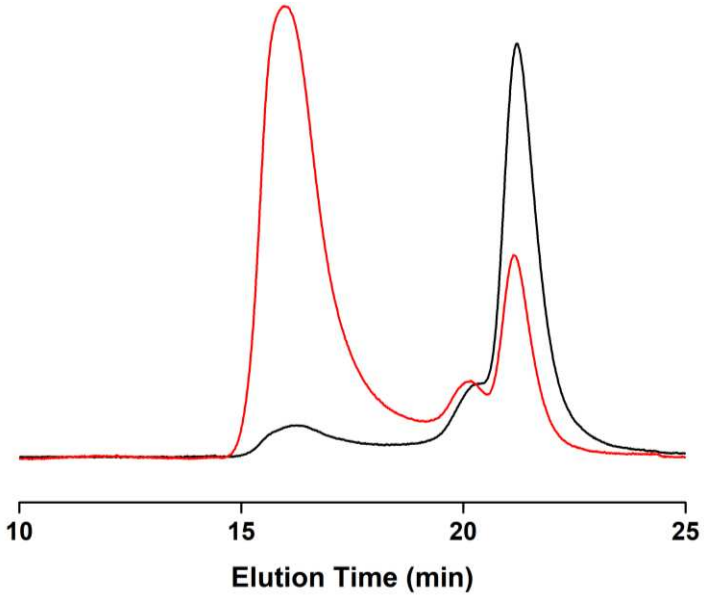

Figure C7. GPC (dRI black, LS red) trace of P^{n}BA synthesized by ^{n}BA/MAD/PMe$_3$ = 200/2/1 (Table C1, run 6). Low M_n peak: M_n = 31.7 kg/mol, $Đ$ = 1.18; high M_n peak: M_n = 497 kg/mol, $Đ$ = 1.74, 15 % mass composition.

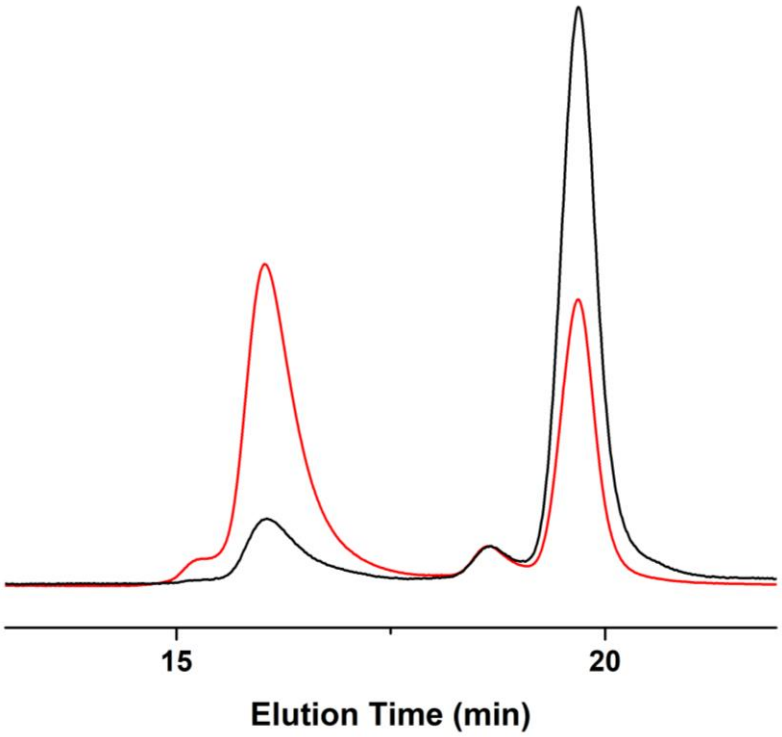

Figure C8. GPC (dRI black, LS red) trace of P^{n}BA synthesized by ^{n}BA/MAD/PMe$_3$ = 800/2/1(Table C2, run 18). Low M_n peak: M_n = 98.6 kg/mol, $Đ$ = 1.01; high M_n peak: M_n = 1130 kg/mol, $Đ$ = 1.12, 15 % mass composition.

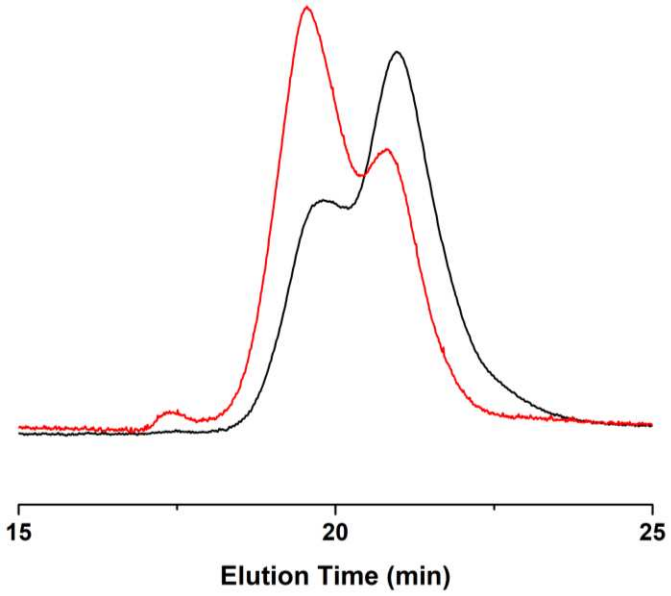

Figure C9. GPC (dRI black, LS red) trace of P^{t}BA-*ran*-P^{n}BA random copolymer synthesized by the LA (^{i}Bu)$_2$Al(OMes) with ^{t}BA/^{n}BA/(^{i}Bu)$_2$Al(OMes)/PMe$_3$ = 100/100/2/1 (Table 4.1, run 1; M_n = 32.3 kg/mol, $Đ$ = 1.68).

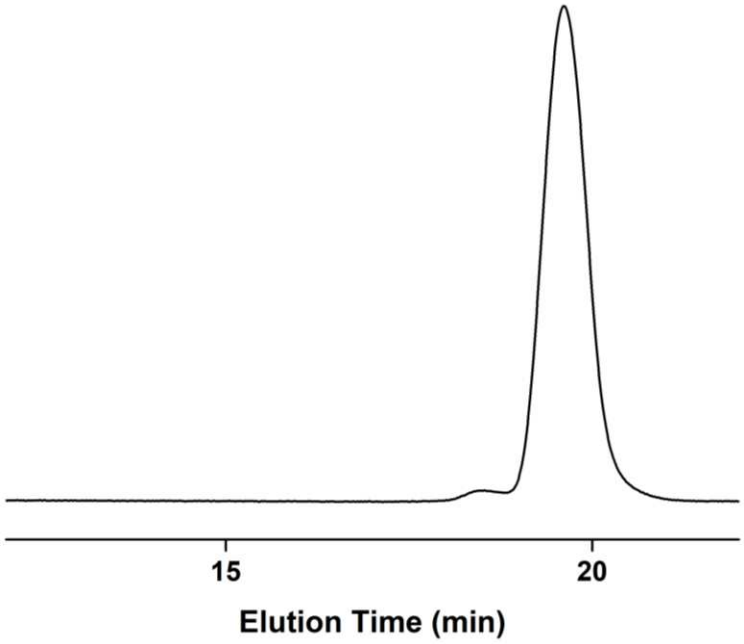

Figure C10. GPC (dRI) trace of P^{t}BA-*b*-P^{n}BA) di-block copolymer, synthesized by the mixed addition protocol, with ^{t}BA/^{n}BA/MAD/PMe$_3$ = 100/900/2/1 (Table 4.1, run 3; M_n = 127 kg/mol, $Đ$ = 1.02).

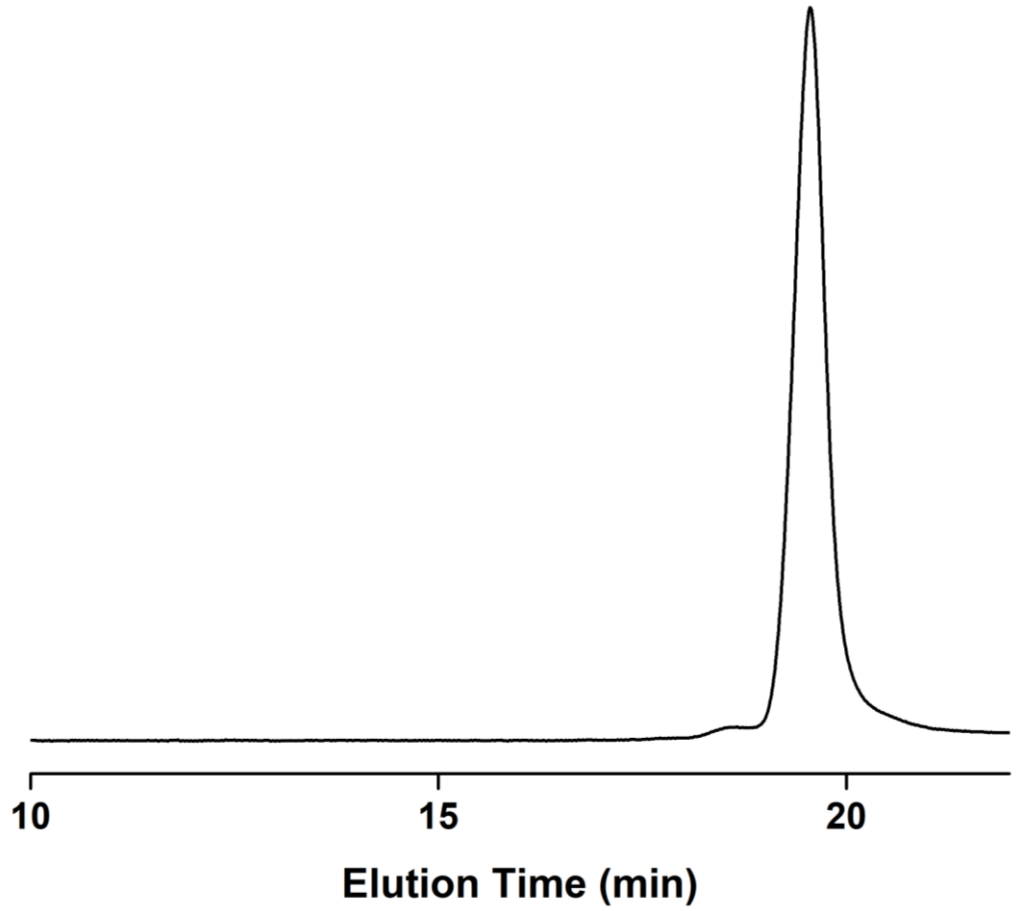

Figure C11. GPC (dRI) trace of P^{t}BA-*b*-P^{n}BA diblock copolymer, synthesized by the mixed addition protocol with ^{t}BA/^{n}BA/MAD/PMe$_3$ = 300/300/2/1 (Table 4.1, run 4; M_n = 90.1 kg/mol, $Đ$ = 1.06).

Selected NMR Spectra of Polymer Products

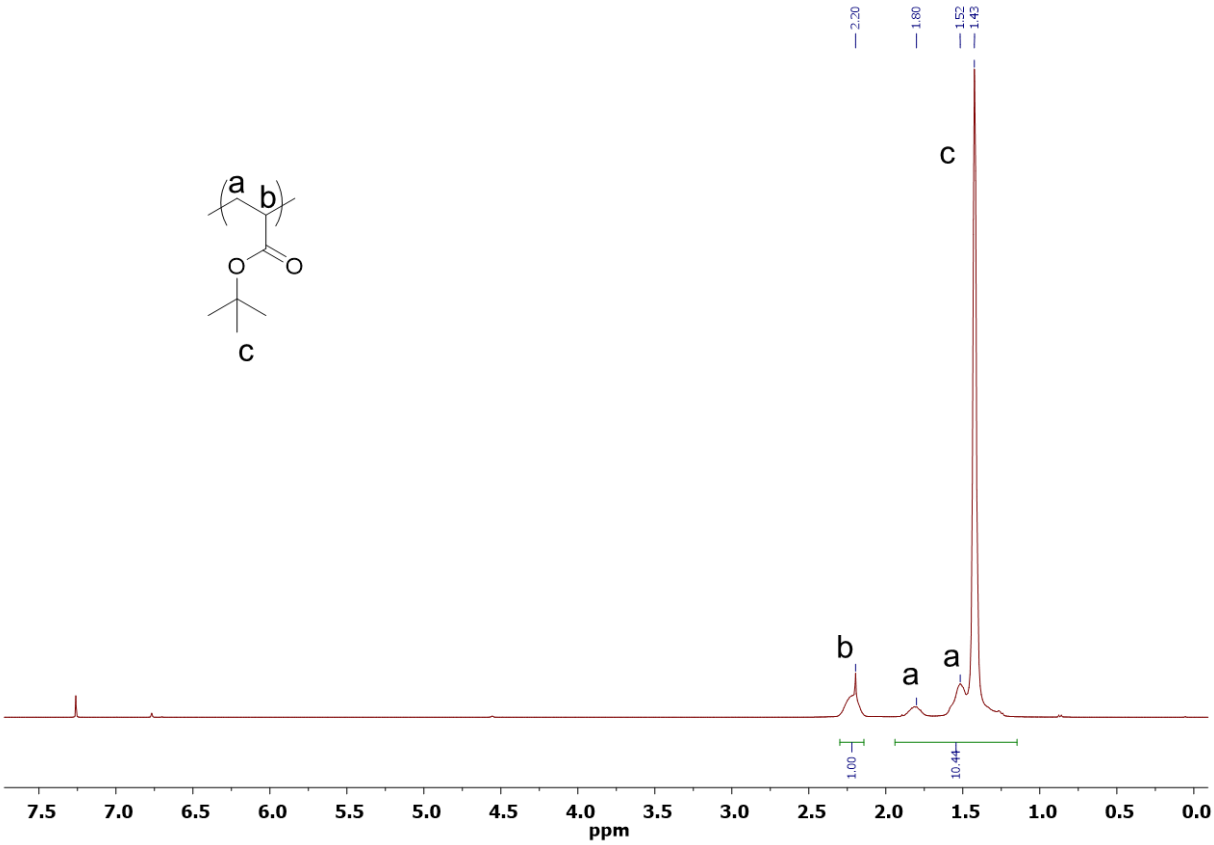

Figure C12. ^{1}H NMR ($CDCl_3$) of P^{t}BA synthesized by (^{i}Bu)$_2$Al(OMes) with ^{t}BA/(^{i}Bu)$_2$Al(OMes)/PMe_3 = 200/2/1 (Table C1, run 1).

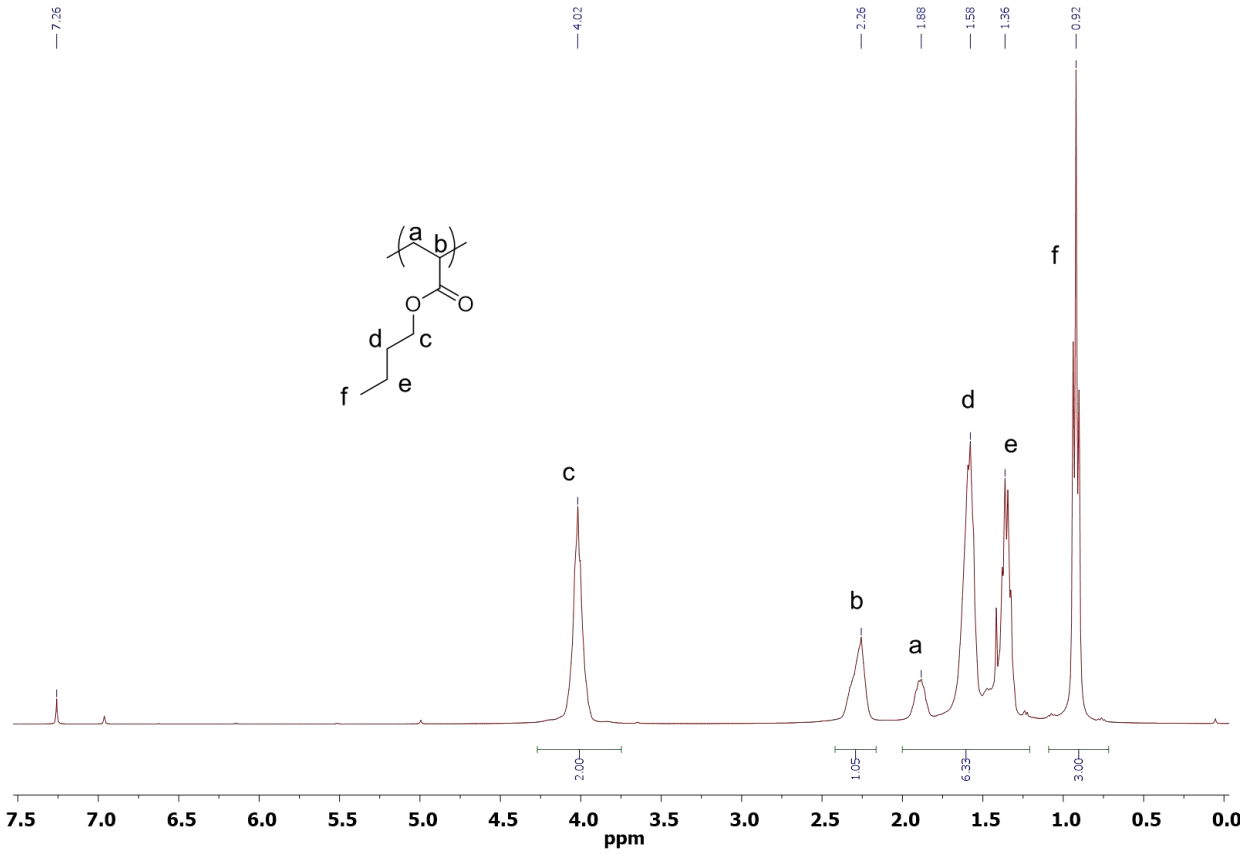

Figure C13. ^{1}H NMR ($CDCl_3$) of P^{n}BA synthesized by MAD with ^{n}BA/MAD/PMe_3 = 200/2/1 (Table C1, run 6).

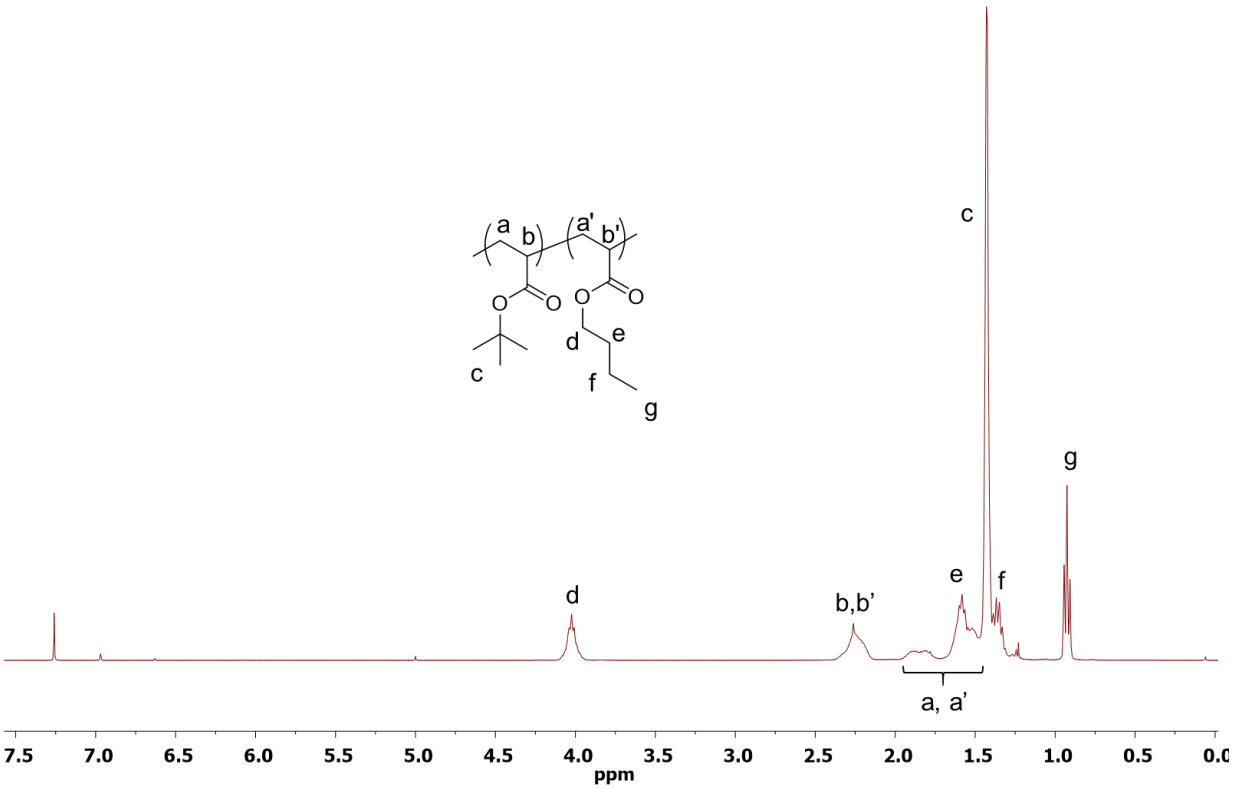

Figure C14. ^{1}H NMR ($CDCl_3$) of P^{t}BA-*b*-P^{n}BA-*b*-P^{t}BA (theoretical DP = 300-300-300) synthesized by sequential addition ^{t}BA/^{n}BA/MAD/PMe_3 = 600/300/2/1 (Table C3, run 20c).

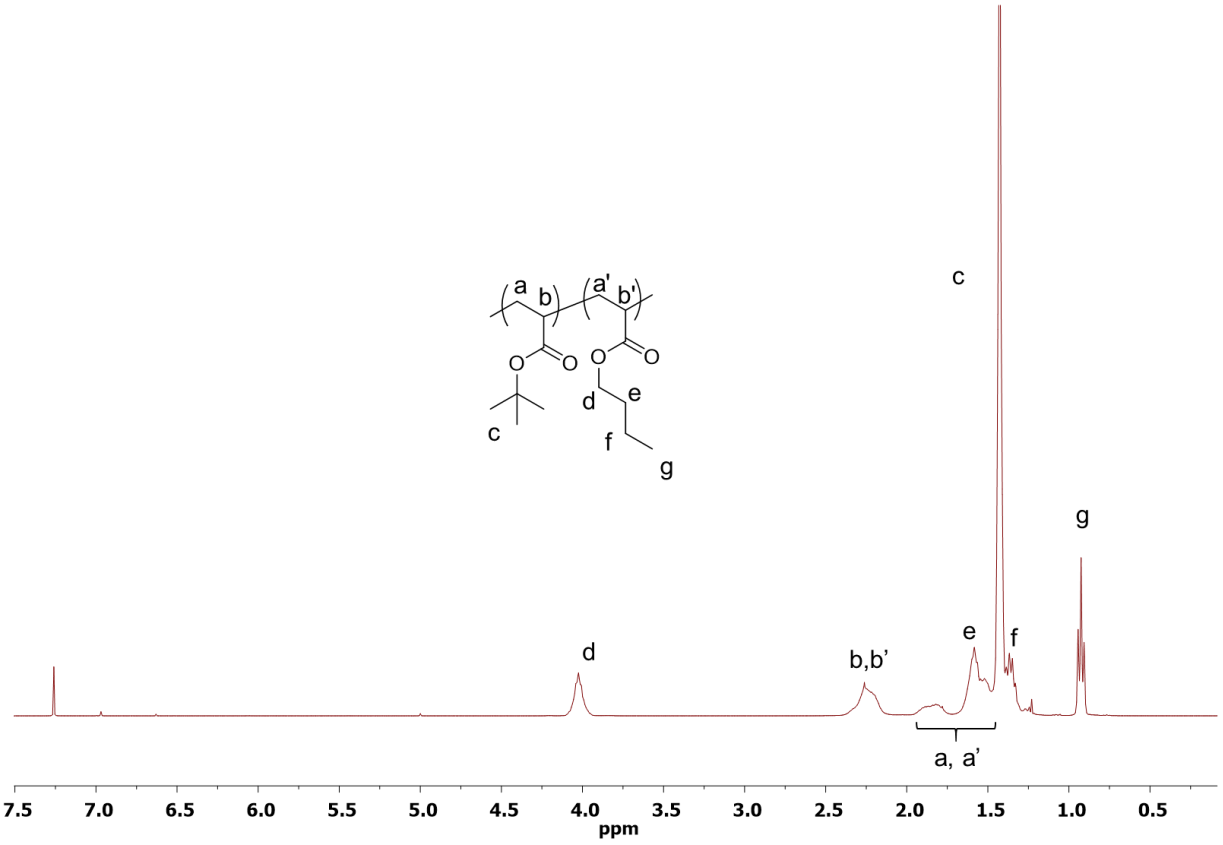

Figure C15. ^{1}H NMR ($CDCl_3$) of P^{t}BA-*b*-P^{n}BA-*b*-P^{t}BA (theoretical DP = 300-300-300) synthesized by mixed addition ^{t}BA/^{n}BA/MAD/PMe_3 = 600/300/2/1 (Table 4.1, run 6).

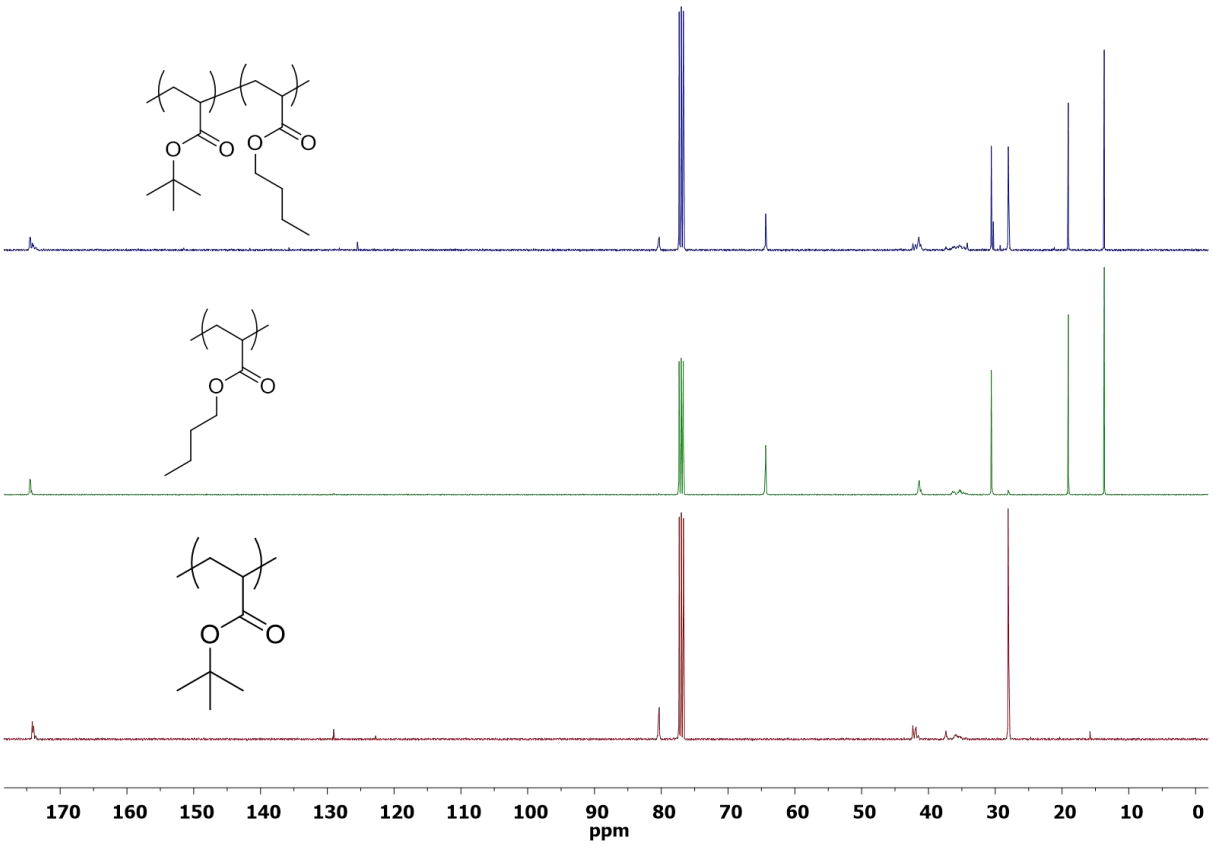

Figure C16. ^{13}C NMR ($CDCl_3$) of P^{t}BA (Table C2, run 2, bottom), P^{n}BA (Table C2, run 16, middle), and P^{t}BA-*b*-P^{n}BA-*b*-P^{t}BA) (theoretical DP = 100-200-100, top) synthesized by sequential addition (Table C3, run 19c).

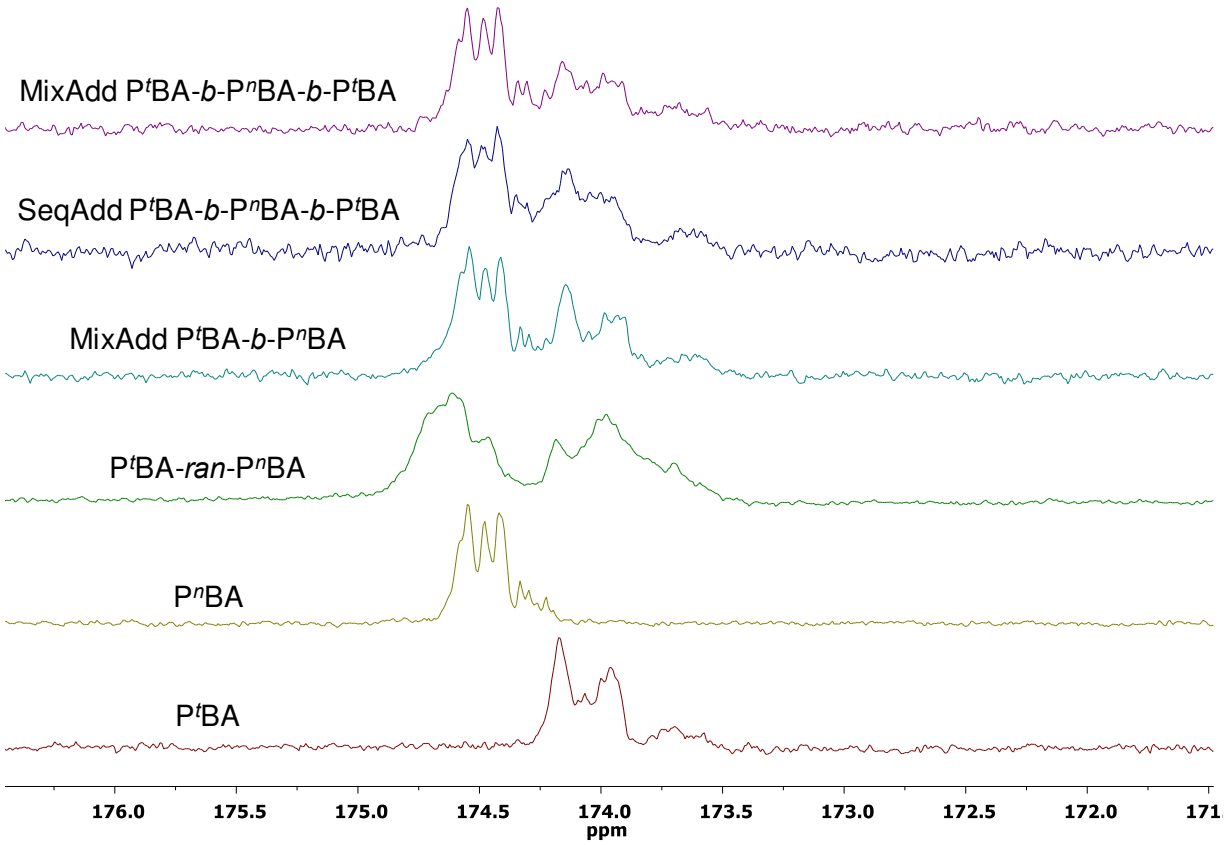

Figure C17. ^{13}C NMR spectra ($CDCl_3$) of the carbonyl region for P^{t}BA, P^{n}BA, P^{t}BA-*ran*-P^{n}BA (Table 4.1, run 1), P^{t}BA-*b*-P^{n}BA by mixed addition (Table 4.1, run 4), P^{t}BA-*b*-P^{n}BA-*b*-P^{t}BA by sequential addition (Table C3, run 19c) and mixed addition (Table 4.1, run 5).

Determination of K_{eq} by Variable Temperature NMR Study

To confirm the proposed prior equilibrium differentiation mechanism exploited by the mixed addition protocol, it was necessary to acertain the K_{eq} between the ^{t}BA/MAD and ^{n}BA/MAD adducts. This can be done by comparison of ^{1}H NMR integration of one of the MAD peaks (we chose to use the Al-CH_3) from a 1/1/1 mixture of ^{t}BA/^{n}BA/MAD. A solution of ^{t}BA/^{n}BA/MAD = 1/1/1 (0.50 mL of 0.008 M ^{t}BA + 0.50 mL of 0.008 M ^{n}BA + 0.50 mL of 0.008 M MAD in toluene-d_8) was prepared in a J-Young type tube. Attempts to perform this experiment at RT were inconclusive because the two species exist as one average peak due to rapid equilibrium exchange between the two species (Figures C18 and C19). Therefore, we used variable temperature NMR to perform the experiment at lower temperatures where the exchange rate would be much lower. To our satisfaction, this technique was successful in slowing down the exchange rate to the extent that both ^{t}BA/MAD and ^{n}BA/MAD signals were visable and well-resolved between -30 and -70 ^{o}C (Figure C20). We calculated K_{eq} based on integration of Al-CH_3 peaks at 5 different temperatures and used this data to generate a Van't Hoff plot (Figure C21). We used this plot to estimate K_{eq} at RT, and determine approximate ΔH_{rxn} and ΔS_{rxn}, shown below.

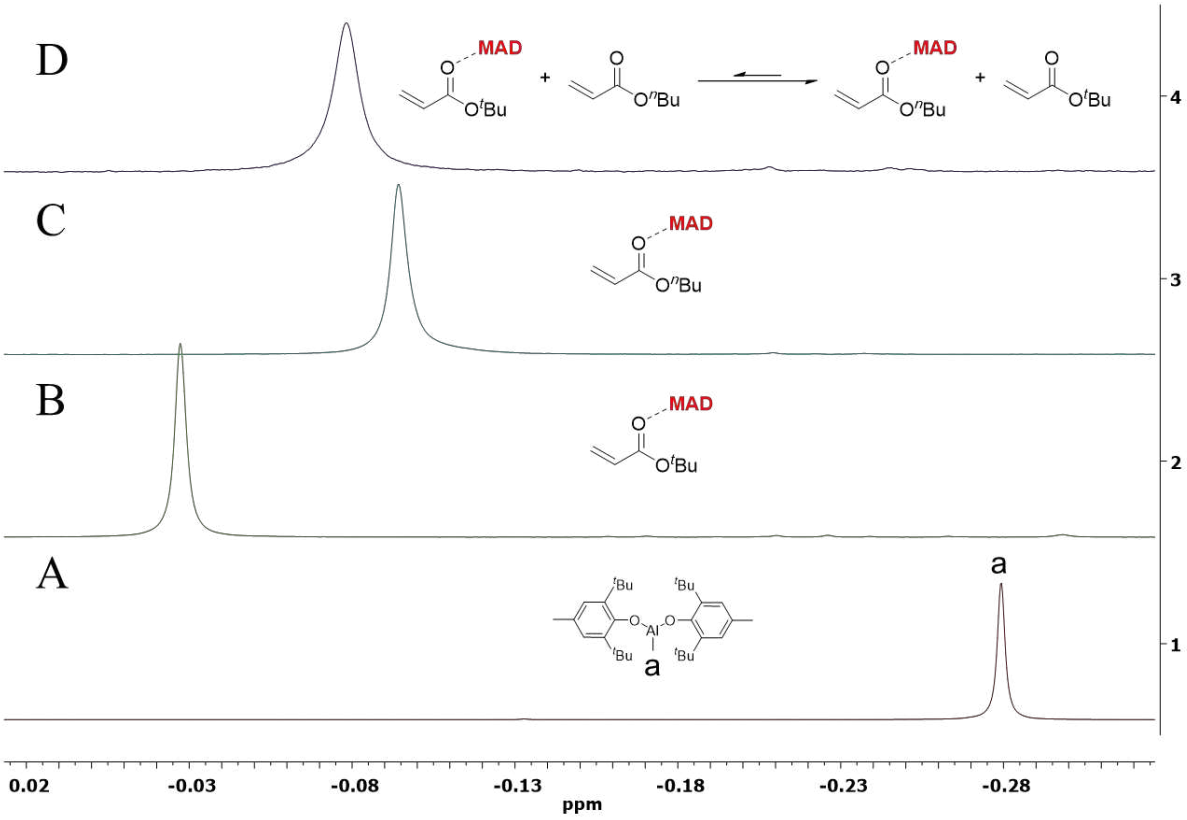

Figure C18. ^{1}H NMR (toluene-d_8) of MAD Al-CH_3 peaks (**A**), overlaid with individual ^{t}BA/MAD (**B**), ^{n}BA/MAD LA/monomer adducts (**C**), and the competing 1/1/1 equilibrium (**D**), showing a shift in the Al-CH_3 peak following coordination, but an averaging of the two monomer-MAD adduct peaks at RT due to rapid equilibrium exchange.

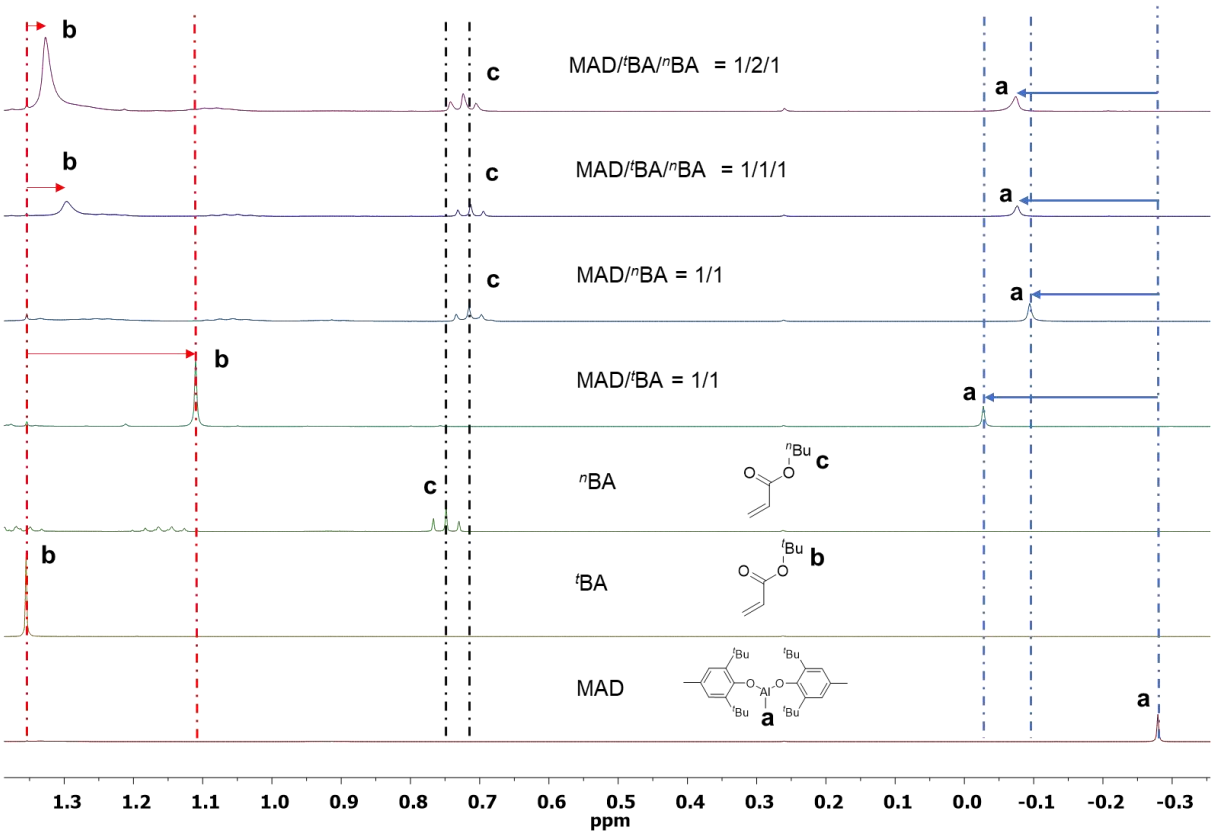

Figure C19. ^{1}H NMR (toluene-d_8) of MAD and monomer adducts ^{t}BA/MAD and ^{n}BA/MAD, showing shifts in MAD Al-CH_3, ^{t}BA O-C(CH_3)$_3$, and ^{n}BA O-CH$_2$CH$_2$CH$_2$CH_3 peaks. An averaging effect on the ppm shift is observed in the 1/1/1 spectrum due to rapid equilibrium exchange.

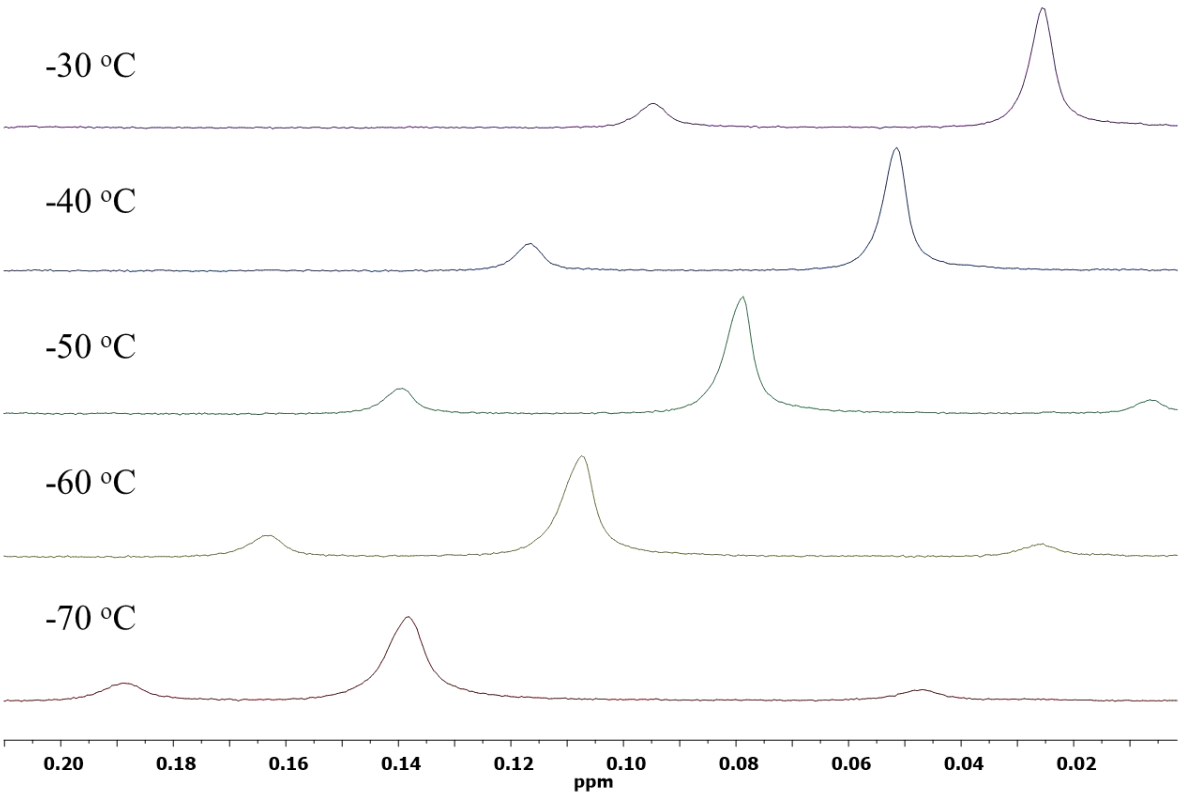

Figure C20. ^{1}H NMR (toluene-d_8) of ^{t}BA/^{n}BA/MAD = 1/1/1 (0.50 mL of 0.008 M ^{t}BA + 0.50 mL of 0.008 M ^{n}BA + 0.50 mL of 0.008 M MAD) in a J-Young type tube, at different low temperatures. Unlike the adducts at RT, the ^{t}BA/MAD (left minor peak) and ^{n}BA/MAD (right major peak) adducts at low temperatures were split into two peaks, which were integrated after reaching equilibrium at each temperature for Van't Hoff calculations.

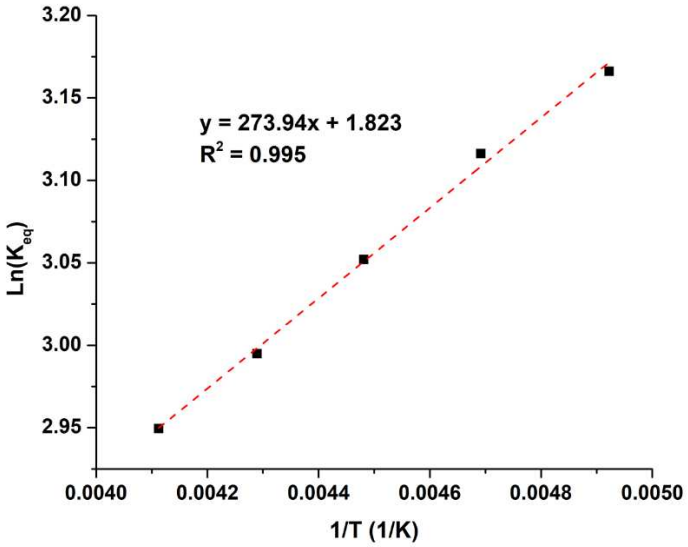

Figure C21. Van't Hoff plot of the K_{eq} values acquired at various temperatures for ^{t}BA/^{n}BA/MAD = 1/1/1 (0.50 mL of 0.008 M ^{t}BA + 0.50 mL of 0.008 M ^{n}BA + 0.50 mL of 0.008 M MAD).

Table C4. Variable temperature ^{1}H NMR Equilibrium study

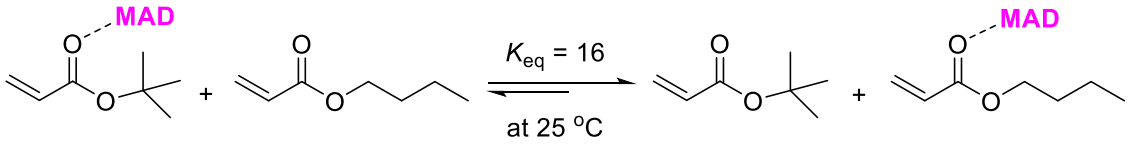

T (°C)	T(K)	1/T	[a]Reactants	[b]Products	[^{n}BA]	[^{t}BA]	[^{n}BA·MAD]	[^{t}BA·MAD]	K_{eq}	Ln(K_{eq})
-70	203.15	0.00492	1	4.87	0.0004429	0.002157	0.002157	0.0004429	23.7	3.17
-60	213.15	0.00469	1	4.75	0.0004522	0.002148	0.002148	0.0004522	22.6	3.12
-50	223.15	0.00448	1	4.60	0.0004643	0.002136	0.002136	0.0004643	21.2	3.05
-40	233.15	0.00429	1	4.47	0.0004753	0.002125	0.002125	0.0004753	20.0	2.99
-30	243.15	0.00411	1	4.37	0.0004842	0.002116	0.002116	0.0004842	19.1	2.95

Conditions: [^{t}BA]$_0$/[^{n}BA]$_0$/[MAD]$_0$ = 1/1/1, (calculated 2.6 mM of each component) in toluene-d_8. [a]Integration of ^{t}BA/MAD (Al-C*H*3) signal, and [b]integration of ^{n}BA/MAD (Al-C*H*3) signal.

The Van't Hoff equation:

1. $$Ln(K_{eq}) = -\frac{\Delta H_{rxn}}{RT} + \frac{\Delta S_{rxn}}{R}$$

By plotting the ln(K_{eq}) vs 1/T values from Table C4, a linear curve was obtained (Figure C21) following the equation y = 273.94x + 1.823 with an R^2 = 0.995. Plugging in the (1/T) value corresponding to 25 °C yielded a K_{eq} value of 16. The ΔH_{rxn} was calculated from the slope to be -2.3 kJ/mol and the ΔS_{rxn} was calculated from the y-intercept to be 15 J K^{-1}mol^{-1}.

COPASI (COmplex PAthway SImulator, Version 4.22, build 170) Kinetic Simulation of Sequences controlled by LPP

1. Chain Growth polymerization

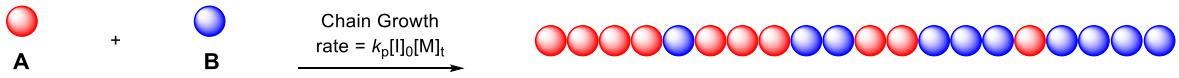

$[A]_0 = [B]_0 = 100$ mmol/mL
(initiator) $[I]_0 = 1$ mmol/mL

$k_{A/A} = 0.1$ mL/(mmol*s)
$k_{A/B} = 0.009$ mL/(mmol*s)
$k_{B/B} = 0.003$ mL/(mmol*s)
$k_{B/A} = 0.05$ mL/(mmol*s)

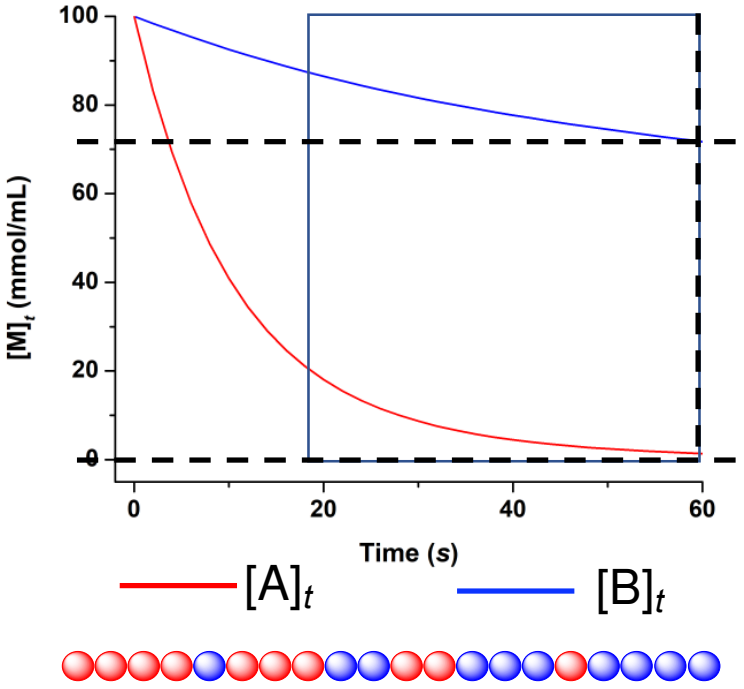

Figure C22. COPASI simulation of mixed copolymerization following rate = $k_p[I]_0[M]_t$, where "I" is the initiating species and "M" is monomer. The simulation shows first-order decay (in $[M]_t$) for both monomers A and B, resulting in a tapered block structure. The X-axis is scaled to the time point (60 s) when monomer A reaches depletion. The tapering phase, where $rate_A \approx rate_B$, is highlighted in red.

Chain Growth settings:

#	Name	Compartment	Type	Initial Concentration (mmol/ml)
1	A	compartment	reactions	100
2	B	compartment	reactions	100
3	PA*	compartment	reactions	1
4	PB*	compartment	reactions	0

#	Name	Reaction	Rate Law	Flux (mmol/s)
1	pro-PA*-A	PA* + A -> PA*	Mass action (irreversible)	10
2	pro-PA*-B	PA* + B -> PB*	Mass action (irreversible)	0.9
3	pro-PB*-A	PB* + A -> PA*	Mass action (irreversible)	0
4	pro-PB*-B	PB* + B -> PB*	Mass action (irreversible)	0

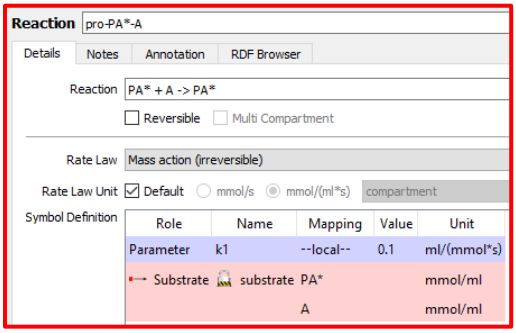

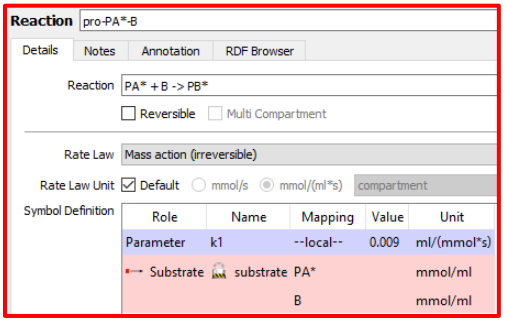

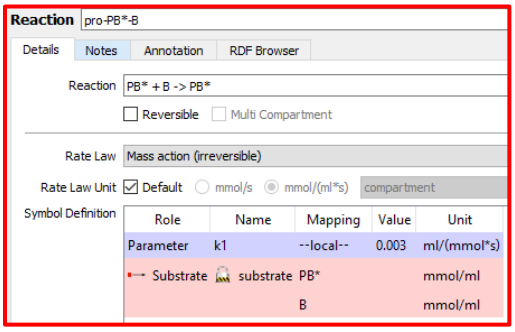

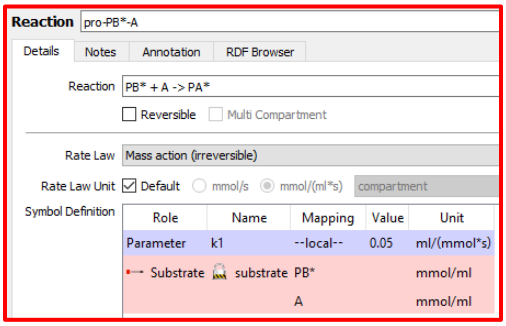

	(pro-PA*-A)	(pro-PA*-B)	(pro-PB*-A)	(pro-PB*-B)
A	-1	0	-1	0
B	0	-1	0	-1
PA*	0	-1	1	0
PB*	0	1	-1	0

2. Differentiating LPP (K_{eq} = 4)

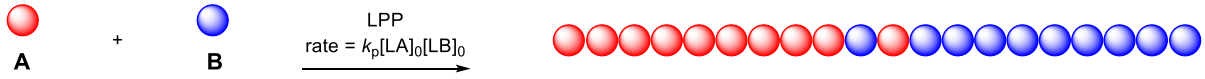

$[A]_0 = [B]_0$ = 100 mmol/mL
(initiator) $[LB]_0$ = 1 mmol/mL
$[LA]_0$ = 1 mmol/mL

K_{eq} = 4

$k_{A/A}$ = 0.1 mL/(mmol*s)
$k_{A/B}$ = 0.009 mL/(mmol*s)
$k_{B/B}$ = 0.003 mL/(mmol*s)
$k_{B/A}$ = 0.05 mL/(mmol*s)

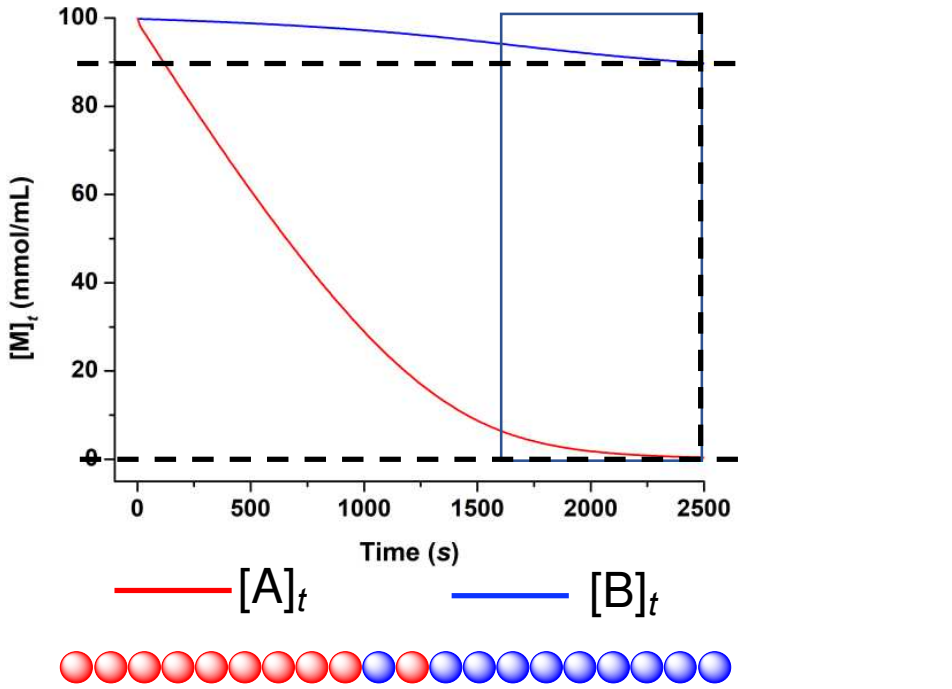

Figure C23. COPASI simulation of mixed copolymerization following rate = $k_p[LA]_0[LB]_0$ with K_{eq} = 4. The simulation shows zero-order decay (in $[M]_t$) for both monomers A and B during a long linear phase, followed by a short tapering phase beginning when $[A]_t \approx [LA]_0$, resulting in a highly resolved block structure. The X-axis is scaled to the time point (2500 s) when monomer A reaches depletion. The tapering phase, where $rate_A \approx rate_B$, is highlighted in red.

Differentiating LPP (K_{eq} = 4) settings:

#	Name	Compartment	Type	Initial Concentration (mmol/ml)
1	A	compartment	reactions	100
2	B	compartment	reactions	100
3	A*	compartment	reactions	0
4	B*	compartment	reactions	0
5	LA	compartment	reactions	1
6	PA*	compartment	reactions	0
7	PB*	compartment	reactions	1

#	Name	Reaction	Rate Law	Flux (mmol/s)
1	A activation	A + LA = A*	Mass action (reversible)	10000
2	B activation	B + LA = B*	Mass action (reversible)	2000
3	pro-PA*/A*	PA* + A* -> PA* + LA	Mass action (irreversible)	0
4	pro-PA*/B*	PA* + B* -> PB* + LA	Mass action (irreversible)	0
5	pro-PB*/B*	PB* + B* -> PB* + LA	Mass action (irreversible)	0
6	pro-PB*/A*	PB* + A* -> PA* + LA	Mass action (irreversible)	0

Reaction A activation

Details | Notes | Annotation | RDF Browser

Reaction: A + LA = A*

☑ Reversible ☐ Multi Compartment

Rate Law: Mass action (reversible)

Rate Law Unit: ☑ Default ○ mmol/s ◉ mmol/(ml*s) compartment

Symbol Definition

Role	Name	Mapping	Value	Unit
Parameter	k1	--local--	100	ml/(mmol*s)
Substrate	substrate	A		mmol/ml
		LA		mmol/ml
Parameter	k2	--local--	0.1	1/s
Product	product	A*		mmol/ml

Reaction B activation

Details | Notes | Annotation | RDF Browser

Reaction: B + LA = B*

☑ Reversible ☐ Multi Compartment

Rate Law: Mass action (reversible)

Rate Law Unit: ☑ Default ○ mmol/s ◉ mmol/(ml*s) compartment

Symbol Definition

Role	Name	Mapping	Value	Unit
Parameter	k1	--local--	20	ml/(mmol*s)
Substrate	substrate	B		mmol/ml
		LA		mmol/ml
Parameter	k2	--local--	0.1	1/s
Product	product	B*		mmol/ml

Reaction pro-PA*/A*

Details | Notes | Annotation | RDF Browser

Reaction: PA* + A* -> PA* + LA

☐ Reversible ☐ Multi Compartment

Rate Law: Mass action (irreversible)

Rate Law Unit: ☑ Default ○ mmol/s ◉ mmol/(ml*s) compartment

Symbol Definition

Role	Name	Mapping	Value	Unit
Parameter	k1	--local--	0.1	ml/(mmol*s)
Substrate	substrate	PA*		mmol/ml
		A*		mmol/ml

Reaction pro-PA*/B*

Details | Notes | Annotation | RDF Browser

Reaction: PA* + B* -> PB* + LA

☐ Reversible ☐ Multi Compartment

Rate Law: Mass action (irreversible)

Rate Law Unit: ☑ Default ○ mmol/s ◉ mmol/(ml*s) compartment

Symbol Definition

Role	Name	Mapping	Value	Unit
Parameter	k1	--local--	0.009	ml/(mmol*s)
Substrate	substrate	PA*		mmol/ml
		B*		mmol/ml

Reaction pro-PB*/B*

Details | Notes | Annotation | RDF Browser

Reaction: PB* + B* -> PB* + LA

☐ Reversible ☐ Multi Compartment

Rate Law: Mass action (irreversible)

Rate Law Unit: ☑ Default ○ mmol/s ◉ mmol/(ml*s) compartment

Symbol Definition

Role	Name	Mapping	Value	Unit
Parameter	k1	--local--	0.003	ml/(mmol*s)
Substrate	substrate	PB*		mmol/ml
		B*		mmol/ml

Reaction pro-PB*/A*

Details | Notes | Annotation | RDF Browser

Reaction: PB* + A* -> PA* + LA

☐ Reversible ☐ Multi Compartment

Rate Law: Mass action (irreversible)

Rate Law Unit: ☑ Default ○ mmol/s ◉ mmol/(ml*s) compartment

Symbol Definition

Role	Name	Mapping	Value	Unit
Parameter	k1	--local--	0.05	ml/(mmol*s)
Substrate	substrate	PB*		mmol/ml
		A*		mmol/ml

	(A activation)	(B activation)	(pro-PA*/A*)	(pro-PA*/B*)	(pro-PB*/B*)	(pro-PB*/A*)
LA	-1	-1	1	1	1	1
PA*	0	0	0	-1	0	1
B*	0	1	0	-1	-1	0
A	-1	0	0	0	0	0
B	0	-1	0	0	0	0
A*	1	0	-1	0	0	-1
PB*	0	0	0	1	0	-1

Differentiating LPP (K_{eq} = 100)

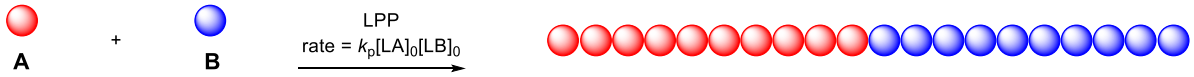

$[A]_0 = [B]_0$ = 100 mmol/mL
(initiator) $[LB]_0$ = 1 mmol/mL
$[LA]_0$ = 1 mmol/mL

K_{eq} = 100

$k_{A/A}$ = 0.1 mL/(mmol*s)
$k_{A/B}$ = 0.009 mL/(mmol*s)
$k_{B/B}$ = 0.003 mL/(mmol*s)
$k_{B/A}$ = 0.05 mL/(mmol*s)

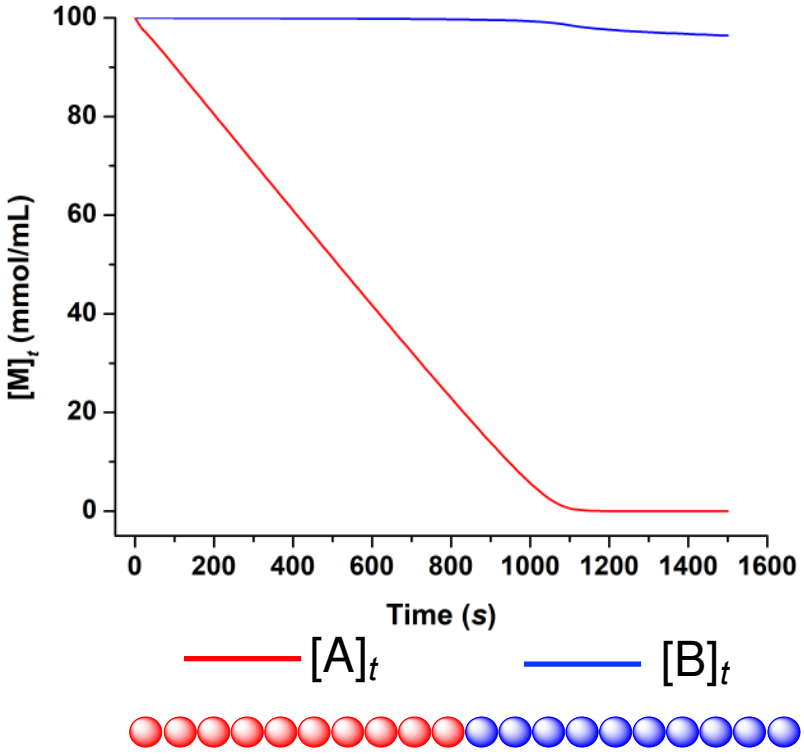

Figure C24. COPASI simulation of mixed copolymerization following rate = $k_p[LA]_0[LB]_0$ with K_{eq} = 100. The simulation shows zero order decay (in $[M]_t$) for both monomers A and B during a long linear phase that does not taper, even when $[A]_t \approx [LA]_0$, *resulting in a perfectly resolved block structure*. This shows that block resolution is a function of K_{eq} in differentiating LP copolymerizations. The X-axis is scaled to the time point (1600 seconds) shortly after monomer A reaches depletion.

Differentiating LPP (K_{eq} = 100) settings:

#	Name	Compartment	Type	Initial Concentration (mmol/ml)
1	A	compartment	reactions	100
2	B	compartment	reactions	100
3	A*	compartment	reactions	0
4	B*	compartment	reactions	0
5	LA	compartment	reactions	1
6	PA*	compartment	reactions	0
7	PB*	compartment	reactions	1

#	Name	Reaction	Rate Law	Flux (mmol/s)
1	A activation	A + LA = A*	Mass action (reversible)	10000
2	B activation	B + LA = B*	Mass action (reversible)	100
3	pro-PA*/A*	PA* + A* -> PA* + LA	Mass action (irreversible)	0
4	pro-PA*/B*	PA* + B* -> PB* + LA	Mass action (irreversible)	0
5	pro-PB*/B*	PB* + B* -> PB* + LA	Mass action (irreversible)	0
6	pro-PB*/A*	PB* + A* -> PA* + LA	Mass action (irreversible)	0

Reaction A activation

Details | Notes | Annotation | RDF Browser

Reaction: A + LA = A*

☑ Reversible ☐ Multi Compartment

Rate Law: Mass action (reversible)

Rate Law Unit: ☑ Default ○ mmol/s ○ mmol/(ml*s) compartment

Symbol Definition

Role	Name	Mapping	Value	Unit
Parameter	k1	--local--	100	ml/(mmol*s)
Substrate	substrate	A		mmol/ml
		LA		mmol/ml
Parameter	k2	--local--	0.1	1/s
Product	product	A*		mmol/ml

Reaction B activation

Details | Notes | Annotation | RDF Browser

Reaction: B + LA = B*

☑ Reversible ☐ Multi Compartment

Rate Law: Mass action (reversible)

Rate Law Unit: ☑ Default ○ mmol/s ○ mmol/(ml*s) compartment

Symbol Definition

Role	Name	Mapping	Value	Unit
Parameter	k1	--local--	1	ml/(mmol*s)
Substrate	substrate	B		mmol/ml
		LA		mmol/ml
Parameter	k2	--local--	0.1	1/s
Product	product	B*		mmol/ml

Reaction pro-PA*/A*

Details | Notes | Annotation | RDF Browser

Reaction: PA* + A* -> PA* + LA

☐ Reversible ☐ Multi Compartment

Rate Law: Mass action (irreversible)

Rate Law Unit: ☑ Default ○ mmol/s ○ mmol/(ml*s) compartment

Symbol Definition

Role	Name	Mapping	Value	Unit
Parameter	k1	--local--	0.1	ml/(mmol*s)
Substrate	substrate	PA*		mmol/ml
		A*		mmol/ml

Reaction pro-PA*/B*

Details | Notes | Annotation | RDF Browser

Reaction: PA* + B* -> PB* + LA

☐ Reversible ☐ Multi Compartment

Rate Law: Mass action (irreversible)

Rate Law Unit: ☑ Default ○ mmol/s ○ mmol/(ml*s) compartment

Symbol Definition

Role	Name	Mapping	Value	Unit
Parameter	k1	--local--	0.009	ml/(mmol*s)
Substrate	substrate	PA*		mmol/ml
		B*		mmol/ml

Reaction pro-PB*/B*

Details | Notes | Annotation | RDF Browser

Reaction: PB* + B* -> PB* + LA

☐ Reversible ☐ Multi Compartment

Rate Law: Mass action (irreversible)

Rate Law Unit: ☑ Default ○ mmol/s ○ mmol/(ml*s) compartment

Symbol Definition

Role	Name	Mapping	Value	Unit
Parameter	k1	--local--	0.003	ml/(mmol*s)
Substrate	substrate	PB*		mmol/ml
		B*		mmol/ml

Reaction pro-PB*/A*

Details | Notes | Annotation | RDF Browser

Reaction: PB* + A* -> PA* + LA

☐ Reversible ☐ Multi Compartment

Rate Law: Mass action (irreversible)

Rate Law Unit: ☑ Default ○ mmol/s ○ mmol/(ml*s) compartment

Symbol Definition

Role	Name	Mapping	Value	Unit
Parameter	k1	--local--	0.05	ml/(mmol*s)
Substrate	substrate	PB*		mmol/ml
		A*		mmol/ml

	(A activation)	(B activation)	(pro-PA*/A*)	(pro-PA*/B*)	(pro-PB*/B*)	(pro-PB*/A*)
LA	-1	-1	1	1	1	1
PA*	0	0	0	-1	0	1
B*	0	1	0	-1	-1	0
A	-1	0	0	0	0	0
B	0	-1	0	0	0	0
A*	1	0	-1	0	0	-1
PB*	0	0	0	1	0	-1

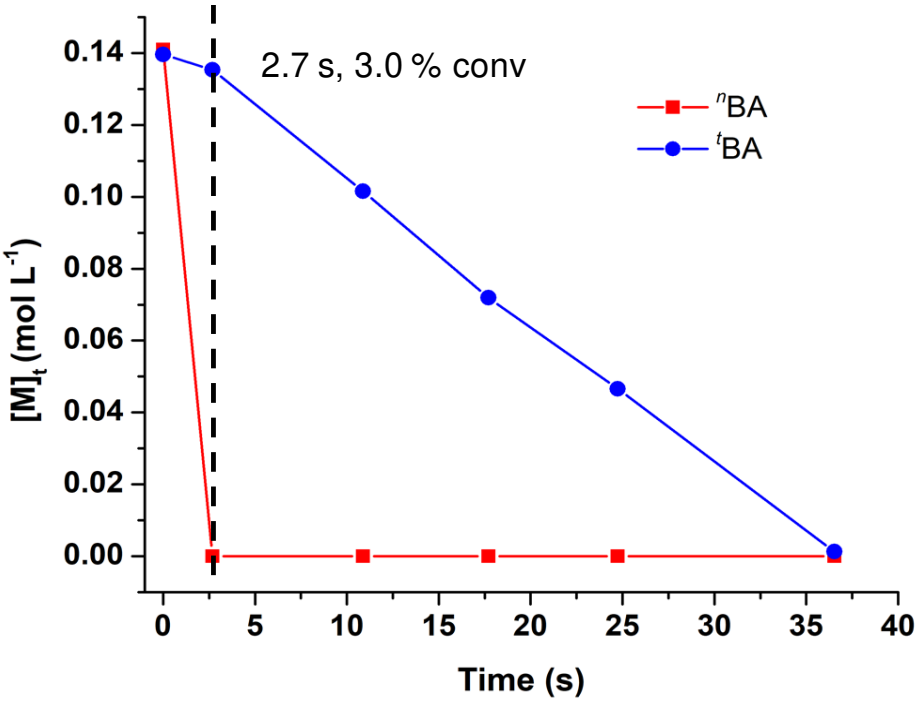

Figure C25. Kinetic profile of a 1/1 ^{n}BA/^{t}BA diblock copolymerization by mixed addition, $[^{n}BA]_0$ = $[^{t}BA]_0$ = 0.141 M in toluene, ^{n}BA/^{t}BA/MAD/PMe_3 = 100/100/2/1, 23 °C, revealing an approximate ^{t}BA misincorporation of <3 %.

References cited in Appendix C

1 (a) Faingol'd, E. E.; Bravaya, N. M.; Panin, A. N.; Babkina, O. N.; Saratovskikh, S. L.; Privalov, V. I. Isobutylaluminum Aryloxides as Metallocene Activators in Homo- and Copolymerization of Olefins. *J. Appl. Polym.* **2016**, *133*, 43276 (1-8). (b) Shreve, A. P.; Mulhaupt, R.; Fultz, W.; Calabrese, J.; Robbins, W.; Ittel, S. Sterically Hindered Aryloxide-Substituted Alkylaluminum Compounds. *Organometallics* **1988**, *7*, 409–416. (c) Skowronska-Ptasinska, M.; Starowieyski, K. B.; Pasynkiewicz, S.; Carewska, M. Phenoxyaluminium Compounds : VII. Reactions of Organoaluminium Compounds with Hindered Phenols. *J. Organomet. Chem.* **1978**, *160*, 403–409. (d) Starowieyski, K. B.; Pasynkiewicz, S.; Skowronska-Ptasinska, M. Phenoxyaluminium Compounds IV. Syntheses and Structures of Monomeric (2,6-DI-t-Butyl-4-methylphenoxy)aluminium Compounds. *J. Organomet. Chem.* **1975**, *90*, C43–C44.

Appendix D
Supplementary Information Corresponding to Chapter 5

Taken verbatim from:

McGraw, M. L.; Clarke, R. W.; Chen, E. Y.-X. Synchronous Control of Chain Length/Sequence/Topology for Precision Synthesis of Cyclic Block Copolymers from Monomer Mixtures. *J. Am. Chem. Soc.* **2021**, *143*, 3318–3322.

Materials

Methyl Methacrylate (MMA), ethyl sorbate (ES), and *n*-butyl acrylate (^{n}BA) were purchased from TCI and dried over calcium hydride for several hours in the absence of light before vacuum distillation on a Schlenk line under N_2. The distillates were moved into an argon filled glovebox, transferred to amber bottles and stored in the dark at –30 °C. *N*-heterocyclic carbene (NHC) 1,3-di-*tert*-butylimidazolin-2-ylidene (I^{t}Bu) was purchased from TCI and used as received. Tricyclohexyl phosphine (PCy_3) was purchased from Alfa Aesar and used as received. Toluene was dried over NaK alloy and filtered through a 0.2 μm filter just prior to use. Methyl aluminum di(2,6-di-*tert*-butyl-4-methylphenoxy) (MAD) was synthesized by known literature methods.
[1]

Analytical Methods

NMR Spectroscopy. Monomer conversion as well as structure characterizations of polymers were carried out by ^{1}H NMR experiments using a Bruker Advance NEO 400 MHz (FT 400 MHz, ^{1}H; 100 MHz, ^{13}C) or a or Bruker AVIII 400 MHz spectrometer (400 MHz, ^{1}H; 100 MHz, ^{13}C). Chemical shifts were referenced to internal solvent resonances corresponding to 7.26 ppm (chloroform), 2.13 ppm (toluene), and 7.16 ppm (benzene) and reported as parts per million relative to $SiMe_4$.

Gel Permeation Chromatography (GPC). Measurements of polymer absolute weight-average molecular weight (M_w), number-average molecular weight (M_n), and molecular weight distributions or dispersity indices ($Đ = M_w/M_n$) were performed via GPC. The GPC instrument consisted of an Agilent HPLC system equipped with one guard column and three PL gel 5 μm mixed-C gel permeation columns and coupled with a Wyatt DAWN HELEOS II multi (3)-angle light scattering detector and a Wyatt Optilab TrEX dRI detector; the analysis was performed at 40 °C using THF as the eluent at a flow rate of 1.0 mL/min. Viscometry experiments were performed in a similar way using a Wyatt DAWN HELEOS II multi (18)-angle light-scattering detector, Wyatt Optilab TrEX dRI detector, and a Wyatt Viscostar III viscometer. Wyatt ASTRA 7.1.2 molecular weight characterization software. The refractive index increment (d*n*/d*c*) of the P^{n}BA-*b*-PMMA cyclic and linear copolymers were determined individually by batch experiments involving the dissolution of a particular polymer to four or five specific concentrations ranging from 0.50 to 5.00 mg/mL and measuring the differential refractive index at each concentration to generate a calibration curve with the slope being the d*n*/d*c* of that polymer.

Thermal Characterization

Differential scanning calorimetry (DSC). All block copolymer samples compared by DSC were measured with the same procedure. Roughly 5 – 10 mg of a thoroughly dried polymer sample was placed into an Auto Q20 DSC in aluminum TZero pans topped with TZero lids (TA Instrument). Plotted data represents the second heating scan against an empty aluminum reference pan. Heating scans were performed at 15 °C/min to 200 °C while cooling scans were performed at 10 °C/min to –80 °C. All raw data collected on the DSC was analyzed on the Universal Analysis software (TA Instruments).

Rheology

Viscosity Experiments. Viscosity experiments by rheology were performed on thoroughly dried linear and cyclic block copolymers prepared by heated compression molding at 195 °C (between two steel plates, a 38.1×12.7×1 mm steel mold, and non-stick Teflon sheets) inside a Carver Bench Top Laboratory Press (Model 4386). A Small circular-cut (8 mm diameter) samples were loaded between two 8 mm steel electrically heated platen (EHP) loading discs within a Discovery Series HR-2 (Hybrid Rheometer) (TA Instruments) under nitrogen gas flow (30 psi) connected to the TRIOS software (TA Instruments). Viscosity was studied under the flow testing option and amplitude setting. Experiments were run at 195 °C with shear rates varying between 10^{-3} and 10^{-1} rad/*s*. The axial force was controlled within a negligible ± 0.1 *N* to prevent non-frictional forces.

Microscopy and Surface Imaging

Transmission Electron Microscopy (TEM). Thin films of linear and cyclic high molecular weight $PAMA_g$-*b*-P^{n}BA were prepared by drop-casting a 0.1 mg/mL polymer solution in toluene onto DI water in a 20 mL scintillation vial. The samples were left uncapped in a closed fume-hood overnight, yielding a suitable specimen. A 200 mesh TEM grid was used to sweep under the film and capture sample by lifting it out of the water from below. The grid was left to dry in a desiccator for 1 h before placing it on the microscope. The transmission electron microscope imaging was done at 200 kV using a JEOL 2100F transmission electron microscope. The incident beam illuminating conditions were adjusted for minimum beam current and therefore to minimize radiation damage to the samples. An objective aperture was used to maximize contrast in bright field conditions (but also reduced beam damage). Exposure time for all images was 0.5 seconds, again to minimize the effect of beam damage. The images are representative of the entire sample as they are from a number of different grid openings and not specialized areas. All images were fitted with a scale bar using the publicly available tool ImageJ (NIH).

Experimental details

All syntheses and storage of air-sensitive materials were handled in an Argon filled glovebox or in a flame dried dual manifold Schlenk line.

Characterization of ^{n}BA/MMA/MAD equilibrium

In toluene-d_8, 0.080 M stock solutions were prepared of ^{n}BA, MMA, and MAD. Then, in four J-Young type NMR tubes, the following samples were prepared: (**1**) MAD alone 0.080 M in toluene; (**2**) MAD (0.30 mL of 0.080 M) + ^{n}BA (0.30 mL of 0.080 M); (**3**) MAD (0.30 mL of 0.080 M) + MMA (0.30 mL of 0.080 M); (**4**) MAD (0.20 mL of 0.080 M) + ^{n}BA (0.20 mL of 0.080 M) + MMA (0.20 mL of 0.080 M). Each sample was sealed and analyzed by ^{1}H NMR.

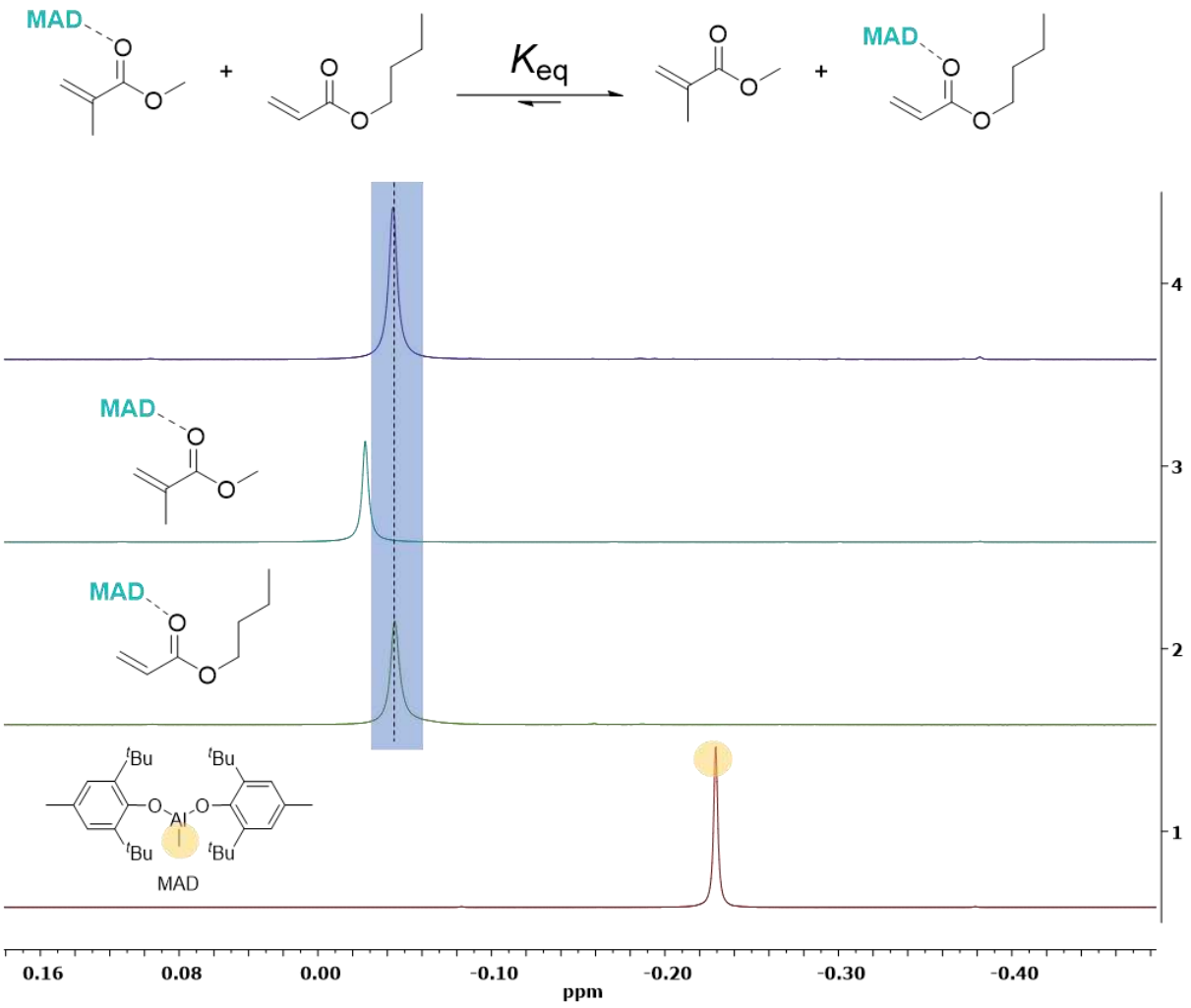

Figure D1. ^{1}H NMR (toluene-d_8, RT) equilibrium study of MMA vs ^{n}BA LA affinity with MAD. Using the Al-CH_3 shift as the dependent variable, from bottom to top: (**1**) MAD; (**2**) MAD/^{n}BA = [1]/[1]; (**3**) MAD/MMA = [1]/[1]; (**4**) MAD/^{n}BA/MMA = [1]/[1]/[1].

Preparation of ES/I^{t}Bu/MAD mixture (1)

The preparation of mixture **1** was carried out by a similar method published by Takasu.[2] Individual 0.24 M stock solutions were prepared of I^{t}Bu, MAD, and ethyl sorbate (ES) in DCM. These solutions were put in a –30 °C freezer for 1 h. Then, 1.00 mL of the ES solution was added to 1.00 mL of the MAD solution, giving a brilliant orange/yellow color. Then, 1.00 mL of the combined MAD/ES solution (now only 0.12 M) was added to 0.50 mL of I^{t}Bu solution dropwise over 1 min,

generating the titled mixture at a theoretical concentration 0.080 M. The concentrations of the stock solutions were manipulated so that 0.10 mL of the final **1** solution would correspond to a quantity of initiator appropriate for each particular reaction.

Judging the degree of sequence control between comonomers ^{n}BA and MMA

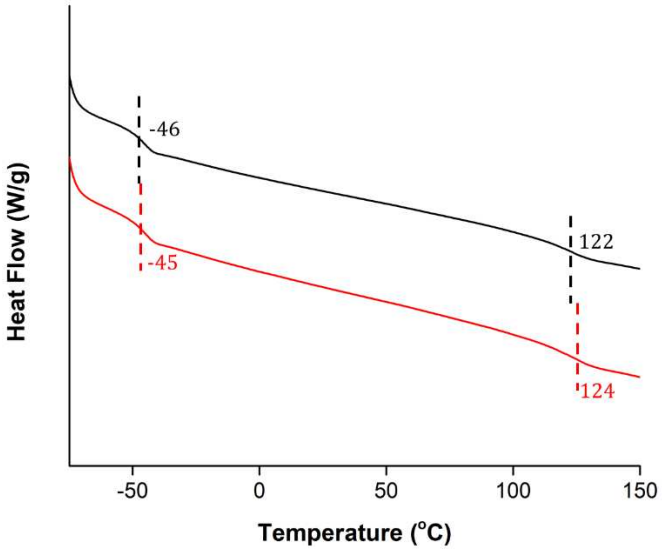

Figure D2. Comparative DSC overlay of P^{n}BA-*b*-PMMA linear (Table D1, run 1, black) and cyclic (Table D1, run 3, red) copolymers. Both polymers show two glass transition temperatures (T_g) indicating two distinct polymer domains (associated with P^{n}BA and PMMA).

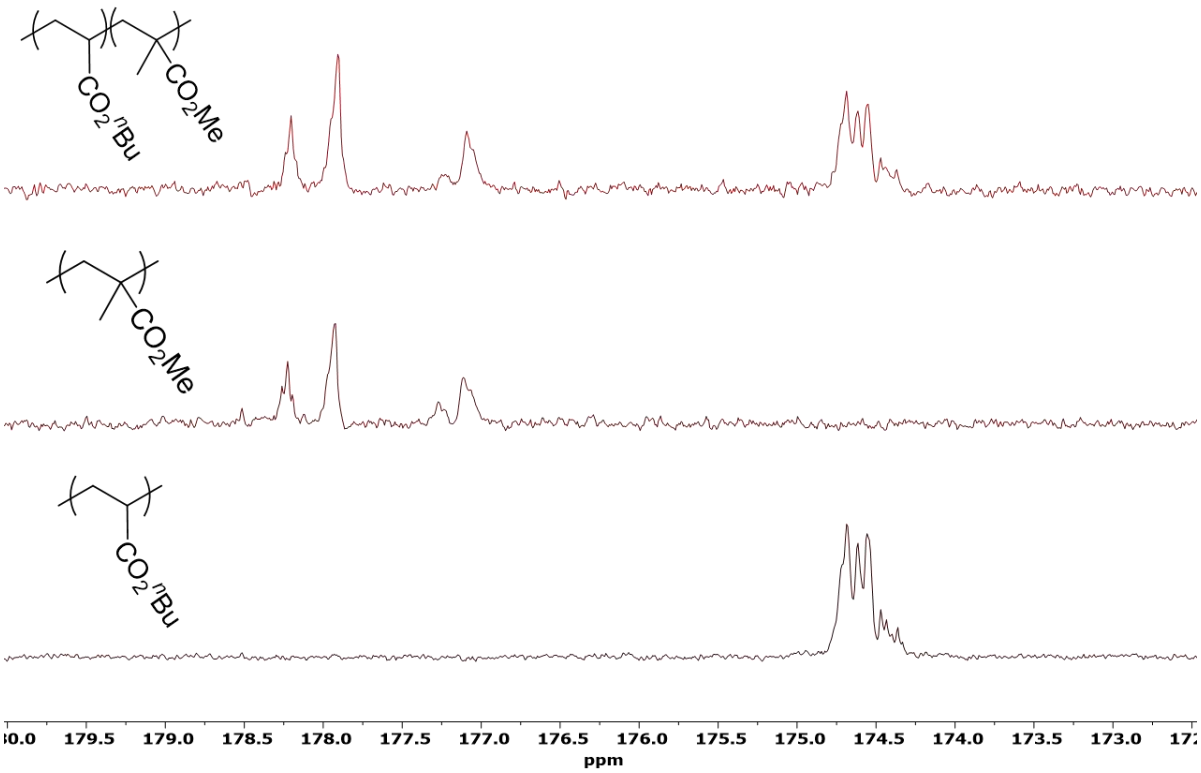

Figure D3. ^{13}C NMR ($CDCl_3$) overlay expanded to the carbonyl region of P^{n}BA homopolymer (bottom), PMMA homopolymer (middle), and high MW linear P^{n}BA-*b*-PMMA (Table D1, run 2, top), all synthesized by MAD/PCy_3 LPs.

Polymerization procedures and characterization

Synthesis and characterization of medium molecular weight linear diblock P^{n}BA-*b*-PMMA (Table D1, run 1)

In a 25 mL vial, 0.0511 g of MAD was weighted out precisely. Then 1.00 mL of MMA and 1.00 mL of ^{n}BA and 12 mL of toluene were added to MAD to make a brilliant yellow solution. A magnetic stir bar was added. Then 0.0149 g of PCy_3, as 0.10 mL of a 0.53 M stock solution in toluene, was injected into the solution, with vigorous stirring to make the overall compositional ratio [^{n}BA]/[MMA]/[MAD]/[PCy_3] = [130]/[168]/[2]/[1]. The yellow color of the reaction dimmed slightly following the injection of PMe_3 signaling the generation of an active species.

Then, 1 to 2 seconds later, the reaction dimmed again signaling the consumption of ^{n}BA. Then, 1 to 2 mins later, the reaction went completely clear signaling full consumption of MMA. An aliquot was taken for conversion calculation by ^{1}H NMR analysis, showing no monomer for quantitative conversion for both monomers.

The reaction was then quenched by adding 1 mL of methanol spiked with 100 ppm benzoic acid. Solvents were removed by rotary evaporation. Then, 5-10 mL of methanol was added. PMMA/P^{n}BA copolymers in general did not suddenly crash from methanol but rather swelled up as a gel. About half the solvent volume was then removed by rotary evaporation, which caused the polymers to stick to the walls of the vial, at which point the remaining methanol was decanted. Further purification was achieved by repeated dissolution in chloroform then precipitation in cold methanol assisted by centrifuge. Polymer products were dried in a vacuum oven at 100 ^{o}C for at least 6 h.

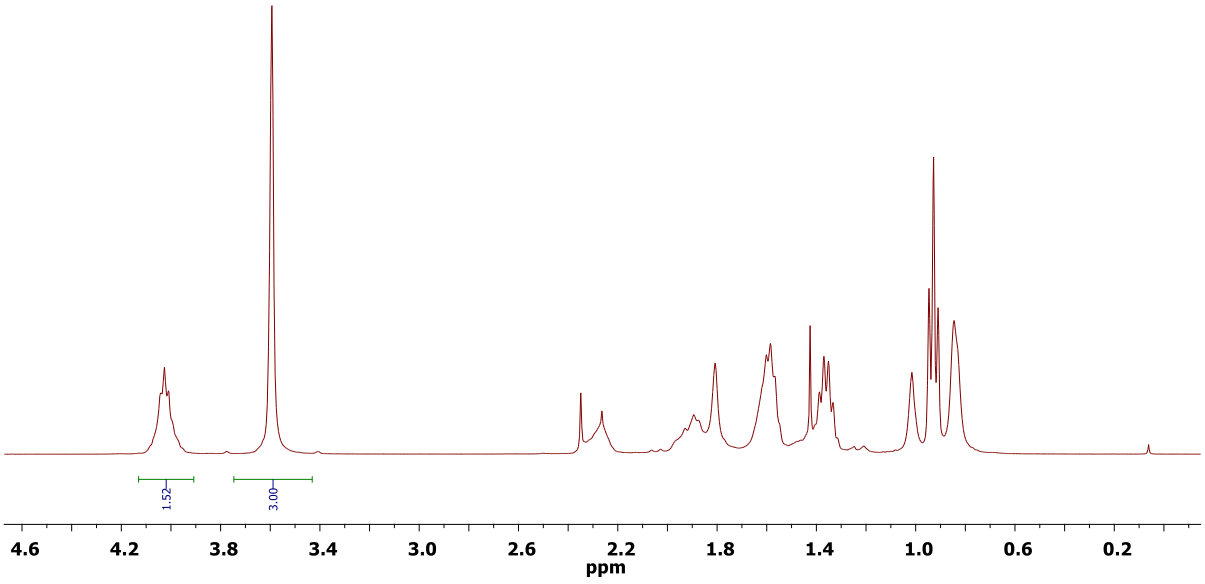

Figure D4. ^{1}H NMR ($CDCl_3$) of linear P^{n}BA-*b*-PMMA (Table D1, run 1) with a theoretical comonomer incorporation MMA/^{n}BA = 168/130, which should correspond to MMA/^{n}BA

integration ratio of 3.00/1.48 for MMA alkoxy methyl at 3.59 ppm and ^{n}BA alkoxy methylene at 4.02 ppm, respectively.

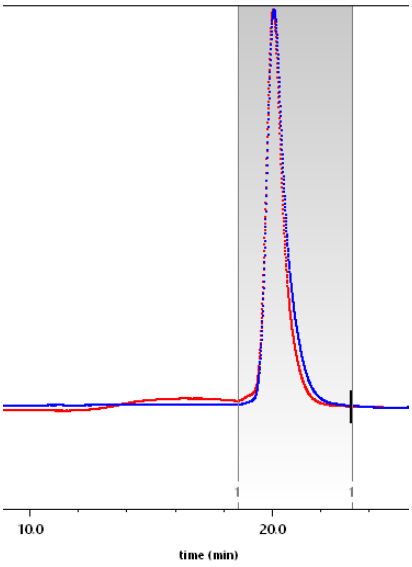

Figure D5. GPC trace (red, LS; blue dRI) of linear P^{n}BA-*b*-PMMA (Table D1, run 1). Shaded region indicates data included in MW calculation. d*n*/d*c* = 0.0737 mL/g; M_n = 73.1 kg/mol; $Đ$ = 1.06.

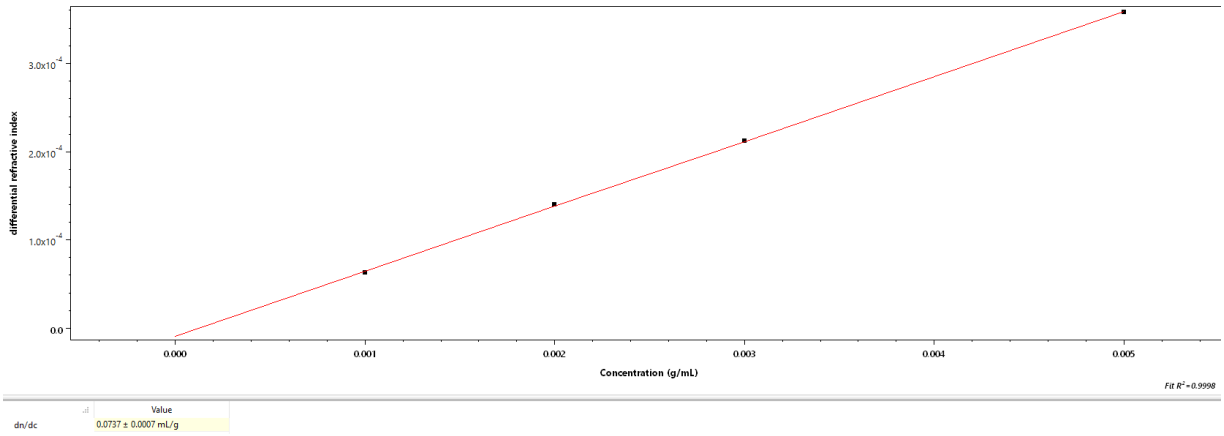

Figure D6. dRI vs concentration plot used to measure exact d*n*/d*c* value for linear P^{n}BA-*b*-PMMA (Table D1, run 1) in THF, with calculated d*n*/d*c* = 0.0737 mL/g.

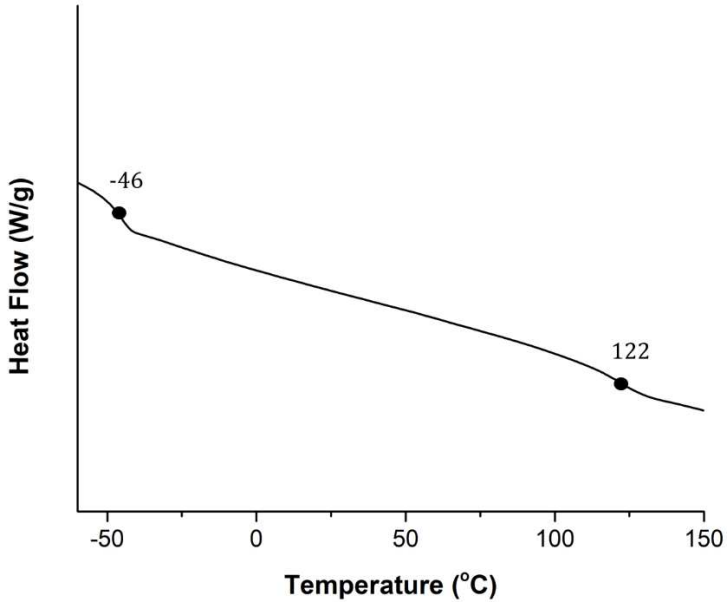

Figure D7. DSC trace (2nd heating scan) of linear P^{n}BA-*b*-PMMA (Table D1, run 1) showing two T_g's at –46 and 122 °C.

Synthesis and characterization of high molecular weight linear diblock P^{n}BA-*b*-PMMA (Table D1, run 2)

In a 50 mL round-bottom flask, 0.1128 g of MAD was weighted out precisely. Then 2.00 mL of MMA and 4.05 mL of ^{n}BA and 36 mL of toluene were added to MAD to make a brilliant yellow solution. A magnetic stir bar was added. Then 0.0066 g of PCy_3, as 0.10 mL of a 0.235 M stock solution in toluene, was injected into the solution with vigorous stirring to make the overall compositional ratio [^{n}BA]/[MMA]/[MAD]/[PCy_3] = [1200]/[800]/[10]/[1]. The yellow color of the reaction dimmed after 10 to 15 seconds signaling the consumption of ^{n}BA. Then, about 20 min later, the reaction went clear signaling full consumption of MMA. An aliquot was taken for conversion calculation by ^{1}H NMR analysis, showing no monomer for quantitative conversion for both monomers.

The reaction was then quenched by adding 3 mL of methanol spiked with 100 ppm benzoic acid. Solvents were then removed by rotary evaporation. Then, 15-20 mL of methanol was added.

PMMA/P^{n}BA copolymers in general did not suddenly crash from methanol but rather swelled up as a gel. About half the solvent volume was removed by rotary evaporation which caused the polymers to stick to the walls of the vial, at which point the remaining methanol was decanted. Further purification can be achieved by repeated dissolution in chloroform then precipitation in cold methanol assisted by centrifuge. Polymer products were dried in a vacuum oven at 100 ^{o}C for at least 6 h.

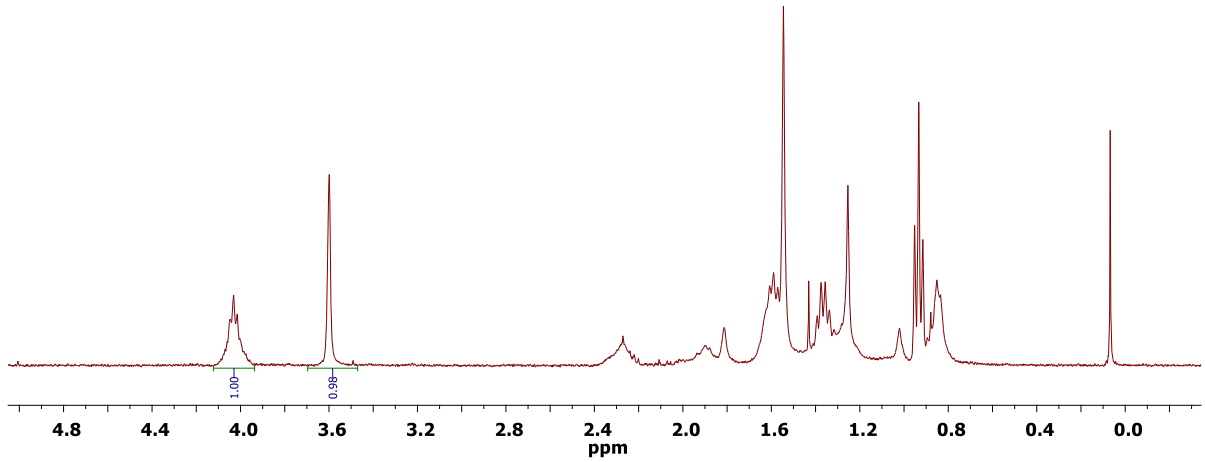

Figure D8. ^{1}H NMR ($CDCl_3$) of linear high MW P^{n}BA-*b*-PMMA (Table D1, run 2) with a theoretical comonomer incorporation MMA/^{n}BA = 800/1200, which should correspond to MMA/^{n}BA integration ratio of 1/1 for MMA alkoxy methyl at 3.59 ppm and ^{n}BA alkoxy methylene at 4.02 ppm, respectively.

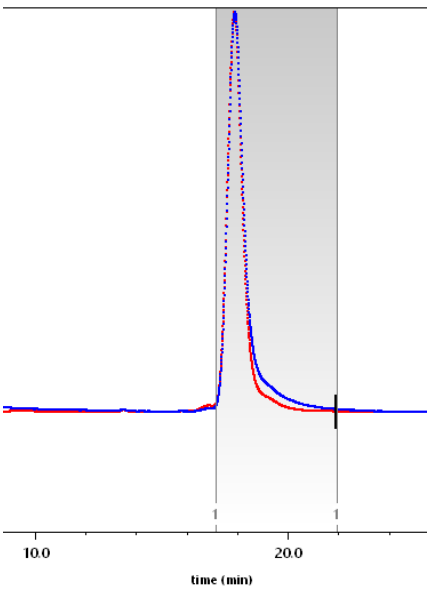

Figure D9. GPC trace (red, LS; blue dRI) of linear P^{n}BA-*b*-PMMA (Table D1, run 2). Shaded region indicates data included in MW calculation. d*n*/d*c* = 0.0791 mL/g; M_n = 286 kg/mol; $Đ$ = 1.12.

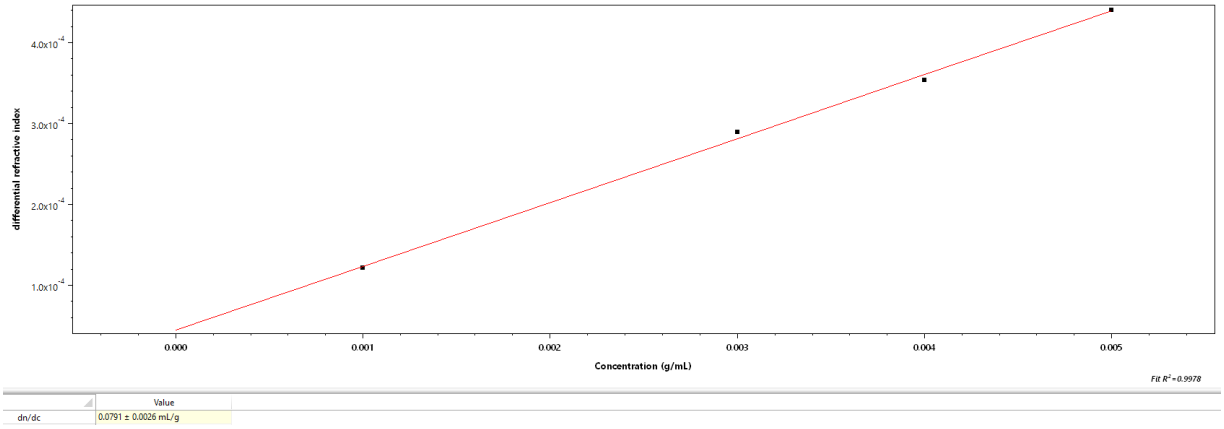

Figure D10. dRI vs concentration plot used to measure exact d*n*/d*c* value for linear high MW P^{n}BA-*b*-PMMA (run 2), with calculated d*n*/d*c* = 0.0791 mL/g.

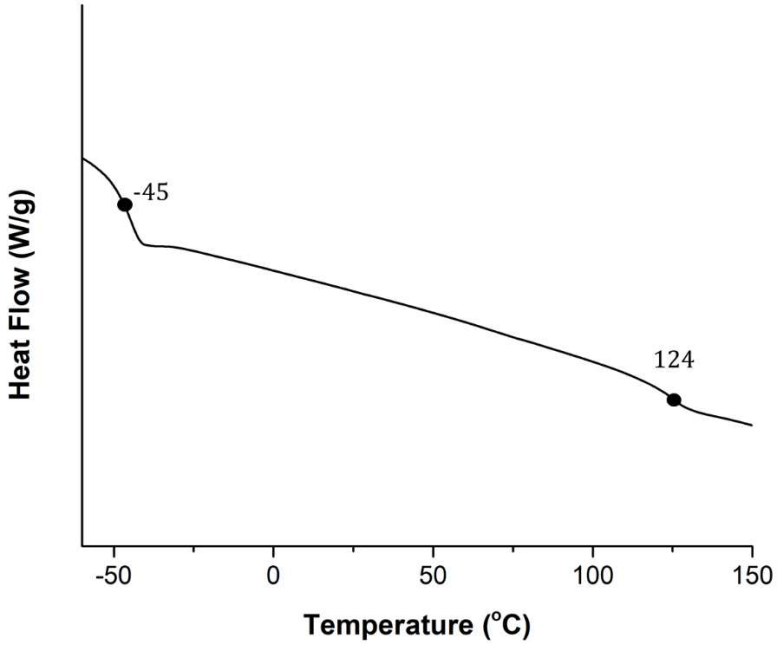

Figure D11. DSC trace (second heating scan) of linear high MW P^{n}BA-*b*-PMMA (Table D1, run 2) showing two T_g's at –45 and 124 °C.

Synthesis and characterization of medium molecular weight cyclic diblock P^{n}BA-*b*-PMMA (Table D1, run 3)

In a 25 mL vial, 0.0214 g of MAD was weighted out precisely. Then 1.00 mL of MMA and 1.00 mL of ^{n}BA and 12 mL of toluene were added to MAD to make a brilliant yellow solution. A magnetic stir bar was added. Then 0.0239 g of **1** (combined mass of ES, MAD, and I^{t}Bu 1/1/1 molar ratio) was injected into the solution, as 0.10 mL of a 0.30 M stock solution in dichloromethane, with vigorous stirring to make the overall compositional ratio [^{n}BA]/[MMA]/[MAD]/[**1**] = [300]/[233]/[2]/[1]. The yellow color of the reaction dimmed after 1 to 2 seconds signaling the consumption of ^{n}BA. Then, 1-2 min later, the reaction went clear signaling full consumption of MMA. Unlike the linear analogue (Table D1, run 1), a slight yellow tint remained in the reaction even after full conversion. The reaction was allowed to stir for 3 h following complete conversion to ensure complete cyclization. An aliquot was taken for conversion calculation by ^{1}H NMR analysis, showing no monomer for quantitative conversion for

both monomers. The quenching and workup procedures are the same as those already described for the linear di-BCP.

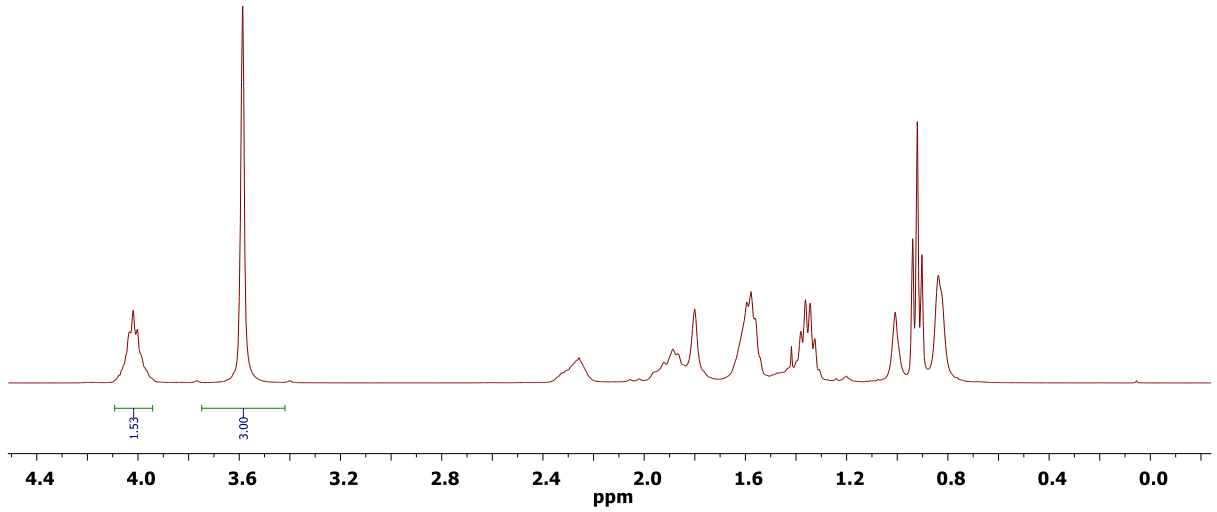

Figure D12. ^{1}H NMR ($CDCl_3$) of cyclic P^{n}BA-*b*-PMMA (Table D1, run 3) with a theoretical comonomer incorporation MMA/^{n}BA = 300/233, which should correspond to MMA/^{n}BA integration ratio of 3.00/1.48 for MMA alkoxy methyl at 3.59 ppm and ^{n}BA alkoxy methylene at 4.02 ppm, respectively.

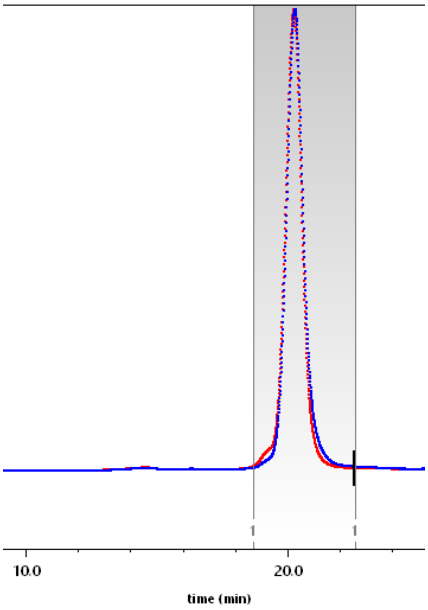

Figure D13. GPC trace (red, LS; blue dRI) of cyclic P^{n}BA-*b*-PMMA (Table D1, run 3). Shaded region indicates data included in MW calculation. d*n*/d*c* = 0.0643 mL/g; M_n = 82.6 kg/mol; $Đ$ = 1.04.

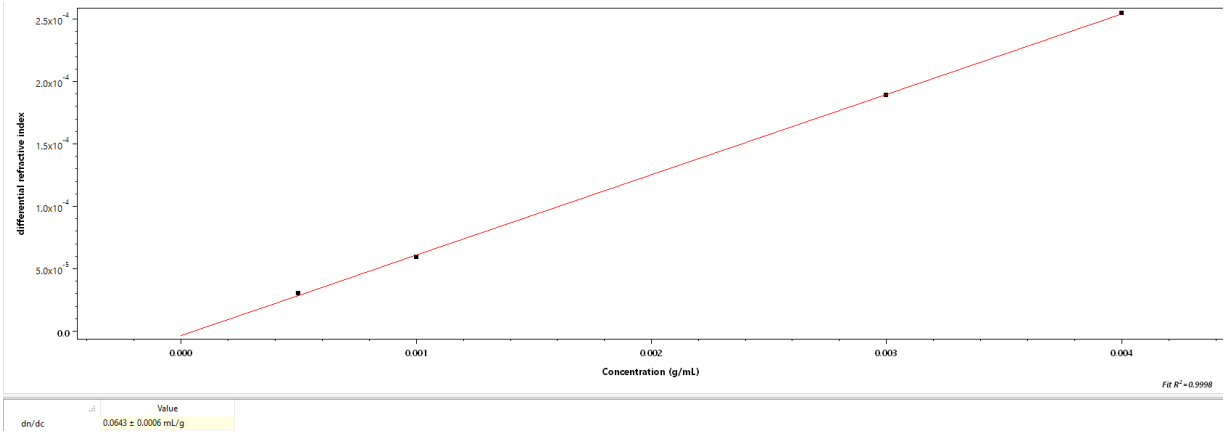

Figure D14. dRI vs concentration plot used to measure exact dn/dc value for cyclic P^{n}BA-*b*-PMMA (Table D1, run 3), with calculated dn/dc = 0.0643 mL/g.

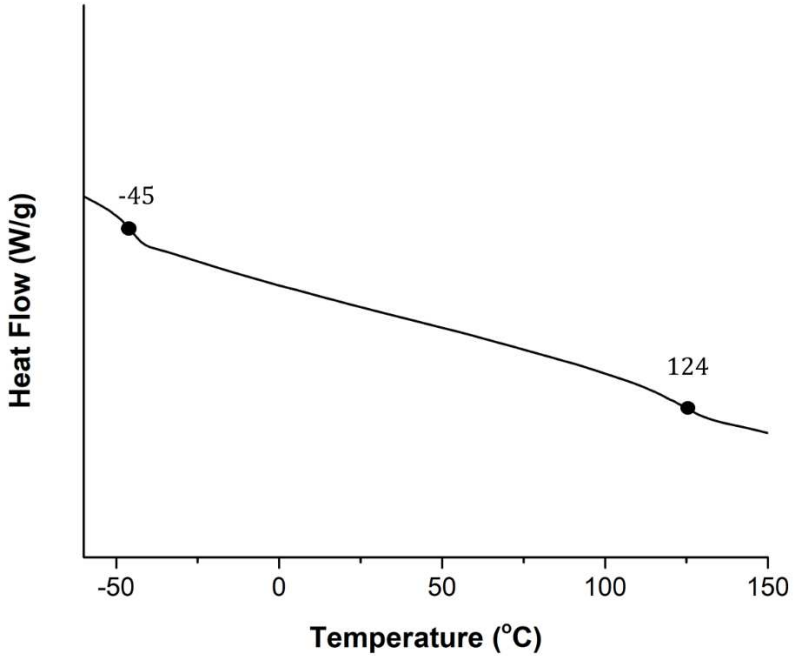

Figure D15. DSC trace (2nd heating scan) of cyclic P^{n}BA-*b*-PMMA (Table D1, run 3) showing two T_g's at –45 and 124 °C.

Synthesis and characterization of high molecular weight cyclic diblock P^{n}BA-*b*-PMMA (Table D1, run 4)

In a 25 mL vial, 0.0277 g of MAD was weighted out precisely. Then 0.49 mL of MMA and 1.00 mL of ^{n}BA and 9 mL of toluene were added to MAD to make a brilliant yellow solution. A magnetic stir bar was added. Then 0.0046 g of **1** (combined mass of ES, MAD, and I^{t}Bu 1/1/1 molar ratio) was injected into the solution, as 0.10 mL of a 0.0579 M stock solution in dichloromethane, with vigorous stirring to make the overall compositional ratio [^{n}BA]/[MMA]/[MAD]/[**1**] = [1200]/[800]/[10]/[1]. The yellow color of the reaction dimmed after 10 to 15 seconds signaling the consumption of ^{n}BA. Then, about 20 min later, the reaction went clear signaling full consumption of MMA. The reaction was given an additional 3 h of stirring for cyclization. An aliquot was taken for conversion calculation by ^{1}H NMR analysis, showing no

monomer for quantitative conversion for both monomers. The quenching and workup procedures are the same as those already described for the linear di-BCP.

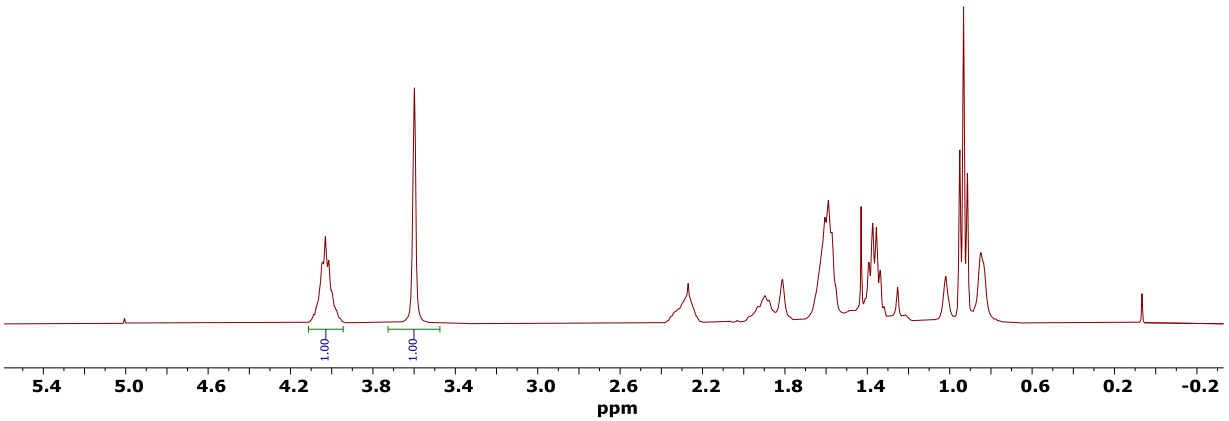

Figure D16. ^{1}H NMR ($CDCl_3$) of cyclic P^{n}BA-*b*-PMMA (Table D1, run 4) with a theoretical comonomer incorporation MMA/^{n}BA = 800/1200, which should correspond to MMA/^{n}BA integration ratio of 1/1 for MMA alkoxy methyl at 3.59 ppm and ^{n}BA alkoxy methylene at 4.02 ppm, respectively.

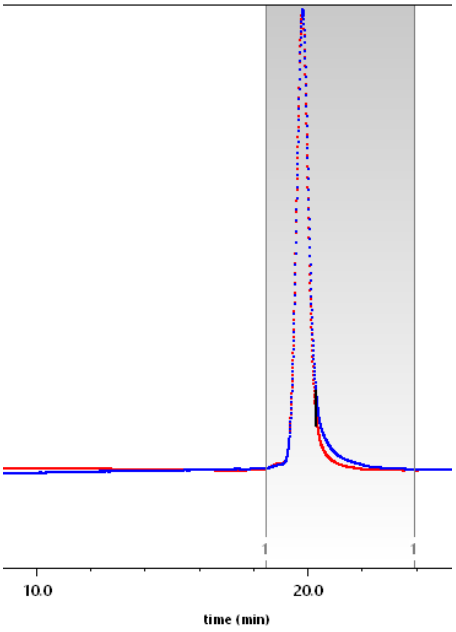

Figure D17. GPC trace (red, LS; blue dRI) of cyclic P^{n}BA-*b*-PMMA (Table D1, run 4). Shaded region indicates data included in MW calculation. d*n*/d*c* = 0.0670 mL/g; M_n = 247 kg/mol; $Đ$ = 1.04.

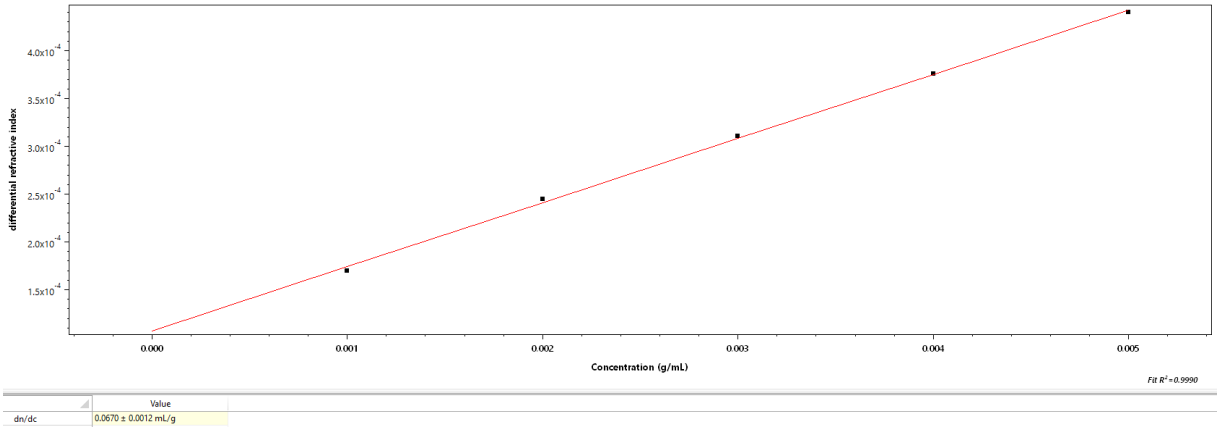

Figure D18. dRI vs concentration plot used to measure exact dn/dc value for cyclic high MW P^{n}BA-*b*-PMMA (Table D1, run 4), with calculated d*n*/d*c* = 0.0670 mL/g.

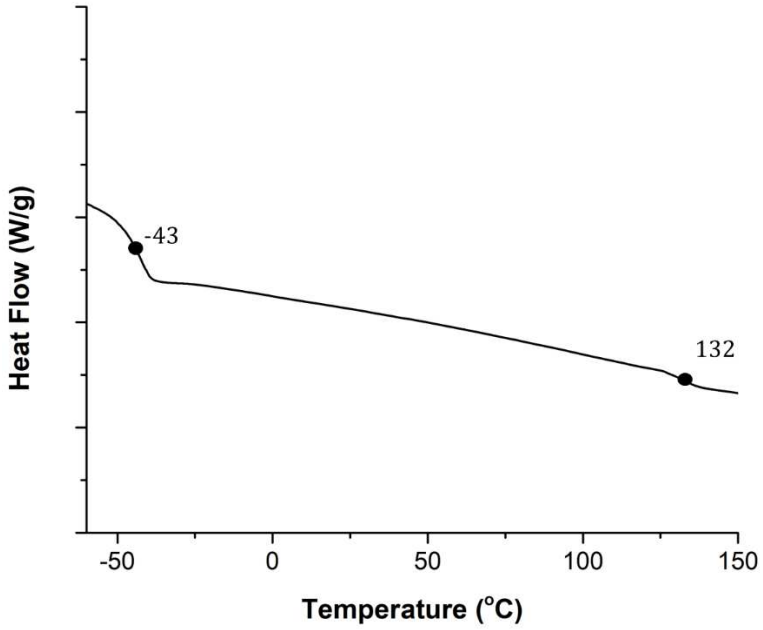

Figure D19. DSC trace (2nd heating scan) of cyclic high MW P*n*BA-*b*-PMMA (Table D1, run 4) showing two T_g's at –43 and 132 °C.

Comparative GPC studies on medium MW linear and cyclic P^{n}BA-*b*-PMMA (Table D1, runs 1 and 3)

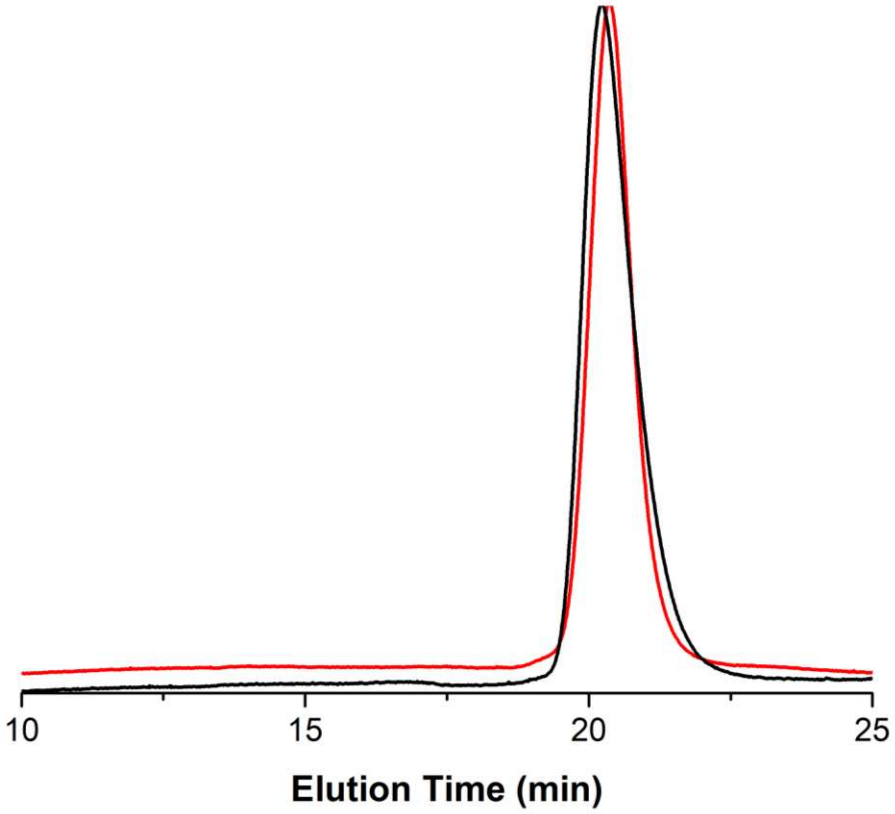

Figure D20. Overlaid GPC traces of medium MW linear and cyclic P^{n}BA-*b*-PMMA (Table D1, run 1, linear, black; and Table D1, run 3, cyclic, red).

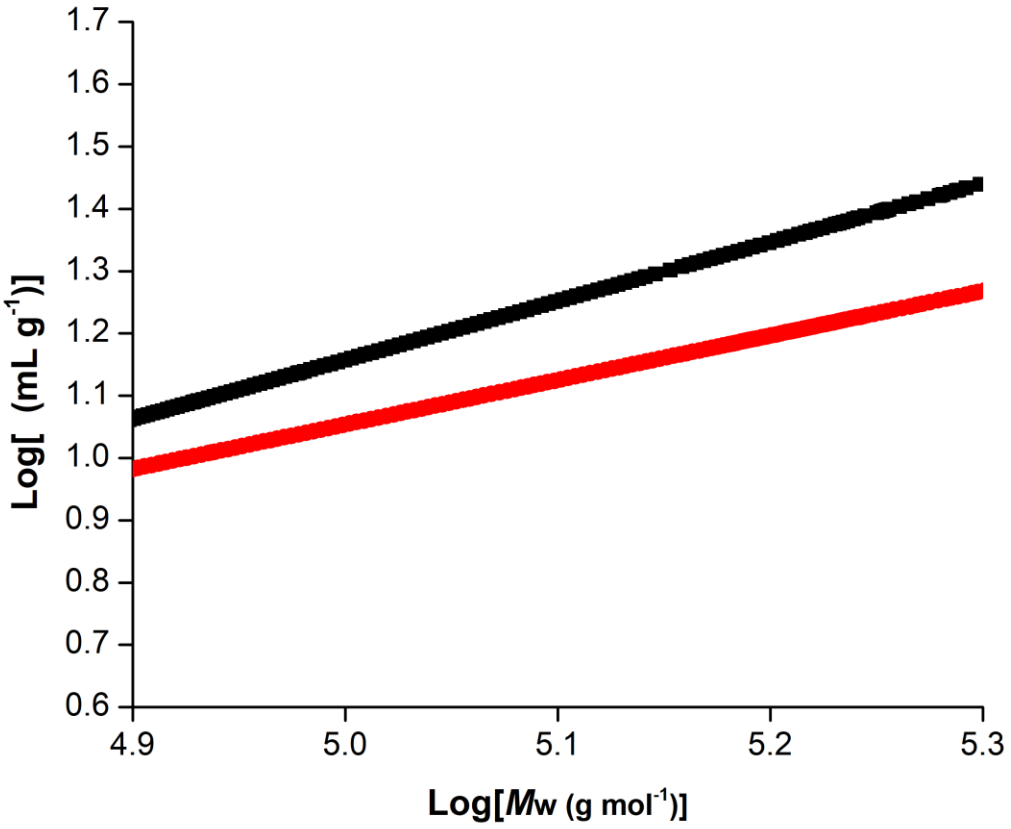

Figure D21. GPC-viscometry plots of viscosity vs weight-average MW (M_w) for medium MW linear and cyclic P^{n}BA-*b*-PMMA (Table D1, run 1, linear, black; and Table D1, run 3, cyclic, red), with the linear analogue showing a higher viscosity over a broad range of MWs.

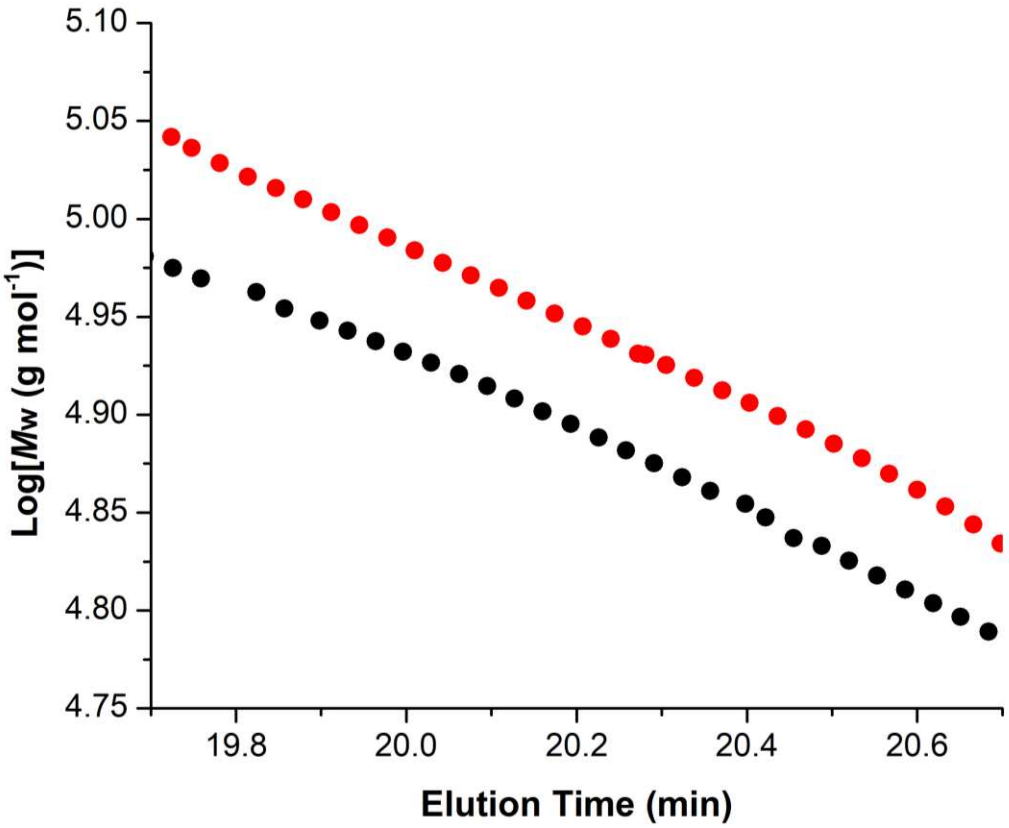

Figure D22. GPC MW vs elution time plots for medium MW linear and cyclic P^{n}BA-*b*-PMMA (Table D1, run 1, linear, black; and Table D1, run 3, cyclic, red), with higher MW cyclic polymer eluting at the same time as lower MW linear polymer, indicating that lower hydrodynamic radii of cyclic polymers.

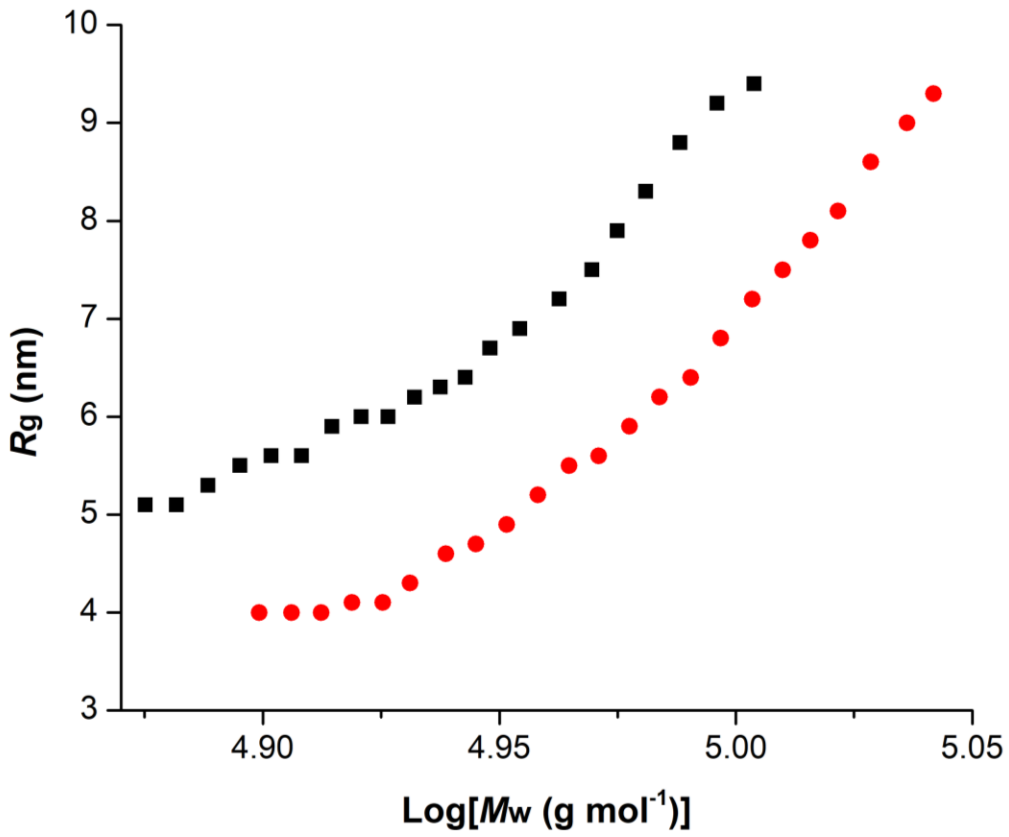

Figure D23. GPC radius of gyration (R_g, determined by 3-angle light scattering) vs MW plots for medium MW linear and cyclic P^{n}BA-*b*-PMMA (Table D1, run 1, linear, black; and Table D1, run 3, cyclic, red), with linear polymers exhibiting higher R_g compared to cyclic polymers of similar MW.

Comparative GPC studies on high MW linear and cyclic PnBA-b-PMMA (Table D1, runs 2 and 4)

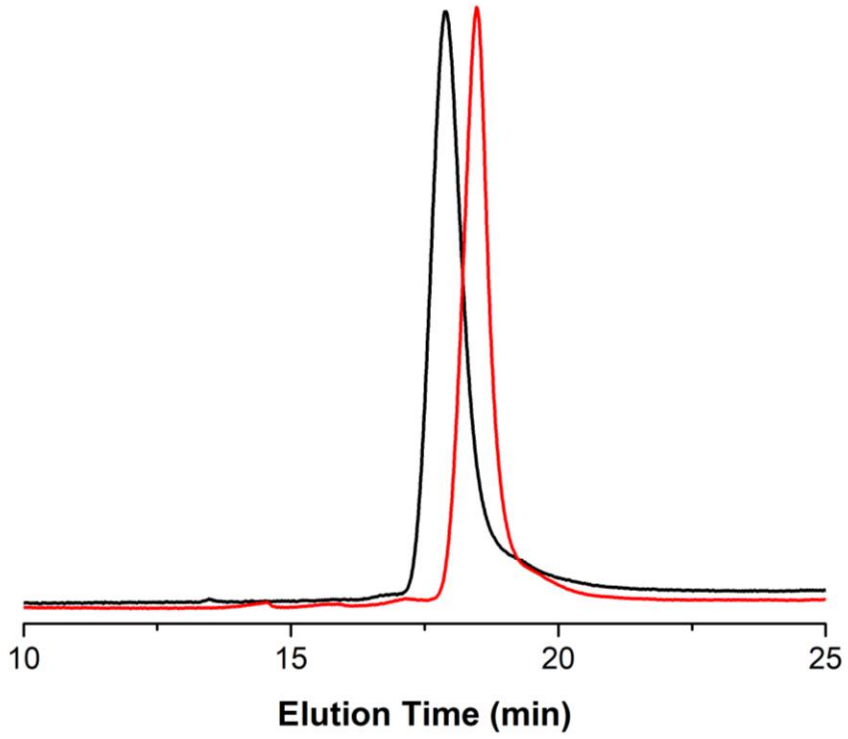

Figure D24. Overlaid GPC traces of high MW linear and cyclic P^{n}BA-*b*-PMMA (Table D1, run 2, linear, black; and Table D1, run 4, cyclic, red).

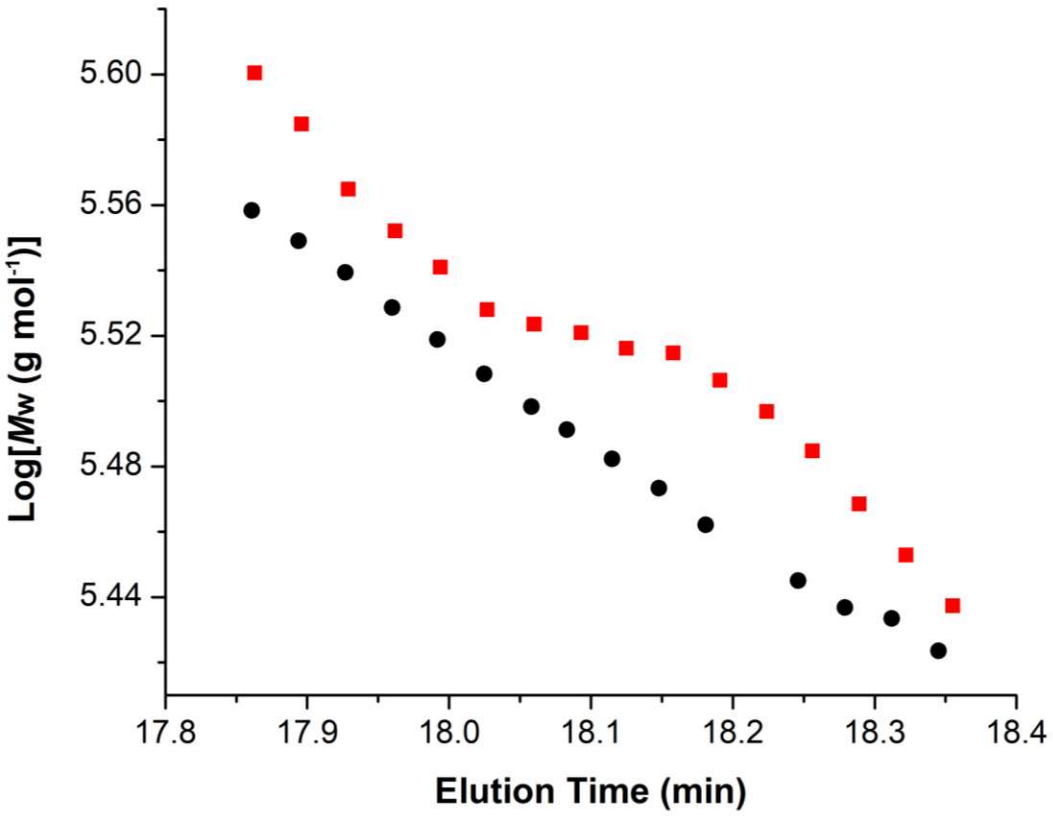

Figure D25. GPC MW vs elution time plots for high MW linear and cyclic P^{n}BA-*b*-PMMA (Table D1, run 2, linear, black; and Table D1, run 4, cyclic, red), with higher MW cyclic polymer eluting at the same time as lower MW linear polymer, suggesting that lower hydrodynamic radii of cyclic polymers.

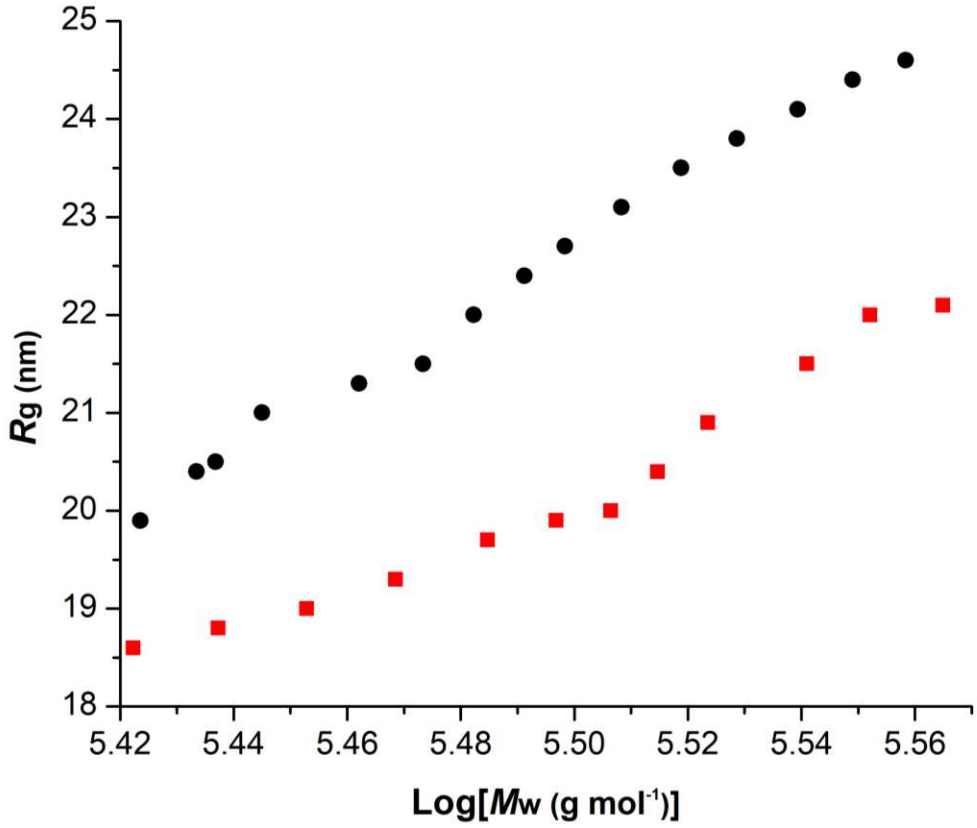

Figure D26. GPC radius of gyration (R_g, determined by 3-angle light scattering) vs MW plots for high MW linear and cyclic P^{n}BA-*b*-PMMA (Table D1, run 2, linear, black; and Table D1, run 4, cyclic, red), with linear polymers exhibiting higher R_g compared to cyclic polymers of similar MW.

Rheological viscosity comparison of linear and cyclic P^{n}BA-*b*-PMMA

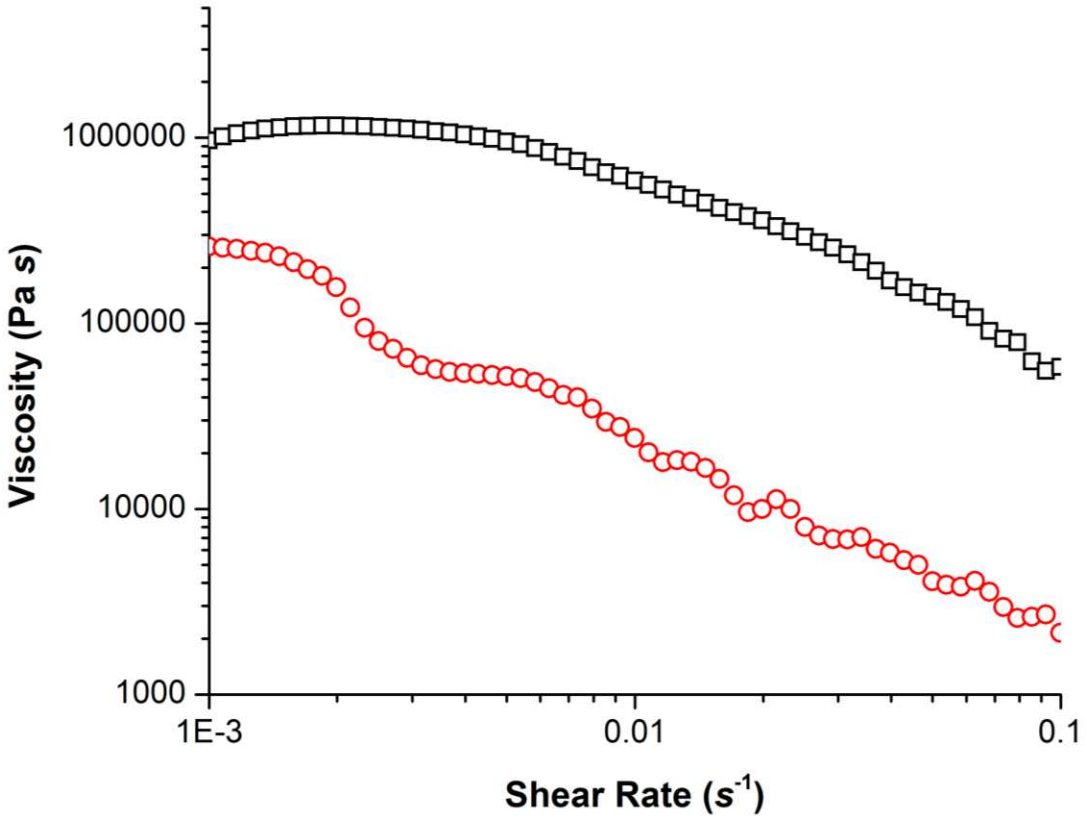

Figure D27. Rheological viscosity comparison of linear (Table D1, run 2, black) and cyclic (Table D1, run 4, red) high MW P^{n}BA-*b*-PMMA.

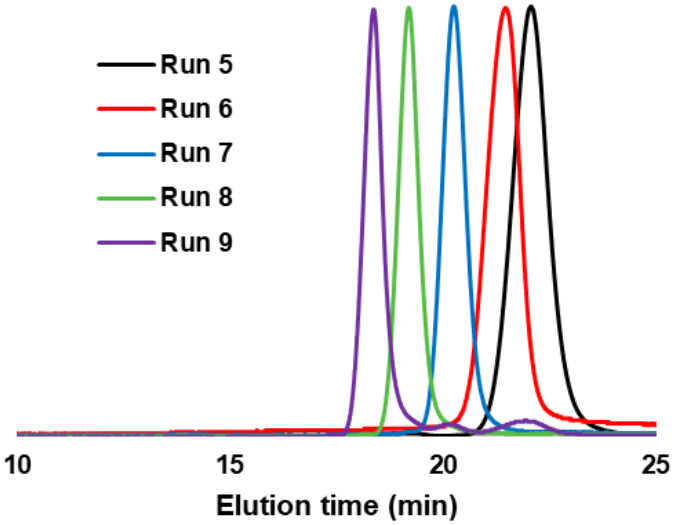

Figure D28. GPC trace overlay of *c*BCPs reported in Table D2.

Synthesis and characterization of cyclic and linear P^{n}BA-*b*-PAMA [poly(allyl methacrylate)]

In a 25 mL vial, 1.00 mL of ^{n}BA, 0.93 mL of AMA, and 0.0222 g of MAD were mixed with 12 mL of toluene. A stir bar was added. Then, with vigorous stirring, 0.0185 g of **1** was added as 0.30 mL of a 0.077 M stock solution to make a ^{n}BA/AMA/MAD/I^{t}Bu molar ratio of 300/300/2/1. The reaction was given 3 h to react before quenching with MeOH spiked with 100 ppm of benzoic acid. An aliquot was removed and analyzed by ^{1}H NMR, observing no monomer peaks left.

The same procedure was used to synthesize the linear counterpart, except that 0.0065 g of PCy_3 was used, instead of **1**, and the reaction was quenched after 5 min instead of 3 h.

Solvents were removed by rotary evaporation. Then, 5-10 mL of methanol was added. PAMA/P^{n}BA copolymers in general did not suddenly crash from methanol but rather swelled up as a gel. About half the solvent volume was removed by rotary evaporation, which caused the polymers to stick to the walls of the vial, at which point the remaining methanol was decanted. Further purification can be achieved by repeated dissolution in chloroform then precipitation in cold methanol assisted by centrifuge. Polymer products were dried in a vacuum oven at 100 ^{o}C for at least 6 h.

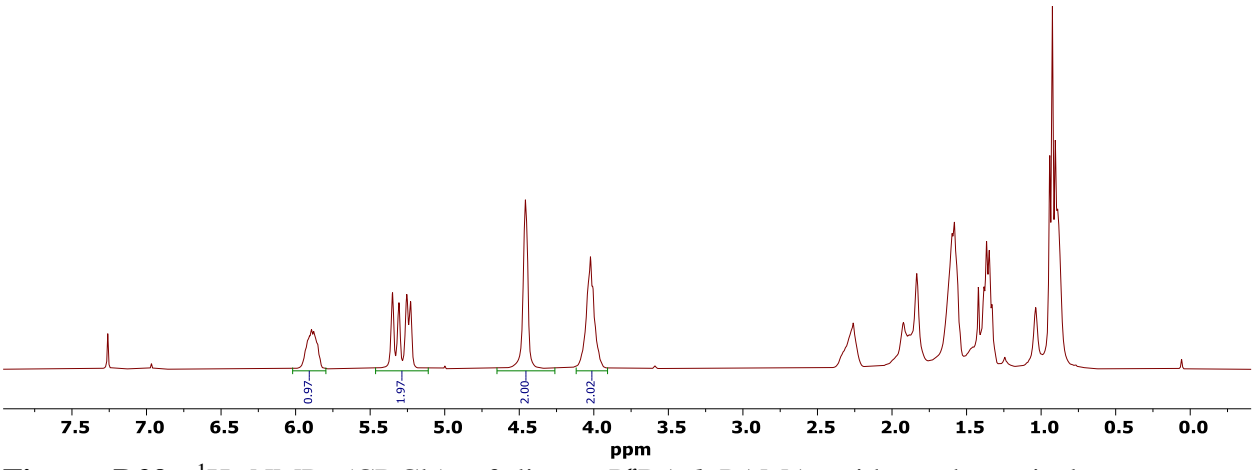

Figure D29. ^{1}H NMR ($CDCl_3$) of linear P^{n}BA-*b*-PAMA with a theoretical comonomer incorporation AMA/^{n}BA = 300/300, which should correspond to AMA/^{n}BA integration ratio of 2/2 for AMA alkoxy methylene at 4.46 ppm and ^{n}BA alkoxy methylene at 4.02 ppm.

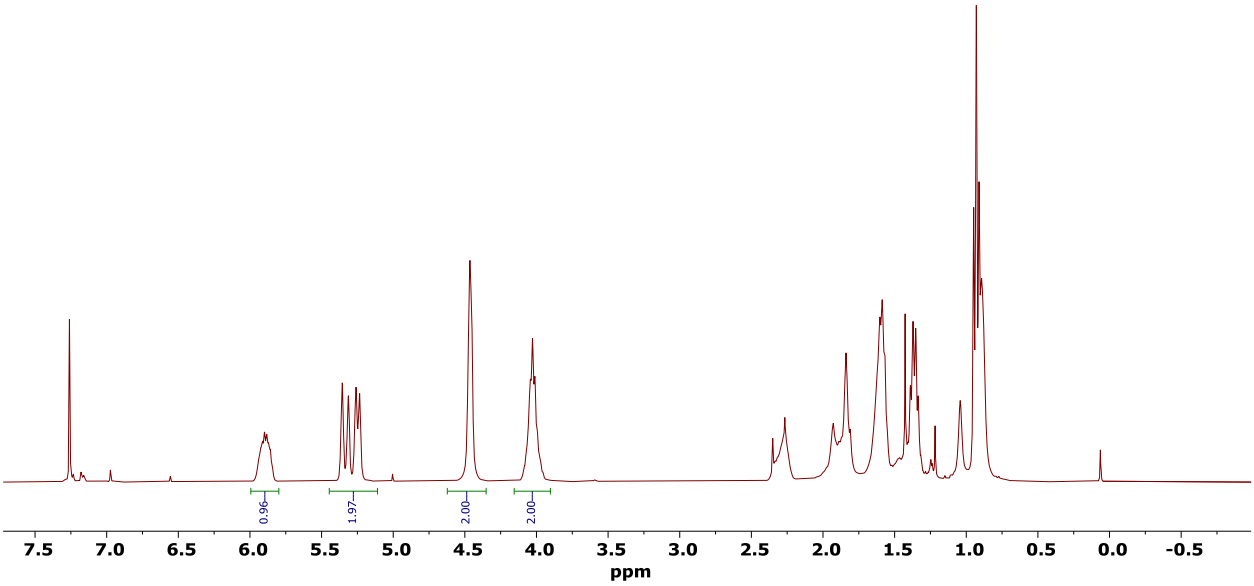

Figure D30. ^{1}H NMR ($CDCl_3$) of cyclic P^{n}BA-*b*-PAMA with a theoretical comonomer incorporation AMA/^{n}BA = 300/300, which should correspond to MMA/^{n}BA integration ratio of 2/2 for AMA alkoxy methylene at 4.46 ppm and ^{n}BA alkoxy methylene at 4.02 ppm.

Post functionalization of P^{n}BA-*b*-PAMA to P^{n}BA-*b*-PAMA$_g$ [poly(allyl methacrylate-*graft*-octadecanethiol)]

In an argon filled glovebox, a glass 500 mL high-pressure reactor was charged with 0.502 g of P^{n}BA-*b*-PAMA, 5.69 g of octadecane thiol, 0.23 g of DMPA (2,2-dimethoxy-2-phenylacetophenone), a stir bar, and 75 mL of anhydrous toluene. The reactor was sealed and put inside a photoreactor equipped with a stir plate. The reaction was irradiated with UV wavelengths for 3 h. The crude reaction mixture was precipitated with ethyl acetate and filtered. The solid product was washed three times with 50 mL tetrahydrofuran. It was then dried in a vacuum oven at 100 ^{o}C for 3 h until a constant mass was achieved.

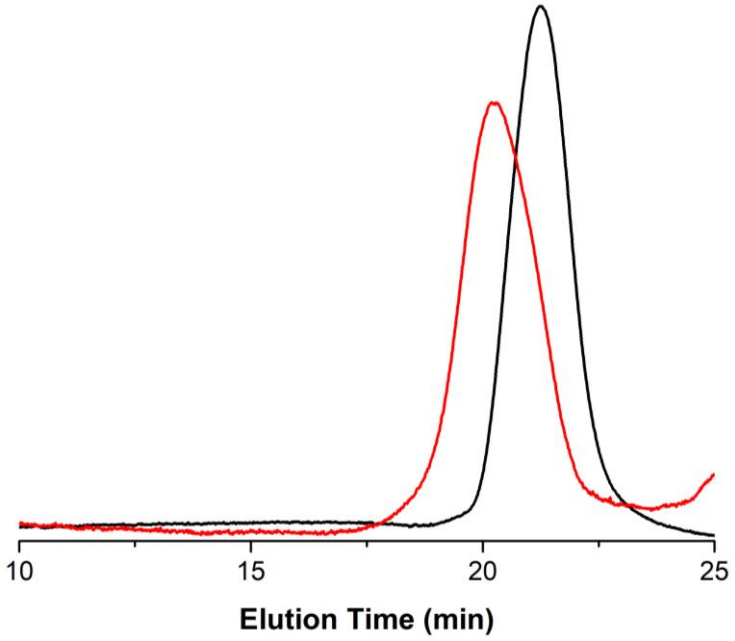

Figure D31. Overlayed GPC trace of linear P^{n}BA-*b*-PAMA (black) and P^{n}BA-*b*-PAMA$_{g}$ (red) before and after grafting.

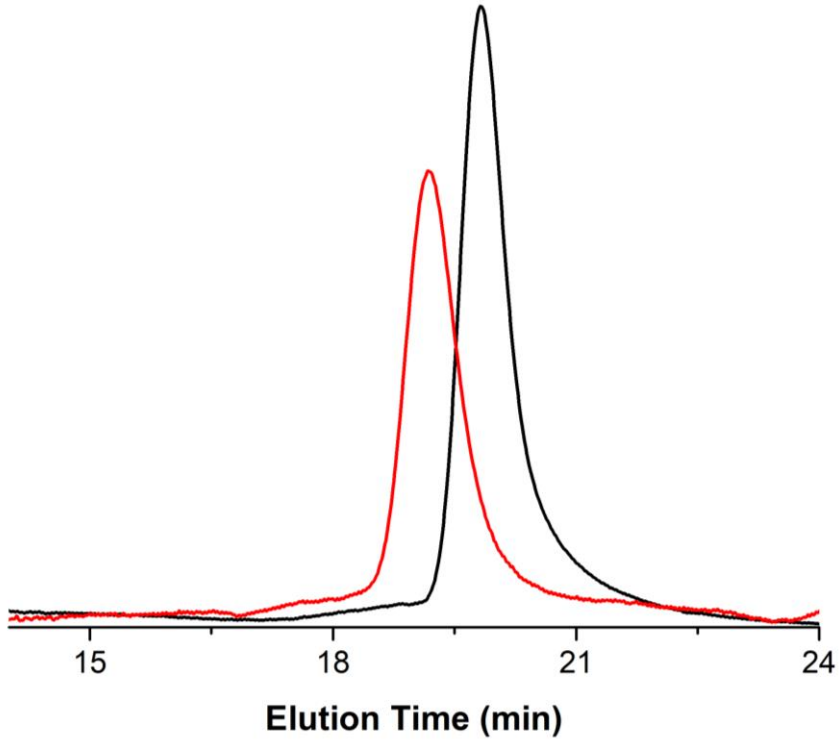

Figure D32. Overlayed GPC trace of cyclic P^{n}BA-*b*-PAMA (black) and P^{n}BA-*b*-PAMA$_{g}$ (red) before and after grafting.

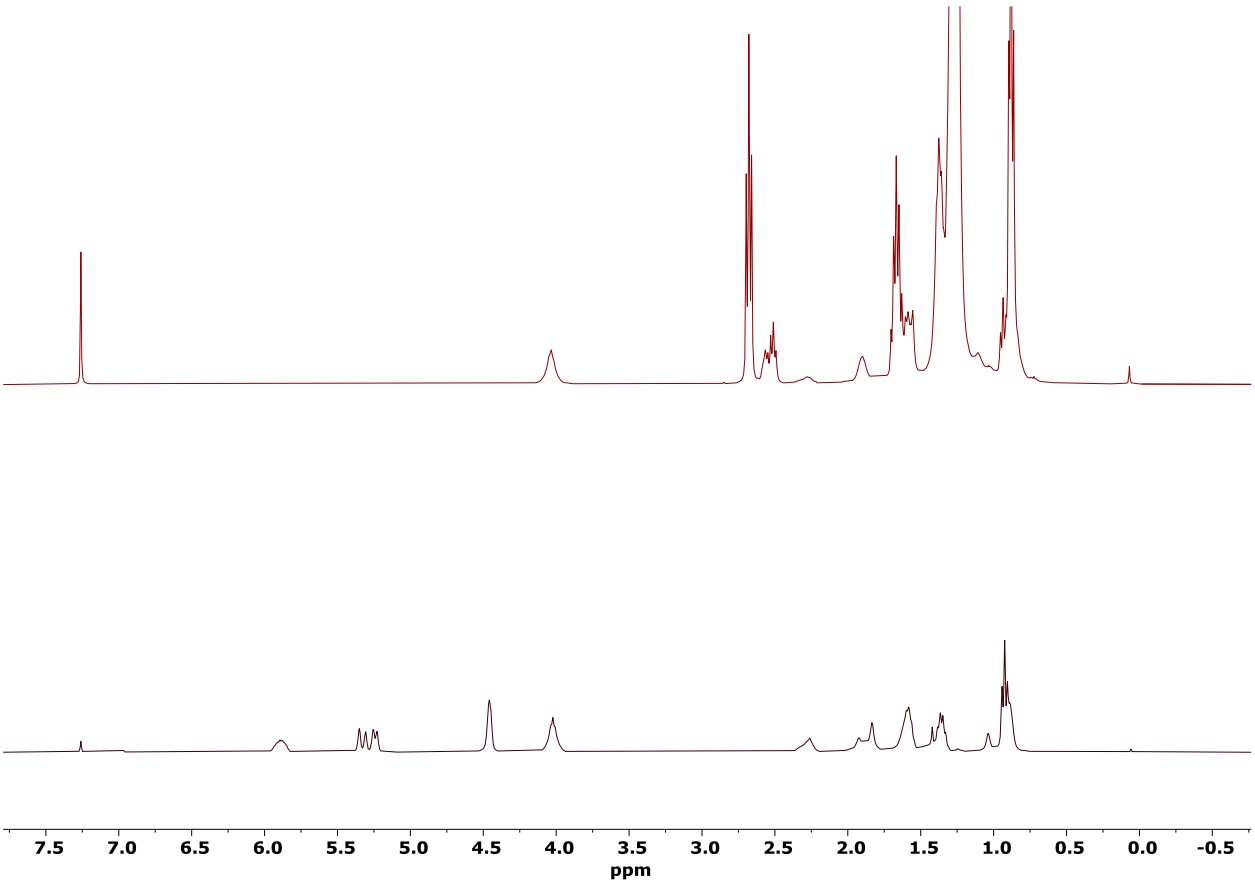

Figure D33. ^{1}H NMR ($CDCl_3$) overlay of linear P^{n}BA-*b*-PAMA (bottom) and P^{n}BA-*b*-PAMA$_g$ (top) showing complete disappearance of allyl peaks following thiol-ene click reaction.

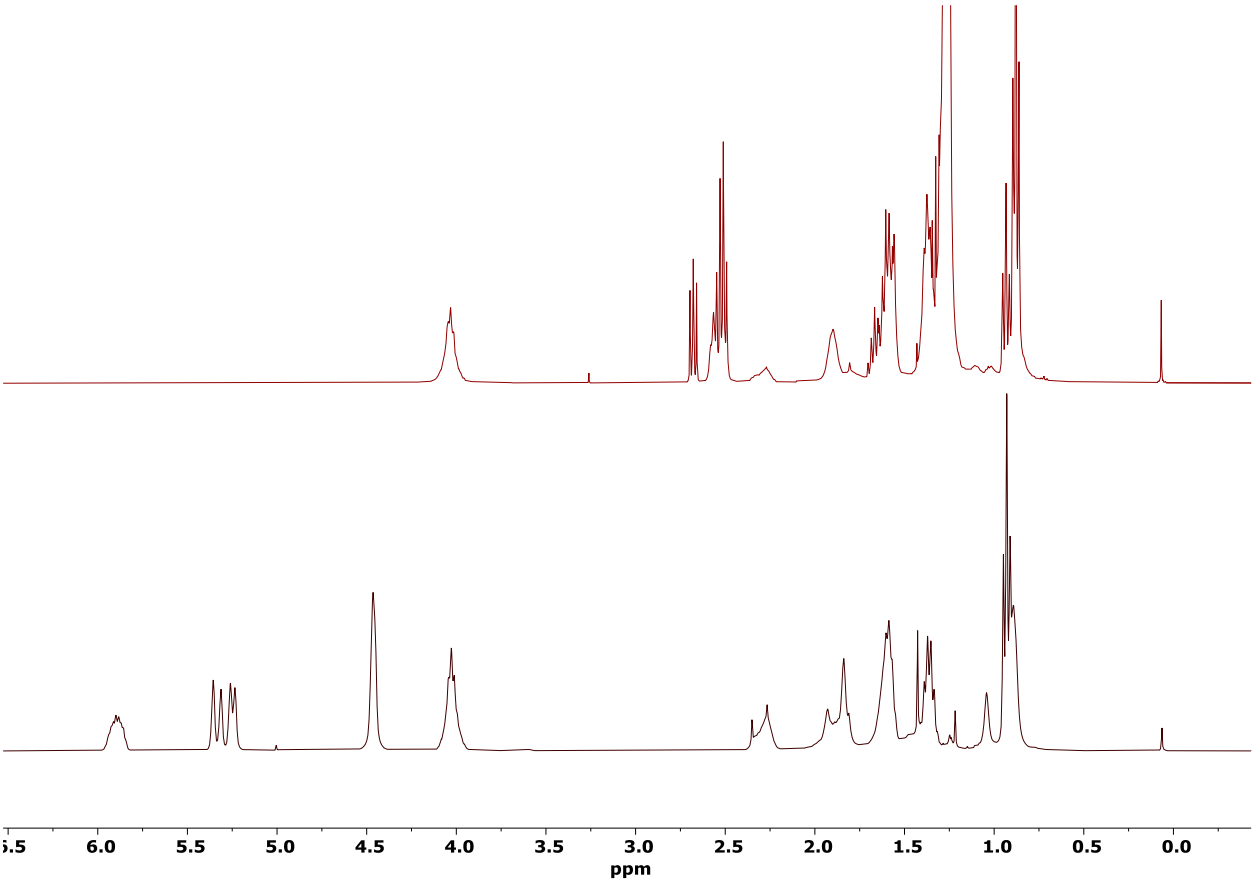

Figure D34. ^{1}H NMR overlay of cyclic P^{n}BA-*b*-PAMA (bottom) and P^{n}BA-*b*-PAMA$_{g}$ (top) showing complete disappearance of allyl peaks following thiol-ene click reaction.

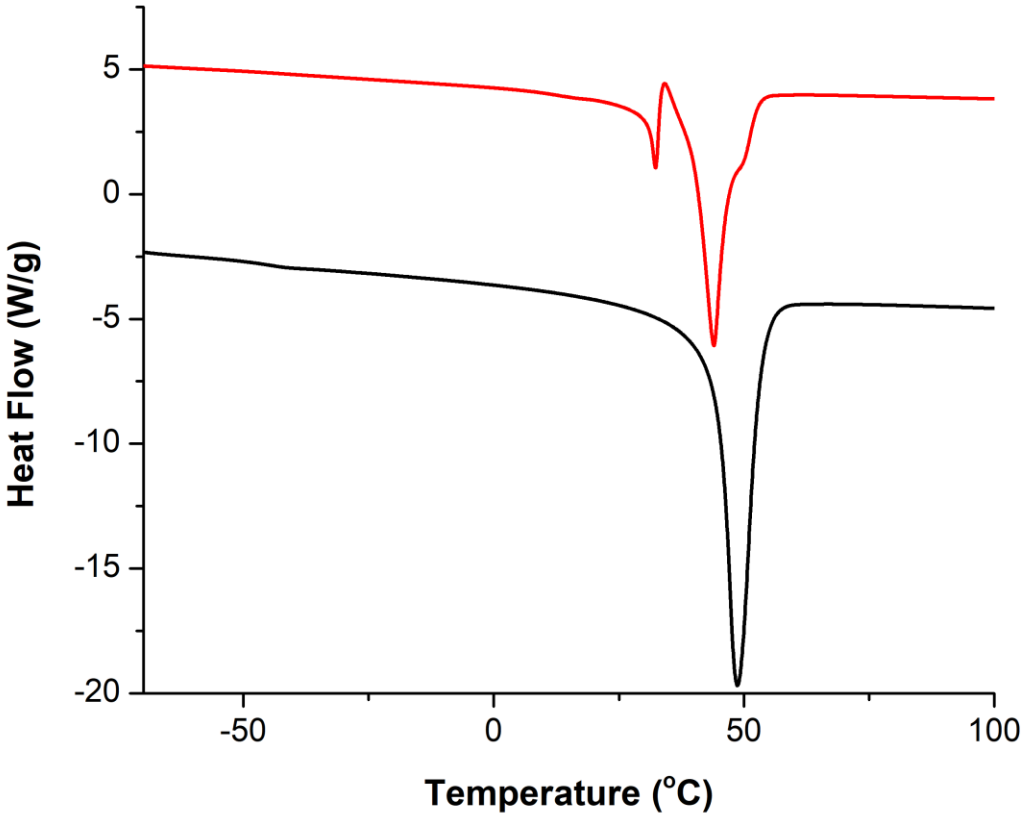

Figure D35. DSC trace (2nd heating scan) of linear (black) and cyclic (red) P^{n}BA-*b*-PAMA$_{g}$ showing melting transitions at 48.7 °C and 44.0 °C, respectively.

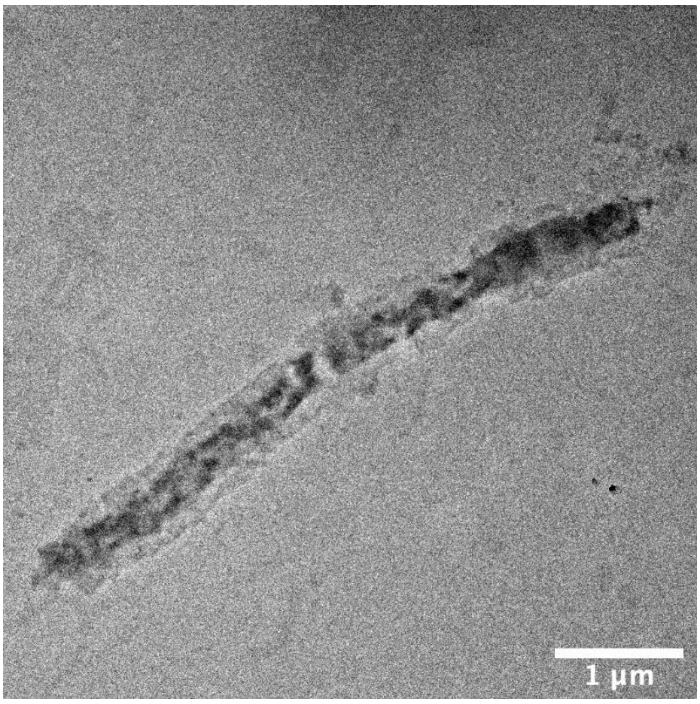

Figure D36. TEM image of linear P^{n}BA-*b*-PAMA$_{g}$ copolymer drop-casted thin film at a 1 micrometer scale highlighting contrasting crystalline worm-like structures.

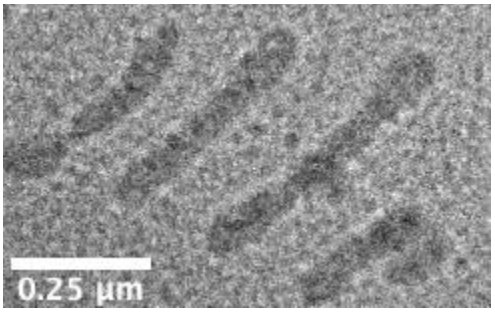

Figure D37. TEM surface image of linear P^{n}BA-*b*-PAMA$_{g}$ copolymer drop-casted thin film at a 250 nm scale highlighting contrasting crystalline worm-like structures at high resolution.

Table D1. Selected results for the synthesis of linear and cyclic di-BCPs by CSC-LPP [a]

Run #	I	^{n}BA/MMA/MAD/I	t (min)	M_n [b] (kg/mol)	$Đ$ [b]	T_g (°C)
1	PCy_3	130/168/2/1	5	73.1	1.06	-46, 122
2	PCy_3	1200/800/10/1	20	286	1.12	-45, 124
3	**1**	233/300/2/1	180	82.6	1.04	-45, 124
4	**1**	1200/800/10/1	180	247	1.04	-43, 132

[a] Conditions: ^{n}BA, MMA, and MAD were dissolved in toluene, so that M/toluene = 1 mL/6 mL (where M = ^{n}BA + MMA). Then PCy_3 or mixture **1** was added as 0.10 mL of a dichloromethane stock solution. [b] M_n and $Đ$ determined by GPC with a d*n*/d*c* method utilizing a Wyatt DAWN HELEOS II 18-angle light scattering detector and a Wyatt Optilab TrEX dRI detector.

Table D2. Demonstration of molecular weight control by tuning $[M]_0/[\mathbf{1}]_0$ ratio

Run #	^{n}BA/MMA/MAD/**1**	Conv	M_n	$Đ$
5	50/33/1/1	100	16.6	1.12
6	100/66/2/1	100	28.7	1.09
7	300/200/6/1	100	68.5	1.04
8	600/400/12/1	100	153	1.03
9	1200/800/24/1	100	267	1.03

Conditions: nBA, MMA, and MAD were all added to toluene so that nBA/MMA/MAD = [50]/[33]/[1], and [nBA]0 = 0.32 M. Initiator mixture 1 was added as appropriate volumes of a 0.10 M stock solution in dichloromethane. All reactions were given 12 h to proceed. Mn and Đ values were estimated using the dn/dc value measured from Table D1, run 4 (0.0670 mL/g in THF).

References cited in Appendix D

[1]. Shreve, A. P.; Mulhaupt, R.; Fultz, W.; Calabrese, J.; Robbins, W.; Ittel, S. Sterically Hindered Aryloxide-Substituted Alkylaluminum Compounds. *Organometallics* **1988**, *7*, 409–416.

[2]. Oga, Y.; Hosoi, Y.; Takasu, A. Synthesis of cyclic Poly(methyl methacrylate) via N-Heterocyclic carbene (NHC) initiated-anionic polymerization and subsequent ring-closing without need of highly dilute conditions. *Polymer* **2020**, *186*, 122019.

Appendix E
Supplementary Information Corresponding to Chapter 6

Taken from:

Towards Spatial and Temporal Control in Precision Cyclic Polymer Synthesis by Lewis Pair Polymerization

Michael L. McGraw, Liam T. Reilly, Ryan W. Clarke, Luigi Cavallo, Laura Falivene, and Eugene Y.-X. Chen

*Under review for publication during the time of writing this dissertation

Materials

Methyl Methacrylate (MMA), allyl methacrylate (AMA), methyl sorbate (MS), ethyl sorbate (ES), and methyl crotonate (MC) were purchased from TCI and dried over calcium hydride for several hours before vacuum distillation on a Schlenk line under N_2. The distillates were immediately transferred under vacuum into an argon atmosphere glovebox and filtered into to amber bottles using a 0.2 μm nylon syringe filter. *N*-heterocyclic carbene (NHC) 1,3-di-tert-butylimidazolin-2-ylidene (I^{t}Bu) was purchased from TCI and used without further purification. Tricyclohexyl phosphine (PCy_3) was purchased from Alfa Aesar and used as received. NHC 1,3,4-triphenyl-4,5-dihydro-1H-1,2,4-tiazol-5-ylidene (TPT) was synthesized by known literature methods.[1] Toluene was dried over Na/K alloy and filtered through a 0.2 μm nylon syringe filter just prior to use. Methyl aluminum di(2,6-di-tert-butyl-4-methylphenoxy) (MAD) was synthesized by known literature methods. All aforementioned materials, with the exception of solvents and PCy_3, were stored in the dark at –30 °C.

Analytical Methods

NMR Spectroscopy

Monomer conversion as well as structure characterizations of mechanistic intermediates were carried out by ^{1}H NMR experiments using a Bruker Advance NEO 400 MHz (FT 400 MHz, ^{1}H) or a or Bruker AVIII 400 MHz spectrometer (400 MHz, ^{1}H). Chemical shifts were referenced to internal solvent resonances corresponding to 7.26 ppm (chloroform) and 7.16 ppm (benzene) and reported as parts per million relative to $SiMe_4$.

Time of Flight Mass Spectrometry (TOF-MS)

Measurements of mass spectrums were collected using an Agilent 6230 TOF LC/MS "BTOF". A solution of **1** was prepared in toluene and directly injected into the detector system, without preliminary column separation, with acetonitrile as the mobile phase and in the absence of any external ionization agent. Owing to the nature of the intended analysis of the ion pair, the sample was analyzed in both positive and negative modes.

Matrix Assisted Laser Desorption Ionization Time of Flight Mass Spectrometry (MALDI-TOF)

MALDI−TOF MS was used to analyze low molecular weight samples, using an Ultraflex MALDI-TOF mass spectrometer (Bruker Daltonics) operated in positive ion, reflector mode using a Nd:YAG laser at 355 nm and 25 kV accelerating voltage. A thin layer of a 1% NaI solution was first deposited on the target plate, followed by 0.6 μL of both PMC (2 mg/ml in $CHCl_3$) and matrix (dithranol, 20 mg/mL in $CHCl_3$). External calibration was done using a peptide calibration mixture (8 peptides) on a spot adjacent to the sample. The raw data was processed in the FlexAnalysis software (version 2.4, Bruker Daltonics), and the Figures were plotted using mMass software.

Gel Permeation Chromatography (GPC).

Measurements of polymer absolute weight-average molecular weight (M_w), number-average molecular weight (M_n), and molecular weight distributions ($Đ = M_w/M_n$) were performed by GPC.

The GPC instrument consisted of an Agilent HPLC system equipped with one guard column and three PL-gel 5 µm mixed-C gel permeation columns running THF as eluent at 1.0 mL/min at 40 °C. The detectors used were a Wyatt Technology TrEX differential refractometer (dRI) and a Wyatt Technology miniDAWN Treos light scattering detector (MALS). The d*n*/d*c* value used for *c*PMMA was 0.0840 mL/g. The *c*PAMA sample used the "assume 100 % mass recovery option" which calculates an approximate d*n*/d*c* internally based on a precisely known polymer concentration of the sample prior to injection, which was 2.50 mg/mL. The approximated d*n*/d*c* according to this measurement was 0.0848 mL/g (note that this value is prone to error and should not be used as a reference d*n*/d*c* for future GPC measurements of PAMA).

Thermal Analysis.

Differential Scanning Calorimetry (DSC) was performed on thoroughly dried polymer samples on an Auto Q20, TA Instrument. DSC Plots represent the data obtained from a second heating scan after the thermal history was removed on the first heating scan. The second heating scan was performed at a heating rate of 20 °C/min following a cooling scan at a rate of 10 °C/min.

Microscopy and Surface Imaging

Transmission Electron Microscopy (TEM)

A thin film of cyclic PAMAg synthesized by the MC initiator (see below) was prepared by drop-casting five drops from a 0.1-0.01 mg/mL polymer solution in toluene onto DI water in a 20 mL scintillation vial. The sample was left uncapped in a closed fume-hood overnight, yielding a semi-visible but suitable specimen. A 200 copper mesh TEM grid was used to retrieve and capture the sample by lifting it out of the water from below. The grid was left to dry in a desiccator for 1 h

before placing it on the microscope. The transmission electron microscope imaging was done at 200 kV using a JEOL 2100F transmission electron microscope. The incident beam illuminating conditions were adjusted for minimum beam current and therefore to minimize radiation damage to the samples. An objective aperture was used to maximize contrast in bright field conditions (but also reduced beam damage). Exposure time for all images was 0.5 seconds, again to minimize the effect of beam damage. The images are representative of the entire sample as they are from a number of different grid openings. All images were fitted with a scale bar using the publicly available microscopy program ImageJ (NIH).

Experimental Details

All syntheses and storage of air-sensitive materials were handled in an Argon filled glovebox or in a flame dried dual manifold Schlenk line.

Preparation of Ion Pair Cyclic Polymer Initiators

A range of β-substituted acrylate ion pairs were generally prepared through the stoichiometric combination of each unique β-substituted acrylate (ES, MS, MC), MAD, and I^{t}Bu (1:1:1, respectively). A general preparation required 0.3 M stock solutions of each component. The β-substituted acrylate stock was first combined with an equivalent amount of the MAD stock and mixed thoroughly. The resulting solution (yellow in color, varying in intensity depending on the solvent used and the identity of the β-substituted acrylate), was added drop wise into the I^{t}Bu stock solution while stirring.

As an example, 1 mL of 0.3 M ethyl sorbate stock solution was combined with 1 mL of 0.3 M MAD stock solution. The resulting 2 mL solution of MAD activated ethyl sorbate (0.15 M) was added dropwise to 1 mL of the 0.3 M I^{t}Bu stock solution – resulting in a 3 mL of 0.1 M ethyl sorbate ion pair stock solution.

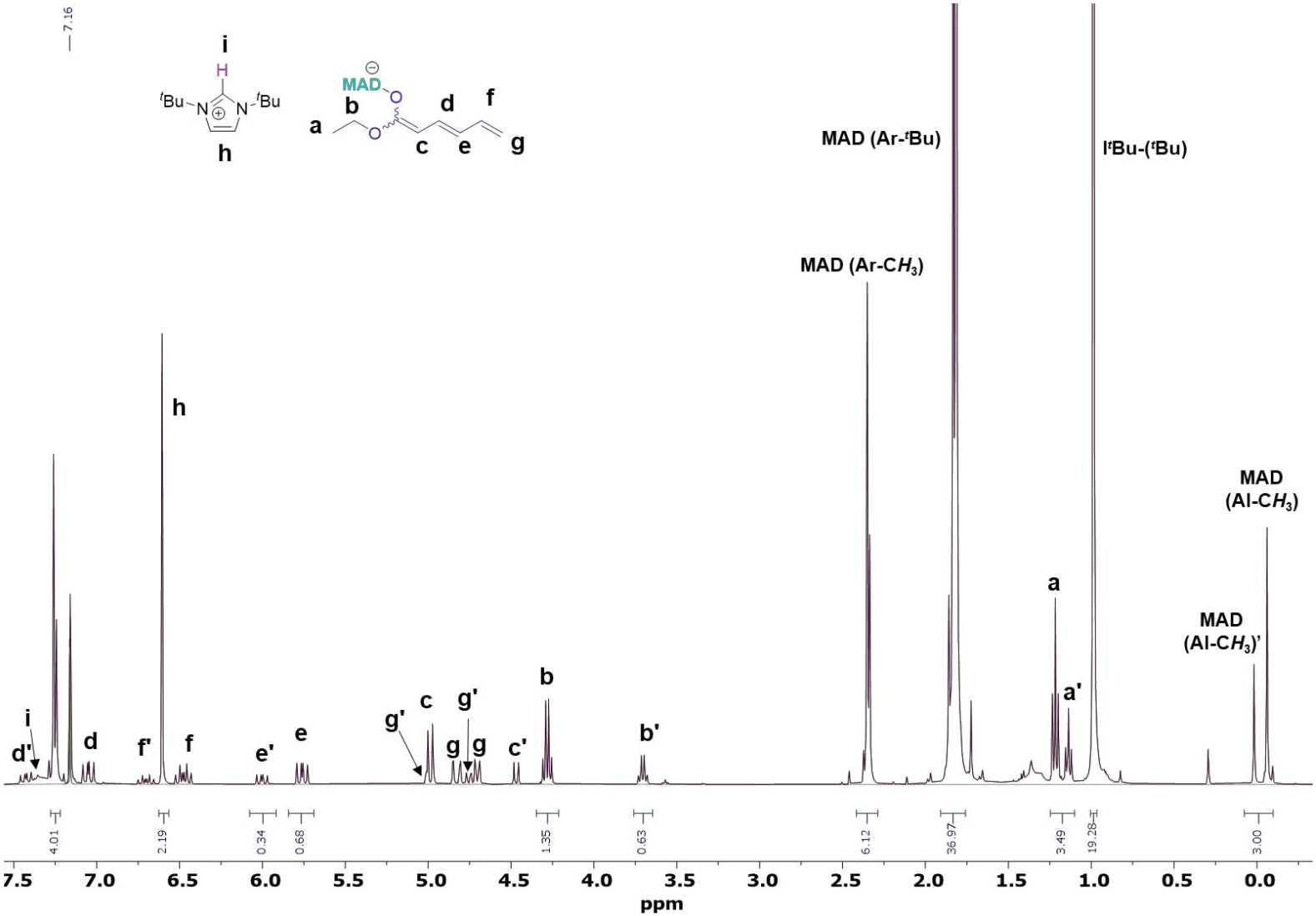

Figure E1. Assigned ^{1}H NMR (C_6D_6) of ethyl sorbate ion pair (**1**) synthesized using deuterated benzene (C_6D_6) stock solutions.

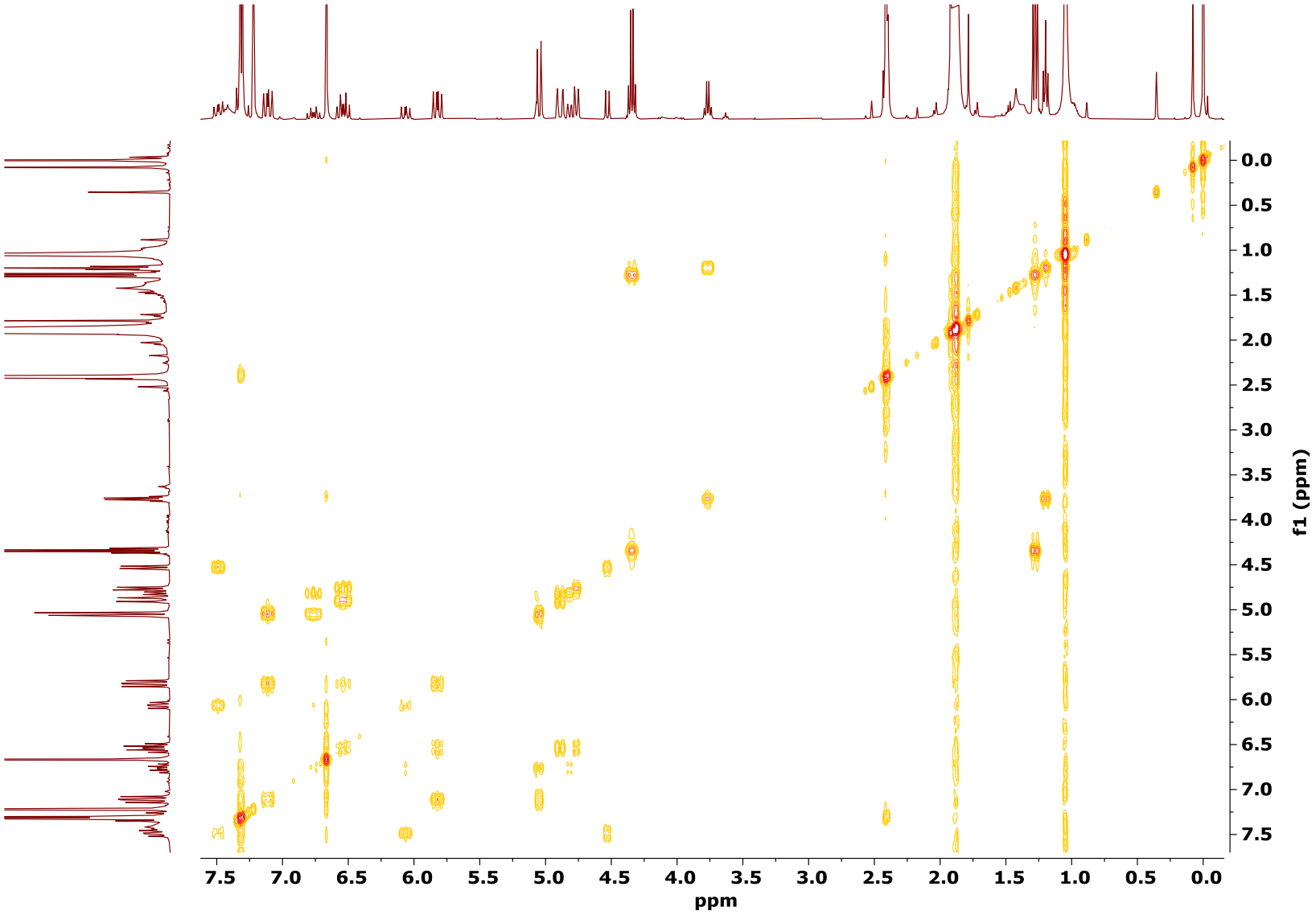

Figure E2. HH COSY NMR (C_6D_6) of ethyl sorbate ion pair (**1**) synthesized using deuterated benzene (C_6D_6) stock solutions.

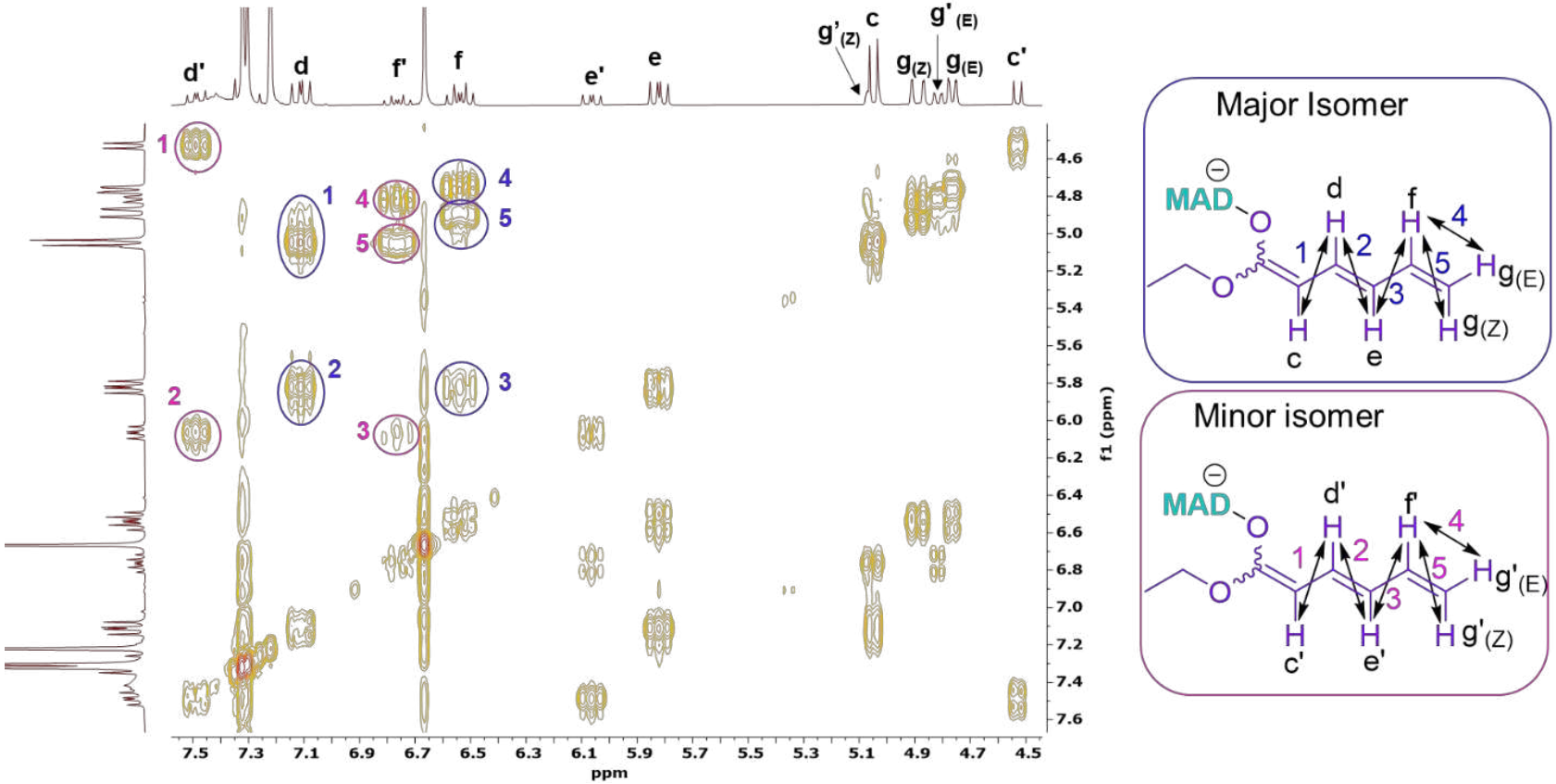

Figure E3. HH COSY NMR (C_6D_6) of ethyl sorbate ion pair (**1**) synthesized using deuterated benzene (C_6D_6) stock solutions, expanded to the alkene region and assigned.

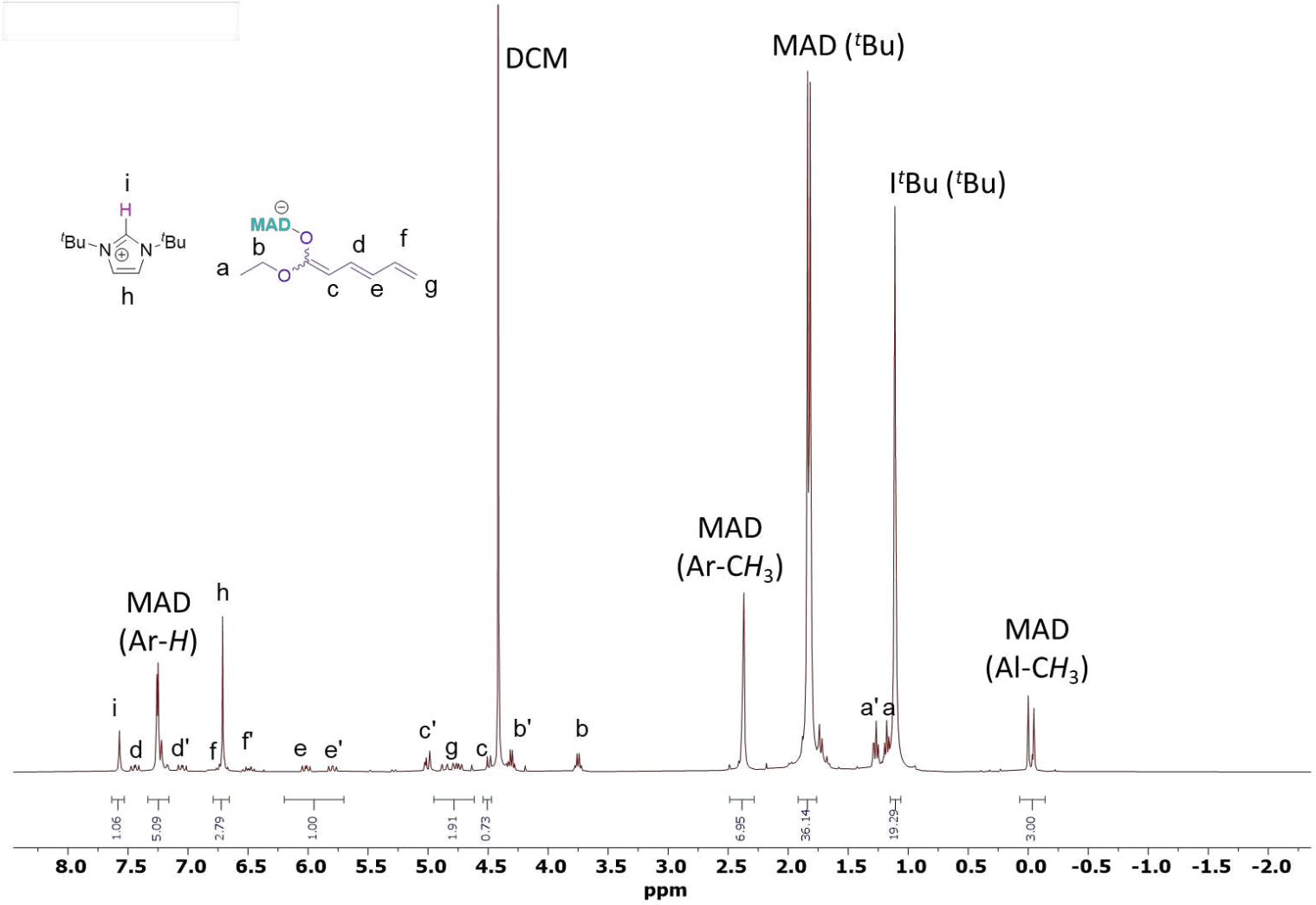

Figure E4. Assigned ^{1}H NMR (C_6D_6) of ethyl sorbate ion pair (**1**) synthesized using DCM stock solutions.

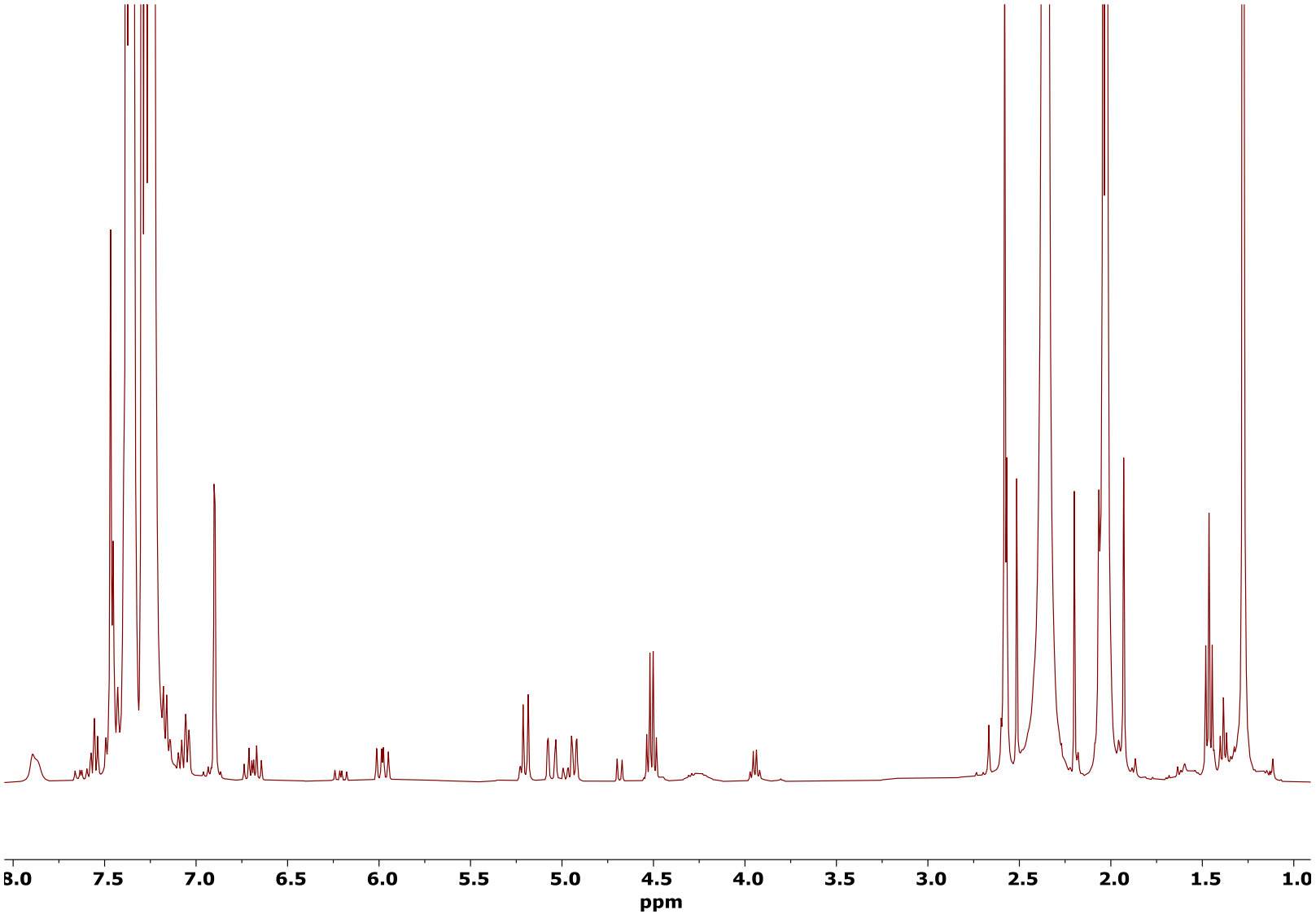

Figure E5. ^{1}H NMR (C_6D_6) of ethyl sorbate ion pair (**1**) synthesized at -30 °C using toluene stock solutions.

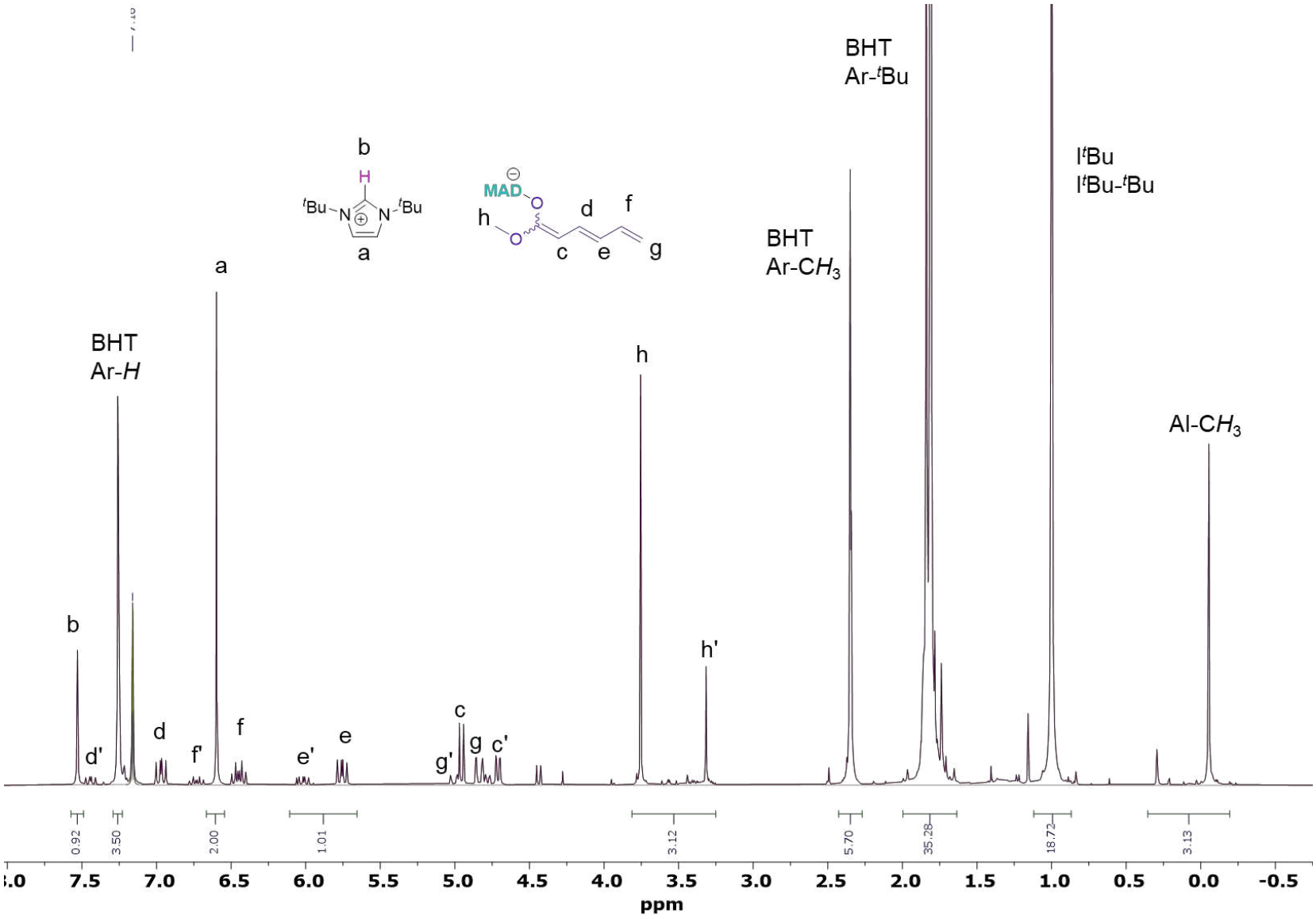

Figure E6. ^{1}H NMR (C_6D_6) of methyl sorbate ion pair synthesized using deuterated benzene (C_6D_6) stock solutions.

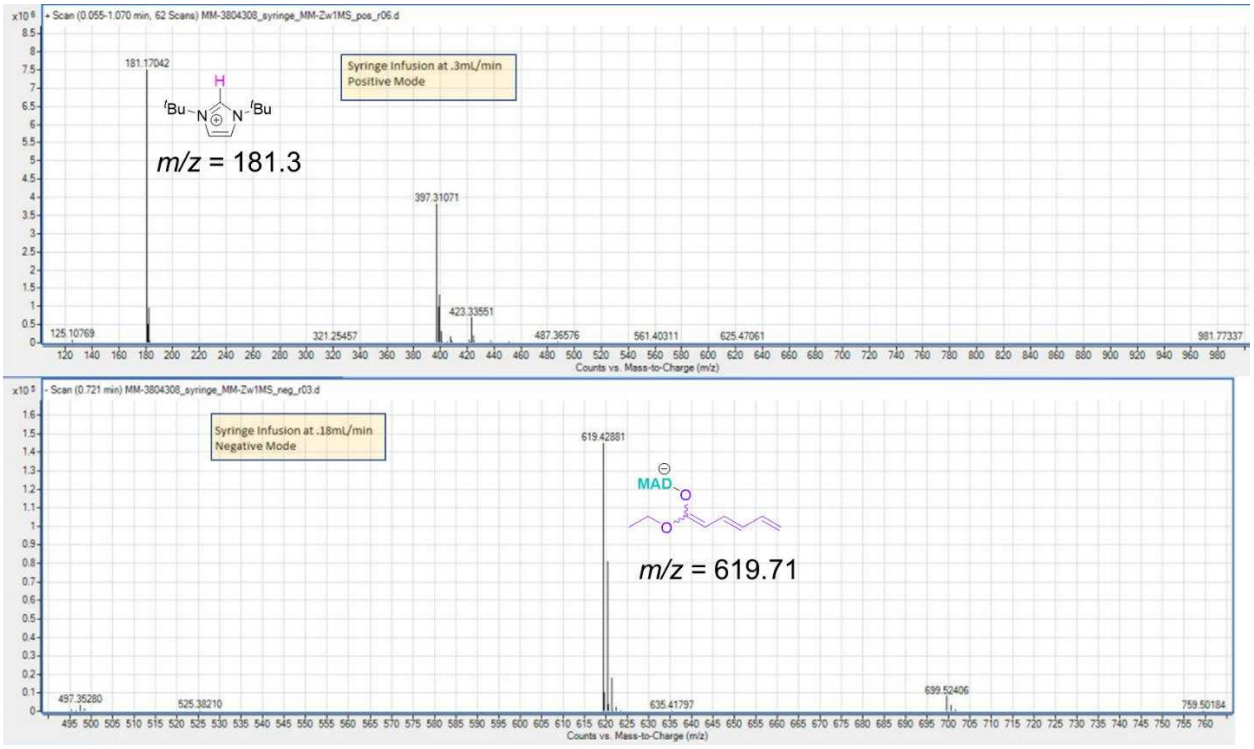

Figure E7. Mass spectrum of ethyl sorbate ion pair (**1**) collected in positive (above) and negative (below) modes respectively, revealing the H-I^{t}Bu$^+$ and ES$^-$ ion pair counter parts, respectively.

Preparation of Ethyl Sorbate-TPT Zwitterion

The zwitterion cocktail (**2**) was prepared identically to the ion pair **1**, with the exception that NHC TPT was substituted for NHC I^{t}Bu. Stock solutions were prepared in C_6D_6 at 0.080 M. Ethyl sorbate stock solution (0.20 mL, 16 μmol) was mixed with MAD stock solution (0.20 mL, 16 μmol). Then the ES/MAD mixture (0.2 mL) was added to the TPT stock solution (0.20 mL, 16 μmol) with stirring. This 1/1/1 mixture was immediately sent for NMR analysis.

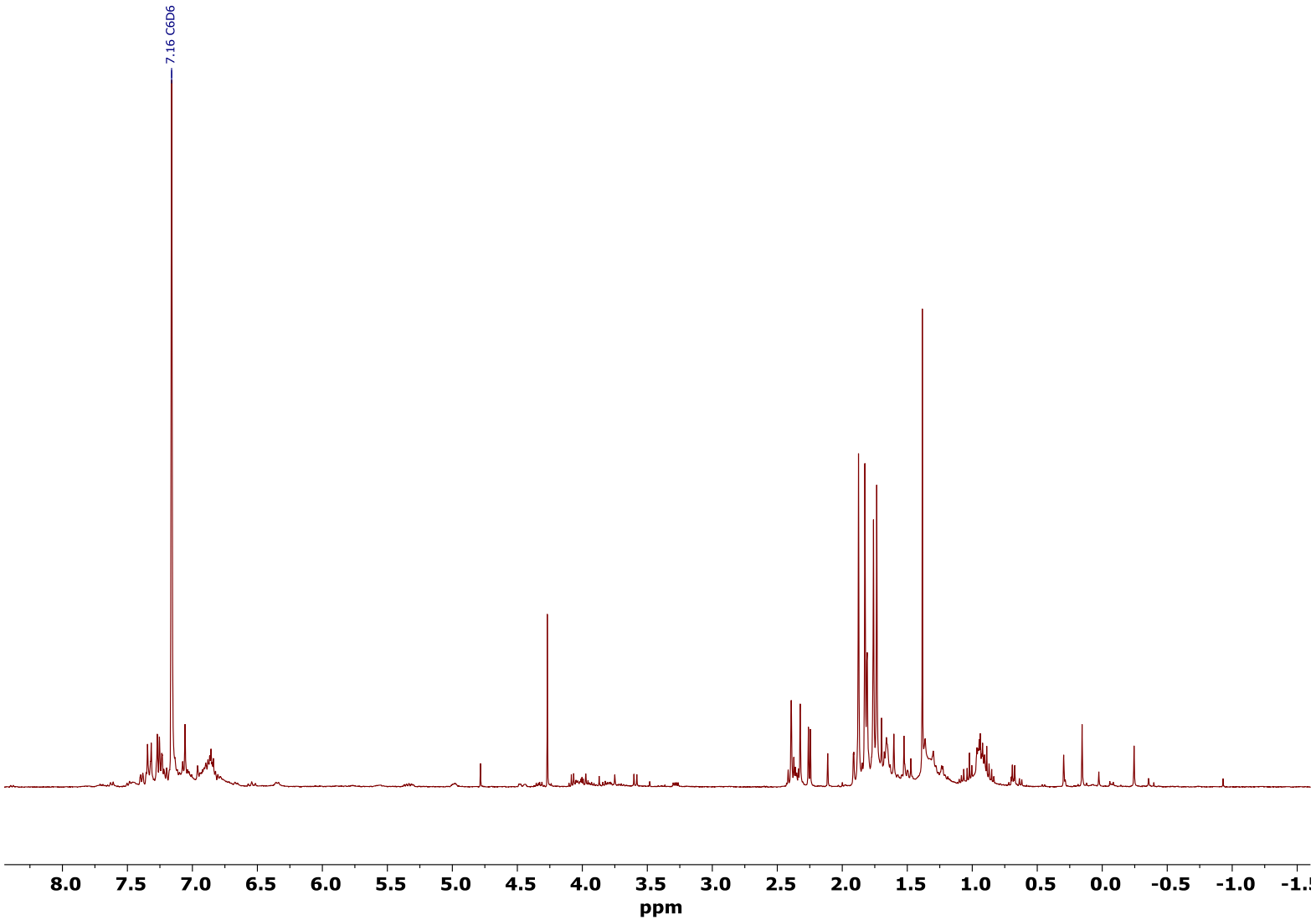

Figure E8. ^{1}H NMR (C_6D_6) of ethyl sorbate-TPT zwitterion cocktail (**2**).

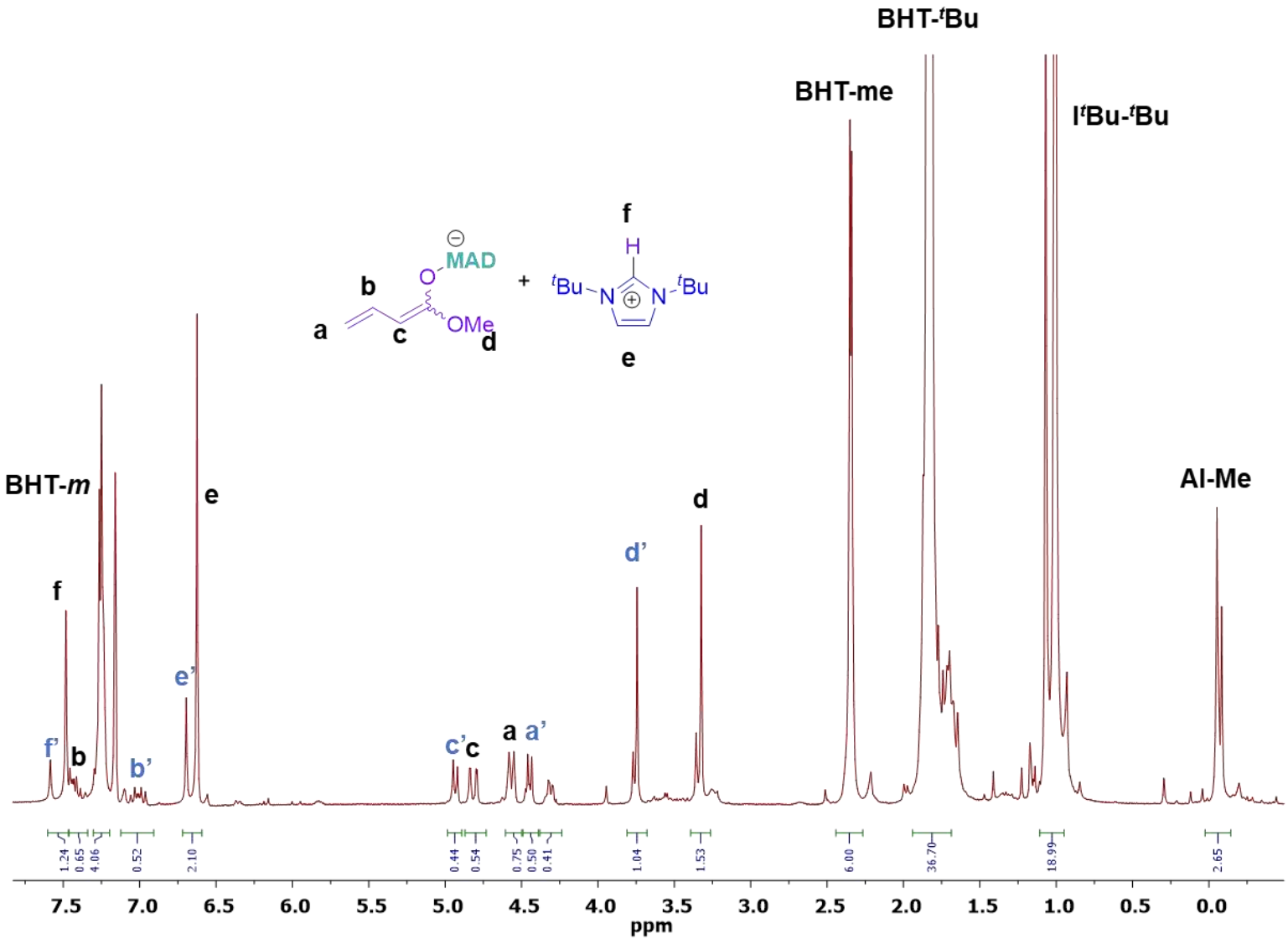

Figure E9. ^{1}H NMR (C_6D_6) of methyl crotonate ion pair (**3**).

General Polymerization Procedure for the preparation of cyclic polymers by LPP

A typical polymerization was carried out as follows. In an argon filled glovebox, monomer (MMA, BMA, AMA, ES) was premixed in toluene with MAD at appropriate concentrations and stirred vigorously. Then, the initiator (**1**, **2**, **3**) was injected as an appropriate volume (usually 0.20 mL) of a stock solution (usually DCM, as I^{t}Bu solubility is problematic in toluene) prepared at an appropriate concentration. For cyclic polymers, we prefer 24 h as a suitable timeframe to allow full cyclization. In some cases, we pipette a desired volume of the reaction directly into powdered benzoic acid (~100 mg) to quench prematurely. Otherwise, after 24 h, we removed the reactor from the glovebox and directly added 100-200 mg of benzoic acid. We then preserve an aliquot to check conversion by NMR and proceed to remove the toluene by rotary evaporation. A minimal volume of chloroform was used to re-dissolve the dry polymer/ reaction mixture. This chloroform solution is then added to cold methanol (chilled with dry ice for best results) dropwise with stirring. The white solid precipitant was collected by filtration, then re-dissolved in chloroform, at which point a cloudy solid was visible. The chloroform solution was filtered through a 0.20 μm syringe filter and was finally dried by rotary evaporation followed by 12-24 h in a 60 ^{o}C vacuum oven.

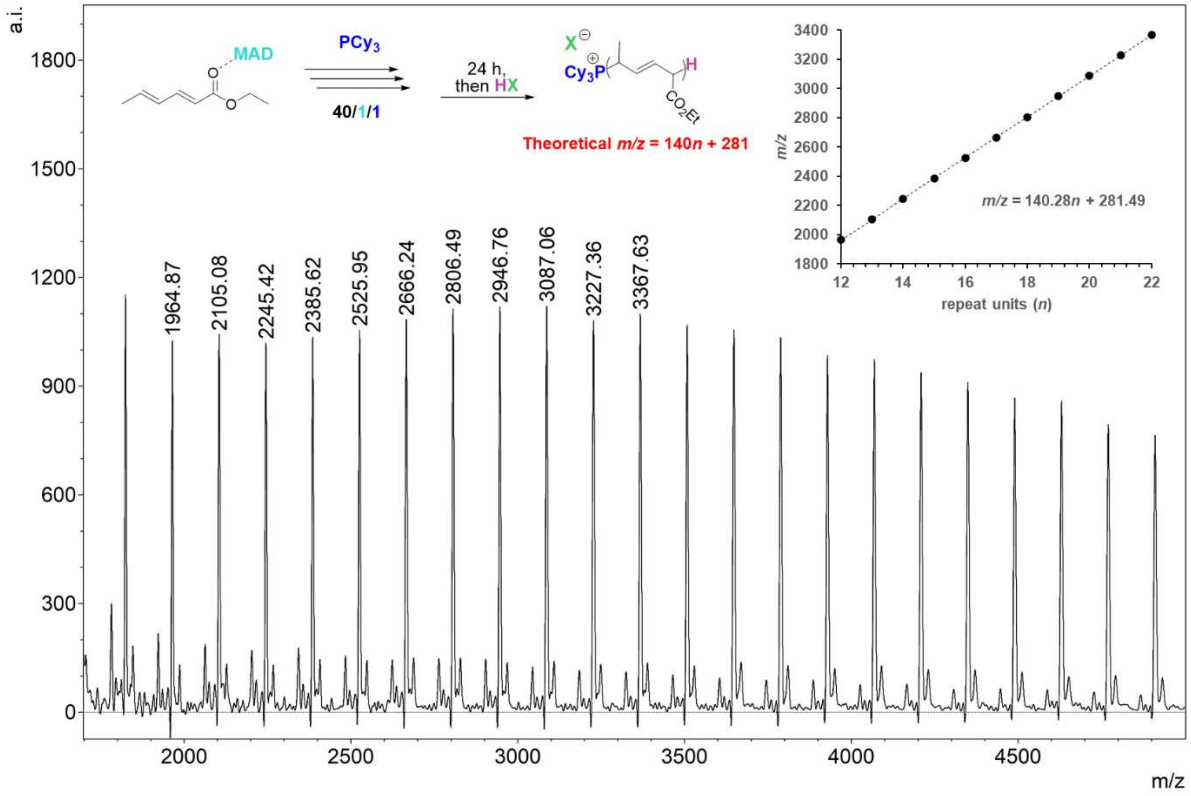

Figure E10. MALDI-TOF spectrum and end group analysis of ethyl sorbate PCy_3 zwitterion PES. Demonstrating the zwitterionic nature of the polymerization.

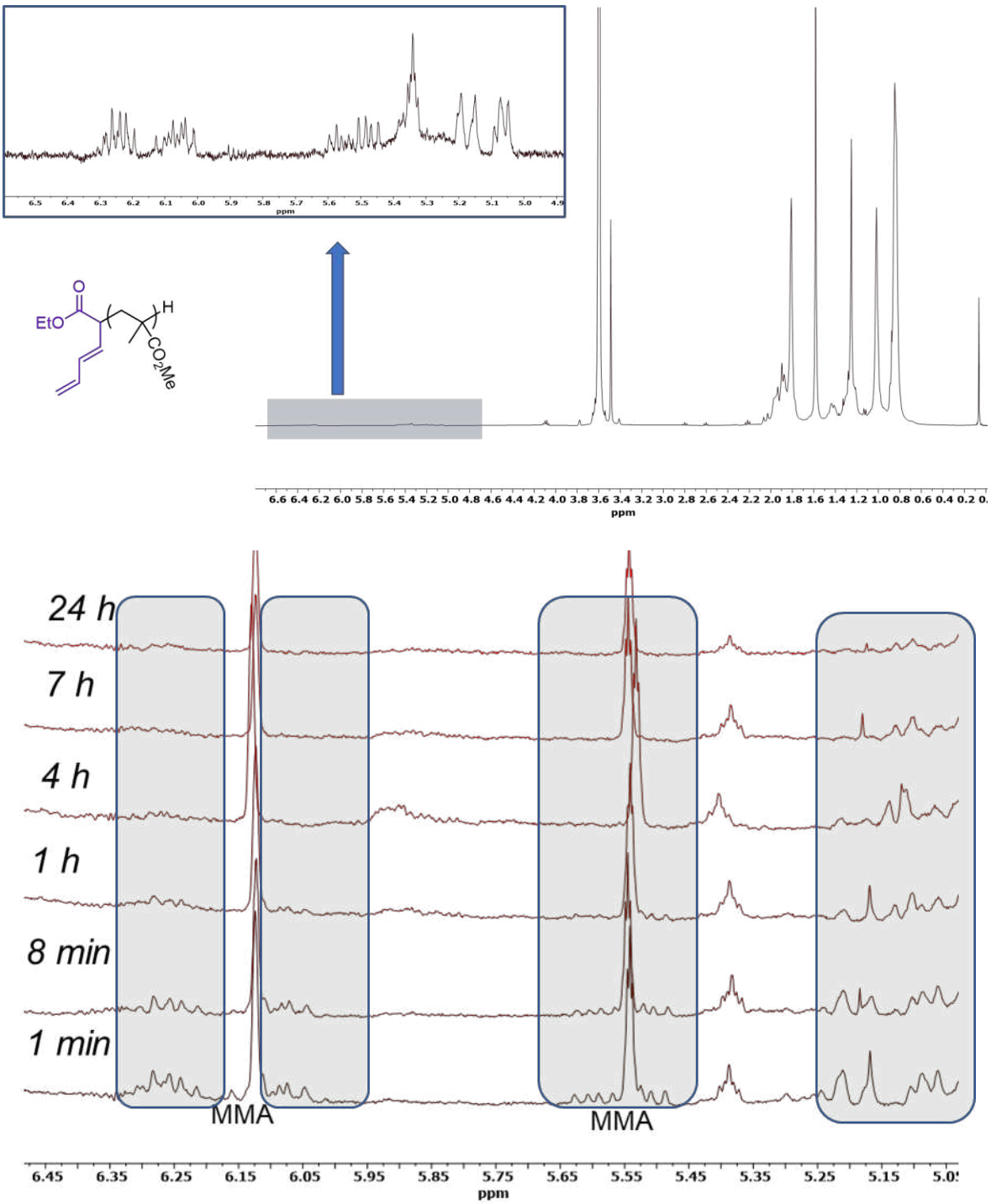

Figure E11. (Top) ^{1}H NMR ($CDCl_3$) spectrum and end group analysis of *l*-PMMA prepared by **1** at an MMA/MAD/**1** molar ratio of 25/0.50/1.00, quenched after one minute to prevent any cyclization, expanded to alkenyl region to show abundance of alkene peaks attributed to sorbate terminus. (Bottom) ^{1}H NMR of an identical polymerization quenched at various time points,

expanded to the alkenyl region to show time dependent disappearance of alkenyl peaks presumably associated cyclization according to our proposed H-transfer/then conjugate addition mechanism.

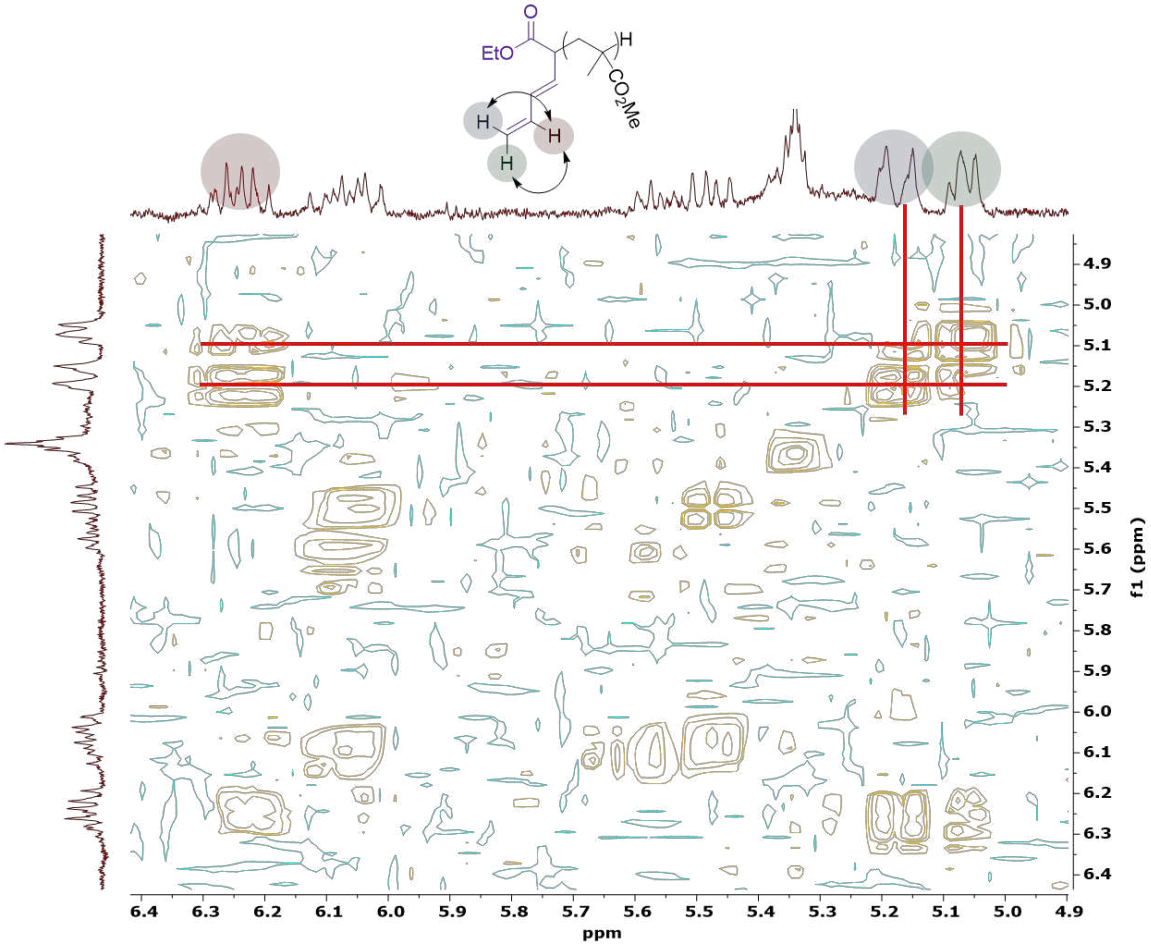

Figure E12. HH COSY NMR ($CDCl_3$) spectrum and end group analysis of *l*-PMMA prepared by **1** at an MMA/MAD/**1** molar ratio of 25/0.50/1.00, quenched after one minute to prevent any cyclization, expanded to alkenyl region to show NOE between alkene peaks suggestive of terminal alkene.

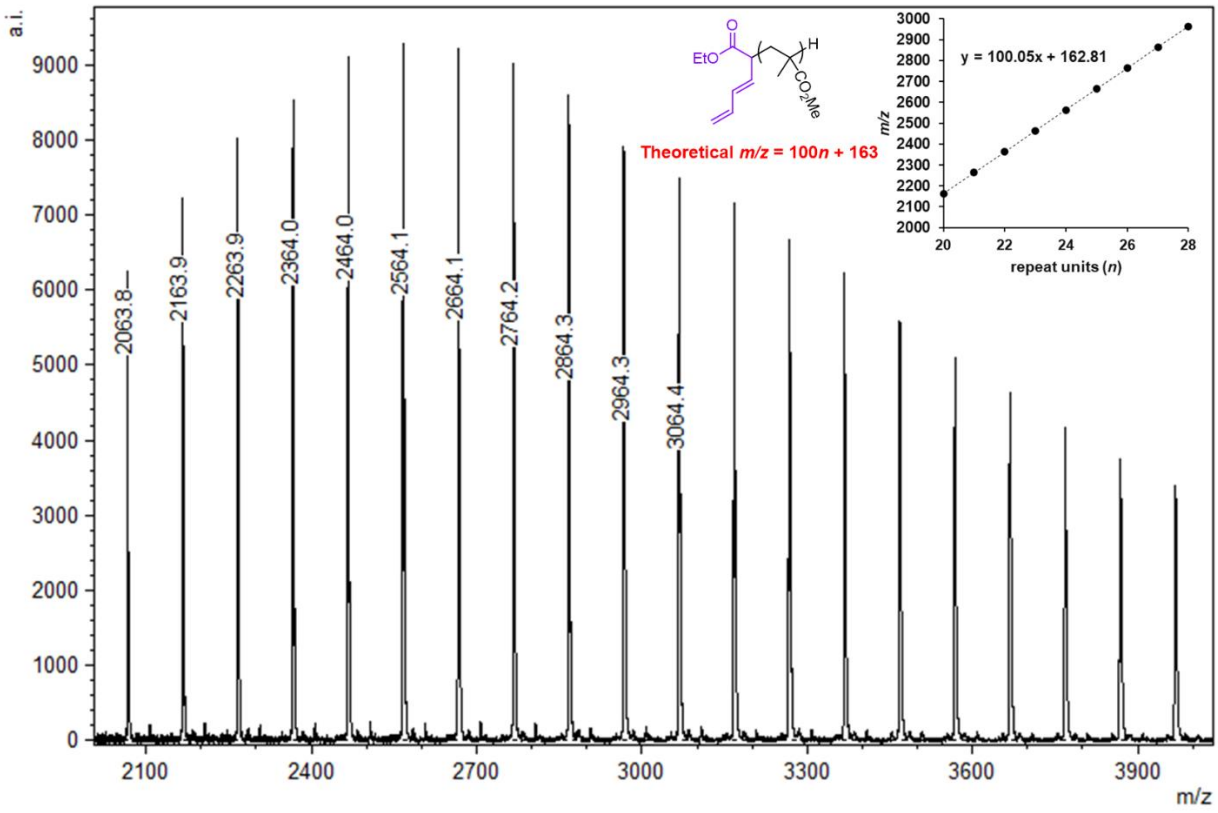

Figure E13. MALDI-TOF spectrum and end group analysis of *l*-PMMA prepared by **1** at an MMA/MAD/**1** molar ratio of 25/0.50/1.00, quenched after one minute to prevent any cyclization.

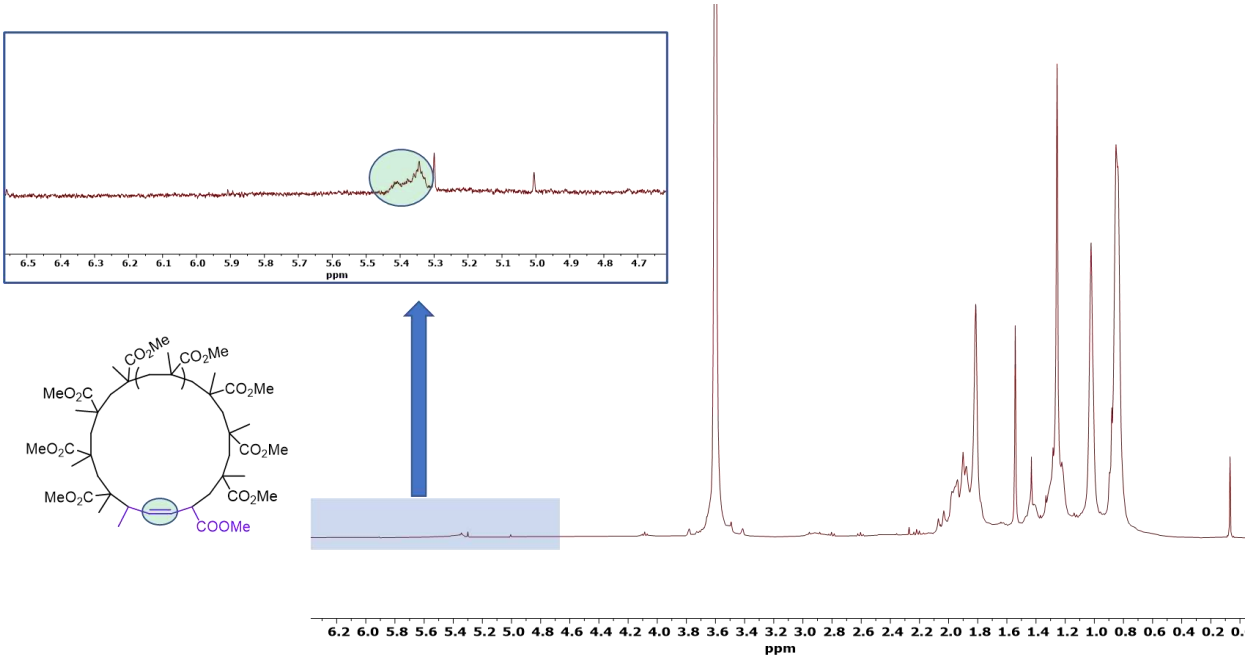

Figure E14. ^{1}H NMR ($CDCl_3$) spectrum and end group analysis of *c*-PMMA prepared by **1** at an MMA/MAD/**1** molar ratio of 25/0.50/1.00, quenched after 24 h to allow full cyclization, expanded to alkenyl region to show disappearance of alkenyl peaks observed in Figure E11.

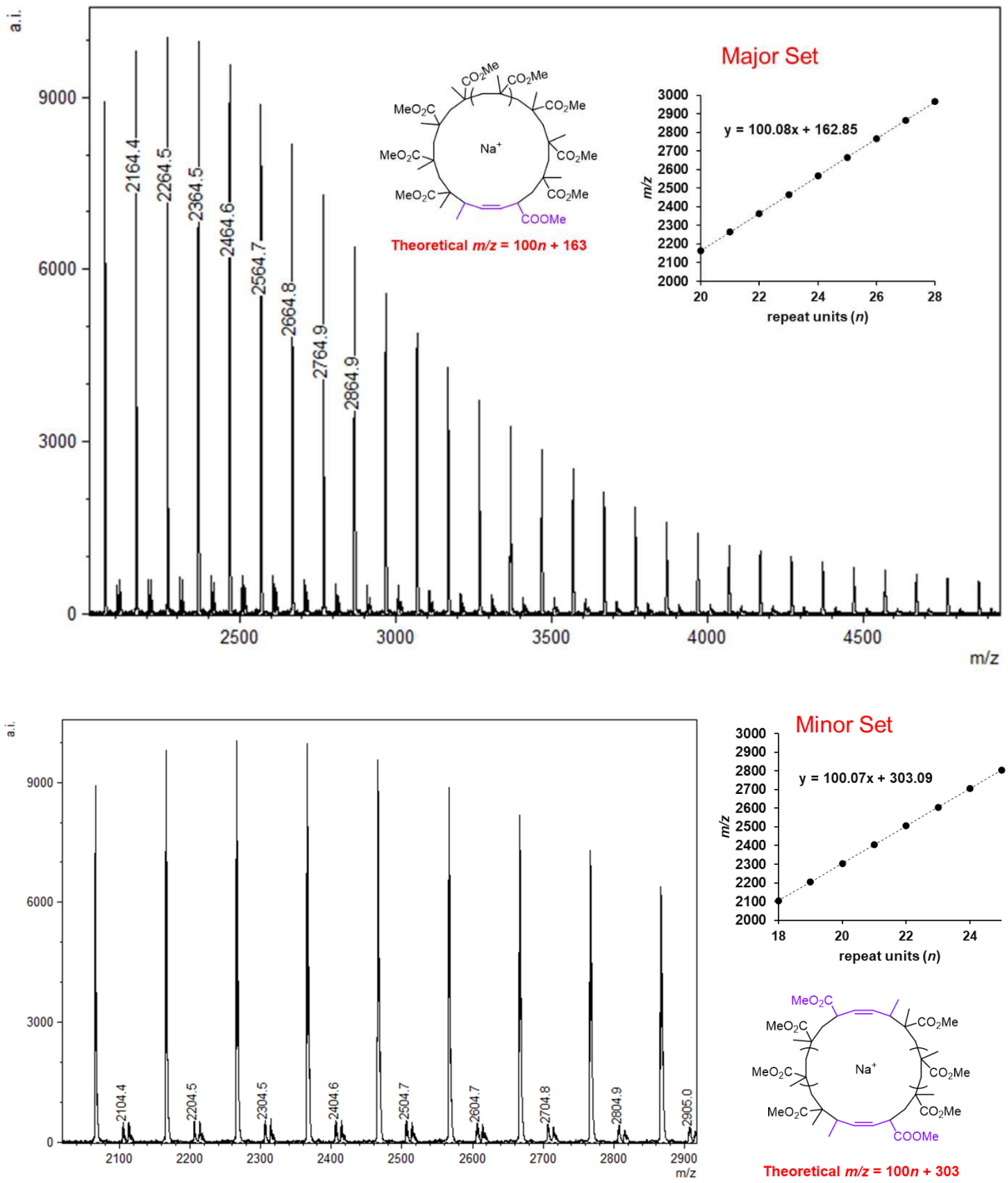

Figure E15. MALDI-TOF spectrum and end group analysis of *c*-PMMA prepared by **1** at an MMA/MAD/**1** molar ratio of 25/0.50/1.00, given 24 h for full cyclization.

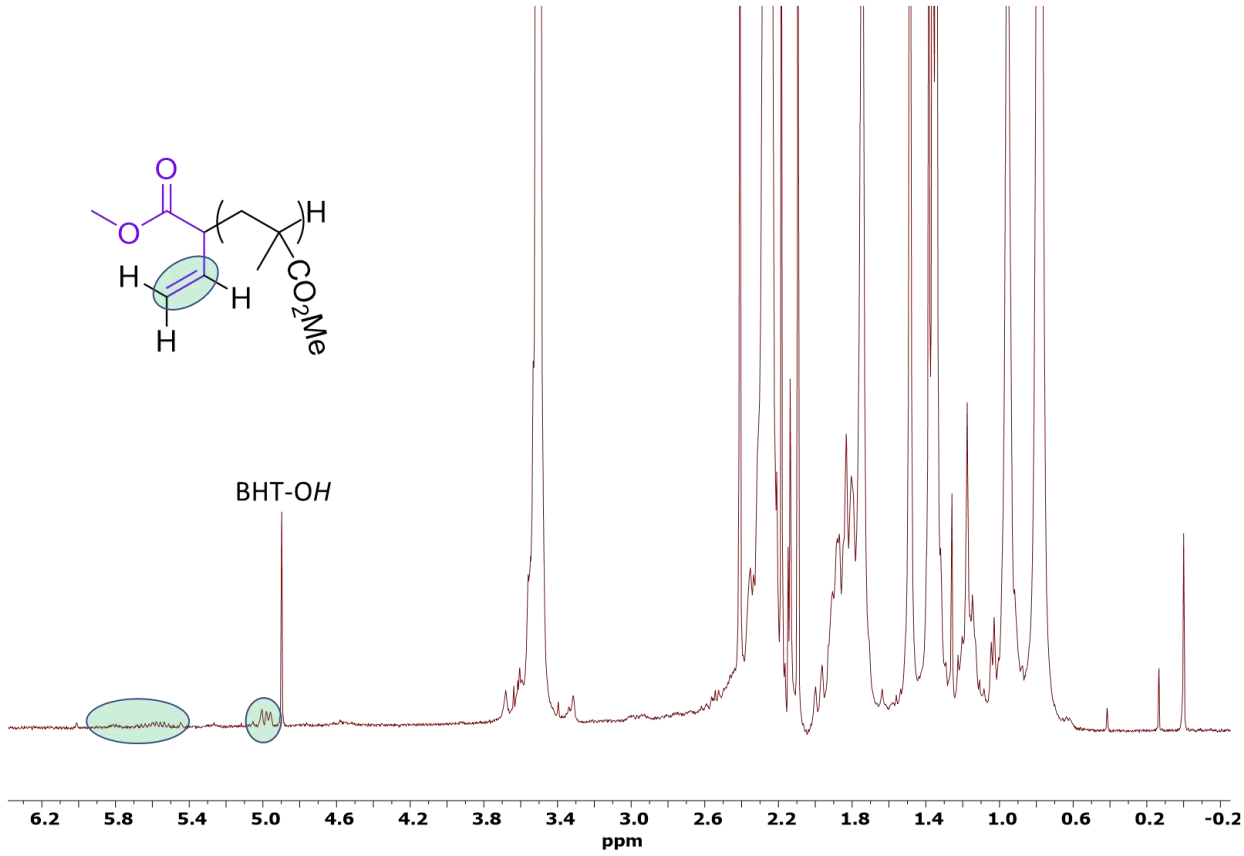

Figure E16. ^{1}H NMR ($CDCl_3$) spectrum and end group analysis of *l*-PMMA prepared by **3** at an MMA/MAD/**3** molar ratio of 25/0.50/1.00, quenched after 3 min to prevent any cyclization, showing alkenyl peaks attributed to crotonate terminus.

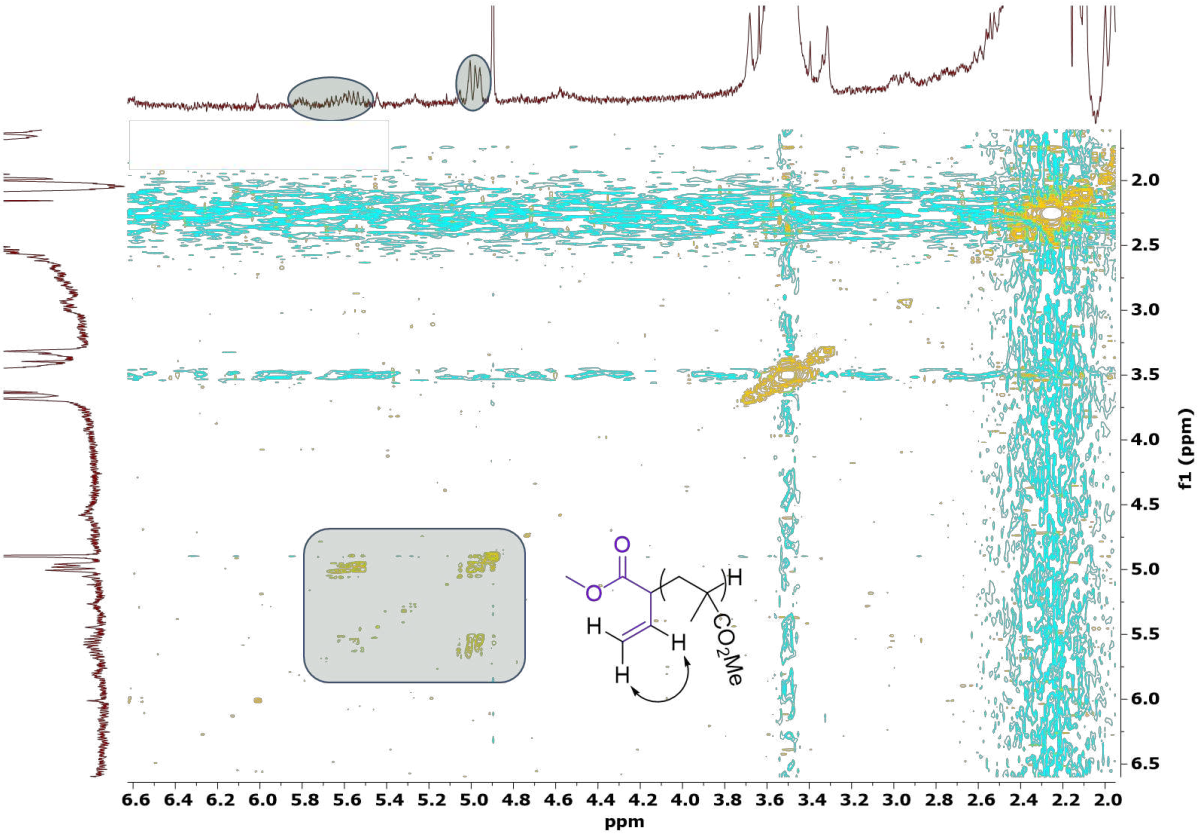

Figure E17. HH COSY NMR ($CDCl_3$) spectrum and end group analysis of *l*-PMMA prepared by **3** at an MMA/MAD/**3** molar ratio of 25/0.50/1.00, quenched after 3 min to prevent any cyclization, expanded to alkenyl region to show NOE between alkene peaks suggestive of terminal alkene.

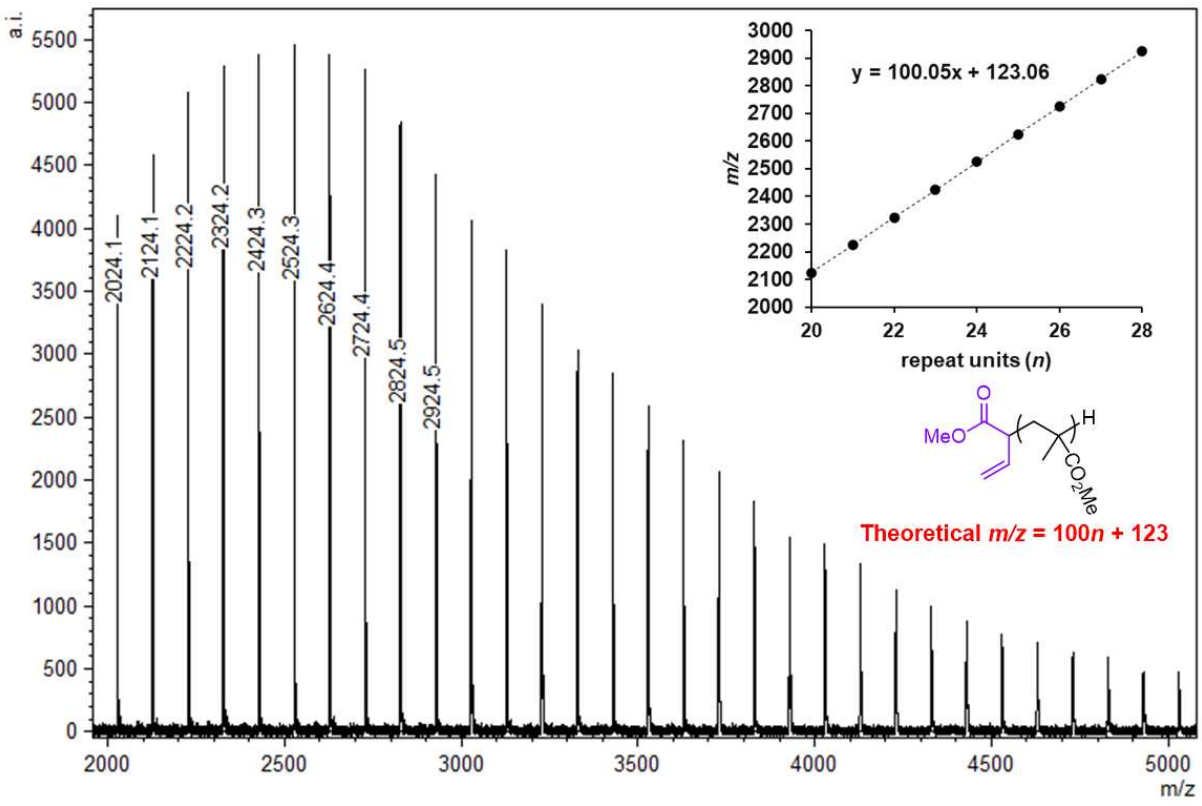

Figure E18. MALDI-TOF spectrum and end group analysis of *l*-PMMA prepared by **3** at an MMA/MAD/**3** molar ratio of 25/0.50/1.00, quenched after 3 min to prevent any cyclization.

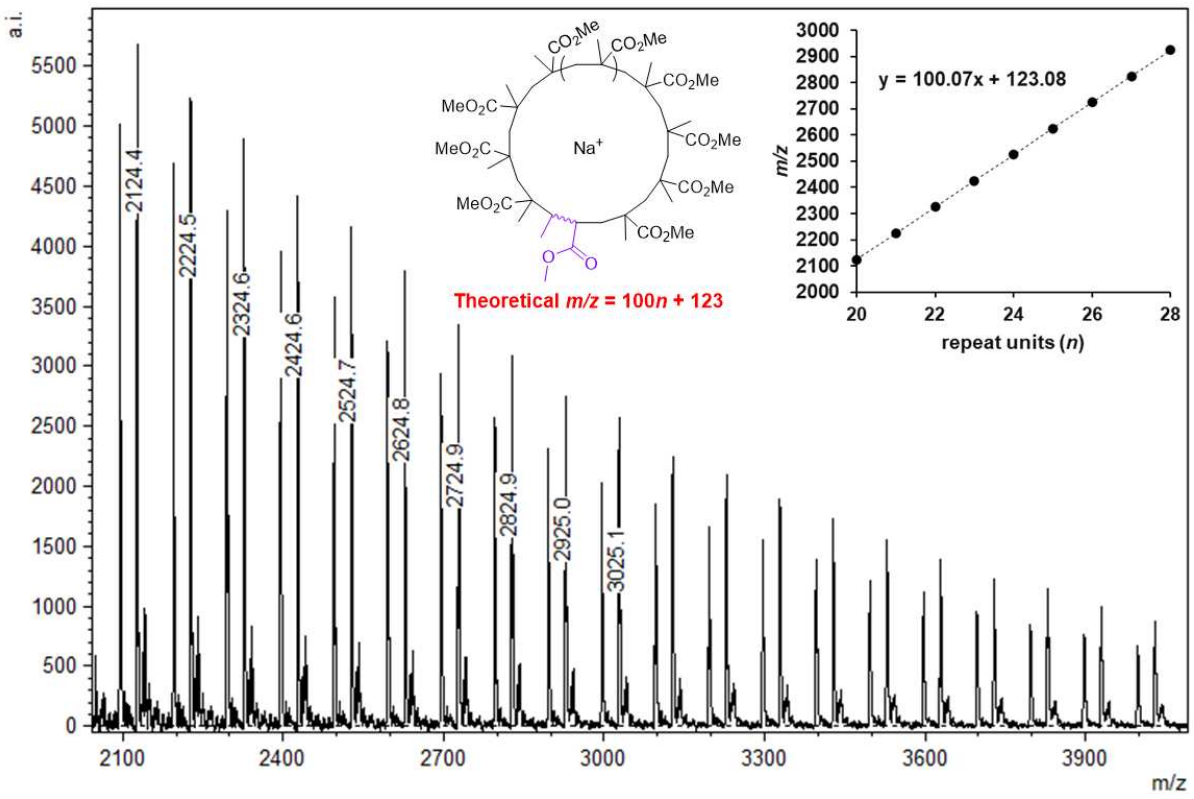

Figure E19. MALDI-TOF spectrum and end group analysis of *c*-PMMA prepared by **3** at an MMA/MAD/**3** molar ratio of 25/0.50/1.00, quenched after 24 h to allow full cyclization. Labeled peaks and accompanying plot correspond to the major set of peaks representing the cyclized structure.

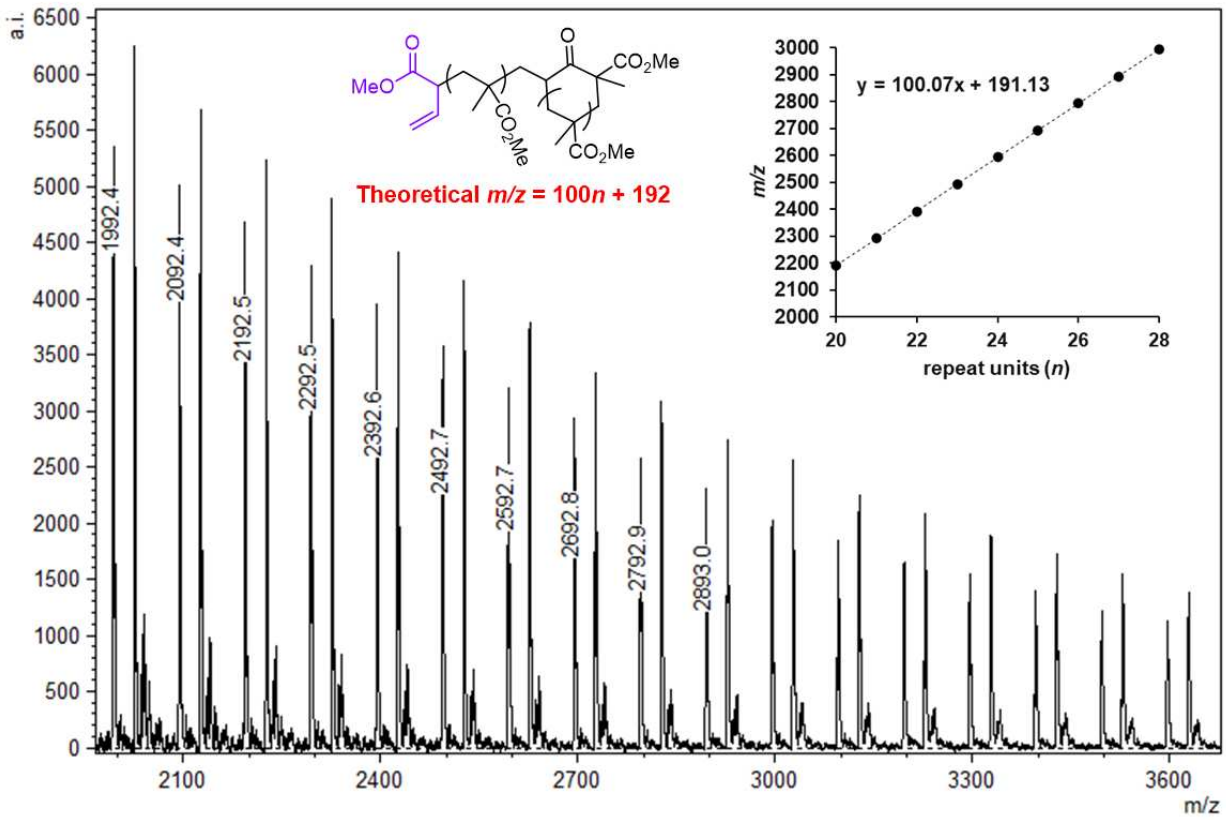

Figure E20. MALDI-TOF spectrum and end group analysis of *c*-PMMA prepared by **3** at an MMA/MAD/**3** molar ratio of 25/0.50/1.00, quenched after 24 h to allow full cyclization. Labeled peaks and accompanying plot correspond to the minor set of peaks representing the Claisen-type terminated polymer (This is the same spectrum as shown in Figure E19).

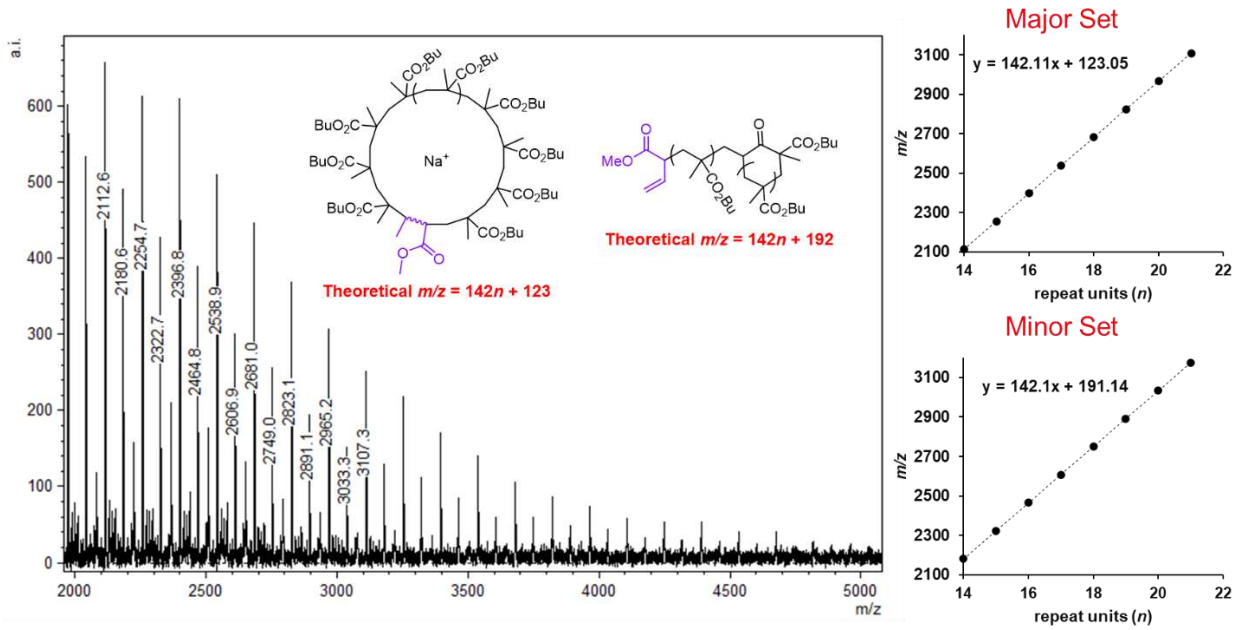

Figure E21. MALDI-TOF spectrum and end group analysis of *c*-PBMA prepared by **3** at an BMA/MAD/**3** molar ratio of 25/0.50/1.00, quenched after 24 to allow full cyclization. The major set of peaks give an end group identical to the analogous MMA run (Figure E19) while the minor set gives a Claisen-type termination product identical to the analogous MMA run (Figure E20).

Preparation of 1-octadecanethiol-Grafted Cyclic Poly(allyl methacrylate) (*c*-PAMA$_g$)

A 100 mL round bottom flask was charged with *c*-PAMA (1.0 g, M_n = 55.2 kg mol^{-1}), excess 1-octadecanethiol (5.8 g), 2,2-dimethoxy-2-phenylacetophenone (DMPA, 0.149 g, excess), 75 mL of non-stabilized tetrahydrofuran, and a stir bar. The mixture was stirred vigorously until all components were dissolved, at which time the reaction vessel was moved to a UV reactor (365 nm) and irradiated for 8 h. Volatiles were removed via roto-vap. The dried products were re-dissolved in chloroform, cooled to 0 ^oC, and precipitated with diethyl ether. The precipitated PAMA$_g$ was collected by filtration, washed with ether three times, and dried in a vacuum oven at 40 ^oC until a constant mass was achieved. This procedure has been found successful for removing detectable 1-octadecanethiol remnants.

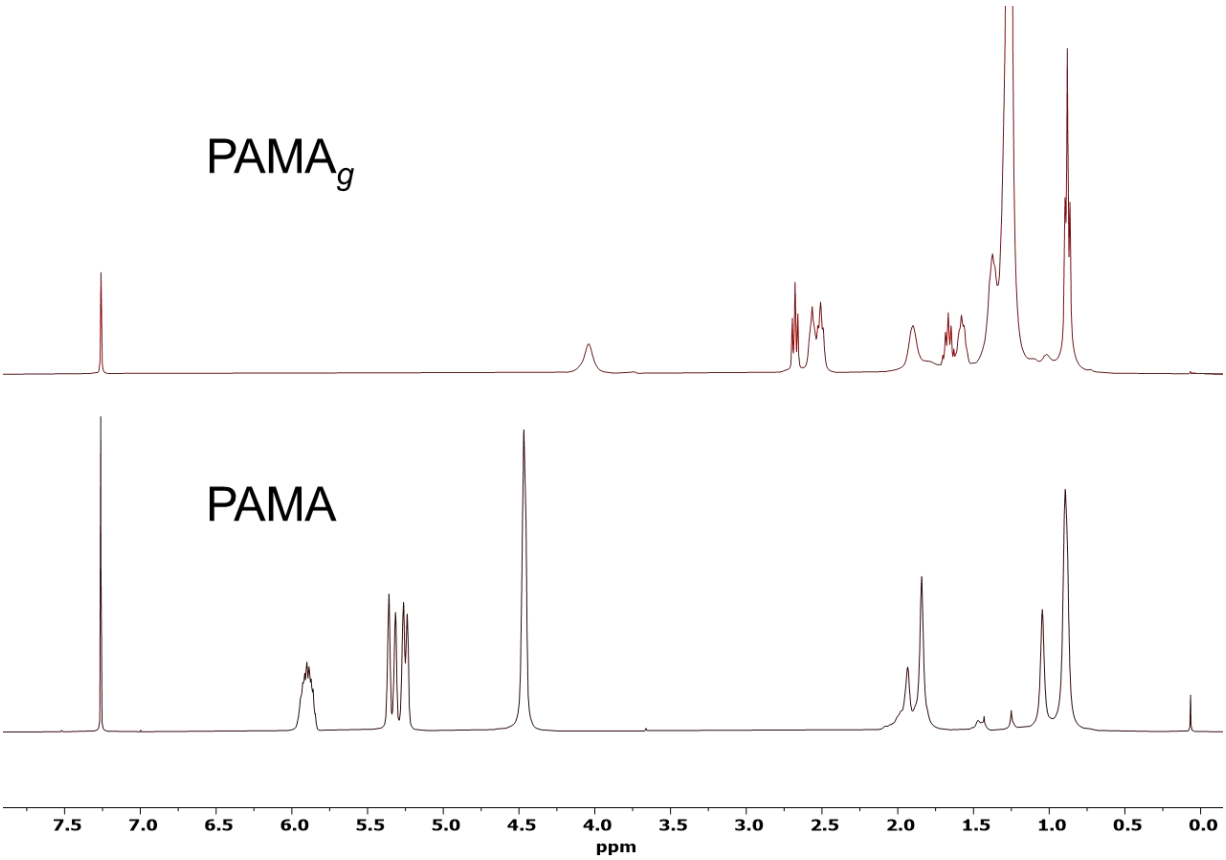

Figure E22. Overlayed ^{1}H NMR ($CDCl_3$) spectra of PAMA before (PAMA) and after ($PAMA_g$) thiol-ene click grafting of 1-octadecanethiol.

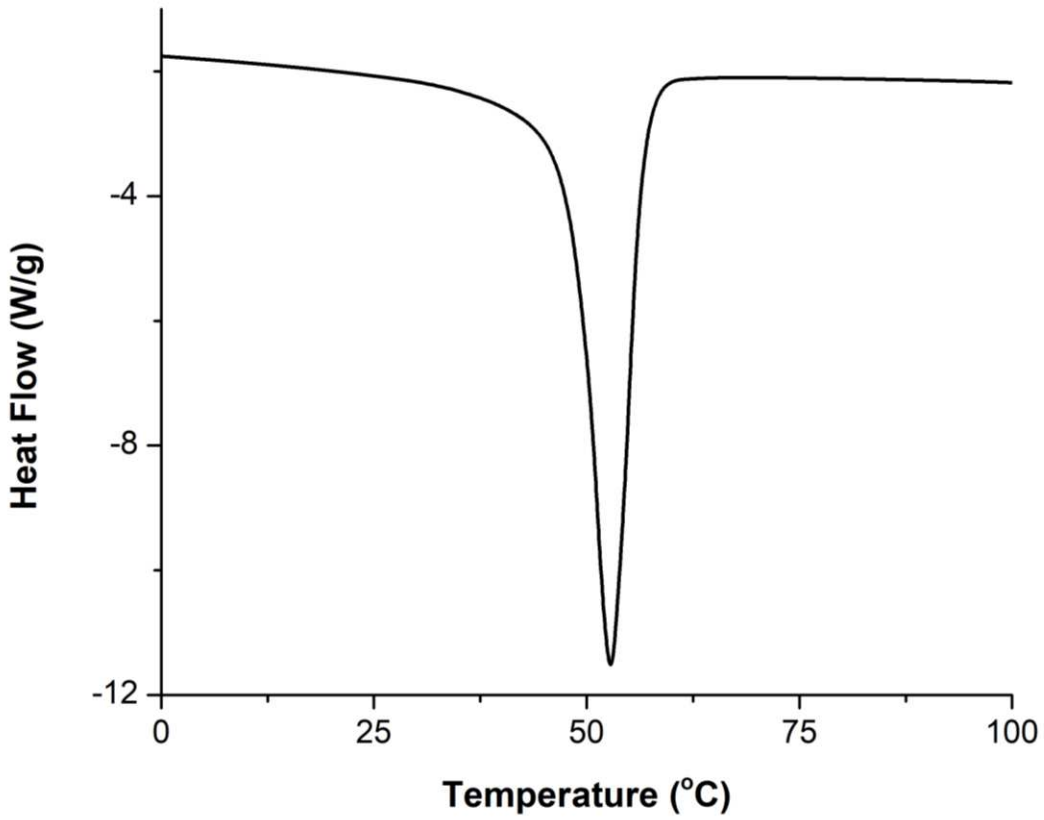

Figure E23. DSC heating scan (endo down) for PAMA$_g$ highlighting the introduced T_m (53 °C) from the crystalline grafted 1-octadecanethiol units.

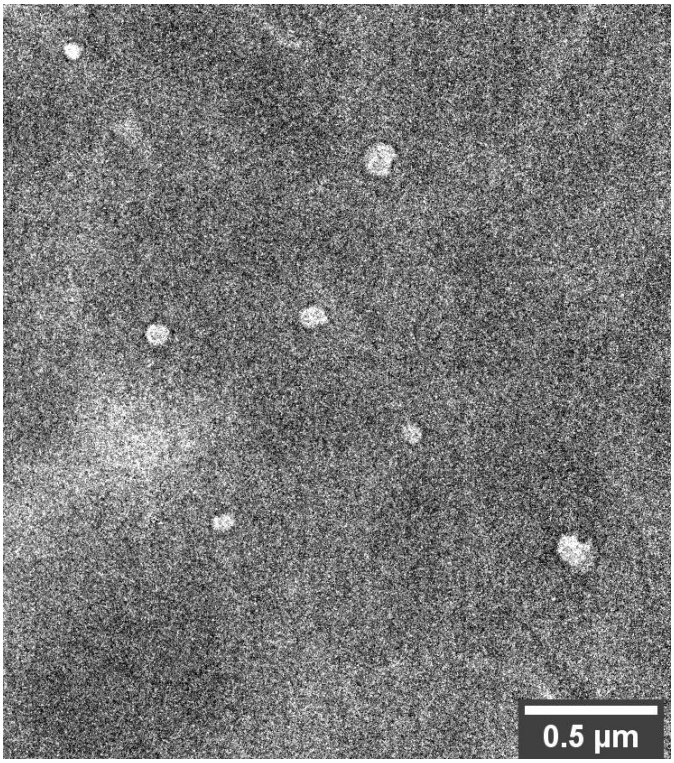

Figure E24. TEM image of *c*-PAMA$_g$ drop-casted thin film at 0.5 µm scale.

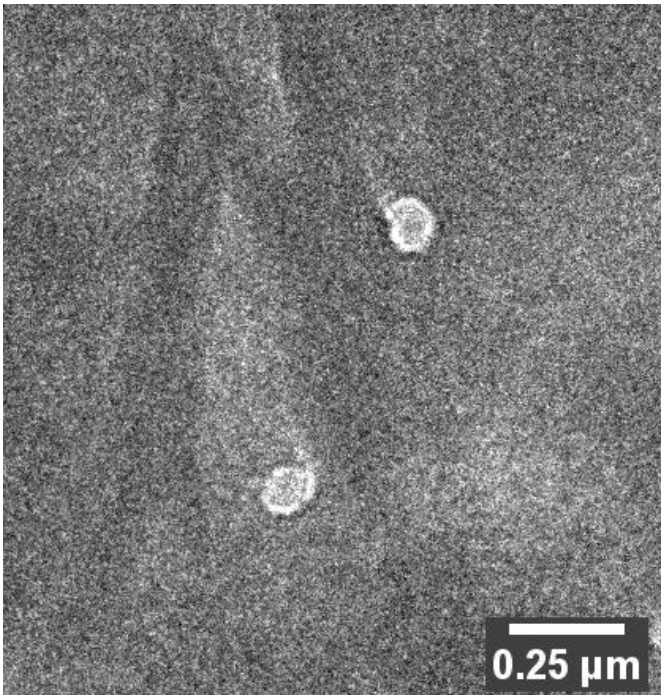

Figure E25. TEM image of *c*-PAMA$_g$ drop-casted thin film at 0.25 µm scale.

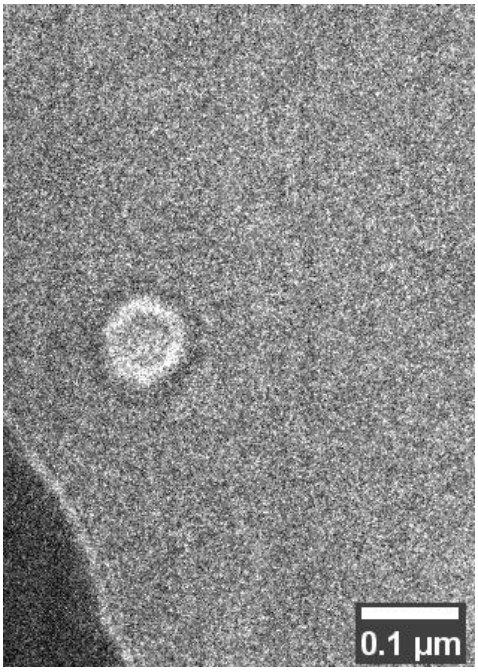

Figure E26. TEM image of *c*-PAMA$_g$ drop-casted thin film at 0.1 µm scale.